Fall 2014

# Syntheses of Aminyl Diradicals and Nitroxide Tetra- and Octaradicals

Arnon Olankitwanit
*University of Nebraska-Lincoln*, arnon@huskers.unl.edu

Syntheses of Aminyl Diradicals and Nitroxide Tetra- and Octaradicals

by

Arnon Olankitwanit

A DISSERTATION

Presented to the Faculty of

The Graduate College at the University of Nebraska

In Partial Fulfillment of Requirements

For the Degree of Doctor of Philosophy

Major: Chemistry

Under the Supervision of Professor Andrzej Rajca

Lincoln, Nebraska

October, 2014

Syntheses of Aminyl Diradicals and Nitroxide Tetra- and Octaradicals

Arnon Olankitwanit, Ph.D.

University of Nebraska, 2014

Advisor: Andrzej Rajca

This dissertation comprises of two main research projects: aminyl diradicals and calix[4]arene nitroxide tetra- and octaradicals. The design, multi-step synthesis and characterization, including NMR, EPR spectroscopy, magnetic measurements and X-ray crystallography of precursors and target compounds will be discussed.

Aminyl radicals, nitrogen-centered radicals, are typically short-lived and considered as reactive intermediates. Because of their unique magnetic properties, aminyls are attractive building blocks for high-spin di-and polyradicals. The challenge is in the design and synthesis of aminyls with increased stability. In this chapter, we have prepared triplet ($S = 1$) ground state aminyl diradicals, which are derivatives of aza-$m$-xylylene diradicals. Triplet ($S = 1$) ground state these aminyl diradicals are predicted to possess singlet-triplet energy gap, $\Delta E_{ST} \approx 10 - 14$ kcal mol$^{-1}$. Kinetics experiments for these aminyl diradicals are carried out in solution of 2-methyltetrahydrofuran at room temperature with the half-life measured in minutes.

Nitroxides are one of the most studied stable radicals in chemistry and in other related fields because of their stability. To explore potential of nitroxides as paramagnetic contrast agents for magnetic resonance imaging (MRI), we designed and synthesized 1,3-

alternate calix[4]arenes nitroxide tetraradical and octaradical. Attachment of nitroxides on a rigid, well-defined framework such as calix[4]arene locked in 1,3-alternate conformation allow for study of the exchange coupling through bond and through space. In this chapter, 1,3-alternate calix[4]arenes with phenylene spacers connecting mononitroxides and high-spin ($S = 1$) dinitroxides on the upper rim providing calix[4]arene nitroxide tetraradicals and octaradicals, respectively, are synthesized and characterized by ^{1}H NMR and EPR spectroscopy. With the desire in biological applications, calix[4]arene nitroxide tetraradical and octaradical with hexaethylene glycol methyl ether (HEG) are also synthesized and characterized.

## Acknowledgement

Table of Contents

**CHAPTER 1**

**AMINYL DIRADICALS**

Portions of the work described in this chapter have been reported: (1) Rajca, A.; Olankitwanit, A.; Rajca, S. "Triplet Ground State Derivative of Aza-*m*-xylylene diradical with large singlet–triplet energy gap", *J. Am. Chem. Soc.* **2011**, *133*, 4750–4753. (2) Olankitwanit, A.; Pink, M.; Rajca, S.; Rajca, A. "Synthesis of aza‑*m*‑xylylene diradicals with large singlet–triplet energy gap and statistical analyses of their EPR spectra", *J. Am. Chem. Soc.* **2014**, *136*, 14277−14288.

## 1.1. Introduction

Organic radicals and polyradicals, molecules containing unpaired electrons, are an important class of organic compounds that are studied in a wide range of multidisciplinary fields. Applications of organic radicals include sensing, switching devices, contrast agents for magnetic resonance imaging, spin labels, and mediators for radical polymerizations. There are many other classes of radical containing compounds, including triphenylmethyl radicals (trityls), triplet carbenes, nitrenes and relatively stable and well-studied nitroxide radicals. However, this chapter will provide general background on the subclass of high-spin organic radicals with a particular focus on triplet ground state diradicals.

### 1.1.1. Background on diradicals

The interest in organic radicals accelerated with the breakthrough discovery of the first stable carbon-based radical, triphenylmethyl radical, by Gomberg[1] in 1900 (Figure

1.1).   The propeller-twisted phenyl rings in triphenylmethyl radical impose a large steric

hindrance near the α-carbon but twist angle is moderate enough to allow for significant

delocalization of the spin density into the phenyl rings.  At room temperature under inert

atmosphere, solution of triphenylmethyl contains radical that exists in equilibrium with its

dimer; e.g., in benzene solution, the percentages of the radical and the dimer are

approximately 1% and 99%, respectively.
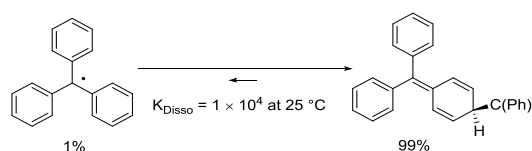


**Figure 1.1.**  Gomberg triphenylmethyl radical.

Radicals, free radicals or monoradicals typically refer to molecules containing an

unpaired electron, such compounds are usually highly reactive and short-lived.  In quantum

mechanics, each electron has a spin (an intrinsic angular momentum), which is assigned to

have a spin quantum number $S = 1/2$, correlating with the magnitude of the spin angular

momentum.  Since an electron is a spinning charge, it creates a small magnetic field at

which the magnetic moment ($\mu_e$) is proportional to spin angular momentum (**S**).

$$\mu_e = g_e\,\mu_B\,\mathbf{S} \qquad\qquad \text{(eq. 1)}$$

$g_e$ is the *g factor*, which is 2.0023 for a free electron and $\mu_B$ is called the Bohr

magneton $= (-e)h/4\pi m_e = -9.274 \times 10^{-24}$ J T$^{-1}$, where $m_e$ is the electron mass; $e$ is the

electron charge; $h$ is the Planck constant $= 6.626 \times 10^{-34}$ J s.

An electron spin can be in two states, either α or β.  In the presence of external

magnetic field ($B$), the magnetic moment of the electron spin aligns itself in either the same

(parallel, assigned α spin) or opposite (antiparallel, assigned β spin) direction to the B

direction. Each magnetic spin quantum number ($m_s$) equals ½ (denote α spin) or −½ (denote β spin). The interaction of external field and electron spin's magnetic moment is called *Zeeman interaction* which gives rise to the splitting of the spin energy level into two levels (Zeeman's effect) as illustrated in Figure 1.2.
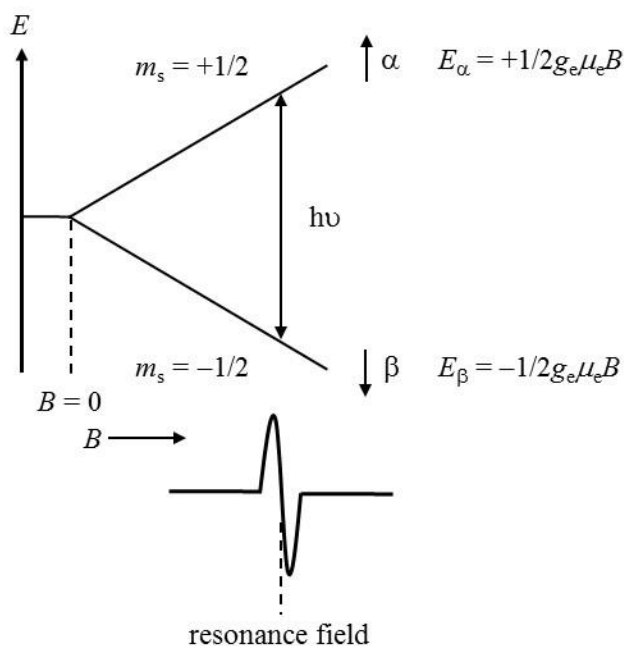


**Figure 1.2.** Energy diagram and EPR spectrum for $S = $ ½ radical.

The interaction energy ($E_\alpha$ and $E_\beta$) of the electron spin with the external field is given by $E = g_e\mu_e m_s B$, where $g_e$ is g factor (2.0023 for a free electron), $\mu_e$ is the Bohr magnetron, and $B$ is the strength of applied magnetic field. Therefore, the Zeeman energy difference between the two energy levels ($E_\alpha$ and $E_\beta$) is given by $\Delta E = E_\alpha - E_\beta = g_e\mu_e B$. When a frequency is matched with the energy separation between the two energy levels, an absorption which causes the transition between the two energy levels occurs. The equation is $h\upsilon = \Delta E = g_e\mu_e B$. This absorption can be monitored and converted to a spectrum by electron paramagnetic resonance (EPR) spectroscopy, sometimes referred to as electron spin resonance (ESR) spectroscopy.

According to the multiplicity rule $2S + 1$, the spin multiplicity of a radical containing one unpaired electron ($S = 1/2$, $m_s = 1/2$ or $-1/2$) is 2, indicating that there are two magnetic spin quantum number ($m_s$) energy sublevels (Figure 1.2). In a more general case of a diradical or polyradical, containing two or more unpaired electrons, the spin quantum number, $S \geq 1$, is possible for some of the electronic states; the multiplicity, $2S+1$, represents the number of the $m_s$ energy subleveles with $m_s = S, S-1, \ldots -S$.

**High Spin Diradicals**

In case of two-electron system, the total spin, $S$, can be either $S = 1$ (triplet) or $S = 0$ (singlet) according to the spin multiplicities, $2S + 1$. For triplet ($S = 1$) ground state diradical, the exchange coupling between two electrons is called ferromagnetic coupling; antiferromagnetic coupling gives rise to a singlet ($S = 0$) ground state. The strength of the exchange coupling is proportional to the energy difference between the singlet and triplet states ($\Delta E_{ST} = E_S - E_T$). The positive value of $\Delta E_{ST}$ is obtained if the triplet is lower in energy (triplet ground state) as shown in Figure 1.3.
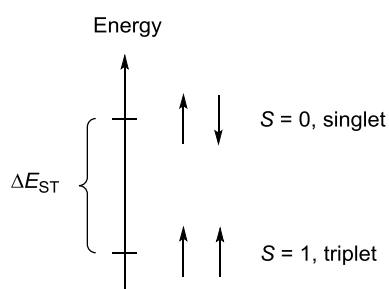


**Figure 1.3.** The energy difference between singlet and triplet states in case of ferromagnetic coupling.

The preference of ferromagnetic or antiferromagnetic coupling in case of non-Kekulé diradicals is considered. Non-Kekulé structures are fully conjugated hydrocarbons

and contain at least two atoms that are not $\pi$–bonded.[2] For example, trimethylenemethane (TMM) is a diradical, in which unpaired electrons are located in degenerate singly occupied NBMOs. These NBMOs are non-disjoint because their atomic spin densities have at least an atom in common. Therefore, TMM has triplet ground state (Figure 1.4).

In contrast to TMM, tetramethylenethane (TME), which is also a non-Kekulé molecule, possesses singlet ground state. In TME, the NBMOs are disjoint, i.e., there is no spin density on any atoms in common. Thus, topology (connectivity) is crucial to determine spin coupling (Figure 1.4).
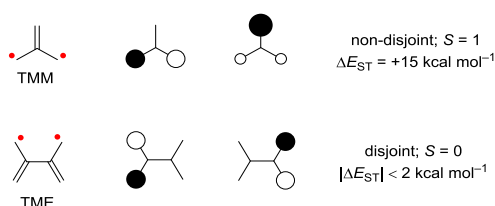


**Figure 1.4.** Diradicals with non-disjoint (TMM) and disjoint (TME) non-bonding MOs.

Another simple approach to determining the spin of the ground state is developed by Ovchinnikov.[3] We considered *m*-xylylene (Figure 1.5). Using a similar approach to Ovchinikov, the spin densities at the adjacent atoms in $\pi$-system are in alternating mode of $\alpha\beta\alpha\beta$ pattern throughout the molecule. The preference of spin at ground state is obtained by $S = (n_\alpha - n_\beta)/2$ in which $n_\alpha$ is a number of $\alpha$ centers and $n_\beta$ is a number of $\beta$ centers. As illustrated in Figure 1.5, *m*-xylylene is the $S = (5-3)/2 = 1$. This method can also be applied for TMM, which indicated triplet $S = 1$ ground state. Conceptually, diradicals with the ferromagnetic couplings may be viewed in terms of ferromagnetic coupling units (fCU) as illustrated in Figure 1.5.
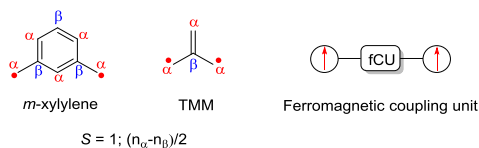
**Figure 1.5.** *m*-Xylylene and TMM by Ovchinnikov's method.

*m*-Xylylene is a non-disjoint diradical that is commonly used as a template for high-spin coupling molecules that are typically found in the triplet ground state. In order to design novel compounds, the methylene radicals are replaced with other radicals. This approach has led to the concept of using *m*-phenylene as a ferromagnetic coupling unit (fCU). The fCU may be defined as a spacer that allows the exchange coupling between the unpaired electrons to occur and still prevent the electrons from pairing. In comparison, the molecules such as *ortho*- and *para*-xylylenes allow the spin to pair together in the Kekulé form as illustrated in Figure 1.6.
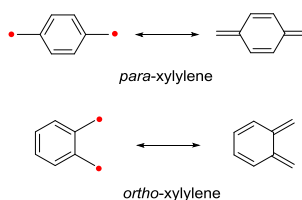


**Figure 1.6.** *p*-Xylene and *o*-xylene.

More extensive insights into diradicals may be found in these excellent reviews[4-6] and textbook.[7]

The relationship between the high-spin ground state and topology (connectivity) may be related to the spin polarization of the unpaired electrons. The concept of spin polarization is first illustrated in methyl radical, where the unpaired electron occupying a 2p orbital is orthogonal to σ MO of C–H bond. The spin alignment has two alternatives, as is shown in Figure 1.7. The unpaired electron spin polarizes the two paired electron

spins in the σ orbital which makes the alignment in Figure 1.7 (A) slightly more favorable than the alignment in Figure 1.7 (B).[8] The preference for the spin alignment in Figure 1.7 (A) is also supported by the Pauli Exclusion Principle,[9] which indicates that the electron repulsion of the same spin is relatively smaller than that of the opposite spin. This "spin polarization" effect implies that the opposite spin density (or negative spin density) is greater on hydrogen, which results in a negative value of the $^1$H hyperfine coupling constant.
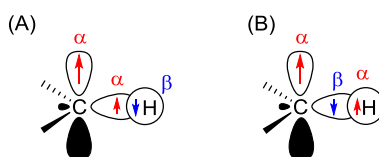


**Figure 1.7.** Spin polarization on an adjacent hydrogen atom induced by spin density on carbon.

In a more complex structure as allyl radical in Figure 1.8, this spin polarization effect also explains the sign of the coupling constant or negative spin density at C2 which is opposite to C1/C3. If we assumed that the unpaired electron spin is α (positive sign or spin up, ↑), based on the spin polarization the β spin density (negative sign or spin down, ↓) should avoid the C1/C3 position and the α spin would tend to increase at C1/C3. When the β spin on C2 polarizes the spins of the C2-H8 bond, the α spin at H8 is obtained resulted in positive sign of hyperfine coupling constant at H8. In contrast, the hyperfine coupling constants of hydrogen (H4, H5, H6 and H7) connecting to C1/C3 are negative. In fact, the sign of experimental hyperfine coupling constant of allyl radical is in agreement with this explanation.[10]

$a_{H4}$, $a_{H6}$ = -1.48
$a_{H5}$, $a_{H7}$ = -1.39
$a_{H8}$ = +0.41

○ positive spin density

○ negative spin density
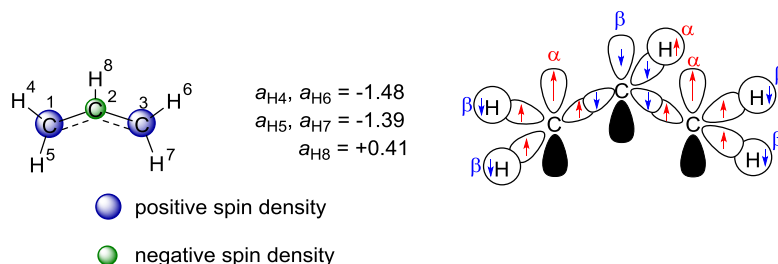
**Figure 1.8.** Hyperfine coupling of hydrogen on allyl radical and MO showing spin polarization.

### 1.1.2. Background on aminyl radicals

The term "aminyl radical" denotes a neutral nitrogen-centered radical in which the nitrogen atom is substituted by two groups, an unpaired electron and a non-bonding pair of electrons. Substituents (hydrogen, alkyl, phenyl or heteroatoms) on nitrogen play an important role in the stability, electronic structure and properties. The ground state is predicted to have a planar structure with electronic configuration, in which an unpaired electron on nitrogen atom can be either in $\pi$- or $\sigma$-type radical (Figure 1.9).[11] For $\pi$ radical, the unpaired electron resides primarily in a nitrogen $2p_z$ orbital. On the other hand, the unpaired electron located in a *sp²* hybridization.
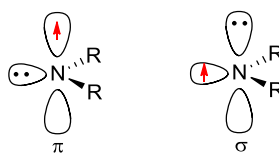


**Figure 1.9.** Possible electronic ground states of aminyl radicals.

In order to distinguish between the two states, hyperfine coupling is utilized in EPR spectroscopy to provide such information. Hyperfine coupling (*a*) is caused by the interaction between unpaired electron and neighboring nuclear dipole monents. A large

hyperfine coupling constant may indicate that the wavefunction of the unpaired electron has probability density at the nucleus; therefore, *s*-orbital is considered. For example, a pure *s*-orbital would yield a $^{14}$N hyperfine coupling, $a^N$, ~600 G.[8] An *sp²* hybrid for a trigonal planar configuration would yield 33% of 600 G; that is 200 G. For alkyl and aryl aminyl radicals, $a^N$ values are in the range of 10 G to 20 G. For instance, $a^N$ value for •N(CH$_3$)$_2$ is 14.78 G.[12] This indicates π-type radical that the unpaired electron resides in a $2p_z$ orbital. Many aminyl radicals are reported as a π-type radical.[11]

The first aminyl radical, diphenylaminyl, was discovered more than a hundred years ago in 1911 by Wieland.[13] It was formed by homolysis of tetraphenylhydrazine either by heating to 100 °C or by the UV irradiation (Scheme 1.1). However, aminyl radicals have attracted little attention over the course of the past century. One of the most challenging problems is that most aminyl radicals are highly reactive and short-lived; they often undergo dimerization and hydrogen atom abstraction. As shown in Scheme 1.1, flash photolysis of the tetraphenylhydrazine in benzene solution at room temperature yielded diphenylaminyl radical. Diphenylaminyl radical was quenched with a second order rate constant of $2.5 \times 10^7$ L mol$^{-1}$ s$^{-1}$.[14]

**Scheme 1.1.** Formation of diphenylaminyl radical from tetraphenylhydrazine.



Tetraphenylhydrazine        Diphenylaminyl radical
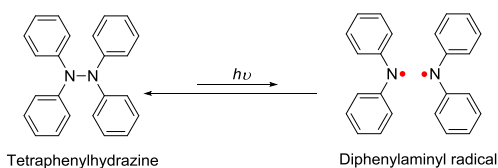
Most aminyl radicals reported are generally not isolable at room temperature. However, with proper design, stable aminyl radicals can be generated to avoid the decomposition pathways. This led to the study of the factors affecting the stability. As exemplified by diphenylaminyl radical, the unpaired electron can be delocalized to the two

phenyl rings which results in large positive spin density on alternate carbon atoms as shown in Figure 1.10. In the absence of significant steric shielding at these positions, the radicals may form a bond (forming a sigma-bonded dimer), initiating a decomposition via dimerization.
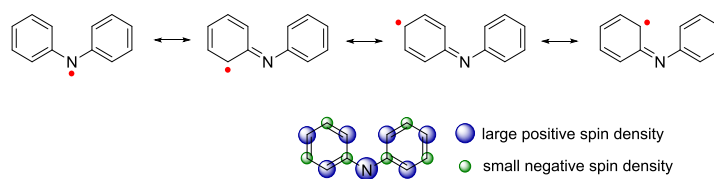


**Figure 1.10.** Resonance structures and spin density of diphenylaminyl radical.

To avoid those chemical degradations, Neugebauer and co-workers[15] modified the structure in two ways. Firstly, *tert*-butyl groups were substituted at positions 1, 3, 6 and 8, i.e. large positive spin density positions by delocalization from aminyl radical. These large groups stabilize the unpaired electron at the position of large positive spin density and prevent dimerization. Secondly, as illustrated in Figure 1.11, the carbazole structure is planar causing increased resonance stability. With this careful design, 1,3,6,8-tetra-*t*-butylcarbazole aminyl radical was synthesized by oxidation a solution of the lithium salt of starting amine in benzene using iodine and isolated as a blue-black crystals.



1,3,6,8-tetra-*t*-butylcarbazole aminyl radical
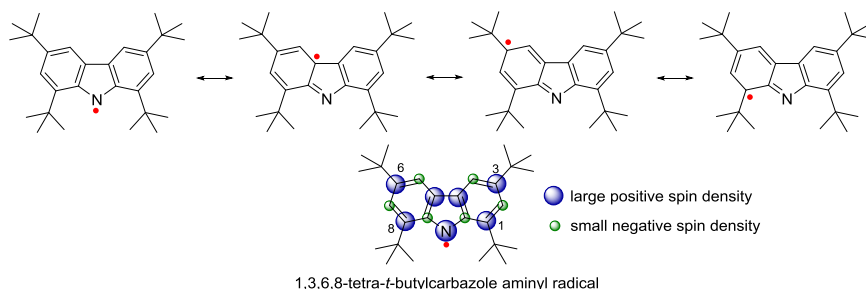
**Figure 1.11.** Resonance structures and spin density of 1,3,6,8-tetra-*t*-butylcarbazole aminyl radical.

In another example in 1974, Ballester and co-workers[16] reported the syntheses and isolation of perchlorodiphenylaminyl radical, as is shown in Scheme 1.2. This radical could be synthesized by either oxidation of decachlorodiphenylamine using an aqueous, alkaline solution of potassium ferricyanide (or using silver (II) oxide) or dechlorination of perchloro-*N*-phenylcyclohexan-2,5-dienimine using silver (Ag$^0$). The *ortho*-chlorines on the aryl rings effectively shielded the radical site; the resulting perchlorodiphenylaminyl radical is air stable for months.

**Scheme 1.2.** Synthesis of perchlorodiphenylaminyl radical.



Decachlorodiphenylamine          Perchlorodiphenylaminyl radical          Perchloro-*N*-phenylcyclohexan-2,5-dienimine
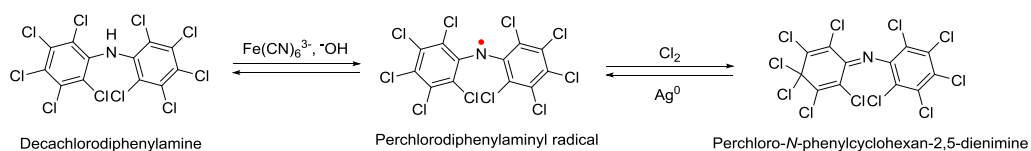
### 1.1.3. Background on aminyl diradicals

Although, many aminyl monoradicals have been widely studied and isolated, only a few high spin ($S$ = 1) aminyl diradicals have been reported. In 1989, Platz and co-workers[17] reported the EPR spectra for an *m*-phenylene-connected aminyl diradical (Figure 1.12) in a rigid 2-MeTHF matrix at 77 K (−196 °C). The diradical, containing fluorine substituents at *ortho*/*para*, *para*/*ortho* and *ortho*/*ortho* positions (positive spin density) on a benzene ring (Figure 1.12), was generated from the nitrene precursor, which was obtained from the corresponding azide by photolysis at 77 K. However, there was no evidence for triplet ground state for this diradical.
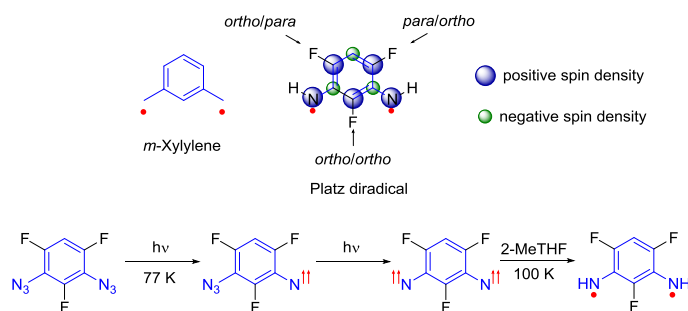
**Figure 1.12.** Platz aminyl diradical.

In 2007, Rajca and co-workers[18] reported the synthesis of *m*-phenylene-connected aminyl diradical **1** from diamine precursor **2**. Deprotonation using *n*-BuLi, followed by oxidation of the corresponding dianion using iodine, yielded the radical **1**. Aminyl diradical **1** consists of five linearly-fused six-membered rings (diazapentacene derivative) with a (4-*tert*-butylphenyl) pendant, as is shown in Figure 1.13. Hydrogen atoms at positions with significant spin density are replaced with bulky substituents that do not intrtfere with the planar geometry for spin delocalization; the X-ray crystal structure of diamine precursor **2** shows that planarity is maintained. The EPR spectra (X-band) of aminyl diradical **1** in a 2-MeTHF matrix at 133 K showed $|\Delta m_s| = 1$ and $|\Delta m_s| = 2$ transitions. Superconducting QUantum Interference Device (SQUID) magnetic studies for diradical **1** in the THF matrix established the triplet ground state ($S = 1$). SQUID magnetometry also provided a measurement of a lower limit for the singlet-triplet energy gap ($\Delta E_{ST}$) for **1** $\geq 0.4$ kcal mol$^{-1}$. In addition, aminyl diradical **1** in 2-MeTHF is persistent at about $-100$ °C and is inert toward dry oxygen at about $-108$ °C (165 K).
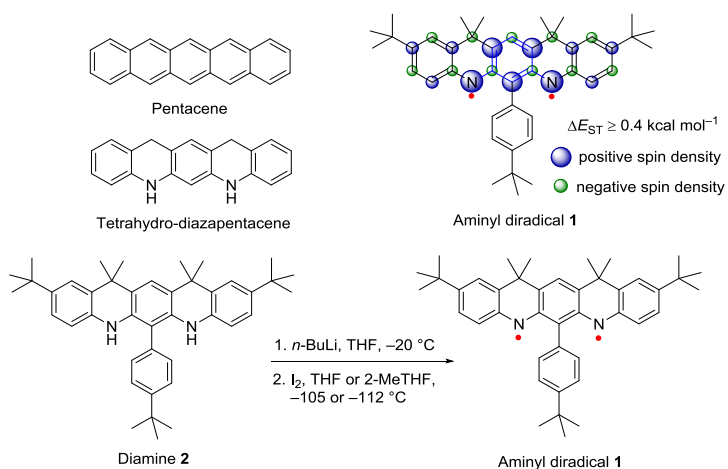
**Figure 1.13.** Structure of aminyl diradical **1**.

In 2010, Rajca and co-workers[19] reported the synthesis of *m*-phenylene-connected aminyl diradicals **3** and **4**. Aminyl diradical **3** and **4** were prepared by deprotonation of diamine **5** and **6** using *n*-BuLi and oxidation of the corresponding dianions using iodine. Additional sterically hindered *tert*-undecylphenyl pendants at *ortho*-positions with respect to aminyl radical, where significant spin density is expected, improved the solubility in organic solvents and persistence of aminyl diradical **4** (Figure 1.14). This exceptional persistence encouraged them to isolate **4** as a solid. The EPR spectra (X-band) of aminyl diradical **1** in 2-MeTHF matrix at 132 K showed $|\Delta m_s| = 1$ and $|\Delta m_s| = 2$ transitions. SQUID magnetic studies for diradical **4** in 2-MeTHF matrix established its triplet ground state ($S = 1$). SQUID magnetometry also provided a measurement of a lower limit for the value of $\Delta E_{ST}$ for **4** $\geq 2$ kcal mol$^{-1}$, which is in agreement with the value of $\Delta E_{ST} \approx 7$ kcal mol$^{-1}$ for DFT-computed **3**, using the UB3LYP/6-31(d) level of theory. For persistence of **4**, the concentration of isolated solid **4** under argon atmosphere at room temperature decreased to 60% after five days. In addition, the half-life ($\tau$) of aminyl diradical **4** in 2-MeTHF at room

temperature was ≈ 3 h.  Aminyl diradical **4** in 2-MeTHF is sensitive toward an excess of

iodine and oxygen at about −26 and −78 °C, respectively.
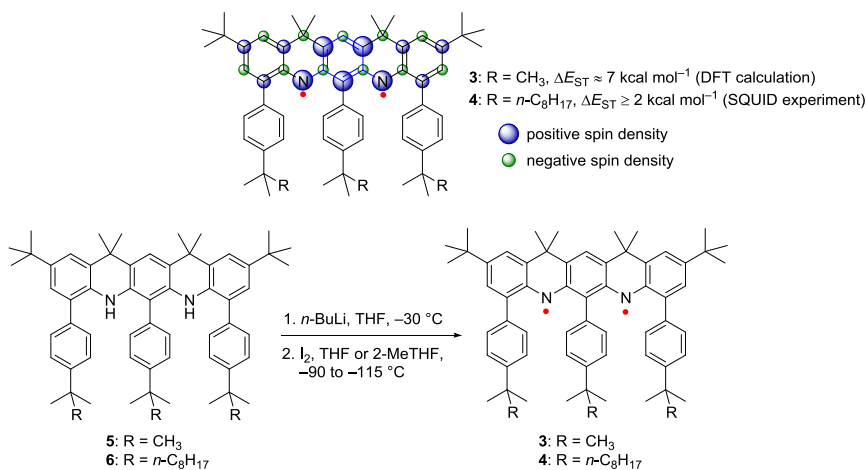


**Figure 1.14.**  Structures of aminyl diradical **3** and **4**.

Based on the above report, aminyl diradicals based on *m*-phenylene as a

ferromagnetic coupling unit are certainly good building blocks for the design of high spin

molecules.

## 1.2. Results and Discussion

Our objective was to synthesize triplet ($S = 1$) ground state diradicals that possess

a large singlet-triplet energy gap ($\Delta E_{ST}$) and persist at room temperature.  As described in

the earlier section, we were interested in the design and synthesis of aminyl diradicals based

on *m*-phenylene as a ferromagnetic coupling unit (aza-*m*-xylylene), since *m*-xylylene, a

high-spin diradical, is one of the well-known reactive intermediates with a strong spin-spin

interaction.  The triplet ground state of *m*-xylylene is lower in energy than the singlet state

($\Delta E_{ST} = E_S − E_T$) by $9.6 \pm 0.2$ kcal mol$^{-1}$.[20,21]  This $\Delta E_{ST}$ value is much greater than the

thermal energy at room temperature which is ~ 0.6 kcal kcal mol$^{-1}$. In the initial stages of the design of novel high spin molecules, we estimated the $\Delta E_{ST}$ values using broken-symmetry (BS-DFT) method.[22] Interestingly, the calculated value for aza-*m*-xylylene (15.8 kcal mol$^{-1}$) is comparable to *m*-xylylene (12.0 kcal mol$^{-1}$). We designed the aminyl diradicals connected through the *m*-phenylene with concerning of two main factors: (1) an effective overlap of the N-centered $2p_{\pi}$-orbitals of aminyl moieties and C-centered $2p_{\pi}$-orbitals of *m*-phenylene for enhancing spin-spin interaction and (2) sufficient protection of the atoms (carbon and nitrogen) with significant spin density for stability of diradicals. Hexahydropyrrolo[3,2-*f*]indole (HHPI) and octahydropyrido[3,2-*g*]quinoline (OHPQ) aminyl diradicals, considered as models were reported to have a similarly large $\Delta E_{ST}$ value at 9.2[23] and 13.5[23,24] kcal kcal mol$^{-1}$, respectively (Figure 1.15).

HHPI- and OHPQ-derivatived aminyl diradicals **7** and **8**, in which π-delocalization is confined to the center *m*-phenylene ring to maximize the spin-spin interaction with alkyl substituents for protection of large spin density atoms to enhance the stability, showed large $\Delta E_{ST}$ gaps, = 11.0 and 14.0 kcal mol$^{-1}$, respectively, which are comparable to *m*-xylylene diradical (Figure 1.15).

In comparison, a smaller gap ($\Delta E_{ST} \approx 7$ kcal mol$^{-1}$) is reported for extended conjugated π-system aminyl diradical **3**.[19] This discrepancy can be explained by the distribution of spin density from the *m*-phenylene (center ring) throughout π-system in the neighboring rings.

Recently, Barone and co-workers[25] applied their state-of-the-art and computationally intensive method for calculation of $\Delta E_{ST}$ for **3** and **7** (4.7 and 9.5 kcal mol$^{-1}$, Figure 1.15). The values of $\Delta E_{ST}$ are lower (~ 2 kcal mol$^{-1}$) compared to BS-DFT

method, which tends to overestimate the value of $\Delta E_{ST}$ for triplet ground state molecules.[19]

However, the value of $\Delta E_{ST}$ of **7** is still comparable to *m*-xylylene. They also showed that

the values of $\Delta E_{ST}$ for **7** and **9**, in which two methyl groups were substituted by propyl

groups, were comparable. Moreover, this method was also applied to calculation of $\Delta E_{ST}$

for triplet ground state nitroxide diradical.[25]



*m*-Xylylene: R = CH$_2$, $\Delta E_{ST}$ = 12.0 kcal mol$^{-1}$
Aza-*m*-xylylene: R = NH, $\Delta E_{ST}$ = 15.8 kcal mol$^{-1}$

Hexahydropyrroloindole
aminyl diradical (HHPI)
$\Delta E_{ST}$ = 9.2 kcal mol$^{-1}$

Octahydropyridoquinoline
aminyl diradical (OHPQ)
$\Delta E_{ST}$ = 13.5 kcal mol$^{-1}$

**3**
BS-DFT: $\Delta E_{ST}$ = 7 kcal mol$^{-1}$
DDCI: $\Delta E_{ST}$ = 4.7 kcal mol$^{-1}$

○ positive spin density
○ negative spin density

**7** (R = Me)
BS-DFT: $\Delta E_{ST}$ = 11.0 kcal mol$^{-1}$
DDCI: $\Delta E_{ST}$ = 9.5 kcal mol$^{-1}$
**9** (R = Pr)
DDCI: $\Delta E_{ST}$ = 10.0 kcal mol$^{-1}$

**8**
$\Delta E_{ST}$ = 14.0 kcal mol$^{-1}$

**Figure 1.15.** Structures and calculated $\Delta E_{ST}$ values of triplet ground state diradicals.

Here we report the synthesis of aminyl diradicals **9**, **10** and **11** and characterization

of their EPR spectra, thermal persistence and reactivity (with iodine and oxygen). In

section 1.2.1, the synthesis of their diamine precursors are discussed.



**9**

**10**

**11**
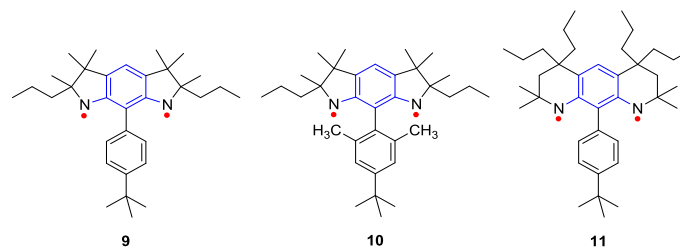
**1.2.1.  Synthesis of diamine 12 as a precursor for aminyl diradical 9**

**Synthetic plan for diamine 12**

As shown in Scheme 1.3, the retrosynthesis of **12** involves the disconnection of the *p-tert*-butylphenyl substituent and bromodiamine **13** via Suzuki-Miyaura cross-coupling reaction.  The bromodiamine **13** could be produced from **14** by allylation, hydrogenation and bromination reactions, respectively.  Fischer indole synthesis was selected to construct **14** from commercially available 1,3-phenylenediamine.   The synthetic steps and characterization are discussed in details in the following section.

**Scheme 1.3.** Retrosynthesis of diamine **12**.
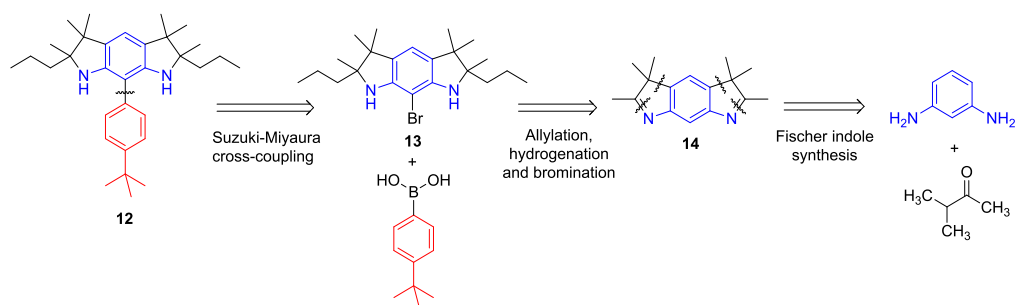


**Synthesis of diamine 12**

Diamine **12** was successfully synthesized in 5 steps from commercially available 1,3-phenylenediamine as shown in Scheme 1.4.  The results and discussion for each step are described below.

**Scheme 1.4.** Synthesis of diamine **12**.
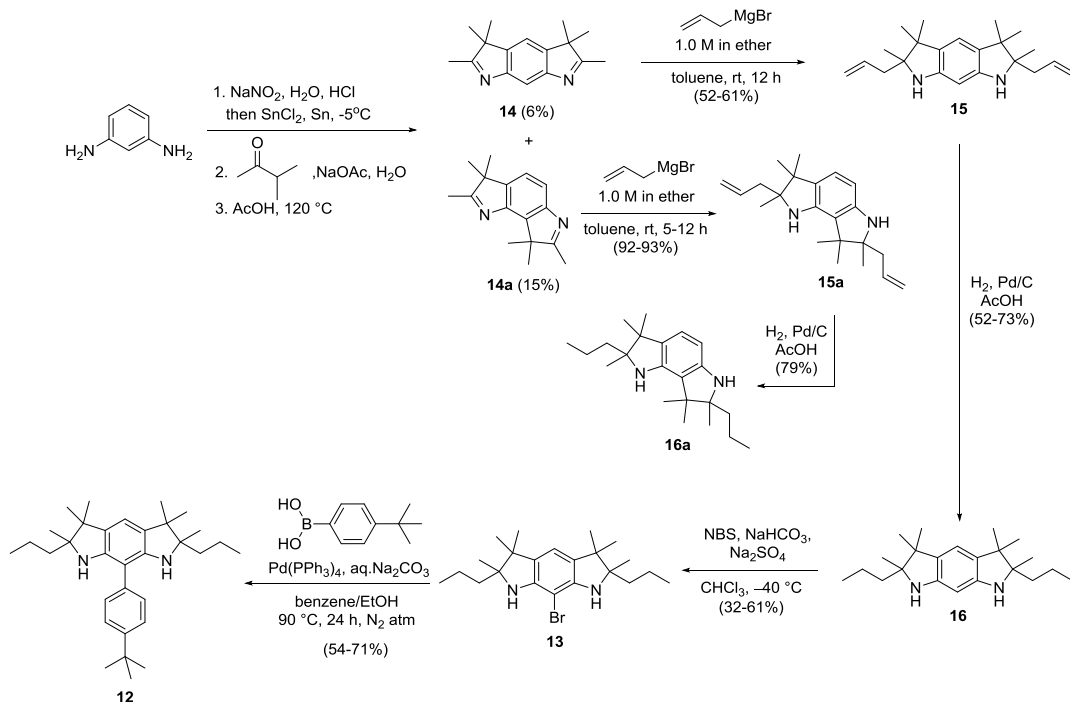


Nitrogen-containing heterocyclic molecules are found in many natural products. Indole and indolenine alkaloids, in particular, are important heterocyclic components in pharmaceutical agents. The synthesis and functionalization of indole and its derivatives have been reported extensively.[26-28] One of the oldest useful and well-known methods is the Fischer indole synthesis.[29]

Indolenines are known as useful building blocks in the synthesis of complex indole alkaloids and related compounds using the imine as an electrophile. Our plan was to construct an indolenine moiety in a *m*-phenylene framework as a model for synthesis of **15** with quaternary carbon at C3 and C2 positions, in which quaternary C2 could be created by the addition of carbon nucleophiles to the imines.
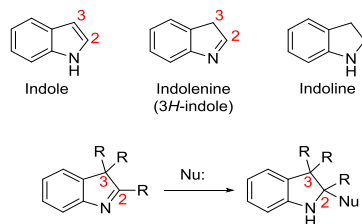
Buchwald and co-workers[30] showed the synthesis of 2,3,3,4,6-pentamethyl-*3H*-indole in very good yield (Scheme 1.5). This modified Fischer indole reaction used the *N*-aryl benzophenone hydrazone as a precursor to convert to indole product via an in situ hydrolysis and Fischer cyclization using a strong Lewis acid, *p*-toluenesulfonic acid (*p*-TsOH).

**Scheme 1.5.** Synthesis of 2,3,3,4,6-pentamethyl-3*H*-indole.
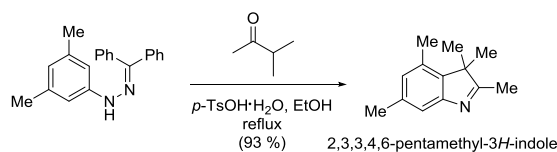


This protocol was applied for the synthesis of **14** (Scheme 1.6). With several attempts, however, the crude reaction provided a mixture of unknown products based on thin-layer chromatography (TLC) and $^1$H NMR spectra. There was no further attempt to investigate the mixture.

**Scheme 1.6.** Initial attempts for synthesis of **14**.
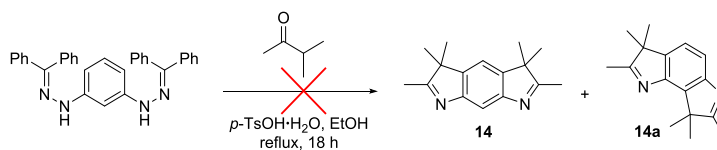
This unsuccessful reaction led us to survey the literature for synthesis of **14**. In 1971, Mikhailenko[31] reported that two isomer products (**14** and **14a**) obtained by a two-step synthesis: (1) preparation of tin salts of 1,3-phenylenedihydrazine[32-33] by mixing 1,3-phenylenediamine dihydrochloride with $NaNO_2$ in concentrated hydrochloric acid at −10 to −5 °C followed by reduction with $SnCl_2$ in presence of Sn metal, and (2) Fischer indole synthesis of 1,3-phenylenedihydrazine with methyl isopropyl ketone in acetic acid. The purification step was performed by acidification of the crude product in perchloric acid to give crystalline perchlorate salts of **14** and **14a** after vacuum sublimation and recrystallization from heptane in 25 and 51%, respectively. We followed this method except for the purification step. The product **14** and **14a** were isolated by column chromatography in 6% and 15% yield, respectively (Scheme 1.4).

In 2012, Solé and co-workers[34] demonstrated an alternative preparation of **18** from **17** using a palladium-catalyzed acylation reaction (Table 1.1). Addition of a carbon nucleophile, such as alkyl Grignard reagent to the carbonyl groups of **18**, might provide a promising model for an alternative method to construct the diamine precursor. However, with limited time, we did not attempt this method.

**Table 1.1.** Palladium-catalyzed reactions of **17**
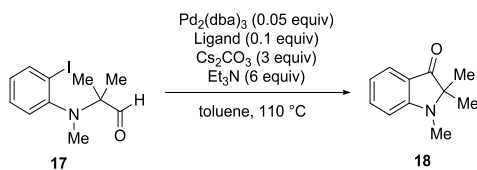


| ligand | time (h) | yield (%) |
|---|---|---|
| dtpf | 36 | 80 |
| $(^tBu)_3PH \cdot BF_4$ | 28 | 82 |
| $(o\text{-tolyl})_3P$ | 36 | 75 |

dtpf = 1,1′-bis(di-tert-butylphosphino)ferrocene

The next step of synthesis is nucleophilic addition to construct a quaternary carbon center at C2. At the beginning, we had planned to synthesize aminyl diradical **7**. Thus, addition of methyl nucleophiles to C=N electrophiles became a crucial step based upon our synthetic plan. We used commercially available 2,3,3-trimethyl indolenine as a model to preserve the amount of precious indolenine **14**, since it was produced in low yields from the previous step. It is well known that organometallic reagents can undergo nucleophilic addition to the C=N bond of imine derivatives.[35] However, due to the poor reactivity of the azomethine carbon and the possible formation of enamines by deprotonation, several approaches have been developed to overcome these limitation. Generally, these limitations are overcome by increasing the reactivity of the imine (C=N bond) with Lewis acids and optimizing the organometallic reagents.

Our initial attempt was performed by the addition of methyl lithium solution (3 equiv of MeLi) to the solution of 2,3,3-trimethyl indolenine in toluene at 0 °C. However, after it was stirred at room temperature for overnight, the crude reaction mainly contained unreacted strating material, as was determined by $^1$H NMR spectra and GC-MS. A trace amount of a compound with *m/z* 176, which may correspond to the product, was also observed by GC-MS. Prolonging the reaction time to two days and increasing the reaction temperature to about 40-50 °C gave no improvement (Scheme 1.7). Addition to 2,3,3-trimethyl indolenine using Grignard reagent, e.g. methylmagnesium bromide (MeMgBr), also provided the same result as MeLi. The similarly unsuccesful addition reaction by these reagents to imines were reported previously.[36]

**Scheme 1.7.** Attempted addition reaction of MeLi to 2,3,3-trimethyl indolenine.
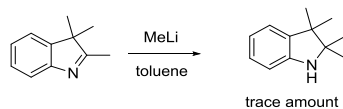


Our second approach to improve the yield was the activation of the aromatic imine using a Lewis acid. Szymoniak and co-workers[37] reported that zirconium complex (Cp$_2$ZrCl$_2$) catalyzed the addition of an alkyl organomagnesium reagent, such as ethylmagnesium chloride (EtMgCl), to many poor electrophiles and enolizable imines in good yields (Scheme 1.8).

**Scheme 1.8.** Zirconium-catalyzed ethylation of imine.
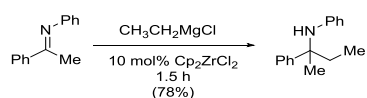


However, the addition of **14** and **14a** with ethylmagnesium bromide (EtMgBr) in presence of Cp$_2$ZrCl$_2$ according to the published procedure,[37] mainly showed unreacted strating material in crude reaction. ESI MS showed a trace amount of the fragment with *m/z* 271 which may correspond to the mono-ethylated products along with unreacted starting material and other unknown materials (Scheme 1.9).

**Scheme 1.9.** Attempted zirconium-catalyzed ethylation of **14a** and **14**.
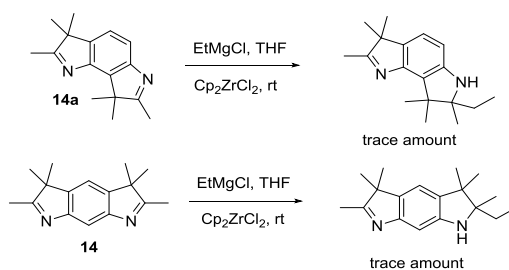
Our hypothesis for these unsuccessful attempts was that alkyl organolithium and magnesium reagents are prone to undergo protonation by imine (**14** and **14a**) or imine reduction rather than addition to the imine. Also, the poor electrophilicity of the carbon atom of the C=N bond may be one of the factors. Since it is known that resonance-stabilized allyl organometallics are more reactive toward imine addition reaction than typical organometallic reagents due to a greater ionization of the carbon-metal bond, we postulated that allylation might be the alternative method for creating quaternary carbon at C2 position. Allyl organometallics are less basic than alkyl organometallics, and consequently may be less prone to undergo protonation reactions by imines such as **14** and **14a**.

Rodríguez and co-workers[36] reported an extremely useful method for addition of allyl Grignard to sterically shielded imine. As presented in Scheme 1.10, the allylation reaction of spiroindolenine **19** using allylmagnesium chloride produced the allylated product **20** in excellent yield.

**Scheme 1.10.** Addition of allylmagnesium chloride to spiroindolenine.
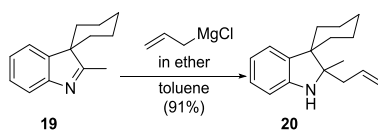


Based on this approach to imine allylation, the reaction of 2,3,3-trimethyl indolenine with allylmagnesium bromide (1.0 M in diethyl ether) in toluene at room temperature was investigated as a synthetic model. The target product, allylated indoline **21**, was obtained and isolated in 83% yield as shown in Scheme 1.11.

**Scheme 1.11.** Addition of allylmagnesium bromide to 2,3,3-trimethyl indolenine.
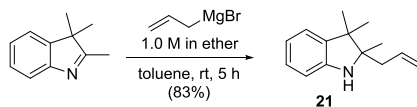


Followed the same conditions as in Scheme 1.11, the reaction of **14** and **14a** with allylmagnesium bromide in toluene at room temperature successfully provided allylated diamine **15a** in 92-93% yield and **15** in 54-61% yield. Both products were isolated as a mixture of diastereomers (Scheme 1.12).

**Scheme 1.12.** Addition of allylmagnesium bromide to **14** and **14a**.
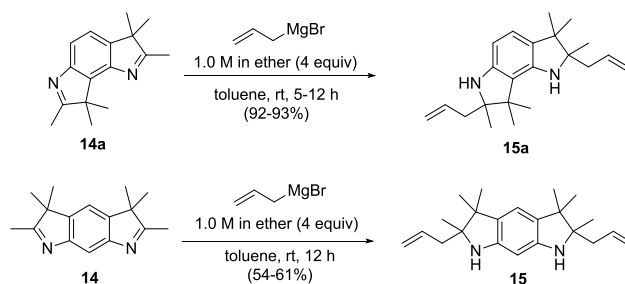


In the next step, reduction of allyl to *n*-propyl groups was investigated using **15a** as a model compound to preserve the amount of **15**. Catalytic hydrogenation reaction in Schlenk vessel of a solution of **15a** in acetic acid using H$_2$ (1 atm) in the presence of 10 mol% of Pd/C successfully produced **16a** in 79% yield (Scheme 1.13). Hydrogenation reaction of allylated diamine **15** using H$_2$ (1 atm) in the presence of 10 mol% of Pd/C in acetic acid yielded *n*-propyl diamine **16** in 52-73% yield (Scheme 1.13).

**Scheme 1.13.** Catalytic hydrogenation of **15a** and **15**.
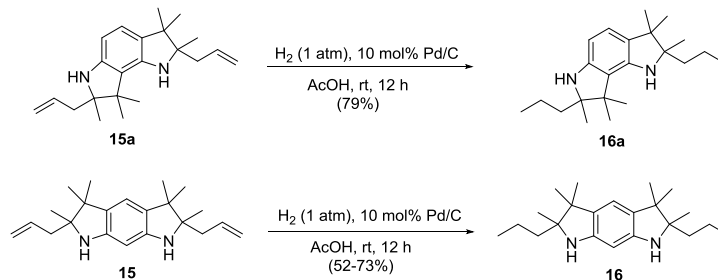


The bromination reaction of propyldiamine **16** with *N*-bromosuccinimide (NBS) in the presence of NaHCO$_3$ and Na$_2$SO$_4$ in CHCl$_3$ at −40 °C produced bromodiamine **13** in 32-61% yield.[18]  Carbon–carbon bond formation between bromodiamine **13** and commercially available 4-*tert*-butylphenyl boronic acid was achieved by Suzuki-Miyaura cross-coupling reaction in the presence of catalytic amount (10 mol%) of Pd(PPh$_3$)$_4$ and Na$_2$CO$_3$ in benzene/EtOH (4:1) at 90 °C for 24 h to provide diamine **12** in 54-71% yield (Scheme 1.4).

Diamine **12** was characterized by NMR spectroscopy, IR spectroscopy, mass spectrometry and melting point.  The structure of diamine **12** was confirmed by the assignment of $^1$H and $^{13}$C NMR spectra in chloroform-*d* using standard 2D NMR spectroscopy, including $^1$H–$^{13}$C HSQC, $^1$H–$^{13}$C HMBC, $^1$H–$^1$H COSY, $^1$H–$^1$H NOESY, and $^1$H–$^{15}$N HSQC (Figures B7-B11 in Appendix B).  Two diastereomers (*meso*-**12** and *dl* pair-**12**) as is shown in Figure 1.16 are expected to be observed by NMR spectroscopy.  $^1$H NMR (500 MHz, chloroform-*d*, Figure 1.17) spectrum showed AB patterns at $\delta$ = 7.427, 7.375 ppm (ABq, $\Delta v$ = 25.6 Hz, $J_{AB}$ = 7.8 Hz, 2H, diastereomer 1)/7.427, 7.337 ppm (ABq, $\Delta v$ = 45.3 Hz, $J_{AB}$ = 8.0 Hz, 2H, diastereomer 2) corresponding to 2H$_a$ and 2H$_b$ for two diastereomers.  It is assumed that a very small amount of benzene residue ($\delta$ = 7.36 ppm in chloroform-*d*)[38] may interfere with the AB spectral pattern.  In fact, $^1$H NMR (600 MHz,

chloroform-$d$, Figure A21 in Appendix A, label: AO-2-52-suzuki-CDCl3) spectrum from different experiment unequivocally showed AB pattern at $\delta$ = 7.418, 7.365 ppm (ABq, $\Delta\nu$ = 31.4 Hz, $J_{AB}$ = 7.8 Hz, 2H, diastereomer 1)/7.418, 7.329 ppm (ABq, $\Delta\nu$ = 53.4 Hz, $J_{AB}$ = 7.8 Hz, 2H, diastereomer 2). This assignment for aromatic protons (Ar-**H**) on 4-*tert*-butylphenyl pendant is confirmed by $^1$H–$^1$H COSY spectra. A singlet peak at $\delta$ = 6.570 ppm (1H$_c$) assigned for aromatic proton on diamine moiety. A broad singlet peak at $\delta$ = 3.528 ppm (2H$_d$) assigned to N-**H** resonances. In acetone-$d_6$, the singlet corresponding to the N-**H** group was found at $\delta$ = 3.881 ppm (2H$_d$). This assignment was confirmed by a cross-peak between $^1$H and $^{15}$N in $^1$H–$^{15}$N HSQC spectra in acetone-$d_6$ showing the N-**H** connectivity (Figure B7 in Appendix B). The $^{15}$N NMR chemical shift is in the $\delta$ = −287.4 ppm (relative to nitromethane at 0.0 ppm), which is in the same range for secondary diamine **2** ($\delta$ = −286 ppm).[39] Additional evidence for the N-**H** was obtained from D$_2$O exchange experiment in benzene-$d_6$ (Figure A24 in Appendix A); $^1$H NMR spectrum showed two overlapping singlets at $\delta$ = 3.708 and 3.646 ppm assigned to N-**H** (from two diastereomers), which after addition of a drop of D$_2$O rapidly underwent a complete H/D exchange.

As shown in Figure 1.17, multiplets at $\delta$ = 1.616-1.150 ppm (4H$_e$ and 4H$_g$, overlapping signal) were assigned to CH$_2$ protons on *n*-propyl groups. A singlet at $\delta$ = 1.359 ppm (9H$_f$) were assigned to *t*-Bu group. Two singlet peaks at $\delta$ = 1.175 ppm (6H$_h$) and 1.133 ppm (6H$_h'$) were assigned to diastereotopic CH$_3$ groups. Two singlet peaks at $\delta$ = 1.072 and 1.042 ppm (6H$_i$) ppm were assigned to two diastereomers (*meso*-H$_i$ and *dl* pair-H$_i$). Two triplets at $\delta$ = 0.935 and 0.907 ppm (6H$_j$) ppm were assigned to two diastereomers (*meso*-H$_j$ and *dl* pair-H$_j$).
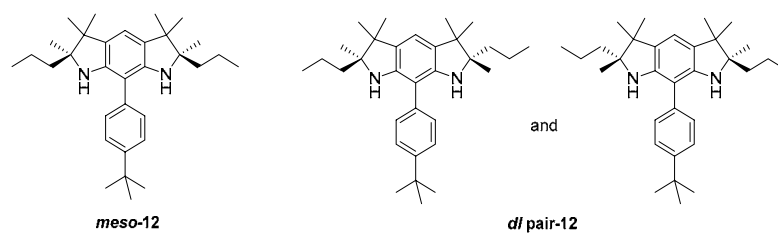
**Figure 1.16.** Structures of *meso*-**12** and *dl* pair-**12**.
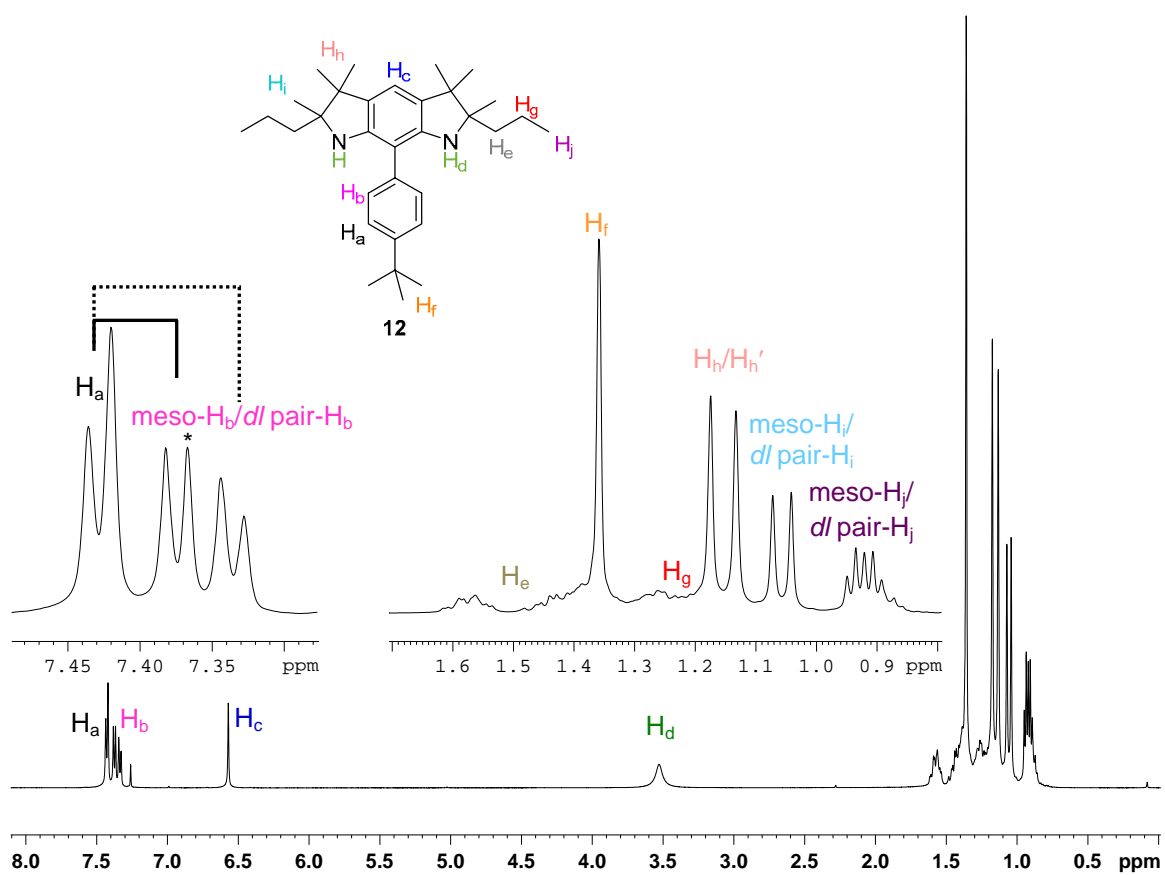


**Figure 1.17.** $^1$H NMR (500 MHz, chloroform-*d*, label: AO-9-55-flt-5) spectrum of the diamine **12**. *benzene residue

$^{13}$C NMR (100 MHz, chloroform-*d*, Figure A25 in Appendix A) spectrum is in agreement with the structure of diamine **12**. IR (ZnSe, Figure A27 in Appendix A) spectrum showed the absorption of amine groups at 3363 cm$^{-1}$.

Additional structural evidence for diamine **12** was obtained from the correlation between the DFT-calculated ($\delta_{DFT}$) and experimental ($\delta_{expt}$) $^1$H and $^{13}$C NMR chemical shifts (Figure B3 in Appendix B). The correlation coefficients, $R^2$ = 0.9946 and 0.9986 (Figure B3, Table B1 and Table B2 in Appendix B), are obtained for $^1$H and $^{13}$C NMR chemical shifts using the calculated chemical shift for simplified structure of **12**, in which the *n*-propyl groups are replaced with methyl groups (**12a**). The relationship between computed and experimental NMR chemical shift is further illustrated by appling the correlations to scale linearly ($\delta_{DFT}$) to provide ($\delta_{scaled}$). The plot of the differences between the scaled and experimental NMR chemical shift ($\delta_{scaled} - \delta_{expt}$) for each hydrogen or carbon atom in the structure confirm good agreement between theory and experiment, indicated by the low value of statistical error parameters for $^1$H and $^{13}$C NMR chemical shift (Table B1 in Appendix B).

### 1.2.2. Synthesis of diamine 22 as a precursor for aminyl diradical 10

We hypothesized that a more sterically hindered group near the radical sites could improve the stability of diradical. Therefore, we proposed two adding pendant groups: 2,4,6-tri-*tert*-butylphenyl and 2,6-dimethyl-4-*tert*-butylphenyl pendants. 2,4,6-Tri-*tert*-butylphenyl substituent would be an ideal design for sterically shielded diradical. However, the coupling reaction between this substituent group and diamine moiety was anticipated to be very difficult. The less sterically hindered, 2,6-dimethyl-4-*tert*-butylphenyl, was thought to be more amenable to cross-coupling with the bromodiamine **13**; however, the presence of benzylic hydrogens (BDE = 89.9 kcal mol$^{-1}$)[40] in this aryl

group could potentially provide an additional pathway for the decay of the aminyl diradical via intramolecular (or intermolecular) H-atom abstraction.

### Synthetic plan for diamine 22

Our synthetic plan was based on Suzuki-Miyaura cross-coupling reaction between sterically hindered aryl boronic esters (**24** or **25**) and bromodiamine **13** (Scheme 1.14).

**Scheme 1.14.** Retrosynthesis of sterically hindered diamines **22** and **23**.
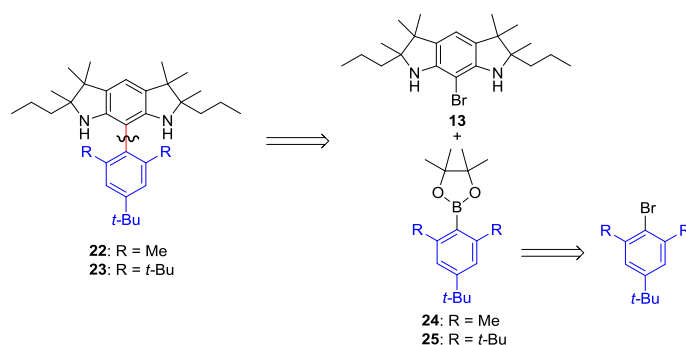


We considered that the cross-coupling reactions of sterically hindered boronate esters are rare and that the bromodiamine **13** is both sterically hindered and electron rich aryl halide. During the past decades, significant efforts have been devoted to developing new palladium/ligand catalyst for sterically hindered Suzuki-Miyaura cross-coupling reaction. The syntheses of tetra-*ortho*-substituted biaryls bearing methyl *ortho* substituents successfully employed by Suzuki-Miyaura cross-coupling using *N*-heterocyclic carbene-Pd complexes[41-45] and bulky, electron-rich phosphines.[46-49] To the best of our knowledge, there is only one example with tetra-*ortho*-substituent bearing secondary alkyl *ortho* substituent, e.g. *iso*-propyl groups in Suzuki-Miyaura cross-coupling reaction (Scheme 1.15).[50]

**Scheme 1.15.** Sterically hindered Suzuki-Miyaura cross-coupling reaction.
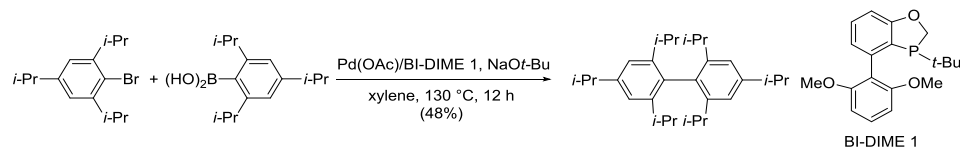


### Synthesis of diamine 22

The pinacolboronate **24** and **25** were successfully prepared by a known procedure,[19]

through Br/Li exchange using *t*-BuLi (2.1 equiv) in THF at –78 °C of the corresponding

aryl bromides, 1-bromo-2,6-dimethyl-4-*tert*-butylbenzene **26** and 1-bromo-2,4,6-tri-*tert*-

butylbenzene **27**, followed by borylation reaction using 2-isopropoxy-4,4,5,5-tetramethyl-

1,3,2-dioxoborolane as shown in Scheme 1.16.

**Scheme 1.16.** Synthesis of boronate esters **24** and **25**.
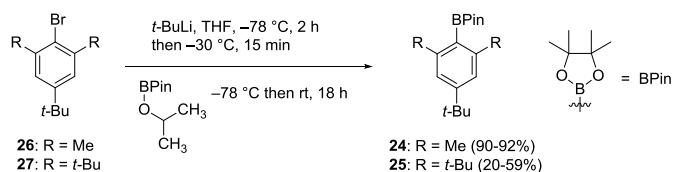


With the boronate esters in hand, we first followed a standard procedure of Suzuki-

Miyaura cross-coupling reaction between bromodiamine **12** and boronate ester **24** using a

palladium(0) complex, tetrakis(triphenylphosphine)palladium(0) (Pd(Ph$_3$)$_4$), as a catalyst

and sodium carbonate as a base. After stirring the reaction at 90 °C for 24 h, $^1$H NMR (400

MHz, benzene-$d_6$, label: AO-4-43-crd, Figure A34 in Appendix A) spectrum of crude

mixture showed unreacted boranate **24**, diamine **16** and other baseline materials. However,

the CC-bond cross-coupling product was not observed. Diamine **16** was recovered in 46%

after column chromatography (Scheme 1.17).

**Scheme 1.17.** Attempted synthesis of diamine **22**.
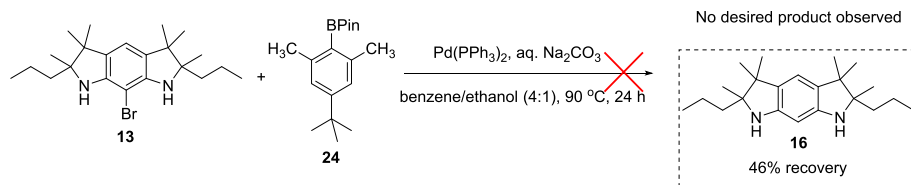


The Suzuki-Miyaura cross-coupling reaction between **13** and **24** was unsuccesful possibly due to steric hindrance of the large *ortho* substituents of aryl boronate ester. In general, palladium-catalyzed cross-coupling reactions can be improved by ligand modification since the reactivity and stability of metal catalysts depended greatly on the ligand coordination. Therefore, we searched the literature for the preparation of sterically hindered biaryls by Suzuki-Miyaura cross-coupling reaction and found a procedure in 2005 reported by the Buchwald group.[51] The authors reported the use of $Pd_2(dba)_3$ and a highly reactive phosphine ligand, Sphos, to couple a wide range of sterically hindered substrates; an example is shown in Scheme 1.18.

**Scheme 1.18.** Suzuki-Miyaura cross-coupling reaction of sterically hindered substrates.
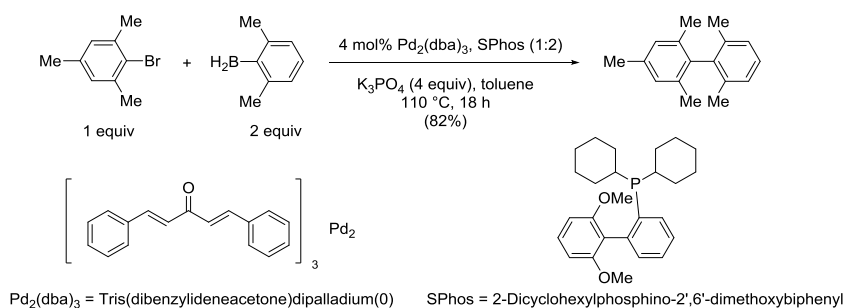


These conditions were applied to our synthesis; however, $^1$H NMR spectrum of the crude reaction showed a mixture of unknown products. (Scheme 1.19) There was no further attempt to investigate the composition of the mixture.

**Scheme 1.19.** Attempts of synthesis of diamine **22**.
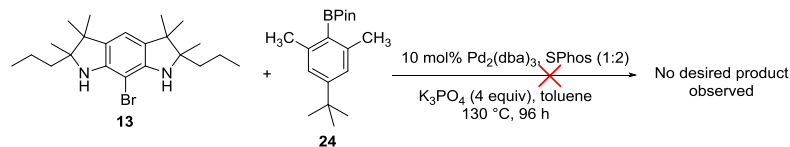


Another highly reactive ligand that has been used to cross-couple a variety of sterically hindered substrates as well as electron rich aryl halides was P($^t$Bu)$_3$ reported in 2000 by Fu group.[52] The authors investigated many catalysts, ligands, and bases to find an optimized set of conditions and found that the combination of Pd$_2$(dba)$_3$/P(*t*-Bu)$_3$ catalyst system, using KF as a base, was the most effective (Scheme 1.20).

**Scheme 1.20.** Suzuki-Miyaura cross-coupling reaction of sterically hindered substrates.
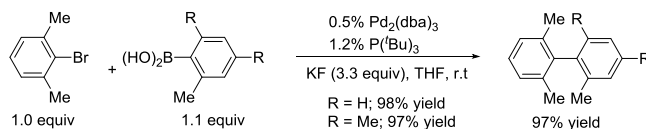


Due to the availability of the catalyst and base in our lab, we adapted these conditions to couple bromodiamine **12** and boronated ester **24** using [PdP(*t*-Bu$_3$)]$_2$ as a catalyst in the presence of K$_3$PO$_4$ in toluene (Scheme 1.21).

**Scheme 1.21.** Synthesis of diamine **22**.
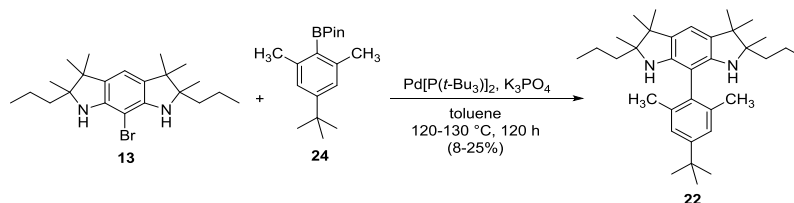


After stirring at 120-130 °C for 5 days, the crude mixture was purified by column chromatography to give diamine **22** in 8-25% yield. No optimization of the reaction conditions was further investigated.

Diamine **22** was characterized by NMR spectroscopy, IR spectroscopy, mass spectrometry and melting point. The structure of diamine **22** is confirmed by the assignment of $^1$H and $^{13}$C NMR spectra in chloroform-*d* using standard 2D NMR spectroscopy, including $^1$H–$^{13}$C HSQC, $^1$H–$^{13}$C HMBC, $^1$H–$^1$H COSY, $^1$H–$^1$H NOESY and $^1$H–$^{15}$N HSQC (Figure B12-B16 in Appendix B). Two diastereomers (*meso*-**22** and *dl* pair-**22**) as shown in Figure 1.18 are expected to be observed by NMR spectroscopy. $^1$H NMR (500 MHz, chloroform-*d*, Figure 1.19) spectrum showed a broad singlet at $\delta = 7.095$ ppm (2H$_a$) and a singlet at 6.589 ppm (1H$_b$) assigned for aromatic protons (Ar-**H**) on 4-*tert*-butylphenyl pendant and diamine moiety, respectively.

$^1$H NMR (700 MHz, chloroform-*d*, Figure 1.20) spectrum of **22** from the same compound revealed a better resolution for the broad singlet at $\delta = 7.095$ ppm (2H$_a$) which was split into three singlet peaks at $\delta = 7.089$, 7.083 and 7.078 ppm (2H$_a$). The center singlet peak at $\delta = 7.083$ ppm may correspond to *dl* pair-**22** because two aromatic protons (H$_a$) are effectively homotopic. Two outer singlet peaks $\delta = 7.089$ and 7.078 ppm may correspond to *meso*-**22** because two aromatic protons (H$_a$) are effectively diastereotopic.

Based on the assignment in the aromatic region (preceding paragraph), three singlet peaks at $\delta = 2.053$, 2.043 and 2.033 ppm (6H$_d$) may be assigned by the same principle to CH$_3$ groups of 2,6-dimethyl-4-*tert*-butylphenyl pendant. The center peak at 2.043 ppm may correspond to *dl* pair-**22** because two CH$_3$ groups are homotopic. Two outer singlet peaks $\delta = 2.053$ and 2.033 ppm may correspond to *meso*-**22** because two CH$_3$ groups are diastereotopic. A broad singlet peak at $\delta = 2.931$ ppm (2H$_c$) is assigned to the N-**H** group. This assignment was confirmed by a cross-peak between $^1$H at $\delta = 3.216$ ppm (2H$_c$) and $^{15}$N in $^1$H–$^{15}$N HSQC spectra in acetone-*d$_6$* showing N-**H** group. The $^{15}$N NMR chemical

shift is in the $\delta = -288.2$ ppm (relative to nitromethane at 0.0 ppm). Additional evidence

for N-**H** was obtained from $D_2O$ exchange experiment in benzene-$d_6$ (Figure A39 in

Appendix A). After addition of a drop of $D_2O$, $^1$H NMR spectrum showed a rapid and

complete H/D exchange of the singlet at $\delta = 3.051$ ppm ($2H_c$) corresponding to the N-**H**

group.

As shown in Figure 1.19, multiplets at $\delta = 1.547\text{-}1.100$ ppm ($4H_e$ and $4H_g$,

overlapping signal) were assigned to $CH_2$ protons of *n*-propyl groups. A singlet at $\delta =$

1.343 ppm ($9H_f$) was assigned to *t*-Bu group. Two singlet peaks at $\delta = 1.165$ ppm ($6H_h$)

and 1.121 ppm ($6H_h'$) were assigned to diastereotopic $CH_3$ protons. Two singlet peaks at

$\delta = 1.033$ and 1.027 ppm ($6H_i$) ppm were assigned to two diastereomers (*meso*-$H_i$ and *dl*

pair-$H_i$). A triplet peak at $\delta = 0.883$ ppm ($6H_j$) ppm was assigned to $CH_3$ on *n*-propyl

groups. $^1$H NMR (700 MHz, chloroform-*d*, Figure 1.20) spectrum clearly revealed two

diastereomers in this aliphatic regions because of better resolution.

$^{13}$C NMR (100 MHz, chloroform-*d*, Figure A40 in Appendix A) spectrum is in

agreement with the structure of diamine **22**. IR spectrum showed the absorption peak at

$\nu_{N-H} = 3375$ cm$^{-1}$ (Figure A41 in Appendix A).
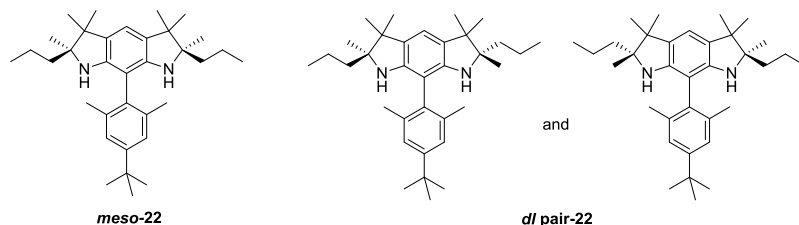


**Figure 1.18.** Structures of *meso*-**22** and *dl* pair-**22**.
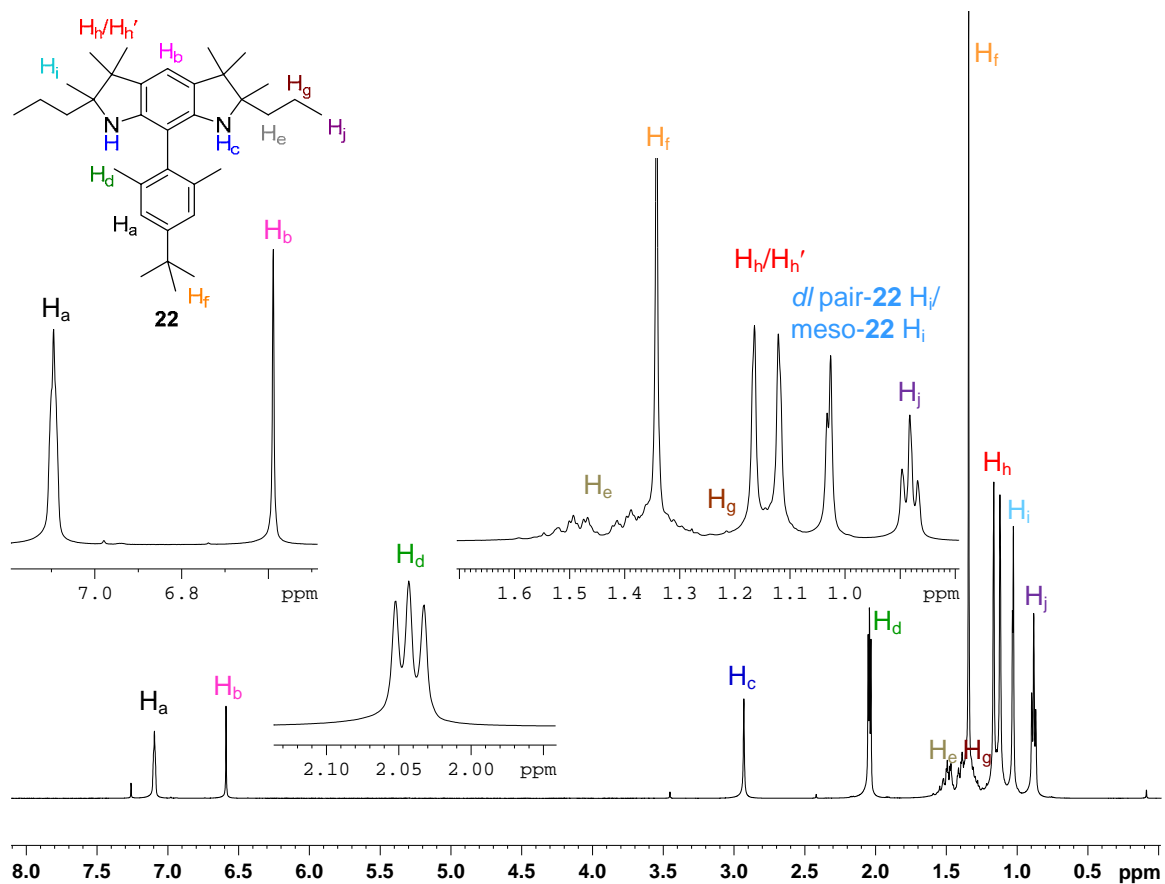
**Figure 1.19.** ¹H NMR (500 MHz, chloroform-*d*, label: AO-9-28-wsh4) spectrum of the diamine **22**.
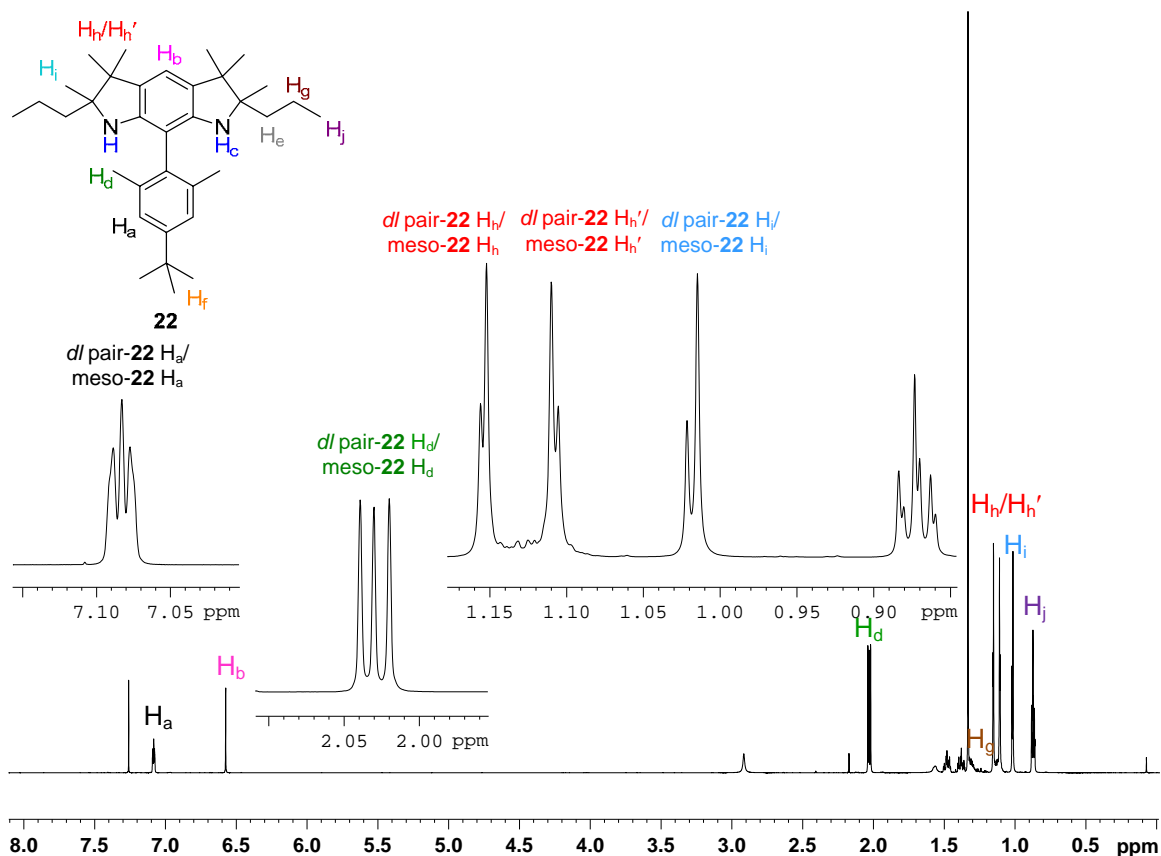
**Figure 1.20.** ^{1}H NMR (700 MHz, chloroform-*d*, label: AO-9-28-wsh6) spectrum of the diamine **22**.

Additional structural evidence for diamine **22** was obtained from the correlation between the DFT-calculated ($\delta_{DFT}$) and experimental ($\delta_{expt}$) ^{1}H and ^{13}C NMR chemical shifts (Figure B3 in Appendix B). The correlation coefficients, $R^2$ = 0.9934 and 0.9989 (Figure B4, Table B1, Table B2 in Appendix B), are obtained for ^{1}H and ^{13}C NMR chemical shifts using the calculated chemical shift for simplified structure of **22**, in which the *n*-propyl groups are replaced with methyl groups (**22a**). The relationship between computed and experimental NMR chemical shift is further illustrated by appling the correlations to scale linearly ($\delta_{DFT}$) to provide ($\delta_{scaled}$). The plot of the differences between the scaled and experimental NMR chemical shift ($\delta_{scaled} - \delta_{expt}$) for hydrogen or

carbon atom in the structure confirm good agreement between theory and experiment, indicated by the low value of statistical error parameters for $^1$H and $^{13}$C NMR chemical shift (Table B1 in Appendix B).

The attempted synthesis of the sterically hindered diamine **23** by the coupling reaction between 4,4,5,5-tetramethyl-2-(2,4,6-tri-*tert*-butylphenyl)-1,3,2-dioxaborolane **25** and bromodiamine **13** using Pd[P(*t*-Bu$_3$)]$_2$ as a catalyst in presence of K$_3$PO$_4$ as a base in toluene at 120-130 °C for 5 d (Scheme 1.22).  However, the diamine product **23** was not obtained.  $^1$H NMR (600 MHz, chloroform-*d*, label: AO-5-85-crd, Figure A42 in Appendix A) spectrum of the crude mixture showed unreacted boronate **25**, diamine **16** along with unknown compounds.  ESI-MS (label: AO585crd, Figure A43 in Appendix A) of the crude mixture showed *m/z* 329.5 and 655.8 which may correspond to diamine **16** and its dimer, **16-dimer**, respectively.  After separation by preparative TLC, ESI-MS of the fraction 3 (R$_f$ = 0.55, 3% deactivated silica plate, 3% ether/pentane) showed only *m/z* 655.7.  ESI-MS of the residue fraction from the washing the silica showed *m/z* 329.4 and unknown product *m/z* 505.5 (Figure A43 in Appendix A).

**Scheme 1.22.**  Attempted synthesis of diamine **23**.
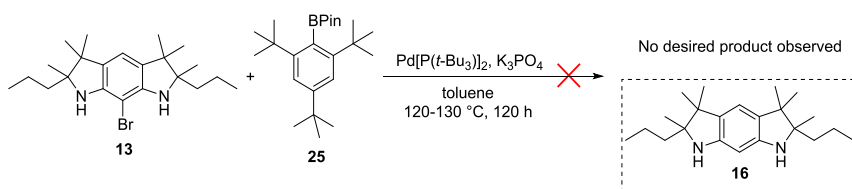


### 1.2.3.   Synthesis of diamine 28 as a precursor of aminyl diradical 11

### Synthetic plan for diamine 28

Our retrosynthetic analysis, as illustrated in Scheme 1.23, involved the disconnection of the *p-tert*-butylphenyl pendant and bromodiamine **29** via Suzuki-Miyaura

cross-coupling reaction. The bromodiamine **29** could be transformed from **30** by allylation, hydrogenation and bromination reactions, respectively. **30** could be prepared by Sonogashira cross-coupling between 1,3-dibromo-4,6-bis(acetamido)benzene and 2-methyl-3-butyn-2-ol followed by acid-catalyzed cyclization. 1,3-Dibromo-4,6-bis(acetamido)benzene was converted from commercially available 1,3-phenylenediamine by bromination and acetylation reactions, respectively. The synthesis and characterization are discussed in detail in the following section.

**Scheme 1.23.** Retrosynthesis of diamine **28**.
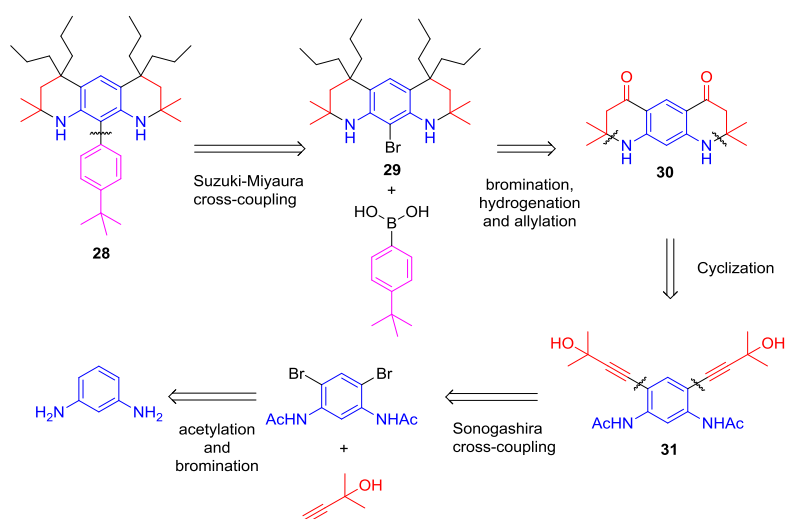


**Synthesis of diamine 28**

We successfully synthesized diamine precursor **28** in eight steps from commercially available 1,3-phenylenediamine as shown in Scheme 1.24. The results and discussion for each step is described below.

**Scheme 1.24.** Synthetic of diamine **28**.
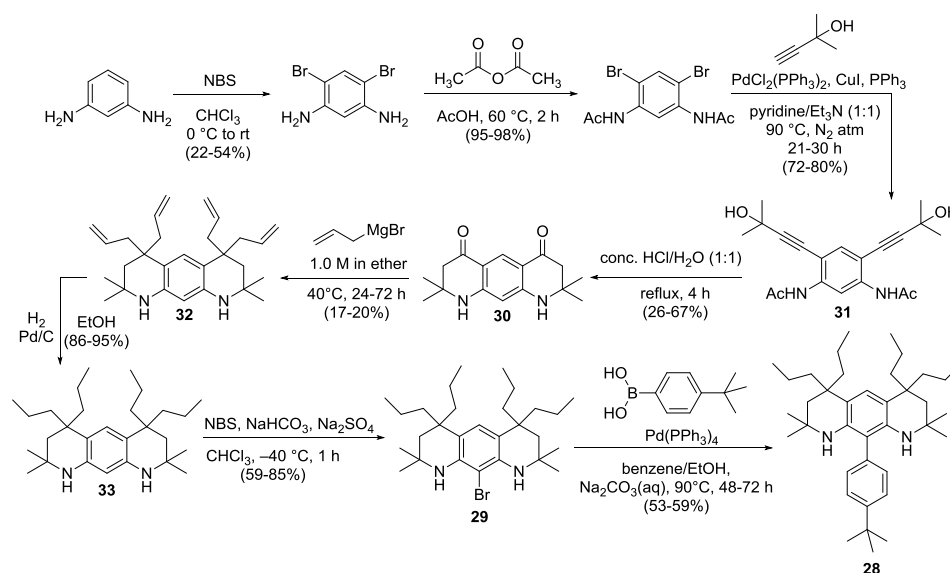
Several approaches to the construction of tetrahydroquinoline have been reported.[53,54] However, the reports of the synthesis of octahydropyrido[3,2-*g*]quinoline (OHPQ) are very limited. The OHPQ ring may be construct by generating two new bond as illustrated in Figure 1.21. The tetrahydroquinoline and OHPQ examples shown in the following section focus on N1-C2 bond formation.
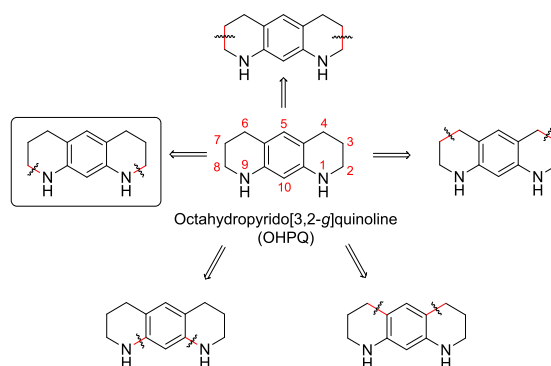


**Figure 1.21.** Disconnections of the OHPQ framework.

Hamann and co-workers[55] reported the synthesis of tricyclic pyridonoquinoline **34** from 7-amino-4-methyl-2-hydroxyquinoline (Carbostyril 124) with acetone and iodine (Scheme 1.25). The main concern for this synthetic pathway is the requirement of harch

conditions e.g., high temperature and sealed tube conditions, low yields and poor regioselectivity.

**Scheme 1.25.** Synthesis of pyridonoquinoline **34**.
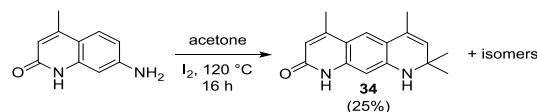


Yoo and co-workers[56] reported the synthesis of 3-iodotetrahydroquinoline **35** from arylamine **36** with iodine and sodium carbonate by intramolecular aminoiodination (Scheme 1.26). The reaction mechanism of this reaction may proceed though three-membered intermediate **37**. Another example shown three-membered intermediate reported by Morimoto and co-workers.[57] **38** was prepared from epoxide **39** under acid condition, e.g. trifluoroacetic acid via three-membered intermediate **40** (Scheme 1.26).

**Scheme 1.26.** Synthesis of **37** and **40** via three-membered intermediates.
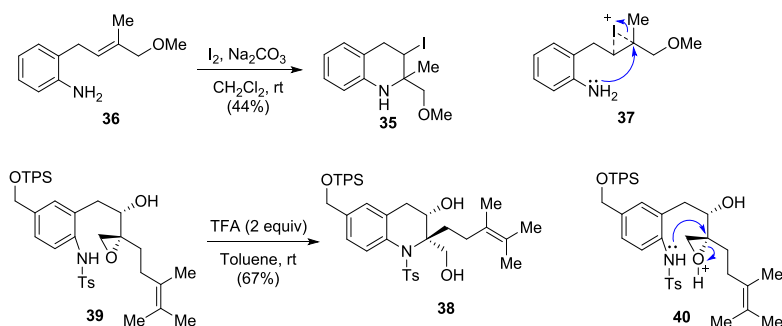


Bunce and co-workers[58] reported the tandem reduction-Michael addition synthesis of **41a** and **41b** using iron powder in glacial acetic acid at 115 °C for 30 min (Scheme 1.27). The reaction started with the reduction of the nitro group to an amine, followed by Michael addition to the acrylate by a favorable *six-exo-trig* process.[59]

**Scheme 1.27.** Synthesis of **41a** and **41b**.
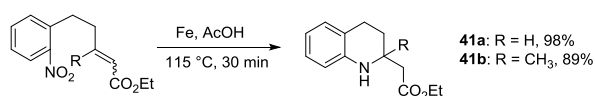
These examples may considered as tetrahydroquinoline or OHPQ frameworks. However, quaternary carbons at C2, C4, C6 and C8 positions are required for stability of aminyl diradicals.

Pisaneschi and co-workers[60] reported the synthesis of 2-substituted-2,3-dihydro-1*H*-quinolin-4-ones. The synthesis can be accomplished by two-step reaction from anilines involving Sonogashira cross-coupling reaction with a 2-methyl-3-butyn-2-ol and acid-catalyzed cyclization (Scheme 1.28).

**Scheme 1.28.** Synthesis of 2,2-dimethyl-2,3-dihydro-1*H*-quinolin-4-one.
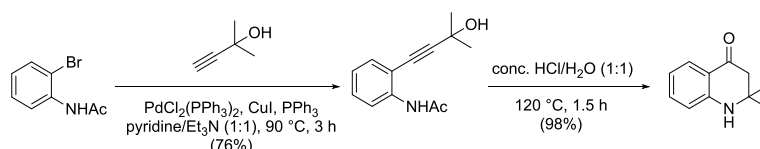


The mechanism for acid-catalyzed cyclization, proposed by the authors,[60] involves regioselective rearrangement of the 2-methyl-3-butyn-2-ol to the $\alpha,\beta$-unsaturated ketone (Rupe rearrangement) and 6-*endo*-trig ring closure as shown in Scheme 1.29. This mechanism is supported by the isolation of an approximately 1:1 mixture of quinolin-4-one (OCF$_3$) and $\alpha,\beta$-unsaturated ketone intermediate as illustrated in Scheme 1.29.

**Scheme 1.29.** Proposed mechanism for acid-catalyzed cyclization.[60]
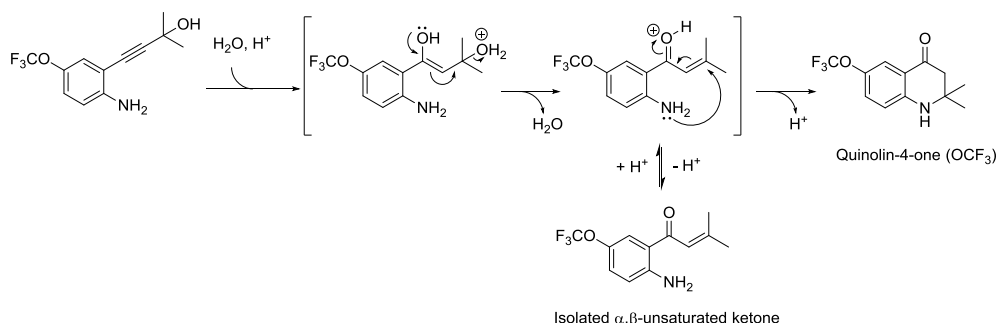


We envisioned that we could applied this useful method reported by Pisaneschi and co-workers[60] to the synthesis of diamine **30**. The construction of quaternary carbon C4 and

C6 may be acheieved by the addition of organometallic nucleophiles to carbonyl groups. According to Pisaneschi's synthesis, diamine **30** could be prepared from 1,3-dibromo-4,6-bis(acetamido)benzene, which is obtained from 1,3-dibromo-4,6-diaminobenzene (Scheme 1.24). 1,3-Dibromo-4,6-diaminobenzene and 1,3-dibromo-4,6-bis(acetamido)benzene were previously reported and prepared from 1,3-dibromobenzene by the following sequence of reactions: (1) dinitration of 1,3-dibromobenzene with fuming $HNO_3$/fuming $H_2SO_4$, (2) reduction of 1,3-dibromo-4,6-dinitrobenzene with Fe/AcOH, (3) acetylation of 1,3-dibromo-4,6-diaminobenzene using acetic anhydride in dichloromethane.[61]

**Scheme 1.30.** Reported synthesis of 1,3-dibromo-4,6-bis(acetamido)benzene.
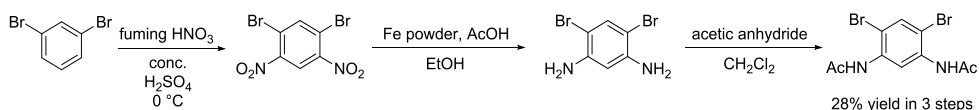


We chose a more straightforward route by bromination reaction of commercially available 1,3-phenylenediamine with *N*-bromosuccinimide (NBS) at 0 °C in CHCl$_3$ to obtain 1,3-dibromo-4,6-diaminobenzene in 22-54% yield after isolation by column chromatography along with undesired 1,3,5-tribromo-4,6-diaminobenzene in 29-54% yield. The amine groups of 1,3-dibromo-4,6-diaminobenzene were protected by acetylation reaction using acetic anhydride in acetic acid at 60 °C to yield 1,3-dibromo-4,6-bis(acetamido)benzene in 78-98% yield (Scheme 1.31). $^1$H NMR (Figure A42 and A45 in Appendix A) spectra of 1,3-dibromo-4,6-diaminobenzene and 1,3-dibromo-4,6-bis(acetamido)benzene are in good agreement with the previous report.[61]

**Scheme 1.31.** Synthesis of 1,3-dibromo-4,6-bis(acetamido)benzene.
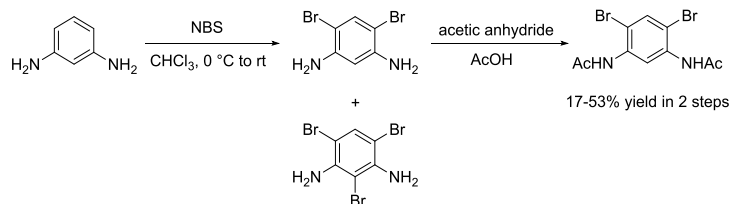


1,3-Dibromo-4,6-bis(acetamido)benzene was subjected to Sonogashira cross-coupling reaction with 2-methyl-3-butyn-2-ol, using $PdCl_2(PPh_3)_2$ as a catalyst and CuI as a co-catalyst, in a $N_2$-bubbled solution of triethylamine/pyridine (1:1, 0.1 M) at 90 °C, to give the diamine **31** in 72-80% yield. Diamine **31** was characterized by ^{1}H, ^{13}C and IR spectroscopy (Figure A48-A50 in Appendix A). The solution of diamine **31** in concentrated $HCl/H_2O$ (1:1, 0.1 M) was then heated under reflux to form diketone-diamine **30** in 26-67 % yield by acid-catalyzed cyclization reaction.

**Scheme 1.32.** Synthesis of diketone-diamine **30**.
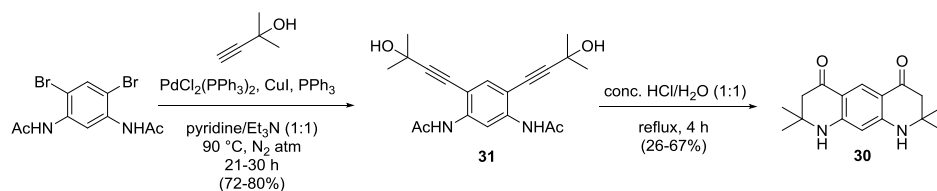


Diketone-diamine **30** was characterized by ^{1}H, ^{13}C NMR and IR spectroscopy (Figure A52-A54 in Appendix A). The structure of **30** was confirmed by single crystal X-ray crystallography (Figure 1.22).

(A)                                                    (B)
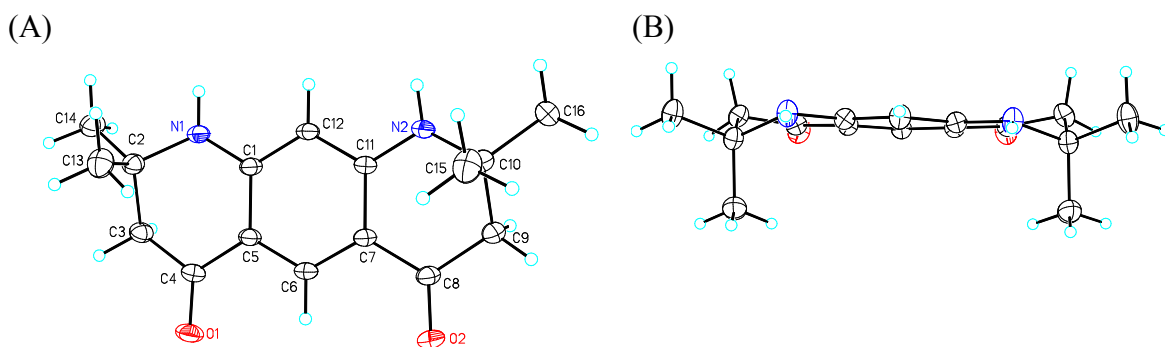
**Figure 1.22.** Molecular structure and conformation of diketone-diamine **30**: (A) top view, (B) side view. Carbon, nitrogen and oxygen atoms are depicted with thermal ellipsoids set at the 50% probability level; disorder is omitted for clarity. Reproduced from Ref. 83 with permission from American Chemical Society.

X-ray crystallographic data for **30** are summarized in Table A1 in Appendix A. Diketone-diamine **30** has an approximate $C_s$ point group. The lateral rings adopt *syn*-half chair conformations in which the carbon atoms next to nitrogen (C2 and C10 in Figure 1.22 A) are on the same sides with respect to the *m*-phenylene plane as illustrated in Figure 1.22 B. Crystal packing of **30** includes hydrogen bonding network with the N–H-----O hydrogen bonds possessing distances of 2.121 and 2.077 Å (Figure 1.23 and Table A2 in Appendix A).

(A)  (B)
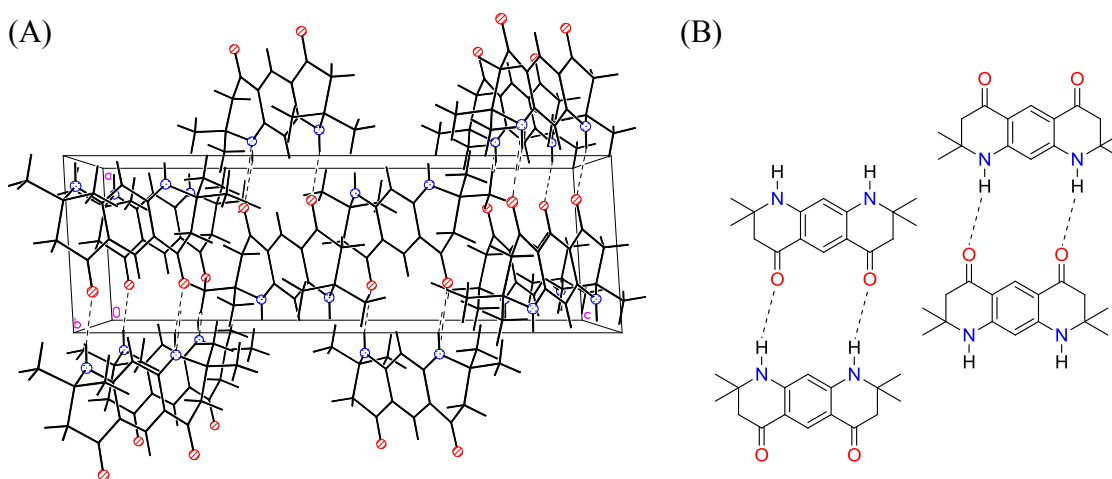


**Figure 1.23.** (A) A view of crystal packing of diketone-diamine **30** along *b* axis, showing H-bonding network. (B) Schematic representation of H-bonding pattern observed in X-ray crystallography.

The replacement of the carbonyl oxygen of diketone-diamine **30** by *gem*-dialkyl groups generating the quaternary carbon centers is investigated in this section. Typically, the transformation depends on the nature of the carbonyl compound. Two important carbonyl compound for *gem*-dialkylation are ketone and amide. More descriptive details can be found in minireview by Seebach.[62]

For the ketone, quaternary carbon center can be constructed directly by treatment with trimethylaluminum (AlMe$_3$),[63] or Me$_2$TiCl$_2$.[64] For example, 1,1-dimethylindane was prepared from indan-1-one by treatment with AlMe$_3$ at 180 °C as illustrated in Scheme 1.33.[63]

**Scheme 1.33.** Synthesis of 1,1-dimethylindane.
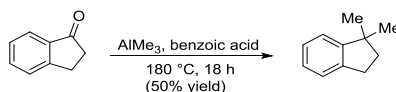


We first chose a more straightforward method for *gem*-dimethylation by treatment diketone-diamine **30** with an excess of AlMe$_3$ (2.0 M in toluene, 5-20 equiv) at 150 °C in a closed Schlenk vessel. $^1$H NMR spectra of the crude reaction were quite messy and complicated. ESI-MS of the crude reaction did not showed any promising fragment that might correspond to methylation product (Scheme 1.34). No attempt was made to investigate the reaction mixtures further.

**Scheme 1.34.** Attempted *gem*-dimethylation reaction of **30**.
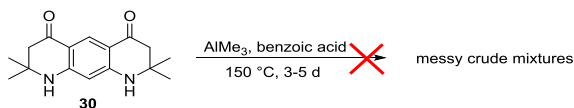
The *gem*-dimethylation reaction of ketone by AlMe₃ may depend on the nature of ketone. Diketone-diamine **30** may also be viewed as "vinyl homologoue" of amide, and therefore AlMe₃ may not be suitable for this type of amide.

In case of amide, typical method to achieve *gem*-dialkylation consists of two-step reaction: (1) the activation of amide and (2) the addition of organometallic nucleophiles (RMgX, RLi, etc.) to the activated form. For example, treatment of 2-pyrrolidone with triehyloxonium fluoroborate, followed by the addition of 2-ethoxypyrroline with an excess of allylmagnesium bromide provided 2,2-diallylpyrrolidine in 57% yield from two steps (Scheme 1.35).[65]

**Scheme 1.35.** Synthesis of 2,2-diallylpyrrolidine.
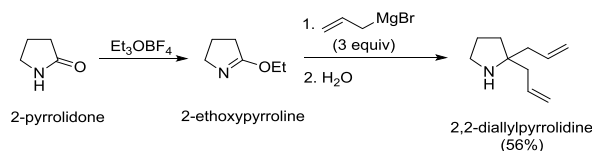


Additional example for preparation of benzyl-protected diallylpyrrolidine using triflic anhydride (Tf₂O) as an amide activator in the presence of 2,6-di-*t*-butyl-4-methylpyridine (DTBMP) as a base, followed by addition of allylmagnesium bromide to activated derivative. Benzyl-protected diallylpyrrolidine was obtained in 85% yield (Scheme 1.36).[66]

**Scheme 1.36.** Synthesis of benzyl-protected diallylpyrrolidine.
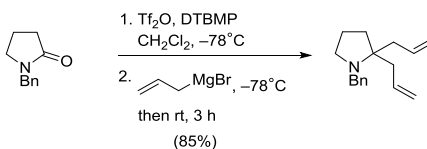
In 2000, Bubnov and co-workers[67] also prepared 2,2-diallylpyrrolidine in 90% yield by treatment of 2-pyrrolidone with triallylborane in THF. The possible mechanism, proposed by the authors, proceeded through the pathway as illustrated in Scheme 1.37.

**Scheme 1.37.** Proposed mechanism of the reductive diallylation.
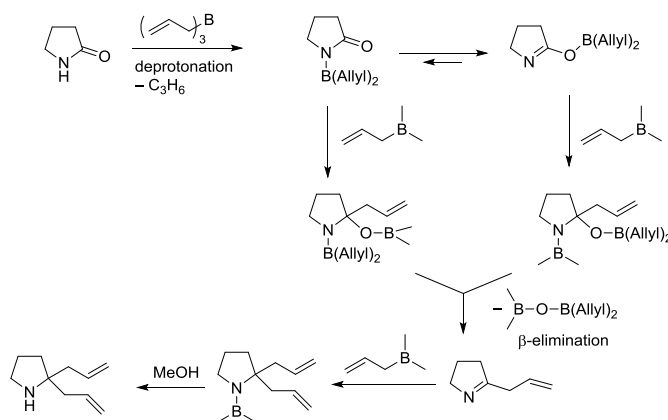


We initially investigated the reaction of diketone-diamine **30** with an excess MeMgBr at room temperature and with an excess MeMgCl at 75 °C. $^{1}$H NMR spectra of the crude reaction showed mainly starting material diketone-diamine **30**.

Subsequently, addition of diketone-diamine **30** using an excess (20 equiv) of allylmagnesium bromide (1.0 M in diethyl ether) was investigated. After stirring the reaction at room temperature for several days, bis(*gem*-diallyl)diamine **32** was obtained in low yield (~ 10% yield after tedious purification by column chromatography from crude mixture). The low solubility of **30** in organic solvents such as ether and THF might be the limitation. The reaction temperature was increased to 40-65 °C which resulted in 20% yield after stirring for 3 days. Prolonging the reaction time to 7 days did not improve the yield of **32**.

The plausible mechanism of the transformation from our diketo-diamine **30** to bis(*gem*-diallyl)diamine **32** may be demonstrated in Scheme 1.38.  The first allylation of the ketone generates an alkoxide intermediate, which is dearomatized to eliminate the MgBrOH fragment to produce imines.  The second allylation on the same position then allow to rearomatize the phenyl ring.

**Scheme 1.38.**  Plausible mechanism of allylation reaction.
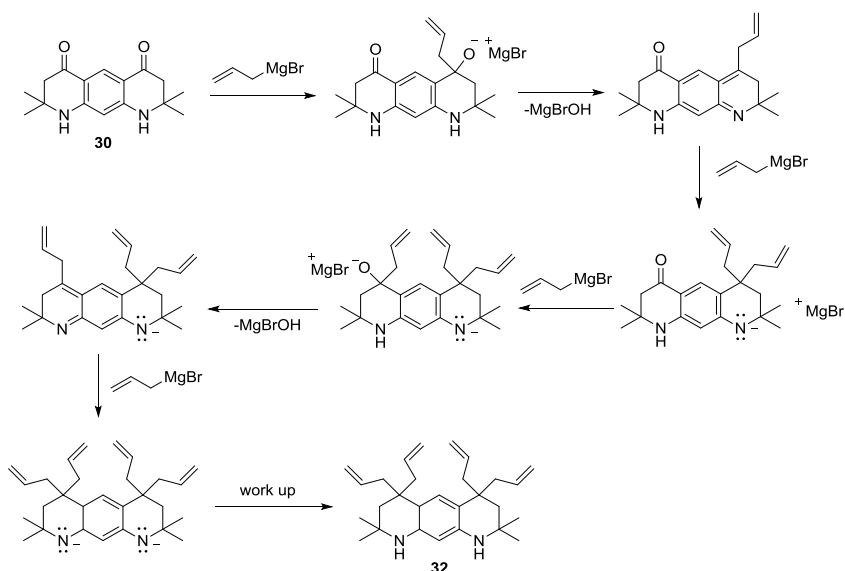


We further investigated to improve the yield of our reaction.  Zhang and Li[68] reported direct approach for diallylation forming quaternary carbon center using allylsamarium bromide.  They prepared allylsamarium bromide *in situ* by mixing allylbromide (2.5 equiv) and samarium powder (2.2 equiv) in dry THF under $N_2$ atmosphere.  After addition of various lactones and lactams to allylsamarium bromide solution and mixing at room temperature within 5 min, diallylated products were formed (Scheme 1.39).

**Scheme 1.39.** Allylation reaction of cyclic amide using allylsamarium bromide.
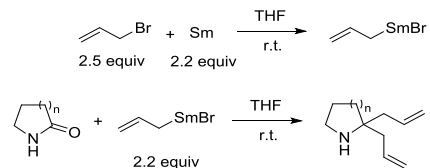


We envisioned that using allylsamarium reagents, which are less basic than Grignard reagents, might give us better yields by reducing undesired reactions such as deprotonation. However, $^1$H NMR spectra of the crude reaction showed starting diamine and unknown materials. No attempt to investigate of the composition of the crude reaction was made.

After successful preparation of bis(*gem*-diallyl)diamine **32**, the rest of the synthesis is straight forward. First, hydrogenation of bis(*gem*-diallyl)diamine **32** in ethanol under $H_2$ atmosphere with catalytic amount of Pd/C gave bis(*gem*-di-*n*-propyl)diamine **33** in 86-95% yield. Second, bromination of diamine **33** using NBS in chloroform at –40 °C furnished bromo-substituted diamine **29** in 59-62% yield. Finally, bromodiamine **29** was reacted with *p-tert*-butylphenyl boronic acid in aqueous solution of $Na_2CO_3$ and 0.1 M solution of benzene/ethanol (4:1) by Suzuki-Miyaura cross-coupling reaction, using $Pd(PPh_3)_4$ as a catalyst, to yield diamine **28** in 39-55% yield.

Diamine **28** was characterized by NMR spectroscopy, IR spectroscopy, mass spectrometry and melting point. The structure of diamine **28** is confirmed by the assignment of $^1$H and $^{13}$C NMR spectra in chloroform-*d* using standard 2D NMR spectroscopy, including $^1$H–$^{13}$C HSQC, $^1$H–$^{13}$C HMBC, $^1$H–$^1$H COSY, $^1$H–$^1$H NOESY and $^1$H–$^{15}$N HSQC (Figure B17-B21 in Appendix B). $^1$H NMR (500 MHz, chloroform-*d*, Figure 1.24) spectrum showed AB pattern at $\delta = 7.461, 7.132$ ppm ($J_{AB} = 8.3$ Hz, 2H$_a$, 2H$_b$)

assigned to four aromatic protons (Ar-**H**) on 4-*tert*-butylphenyl pendant. This assignment is confirmed by $^1$H–$^1$H COSY spectra. A singlet peak at $\delta$ = 6.806 ppm (1H$_c$) assigned to aromatic proton on diamine moiety. A broad singlet peak at $\delta$ = 2.988 ppm (2H$_d$) assigned to N-**H** resonances. This assignment was confirmed by a cross-peak between $^1$H (the broad peak at $\delta$ = 3.034 ppm; N-**H**) correlated to $^{15}$N (the broad peak at $\delta$ = –287.9 ppm, relative to nitromethane at 0.0 ppm) in $^1$H–$^{15}$N HSQC spectra in acetone-$d_6$ (Figure B17 in Appendix B) showing N-**H** group. Additional evidence for N-**H** was obtained from D$_2$O exchange experiment in benzene-$d_6$ (Figure A68 in Appendix A). After addition of a drop of D$_2$O, $^1$H NMR spectrum showed a rapid and complete H/D exchange of the singlet at $\delta$ = 3.322 ppm (2H$_d$) corresponding to the N-**H** group.

As shown in Figure 1.24, a singlet peak at $\delta$ = 1.644 ppm (4H$_e$) was assigned to CH$_2$ protons. Multiplets at $\delta$ = 1.650-1.536 ppm and 1.293-1.196 ppm (4H$_f$, overlapping signal and 4H$_h$) were assigned to CH$_2$ protons on *n*-propyl groups. Two singlets at $\delta$ = 1.363 ppm (9H$_g$) and 1.080 ppm (12H$_i$) were assigned to *t*-Bu group and CH$_3$ groups, respectively. A triplet peak at $\delta$ = 0.868 ppm (12H$_j$) was assigned to CH$_3$ on *n*-propyl groups.

Additional structural evidence for diamine **28** was obtained from the correlation between the DFT-calculated ($\delta_{DFT}$) and experimental ($\delta_{expt}$) $^1$H and $^{13}$C NMR chemical shifts (Figure B3 in Appendix B). The correlation coefficients, $R^2$ = 0.9959 and 0.9938 (Figure B5, Table B1, Table B2 in Appendix B), are obtained for $^1$H and $^{13}$C NMR chemical shifts using the calculated chemical shift for simplified structure of **28**, in which the *n*-propyl groups are replaced with methyl groups (**28a**). The relationship between computed and experimental NMR chemical shift is further illustrated by appling the

correlations to scale linearly ($\delta_{DFT}$) to provide ($\delta_{scaled}$). The plot of the differences between the scaled and experimental NMR chemical shift ($\delta_{scaled} - \delta_{expt}$) for each hydrogen or carbon atom in the structure confirm good agreement between theory and experiment, indicated by the low value of statistical error parameters for $^{1}$H and $^{13}$C NMR chemical shift (Table B1 in Appendix B).
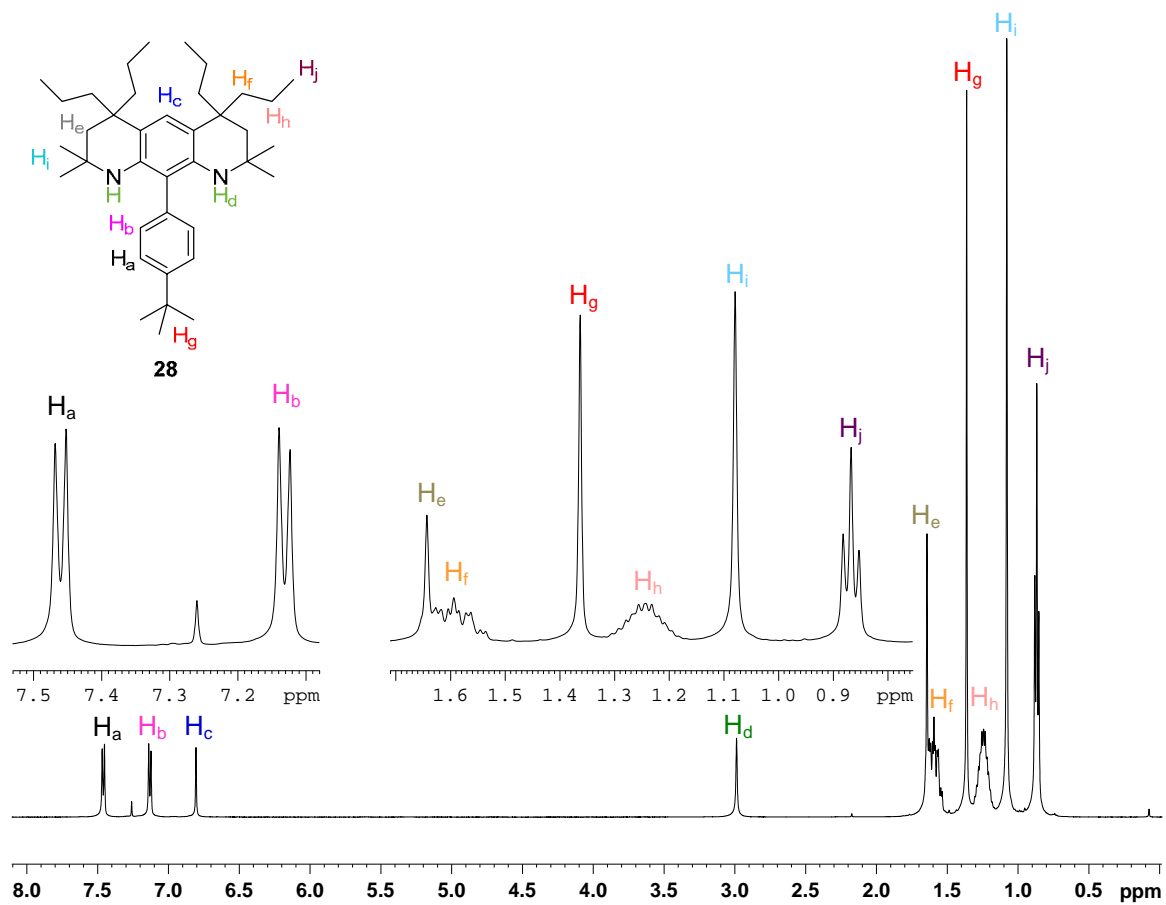


**Figure 1.24**. $^{1}$H NMR (500 MHz, chloroform-*d*, label: AO-9-32-2) spectrum of diamine **28**.

$^{13}$C NMR (100 MHz, chloroform-*d*, Figure A69 in Appendix A) spectrum, which supported the structure of **28**, showed expected 8 resonances in the aromatic carbon region corresponding to two aromatic ring in the molecule and expected 9 resonances in

aliphatic carbon region. IR (diamond, cm$^{-1}$, Figure A70 in Appendix A) spectrum exhibited the absorption at $\nu_{N-H}$ = 3379 cm$^{-1}$.

Using DFT-optimized geometry, $^{15}$N NMR isotropic shieldings for simplified structures of diamine **12**, **22** and **28**, in which the *n*-propyl groups are replaced with methyl groups (**12a**, **22a** and **28a**), were calculated at the GIAO/B3LYP/6-31G(d,p) level of theory with the IEF-PCM-UA0 solvent model for acetone (Gaussian 09),[69] in order to obtain calculated $^{15}$N NMR chemical shift $\delta_{DFT}$($^{15}$N) for direct comparison with the experimental $^{15}$N NMR chemical shift $\delta_{expt}$($^{15}$N) in acetone-*d*$_6$. (Figure 1.25) These values, which are summarized in Figure 1.25, are in good agreement with those repoted in diamine **2** in acetone-*d*$_6$ ($\delta$ = −285.9 ppm)[39], relative to nitromethane at $\delta$ = 0.0 ppm and in tetraamine **42** in benzene-*d*$_6$ ($\delta$ = −283.2 and −286.6 ppm)[70], relative to nitromethane at $\delta$ = 0.0 ppm as illustrated in Figure 1.25.



**12a**: R = Me, $\delta_{DFT}$ −287.7 ppm$^a$     **22a**: R = Me, $\delta_{DFT}$ −287.7 ppm$^a$     **28a**: R = Me, $\delta_{DFT}$ −292.1 ppm$^a$
**12**: R = *n*-Pr, $\delta_{expt}$ −287.4 ppm$^b$     **22**: R = *n*-Pr, $\delta_{expt}$ −288.2 ppm$^b$     **28**: R = *n*-Pr, $\delta_{expt}$ −287.9 ppm$^b$

$^a$ $^{15}$N chemical shift determined by DFT calculation
$^b$ $^{15}$N chemical shift determined by experiment

**2**: $\delta_{DFT}$ −286.4 ppm$^a$     **42a**: R = Me, $\delta_{DFT}$ −283.2 and −287.2 ppm$^a$
**2**: $\delta_{expt}$ −285.9 ppm$^b$     **42**: R = Octyl, $\delta_{expt}$ −283.2 and −286.6 ppm$^b$
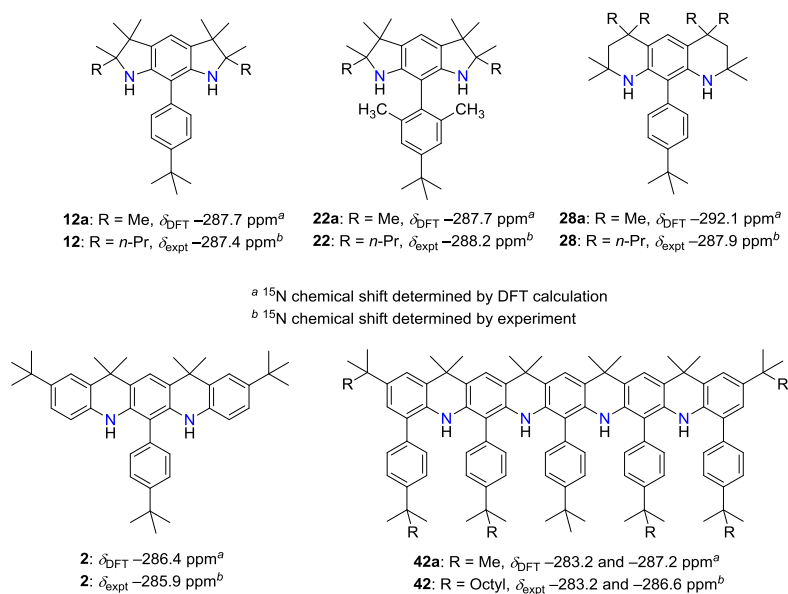
**Figure 1.25.** Experimental and calculated $^{15}$N NMR chemical shifts of diamines in acetone-*d*$_6$.

The molecular structure of diamine **28** was confirmed by X-ray crystallography as shown in Figure 1.26. X-ray crystallography data for diamine **28** is summarized in Table A1 in Appendix A. The moiety of three collinearly fused six-membered rings adopts an approximate $C_s$ point group. The piperidine rings are in *syn* half-chair conformations, in which the carbon atoms (C2 and C10 in Figure 1.26) are on the same sides of the *m*-phenylene plane. In comparison, the optimized geometry of simplified structure diamine **28a** at UB3LYP/6-31G(d,p) level, obtained by replacing *n*-propyl with methyl groups, belonged to the $C_1$ point group. The piperidine rings are in *anti* half-chair conformations, in which the carbon atoms (C2 and C10) are on the opposite sides of the *m*-phenylene plane.

In the structure of **28**, the *p-tert*-butylphenyl pendant is twisted out of *m*-phenylene plane as indicated by the torsion angles of 64.2(3)° (C1-C12-C29-C35 in Figure 1.26) and 66.3(3)° (C11-C12-C29-C30 in Figure 1.26). The computed structure of **28a** revealed the torsion angles between *tert*-butylphenyl pendant and the π-system around 69.3° which was in good agreement with those obtained from X-ray crystal structure of diamine **28**.
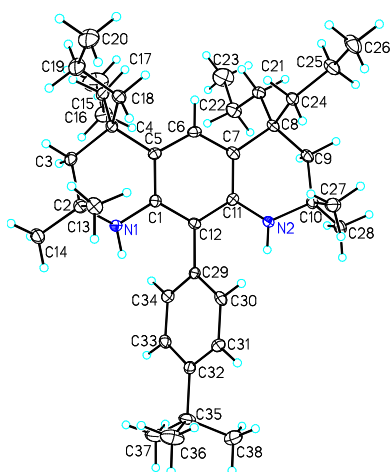


**Figure 1.26.** Molecular structure and conformation of diamine **28**. Carbon and nitrogen atoms are depicted with thermal ellipsoids set at the 50% probability level; disorder is

omitted for clarity.  Reproduced from Ref. 83 with permission from American Chemical Society.

The X-ray crystal structure diamine **28** also revealed the nitrogen-nitrogen distance ($r_{NN}$, Å) of 4.84 Å which is in good agreement with computed diamine **28a** (4.86 Å; B3LYP/6-31G(d,p)).

The molecular geometry of diamine **28a** also provided a vibrational mode with the lowest frequency which may compared to experimental IR spectrum of diamine **28**.  After correcting with vibrational scaling factor of 0.9614 at B3LYP/6-31G(d) level,[71] the calculated IR spectrum is shown in Figure 1.27, which is in good agreement with IR spectrum for **28** (Figure A70 in Appendix A).
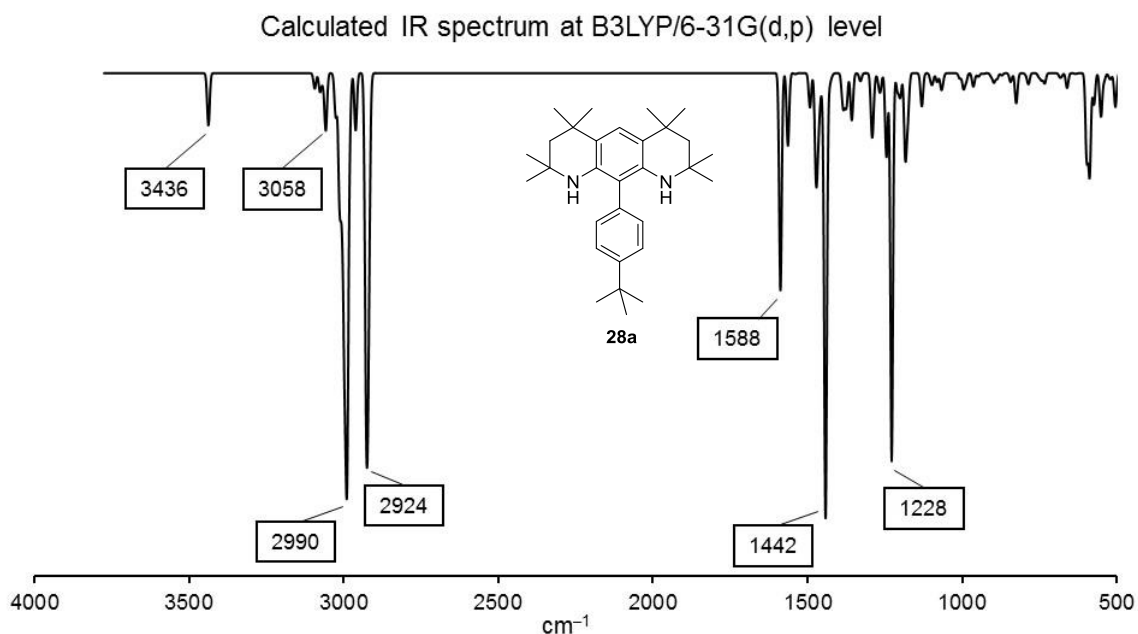


**Figure 1.27.**  Calculated harmonic vibration frequency of diamine **28a** at B3LYP/6-31G(d,p) corrected by vibrational scaling factor of 0.9614 at B3LYP/6-31G(d) level.[71]

### 1.2.4. Cyclic Voltammetry (CV) and Square Wave Voltammetry (SWV)

Diamine **12**, **22** and **28** provided us with an opportunity not only to prepare novel aminyl diradicals but also to explore the feasibility of the corresponding aminium diradical dications. Electrochemical studies using cyclic voltammetry (CV) and square wave voltammetry (SWV) techniques were performed to examine the redox behavior of diamine **12**, **22** and **28** including the stability of the different redox states.

Electrochemical studies of diamines **12**, **22** and **28** were carried out at room temperature in dichloromethane ($CH_2Cl_2$) with 0.1 M tetrabutylammonium tetrafluoroborate (*n*-$Bu_4NPF_6$) supporting electrolyte, and decamethyl ferrocene ($Cp*_2Fe$) as an internal standard, under argon atmosphere. Cyclic voltammograms of **12** and **22** showed reversible one-electron oxidation waves, which are associated with the formation of aminium radical cation **12**$^{\cdot+}$ and **22**$^{\cdot+}$. The first oxidation potentials, $E^{+/0}$ are similar for **12**, $E^{+/0} = 0.32$ V and **22**, $E^{+/0} =$ at 0.31 V (Figure 1.28 and Table 1.2) vs saturated calomel electrode (SCE) (based on average values from multiple voltammograms with the scanning rates in the 50-500 mV s$^{-1}$ and 50-200 mV s$^{-1}$, respectively). The effect of scan rates (50-500 mV s$^{-1}$) on peak current was evaluated. As illustrated in Figure 1.29, the good linearity of the plot of peak current versus the square root of scan rates is observed, which indicates a reversible process. Square-wave voltammograms also showed the first oxidation potential $E^{+/0}$ at 0.32 V for **12** and 0.30 V for **22** vs. SCE (Figure 1.28 and Table 1.2). From these measurement, it can be concluded that the singly oxidized **12**$^{\cdot+}$ and **22**$^{\cdot+}$ are stable under these circumstances.

Meanwhile, cyclic voltammograms of **28** revealed only a partially reversible first oxidation step, indicating the first oxidation potential $E^{+/0}$ at 0.46 V vs. SCE (based on

average values from multiple voltammograms with the scanning rates in the 100-200 mV $s^{-1}$). The quasi-reversible wave with the peak-to-peak difference between cathodic and anodic waves ~ 288 mV, which is significantly larger than the theoretical value of 59 mV, implies that the singly oxidized radical cation $\mathbf{28}^{\cdot+}$ is only moderately stable under these circumstances. Square-wave voltammograms also showed the first oxidation potential $E^{+/0}$ at 0.43 V vs. SCE for **28**.

Upon further oxidation, e.g. the second oxidation, the partially reversible oxidation waves from cyclic voltammograms were observed for $\mathbf{12}^{2\cdot2+}$, $\mathbf{22}^{2\cdot2+}$ due to limited stability of those diradical dications under this condition. Square-wave voltammograms also revealed additional peaks appearing in both **12** and **22** (Figure 1.28). However, the second oxidation potentials, $E^{2+/+}$ may be estimated by adding the average values of first oxidation potential to the difference between the first and second oxidation waves from cyclic voltammograms. This extrapolation provided $E^{2+/+} \approx 1.41$ V for **12** and $E^{2+/+} \approx 1.45$ V for **22**. In case of **28**, the completely irreversible wave was found for $\mathbf{28}^{2\cdot2+}$ corresponding to the formation of unstable diradical dication (Figure 1.28). Thus, the estimation of the second oxidation potential for **28** was not attempted.
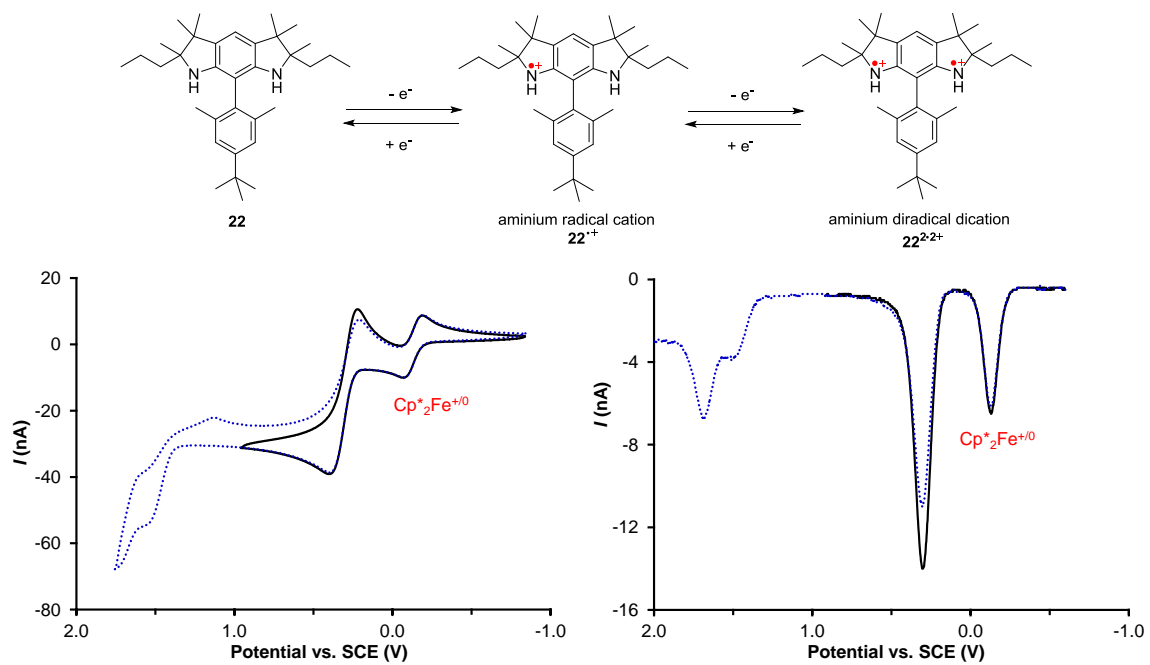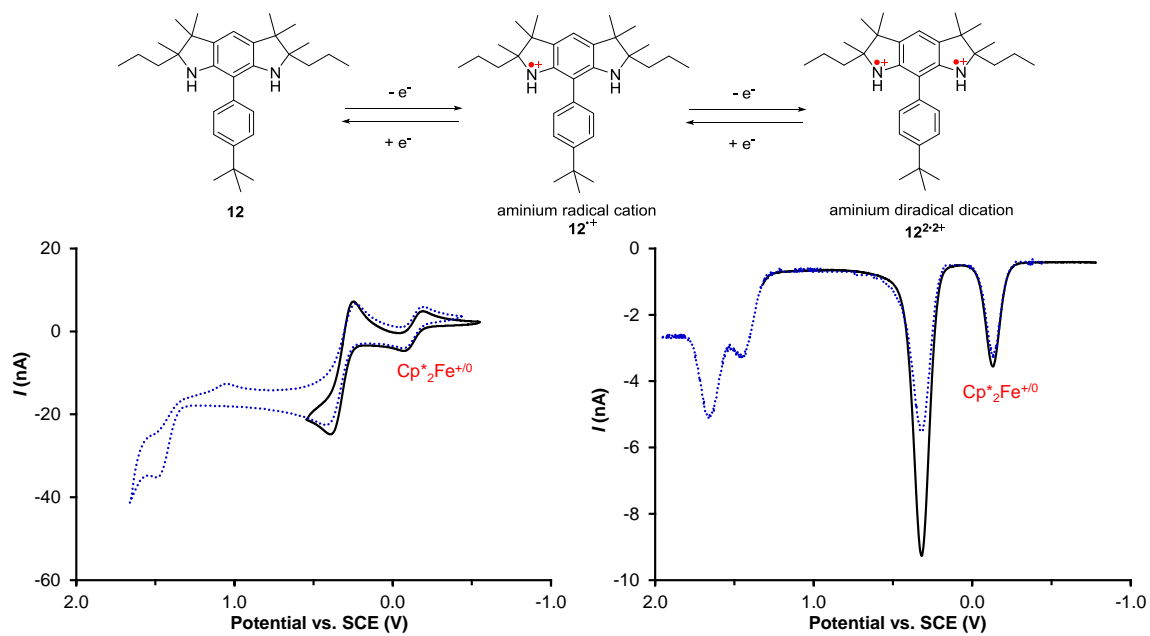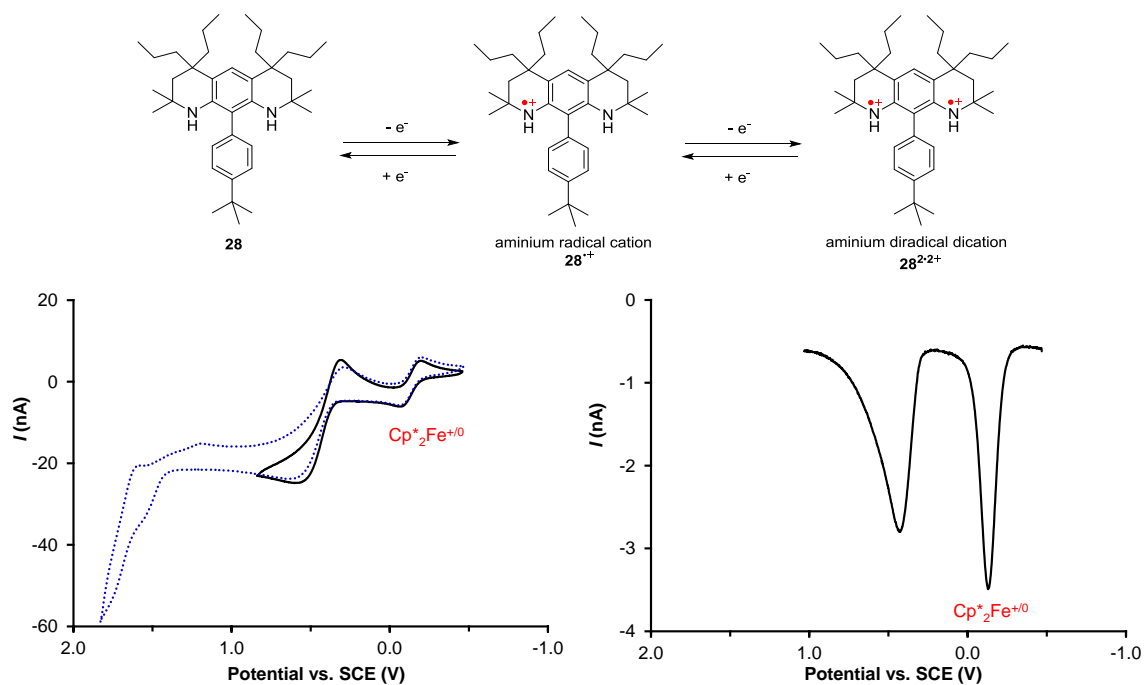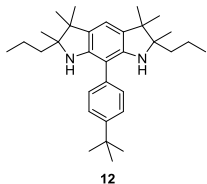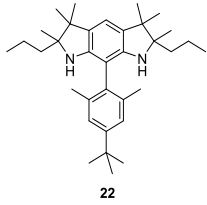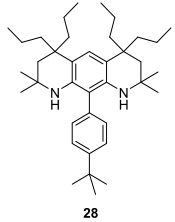
**Figure 1.28.** Cyclic voltammograms (CV, scan rate 200 mV s$^{-1}$) and square-wave voltammograms (SWV, 10 Hz, pulse height 25 mV) for diamine **12**, **22** and **28** in 0.1 M *n*-Bu$_4$NPF$_6$ in CH$_2$Cl$_2$ and internally reference to Cp*$_2$Fe$^{+/0}$ (–0.130 V vs. SCE).

**Table 1.2.** Oxidation potentials of diamines **12**, **22** and **28** [a]

| Compound | Oxidation potentials | CV $E_{1/2}^{ox}$ (V) | SWV $E_p^{ox}$ (V) |
|---|---|---|---|
| **12** | $E^{+/0}$ | 0.322 ± 0.002 (4) | 0.320 ± 0.001 (6) |
|  | $E^{2+/+}$ | 1.410 ± 0.015[b] (5) | - |
| **22** | $E^{+/0}$ | 0.310 ± 0.003 (8) | 0.302 ± 0.002 (6) |
|  | $E^{2+/+}$ | 1.450 ± 0.003[b] (3) | - |

| | | | |
|---|---|---|---|
|  **28** | $E^{+/0}$ | 0.459 ± 0.007 (6) | 0.426 ± 0.002 (4) |

[a] Potentials (vs SCE) from CV and SWV reported as arithmetic mean ± standard deviation (*n*), where *n* is the number of voltammograms with different scan rates or number of square-wave voltammograms.    The voltammograms were recored with scan rates of 50-500 for **12**, 50-200 for **22**, or 100-200 mV s$^{-1}$ for **28** (and with frequency of 10 Hz) in 0.1 M [*n*-Bu$_4$N]$^+$[PF$_6$]$^-$ in dichloromethane; 100 micron Pt-disk as working electrode.  The potentials are calibrated with decamethylferrocene (Cp*$_2$Fe) as the internal standard (–0.130 V vs SCE for Cp*$_2$Fe$^{+/0}$ in dichloromethane).[72] [b] The second oxidation was estimated by the method described in the discussion section (discussed in the decay kinetic experiment of **11**).
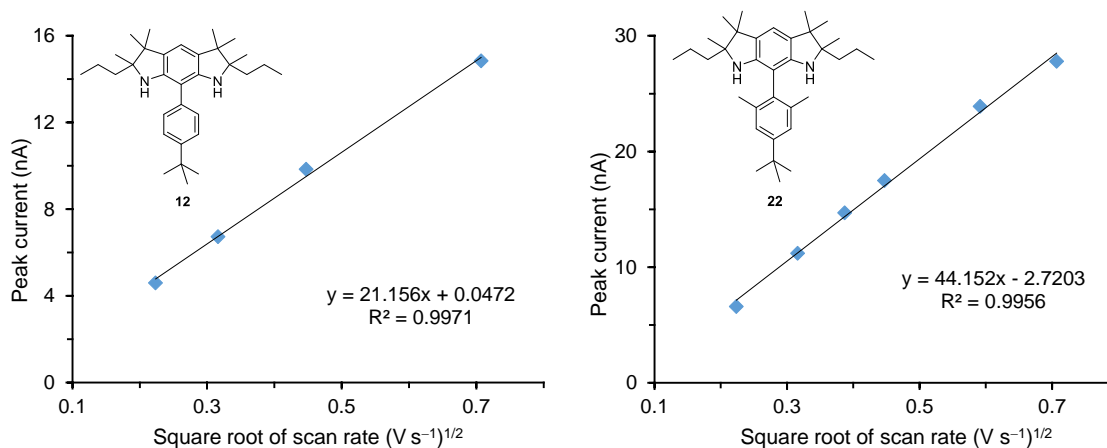


**Figure 1.29.**  Plots of oxidation peak current vs. square root of scan rates for **12** and **22**.

In conclusion, the generation of aminium diradical dication **12$^{2\cdot2+}$**, **22$^{2\cdot2+}$** and **28$^{2\cdot2+}$** are not feasible due to the lack of stability at room temperature.  Aminium radical cation **12$^{\cdot+}$** and **22$^{\cdot+}$** is stable on time scale of the the experiment under this condition but radical

cation **28**$^{\cdot+}$ is barely stable at room temperature. The limited stability of **28** may come from the same origin found in the generation of aminyl diradical **11** (vide infra).

### 1.2.5. Aza-*m*-xylylene diradical derivatives 9, 10 and 11

Aminyl diradicals **9**, **10** and **11** were prepared in custom-made 5-mm EPR or SQUID sample tube using the procedure, as described for the synthesis of aminyl diradicals **1**, **3** and **4**.[18,19] The synthesis of aminyl diradical using very small amount of starting materials (0.4-1.3 mg, μmol scale) proved to be an experimental challenge. It requires skills for handling highly sensitive materials at low temperature using high-vacuum techniques due to the air sensitivity and thermal instability of the diradicals. Typical EPR and SQUID vessels including detailed description of the generation of diradicals are shown in Figure 1.30.
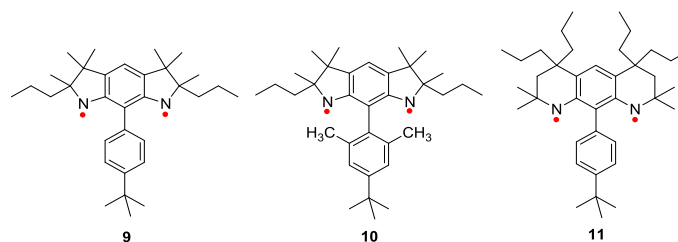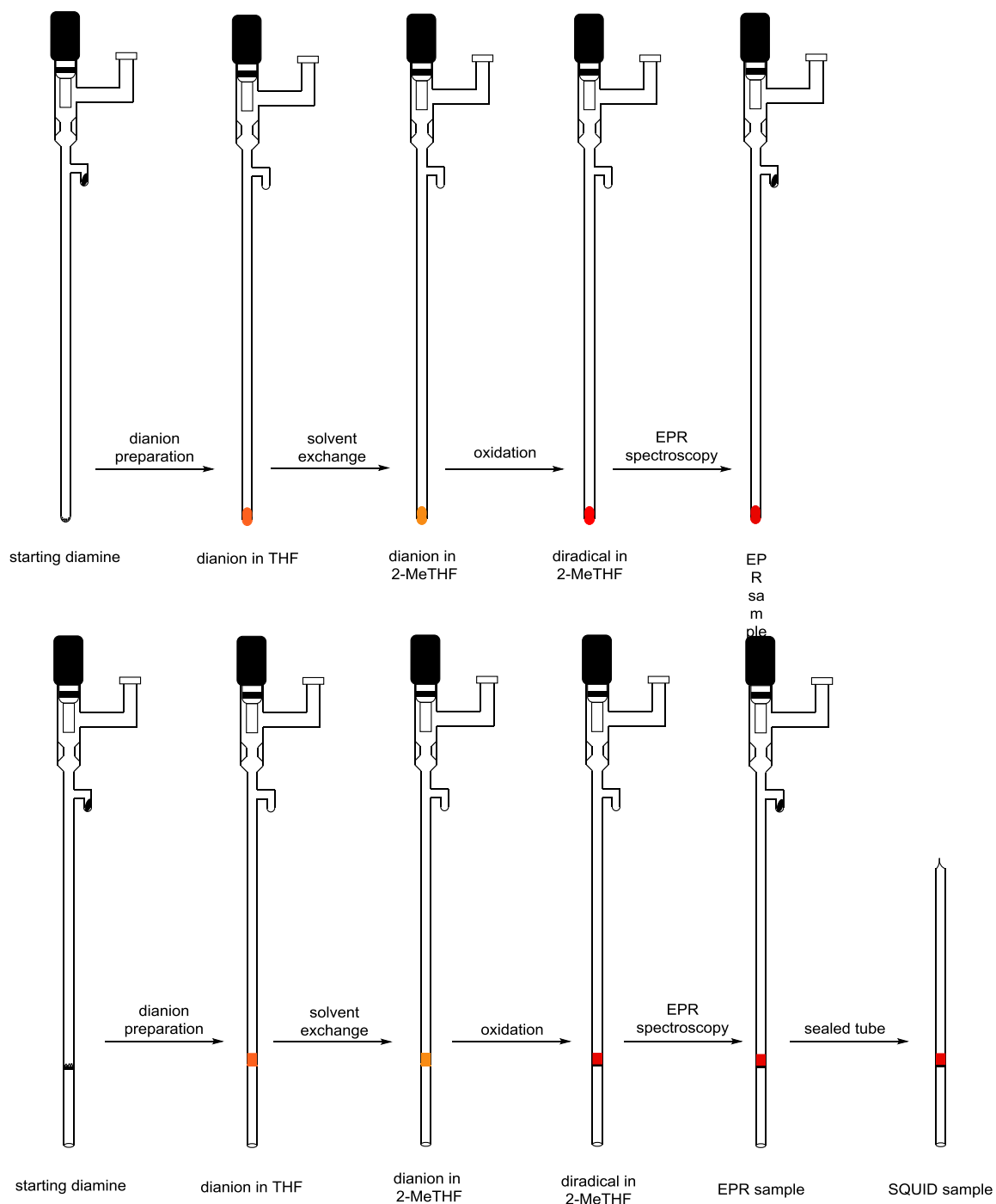
**Figure 1.30.** Custom-made EPR and SQUID vessels with the detailed description for generation of diradicals. Colors shown in the figure are represented for the generation of aminyl diradical **9**.

**Synthesis of aminyl diradical 9, 10 and 11**

As illustrated in Scheme 1.40, treatment of diamine **12**, **22** and **28** with *n*-BuLi at –30 to –50 °C to produce the corresponding dianion, followed by oxidation of the dianion with iodine at –115 °C, yielded aminyl diradical **9**, **10** and **11**, respectively. The corresponding dianions were generated in THF solution by adding a slightly more than stoichiometric amount of dilute 0.15-0.25 M *n*-BuLi in hexane (2.1-2.4 equiv, 12-20 µL) at –30 °C using microsyringes. The temperature and time for preparation of dianions were optimized. Prior to the oxidation step, THF (m.p. –108 °C) and hexane were removed and replaced by 2-MeTHF (m.p. –136 °C) via multiple vacuum transfers of solvents. The oxidation step of the dianions was carried out using EtOH slush bath (–115 °C). One of the very challenging tasks is the addition of stoichiometric amount of iodine by vacuum transfer. It was helpful to certain extent to monitor the color changes during the oxidation. For example, an orange solution of dianion resulted in a red solution of **9**, a green solution of **10**, and a green solution of **11**.

**Scheme 1.40.** Synthesis of aminyl diradical **9, 10** and **11**.
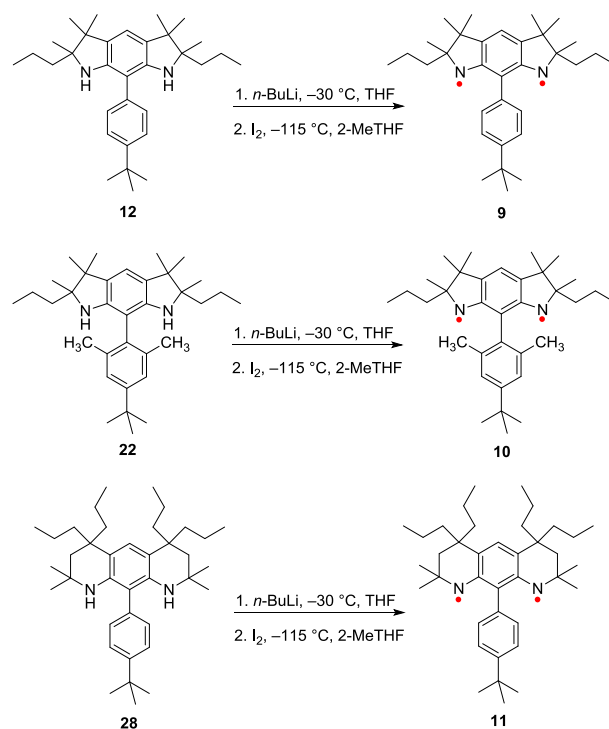


**EPR spectra of aminyl diradical 9, 10 and 11**

The EPR (X-band) spectra of aminyl diradical **9**, **10** and **11** (Figure 1.31-1.33) in a glassy matrix of 2-MeTHF at 132 K showed six symmetrically disposed side peaks corresponding to diradical ($|\Delta m_s| = 1$). Also, a half-field transition ($|\Delta m_s| = 2$), which was the evidence of the triplet state was observed. The center lines are assigned to monoradical.

The EPR spectra of aminyl diradical **9**, **10** and **11** in glassy 2-MeTHF at 132 K can be simulated and fitted to the $S = 1$ state (Figure 1.31, Table 1.4). For **9**, the $S = 1$ diradical is the predominant species corresponding to 85% of doubly integrated EPR intensity. For the best samples of **10** and **11**, the $S = 1$ diradical species correspond to 40-60% of doubly integrated EPR intensity.
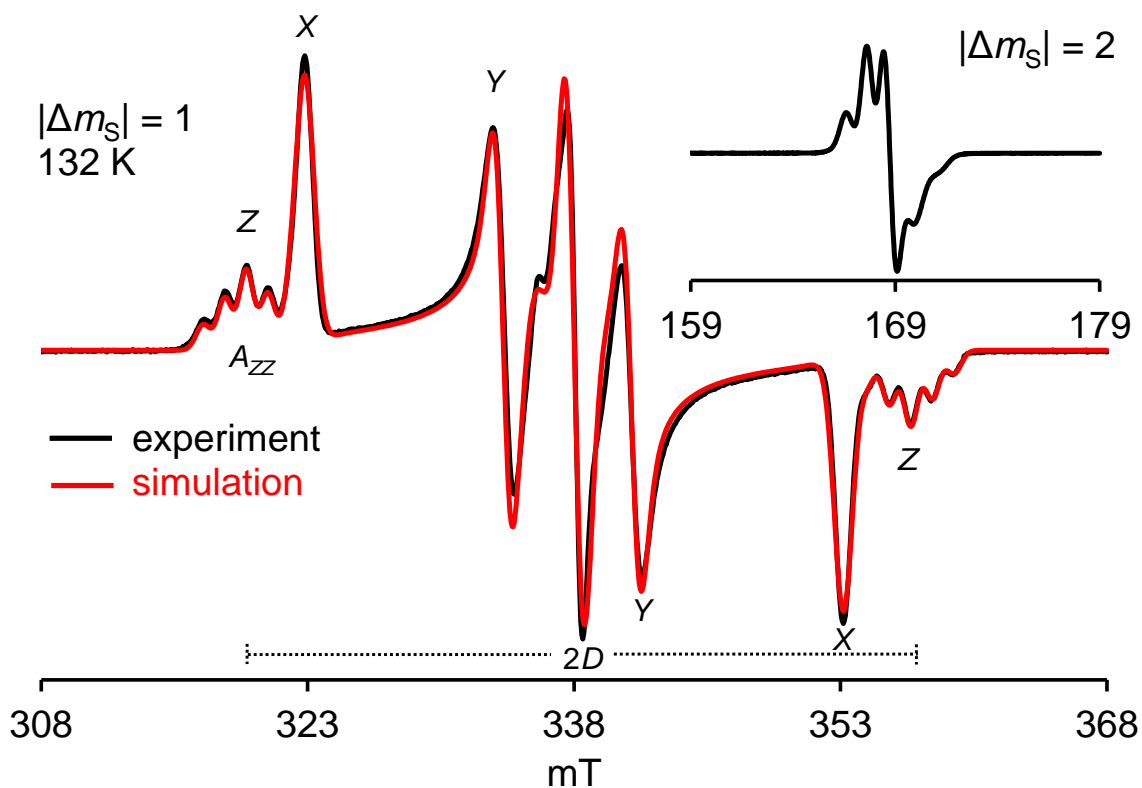
**Figure 1.31.** EPR (X-Band, $v$ = 9.4780 GHz) spectrum of aminyl diradical **9** in 2-MeTHF

at 132 K (15 mM, label: AO335r3/r4); inset plot: $|\Delta m_s|$ = 2 region, $v$ = 9.4782 GHz. The

simulation parameters for the $S$ = 1 state are: $|D/hc|$ = 17.5 × 10$^{-3}$ cm$^{-1}$, $|E/hc|$ = 3.60 × 10$^{-3}$

cm$^{-1}$, $|A_{zz}/2hc|$ = 1.13 × 10$^{-3}$ cm$^{-1}$, $g_x$ = 2.0046, $g_y$ = 2.0030, $g_z$ = 2.0019, Gaussian line ($L_x$

= 0.90, $L_y$ = 1.05, $L_z$ = 0.80 mT). The center lines correspond to an $S$ = ½ (monoradical)

by-product simulated with the identical $g$-values, $|A_{zz}/hc|$ = 2.40 × 10$^{-3}$ cm$^{-1}$ and Gaussian

line ($L_x$ =1.05, $L_y$ = 1.00, $L_z$ = 1.40 mT). Adapted from Ref. 23 with permission from

American Chemical Society.
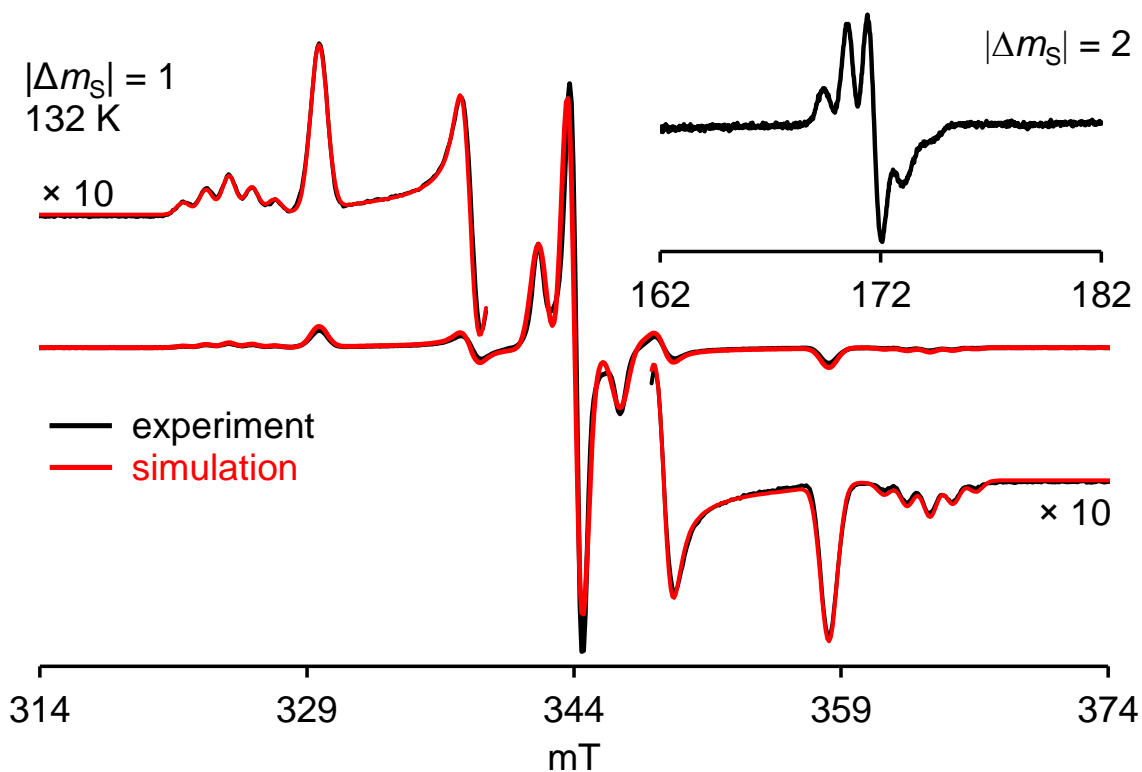
**Figure 1.32.** EPR (X-Band, $\nu = 9.6451$ GHz) spectrum of aminyl diradical **10** in 2-MeTHF at 132 K (8 mM, label: AO552r3/r4); inset plot: $|\Delta m_s| = 2$ region, $\nu = 9.6449$ GHz. The simulation parameters for the $S = 1$ state are: $|D/hc| = 18.4 \times 10^{-3}$ cm$^{-1}$, $|E/hc| = 2.77 \times 10^{-3}$ cm$^{-1}$, $|A_{zz}/2hc| = 1.20 \times 10^{-3}$ cm$^{-1}$, $g_x = 2.0045$, $g_y = 2.0027$, $g_z = 2.0014$, Gaussian line ($L_x = 0.84$, $L_y = 0.94$, $L_z = 0.76$ mT). The center lines correspond to an $S = \frac{1}{2}$ (monoradical) by-product simulated with the identical $g$-values, $|A_{zz}/hc| = 2.15 \times 10^{-3}$ cm$^{-1}$ and Gaussian line ($L_x = 0.80$, $L_y = 0.80$, $L_z = 0.90$ mT).
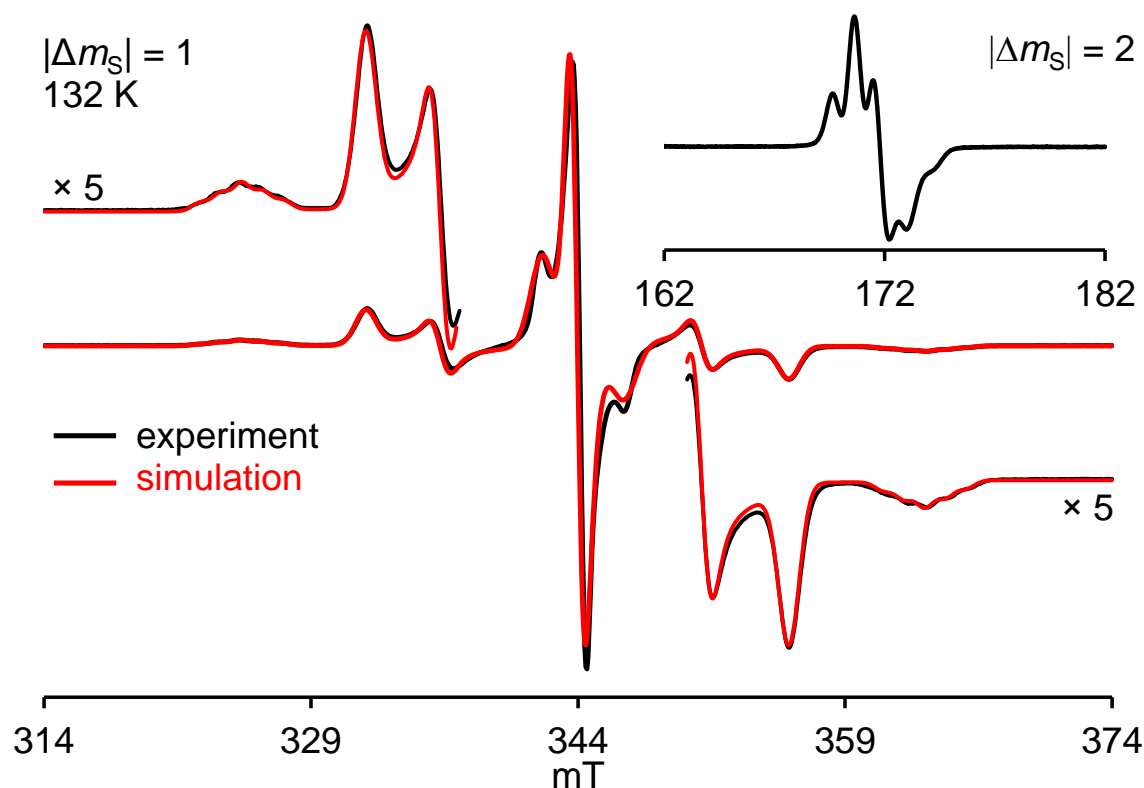
**Figure 1.33.** EPR (X-Band, $\nu = 9.6463$ GHz) spectrum of aminyl diradical **11** in 2-MeTHF at 132 K (19.3 mM, label: AO983r1/r2); inset plot: $|\Delta m_s| = 2$ region, $\nu = 9.6463$ GHz. The simulation parameters for the $S = 1$ state are: $|D/hc| = 17.9 \times 10^{-3}$ cm$^{-1}$, $|E/hc| = 1.42 \times 10^{-3}$ cm$^{-1}$, $|A_{zz}/2hc| = 1.08 \times 10^{-3}$ cm$^{-1}$, $g_x = 2.0050$, $g_y = 2.0031$, $g_z = 2.0018$, Gaussian line ($L_x = 0.95$, $L_y = 1.17$, $L_z = 0.97$ mT). The center lines correspond to an $S = \frac{1}{2}$ (monoradical) by-product simulated with the identical $g$-values, $|A_{zz}/hc| = 2.25 \times 10^{-3}$ cm$^{-1}$ and Gaussian line ($L_x = 0.75$, $L_y = 0.70$, $L_z = 1.35$ mT). Reproduced from Ref. 83 with permission from American Chemical Society.

As shown in Figure 1.33, the EPR spectra of **11** revealed a mixture of diradical and monoradical. Reaction time (2-6 h) and temperature (−30 °C or −22 °C) for preparation of corresponding dianion were optimized. The oxidation step was also investigated using

various oxidizing agents, i.e., I$_2$, Cp$_2$FeBF$_4$, AgBF$_4$, tris-4-bromophenylammoniumyl

hexachloroantimonate ((4-Br-Ph)$_3$NSbCl$_6$) as well as a sequence of oxidation using I$_2$

followed by Cp$_2$FeBF$_4$ to improve the content of diradical, as describe in detail in

experimental section.

The oxidation of the corresponding dianion by I$_2$ showed the diradical content to

about 40%. After addition of Cp$_2$FeBF$_4$ to the reaction mixture, EPR spectra provided a

content of diradical up to 60%. However, the diradical disappeared completely after

annealing the sample at room temperature (21 °C) for 5 min; and only monoradical was

observed by EPR spectroscopy (Scheme 1.42). According to oxidation potentials of

Cp$_2$FeBF$_4$ and I$_2$,[73] Cp$_2$FeBF$_4$ may reoxidize I$_3^-$ to produce more iodine which may rapidly

deteriorate diradical due to sensitivity of diradical to I$_2$ at room temperature.

**Scheme 1.41.** Synthesis of aminyl diradical **11**.
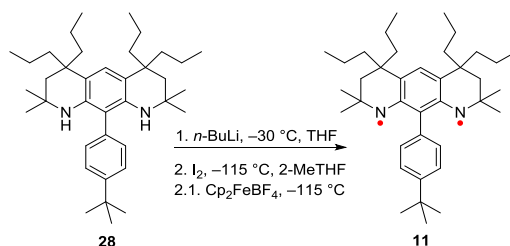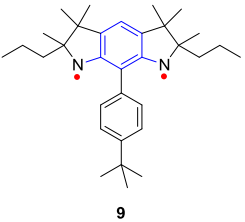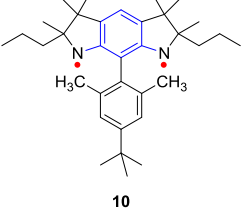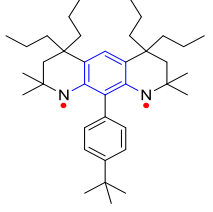


**Scheme 1.42.** Generation of diradical using I$_2$ followed by Cp$_2$FeBF$_4$ showing % diradical

content[a] and color in 2-MeTHF solution monitored by EPR spectroscopy.
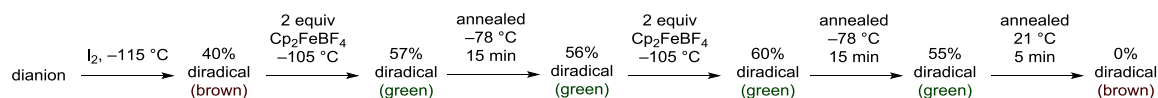


[a] % diradical determined by double integration

**Table 1.3.** Summary of % diradical in mixtures obtained from selected experiments of diradical **9**, **10** and **11**

| Diradical | Label | % diradical[a] |
|---|---|---|
|  **9** | AO-3-35 | 85 |
| | AO-3-52 | 85 |
| | AO-3-58 | 85 |
|  **10** | AO-5-52 | 40 |
| | AO-5-74 | 27 |
| | AO-9-15 | 26 |
|  **11** | AO-9-43 | 60 |
| | AO-9-83 | 51 |
| | AO-9-36 | 48 |
| | AO-9-80 | 46 |
| | AO-9-88 | 45 |

[a] % $S = 1$ diradical obtained from double integration of EPR spectra

The zero-field splitting (zfs) parameters ($D$ and $E$) of aminyl diradicals **9**, **10** and **11** are reported and compared with previously reported aminyl diradical **1** and **4** as illustrated in Figure 1.34. The $|D/hc|$ values for aminyl diradicals **9**, **10** and **11** = 17.5 − 18.4 × 10$^{-3}$ cm$^{-1}$, correspond to the spectral width of 2$|D/hc|$, which is approximately two times greater than those of **1** and **4** (9.18 and 8.60 × 10$^{-3}$ cm$^{-1}$, respectively). The increasing values of $|D/hc|$ suggest that the average distances of spin densities for **9-11** become closer than those for **1** and **4**. As illustrated in Figure 1.34, the spin densities for diradical **9**, **10** and **11** are distributed only in *m*-phenylene unit, while the spin densities for diradical **1** and **4** are distributed to the neighboring benzene rings. In addition, the $|A_{zz}/2hc|$ values corresponding to $^{14}$N-splitting of aminyl diradical **9**, **10** and **11** are in the same range (1.10–

1.20) and in good agreement with the value observed in aminyl diradical **1** and **4** (0.99–1.00). The isotropic *g*-values of **9**, **10** and **11**, are in the range of 2.0029–2.0033, which is in good agreement with those for aminyl diradicals **1** and **4** (2.0030–2.0031).[18,19] The EPR parameters of these diradicals are summarized in Table 1.4.



**9** (R$_1$ = *n*-Pr, R$_2$ = H): |*D/hc*| = 17.5 × 10$^{-3}$ cm$^{-1}$
**10** (R$_1$ = *n*-Pr, R$_2$ = Me): |*D/hc*| = 18.4 × 10$^{-3}$ cm$^{-1}$

**11** (R$_1$ = *n*-Pr): |*D/hc*| = 17.9 × 10$^{-3}$ cm$^{-1}$

**1** : |*D/hc*| = 9.18 × 10$^{-3}$ cm$^{-1}$

**4** (R = *n*-C$_8$H$_{17}$): |*D/hc*| = 8.60 × 10$^{-3}$ cm$^{-1}$
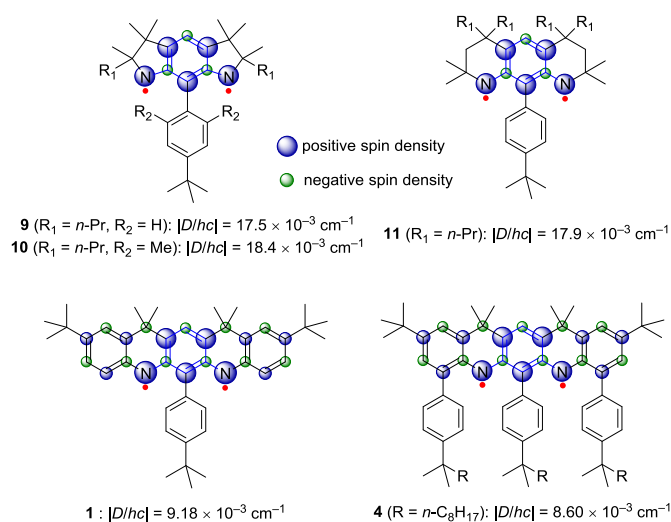
**Figure 1.34.** Summary of aminyl radicals showing spin density distribution with |*D/hc*| values.

**Table 1.4.** Summary of analyses of EPR spectra for aminyl diradicals in 2-MeTHF at 132–133 K

| Diradical | Label | Conc.[a] (mM) | *v* (GHz) | \|*D/hc*\| (10$^{-3}$ cm$^{-1}$) | \|*E/hc*\| (10$^{-3}$ cm$^{-1}$) | \|*A$_{ZZ}$/2hc*\| (10$^{-3}$ cm$^{-1}$) | $g_X$ | $g_Y$ | $g_Z$ | *g* |
|---|---|---|---|---|---|---|---|---|---|---|
| 1 | KS | - | 9.6376 | 9.18 | 2.10 | 1.00 | 2.0030 | 2.0042 | 2.0019 | 2.0030 |
| 4 | PB | - | 9.4743 | 8.60 | 1.95 | 0.99 | 2.0030 | 2.0043 | 2.0019 | 2.0031 |
| 9 | 335 | 9.41 | 9.4780 | 17.5 | 3.60 | 1.13 | 2.0046 | 2.0030 | 2.0019 | 2.0032 |
| 10 | 552r3 | 8.02 | 9.6451 | 18.4 | 2.77 | 1.20 | 2.0045 | 2.0027 | 2.0014 | 2.0029 |
| 11 | 943r10 | 12.2 | 9.6487 | 17.9 | 1.42 | 1.08 | 2.0050 | 2.0031 | 2.0018 | 2.0033 |
| 11 | 983r5 | 5.09 | 9.6415 | 17.9 | 1.42 | 1.08 | 2.0050 | 2.0031 | 2.0018 | 2.0033 |
| 11 | 980r6 | 2.23 | 9.6410 | 17.9 | 1.42 | 1.08 | 2.0050 | 2.0031 | 2.0018 | 2.0033 |
| 11 | 988r4 | 3.08 | 9.6407 | 17.9 | 1.42 | 1.08 | 2.0050 | 2.0031 | 2.0018 | 2.0033 |

[a] Concentration based on the mass of precursor diamine **9**, **10** and **11**, respectively and volume of the solvent.

According to point dipole approximation, the parameter $D$ is inversely proportional to the cube of the average distance ($r^3$) between two unpaired electrons, as shown in eq. 2.[74]

$$D = 2781/r^3 \qquad \text{(eq. 2)}$$

where $D$ is the dipolar splitting parameter in mT unit, and $r$ is the average distance between the unpaired electrons in Å unit. For example, the parameter $|D/hc| = 17.5 \times 10^{-3}$ cm$^{-1}$ ($|D/g\mu_B| = 18.7$ mT) for aminyl diradical **9** corresponds to a distance between nitrogen radicals ($r_{NN}$) ~ 5.30 Å.

The $r_{NN}$ distances estimated by point-dipole approximation of **9**, **10** and **11** are in a range of 5.21–5.30 Å, which are slightly longer than those of DFT computed diradical **7**, **10a** and **8** (~4.74–4.90 Å). The distances between two nitrogen radicals of these diradicals are summarized in Figure 1.35.



**7**: R = Me, 4.90 Å$^a$
**9**: R = $n$-Pr, 5.30 Å$^b$

**10a**: R = Me, 4.87 Å$^a$
**10**: R = $n$-Pr, 5.21 Å$^b$

**8**: R = Me, 4.74 Å$^a$
**11**: R = $n$-Pr, 5.26 Å$^b$

$^a$ $r_{NN}$ determined by DFT calculation
$^b$ $r_{NN}$ determined by point dipole approximation
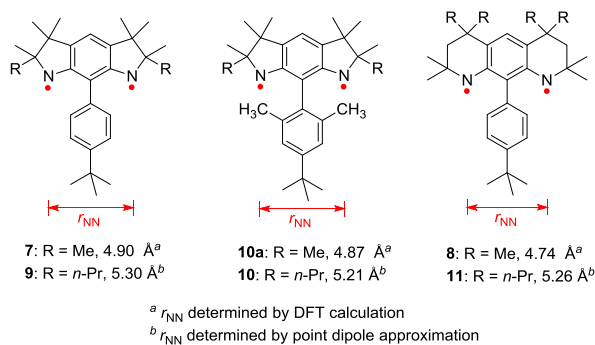
**Figure 1.35.** Summary of nitrogen-nitrogen distance ($r_{NN}$, Å) of computed diradical **7**, **10a** and **8** determined by DFT calculation and diradical **9**, **10** and **11** determined point-dipole approximation.

**Magnetic measurement of aminyl diradical 9**

The SQUID magnetic studies require near-perfect samples, e.g. very high content of diradical. As shown in Table 1.3, only diradical **9** (up to 85% diradical) was eligible for magnetic study. Studies of diradical **10** and **11** were not attempted because all their samples had low content of diradical.

The magnetic studies of aminyl diradical **9** were carried out in 2-MeTHF solution by SQUID magnetometry. The plot between $\chi T$ and $T$ where $\chi$ is molar paramagnetic susceptibility and $T$ is temperature in Kelvin for diradical **9** (~20 mM in 2-MeTHF) showed the value of $\chi T = 0.89$ emu K mol$^{-1}$ (Figure 1.36). After correction for spin concentration, $\chi T \approx 1.0$ emu K mol$^{-1}$ was obtained. The pure diradical with $S = 1$ is expected to have $\chi T = 1.0$ emu K mol$^{-1}$. The value of $\chi T$ ($\chi T \approx 1.0$ emu K mol$^{-1}$) indicated the pure sample of aminyl diradical **9**. Also, the plot between $M/M_{sat}$ and $H/(T+0.2)$ at 1.8, 3 and 5 K ($M_{sat}$, magnetization at saturation) followed $S = 1$ Brillouin function. The curvature of the plot suggested the $S = 1$ ground state of diradical **9**.
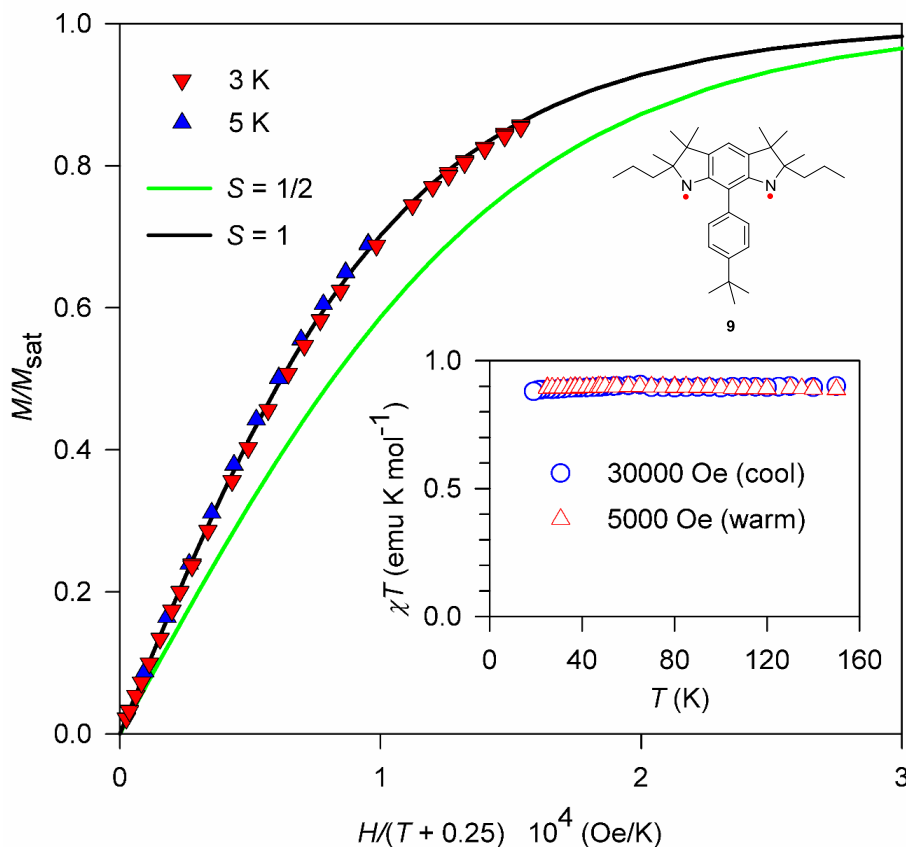
**Figure 1.36.** SQUID magnetometry of aminyl diradical **9**. Reproduced from Ref. 23 with permission from American Chemical Society.

**Decay kinetics of aminyl diradical 9, 10 and 11**

The decay kinetics of **9**, **10** and **11** in 2-MeTHF were investigated by EPR spectroscopy at 132 K, as is described extensively in the experimental section. In addition, the decay kinetics for **9** in THF were studied by SQUID magnetometry.

As previously reported by our group, aminyl diradical **4** was sensitive to an excess of iodine at −26 °C and oxygen at −78 °C.[19] To compare the reactivity with an excess of iodine among aminyl diradicals **9**, **10**, **11** and **4**, and to prove an absence of oxygen and to remove any excess of iodine in the sample, the samples were annealed at −78 °C (195 K)

and –27 °C (246 K) for some certain amount of time until diradical intensity of EPR spectra remained unchanged.  Subsequently, the samples were annealed at 22 °C (295 K).

We used two methods to determine the half-life of aminyl diradicals: (1) we followed the decay of % diradical content in the reaction mixture and (2) we followed the decay of the measured EPR peak heights corresponding to diradicals.

For the first method, the percentage of diradical in a mixture of monoradical/diradical was estimated by double integration of EPR spectra.  The EPR spectra, including spectral simulation were double integrated in three sections: 310-325 mT (side), 325-350 mT (center) and 350-365 mT (side) for aminyl diradical **9**; 320-339 mT (side), 339-349 mT (center) and 349-368 mT (side) for aminyl diradical **11**.  It was assumed that only the diradical contributed to the EPR intensity in the "side" regions, while both diradical and monoradical contributed in the "center" region.  After correcting the contribution of $S =1/2$ monoradical and $S =1$ diradical to the EPR double integrated intensity with $S(S+1)$ factor, the diradical in the diradical/monoradical mixtures were estimated for each sample.

For the second method, the average of measured EPR peak heights corresponding to diradical at ~ 329 and 359 mT for **9** and ~ 332 and 356 mT for **11** were determined.  For reference, double integration of EPR spectra for TEMPONE or TEMPOL (1.0 mM in 2-MeTHF) was used for correction of peak height of the sample.

Initially, the decay experiment for aminyl diradical **9** was carried out by the first method with only 2 points of data, e. g. at 10 and 20 min.  The half-life of ~4.6 mM diradical **9** in 2-MeTHF at room temperature ~ 7 min.

Additional experiments to estimate the half-life of ~2.5 mM aminyl diradical **9** in 2-MeTHF using the second method was developed.  EPR spectra of the sample annealed at 295 K (22 °C) for 120, 240, 360, 480, 600 s (total time) showed consecutively decrease of peak height intensity in EPR signal corresponding to diradical.  The linear regression for –ln peak height vs. time revealed the first order kinetics with a half-life 624 ± 146 s in 2-MeTHF at room temperature (Figure C1 in Appendix C).

The decay kinetics of **9** was also carried out in THF monitored by SQUID magnetometry.  Magnetic measurements of **9** annealed at 246 K (–27 °C) for 30 min showed data corresponding diradical.  The sample was annealing at 273 K (0 °C) for 30 min, 295 K (22 °C) for 30 min and 295 K (22 °C) for additional 30 min, respectively.  The data were in agreement with EPR experiment with a sharp decrease of diradical signal.  In addition, the trace of diradical was detectable after annealing at 295 K (22 °C) for 60 min.  The half-life at 295 K ~ 10 min is estimated.

Aminyl diradical **10** is significantly less persistent than diradical **9**.  The sample annealed at –30 °C for 15, 30 and 60 min showed a decrease of diradical EPR signal intensity.  Only a trace amount of diradical was observed by EPR spectroscopy after annealing for 60 min at –30 °C (Figure C2 in Appendix C).

The decay kinetic experiments for aminyl diradical **11** were carried out using the second method.  EPR spectra of ~5 mM aminyl diradical **11** annealed at 195 K (–78 °C) for 15, 30 min (total time) and at 246 K (–27 °C) for 15, 30, 45, 60 min (total time) revealed no significant change (Figure C3 in Appendix C).  Subsequently, EPR spectra of the sample annealed at 295 K (22 °C) for 60, 120, 180, 240, 300, 360, 420, 480, 600, 720 s (total time) showed consecutively decrease of peak height intensity in EPR signal corresponding to

diradical at ~ 332 and 356 mT.  The linear regression for −ln peak height (after correction)
vs. time revealed the first order kinetics with a half-life ~214 ± 11 s in 2-MeTHF at room
temperature. (Figure 1.37 and Figure C4 in Appendix C).  EPR spectra of decay kinetics
are illustrated in Figure 1.37.  Additional decay kinetics of ~2.8 mM aminyl diradical **11**
in 2-MeTHF revealed a half-life ~ 246 ± 33 s at room temperature (Figure C5 in Appendix
C).
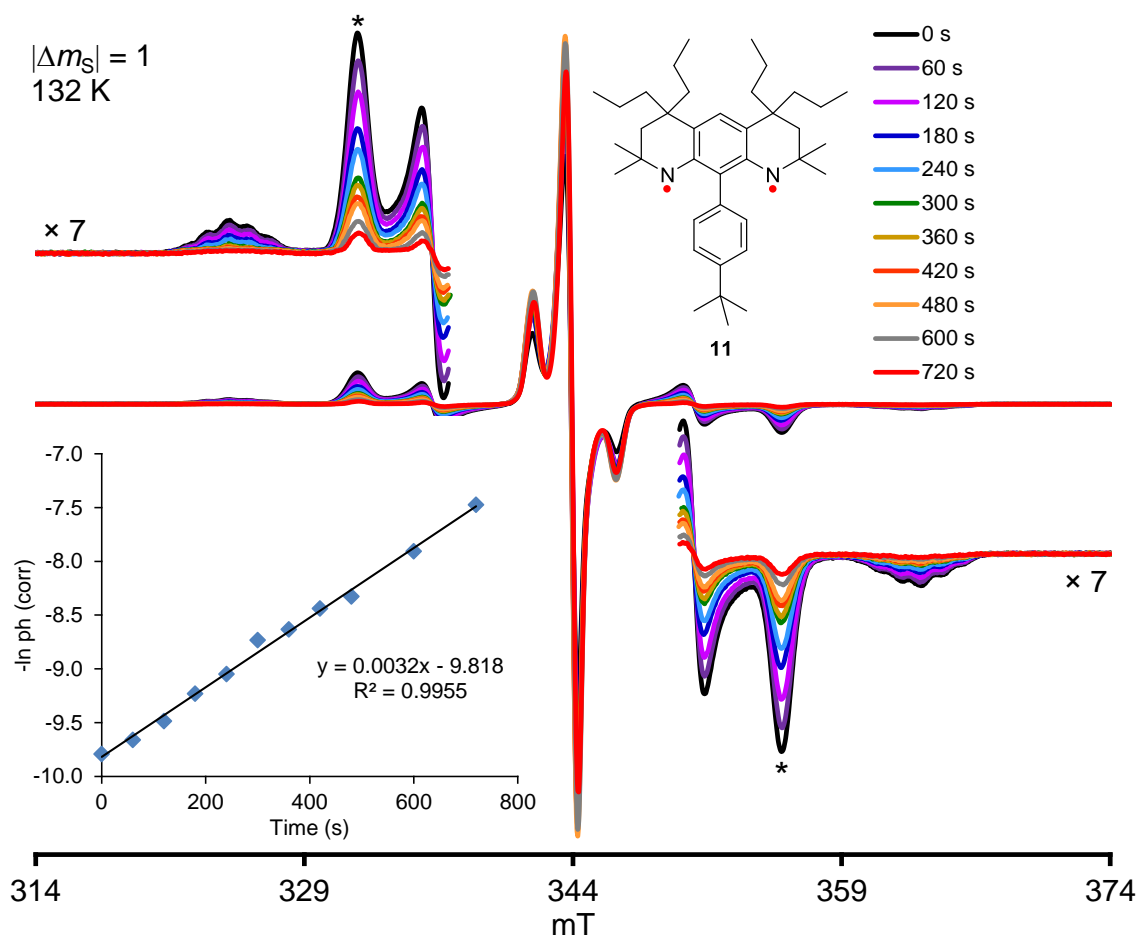


**Figure 1.37.**  Summary of EPR (X-band, $|\Delta m_S|$ = 1, label: AO-9-83) spectra at 132 K for
decay kinetics of **11** (5 mM) in 2-MeTHF at room temperature.  Inset plot: decay kinetics
of **11** in 2-MeTHF at room temperature, with the average of the −ln (measured EPR peak

heights after correction) at ~332 and 356 mT (starred, *). Reproduced from Ref. 83 with permission from American Chemical Society.

The decay kinetics of diradical **9** and **11** in 2-MeTHF at room temperature are summarized in Table 1.**5**. Experiment AO968 showed significantly lower half-life for **11** because the interference of an excess of iodine in the reaction mixture that rapidly quenches the diradical at room temperature.

**Table 1.5**. Summary of decay kinetics of aminyl diradical **9** and **11** in 2-MeTHF at room temperature

| Diradical | Label | $n^a$ | $R^2$ | $k$ (s$^{-1}$) | 95% Confidence limits ($k$) | | $t_{1/2}$ (s)$^b$ |
|---|---|---|---|---|---|---|---|
| | | | | | Lower (s$^{-1}$) | Upper (s$^{-1}$) | |
| **9** | AO953 | 6 | 0.9750 | $(1.11 \pm 0.25) \times 10^{-3}$ | $0.86 \times 10^{-3}$ | $1.36 \times 10^{-3}$ | $624 \pm 139$ |
| **11** | AO936 | 9 | 0.9792 | $(2.81 \pm 0.37) \times 10^{-3}$ | $2.45 \times 10^{-3}$ | $3.18 \times 10^{-3}$ | $246 \pm 32$ |
| | AO983 | 10 | 0.9946 | $(3.26 \pm 0.16) \times 10^{-3}$ | $3.07 \times 10^{-3}$ | $3.40 \times 10^{-3}$ | $214 \pm 13$ |
| | AO968 | 6 | 0.9567 | $(8.67 \pm 2.56) \times 10^{-3}$ | $6.11 \times 10^{-3}$ | $11.2 \times 10^{-3}$ | $80 \pm 24$ |

$^a$ number of data points  $^b$ mean ± 95% confidence interval

The half-life of aminyl radicals **9** and **11** in 2-Me-THF at room temperature are ~ 10 min and 4 min, respectively, which are significantly shorter than that for aminyl radical **4** (half-life ~ 3 h) in 2-MeTHF at room temperature because **4** has greater distribution of spin density and sterically hindered protection.

After annealing diradical **9** and **10** at room temperature with exclusion of light for 3-7 d, the crude mixture of the reaction was transferred to a vial; and the solvents were evaporated under nitrogen flow. The crude mixture was evacuated on high vacuum for overnight. $^1$H NMR spectra and mass spectrometry (ESI-MS) of the crude mixture showed predominantly diamine precursors, **12** and **22** and baseline materials (Figure C6 and C7 in

Appendix C).  The conversion of aminyl diradicals to diamines may primarily undergo via a hydrogen-atom abstraction mechanism because of low C–H bond dissociation energy of solvent such as 2-MeTHF or THF.[40]  This observation was similar to that seen for aminyl diradical **4**.[19]

In contrast to aminyl diradicals **9** and **10**, ^{1}H NMR spectra of the crude mixture, after annealing aminyl diradical **11** at room temperature for 3-4 d, showed two major components: diamine **28** and by-product **43** as illustrated in Figure 1.38.  The plausible mechanism for formation of by-product **43** is shown in Scheme 1.43.

**Scheme 1.43.** Proposed mechanism for by-product **43.** Adapted from Ref. 83 with permission from American Chemical Society.
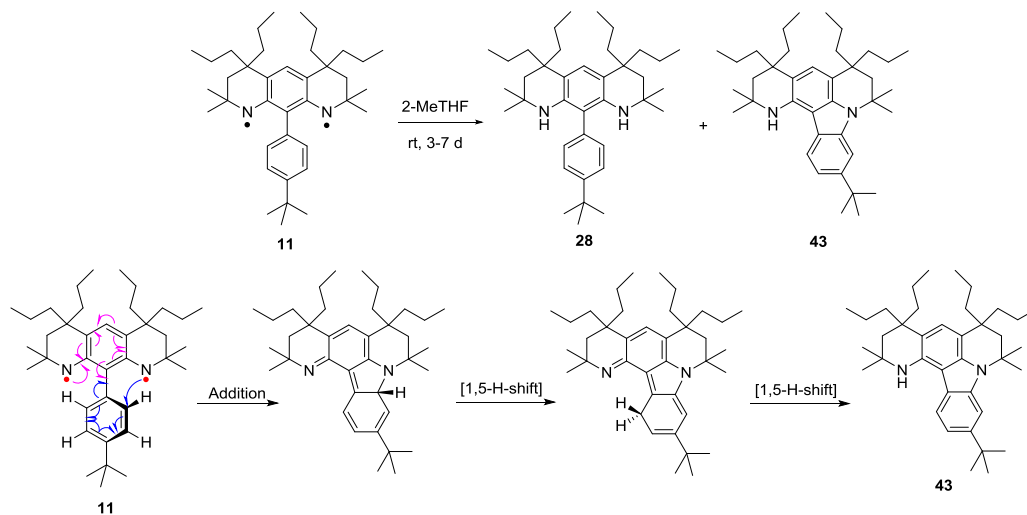


The molar ratio of diamine **28** and by-product **43** was determined by integrated intensity of signals corresponding to diamine **28** and by-product **43** in ^{1}H NMR spectra as shown in Table 1.6.  In typical ^{1}H NMR (500 MHz, acetone-$d_6$) spectra of the crude reaction, doublets at $\delta$ 7.569 ppm (2H), $\delta$ 7.125 ppm (2H) and a singlet at $\delta$ 6.878 ppm (1H) were assigned to diamine **28**; and doublet at $\delta$ 7.988 ppm (1H), singlet at $\delta$ 7.688 ppm (1H), doublet at $\delta$ 7.213 ppm (1H), and singlet at $\delta$ 7.054 ppm (1H) were assigned to by-

product **43** as illustrated in Figure 1.38. The relative integrations of these peaks provided an approximate composition of the crude mixtures. The molar fraction ratios of diamine **28**/by-product **43** in selected experiments are shown in Table 1.6.
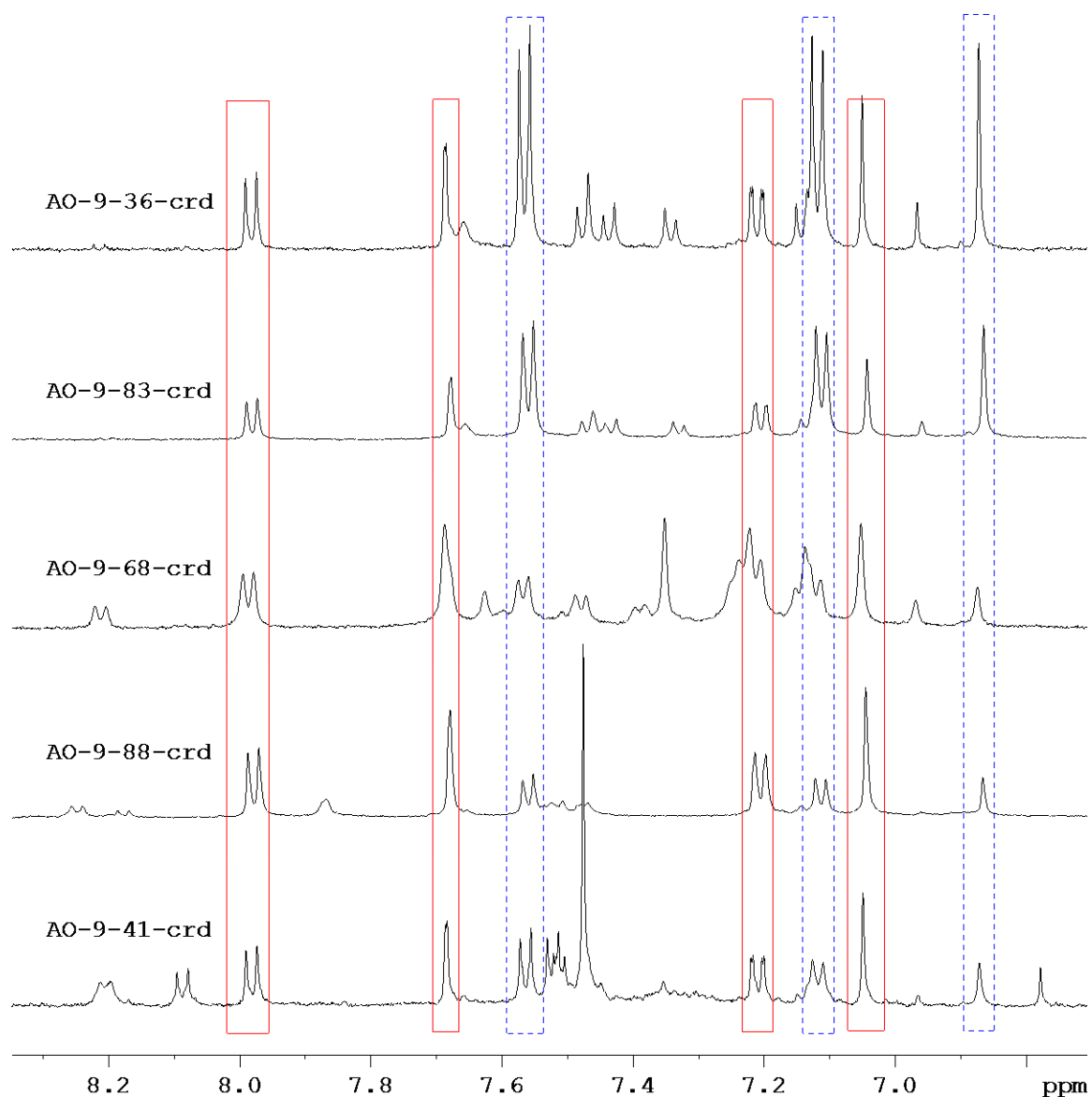


**Figure 1.38.** ^{1}H NMR spectra of crude mixtures after annealing diradical **11** at room temperature for 4-7 d. The mixtures contained by-product **43** (solid line) and diamine **28** (dotted line). Reproduced from Ref. 83 with permission from American Chemical Society.

**Table 1.6.** Integration of diamine **28** and by-product **43** in crude $^1$H NMR spectra

| Run | Label | Conc. (mM) | Diamine **28** | | | avg | By-product **43** | | | | avg | Ratio of **43/28** |
|---|---|---|---|---|---|---|---|---|---|---|---|---|
| | | | 7.569 (d, 2H) | 7.125 (d, 2H) | 6.878 (s, 1H) | | 7.988 (d, 1H) | 7.688 (s, 1H) | 7.213 (d, 1H) | 7.054 (s, 1H) | | |
| 1 | AO936 | 2.84 | 2.08 | 2.19 | 1.00 | 1.05 | 0.67 | 0.73 | 0.79 | 0.69 | 0.72 | 0.69 |
| 2 | AO983 | 5.09 | 2.02 | 2.16 | 1.00 | 1.03 | 0.59 | 0.61 | 0.69 | 0.72 | 0.65 | 0.63 |
| 3 | AO968 | 2.49 | 2.45 | $a$ | 1.00 | 1.11 | 2.52 | $a$ | $a$ | 2.71 | 2.62 | 2.35 |
| 4 | AO988 | 3.08 | 1.84 | 1.92 | 1.00 | 0.96 | 2.70 | 2.67 | $a$ | 2.89 | 2.75 | 2.87 |
| 5 | AO941 | 12.7 | 2.60 | 2.67 | 1.00 | 1.21 | 2.03 | 1.85 | $a$ | 1.85 | 1.91 | 1.58 |

$a$ Integration cannot be determined properly due to overlapping signals

Separation of the crude reaction mixture by preparative TLC yielded fraction 1 ($R_f$ = 0.56, 3% ether/pentane) as isolated by-product **43** and fraction 2 ($R_f$ = 0.33, 3% ether/pentane) as diamine **28**. $^1$H NMR (500 MHz, acetone-$d_6$, label: AO-9-36-fr2, Figure C8 in Appendix C) spectrum and LR ESI-MS: $m/z$ 545.8 (M+H)$^+$ confirmed the structure of diamine **28**. $^1$H NMR (500 MHz, acetone-$d_6$, label: AO-9-36-fr1, Figure C9 in Appendix C) spectrum corresponds to by-product **43**. For structural assignment of by-product **43**, $^1$H and $^{13}$C NMR spectra in chloroform-$d$ using standard 2D NMR spectroscopy, including $^1$H–$^{13}$C HSQC, $^1$H–$^{13}$C HMBC, $^1$H–$^1$H COSY, $^1$H–$^1$H NOESY and $^1$H–$^{15}$N HSQC (Figure B22-B26 in Appendix B) were carried out on a combined sample (experiment AO980, AO983 and AO988). $^1$H NMR (700 MHz, chloroform-$d$, label: AO-9-88-fr1-cb2, Figure 1.39 and A69 in Appendix A) spectrum of combined by-product **43** in chloroform-$d$ showed a doublet at 7.850 ppm ($J$ = 8.4 Hz, 1H$_a$), a doublet at 7.619 ppm ($J$ = 1.4 Hz, 1H$_b$), a doublet of doublet at 7.229 ppm ($J$ = 1.4, 8.4 Hz, 1H$_c$) and a singlet at 6.959 ppm (1H$_d$). A broad singlet peak at $\delta$ = 4.200 ppm (2H$_e$) was assigned to N-**H** resonances. This assignment was confirmed by a cross-peak between $^1$H (the broad peak at $\delta$ = 4.557 ppm; N-**H**) correlated to $^{15}$N (the broad peak at $\delta$ = –287.5 ppm, relative to nitromethane at 0.0

ppm) in $^1$H–$^{15}$N HSQC spectra in acetone-$d_6$ showing N-**H** group (Figure B22 in Appendix B).

Singlets at $\delta = 2.086$ and 1.835 ppm (2H$_f$ and 2H$_f'$) were assigned to CH$_2$ protons. Singlets at $\delta = 1.796$ and 1.348 ppm (6H$_g$ and 6H$_g'$) were assigned to four methyl groups. Multiplets at $\delta = 1.747$-1.658 ppm (4H$_h$ and 4H$_h'$) were assigned to CH$_2$ protons on $n$-propyl groups next to quarternary carbon atoms. Singlet at $\delta = 1.430$ ppm (9H$_i$) was assigned to $t$-Bu group. Multiplets at 1.395-1.115 ppm (4H$_j$ and 4H$_j'$) were assigned to CH$_2$ protons on $n$-propyl groups. Two triplets at $\delta = 0.872$ and 0.848 ppm (6H$_k$ and 6H$_k'$) were assigned to CH$_3$ on $n$-propyl groups.
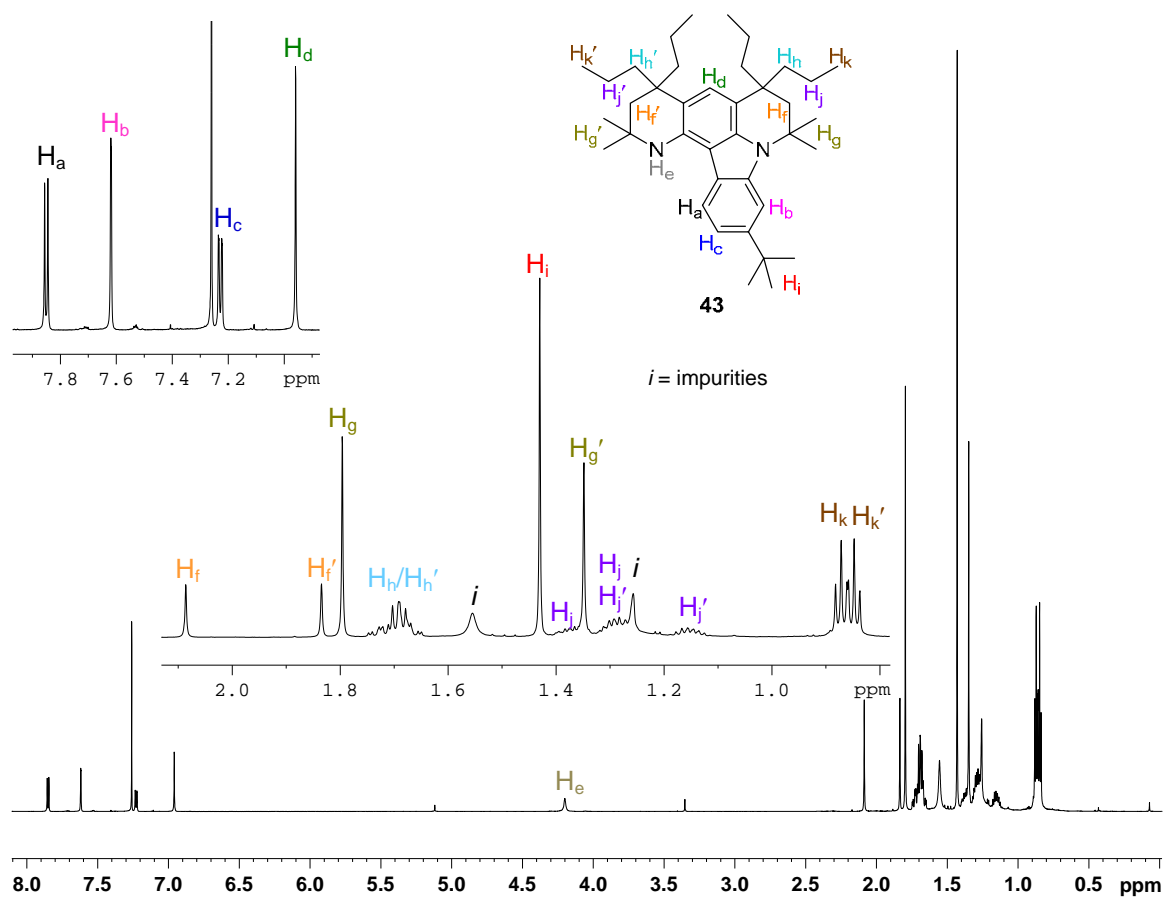


**Figure 1.39.** $^1$H NMR (700 MHz, chloroform-$d$, label: AO-9-88-fr1-cb2) spectrum of by-product **43**.

**Reaction with iodine of aminyl diradical 9 and 11**

The reactivity of aminyls **9** and **11** with an excess of iodine was investigated. The experiment with aminyl **10** was not attempted because of the lack of stability of **10** at room temperature. Aminyl diradicals **9** and **11** in 2-MeTHF were generated as describe in the experimental section. After mixing with an excess iodine, the sample was annealed at −78 °C for 10 min. EPR spectra at 132 K of **9** and **11** showed no significant change. After annealing at −25 °C for 10 min, EPR spectra of **9** showed disappearance of diradical signal. Only monoradical signal was observed (Figure C10 in Appendix C). In contrast, EPR spectra of **11** after annealing at −27 °C for 120 min showed no significant change (Figure C11 in Appendix C).

To sum up, aminyl diradical **9** reacted with an excess of iodine at −27 °C, which also found in previous report for aminyl diradical **4**, whereas aminyl diradical **11** surprisingly proved to be inert toward an excess of iodine at temperature as low as −27 °C. However, a brief warm up to room temperature for ~5 min resulted in immediate disapperance of diradical.

**Reaction with oxygen of aminyl diradical 9 and 11**

The reactivity of aminyl diradicals **9** and **11** with oxygen was investigated. The solution of **9** and **11** in 2-MeTHF was saturated under dry oxygen atmosphere at −108 °C for 15 min. EPR spectra at 132 K of **9** and **11** showed disappearance of diradical signal, though monoradical and unidentified intermediates were observed (Figure C12 in Appendix C). The mixtures of crude reaction were isolated by chromatography presenting corresponding diamines and new diamagnetic products.

For **9**, ^{1}H NMR spectra and mass spectra of the isolated products showed "diol product". Hydroxyl (–OH) groups are indicated by $D_2O$ exchange experiment in benzene-$d_6$ (Figure C13 in Appendix C). After addition of a drop of $D_2O$, ^{1}H NMR spectrum showed a rapid and complete H/D exchange of two singlet peaks at $\delta$ 3.24 and 3.75 ppm (2H) corresponding to the O-**H** groups.

For **11**, ^{1}H NMR (Figure C14 in Appendix C) spectra of the isolated products showed the addition of $O_2$ product to aminyl diradical **11**. This observation was similar to aminyl diradical **4** that new diamagnetic product was observed in place of corresponding nitroxide. In the presence of oxygen, the nitroxide would expected because *N-tert*-butylanilino monoradicals react with oxygen to produce corresponding nitroxides.[75]

The previous report showed that aminyl diradicals **1** and **4** are inert toward oxygen at −108 °C, though **4** reacted with $O_2$ at −78 °C.[18,19] Meanwhile, aminyl diradicals **9** and **11** are sensitive to oxygen at −108 °C as indicating by disappearance of diradical EPR signal. Aminyl diradicals **9** and **11** are more reactive than **1** and **4** may result from the increased spin density at the center ring (*m*-phenylene). On the other hand, the spin density on the centered ring in **1** and **4** is distributed through the cross-conjugated $\pi$-system. The proposed mechanism for aminyl diradical **11**, reacting with oxygen is presented in Figure 1.40.
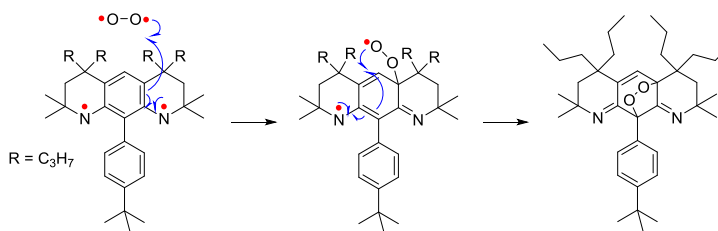


**Figure 1.40.** Proposed mechanism for aminyl diradical **11** reacting with oxygen.

The proposed structures of the products, obtained after the reaction of aminyl diradical **9** and **11** with oxygen as shown in Figure 1.41, are based on the analysis of $^1$H NMR spectra and high resolution mass spectra.

For the reaction of **9** with oxygen, $^1$H NMR (Figure C13 in Appendix C) spectra showed two doublets at ~ 7.6 and 7.3 ppm, which may correspond to aromatic protons on 4-*tert*-butylphenyl group. Singlet at ~5.7 ppm may be assigned to a vinylic proton. An evidence for the O-**H** was obtained from D$_2$O exchange experiment in benzene-$d_6$ (Figure C13D in Appendix C); $^1$H NMR spectrum showed two singlet peaks at 3.24 and 3.75 ppm, assigned to O-**H**, which after addition of a drop of D$_2$O rapidly underwent a complete H/D exchange. HR EI mass spectrum (Figure C13(E) in Appendix C) shows *m/z* 492.3710 [M]$^{+\bullet}$, which is in agreement with the expected molecular ion.

For the reaction of **11** with oxygen, $^1$H NMR (Figure C14(D) in Appendix C spectra) spectrum for the isolated product is inconclusive for assignment which may due to unknown impurities. However, HR ESI mass spectrum (Figure C33-C34 in Appendix C) shows *m/z* 597.4369 [M+Na]$^{+\bullet}$, which may correspond to the expected molecular ion. The product obtained after the reaction of **11** with O$_2$ is analogous to that obtained from the reaction of **4** with O$_2$ at −78 °C.
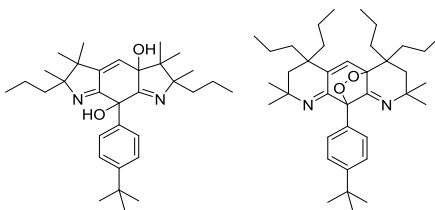


**Figure 1.40.** Proposed structures of the products obtained after reaction of aminyl diradical **9** and **11** with oxygen.

**1.3. Conclusions**

Triplet ground-state aminyl diradicals **9**, **10** and **11**, which were predicted to possess a large $\Delta E_{ST} \approx 10–14$ kcal mol$^{-1}$, were successfully prepared in solution and characterized by EPR spectroscopy. The aminyl diradicals **9** is persistent in 2-MeTHF solution at room temperature with the half-life ~10 min. The aminyl diradical **10** with sterically hindered 2,6-dimethyl-4-*tert*-butylphenyl pendant is not persistent in 2-MeTHF solution even at −30 °C which may due to the weak C-H bonds at benzylic positions on the pendant substituent. The aminyl diradical **11** is persistent in 2-MeTHF solution at room temperature with the half-life ~1-4 min. The shorter half-life at room temperature (vs. **9**) observed in aminyl radical **11** may result from the additional pathway of decay of diradical as suggested by the observation of a significant amount of by-product **43**.

**1.4. Experimental Section**

**General procedures and materials**

For small scale reactions, tetrahydrofuran (THF) and 2-methyltetrahydrofuran (2-MeTHF) were vacuum transferred from sodium/benzophenone directly to the reaction vessel. All vacuum transfers, including those of iodine (99.999%, ultra dry, Alfa), were carried out using liquid nitrogen baths, unless indicated otherwise. *t*-BuLi (pentane) and *n*-BuLi (hexane) were obtained from Aldrich; prior to use, the concentration was determined by titration with *N*-pivaloyl-*o*-toluidine.[76] For large scale reactions, all solvents were freshly distilled, e.g., toluene (from sodium), ether and THF (from sodium benzophenone), or alternatively obtained from solvent purification system. Per-deuterated solvents for NMR spectroscopy were obtained from Cambridge Isotope Laboratories. All

other commercially available chemicals were obtained from either Aldrich or Acros, unless indicated otherwise. Column chromatography (0–20 psig pressure) was carried out on silica gel or silica gel or deactivated silica gel (typically 3% triethylamine in pentane). Analytical and preparative TLC plates (Analtech silica plates, tapered with a preadsorbent zone) were typically deactivated with 3% triethylamine in pentane immediately before use. Standard techniques for synthesis under inert atmosphere, using Schlenk glassware and gloveboxes (Vacuum Atmospheres), were employed.

**NMR spectroscopy**

NMR spectra were obtained with a Bruker spectrometer ($^1$H, 300, 400, 500 and 600 MHz) using chloroform-$d$ (CDCl$_3$), benzene-$d_6$ (C$_6$D$_6$), dimethyl sulfoxide-$d_6$ (DMSO-$d_6$) and acetone-$d_6$ as solvent. The chemical shift references were as follows: ($^1$H) chloroform-$d$, 7.26 ppm; ($^{13}$C) chloroform-$d$, 77.00 ppm (chloroform-$d$), ($^1$H) benzene-$d_5$, 7.15 ppm; ($^{13}$C) benzene-$d_5$, 128.39 ppm (benzene-$d_6$), ($^1$H) dimethyl sulfoxide-$d_5$, 2.50 ppm; ($^{13}$C) dimethyl sulfoxide-$d_5$, 39.50 ppm (dimethyl sulfoxide-$d_6$), ($^1$H) acetone-$d_5$, 2.05 ppm; ($^{13}$C) acetone-$d_5$, 29.92 ppm (acetone-$d_6$). Typical 1D FID was subjected to exponential multiplication with a line broadening exponent (LB) of 0.3 Hz (for $^1$H) and 1.0 – 2.0 Hz (for $^{13}$C). For selected spectra, smaller (or negative) values of LB and additional Gaussian multiplication (GB) were used, to resolve closely spaced resonances, as indicated in the spectral data summaries. IR spectra were obtained using a Nicolet Avatar 360 FT-IR instrument, equipped with an ATR sampling accessory (Spectra Tech, Inc.). A few drops of the compound in CH$_2$Cl$_2$ were applied to the surface of a ZnSe ATR plate horizontal parallelogram (45°, Wilmad). After the solvent evaporated, the spectrum was acquired (2-cm$^{-1}$ resolution).

**Mass spectrometry**

FAB MS analyses were carried out in 3-nitrobenzyl alcohol (3-NBA) or glycerol matrices at the Nebraska Center for Mass Spectrometry.  EI and ESI MS analyses were carried out at the Nebraska Center for Mass Spectrometry.

**Electrochemistry**

Voltammetry data for diamines **12**, **22**, and **28** were obtained in a glovebag under argon gas atmosphere. (The supply gas was a commercial ultra-high purity argon, certified to contain < 1 ppm of $O_2$ and < 1 ppm of $H_2O$.) The home-made electrochemical cell, all solid reagents, syringes, needles, etc. were extensively evacuated in Schlenk vessels (typical pressure ≤ 1 mTorr, temperature 20–70 °C), prior to the transfer to the glovebag. Dichloromethane ($CH_2Cl_2$) was obtained from commercial solvent purification system, then distilled from calcium hydride under nitrogen, and stored in the absence of light in a Schlenk vessel on a vacuum line; just prior to the use, the solvent was vacuum transferred as needed. Commercial potentiostat/galvanostat was used.  About 1 mg of diamines **12**, **22** and **28** was dissolved in the supporting electrolyte solution (2.4 mL), 0.1 M tetrabutylammonium hexafluorophosphate ($n$-$Bu_4NPF_6$) in anhydrous DCM, and then transferred to a custom-made cell equipped with quasi-reference (Ag wire), counter (Pt foil), and working (100 μm Pt-disk) electrodes.  The concentrations of an elcetroactive solute for **12**, **22** and **28** were 1.1, 1.0 and 0.9 mM, respectively.  A small amount (10-25 drops) of solution of decamethylferrocene (ca. 0.7 mg of $Cp*_2Fe$) in the supporting electrolyte (ca. 0.8 mL) was added to the cell.  The redox potentials were referenced to SCE using an internal decamethylferrocene (–0.130 V vs SCE for $Cp*_2Fe/Cp*_2Fe^+$ in $CH_2Cl_2$).[73,77]  For each compound, plots of peak current vs square root of scan rate (50–500

or 20–500 mV/s) in cyclic voltammetry were linear. Diamines **12**, **22**, and **28** were examined by square wave voltammetry (frequency 10 Hz, pulse height 25 mV).

**Generation of aminyl diradicals 9, 10 and 11 for EPR measurement**

Diamines **12**, **22** and **28** (0.70 – 1.32 mg, 1.28 – 2.42 μmol) were placed in a custom made Schlenk-EPR-tube (5-mm OD) and then they were placed under high vacuum ($10^{-4}$ mTorr). The whole EPR sample tube was wrapped by heating tape and heated at 70 °C for overnight. The next day, the heating tape was raised up above the sample and heated the remaining part of EPR tube at 110 – 120 °C for overnight. THF (~0.1 mL, ~10-mm height) was added to the vessel by vacuum transfer, and then the solution was stirred for 30 min at –30 °C. *n*-BuLi (0.14 – 0.26 M in hexane, 12 – 27 μL, 3.08 – 5.81 μmol, 2.1 – 2.4 equiv) was added to produce corresponding dianion. After stirring at –30 °C for 3 – 5 h, the orange reaction mixture was evaporated at –45 °C then immersed in liquid nitrogen. 2-MeTHF (~0.1 mL) was added to the reaction mixture by vacuum transfer, and then the reaction mixture (under vacuum) was immersed in liquid nitrogen. Subsequently, iodine was vacuum transferred to the sample tube wall, just above the reaction mixture. Iodine was mixed into the reaction mixture at –115 °C, and then the solution was stirred at –115 °C for 1 h. The resultant green solution was stored in liquid nitrogen; EPR spectra were obtained at 132 K.

**Generation of aminyl diradicals 9 for SQUID measurement**

Diamine **12** (0.57 – 0.74 mg, 1.24 – 1.60 μmol) was placed in the custom-made SQUID sample tube (5-mm O.D. EPR quartz tube with a thin bottom ~6 cm from the end of the tube); and then it was placed under high vacuum ($10^{-4}$ mTorr). The whole EPR sample tube was wrapped by heating tape and heated at 70 °C for overnight. The next day,

the heating tape was raised up above the sample and heated the remaining part of EPR tube at 150 °C for 2 d. THF (~0.1 mL, ~8-mm height) was added to the vessel by vacuum transfer, and then stirred for 30 min at −30 °C. *n*-BuLi (0.192 − 0.231 M in hexane, 12 − 17 µL, 2.59 − 3.85 µmol, 2.1 − 2.4 equiv) was added to produce initially the orange homogeneous solution. After stirring at −30 °C for 1 h, the deep red reaction mixture was concentrated at −30 °C until the volume decreased to about 0.025 mL (~2-mm height). THF (~0.1 mL) was added to the concentrated reaction mixture by vacuum transfer, and then the reaction mixture was stirred for 5 min at −30 °C. This sequence of solvent removal under vacuum, followed by addition of THF by vacuum transfer was repeated another two times (total of three times). Finally, 2-MeTHF (~0.06 − 0.08 mL) was added to the reaction mixture by vacuum transfer, and then the reaction mixture (under vacuum) was immersed in liquid nitrogen. Subsequently, iodine was vacuum transferred (for 10 − 20 s) to the sample tube wall, just above the reaction mixture. Iodine was mixed into the reaction mixture at −115 °C, and then the dark red solution was stirred at −115 °C for 1 h. The resultant dark red solution was stored in liquid nitrogen; EPR spectra were obtained at 132 K. After recording the EPR spectra, the sample tube was re-attached to vacuum line, and the sample tube was flame sealed. Subsequently, the sample tube, which was kept in liquid nitrogen, was transferred to a helium filled glove bag, and then rapidly inserted (<15 s) into the sample chamber of SQUID magnetometer at 10 K.

**EPR spectroscopy**

CW X-band EPR spectra for aminyl diradicals **9**, **10** and **11** in 2-MeTHF were acquired on Bruker EMX instrument, equipped with a frequency counter and nitrogen flow temperature control (130–300 K). The samples, which were contained 5-mm EPR sample

tubes, or in SQUID sample tubes (see: next paragraph), were inserted into the pre-cooled cavity at 132–133 K. The spectra were obtained using either a conventional perpendicular mode cavity or a dual mode cavity, with an oscillating magnetic field either perpendicular ($TE_{102}$) or parallel ($TE_{012}$) to the swept magnetic field. Most of the spectra were obtained in perpendicular mode. DPPH powder ($g = 2.0037$) was used as a $g$-value reference.

**SQUID magnetometry.**

Quantum Design (San Diego, CA) MPMS5S (with continuous temperature control) was used. All solution samples were contained in home-made 5-mm O.D. EPR quality quartz tubes, modified to possess a thin bottom, which is about 6 cm from the end of the tube (referred to as "SQUID tubes").[78,79] All SQUID tubes were flame-sealed.

The SQUID tubes, kept in liquid nitrogen, were rapidly inserted (<15 s) to the magnetometer at low temperature (typically 10 K) under a helium atmosphere, and then evacuated and purged with helium in the sample chamber at 90 K. Following the sequence of magnetic measurements, the samples were rapidly withdrawn from the sample chamber of the magnetometer; e.g., without melting the THF matrix. Following the EPR studies at low temperatures, the samples were carefully reinserted into the magnetometer at low temperature, as described above, and subjected to another sequence of measurements. Selected samples were annealed in the SQUID sample chamber at specified temperatures, and then subjected to another sequence of measurements. For samples in THF, correction for diamagnetism was carried out by extrapolation of the $\chi$ versus $1/T$ plots in the 70–140 range; for samples in 2-MeTHF, typical temperature range used for the correction for diamagnetism was 40–100 K.

Adequate measurements of samples in 2-MeTHF can be very time consuming, due to the matrix effects. The magnetization measurements at 1.8 K (or 2 K), 3 K, and 5 K, required slow annealing to the final temperature, followed by annealing at the final temperature for up to 3 h. For variable temperature measurements, progressively longer time delays were used at lower temperatures; for example, delays of 20+ min were used at each temperature below 25 K. Such precautions were usually sufficient to anneal measurements in the cooling mode.

**Spectral simulations and numerical curve fitting**

The WINEPR SimFonia program (Version 1.25, Bruker) was used for spectral simulations of aminyl diradicals **9**, **10** and **11** in rigid matrices.

The SigmaPlot for Windows software package was used for numerical curve fitting of the magnetic data. The reliability of a fit is measured by the parameter dependence, which is defined as follows: *dependence = 1 − ((variance of the parameter, other parameters constant)/(variance of the parameter, other parameters changing))*. Values close to 1 indicate an overparametrized fit.

*M* versus *H* data at low temperatures ($T = 1.8, 3, 5$ K) were analyzed with Brillouin functions (with mean-field parameters) as described in the text. Values of parameter dependence were 0.47–0.64, 0.81–0.88, and 0.97–0.98 at 1.8, 3, and 5 K, respectively.

The values $S$ obtained from the numerical fits to the Brillouin functions were also used to estimate half-life ($\tau_{1/2}$) for diradical **9** in THF. For a mixture of $S = 1$ diradical and $S = \frac{1}{2}$ monoradical, such values of $S$ correspond to spin-average spin ($S_s$),[80] described by eq. 3. Because the values of $S_s$, derived from the curvature of the magnetization plot, are

independent of mass balance, the molar factions of $S = 1$ diradical ($x_D$) are readily obtained using eq. 3.

$$S_s = [(1 - x_D)(0.5)^2 + x_D(1.0)^2]/[(1 - x_D)(0.5) + x_D(1.0)] \qquad \text{(eq. 3)}$$

Applying standard first order kinetics to the decay of $x_D$ (with formation of the monoradical) and assuming that the monoradical does not decay on the time scale of the experiment, an order of magnitude estimates for $\tau_{1/2}$ for diradical **9** in THF were carried out. For example, $\tau_{1/2}$ of the order of 10 min at 295 K was estimated.

Similar $\tau_{1/2}$ of the order of 10 min for diradical **9** in 2-MeTHF at room temperature was obtained based upon EPR spectra in Figure C1 in Appendix C, by applying standard first order kinetics to the decay of $x_D$ and assuming that the monoradical does not decay on the time scale of the experiment. In order to obtain values of $x_D$ for each spectrum, the spectra, as well as spectral simulation for diradical **9**, were double integrated in three sections 310-325 mT, 325-350 mT, and 350-365 mT; it was assumed that only diradical contributes to the EPR intensity in the 310-325 mT and 350-365 mT sections, while both diradical and monoradical contribute in the 325-350 mT section. Using $S(S+1)$ factors to correct the contributions of $S = \frac{1}{2}$ monoradical and $S = 1$ diradical to the EPR double integrated intensity, the values of $x_D$ for $S = 1$ diradical in the diradical/monoradical mixtures were estimated for each sample in Figure C1 in Appendix C.

**1.4.1. Syntheses of compounds 14, 14a, 15, 15a, 16, 16a, 13, 12 and aminyl diradical 9.**

**2,3,3,5,5,6-hexamethyl-3,5-dihydropyrrolo[3,2-*f*]indole 14.**
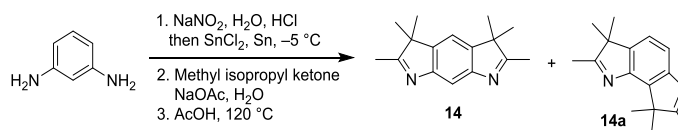


**Summary for step 1**

| Run | *m*-Phenylenediamine (g/mmol) | NaNO$_2$ (g/mmol) | SnCl$_2$ (g) |
|---|---|---|---|
| AO-1-80 | 2.17/20.1 | 2.89/41.9 | 17.5 |
| AO-1-85 | 8.65/80.0 | 11.52/167 | 70 |
| AO-2-55 | 4.33/40.0 | 5.76/83.5 | 35 |
| AO-2-58 | 4.32/40.0 | 5.76/83.5 | 35 |
| AO-2-59 | 8.66/80.0 | 11.5/167 | 70 |
| AO-5-05 | 17.3/160 | 23.2/336 | 140 |

**Summary for steps 2 and 3**

| Run | *m*-Phenylene dihydrazine salts (g/mol) | Methyl isopropyl ketone (mL/mmol) | NaOAc (g/mmol) | Yield of **14a** (g/%) for steps 1 – 3 | Label of **14a** | Yield of **14** (g/%) for steps 1 – 3 | Label of **14** |
|---|---|---|---|---|---|---|---|
| AO-1-83 | 2.15/4.79 | 1.28/11.9 | 3.26/24.0 | 0.385/8 | AO-1-83-spot1 | 0.169/3 | AO-1-83-spot2 |
| AO-1-93 | 4.00/8.92 | 2.39/22.3 | 6.07/44.6 | 0.436/2 | AO-1-93-up | 0.251/1 | AO-1-93-dw |
| AO-2-56 | NA/0.04 | 10.7/0.1 | 27.2/0.2 | 2.65/7 | AO-2-61-up | 1.47/4 | AO-2-61-dw |
| AO-2-60 | NA/0.04 | 10.7/0.1 | 27.2/0.2 | | | | |
| AO-2-61 | NA/0.08 | 21.4/0.2 | 54.4/0.4 | | | | |
| AO-5-06 | NA/0.16 | 42.9/0.4 | 108.9/0.8 | 5.86/15 | AO-5-06-up | 2.42/6 | AO-5-06-dw |

*Step 1*. Our procedure follows previous reports on preparation of HCl salt of *m*-phenylenedihydrazine *via* azotization of *m*-phenylenediamine, and then reduction of the resultant bis-diazonium salt.[32,33] HCl (conc., 78 mL) was added to a solution of *m*-phenylenediamine (MW = 108.1, 2.17 g, 0.02 mmol) in water (22 mL). The reaction mixture was stirred at −5 °C. A solution of NaNO$_2$ (MW = 69, 2.89 g, 0.04 mol) in water (20 mL) was added to the reaction mixture dropwise. The reaction was stirred at −5 °C for 45 min. A solution of SnCl$_2$ (17.5 g) and Sn (0.1 g) in HCl (conc., 40 mL) was heated until Sn was dissolved. The diazonium salt mixture was added to tin solution at −5 °C. HCl

(conc., 45 mL) was added and then stirred at −5 °C for 1 h. The solid was filtered off and washed with cold mixture of conc. HCl (25 mL) and water (10 mL) followed with ethanol and diethyl ether. The light pink solid (AO-1-80) was dried over CaO in a dessicator for 24 h, to yield salt of *m*-phenylenedihydrazine.

*Steps 2 and 3.* Our modified procedure for steps 2 and 3 is based upon the method of Mikhailenko, and Boguslavskaya.[81] The solid from step 1 was dissolved in water (300 mL), and then methyl isopropyl ketone (MW = 86.1, 42.85 mL, 0.4 mol) and NaOAc (MW = 136.1, 108.860 g, 0.8 mol) were added to the solution. The reaction was stirred for 5 min and then extracted with chloroform (3 × 150 mL). The organic phase was dried over anhydrous $Na_2SO_4$ and concentrated *in vacuo*. AcOH (50 mL) was added to the crude mixture. The reaction mixture was heated carefully until it began to boil for 15 min. AcOH was removed and the reaction was neutralized with $NH_4OH$. The reaction was extracted with chloroform (3 × 100 mL), dried over anhydrous $Na_2SO_4$ and evaporated *in vacuo*. The crude product was purified by column chromatography (silica gel, 80% EA:Hexane) to give the target product **14** (2.42 g, 6%, AO-5-06) as a brown solid. A small sample for melting point was recrystallized from heptane, to provide a light yellow solid: m.p. 140–145 °C (AO-5-06-recrys, lit. 149 °C (heptane)[81]), ^{1}H NMR (400 MHz, chloroform-*d*, AO-1-93-dw): $\delta$ = 7.671 (s, 1H), 7.127 (s, 1H), 2.251 (s, 6H), 1.289 (s, 12H). ^{13}C NMR (100 MHz, chloroform-*d*, AO-1-93-dw): $\delta$ = 187.85, 153.41, 143.04, 113.94, 111.78, 53.08, 23.33, 15.41. IR (ZnSe, $cm^{-1}$, AO-5-06-recrys): 2964, 2926, 2865, 1573, 1462, 1449, 1428, 1378, 1362, 1276, 1238, 1140, 1120. LR-FABMS (3-NBA matrix, AO-1-93-dw): *m/z* ion type (%RA for *m/z* = 200-1000): 241 $[M+H]^+$ (100%). HR-FABMS (3-NBA, AO-1-93-dw): *m/z* ion type (%RA for *m/z* = 239-243): 239.1545 $[M–H]^+$ (4%, 1.3 ppm for

$^{12}C_{16}{}^{1}H_{19}{}^{14}N_2$), 240.1615 [M]$^+$ (27%, 4.7 ppm for $^{12}C_{16}{}^{1}H_{20}{}^{14}N_2$), 241.1699 [M+H]$^+$ (100%, 2.3 ppm for $^{12}C_{16}{}^{1}H_{21}{}^{14}N_2$), 242.1736 [M+H+1]$^+$ (17%, 0.8 ppm for $^{12}C_{15}{}^{13}C_1{}^{1}H_{21}{}^{14}N_2$). Another isomer **14a** (5.86 g, 15%, AO-5-06-1) was also obtained after column chromatography as a brown solid. A small sample for melting point was recrystallized from heptane, to provide a light yellow solid: m.p. 130–135 °C (AO-5-06-recrys2, lit.[81] 135 °C (hexane)), $^{1}$H NMR (400 MHz, chloroform-*d*, AO-1-93-up): $\delta$ = 7.344, 7.166 (ABq, $J_{AB}$ = 7.6 Hz, 2H), 2.288 (s, 3H), 2.266 (s, 3H), 1.510 (s, 6H), 1.286 (s, 6H). $^{13}$C NMR (100 MHz, chloroform-*d*, AO-1-93-up): $\delta$ = 189.02, 187.66, 154.14, 148.55, 143.05, 135.52, 119.87, 116.06, 54.01, 52.60, 23.49, 22.31, 15.59 15.09. IR (ZnSe, cm$^{-1}$, AO-1-93-up): 2962, 1581, 1465, 1429, 1360, 1274, 1193. LR-FABMS (3-NBA matrix, AO-1-75-fr2): *m/z* ion type (%RA for *m/z* = 200-1500): 241 [M+H]$^+$ (100%). HR-FABMS (3-NBA, AO-1-75-fr2): *m/z* ion type (%RA for *m/z* = 239-243): 241.1709 [M+H]$^+$ (100%, −1.8 ppm for $^{12}C_{16}{}^{1}H_{21}{}^{14}N_2$)

**Diallyldiamine 15.**
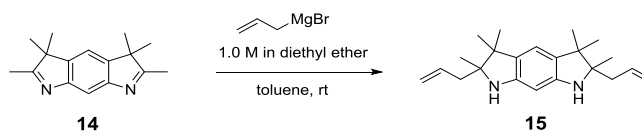


| Run | SM (g/mmol) | AllylMgBr (1.0 M in diethyl ether) (mL/mmol) | Yield (g/%) | TM Label |
|---|---|---|---|---|
| AO-2-10 | 0.231/0.964 | 3.9/3.86 | 0.191/61 | AO-2-10-flt1 |
| AO-2-64 | 1.61/6.70 | 26.8/26.8 | 1.17/54 | AO-2-64-col |
| AO-5-04 | 2.04/8.56 | 34.2/34.2 | 1.45/52 | AO-5-04-fr1/2 |

A solution of allylmagnesium bromide in diethyl ether (3.9 mL, 1.0 M, 3.85 mmol) was added dropwise to a solution of **14** (AO-1-93-dw, MW = 240.3, 0.23 g, 0.96 mmol) in anhydrous toluene (12 mL). The reaction mixture was stirred at room temperature for 12 h and then hydrolyzed with a saturated aqueous ammonium chloride solution (15 mL) and extracted with dichloromethane (3 × 50 mL). The solvent was removed and the brown

residue was purified by filtering through a plug of deactivated silica gel (30% EA:Hexane) to give the target diallyldiamine **15** (191 mg, 61%, label: AO-2-10) as a brown oil. $^1$H NMR (400 MHz, chloroform-*d*, AO-2-10-flt1): $\delta$ = 6.598 (s, 1H), 5.929-5.816 (m, 3H), 5.146-4.926 (m, 4H), 3.472 (br, 2H), 2.317-2.063 (m, 4H), 1.134-1.070 (m, 18H). $^{13}$C NMR (100 MHz, chloroform-*d*, LB = –0.2 Hz, GB = 0.5 Hz, AO-2-10-flt1): aromatic region, expected 12 resonances, found 12 resonances for 2 diastereomers at $\delta$ = 147.34, 147.33, 138.91, 135.17, 135.14, 129.22, 118.75, 118.65, 115.99, 114.35, 92.88, 92.86; aliphatic region expected 12 resonances, found 12 resonances at $\delta$ = 67.86, 67.82, 45.97, 45.96, 40.07, 40.00, 24.61, 24.39, 22.85, 22.65, 20.36, 20.19. $^1$H NMR (400 MHz, acetone-*d*$_6$, AO-2-64-col): $\delta$ = 6.640 (s, 1H), 6.001-5.896 (m, 2H), 5.853 (s, 1H), 5.078-4.971 (m, 4H), 4.242 (br, 2H), 2.329-2.140 (m, 4H), 1.100 (s, 12H), 1.058 (s, 6H). $^{13}$C NMR (100 MHz, acetone-*d*$_6$, LB = –0.2 Hz, GB = 0.5 Hz, AO-2-64-col): aromatic region, expected 12 resonances, found 11 resonances for 2 diastereomers at $\delta$ = 149.06, 149.05, 136.53, 128.63, 128.62, 118.05, 118.04, 116.16, 116.15, 92.90, 92.88; aliphatic region expected 12 resonances, found 10 resonances at $\delta$ = 68.46, 46.49, 41.18, 41.17, 24.18, 24.16, 23.66, 23.66, 20.84, 20.81. IR (ZnSe, cm$^{-1}$, AO-2-10-flt1): 3359, 3072, 2957, 2931, 2868, 1613, 1484, 1457, 1444, 1382, 1359, 1315, 1300, 1149, 1110, 1000, 913, 880, 825, 811. LR-FABMS (Glycerol matrix, AO-2-10-filter2): *m/z* ion type (%RA for *m/z* = 300-1500). HR-FABMS (Glycerol matrix, AO-2-10-filter2): *m/z* ion type (%RA for *m/z* = 322-328): 325.2638 [M+H]$^+$ (67%, 1.7 ppm for $^{12}$C$_{22}$$^1$H$_{33}$$^{14}$N$_2$).

**Diallyldiamine 15a.**
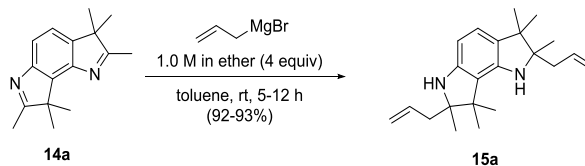


| Run | SM (mg/mmol) | AllylMgBr (1.0 M in diethyl ether) (mL/mmol) | Yield (mg/%) | TM Label |
|---|---|---|---|---|
| AO-1-89 | 40.0/0.166 | 0.67/0.67 | 50.3/93 | AO-1-89 |
| AO-1-100 | 250/1.04 | 4.16/4.16 | 308/92 | AO-1-100-flt1 |

A solution of allylmagnesium bromide in diethyl ether (4.2 mL, 1.0 M, 4.16 mmol) was added dropwise to a solution of **14a** (AO-1-83, MW = 240.3, 250 mg, 1.04 mmol) in anhydrous toluene (6 mL).  The reaction mixture was stirred at room temperature for 12 h and then hydrolyzed with a saturated aqueous ammonium chloride solution (10 mL) and extracted with dichloromethane (3 × 50 mL).  The solvent was removed in vacuo and the brown residue was purified by filtering through a plug of deactivated silica gel (10% EtOAc:Hexane) to give the target diallyldiamine **15a** (308 mg, 92%, label: AO-1-100-filter1) as a brown oil.  $^1$H NMR (400 MHz, chloroform-$d$, AO-1-100-flt1): $\delta$ = 6.655-6.619 (m, 1H), 6.015-5.979 (m, 1H), 5.927-5.775 (m, 2H), 5.170-4.931 (m, 4H), 3.534 (br, 2H), 2.337-2.050 (m, 4H), 1.415-1.082 (m, 18H).  $^{13}$C NMR (100 MHz, chloroform-$d$, AO-1-100-flt1): $\delta$ = 148.26, 148.04, 144.11, 143.87, 138.86, 134.95, 131.03, 130.95, 120.30, 120.16, 119.13, 114.39, 99.95, 99.82, 68.05, 67.79, 46.15, 46.03, 45.08, 40.34, 39.57, 35.20, 33.78, 29.69, 25.49, 24.20.  HR-FABMS (Glycerol matrix, AO-1-100-filter1): $m/z$ ion type (%RA for $m/z$ = 322-328): 325.2641 [M+H]$^+$ (100%, 0.9 ppm for $^{12}C_{22}{}^1H_{33}{}^{14}N_2$).

**Dipropyldiamine 16.**
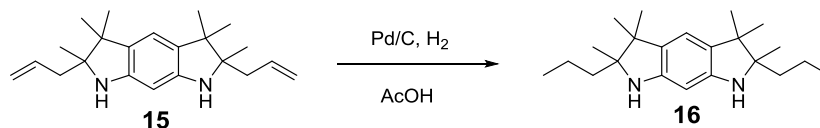


| Run | SM (g/mmol) | Pd/C (g/mmol) | Yield (g/%) | TM Label |
|-----|-------------|---------------|-------------|----------|
| AO-2-22 | 0.132/0.406 | 0.0431/0.0406 | 0.0976/73 | AO-2-22-fr2-hivac |
| AO-2-66 | 0.706/2.18 | 0.231/0.218 | 0.374/52 | AO-2-66-col |
| AO-3-14 | 0.488/1.50 | 0.160/0.150 | 0.177/36 | AO-3-14-pure |
| AO-5-09 | 1.45/4.47 | 0.476/0.447 | 0.220/69 | AO-5-09-fr1/2 |

Pd/C (MW = 106.4, 0.04 g, 0.04 mmol) was added to a solution of **15** (AO-2-10-flt1, MW = 324.5, 0.13 g, 0.40 mmol) in acetic acid (1.5 mL). The reaction was evacuated and then charged with hydrogen gas. The reaction was stirred under hydrogen atmosphere for 24 h then filtered through a plug of deactivated silica gel (40% diethyl ether:pentane) to give the product **16** (97.6 mg, 73%, label: AO-2-22) as a brown oil. $^1$H NMR (400 MHz, acetone-$d_6$, AO-2-22-fr2): $\delta$ = 6.604 (s, 1H), 5.805 (s, 1H), 4.154 (br, 2H), 1.600-1.300 (m, 8H), 1.130/1.127 (s, 6H), 1.052/1.048 (s, 12H), 0.917 (t, $J$ = 7.0 Hz, 6H). $^{13}$C NMR (100 MHz, acetone-$d_6$, LB = –0.2 Hz, GB = 0.5 Hz, AO-2-22-fr2): aromatic region, expected 8 resonances, found 5 resonances for 2 diastereomers at $\delta$ = 149.36, 149.35, 128.69, 116.12, 92.84; aliphatic region expected 16 resonances, found 13 resonances at $\delta$ = 68.93, 68.91, 46.62, 46.61, 39.45, 39.43, 24.82, 24.81, 23.61, 23.59, 21.29, 18.71, 15.70. IR (ZnSe, cm$^{-1}$, AO-2-22-fr2): 3345, 2957, 2933, 2871, 1616, 1485, 1465, 1382, 1367, 1306, 1152, 1125. LR-FABMS (3-NBA matrix, AO-2-22-fr2): $m/z$ ion type (%RA for $m/z$ = 300-1500): 328 [M]$^+$ (100%). HR-FABMS (3-NBA matrix, AO-2-22-fr2): $m/z$ ion type (%RA for $m/z$ = 326-331): 328.2885 [M]$^+$ (100%, –2.0 ppm for $^{12}C_{22}{}^{1}H_{36}{}^{14}N_2$), 329.2941 [M+H]$^+$ (76%, 4.7 ppm for $^{12}C_{22}{}^{1}H_{37}{}^{14}N_2$).

**Dipropyldiamine 16a.**
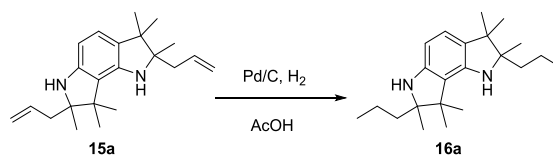


| Run | SM (g/mmol) | Pd/C (g/mmol) | Yield (g/%) | TM Label |
|---|---|---|---|---|
| AO-2-21 | 0.214/0.659 | 0.0701/0.0659 | 0.1976/79 | AO-2-21-fr6 |

Pd/C (MW = 106.4, 0.07 g, 0.07 mmol) was added to a solution of **15a** (AO-1-100-flt1, MW = 324.5, 0.214 g, 0.659 mmol) in acetic acid (1.5 mL). The reaction was evacuated and then charged with hydrogen gas. The reaction was stirred under hydrogen atmosphere for 24 h then filtered through a plug of deactivated silica gel (40% diethyl ether:pentane) to give the product **16a** (0.198 mg, 79%, label: AO-2-21-fr6) as a brown oil.

$^1$H NMR (400 MHz, acetone-$d_6$, AO-2-21-fr6): $\delta$ = 6.529, 5.866 (ABq, $J_{AB}$ = 7.6 Hz, 2H), 4.207/3.995 (br, 2H), 1.600-1.365 (m, 8H), 1.258-1.059 (m, 18H), 0.941-0.880 (m, 6H).

$^{13}$C NMR (100 MHz, acetone-$d_6$, AO-2-21-fr6): $\delta$ = 149.89, 149.05, 130.94, 120.64, 118.44, 100.01, 99.96, 69.13, 68.25, 66.07, 46.71, 45.61, 39.51, 38.86, 38.81, 24.36, 24.24, 24.10, 23.97, 22.51, 22.32, 22.09, 22.00, 20.92, 18.57, 15.58.

**Bromodiamine 13.**
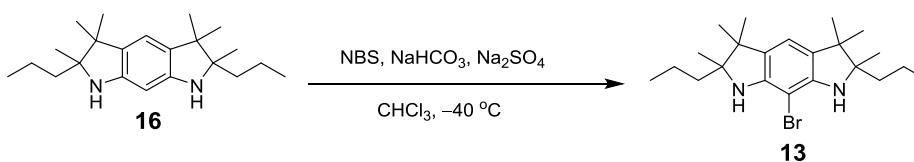


| Run | SM (mg/μmol) | NBS (mg/μmol) | Yield (mg/%) | TM Label |
|---|---|---|---|---|
| AO-2-36 | 6.4/19.5 | 3.9/21.4 | N/A | AO-2-36-flt2fr2UV |
| AO-2-42 | 11.3/34.4 | 6.7/37.8 | 5.0/36 | AO-2-42-flt |
| AO-2-50 | 39.9/121 | 23.8/133 | 15.9/32 | AO-2-50-col |
| AO-3-15 | 64.3/196 | 38.3/215 | 48.9/61 | AO-3-15-flt |
| AO-4-42 | 100.0/304 | 59.6/335 | 69.9/56 | AO-4-42-col |
| AO-4-54[a] | 10.2/31.1 | 6.1/34.2 | 6.2/47 | AO-4-54-flt |
| AO-4-96[b] | 19.3/58.7 | N/A | - | - |
| AO-9-19 | 199.3/607 | 118.8/667 | 138.2/56 | AO-9-19-flt |
| AO-9-54 | 113.5/345 | 67.6/380 | 94.8/60 | AO-9-54-flt |

[a] 0.1 equiv of trifluoroacetic acid was used instead of $NaHCO_3$ and anhydrous $Na_2SO_4$.

[b] Addition of a solution of $Br_2$ in dichloromethane (from solvent purification system) to tetrabutylammonium bromide (TBABr) and diamine **16** in dichloromethane at –44 °C did not produce the corresponding product.

A solution of NBS (MW = 178.0, 38.3 mg, 0.22 mmol) in chloroform (3 mL) was added dropwise to diamine **16** (AO-3-14, MW = 328.5, 64.3 mg, 0.20 mmol) with $NaHCO_3$ (MW = 84.6, 0.20 g, 2.35 mmol) and anhydrous $Na_2SO_4$ (MW = 142, 0.33 g, 2.35 mmol) in chloroform (15 mL) at –40 °C under $N_2$ atmosphere. After stirring at –40 °C for 1 h, excess of $Na_2S_2O_5$ was added and the reaction mixture was allowed to attain room temperature. After the solids were filtered off, the filtrate was concentrated in vacuo and the resultant dark brown oil was purified by column chromatography (deactivated silica gel, diethyl ether/pentane, 1:20), to give the target product **13** (48.9 mg, 61%, label: AO-3-15) as a brown oil. $^1$H NMR (400 MHz, benzene-$d_6$, AO-2-50-col): $\delta$ = 6.737 (s, 1H), 3.746 (br, 1H), 3.738 (br, 1H), 1.541-1.049 (m, 8H), 1.151 (s, 6H), 1.127 (s, 6H), 0.921 (s, 3H), 0.906 (s, 3H), 0.761-0.709 (m, 6H). $^{13}$C NMR (100 MHz, benzene-$d_6$, LB = –0.2 Hz, GB = 0.5 Hz, AO-2-50-col): aromatic region, expected 8 resonances, found 7 resonances for 2 diastereomers at $\delta$ = 146.74, 146.73, 130.00, 115.28, 115.27, 87.83, 87.82; aliphatic region expected 16 resonances, found 15 resonances at $\delta$ = 69.28, 48.31, 48.31, 38.83, 38.83, 24.50, 24.43, 24.25, 24.20, 21.18, 21.14, 18.50, 18.49, 15.30, 15.27. IR (ZnSe, cm$^{-1}$, AO-2-50-col): 3367, 2957, 2931, 2871, 1619, 1466, 1371, 1290, 1158, 1126. LR-FABMS (3-NBA matrix, AO-2-36-ptl2fr2u): $m/z$ ion type (%RA for $m/z$ = 350–1000): 406 [M]$^+$ (100%). HR-FABMS (3-NBA matrix, AO-2-36-ptl2fr2u): 408.1960 [M+1]$^+$ (100%, 0.7 ppm for $^{12}C_{22}{}^1H_{35}{}^{14}N_2{}^{81}Br_1$), 406.1979 [M]$^+$ (94%, 0.5 ppm for $^{12}C_{22}{}^1H_{35}{}^{14}N_2{}^{79}Br_1$).

**4-*tert*-Butylphenyldiamine 12.**
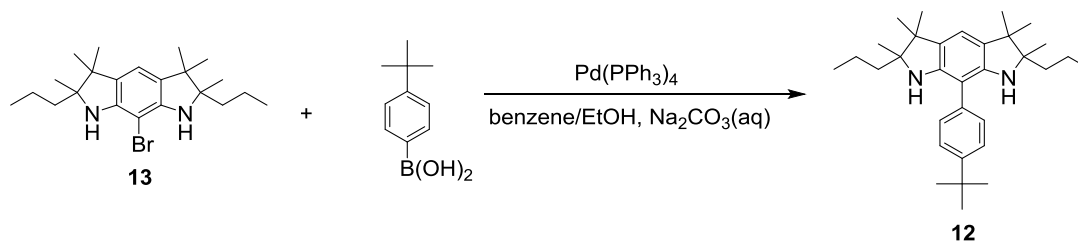


| Run | 13 (mg/μmol) | *p-t*-Butyl boronic acid (mg/μmol) | Yield (mg/%) | TM Label |
|---|---|---|---|---|
| AO-2-45 | 4.7/11.5 | 3.1/17.3 | 10.9/54 | AO-2-52-col2 |
| AO-2-52 | 13.0/31.9 | 8.5/47.9 | | |
| AO-3-18 | 48.5/119 | 31.8/179 | 39.0/71 | AO-3-18-suzuki |
| AO-9-55 | 43.9/108 | 28.8/162 | 26.4/53 | AO-9-55-flt |

Bromodiamine **13** (AO-3-15-flt, MW = 407.4, 48.5 mg, 119 μmol) and 4-*tert*-butylphenylboronic acid (MW = 178.0, 31.8 mg, 179 μmol, 1.5 equiv) were charged into a Schlenk vessel under $N_2$ atmosphere. $Pd(PPh_3)_4$ (13.8 mg, 11.9 μmol, 10 mol%) was added to the vessel in a glove bag under $N_2$ atmosphere. Benzene (4.3 mL), ethanol (1.1 mL), and aqueous $Na_2CO_3$ (1 M, 1.1 mL) were added to the reaction vessel and stirred for 24 h at 90 °C. The reaction mixture was poured into distilled water, and then extracted with benzene (3 × 20 mL). The combined organic extracts were washed with water, dried over anhydrous $Na_2SO_4$, and then concentrated to provide the crude product as light yellow oil. Column chromatography (deactivated silica, diethyl ether/pentane, 1:33) gave the 4-*tert*-butylphenyldiamine **12** as a white solid (39.0 mg, 71%, label: AO-3-18). M.p. 108-112 °C (under air). $^1$H NMR (500 MHz, chloroform-*d*, AO-9-55-flt-5): $\delta$ = 7.427, 7.375 (ABq, $J_{AB}$ = 7.8 Hz, 2H, diastereomer 1), 7.427, 7.337 (ABq, $J_{AB}$ = 8.0 Hz, 2H, diastereomer 2), 6.570 (s, 1H), 3.528 (bs, 2H), 1.616-1.150 (m, 8H, overlapping signals), 1.359 (s, 9H), 1.175 (s, 6H), 1.133 (s, 6H), 1.072/1.042 (s, 6H, two diastereomers), 0.935/0.907 (t, $J$ = 7.0 Hz, 6H, two diastereomers). $^1$H NMR (600 MHz, chloroform-*d*, AO-2-52-suzuki-CDCl3): $\delta$ = 7.418, 7.365 (ABq, $J_{AB}$ = 7.8, Hz, 2H, disastereomer 1), 7.418, 7.329 (ABq, $J_{AB}$ = 7.8, Hz, 2H, disastereomer 2), 6.560 (s, 1H), 3.522 (bs, 2H),

1.608-1.150 (m, 8H, overlapping signals), 1.354/1.351 (s, 9H, two diastereomers), 1.167 (s, 6H), 1.126 (s, 6H), 1.065/1.036 (s, 6H, two diastereomers), 0.928/0.901 (t, $J$ = 7.2 Hz, 6H). $^1$H NMR (500 MHz, benzene-$d_6$, AO-3-18-MeOHwsh): $\delta$ = 7.873 (d, $J$ = 8.5 Hz, 1H), 7.827 (d, $J$ = 8.0 Hz, 1H), 7.452 (d, $J$ = 8.0 Hz, 1H), 7.442 (d, $J$ = 8.0 Hz, 1H), 6.912 (s, 1H), 3.712/3.652 (bs, 2H, two diastereomers), 1.590-1.250 (m, 4H, overlapping signals), 1.285 (s, 6H), 1.259 (s, 6H), 1.230/1.225 (bs, 9H, two diastereomers), 1.101-0.897 (m, 4H, overlapping signals), 0.940/0.848 (s, 6H, two diastereomers), 0.754/0.669 (t, $J$ = 7.2 Hz, 6H, two diastereomers). $^1$H NMR (500 MHz, acetone-$d_6$, AO-9-55-flt2): $\delta$ = 7.457, 7.398 (ABq, $J_{AB}$ = 8.3 Hz, 2H, diastereomer 1), 7.457, 7.376 (ABq, $J_{AB}$ = 7.8 Hz, 2H, diastereomer 2), 6.661 (s, 1H), 3.861 (bs, 2H), 1.615-1.190 (m, 8H, overlapping signals), 1.173/1.168 (s, 6H, two diastereomers), 1.116 (s, 6H), 1.339 (s, 9H), 1.076/1.043 (s, 6H, two diastereomers), 0.905/0.873 (t, $J$ = 7.2 Hz, 6H, two diastereomers). $^1$H-$^{15}$N HSQC experiment (acetone-$d_6$, AO-9-55-flt-2): $\delta$ = −287.4 ppm. $^{13}$C NMR (100 MHz, chloroform-$d$, AO-9-55-flt-4): $\delta$ = 149.08, 149.03, 145.02, 133.89, 133.83, 128.90, 128.42, 128.32, 125.94, 125.85, 114.97, 106.54, 106.46, 68.44, 68.42, 46.27, 38.58, 38.53, 34.53, 31.38, 24.38, 24.07, 23.60, 23.31, 21.24, 21.09, 18.11, 18.03, 15.02, 14.98. $^{13}$C NMR (100 MHz, benzene-$d_6$, LB = −0.2 Hz, GB = 0.5 Hz, AO-2-52-col2): $\delta$ = 150.10, 150.08, 146.44, 146.44, 135.38, 135.36, 129.73, 129.68, 129.66, 126.75, 126.70, 115.73, 115.70, 107.16, 107.12, 69.10, 69.07, 47.12, 47.08, 39.22, 39.11, 34.98, 34.97, 31.80, 25.21, 24.54, 24.53, 23.90, 21.53, 21.25, 18.66, 18.53, 15.41, 15.30. IR (cm$^{-1}$, label: AO-2-52-col2): 3363 (weak), 2960, 2932, 2901, 2870, 1606, 1449, 1400, 1383, 1288, 1265, 1157, 1066, 1045, 742. LR-FABMS (3-NBA matrix, AO-2-52-col2): $m/z$ ion type (%RA for $m/z$ = 300– 1000): 460 [M]$^+$ (100%). HR-FABMS (3-NBA matrix, AO-2-52-col2): $m/z$ ion type

(%RA for *m/z* = 458–463): 461.3851 [M+1]$^+$ (61%, 0.1 ppm for $^{12}C_{31}^{13}C_1^{1}H_{48}^{14}N_2$),

460.3812 [M]$^+$ (100%, 1.1 ppm for $^{12}C_{32}^{1}H_{48}^{14}N_2$).
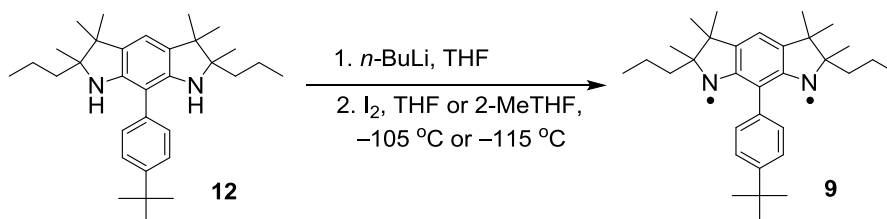
**Representative Preparations of Aminyl Diradical 9.**



**Table 1.7.** Summary of preparation of aminyl diradical **9**

| Run no | label | solvent | **8** (mg) | oxidation temp (°C) | sample type | figures and comments |
|---|---|---|---|---|---|---|
| 1 | AO305 | 2-MeTHF | 0.47 | −115 | EPR | Persistence by EPR |
| 2 | AO309 | THF | 1.69 | −105 | EPR | Sample tube broke |
| 3 | AO317 | 2-MeTHF | 1.05 | −115 | EPR | Failed |
| 4 | AO320 | THF | 0.74 | −105 | EPR/SQUID | Persistence by SQUID |
| 5 | AO321 | 2-MeTHF | 0.43 | −115 | - | Sample tube broke |
| 6 | AO328 | 2-MeTHF | 0.51 | −115 | EPR | Reaction with I$_2$ at −78 °C |
| 7 | AO330 | 2-MeTHF | 0.41 | −115 | EPR | Failed |
| 8 | AO331 | 2-MeTHF | 1.51 | −115 | EPR | I$_2$ added in several portions: diradical-to-monoradical EPR intensity first increases and then decreases. |
| 9 | AO335 | 2-MeTHF | 0.78 | −115 | EPR | Figure 1.31 |
| 10 | AO342 | 2-MeTHF | 0.79 | −115 | EPR | I$_2$ added in two portions: trace amount of diradical after the 1$^{st}$ addition, and no detectable diradical after the 2$^{nd}$ addition. |
| 11 | AO343 | 2-MeTHF | 0.88 | −115 | EPR/SQUID | Repeat SQUID data |
| 12 | AO348 | 2-MeTHF | 0.81 | −115 | EPR | I$_2$ added in three portions: after the 3$^{rd}$ addition, the diradical-to-monoradical EPR intensity decreases. |
| 13 | AO352 | 2-MeTHF | 0.73 | −115 | EPR/SQUID | Repeat SQUID data |
| 14 | AO354 | 2-MeTHF | 0.74 | −115 | EPR | Failed (too much I$_2$) |
| 15 | AO355 | 2-MeTHF | 0.77 | −115 | EPR | I$_2$ added in two portions: diradical-to-monoradical EPR intensity decreases after the 2$^{nd}$ addition. |
| 16 | AO358 | 2-MeTHF | 0.57 | −115 | EPR/SQUID | Repeat SQUID data |
| 17 | AO367 | 2-MeTHF | 1.02 | −115 | EPR | Reaction with O$_2$ |

**Aminyl Diradical 9: EPR Spectra in 2-MeTHF (Figure C15 and C16, label: AO335).**

4-*tert*-Butylphenyldiamine **12** (AO-3-18-suzuki, MW = 460.7, 0.78 mg, 1.69 μmol) was placed into an EPR sample tube (5-mm quartz tube) and evacuated at 50 °C for overnight. THF (0.1 mL, 8-mm height) was added to the vessel by vacuum transfer, and then stirred for 30 min at –30 °C. *n*-BuLi (0.185 M, 20 μL, 3.56 μmol, 2.1 equiv) was added to produce the orange homogeneous solution. After stirring at –30 °C for 1 h, the red mixture was concentrated at –30 °C until the volume decreased to about 0.025 mL (2-mm height). 2-MeTHF (~0.1 mL) was added to the reaction mixture by vacuum transfer.

The reaction mixture was immersed in liquid nitrogen; subsequently, iodine (99.999%, ultra dry, Alfa) was vacuum transferred (for 20 s) to the sample tube wall, just above the reaction mixture. Iodine was mixed into the reaction mixture at –115 °C, and then the dark red solution was shaken at –115 °C for 1 h. The resultant dark red solution was stored in liquid nitrogen; EPR spectra were obtained at 132–134 K (label: AO335r1/r2) as illustrated in Figure C15.

Subsequently, the sample tube was re-attached to the vacuum line, and an additional vacuum transfer of iodine (for 10 s) was carried out, with mixing at –115 °C. The resultant dark red solution was mixed for additional 20 min at –115 °C, and then another set of EPR spectra was obtained at 132–134 K (label: AO335r3–r6); see: Figure 1.31 and Figure C16.

**Aminyl Diradical 9: EPR/SQUID Data in 2-MeTHF (Figures C17–C23, labels: AO358 and AO352).**

4-*tert*-Butylphenyldiamine **12** (AO-3-18-MeOHwsh, MW = 460.7, 0.57 mg, 1.24 μmol) was placed in the custom-made SQUID sample tube (5-mm O.D. EPR quartz tube with a thin bottom ~6 cm from the end of the tube) and evacuated overnight. THF (~0.1

mL, ~8-mm height) was added to the vessel by vacuum transfer, and then stirred for 30 min at −30 °C. $n$-BuLi (0.213 M in hexane, 13 μL, 2.60 μmol, 2.1 equiv) was added to produce initially the orange homogeneous solution. After stirring at −30 °C for 1 h, the deep red reaction mixture was concentrated at −30 °C until the volume decreased to about 0.025 mL (~2-mm height). THF (~0.1 mL) was added to the concentrated reaction mixture by vacuum transfer, and then the reaction mixture was stirred for 10 min at −30 °C. This sequence of solvent removal under vacuum, followed by addition of THF by vacuum transfer was repeated another two times (total of three times). Finally, 2-MeTHF (~0.1 mL) was added to the reaction mixture by vacuum transfer, and then the reaction mixture (under vacuum) was immersed in liquid nitrogen. Subsequently, iodine was vacuum transferred (for 10 s) to the sample tube wall, just above the reaction mixture. Iodine was mixed into the reaction mixture at −115 °C, and then the dark red solution was stirred at −115 °C for 1 h. The resultant dark red solution was stored in liquid nitrogen; EPR spectra were obtained at 132 K (Figure C17, label: AO358r1).

After recording the EPR spectra, the sample tube was re-attached to vacuum line, and the sample tube was flame sealed. Subsequently, the sample tube, which was kept in liquid nitrogen, was transferred to a helium filled glove bag, and then rapidly inserted (<15 s) into the sample chamber of SQUID magnetometer at 10 K. After pumping the chamber at 90 K, the matrix was briefly annealed at 170 K, and then the first set of magnetic data was obtained (AO358s1); however, this set of data was of low quality due to incomplete temperature equilibration of the sample, especially at low temperatures. The second set of magnetic data was obtained after annealing the matrix at 190 K and providing increasingly long time delays at lower temperatures (Figure C18, label: AO358s2).

After the sample was rapidly removed from the sample chamber of SQUID magnetometer at 10 K (total time of about 40 s), another set of EPR spectra was obtained (label: AO358r5-7), as illustrated in Figure C19).

A similar procedure was employed to obtain a repeat sample for the EPR spectra and SQUID magnetic data for aminyl diradical **9** in 2-MeTHF (Figure C20-C22, label: AO352r3/r4, AO352s2G and AO352r5/r6), using 4-*tert*-butylphenyldiamine **12** (AO-3-18-MeOHwsh, 0.73 mg).

**Aminyl Diradical 9: Persistence in 2-MeTHF by EPR Spectroscopic Monitoring (Figure C23, label: AO305/306).**

4-*tert*-Butylphenyldiamine **12** (AO-2-52-col2, MW = 460.7, 0.47 mg, 0.78 mg, 1.02 μmol) was put into an EPR sample tube (5-mm quartz tube) and evacuated at 50 °C for overnight.  THF (0.1 mL, 8-mm height) was added to the vessel by vacuum transfer, and then stirred for 30 min at –30 °C.  *n*-BuLi (0.164 M, 15 μL, 2.45 μmol, 2.4 equiv) was added to produce the orange homogeneous solution.  After stirring at –30 °C for 1 h, the red mixture was concentrated at –30 °C until the volume decreased to about 0.025 mL (2-mm height).  2-MeTHF (~0.1 mL) was added to the reaction mixture by vacuum transfer, and then stirred briefly at –35 °C.

The reaction mixture was immersed in liquid nitrogen; subsequently, iodine was vacuum transferred (for 13 s) to the sample tube wall, just above the reaction mixture. Iodine was mixed into the reaction mixture at –115 °C, and then the dark red solution was stirred at –115 °C for 1 h.  The resultant dark red solution was stored in liquid nitrogen; EPR spectra were obtained at 133–134 K (label: AO306r1/r2). The sample was kept at –27 °C for 10 min, and then EPR spectra at 133–134 K were taken (label: AO306r4−r6).

The sample was warmed up to room temperature (22 °C) for 10 min. During this time the color changed to brown. After obtaining a set of EPR at 133−134 K (label: AO306r7–r8), the sample was kept at room temperature for another 10 min, resulting in changes in color to green. Subsequent EPR spectra were taken at 136-137 K (label: AO306r9–r10, as illustrated in Figure S9). Using these spectra, half-life, $\tau_{1/2}$ of the order of 10 min was estimated for diradical **9** in 2-MeTHF at room temperature (Figure C23).

**Experimental double integrated intensities for diradical (IntD) and monoradical (IntM).** In order to overcome the overlap of bands for diradical and monoradical in the center-band section of the spectra, the following approach was implemented. The experimental spectra and spectral simulations for the $S = 1$ state of diradicals **1** and **2** were double-integrated in three sections: 310-325 mT, 325-330 mT, and 350-365 mT; for some experimental spectra, obtained with a different dewar insert or a different cavity, the fields for individual sections were slightly changed. The parameters for spectral simulations were adjusted to individual spectra to obtain adequate fit, as needed. It was assumed for the experimental spectra that only diradical contributed to the EPR intensity in the 310-325 mT and 350-365 mT side-band sections, while both diradical and monoradical contributed in the 325-350 mT center-band section.

To determine the contribution of the diradical to the 325-350 mT center-band section, the spectral simulation for the diradical was double integrated in these 3 sections to provide the ratio of double integrated intensities for the diradical between the center section and the sum of the side sections: $IntD_{cent}^{sim}/IntD_{sides}^{sim}$. This ratio was then multiplied by $IntD_{sides}^{expt}$ in the experimental spectra, to calculate contribution of the diradical to the center section of the experimental spectra: $IntD_{cent}^{expt} =$

$(IntD_{cent}^{sim}/IntD_{sides}^{sim})*IntD_{sides}^{expt}$. The double integrated intensity totals for the diradical and monoradical were $IntD = IntD_{sides}^{expt} + IntD_{cent}^{expt}$ and $IntM = Int_{cent}^{expt} - IntD_{cent}^{expt}$, respectively.

**Table 1.8.** Decay kinetic of 4.6 mM aminyl diradical **9** at room temperature (295 K)

| EPR file name | Annealing temperature | Time (min) | $IntD_{sides}$ | $IntD_{cent}$ | Center-to-side ratio | Corr $IntD_{cent}$ | IntD | IntM | Corr IntM | Relative diradical (%) |
|---|---|---|---|---|---|---|---|---|---|---|
| Simulation | - | - | 55.53 | 236.57 | 4.26 | 236.57 | 292.10 | 0.00 | 0.00 | 100 |
| AO306r3 | - | 0 | 56.26 | 250.61 | 4.45 | 239.69 | 295.96 | 10.92 | 29.11 | 91 |
| AO306r4 | 246 | 10 | 55.58 | 252.70 | 4.55 | 236.78 | 292.36 | 15.92 | 42.45 | 87 |
| AO306r8 | 294 | 10 | 12.79 | 103.85 | 8.12 | 54.51 | 67.30 | 49.34 | 131.57 | 34 |
| AO306r10 | 294 | 20 | 4.87 | 83.84 | 17.23 | 20.74 | 25.60 | 63.10 | 168.28 | 13 |

[a] $IntD_{sides} = IntD_{sides}/10^6$ at 310-325 and 350-365 mT regions, [b] $IntD_{cent} = IntD_{cent}/10^6$ at 325-350 mT, [c] Center-to-side ratio = $IntD_{cent}/IntD_{sides}$, [d] Calc. diradical in center = $DI_{side}\times$ Center-to-side ratio

    The sample was kept at room temperature, with exclusion of light, for 4 days, and then it was exposed to air for 1 h. After degassing the solution, EPR spectra at 294-295 K (label: AO306r17–18) showed presence of a residual monoradical. The sample was filtered through a cotton plug and evaporated *in vacuo*. ^{1}H NMR (500 MHz, benzene-$d_6$, label: AO-3-07-diaminyl after air) spectrum showed resonances in aromatic region as follows: $\delta$ = 7.851 (dd, $J$ = 8.5, 23.0 Hz, 2H), 7.446 (dd, $J$ = 5.0, 8.0 Hz, 2H), 6.913 (s, 1H) and LR-FABMS ((3-NBA matrix, label: AO-3-05-air): $m/z$ ion type (%RA for $m/z$ = 200 – 2200): 460.4 [M]$^+$ (100%)) of the crude reaction mixture showed almost exclusively one product (Figure C6). The crude was purified by preparative TLC (3% deactivated silica, 3% diethyl ether in pentane). ^{1}H NMR spectrum of the pure product (500 MHz, benzene-$d_6$, label:

AO-3-05-fr1): (aromatic region, $\delta = 7.850$ (dd, $J = 8.4, 22.6$ Hz, 2H), 7.447 (dd, $J = 4.7$, 8.2 Hz, 2H), 6.912 (s, 1H)) is coincident with that for 4-*tert*-butylphenyldiamine **12**.

**Aminyl Diradical 9: Persistence in 2-MeTHF by EPR Spectroscopic Monitoring (Figure C1, label: AO953).**

4-*tert*-Butylphenyldiamine **12** (AO-3-18-suzuki, MW = 460.7, 0.50 mg, 1.09 μmol) was placed into an EPR sample tube (5-mm quartz tube) and evacuated under high vacuum for overnight at 55 °C using heating tape wrapping the whole EPR sample tube. The next day, the heating tape was raised up above the sample and heated the remaining tube at 120 °C for overnight. THF (0.1 mL, 8-mm height) was added to the vessel by vacuum transfer, and then stirred for 30 min at −30 °C. *n*-BuLi (0.171 M, 16 μL, 2.60 μmol, 2.4 equiv) was added to produce an orange homogeneous solution. After stirring at −30 °C for 1 h, the orange mixture was evaporated at −40 °C. 2-MeTHF (~0.1 mL) was added to the reaction mixture by vacuum transfer.

The reaction mixture was immersed in liquid nitrogen; subsequently, iodine (99.999%, ultra dry, Alfa) was vacuum transferred (for 14 s) to the sample tube wall, just above the reaction mixture. Iodine was mixed into the reaction mixture at −115 °C, and then the dark red solution was shaken at −115 °C for 1 h. The resultant dark orange solution was stored in liquid nitrogen; EPR spectra were obtained at 132–133 K (label: AO335r1–r3).

The sample tube was re-attached to the vacuum line, and an additional vacuum transfer of 2-MeTHF (3.5-cm height, 2.52 mM) was carried out. The resultant orange solution was mixed for additional 15 min at −115 °C, and then EPR spectra were obtained at 132–133 K (label: AO953r4–r5).

The sample was annealed at 246 K (–27 °C) for 10 min and at room temperature (22 °C) for 1 min to make sure all iodine is consumed. EPR spectra at 132 K were taken after each annealing (labels: AO953r6 and r8). Subsequently, the sample was annealed at 295 K (22 °C) for 0, 2, 4, 6, 8 and 10 min (total time) to produce yellow solution. EPR spectra were taken after each annealing (labels: AO953r9, 10, 15, 17, 19, 21). For reference, EPR spectra of TEMPOL (1 mM in 2-MeTHF) were taken at 132 K (labels: AO953r7, 11, 14, 16, 18, 20). The summary of kinetics is shown in Table 1.9.

**Table 1.9**. Decay Kinetics of 2.52 mM Aminyl Diradical **9** at 295 K

| Sample | | | | | Reference | | |
|---|---|---|---|---|---|---|---|
| EPR filename | Time (s) | Peak height[a] (PH) | $PH_{cor}$ | -ln $PH_{cor}$ | EPR filename | Double integration (DI) | Correction[b] (%) |
| AO953r9 | 0 | 4136.00 | 4136.00 | -8.327484416 | AO953r7 | 5.016E+07 | 100 |
| AO953r10 | 120 | 3685.50 | 3771.47 | -8.235218961 | AO953r11 | 5.133E+07 | 102 |
| AO953r15 | 240 | 3380.00 | 3266.79 | -8.091564434 | AO953r14 | 4.848E+07 | 97 |
| AO953r17 | 360 | 2921.00 | 2905.86 | -7.974484409 | AO953r16 | 4.990E+07 | 99 |
| AO953r19 | 480 | 2250.50 | 2302.55 | -7.741770336 | AO953r18 | 5.132E+07 | 102 |
| AO953r21 | 600 | 2160.00 | 2237.94 | -7.713312233 | AO953r20 | 5.197E+07 | 104 |

[a] Peak height (PH) for **9** = average of the measured EPR peak height at ~ 329 and 359 mT.

[b] Correction for $PH_{cor}$; Correction = $(DI/DI_{(t=0)})\times100\%$ using double integration of 1 mM TEMPOL.

**Aminyl diradical 9: Persistence in THF Monitored by SQUID Magnetometry (label: AO320).** 4-*tert*-Butylphenyldiamine **12** (AO-2-52-col2, MW = 460.7, 0.74 mg, 1.61 μmol) was placed in the custom-made SQUID sample tube (5-mm O.D. EPR quartz tube with a thin bottom ~6 cm from the end of the tube) and evacuated overnight. THF (~0.1 mL, ~8-mm height) was added to the vessel by vacuum transfer, and then stirred for 30

min at –30 °C. *n*-BuLi (0.231 M in hexane, 17 μL, 3.85 μmol, 2.4 equiv) was added to produce initially the orange homogeneous solution. After stirring at –30 °C for 1 h, the deep red reaction mixture was concentrated at –30 °C until the volume decreased to about 0.025 mL (~2-mm height). THF (~0.15 mL) was added to the concentrated reaction mixture by vacuum transfer, and then the reaction mixture was stirred for 10 min at –30 °C. This sequence of solvent removal under vacuum, followed by addition of THF by vacuum transfer was repeated another two times (total of three times). Finally, the volume of reaction mixture was set to < 0.1 mL (8-mm height, or less), and then the reaction mixture (under vacuum) was immersed in liquid nitrogen. Subsequently, iodine was vacuum transferred (for 23 s) to the sample tube wall, just above the reaction mixture. Iodine was mixed into the reaction mixture at –105 °C, and then the dark red solution was stirred at –105 °C for 1 h. The resultant dark red solution was stored in liquid nitrogen; EPR spectra were obtained at 132 K (label: AO320r1/r2).

After recording the EPR spectra, the sample tube was re-attached to vacuum line, and the sample tube was flame sealed. Subsequently, the sample tube, which was kept in liquid nitrogen, was transferred to a helium filled glove bag, and then rapidly inserted (<15 s) into the sample chamber of SQUID magnetometer at 10 K. After pumping the chamber at 90 K, the first set of magnetic data was obtained without melting the matrix in the 1.8– 150 K range (label: AO320s1); the following parameters were obtained for the magnetization, $M/M_{sat}$ vs. $H/(T - \theta)$, and susceptibility, $\chi T$ vs. $T$ data: $\theta = -0.19$ K, $M_{sat} = 0.52$ $\mu_B$, $S = 0.85$, and $\chi T = 0.49$ emu K mol$^{-1}$. Similar set of magnetic data was obtained after annealing the matrix at 170 K (label: AO320s2).

Following these two sets of magnetic measurements, the sample was sequentially annealed at 195 K for 15 min, 246 K for 30 min, 273 K for 30 min, 295 K for 30 min, and 295 K for an additional 30 min. After each annealing, a set of magnetic data was obtained, (label: AO320s3s4). Using these data, half-life, $\tau_{1/2}$ of the order of 10 min was estimated for diradical **9** at 295 K in THF.

After the sample was rapidly removed, without visible melting of the matrix, from the sample chamber of SQUID magnetometer, another set of EPR spectra was obtained (label: AO320r4).

After 14 months at room temperature (exclusion of light), the sample tube was broken, and then the sample was filtered through a cotton plug and evaporated *in vacuo*. $^1$H NMR spectrum (500 MHz, benzene-$d_6$, label: AO-4-92-flt) and ESI-MS (MeOH + 0.1% of HCO$_2$H, label: AO492flt) data of the crude showed the 4-*tert*-butylphenyldiamine **12**, accompanied by unknown impurities. The crude was purified by preparative TLC (4% deactivated silica, 5% diethyl ether in pentane). $^1$H NMR spectrum (500 MHz, benzene-$d_6$, label: AO-4-92-ptlc-fr1): (aromatic region, $\delta$ = 7.850 (dd, $J$ = 8.0, 22.5 Hz, 2H), 7.446 (m, 2H), 6.912 (s, 1H)) along with HR-EI MS (AO-4-92-ptlc-fr1): 445.3562 [M–CH$_3$]$^+$ (100%, −4.7 ppm for $^{12}$C$_{31}$$^1$H$_{45}$$^{14}$N$_2$), 460.3813 [M]$^+$ (94%, −1.0 ppm for $^{12}$C$_{32}$$^1$H$_{48}$$^{14}$N$_2$) of the pure product was consistent with 4-*tert*-butylphenyldiamine **12**.

**Reaction of Diradical 9 with Iodine (Figure C10, label: AO328).**

4-*tert*-Butylphenyldiamine **12** (AO-3-18-suzuki, MW = 460.7, 0.51 mg, 1.11 μmol) was put into an EPR sample tube (5-mm quartz tube) and evacuated at 40 °C for overnight. THF (0.1 mL, 8-mm height) was added to the vessel by vacuum transfer, and then stirred for 30 min at −30 °C. *n*-BuLi (0.231 M, 12 μL, 2.66 μmol, 2.4 equiv) was added to produce

the orange homogeneous solution.  After stirring at −30 °C for 1 h, the deep orange mixture was concentrated at −30 °C until the volume decreased to about 0.025 mL (2-mm height). 2-MeTHF (~0.15 mL) was added to the reaction mixture by vacuum transfer, and then stirred briefly at −105 °C.

The reaction mixture was immersed in liquid nitrogen; subsequently, iodine was vacuum transferred (for 9 s) to the sample tube wall, just above the reaction mixture.  Iodine was mixed into the reaction mixture at −115 °C, and then the deep orange solution was shaken at −115 °C for 2 h.  The resultant deep orange solution was stored in liquid nitrogen; EPR spectra were obtained at 133–134 K (label: AO328r1/r2).

After obtaining the EPR spectra, the sample tube was re-attached to the vacuum line, and an additional vacuum transfer of iodine (for 2 s) was carried out, with mixing at −115 °C for 30 min.  Another set of EPR spectra was obtained at 133–134 K (label: AO328r3/r4, see Figure C10).

The sample was annealed at −78 °C for 10 min and −25 °C for 10 min.  EPR spectra (label: AO238r5 and r6, see Figure C10) were recorded after each annealing. The sample tube was attached to the vacuum line, and then an excess of iodine (for 10 s) was added to the sample tube. After mixing at −115 °C for 30 min, the sample was annealed at −78 °C for 10 min. Subsequent EPR spectrum at 132 K showed only monoradical (label: AO328r7, see Figure C10).

**Reaction of diradical 9 with oxygen (O$_2$) (Figure C12, label: AO367).**

4-*tert*-Butylphenyldiamine **12** (AO-3-18-suzuki, MW = 460.7, 1.00 mg, 2.17 µmol) was put into an EPR sample tube (5-mm quartz tube) and evacuated at 70 °C for overnight. THF (0.1 mL, 8-mm height) was added to the vessel by vacuum transfer, and then stirred

for 30 min at −30 °C.  *n*-BuLi (0.213 M, 22 μL, 4.56 μmol, 2.1 equiv) was added to produce

the orange homogeneous solution.  After stirring at −30 °C for 1 h, the red mixture was

concentrated at −30 °C until the volume decreased to about 0.025 mL (2-mm height).  2-

MeTHF (~0.1 mL) was added to the reaction mixture by vacuum transfer, and then stirred

for 2 min at −50 °C.

The reaction mixture was immersed in liquid nitrogen; subsequently, iodine was

vacuum transferred (for 10 s) to the sample tube wall, just above the reaction mixture.

Iodine was mixed into the reaction mixture at −115 °C, and then the dark red solution was

stirred at −115 °C for 1 h.  The resultant dark red solution was stored in liquid nitrogen;

EPR spectra were obtained at 132–133 K (label: AO367r1/r2).

The sample tube was warmed up to −27 °C for 10 min, then another EPR spectrum

was obtained at 132−133 K (label: AO367r3). The sample tube was attached to the vacuum

line. The solution was saturated under dry oxygen atmosphere at −105 °C for 15 min,

followed by degassing. The EPR spectrum was obtained at 132–133 K (label: AO367r5);

see: Figure C12. The reaction mixture was warmed up to room temperature (295 K),

filtered through a cotton plug, evaporated *in vacuo*, and placed on high vacuum line.  $^1$H

NMR (500 MHz, benzene-$d_6$, label: AO-3-67-chk): aromatic region $\delta$= 7.65-7.60 (m, 2H),

7.39-7.31 (m, 2H), 5.73-5.70 (m, 1H).  LR-FABMS ((3-NBA matrix, label: AO-3-67-O$_2$):

*m/z* ion type (%RA for *m/z* = 350-800): 493.5 [M+H]$^+$ (100%)) and HR-EI MS (AO-3-67-

chk): 475.3672 [M−OH]$^+$ (100%, −3.4 ppm for $^{12}C_{32}{}^{1}H_{47}{}^{14}N_2{}^{16}O_1$), 492.3710 [M]$^+$ (53%,

−1.2 ppm for $^{12}C_{32}{}^{1}H_{48}{}^{14}N_2{}^{16}O_2$).  The above $^1$H NMR and FABMS data of the crude

reaction mixture are consistent with the diamagnetic "diol product" (mixture of isomers).

The crude was then purified by preparative TLC (3% deactivated silica, 50% diethyl

ether/hexane), to provide three fractions, $R_f$ = 0.56 (Fraction 1), 0.51 (Fraction 2), 0.44 (Fraction 3), with similar $^1$H NMR spectra (500 MHz, benzene-$d_6$): Fraction 1 (label: AO-4-67-ptlc-fr1-bz) aromatic region, $\delta$ = 7.618 (d, $J$ = 8.5 Hz, 2H), 7.359 (d, $J$ = 8.5 Hz, 2H), 5.699 (s, 1H), hydroxyl groups, $\delta$ = 3.24 (br), 3.151 (s); Fraction 2 (label: AO-4-67-ptlc-fr2-bz) aromatic region $\delta$ = 7.647 (d, $J$ = 8.5 Hz, 2H), 7.378 (d, $J$ = 8.5 Hz, 2H), 5.724 (s, 1H), hydroxyl groups, $\delta$ = 3.29 (br), 3.230 (s); Fraction 3 (label: AO-4-67-ptlc-fr3-bz) aromatic region $\delta$ = 7.628 (d, $J$ = 8.0 Hz, 2H), 7.362 (d, $J$ = 8.5 Hz, 2H), 5.734 (s, 1H), hydroxyl groups, $\delta$ = 3.76 (br, exch $D_2O$), 3.247 (s, exch $D_2O$). HR$-$EI MS of these three fractions gave the same exact masses; HR-EI MS for Fraction 1 (label: AO-3-67-ptlc-fr1): 492.3714 [M]$^+$ (31%, $-$0.4 ppm for $^{12}C_{32}{}^1H_{48}{}^{14}N_2{}^{16}O_2$); HR$-$EI MS for Fraction 2 (label: AO-3-67-ptlc-fr2): 492.3727 [M]$^+$ (66%, 2.3 ppm for $^{12}C_{32}{}^1H_{48}{}^{14}N_2{}^{16}O_2$); HR-EI MS for Fraction 3 (label: AO-3-67-ptlc-fr3): 492.3713 [M]$^+$ (14%, $-$0.6 ppm for $^{12}C_{32}{}^1H_{48}{}^{14}N_2{}^{16}O_2$). IR (ZnSe, cm$^{-1}$, AO-3-67-ptlc-fr3) spectrum for Fraction 3: 3368, 2958, 2927, 2872, 2855, 1604, 1465, 1378, 1368, 1269, 1134, 1014. $^1$H NMR spectra for the diamagnetic "diol product" are presented in Figure C13 in Appendix C.

### 1.4.2. Syntheses of compounds 24, 25, 22 and aminyl diradical 10.

### 2-(4-(*tert*-butyl)-2,6-dimethylphenyl)-4,4,5,5-tetramethyl-1,3,2-dioxaborolane 24
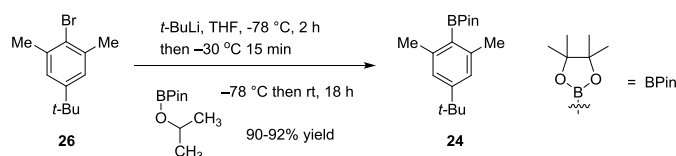


| Run | SM (g/mmol) | *t*-BuLi (mL/mmol) | Borolane (mL/mmol) | Yield (g/%) |
|---|---|---|---|---|
| AO-4-41 | 0.101/0.418 | 0.55/0.879 | 0.12/0.586 | 0.111/92 |
| AO-5-26 | 0.530/2.20 | 3.12/4.62 | 0.63/3.08 | 0.527/90 |

1-Bromo-4-*tert*-butyl-2,6-dimethylbenzene **26** (MT0439C3-I, MW = 241.17, 0.101 g, 0.418 mmol, 1 equiv) was transferred into a Schlenk vessel and evacuated under high vacuum for 10 min. Freshly distilled THF (1.5 mL) was added into the reaction vessel. After stirring at room temperature for 5 min, the reaction was cooled to −78 °C for 15 min. *t*-BuLi (1.59 M, 0.55 mL, 0.879 mmol, 2.1 equiv) was added dropwise to the Schlenk vessel. The reaction mixture was stirred at −78 °C for 2 h to produce milky solution. The reaction was then stirred at −30 °C for 15 min then was cooled down to −78 °C for 15 min. 2-Isopropoxy-4,4,5,5-tetramethyl-1,3,2-dioxoborolane (0.12 mL, 0.586 mmol, 1.4 equiv) was added to the reaction mixture. The reaction was stirred and warmed up to room temperature slowly for overnight. After 18 h, the milky solution was worked up by adding brine solution (2 mL). The crude mixture was extracted with diethyl ether (3 × 25 mL). The organic phase was combined, dried over MgSO$_4$ and evaporated *in vacuo* to give a white solid of the target product **24** (0.111 g, 92% yield, label: AO-4-41-crd). M.p. 162-163 °C. $R_f$ = 0.11 (pentane). $^1$H NMR (400 MHz, chloroform-*d*, AO-4-53-crd1): $\delta$ = 6.992 (s, 2H), 2.433 (s, 6H), 1.384 (s, 12H), 1.293 (s, 9H). $^{13}$C NMR (100 MHz, chloroform-*d*, AO-4-53-crd1): $\delta$ = 152.16, 141.87, 123.66, 83.37, 34.33, 31.18, 24.93, 22.57. IR (cm$^{-1}$,

label: AO-4-53-crd1): 3052, 2962, 2864, 1605, 1373, 1335, 1301, 1265, 1139, 1061, 960, 857, 735.  HR-EI MS (AO-4-53-crd1): *m/z* ion type (%RA for *m/z* = 280–290): 288.2270 [M]$^+$ (100%, 3.3 ppm for $^{12}C_{18}{}^{1}H_{29}{}^{16}O_2{}^{11}B$).

**4,4,5,5-tetramethyl-2-(2,4,6-tri-*tert*-butylphenyl)-1,3,2-dioxaborolane 25**
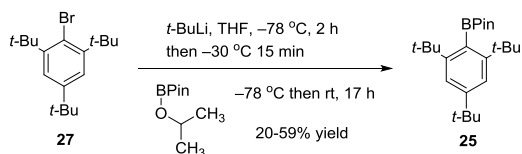


| Run | SM (mg/μmol) | *t*-BuLi (mL/mmol) | Borolane (mL/mmol) | Yield (mg/%) |
|---|---|---|---|---|
| AO-5-80 | 20.6/0.063 | 0.08/0.133 | 0.02/0.089 | 14.0/59 |
| AO-5-82 | 354/1.09 | 1.36/2.29 | 0.31/1.52 | 82.6/20 |

1-Bromo-2,4,6-tri-*tert*-butylbenzene **27** (MW = 325.33, 20.6 mg, 0.063 mmol, 1 equiv) was transferred into a Schlenk vessel and evacuated under high vacuum for 4 h. Freshly distilled THF (1 mL) was added into the Schlenk vessel.  After stirring at room temperature for 5 min, the Schlenk vessel was cooled to −78 °C for 10 min.  *t*-BuLi (1.68 M, 0.08 mL, 0.133 mmol, 2.1 equiv) was added dropwise to the reaction vessel.  The reaction mixture was stirred at −78 °C for 1 h to produce a clear light yellow solution.  The reaction was stirred at −30 °C for 20 min then was cooled down to −78 °C for 10 min.  2-Isopropoxy-4,4,5,5-tetramethyl-1,3,2-dioxoborolane (0.02 mL, 0.089 mmol, 1.4 equiv) was added to the reaction mixture.  The reaction was warmed up slowly to room temperature and stirred for overnight.  After 17 h, the milky solution was quenched by adding brine solution (2 mL) and extracted with diethyl ether (3 × 25 mL).  The organic phase was combined, dried over Na$_2$SO$_4$ and evaporated *in vacuo* to give a crude product. The crude product was filtered through a short silica gel plug with pentane to 1% diethyl ether/pentane to obtain a white solid of the corresponding product **25** (14.0 mg, 59% yield,

label: AO-5-82-flt1). M.p. 175-176 °C. $R_f$ = 0.19 (pentane). ^{1}H NMR (400 MHz, chloroform-*d*, AO-5-82-flt1): $\delta$ = 7.373 (s, 2H), 1.486 (s, 18H), 1.466 (s, 12H), 1.313 (s, 9H). ^{13}C NMR (100 MHz, chloroform-*d*, AO-5-82-flt1): $\delta$ = 154.31, 149.57, 120.47, 83.90, 37.47, 34.89, 32.82, 31.30, 26.38. IR (cm$^{-1}$, label: AO-5-82-flt1): 3001, 2954, 2909, 2869, 1603, 1363, 1317, 1293, 1140, 1057, 964, 857, 691. HR-EI MS (AO-5-80-flt1): *m/z* ion type (%RA for *m/z* = 370–380): 372.3203 [M]$^+$ (100%, 0.9 ppm for $^{12}C_{24}{}^{1}H_{41}{}^{16}O_2{}^{11}B$).

**Attemped synthesis of diamine 23.**
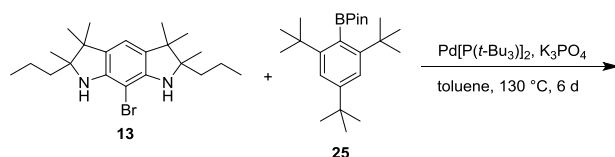


Bromodiamine **13** (AO-4-98-flt, MW = 407.4, 6.1 mg, 15.0 µmol) was transferred into a Schlenk tube and evacuated under high vacuum for overnight. 4,4,5,5-tetramethyl-2-(2,4,6-tri-*tert*-butylphenyl)-1,3,2-dioxaborolane **25** (AO-5-82, MW = 372.39, 16.7 mg, 45.0 µmol, 3 equiv) and anhydrous $K_3PO_4$ (MW = 212.28, 15.9 mg, 74.9 µmol, 5 equiv) were charged into the Schlenk vessel under $N_2$ atmosphere. Pd[P(*t*-Bu$_3$)$_2$ (MW = 511.06, 6.1 mg, 12.0 µmol, 0.8 equiv) was added to the vessel in a glove box. The reaction vessel was evacuated on high vacuum briefly and toluene (0.15 mL) was added to the reaction vessel by vacuum transfer. The reaction was stirred for 6 d (144 h) at 130 °C with exclusion of light. After cooling down to room temperature, the reaction mixture was diluted by chloroform and filtered through a Celite pad to provide the crude mixture. The crude mixture was separated by preparative TLC (3% deactivated silica, diethyl ether/pentane, 1:33) gave the boronate **25**, diamine **16**, and trace amount of its dimer, **16-dimer**, as well as other unidentified by-products.

**2,6-Dimethyl-4-*tert*-butylphenyldiamine 22.**
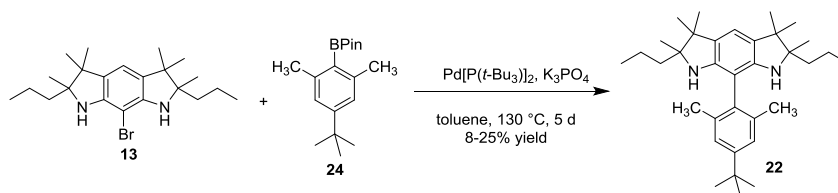


| Run | **13** (mg/μmol) | Boronate **24** (mg/μmol) | Pd[P(*t*-Bu)₃]₂ (mg/μmol) | K₃PO₄ (mg/μmol) | Temperature, reaction time | Yield (mg/%) | TM Label |
|-----|------|-------|------|------|------|------|------|
| AO-5-12 | 4.8/11.8 | 6.8/23.6 | 1.4/1.18 | 10.0/47.1 | 120 °C, 48 h | 0.5/8 | AO-5-20-ptlc |
| AO-5-26 | 35.9/88.1 | 76.2/264 | 36.0/70.5 | 93.5/441 | 130 °C, 120 h | 10.9/25 | AO-5-30-flt-fr3 |
| AO-9-10 | 60.0/155 | 133.7/464 | 63.4/124 | 164.5/775 | 130 °C, 120 h | 6.0/8 | AO-9-10-ptlc3 |
| AO-9-28 | 135.0/331 | 286.5/994 | 135.4/265 | 352.4/1655 | 130 °C, 120 h | 16.3/10 | AO-9-28 |

Bromodiamine **13** (AO-4-98-flt, MW = 407.4, 35.9 mg, 88.1 μmol) was transferred into a Schlenk tube and evacuated under high vacuum for 3 h.   2-(4-(*tert*-Butyl)-2,6-dimethylphenyl)-4,4,5,5-tetramethyl-1,3,2-dioxaborolane **24** (AO-4-53-flt, MW = 288.23, 76.2 mg, 264 μmol, 3 equiv) and anhydrous K₃PO₄ (MW = 212.28, 93.5 mg, 441 μmol, 5 equiv) were charged into the Schlenk vessel under N₂ atmosphere.   Pd[P(*t*-Bu₃)₂ (MW = 511.06, 36.0 mg, 70.5 μmol, 0.8 equiv) was added to the vessel in a glove box under Ar atmosphere.  Toluene (1 mL) was added to the reaction vessel by vacuum transfer.  The reaction was stirred for 5 d (120 h) at 130 °C, exclusion of light.  After cooling down to room temperature, the reaction mixture was diluted by chloroform and filtered through a Celite pad to provide the crude mixture.  Column chromatography (3% deactivated silica, diethyl ether/pentane, 1:33, $R_f$ = 0.79) gave the 2,6-dimethyl-4-*tert*-butylphenyldiamine **22** (10.9 mg, 25% yield, label: AO-5-30-flt-fr-3) as a white solid.   M.p. 152-160 °C (decomposed to brown liquid, under air).  ¹H NMR (500 MHz, benzene-$d_6$, AO-5-30-flt-fr3): $\delta$ = 7.377 (s, 2H), 6.894 (s, 1H), 3.048 (s, 2H), 2.400 (t, $J$ = 2.5 Hz, 6H), 1.408-0.739 (m, 8H), 1.310 (m, 6H), 1.275 (s, 6H), 1.256 (s, 9H), 0.893 (s, 3H), 0.886 (s, 3H), 0.707-

0.669 (m, 6H).  $^1$H NMR (500 MHz, chloroform-*d*, AO-9-28-wsh-4): $\delta$ = 7.095 (bs, 2H), 6.589 (s, 1H), 2.931 (bs, 2H), 2.053-33 (s, 6H), 1.547-1.275 (m, 8H), 1.343 (s, 9H), 1.165 (s, 6H), 1.121 (s, 6H), 1.030 (s, 6H), 0.883 (t, *J* = 7.0 Hz, 6H).  $^1$H NMR (500 MHz, acetone-*d*$_6$, AO-9-28-wsh-3): $\delta$ = 7.165, 7.155, 7.144 (s, 2H, mixture of diastereomers), 6.698 (s, 1H), 3.216 (bs, 2H), 1.568-1.278 (m, 8H), 1.331 (s, 9H), 1.182, (s, 6H), 1.125 (s, 6H), 1.057 (s, 6H), 0.864 (t, *J* = 7.2 Hz, 6H).  $^1$H-$^{15}$N HSQC experiment (acetone-*d*$_6$, AO-9-28-wsh-3): $\delta$ = −287.8 ppm.  $^{13}$C NMR (100 MHz, chloroform-*d*, AO-9-28-wsh-5): $\delta$ = 149.52, 145.03, 137.20, 136,78, 136.40, 131.74, 128.11, 124.66, 124.50, 124.33, 114.21, 105.28, 68.37, 46.41, 38.41, 34.29, 31.45, 23.89, 23.85, 23.53, 20.86, 20.04, 20.02, 19.99, 17.98, 14.91.  IR (cm$^{-1}$, label: AO-5-30-flt-fr3): 3375, 2956, 2932, 2871, 1602, 1435, 1381, 1364, 1301, 1156, 1127, 868, 756.  HR-EI MS (AO-5-20-ptlc): *m/z* ion type (%RA for *m/z* = 480–490): 488.4131 [M]$^+$ (100%, 0.1 ppm for $^{12}C_{34}{}^1H_{52}{}^{14}N_2$).

**Representative Preparations of Aminyl Diradical 10.**
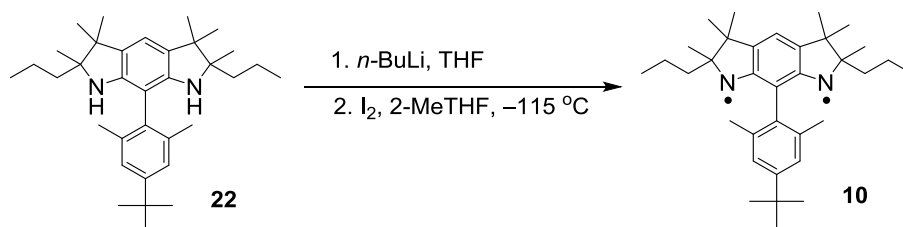


**Table 1.10.** Summary of preparation of aminyl diradical **10**

| Run | SM (mg/μmol) | n-BuLi (μL/μmol) | Conditions for dianion (°C, h) | Comments |
|-----|-----|-----|-----|-----|
| AO552 | 0.62/1.27 | 18/2.66 | −50 °C, 1 h; −30 °C, 1 h | Mono and diradical |
| AO562 | 0.35/0.72 | 11/1.57 | −20 °C, 4 h | No diradical |
| AO565 | 0.68/1.39 | 22/3.20 | −20 °C, 2 h | No diradical |
| AO569 | 0.68/1.39 | 23/3.34 | −70 °C, 3 h | No diradical |
| AO572 | 0.63/1.29 | 19/2.84 | −50 °C, 2 h | Trace of diradical |
| AO574 | 0.60/1.23 | 18/2.70 | −30 °C, 50 min | Mono and diradical, temp persistence |
| AO915 | 0.41/0.84 | 14/2.01 | −40 °C, 1 h;  ; −30 °C, 1 h | Sparteine soln 4.8 eq |

**Aminyl Diradical 10: EPR Spectra in 2-MeTHF (Figure C24); label: AO552.**

4-*tert*-Butyl-2,6-dimethylphenyldiamine **22** (AO-5-30-flt-fr3, MW = 488.8, 0.62 mg, 1.27 μmol) was placed into an EPR sample tube (5-mm quartz tube) and evacuated at 50 °C for overnight then 130 °C for overnight.  THF (0.1 mL, 8-mm height) was added to the vessel by vacuum transfer, and then stirred for 20 min at −30 °C.  *n*-BuLi (0.146 M, 19 μL, 2.66 μmol, 2.1 equiv) was added to produce the orange homogeneous solution.  After stirring at −50 °C for 1 h and at −30 °C for 1 h, the orange mixture was concentrated at −40 °C.  2-MeTHF (~0.2 mL) was added to the reaction mixture by vacuum transfer.  The orange mixture was stirred at −100 °C for 5 min.

The reaction mixture was immersed in liquid nitrogen; subsequently, iodine (99.999%, ultra dry, Alfa) was vacuum transferred (for 8 s) to the sample tube wall, just above the reaction mixture. Iodine was mixed into the reaction mixture at −115 °C, and then the dark green solution was shaken at −115 °C for 1 h. The resultant light brown solution was stored in liquid nitrogen; EPR spectra were obtained at 133 K (label: AO552r1/r2) as illustrated in Figure C24 in Appendix C.

The sample was attached to vacuum line and kept at room temperature for overnight, exclusion of light, and then it was exposed to air. The sample was filtered through 3% deactivated silica (3% diethyl ether in pentane) and evaporated *in vacuo*. ^{1}H NMR spectrum (500 MHz, chloroform-*d*, label: AO-5-52-flt): aromatic region, $\delta = 7.079$ (s, 2H), 6.571 (s, 1H) showed a starting material as a major product (Figure C7).

**Aminyl Diradical 10: Persistence in 2-MeTHF by EPR Spectroscopic Monitoring (Figures C25 in Appendix C, label: AO574).**

4-*tert*-Butyl-2,6-dimethylphenyldiamine **22** (AO-5-30-flt-fr3, MW = 488.8, 0.60 mg, 1.23 μmol) was put into an EPR sample tube (5-mm quartz tube) and evacuated at 50 °C for overnight then at 130 °C for 3 h. THF (0.1 mL, 8-mm height) was added to the vessel by vacuum transfer, and then stirred for 15 min at −30 °C. *n*-BuLi (0.148 M, 18 μL, 2.70 μmol, 2.2 equiv) was added to produce the orange homogeneous solution. After stirring for 50 min at −30 °C, the dark yellow mixture was concentrated at −40 °C. 2-MeTHF (~0.1 mL) was added to the reaction mixture by vacuum transfer, and then stirred 5 min at −100 °C.

The reaction mixture was immersed in liquid nitrogen; subsequently, iodine was vacuum transferred (for 8 s) to the sample tube wall, just above the reaction mixture. Iodine

was mixed into the reaction mixture at −115 °C, and then the yellow solution was stirred for 40 min at −115 °C.  The resultant yellow solution was stored in liquid nitrogen; EPR spectra obtained at 133 K showed only monoradical (label: AO574r1).

Then, the sample tube was re-attached to the vacuum line, and an additional vacuum transfer of iodine (for 8 s) was carried out, with mixing at −115 °C.  The resultant brown solution was mixed for additional 15 min at −115 °C, and then another set of EPR spectra was obtained at 132–134 K (label: AO574r2/r3).

The sample was mixed at −115 °C for additional 1 h, and then another set of EPR spectra was obtained at 136 K (label: AO574r9/r10).  The sample was kept at −78 °C for 10 min, and then EPR spectra at 133 K were taken (label: AO574r14/r15) as illustrated in Figure C28.  The sample was then kept at −30 °C for 15 min, 15 min (30 min total) and 30 min (60 min total), respectively and then EPR spectra at 133 K were taken (label: AO574r16/r17/r22, as illustrated in Figure C25). The sample was attached to vacuum line and kept at room temperature for overnight, with exclusion of light, and then it was exposed to air.  The sample was filtered through 3% deactivated silica (3% diethyl ether in pentane) and evaporated *in vacuo*. $^1$H NMR spectrum (500 MHz, chloroform-*d*, label: AO-5-74-flt): (aromatic region, $\delta$ = 7.079 (s, 2H), 6.571 (s, 1H)) showed a starting material (Figure C7). **Aminyl Diradical 10: EPR Spectra in 2-MeTHF (Figure C26 in Appendix C); label: AO915.**

4-*tert*-Butyl-2,6-dimethylphenyldiamine **22** (AO-5-30-2, MW = 488.8, 0.41 mg, 0.84 μmol) was placed into custom-made SQUID sample tube (5-mm O.D. EPR quartz tube with a thin bottom ~6 cm from the end of the tube) and evacuated at 70 °C for overnight then 120 °C for overnight.  THF (0.1 mL, 8-mm height) was added to the vessel

by vacuum transfer, and then stirred at –30 °C for 15 min.  Under argon flow, a solution of spartine (0.2 M) in THF was added.  Then, *n*-BuLi (0.146 M, 14 µL, 2.01 µmol, 2.4 equiv) was added to produce the orange homogeneous solution.  After stirring at –40 °C for 1 h and at –30 °C for 1 h, the orange mixture was concentrated at –40 °C.  THF (~0.1 mL) was added to the concentrated reaction mixture by vacuum transfer, and then the reaction mixture was stirred briefly at –30 °C.  This sequence of solvent removal under vacuum, followed by addition of THF by vacuum transfer was repeated for additional 2 times (total of 3 times).  Finally, 2-MeTHF (~0.1 mL) was added to the reaction mixture by vacuum transfer.

The reaction mixture was immersed in liquid nitrogen; subsequently, iodine (99.999%, ultra dry, Alfa) was vacuum transferred (for 12 s) to the sample tube wall, just above the reaction mixture.  Iodine was mixed into the reaction mixture at –115 °C, and then the red-brown solution was shaken at –115 °C for 2 h.  The resultant solution was stored in liquid nitrogen; EPR spectra were obtained at 132 K (label: AO915r1/r2) as illustrated in Figure C26.

The sample was annealed at –30 °C for 10 and 20 min.  EPR spectra were obtained after each annealing at 132 K (label: AO915r5-r7) as illustrated in Figure C26.  Finally, the sample was attached to vacuum line and kept at room temperature for 6 d, exclusion of light, and then it was exposed to air.  The brown solution was evaporated under $N_2$ flow and evacuated under high vacuum for overnight.  ^{1}H NMR (500 MHz, chloroform-*d*, label: AO-9-15-crd) spectrum showed a complicated spectra of unidentified mixtures.

### 1.4.3. Syntheses of 1,3-dibromo-4,6-diaminobenzene, 1,3-dibromo-4,6-bis(acetamido)benzene, compounds 31, 30, 32, 33, 29, 28 and aminyl diradical 12

**1,3-Dibromo-4,6-diaminobenzene.**
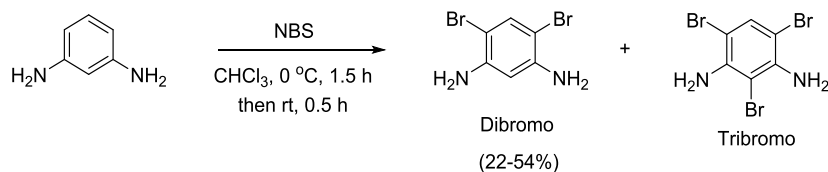


| Run | SM (g/mmol) | NBS (g/mmol) | Yield of dibromo compound (g/%) | Yield of tribromo (g/%) | TM label |
|---|---|---|---|---|---|
| AO-6-24 | 2.00/18.5 | 6.75/37.9 | 2.16/44 | 3.47/54 | AO-6-24-di |
| BDE-1-04 | 2.11/19.5 | 6.95/39.0 | 2.33/35 | 1.76/34 | BDE-1-04-di |
| BDE-1-11 | 17.3/160 | 57.3/178 | 9.27/22 | 22.6/41 | BDE-1-11-di |
| BDE-1-25 | 0.515/4.77 | 1.70/9.53 | 8.07/54 | 5.63/29 | BDE-1-32-di |
| BDE-1-26 | 0.514/4.75 | 1.35/7.60 | | | |
| BDE-1-32 | 6.06/56.1 | 19.8/111 | | | |
| BDE-1-46 | 20.2/189 | 66.3/372 | 13.7/28 | 18.6/29 | BDE-1-46-di |

1,3-Phenylenediamine was dissolved in 40 mL of chloroform in round bottom flask with magnetic stir bar to produce a light brown clear solution. The solution was cooled to 0 °C and *N*-bromosuccinimide (NBS) was slowly added. The reaction was stirred at 0 °C for 1.5 h and at room temperature for 30 min to produce a cloudy dark brown solution. The reaction mixture was washed with water ($2 \times 30$ mL) and brine ($2 \times 30$ mL). The combined organic phase was dried over $Na_2SO_4$ and evaporated *in vacuo*. The crude mixture was purified by flash column chromatography (silica gel, dichloromethane) to give the corresponding product (2.1571 g, 44%, label: AO-6-24-di) as a colorless crystal. $R_f = 0.44$ (dichloromethane). M.p. 133-135 °C; lit.[82] 133-135 °C. $^1$H NMR (600 MHz, dimethyl sulfoxide-$d_6$, label: AO-6-24-di): $\delta = 7.228$ (s, 1H), 6.246 (s, 1H), 5.143 (s, 1H); lit.[82] $^1$H NMR (50 MHz, dimethylsulfoxide-$d_6$): $\delta = 7.22$, 6.24 (s, 2H, *aryl*-C*H*), 5.09 (bs, 4H, N*H*$_2$)

ppm. $^{13}$C NMR (150 MHz, dimethyl sulfoxide-$d_6$, label: AO-6-24-di): $\delta$= 145.69, 133.63, 100.57, 94.82; lit.[82] $^{13}$C{1H} NMR (75 MHz, dimethylsulfoxide-$d_6$): $\delta$ = 145.6, 133.6, 100.6, 94.9 ppm). IR (cm$^{-1}$, label: AO-6-24-di): 3420, 3410, 3329, 3026, 1620, 1487, 1415, 1266, 1036, 872, 825, 689, 658, 633, 591. HR-EI MS (AO-6-24-di): $m/z$ ion type (%RA for $m/z$ = 260-270): 265.8897 [M]$^+$ (100%, 7.4 ppm for $^{12}C_6{}^1H_6{}^{14}N_2{}^{79}Br_1{}^{81}Br_1$).

**1,3-Dibromo-4,6-bis(acetamido)benzene.**
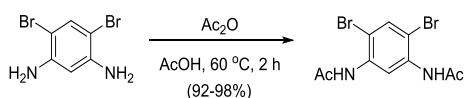


| Run | SM (g/mmol) | Ac$_2$O (mL/mmol) | Yield (g/%) | TM label |
|---|---|---|---|---|
| AO-5-91 | 0.963/3.62 | 1.0/10.9 | 1.21/95 | AO-5-91-crd |
| AO-6-33 | 2.16/8.11 | 2.3/24.3 | 2.77/98 | AO-6-33-crd |
| BDE-1-08 | 1.20/4.53 | 1.4/13.6 | 1.46/92 | BDE-1-08-crd |
| BDE-1-19 | 11.1/41.9 | 12.8/126 | 14.3/98 | BDE-1-19-crd |

1,3-Dibromo-4,6-diaminobenzene (AO-6-24-di, MW 265.93, 2.1571 g, 8.11 mmol, 1 equiv) was weighed and transferred to a 25-mL round bottom flask equipped with magnetic stir bar. Acetic acid was added to produce a cloudy solution. Acetic acid anhydride was added dropwise to the reaction to produce a clear solution for a very short time and then a cloudy solution was observed. The milky solution was stirred at 60 °C for 2 h. After 5 mL of water was added, the crude reaction was filtered and washed with cold water (5 × 25 mL) through the vacuum filtration with filter funnel with fritted disc to give 1,3-dibromo-4,6-bis(acetamido)benzene (2.7650 g, 98%, label: AO-6-33-crd) as a white powder. M.p. 244-246 °C. $^1$H NMR (600 MHz, dimethyl sulfoxide-$d_6$, AO-5-91-flt): $\delta$= 9.516 (s, 2H), 7.939 (s, 1H), 7.880 (s, 1H), 2.070 (s, 6H); lit.[83] $^1$H NMR (200 MHz, dimethylsulfoxide-$d_6$): $\delta$ = 9.52 (br, 2H, NH), 7.94, 7.88 (s, 2H, aryl-CH), 2.07 (s, 6H,

CH$_3$).  $^{13}$C NMR (150 MHz, dimethyl sulfoxide-$d_6$, AO-5-91-flt):  $\delta =$ 168.74, 136.10, 135.11, 124.39, 114.21, 23.36; lit.[83] $^{13}$C NMR (75 MHz, dimethylsulfoxide-$d_6$):  $\delta =$ 168.7 (C=O), 136.1, 135.0, 124.3, 114.2 (aryl-CH), 23.3 (CH$_3$) ppm.  IR (cm$^{-1}$, label: AO-5-91-flt): 3220, 3003, 2900, 1661, 1573, 1517, 1459, 1380, 1291, 1273, 1252, 1060, 1028, 878, 731, 704.  HR-ESI MS (0.05% NaOAc in MeOH/H$_2$O (3:1), AO-5-91-flt): $m/z$ ion type (%RA for $m/z$ = 370-377): 372.8978 [M+Na]$^+$ (100%, $-2.2$ ppm for $^{12}$C$_{10}^{1}$H$_{10}^{14}$N$_2^{16}$O$_2^{23}$Na$_1^{79}$Br$_1^{81}$Br$_1$).

## Sonogashira coupling product 31.
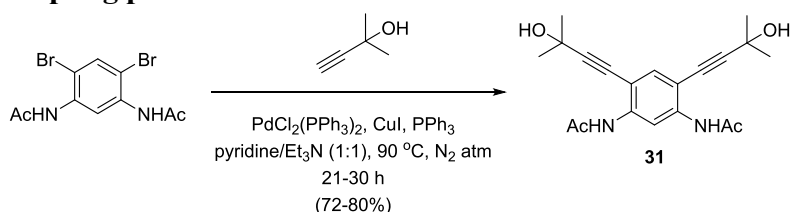


| Run | Dibromo (g/ mmol) | 2-Methyl-3-butyn-2-ol (mL/mmol) | PdCl$_2$(PPh$_3$)$_2$ (mg/μmol) | CuI (mg/μmol) | PPh$_3$ (mg/mmol) | Reaction time (h) | Yield (mg/%)$^a$ | TM label |
|---|---|---|---|---|---|---|---|---|
| AO-6-39 | 0.203/0.579 | 0.17/1.74 | 40.6/57.9 | 11.0/57.9 | 151.9/0.579 | 30 | 165.0/80 | AO-6-39-crd |
| AO-6-43 | 0.202/0.576 | 0.17/1.73 | 40.4/57.6 | 11.0/57.6 | 151.1/0.576 | 21 | 152.0/74 | AO-6-43-crd |
| AO-6-44 | 0.302/0.863 | 0.25/2.59 | 60.6/86.3 | 16.4/86.3 | 226.4/0.863 | 21 | 226.2/74 | AO-6-44-crd |
| AO-6-50 | 0.300/0.858 | 0.25/2.57 | 60.2/85.8 | 16.3/85.8 | 225.0/0.858 | 24 | 231.3/76 | AO-6-50-crd |
| AO-8-57 | 0.401/1.14 | 0.34/3.43 | 80.0/114 | 21.7/114 | 300.1/1.14 | 24 | 285.4/72 | AO-8-57-flt |
| BDE-1-21 | 0.514/1.47 | 0.43/4.40 | 103/146 | 27.9/146 | 385/1.15 | 24 | 400.0/76 | BDE-1-21-flt |
| BDE-1-40 | 0.998/2.85 | 0.72/8.56 | 200/285 | 54.3/285 | 748/2.85 | 24 | 788.1/78 | BDE-1-21-flt |

$^a$ $^1$H NMR spectra of desired product showed the presence of 17-22% of pyridine.  The amount and % yield of product **31** were calculated by subtracting the amount of pyridine.

Our procedure follows previous reports on preparation of 2-(3′-hydroxy-propynyl)aniline.[60]  1,3-Dibromo-4,6-*bis*(acetamido)benzene (AO-6-33-flt, MW 350.01, 0.2027 g, 0.579 mmol, 1 equiv) was weighed, transferred to Schlenk vessel equipped with magnetic stir bar and evacuated under high vacuum for 1 h.  A solution of Et$_3$N/pyridine

(1:1, 0.1 M) was bubbled with nitrogen gas for 10 min. The solution was added to the reaction Schlenk under nitrogen atm. 2-Methyl-3-butyn-2-ol (MW 84.12, 0.17 mL, 1.74 mmol, 3 equiv) was added and the solution was stirred at room temperature for 10 min. PPh$_3$ (MW 262.29, 0.1519 g, 0.579 mmol, 1 equiv), CuI (MW 190.45, 11.0 mg, 0.0579 mmol, 0.1 equiv) and PdCl$_2$(PPh$_3$)$_2$ (MW 701.89, 40.6 mg, 0.0579 mmol, 0.1 equiv) were weighed and added to the reaction Schlenk vessel under nitrogen flow to produce a heterogeneous yellow solution. The reaction was stirred for 30 h at 90 °C, exclusion of light. The heterogeneous orange solution was cooled down to room temperature, filtered through a Celite plug with ethyl acetate. The filtrate was evaporated under reduced pressure. A small amount of heptane was added and evaporated in vacuo to give a light yellow powder. The powder was washed with dichloromethane (2 × 5 mL) to provide diamine **31** (165.0 mg, 80%, label: AO-6-39-crd) as a light yellow powder. M.p. 210–212 °C (under air, decomposed to deep orange liquid). $^1$H NMR (600 MHz, dimethyl sulfoxide-$d_6$, label: AO-6-50-flt): $\delta$ = 9.031 (s, 2H), 8.398 (s, 1H), 7.327 (s, 1H), 5.523 (s, 2H), 2.106 (s, 6H), 1.484 (s, 12H). $^{13}$C NMR (150 MHz, dimethyl sulfoxide-$d_6$, label: AO-6-50-flt): $\delta$ = 168.37, 139.14, 134.13, 134.05, 116.13, 110.68, 101.78, 75.77, 63.85, 23.81. IR (cm$^{-1}$, label: AO-6-50-flt): 3346, 3232, 2978, 1664, 1581, 1539, 1505, 1413, 1361, 1263, 1162, 956, 890, 689. HR–ESI MS (0.05% NaOAc in MeOH/H$_2$O (3:1), label: AO-6-50-flt): $m/z$ ion type (%RA for $m/z$ = 370-380): 379.1616 [M+Na]$^+$ (100%, –4.7 ppm for $^{12}$C$_{10}$$^1$H$_{24}$$^{14}$N$_2$$^{16}$O$_4$$^{23}$Na$_1$).

**Diketone-diamine 30.**
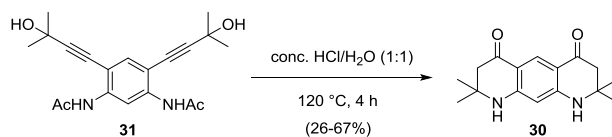


| Run | SM (g/mmol) | Yield (mg/%) | TM label |
|---|---|---|---|
| AO-5-90 | n.a. | n.a. | AO-5-90-3 |
| AO-5-93 | 0.0535/0.150 | 16.1/39 | AO-5-93-wsh2 |
| AO-6-37 | 0.165/0.463 | 33.0/26 | AO-6-37-crd |
| AO-6-51 | 0.152/0.426 | 49.5/43 | AO-6-51-crd |
| AO-6-53 | 0.226/0.635 | 52.8/31 | AO-6-53-crd |
| AO-6-54 | 0.231/0.649 | 88.7/50 | AO-6-54-crd |
| AO-8-59 | 0.275/0.772 | 92.5/44 | AO-8-59-flt |
| BDE-1-41 | 0.400/1.12 | 185/67 | BDE-1-41-flt |
| BDE-1-59 | 3.86/10.8 | 1455/49 | BDE-1-59-flt |

Our procedure follows previous reports on preparation of 2,2-dimethyl-2,3-dihydro-1*H*-quinolin-4-one.[60]  Diamine **31** (AO-6-50-crd, MW 356.42, 0.231 g, 0.649 mmol, 1 equiv) was weighed and transferred to 25 mL round bottom flask with magnetic stir bar.  A solution of conc. HCl and water (1:1) was added to the flask to give a cloudy orange solution.  The reaction was stirred under reflux for 4 h to produce a clear deep orange solution.  The reaction mixture was cooled down to room temperature, basified to pH 11 with 10% solution of sodium hydroxide and extracted with ethyl acetate (3 × 20 mL).  The combined organic layer was dried over $MgSO_4$, evaporated in vacuo, and then evacuated for overnight under high vacuum to give diketone-diamine **30** (88.7 mg, 50%, label: AO-6-54-crd) as a brown powder.  M.p. 150 °C (under air, decomposed to black solid).  $^1$H NMR (400 MHz, dimethyl sulfoxide-$d_6$, label: AO-6-54-crd):  $\delta = 7.981$ (s, 1H), 7.028 (s, 2H), 5.803 (s, 1H), 2.388 (s, 4H), 1.192 (s, 12H); unidentified impurities:  $\delta =$ 8.102, 7.544, 6.496, 4.015 and 1.982 ppm with a relative integration approximately 5

mol%.  $^{13}$C NMR (100 MHz, dimethyl sulfoxide-$d_6$, label: AO-6-54-crd):  $\delta$ = 191.34, 154.34, 127.79, 109.67, 94.90, 52.16, 49.94, 27.47.  IR (cm$^{-1}$, label: AO-5-93-3-sld): 3329, 3318, 2966, 2875, 1646, 1601, 1536, 1278.  HR–ESI MS (0.05% NaOAc in MeOH/H$_2$O (3:1), label: AO-6-37-rsd): *m/z* ion type (%RA for *m/z* = 284-306): 295.1411 [M+Na]$^+$ (100%, −3.9 ppm for $^{12}C_{16}{}^{1}H_{20}{}^{14}N_{2}{}^{16}O_{2}{}^{23}Na_{1}$).

**Bis-(*gem*-diallyl)-diamine 32.**
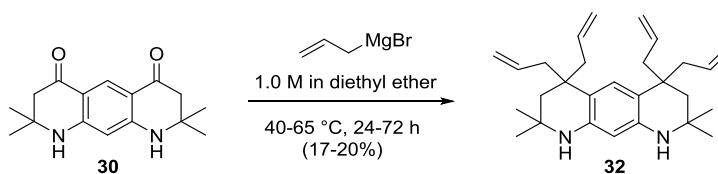


| Run | SM (mg/µmol) | Allylmagnesium bromide (mL/mmol) | Reaction time (d) | Temperature (°C) | Yield (mg/%) | TM label |
|---|---|---|---|---|---|---|
| AO-8-05 | 24.0/87.5 | 1.75/1.75 | 0.5 | 22 | 3.6/10 | AO-8-05-ptlc-fr3 |
| AO-8-48 | 10.6/38.6 | 0.78/0.78 | 7 | 22 | 1.6/10 | AO-8-48-fr2 |
| AO-8-56 | 96.0/350 | 7.0/7.0 | 4 | 22 | 10.8/8 | AO-8-56-col |
| AO-8-62 | 87.5/319 | 6.4/6.4 | 3 | 22 | 8.6/7 | AO-8-62-ptlc |
| Optimized conditions | | | | | | |
| AO-8-95 | 105.0/383 | 11.5/11.5 | 1 | 40 | 26.0/17 | AO-8-95-fr1 |
| AO-9-08 | 450.0/1640 | 33.0/32.8 | 3 | 40 | 131.0/20 | AO-9-08-2 |
| AO-9-25 | 400.2/1460 | 30.0/29.2 | 3 | 65 | 102.2/17 | AO-9-25-fr2 |
| AO-9-26 | 200.0/729 | 14.6/14.6 | 3 | 65 | 52.9/18 | AO-9-26-fr2 |

Diketone-diamine **30** (BDE-1-59-flt, MW 274.34, 450.0 mg, 1.64 mmol, 1 equiv) was evacuated in a Schlenk vessel under high vacuum for overnight.  Allylmagnesium bromide (1.0 M in ether, 33 mL, 32.8 mmol, 20 equiv) was added to the Schlenk to produce a purple color solution.  After 5 min of stirring, the orange solution was observed.  The reaction was stirred at 40 °C for 72 h.  The crude reaction was diluted with diethyl ether (20 mL), and then methanol (1 mL) was added dropwise to the reaction at 0 °C.  The crude was extracted with water (2 × 50 mL), NH$_4$Cl solution (1 × 50 mL) and brine (1 × 50 mL). The combined organic solvent was dried over Na$_2$SO$_4$ and evaporated in vacuo.  The crude product was evacuated on high vacuum for overnight.  The crude was purified by column

chromatography (30% diethyl ether in pentane) to give *gem*-bis(diallyl)diamine **32** (131.0

mg, 20%, label: AO-9-08-2) as sticky dark yellow oil.   $R_f$ = 0.29 (30% diethyl

ether/pentane, 3% deactivated TLC).   $^1$H NMR (600 MHz, acetone-$d_6$, label: AO-8-62-

ptlc):  $\delta$ = 6.948 (s, 1H), 5.770-5.684 (m, 5H), 5.028-4.979 (m, 8H), 4.143 (br, 2H), 2.490-

2.389 (m, 8H), 1.679 (s, 4H), 1.188 (s, 12H).   $^{13}$C NMR (150 MHz, acetone-$d_6$, label: AO-

8-62-ptlc):  $\delta$ =144.38, 137.14, 126.32, 117.46, 117.43, 101.36, 49.83, 46.98, 43.90, 38.67,

31.43.   IR (cm$^{-1}$, label: AO-8-62-ptlc): 3363, 3072, 2972, 2956, 2922, 2859, 1636, 1620,

1511, 1438, 1381, 1363, 1315, 1285, 1234, 1189, 1176, 996, 910, 824.   HR–ESI MS (0.1%

HCOOH in MeOH, label: AO-7-98-ptlc2): *m/z* ion type (%RA for *m/z* = 400–410):

405.3262 [M+H]$^+$ (100%, −1.9 ppm for $^{12}C_{28}{}^1H_{41}{}^{14}N_2$).

**gem-Bis(di-*n*-propyl)diamine 33**.
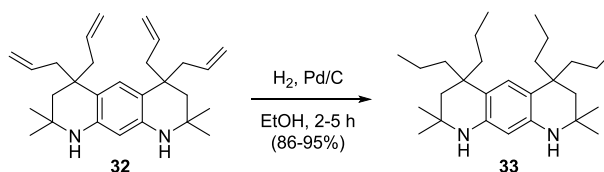


| Run | SM (mg/μmol) | Pd/C (mg/μmol) | Reaction time (d) | Yield (mg/%) | TM label |
|---|---|---|---|---|---|
| AO-8-52 | 1.5/3.71 | 0.4/0.371 | 5 | 1.46/95 | AO-8-52-crd |
| AO-8-55 | 3.5/8.65 | 1.0/0.865 | 4 | 3.4/95 | AO-8-55-crd |
| AO-8-65 | 19.1/47.2 | 5.0/4.72 | 3 | 16.7/86 | AO-8-65-2 |
| AO-8-97 | 26.0/64.3 | 6.8/6.43 | 2 | 25.3/95 | AO-8-97-flt |
| AO-8-98 | 58.2/144 | 15.3/14.4 | 2 | 56.1/94 | AO-8-98-flt |
| AO-9-09 | 125.0/309 | 32.9/30.9 | 2 | 120.8/95 | AO-9-09-crd |
| AO-9-27 | 100.0/247 | 26.3/24.7 | 2 | 92.8/91 | AO-9-27-crd |

A clear yellow solution of *gem*-bis(diallyl)diamine **32** (AO-8-95-fr2, MW 404.63,

26.0 mg, 0.0643 mmol, 1 equiv) in 2 mL of ethanol was transferred into a Schlenk vessel

equipped with magnetic stirring bar.  Pd/C was added into the Schlenk vessel to produce a

heterogeneous solution.  The Schlenk was evacuated briefly by diaphragm pump and

charged with hydrogen gas.  The reaction was stirred at room temperature until completion.

The crude was filtered through a Celite plug with ethyl acetate, evaporated under reduced pressure and evacuated on high vacuum for overnight to produce *gem*-bis(di-*n*-propyl)diamine **33** (25.3 mg, 95%, label: AO-8-97-crd) as a light yellow solid. The crude product was washed with a small portion (3-4 drops) of methanol (3 times) to yield *gem*-bis(di-*n*-propyl)diamine **33** as a white solid (label: AO-8-98-cmb-sld). M.p. 91–92 °C (under air). $R_f$ = 0.30 (30% diethyl ether/pentane, 3% deactivated TLC). $^1$H NMR (400 MHz, acetone-$d_6$, label: AO-8-98-cmb-sld): $\delta$ = 6.763 (s, 1H), 5.696 (s, 1H), 4.007 (br, 2H), 1.655 (s, 4H), 1.610-1.556 (m, 8H), 1.263-1.202 (m, 8H), 1.176 (s, 12H), 0.847 (t, $J$ = 7.2 Hz, 12H). $^{13}$C NMR (100 MHz, acetone-$d_6$, label: AO-8-98-cmb-sld): $\delta$ = 144.04, 125.59, 118.84, 101.39, 49.91, 45.62, 44.44, 38.84, 31.52, 18.14, 15.29. IR (ZnSe, cm$^{-1}$, label: AO-8-65-2): 3350, 2955, 2931, 2870, 1622, 1510, 1456, 1380, 1362, 1315, 1230, 1190, 822. HR–ESI MS (MeOH:H$_2$O, 3:1, label: AO-8-52-crd): *m/z* ion type (%RA for *m/z* = 410–420): 413.3888 [M+H]$^+$ (100%, −1.9 ppm for $^{12}$C$_{28}$$^1$H$_{49}$$^{14}$N$_2$).

**Bromodiamine 29**.
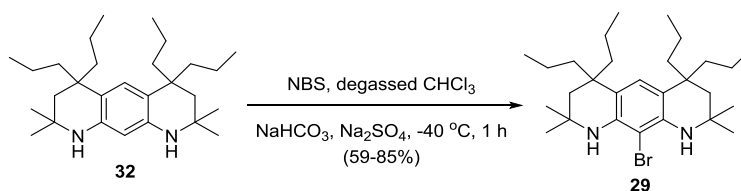


| Run | SM (mg, μmol) | NBS (mg, μmol) | Yield (mg, %) | TM label |
|---|---|---|---|---|
| AO-8-68 | 3.8/9.20 | 1.8/9.67 | 2.8/62 | AO-8-68-up |
| AO-8-69 | 11.2/27.1 | 4.8/27.1 | 7.9/59 | AO-8-69-up |
| AO-9-11 | 30.2/73.2 | 14.3/80.5 | 30.5/85 | AO-9-11-flt1 |
| AO-9-29 | 68.8/167 | 32.6/183 | 54.3/66 | AO-9-29-flt |

NBS (MW = 178.0, 14.3 mg, 0.0805 mmol) in degassed chloroform (1 mL) was added dropwise to a solution of *gem*-bis(di-*n*-propyl)diamine **32** (AO-9-09-sld-wsh3, MW = 412.7, 30.2 mg, 0.0732 mmol) with NaHCO$_3$ (MW = 84.6, 74.3 mg, 0.878 mmol) and

anhydrous $Na_2SO_4$ (MW = 142.0, 124.7 mg, 0.878 mmol) in degassed chloroform (3 mL) at –40 °C under $N_2$ atmosphere to produce a heterogeneous orange solution. After stirring at –40 °C for 1 h, excess of $Na_2S_2O_5$ was added and the reaction mixture was allowed to attain room temperature and stirred for 10 min. After the solids were filtered off, the filtrate was concentrated in vacuo to yield the resultant brown oil. The crude product was filtered through a short plug of silica gel and eluted with 30% diethyl ether/pentane to give a brown film. A small portion of MeOH (3 drops) was added to a brown film and evaporated under $N_2$ to give bromodiamine **29** (30.5 mg, 85%, label: AO-9-11-flt1) as a brown semi-solid. $R_f$ = 0.67 (4% diethyl ether/pentane, 3% deactivated TLC). $^1$H NMR (600 MHz, acetone-$d_6$, label: AO-9-11-flt1): $\delta$ = 6.868 (s, 1H), 4.186 (br, 1H), 1.727 (s, 4H), 1.621 (m, 8H), 1.292-1.187 (m, 8H), 1.261 (s, 12H), 0.850 (t, $J$ = 7.2 Hz, 12H); unidentified impurities: $\delta$ = 7.627, 6.950, 5.611, 4.698 and 4.644 ppm with a relative integration approximately 3 mol%. $^{13}$C NMR (100 MHz, acetone-$d_6$, label: AO-9-11-flt1): $\delta$ = 140.28, 124.71, 119.52, 98.38, 50.62, 45.24, 43.98, 39.55, 31.88, 18.13, 15.22. IR (ZnSe, cm$^{-1}$, label: AO-8-61-fr1): 3384, 2955, 2931, 2870, 1612, 1483, 1466, 1425, 1382, 1363, 1290, 1230, 1200, 1182, 1108, 743. HR–ESI MS (MeOH:$H_2O$, 3:1, label: AO-8-61-fr1): $m/z$ ion type (%RA for $m/z$ = 488–497): 490.2903 [M]$^+$ (100%, –4.0 ppm for $^{12}C_{28}{}^1H_{47}{}^{14}N_2{}^{79}Br_1$), 492.2922 [M]$^+$ (80%, 4.0 ppm for $^{12}C_{28}{}^1H_{47}{}^{14}N_2{}^{81}Br_1$).

***tert*-Butylphenyldiamine 28**.
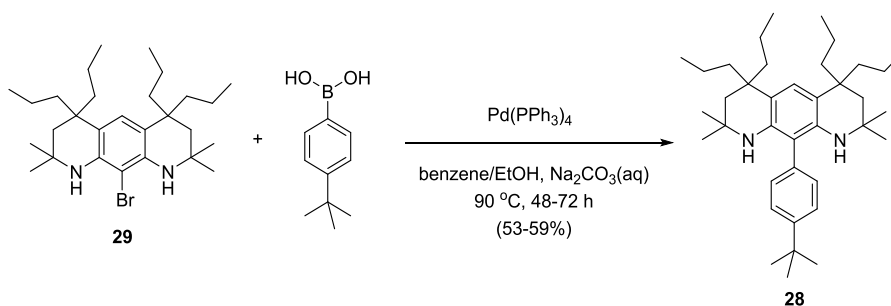


| Run | **29** (mg/µmol) | SM label | *p-t*-Butyl boronic acid (mg/µmol) | Pd(PPh₃)₄ (mg/µmol) | Reaction time (h) | Yield (mg/%) | TM Label |
|---|---|---|---|---|---|---|---|
| AO-8-71 | 4.5/9.15 | AO868/69up | 2.4/13.7 | 1.1/0.92 | 24 | 1.94/39 | AO-8-71-fr3 |
| Optimized conditions | | | | | | | |
| AO-8-74 | 5.7/11.6 | AO868/69dw | 3.1/17.4 | 1.3/1.16 | 48 | 3.45/55 | AO-8-74-fr3 |
| AO-9-21 | 28.5/58.0 | AO911flt1 | 15.5/87.0 | 13.4/11.6 | 72 | 16.9/53 | AO-9-21-sld-wsh |
| AO-9-32 | 54.3/110 | AO929flt | 29.5/165 | 25.4/22.0 | 70 | 35.6/59 | AO-9-32-ptlc |

Bromodiamine **29** (AO-8-68/69dw, MW = 491.6, 5.7 mg, 11.6 µmol) and 4-*tert*-butylphenylboronic acid (MW = 178.0, 3.1 mg, 17.4 µmol, 1.5 equiv) were charged into a Schlenk tube under $N_2$ atmosphere. Pd(PPh₃)₄ (1.3 mg, 1.16 µmol, 10 mol%) was added to the vessel in a glove bag under $N_2$ atmosphere. Benzene (0.5 mL), ethanol (0.15 mL), and aqueous $Na_2CO_3$ (1 M, 0.15 mL) were bubbled by $N_2$ for 10 min and added to the reaction vessel and stirred at 90 °C for 48 h. The reaction mixture was poured into distilled water, and then extracted with benzene. The combined organic layer was washed with 2 M NaOH solution (5 × 4 mL), brine (3 × 4 mL). The combined organic phase was dried over anhydrous $Na_2SO_4$, and then concentrated in vacuo to provide the crude product as a colorless film. Crude mixture was filtered through a short plug of Celite and 3% deactivated silica gel by 10% diethyl ether/pentane. The filtrate was evaporated under reduced pressure and evacuated under high vacuum for overnight. The crude after filtration was purified by PTLC (3% deactivated silica, 2% diethyl ether/pentane) gave the 4-*tert*-butylphenyldiamine **28** as a white solid (3.45 mg, 55%, label: AO-8-74-fr3). $R_f = 0.36$ (3%

diethyl ether/pentane, 3% deactivated TLC). M.p. 120–121 °C (under air). $^1$H NMR (500 MHz, chloroform-*d*, label: AO-9-32-2): $\delta$ = 7.461 (d, *J* = 8.5 Hz, 2H), 7.132 (d, *J* = 8.0 Hz, 2H), 6.806 (s, 1H), 2.988 (br, 2H), 1.664 (s, 4H), 1.627-1.536 (m, 8H), 1.363 (s, 9H), 1.293-1.196 (m, 8H), 1.080 (s, 12H), 0.868 (t, *J* = 7.3 Hz, 12H). $^1$H NMR (400 MHz, acetone-*d*$_6$, label: AO-8-74-fr3): $\delta$ = 7.570 (d, *J* = 8.4 Hz, 2H), 7.125 (d, *J* = 8.4 Hz, 2H), 6.878 (s, 1H), 3.034 (br, 2H), 1.697-1.567 (m, 8H), 1.664 (s, 4H), 1.367 (s, 9H), 1.310-1.217 (m, 8H), 1.059 (s, 12H), 0.869 (t, *J* = 7.2 Hz, 12H). $^1$H NMR (500 MHz, benzene-*d*$_6$, label: AO-9-32-b): $\delta$ = 7.433 (d, *J* = 8.0 Hz, 2H), 7.381 (d, *J* = 8.5 Hz, 2H), 7.161 (s, 1H), 3. 322 (br, 2H, exch. D$_2$O), 1.865-1.739 (m, 8H), 1.689 (s, 4H), 1.445-1.363 (m, 8H), 1.154 (s, 9H), 1.015 (s, 12H), 0.944 (t, *J* = 7.5 Hz, 12H). $^1$H-$^{15}$N HSQC experiment (acetone-*d*$_6$, label: AO-9-32-ptlc): $\delta$ = −287.9 ppm. $^{13}$C NMR (150 MHz, acetone-*d*$_6$, LB = −0.2 Hz, GB = 0.5 Hz, label: AO-8-74-fr3-1): $\delta$ = 151.04, 140.80, 140.77, 134.47, 132.02, 132.01, 127.48, 124.75, 119.28, 119.26, 113.67, 50.33, 50.24, 45.40, 45.38, 44.69, 44.66, 39.29, 35.24, 31.79, 31.75, 18.22, 15.29. $^{13}$C NMR (100 MHz, chloroform-*d*, label: AO-9-32-3): $\delta$ = 149.91, 139.58, 133.31, 131.04, 126.57, 123.89, 118.99, 113.03, 49.71, 44.39, 43.92, 38.42, 34.57, 31.38, 31.37, 17.43, 14.90. IR (cm$^{-1}$, label: AO-9-21-ptlcfr2): 3379, 3084, 3027, 2953, 2930, 2869, 1605, 1476, 1456, 1380, 1361, 1268, 1228, 1201, 1179. HR–ESI MS (MeOH:H$_2$O, 3:1, label: AO-8-71-fr3): *m/z* ion type (%RA for *m/z* = 543–548): 544.4769 [M]$^+$ (100%, 2.3 ppm for $^{12}$C$_{38}$$^1$H$_{60}$$^{14}$N$_2$).
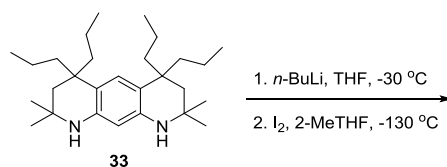
**Attempted preparation of pendant-free aminyl diradical: EPR data in 2-MeTHF (Figure C27, label: AO860).** Bis-(*gem*-di-*n*-propyl)-diamine **33** (AO-8-55-flt, MW = 412.7, 0.41 mg, 0.993 μmol) was placed in the SQUID sample tube (5-mm O.D. EPR quartz tube with a thin bottom ~6 cm from the end of the tube) and evacuated overnight at 55 °C. THF (~0.12 mL, ~10-mm height) was added to the vessel by vacuum transfer, and then stirred for 30 min at −30 °C. *n*-BuLi (0.185 M in hexane, 12 μL, 2.19 μmol, 2.2 equiv) was added to produce very light yellow homogeneous solution. After stirring at −30 °C for 1 h, the reaction mixture was concentrated at −40 °C. THF (~0.12 mL) was added to the concentrated reaction mixture by vacuum transfer, and then the reaction mixture was stirred for 5 min at −40 °C. This sequence of solvent removal under vacuum, followed by addition of THF by vacuum transfer was repeated another two times (total of three times). Finally, 2-MeTHF (~0.1 mL) was added to the reaction mixture by vacuum transfer, and then the reaction mixture (under vacuum) was immersed in liquid nitrogen. Subsequently, iodine was vacuum transferred (for 13 s) to the sample tube wall, just above the reaction mixture. Iodine was mixed into the reaction mixture at −130 °C, and then the yellowish-green solution was stirred at −130 °C for 2 h. The resultant yellowish-green solution was stored in liquid nitrogen; EPR spectra were obtained at 132 K (Figure C27A, label: AO860r1/r2).

Then, the sample tube was re-attached to the vacuum line, and mixed at −115 °C for additional 1 h. The resultant same yellowish-green solution was observed, and then

another set of EPR spectra was obtained at 132 K (label: AO860r7/r8) as illustrated in Figure C27B.

Subsequently, the sample tube was flame sealed. The sample tube was stored in liquid nitrogen and placed in a helium-filled glovebag over the SQUID sample chamber. The sample was then rapidly inserted (over 14 s) into the SQUID sample chamber kept at 10 K, using previously reported protocol.

**Representative Preparations of Aminyl Diradical 11.**
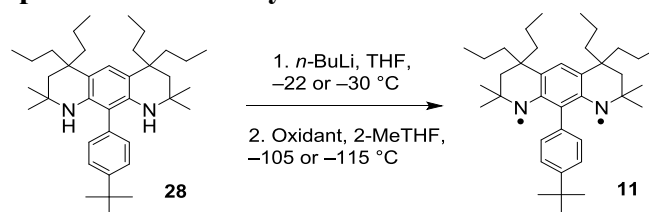


**Table 1.11.** Summary of preparation for aminyl diradical **11**

| run no | label | **28** (mg) | Dianion generation (°C, h) | Oxidants, temperature (°C) | sample type | figures and comments |
|---|---|---|---|---|---|---|
| 1 | AO983 | 1.32 | −30, 5 | I₂, −115 | EPR | **EPR Experiment**: Persistence at 246 and 295 K, followed by the recovery of mixtures, half-life 214 s, di/monoradical 51/49. |
| 2 | AO980 | 0.70 | −30, 5 | I₂, −115 | EPR | **EPR Experiment**: di/monoradical 46/54. |
| 3 | AO988 | 1.05 | −22ᵃ, 6 | I₂, −115 | EPR | **EPR Experiment**: di/monoradical 43/57. |
| 4 | AO943 | 0.83 | −30, 5 | I₂, −115; Cp₂FeBF₄, −105 | EPR | **EPR Experiment**: Figure 1.31, di/monoradical 60/40. |
| 5 | AO936 | 0.85 | −30, 2.5 | I₂, −115 | EPR | **Persistence experiment at 246 and 295 K**: followed by the recovery of mixtures ($^1$H NMR, half-life 246 s, di/monoradical 48/52. |
| 6 | AO876 | 0.88 | −30, 2 | I₂, −115 | EPR | **Reaction with excess I₂** |
| 7 | AO941 | 0.87 | −30, 5 | I₂, −115 | EPR | **Reaction with O₂**: followed by the recovery of mixtures ($^1$H NMR, MS). |
| 8 | AO968 | 0.85 | −30, 3 | I₂, −115 | EPR | **Persistence experiment at 246 and 295 K**: half-life 80 s |
| 9 | AO881 | 0.77 | −30, 2 | I₂, −115 | EPR | 1ˢᵗ and 2ⁿᵈ addition of I₂: Similar EPR spectra showing significant of monoradical impurity. |
| 10 | AO947 | 0.50 | −30, 5 | Cp₂FeBF₄, −105; I₂, −115 | EPR | Addition of Cp₂FeBF₄: no EPR signal, Then followed by I₂: monoradical only. |
| 11 | AO948 | 0.48 | 5 | AgBF₄, −105; I₂, −115 | EPR | Addition of solution of AgBF₄ in THF: no EPR signal, then followed by I₂: di and monoradical. |
| 12 | AO950 | 0.45 | 4 | I₂, −115; Cp₂FeBF₄, −105 | EPR | Addition of I₂ followed by Cp₂FeBF₄ 6.5 equiv): EPR spectra showing significant content of monoradical impurity. |

ᵃ The dianion was prepared in dry ice-CCl₄ bath (−22 °C)

**Aminyl Diradical 11: EPR Data in 2-MeTHF (Figures C28–C29, label: AO943).** 4-*tert*-Butylphenyldiamine **28** (AO-9-21-sld-wsh, MW = 544.9, 0.83 mg, 1.52 μmol) was placed in the EPR sample tube (5-mm O.D. EPR quartz tube) and evacuated overnight at 65 °C then at 110 °C. THF (~0.1 mL, ~8-mm height) was added to the vessel by vacuum transfer, and then stirred for 30 min at −30 °C. *n*-BuLi (0.171 M in hexane, 22 μL, 3.66 μmol, 2.4 equiv) was added to produce initially the yellow homogeneous solution. After stirring at −30 °C for 5 h, the orange reaction mixture was kept in liquid nitrogen for overnight. THF was removed from the orange solution at −50 °C on the next day. 2-MeTHF (~0.08 mL) was then added to the reaction mixture by vacuum transfer, and then the reaction mixture (under vacuum) was stirred at −80 °C for 30 s and immersed in liquid nitrogen. Subsequently, iodine was vacuum transferred (for 14 s) to the sample tube wall, just above the reaction mixture. Iodine was mixed into the reaction mixture at −115 °C, and then the brown solution was stirred at −115 °C for 1.5 h. The resultant brown solution was stored in liquid nitrogen for overnight; EPR spectra were obtained at 132 K on the next day (label: AO943r1/r3, see Figure C28).

Ferrocenium tetrafluoroborate (FeCp$_2$BF$_4$, MW = 272.8, 0.83 mg, 3.04 μmol) was added to the reaction mixture under argon atmosphere at −105 °C. After 5 min, the green solution was observed. The reaction mixture was stirred at −105 °C for 1 h. After obtaining a set of EPR at 132 K (label: AO943r4/r6), the sample was kept at −78 °C for 15 min, resulting in the same green solution. Subsequent EPR spectrum was taken at 132 K (label: AO943r8–r9). FeCp$_2$BF$_4$ (2 equiv) was added for a second time to the reaction mixture at −105 °C. The same green solution was stirred at −105 °C for 1 h. A set of EPR spectra was taken at 132 K (label: AO943r10/r12/r13, see Figure C29). The sample was kept at −

78 °C for 15 min and finally at room temperature (22 °C) for 5 min, EPR spectra at 132 K (label: AO943r14-r15) showed the decrease and disappearance of diradical signal, respectively.

In another 0.45 mg-scale experiments (AO950), EPR spectrum was recorded at 132 K (label: AO950r7) after addition of $I_2$ and 2 portions of $FeCp_2BF_4$ (a total of 6.5 equiv).

In 0.50 mg-scale experiment (AO947) using $FeCp_2BF_4$ as oxidant alone and in 0.48 mg-scale experiment (AO948) using a solution of $AgBF_4$ as oxidant alone, EPR spectra at 132 K are practically undetectable.

**Aminyl Diradical 11: Persistence in 2-MeTHF by EPR Spectroscopic Monitoring (Figures C3–C4, labels: AO983).** 4-*tert*-Butylphenyldiamine **28** (AO-9-21-sld-wsh, MW = 544.9, 1.32 mg, 2.42 μmol) was placed to the bottom of the EPR sample tube and evacuated for overnight at 70 °C using heating tape wrapping the whole EPR sample tube. The next day, the heating tape was raised just above the sample and heated the remaining EPR tube at 110 °C for overnight. THF (~0.1 mL, ~10-mm height) was added to the vessel by vacuum transfer, and then stirred for 30 min at –30 °C. *n*-BuLi (0.261 M in hexane, 22 μL, 5.81 μmol, 2.4 equiv) was added to produce initially the yellow homogeneous solution. After stirring at –30 °C for 5 h, the orange reaction mixture was evaporated at –45 °C then immersed in liquid nitrogen. 2-MeTHF (~0.1 mL) was added to the reaction mixture by vacuum transfer, and then the reaction mixture (under vacuum) was immersed in liquid nitrogen. Subsequently, iodine was vacuum transferred (for 18 s) to the sample tube wall, just above the reaction mixture. Iodine was mixed into the reaction mixture at –115 °C,

and then the green solution was stirred at −115 °C for 1.5 h.  The resultant green solution was stored in liquid nitrogen; EPR spectra were obtained at 132 K (label: AO983r1/r2).

The sample was reattached to vacuum line.  The reaction mixture was diluted by vacuum transferred 2-MeTHF (3.8-cm height, 5.09 mM).  The green solution was mixed at −115°C for 30 min and stored in liquid nitrogen.  EPR spectra of sample were taken at 132 K (label: AO983r5, 6, 9, 10, 13, 14, 17, 18, 21, 22, 25, 26).  For reference, EPR spectra of TEMPONE (1 mM in 2-MeTHF) were taken at 132 K (label: AO983r7, 8, 11, 12, 15, 16, 19, 20, 23, 24, 27, 28).

The sample was annealed at 195 K (−78 °C) for 15 and 30 min (total time) and at 246 K (−27 °C) for 15, 30, 45 and 60 min (total time).  EPR spectra at 132 K were taken after each annealing (labels: AO983r31, 33, 35, 37, 39, 41; Figure C3).  For reference, EPR spectra of TEMPONE (1 mM in 2-MeTHF) were taken at 132 K (labels: AO983r32, 34, 36, 38, 40, 42).  Subsequently, the sample was annealed at 295 K (22 °C) for 1, 2, 3, 4, 5, 6, 7, 8, 10 and 12 min (total time) to produce yellowish green solution.  EPR spectra were taken after each annealing (labels: AO983r43, 45, 47, 49, 51, 53, 55, 57, 59, 61; Figure C4).  For reference, EPR spectra of TEMPONE (1 mM in 2-MeTHF) were taken at 132 K (labels: AO983r44, 46, 48, 50, 52, 54, 56, 58, 60, 62).  Following this experiment, the sample was kept at room temperature for 4 d, and the crude mixture was purified as described in the next section.

**Table 1.12**. Decay kinetics of 5.09 mM aminyl diradical **11** at 295 K

| Sample | | | | | Reference | | |
|---|---|---|---|---|---|---|---|
| EPR filename | Time (s) | Peak height[a] (PH) | PH$_{cor}$ | -ln PH$_{cor}$ | EPR filename | Double integration (DI) | Correction[b] (%) |
| AO983r41 | 0 | 17902.50 | 17902.50 | -9.792695647 | AO983r42 | 4.428E+07 | 100 |
| AO983r43 | 60 | 15315.00 | 15705.83 | -9.661787257 | AO983r44 | 4.541E+07 | 103 |
| AO983r45 | 120 | 13347.00 | 13166.15 | -9.485404143 | AO983r46 | 4.368E+07 | 99 |
| AO983r47 | 180 | 9943.50 | 10217.46 | -9.231853568 | AO983r48 | 4.550E+07 | 103 |
| AO983r49 | 240 | 8936.00 | 8500.10 | -9.04783292 | AO983r50 | 4.212E+07 | 95 |
| AO983r51 | 300 | 5573.00 | 6198.52 | -8.732065047 | AO983r52 | 4.925E+07 | 111 |
| AO983r53 | 360 | 5441.50 | 5618.46 | -8.633812768 | AO983r54 | 4.572E+07 | 103 |
| AO983r55 | 420 | 4478.50 | 4625.15 | -8.439264878 | AO983r56 | 4.573E+07 | 103 |
| AO983r57 | 480 | 4146.00 | 4134.76 | -8.327185587 | AO983r58 | 4.416E+07 | 100 |
| AO983r59 | 600 | 2597.50 | 2714.23 | -7.906265418 | AO983r60 | 4.627E+07 | 104 |
| AO983r61 | 720 | 1710.00 | 1761.75 | -7.474061759 | AO983r62 | 4.562E+07 | 103 |

[a] Peak height for **11** = average of PH at 332.0 and 355.6 mT. [b] Correction for PH$_{cor}$; Correction = (DI/DI$_{(t=0)}$)×100% using double integration of 1 mM TEMPONE.

After annealing the sample (AO-9-83, AO-9-80 and AO-9-88) in the EPR tube at room temperature for 4 d with exclusion of light, the light yellow solution was transferred to a vial and evaporated under N$_2$ flow. The crude was evacuated under high vacuum for overnight. The crude of three experiments was purified by preparative TLC (3% diethyl ether in pentane) to give two fractions. R$_f$ = 0.60, 0.36 for fraction 1 and 2 respectively (3% diethyl ether/pentane). $^1$H NMR (500 MHz, acetone-$d_6$, label: AO-9-88-fr1-cb, Figure C30 (A)) spectrum of the fraction 1: $\delta$ = 7.988 (d, $J$ = 8.0 Hz, 1H), 7.688 (s, 1H), 7.213 (d, $J$ = 8.5 Hz, 1H), 7.054 (s, 1H), 4.557 (s, 2H), 2.135 (s, 2H), 1.870 (s, 2H), 1.817 (s, 6H), 1.755-1.723 (m, 8H), 1.420 (s, 9H), 1.397 (6H), 1.357-1.133 (m, 8H), 0.887 (t, $J$ = 7.0 Hz, 6H), 0.853 (t, $J$ = 7.5 Hz, 6H). Singlets at $\delta$ = 5.109 and 3.303 ppm correspond to unknown imputies. $^1$H-$^{15}$N HSQC experiment (500 MHz, acetone-$d_6$, AO-9-88-fr1-cb): $\delta$ = −287.5 ppm. $^1$H NMR (700 MHz, chloroform-$d$, label: AO-9-88-fr1-cb2, Figure C30 (B))

spectrum of the fraction 1: $\delta = 7.850$ (d, $J = 8.4$ Hz, 1H), 7.619 (d, $J = 1.4$ Hz, 1H), 7.229

(dd, $J = 1.4$, 8.4 Hz, 1H), 6.959 (s, 1H), 4.200 (s, 2H), 2.086 (s, 2H), 1.835 (s, 2H), 1.796

(s, 6H), 1.747-1.650 (m, 8H), 1.430 (s, 9H), 1.395-1.115 (m, 8H), 1.348 (6H), 0.872 (t, $J$

$= 7.0$ Hz, 6H), 0.848 (t, $J = 7.0$ Hz, 6H).  Singlets at $\delta = 5.119$ and 3.353 ppm correspond

to unknown imputies.  Fraction 1 corresponds to by-product **43**.  ^{1}H NMR (400 MHz,

acetone-$d_6$, label: AO-9-88-fr2-cb, Figure C30 (C)) spectrum of the fraction 3 corresponds

to diamine **28**.

**Aminyl Diradical 11: Persistence in 2-MeTHF by EPR Spectroscopic Monitoring (Figure C31, C5, labels: AO936).**  4-*tert*-Butylphenyldiamine **28** (AO-9-21-sld-wsh, MW = 544.9, 0.85 mg, 1.56 µmol) was placed in the EPR sample tube and evacuated overnight at 65 °C and then at 110 °C.  THF (~0.1 mL, ~10-mm height) was added to the vessel by vacuum transfer, and then stirred for 30 min at –30 °C.  *n*-BuLi (0.143 M in hexane, 27 µL, 3.74 µmol, 2.4 equiv) was added to produce initially the yellow homogeneous solution.  After stirring at –30 °C for 2.5 h, the orange reaction mixture was evacuated at –50 °C then immersed in liquid nitrogen.  2-MeTHF (~0.1 mL) was added to the reaction mixture by vacuum transfer, and then the reaction mixture (under vacuum) was immersed in liquid nitrogen.  Subsequently, iodine was vacuum transferred (for 14 s) to the sample tube wall, just above the reaction mixture.  Iodine was mixed into the reaction mixture at –115 °C, and then the greenish–brown solution was stirred at –115 °C for 2 h.  The resultant greenish-brown solution was stored in liquid nitrogen; EPR spectra were obtained at 132 K (label: AO936r1–r3).

The sample was annealed to –78 °C for 15 min.  The same green solution was observed.  After obtaining a set of EPR spectra at 132 K (label: AO936r5–r7), the reaction mixture

was diluted by vacuum transferred 2-MeTHF (4.4-cm-height, 2.84 mM). The yellowish green solution was mixed at –115°C for 30 min and stored in liquid nitrogen. EPR spectrum at 132 K was taken (label: AO936r11). The sample was annealed at –27 °C for 15, 30, 45, 60, 90 and 120 min. EPR spectra at 132 K were taken after each annealing (labels: AO936r14, 16, 18, 20, 22, r24; Figure C31). For reference, EPR spectra of TEMPOL (1.0 mM in 2-MeTHF) were taken at 132 K (labels: AO936r12, 15, 17, 19, 21, 23, 25). Subsequently, the sample was annealed at 22 °C for 4, 6, 8, 10, 12, 14, 16, 20 min to produce brownish green solution. EPR spectra were taken after each annealing (labels: AO936r29, 31, 33, 35, 37, 39, 41, 43; Figure C5). EPR spectra of TEMPOL (1.0 mM in 2-MeTHF) were taken at 132 K (labels: AO936r27, 30, 32, 34, 36, 38, 40, 42, 44).

**Table 1.13.** Decay kinetics of 2.84 mM aminyl diradical **11** at 295 K

| Sample | | | | | Reference | | |
|---|---|---|---|---|---|---|---|
| EPR filename | Time (min) | Peak height[a] (PH) | $PH_{cor}$ | -ln $PH_{cor}$ | EPR filename | Double integration (DI) | Correction[b] (%) |
| AO936r28 | 0 | 10778.50 | 10778.50 | -9.2853 | AO936r27 | 4.943E+07 | 100 |
| AO936r29 | 240 | 3637.50 | 3705.20 | -8.2175 | AO936r30 | 5.035E+07 | 102 |
| AO936r31 | 360 | 2447.50 | 2505.43 | -7.8262 | AO936r32 | 5.060E+07 | 102 |
| AO936r33 | 480 | 1789.00 | 1791.53 | -7.4908 | AO936r34 | 4.950E+07 | 100 |
| AO936r35 | 600 | 1273.00 | 1362.36 | -7.2170 | AO936r36 | 5.290E+07 | 107 |
| AO936r37 | 720 | 938.00 | 959.82 | -6.8667 | AO936r38 | 5.058E+07 | 102 |
| AO936r39 | 840 | 709.50 | 704.05 | -6.5568 | AO936r40 | 4.905E+07 | 99 |
| AO936r41 | 960 | 581.50 | 582.79 | -6.3678 | AO936r42 | 4.954E+07 | 100 |
| AO936r43 | 1200 | 308.00 | 317.66 | -5.7610 | AO936r44 | 5.098E+07 | 103 |

[a] Peak height for **11** = average of PH at 332.0 and 355.6 mT. [b] Correction for $PH_{cor}$; Correction = (DI/DI(t=0))×100% using double integration of 1 mM TEMPONE.

The sample was annealing at room temperature for 7 d, with exclusion of light. The light yellow solution was transferred to a vial and evaporated under $N_2$ flow. The crude

was evacuated under high vacuum for overnight. $^1$H NMR spectrum (500 MHz, acetone-$d_6$, label: AO-9-36-crd, Figure C8 (A)) showed a mixture of two major compounds. The crude was purified by preparative TLC under $N_2$ atm (3% diethyl ether in pentane) to give two fractions. $R_f$ = 0.56, 0.33 for fraction 1 and 2 respectively (3% diethyl ether/pentane). $^1$H NMR (500 MHz, acetone-$d_6$, label: AO-9-36-fr1, Figure C8 (B)) spectrum of the fraction 1: (aromatic region, $\delta$ = 7.988 (d, $J$ = 8.0 Hz, 1H), 7.690 (s, 1H), 7.214 (dd, $J$ = 1.0, 8.0 Hz, 1H), 7.053 (s, 1H)) and ESI MS (0.1% HCOOH/MeOH, label: AO-9-36-fr1) which showed $m/z$ 543.8 may corresponded to by-product **43**. $^1$H NMR (500 MHz, acetone-$d_6$, label: AO-9-36-fr2, Figure C8 (C)) spectrum of the fraction 2: (aromatic region, $\delta$ = 7.569 (d, $J$ = 8.0 Hz, 2H), 7.122 (d, $J$ = 8.0 Hz, 2H), 6.876 (s, 1H)) as well as ESI MS (0.1% HCOOH/MeOH, label: AO-9-36-fr2) which showed $m/z$ 545.8 were coincident with values found in 4-*tert*-butylphenyldiamine **28**.

**Aminyl Diradical 11: Reaction with Iodine (labels: AO876).** 4-*tert*-Butylphenyldiamine **28** (AO-8-71-fr3, MW = 544.9, 0.88 mg, 1.615 μmol) was placed in the custom-made SQUID sample tube (5-mm O.D. EPR quartz tube with a thin bottom ~6 cm from the end of the tube) and evacuated overnight at 55 °C then at 110 °C. THF (~0.1 mL, ~8-mm height) was added to the vessel by vacuum transfer, and then stirred for 30 min at −30 °C. *n*-BuLi (0.161 M in hexane, 22 μL, 3.55 μmol, 2.2 equiv) was added to produce initially the yellow homogeneous solution. After stirring at −30 °C for 1 h, the orange reaction mixture was concentrated at −30 °C until the volume decreased to about 0.025 mL (~2-mm height). THF (~0.1 mL) was added to the concentrated reaction mixture by vacuum transfer, and then the reaction mixture was stirred for 5 min at −30 °C. This sequence of solvent removal under vacuum, followed by addition of THF by vacuum

transfer was repeated another two times (total of three times). Finally, 2-MeTHF (~0.08 mL) was added to the reaction mixture by vacuum transfer, and then the reaction mixture (under vacuum) was immersed in liquid nitrogen. Subsequently, iodine was vacuum transferred (for 14 s) to the sample tube wall, just above the reaction mixture. Iodine was mixed into the reaction mixture at −115 °C, and then the greenish-brown solution was stirred at −115 °C for 2 h. The resultant greenish brown solution was stored in liquid nitrogen; EPR spectra were obtained at 132 K (label: AO876r1−r3).

Subsequently, the sample tube was re-attached to the vacuum line, and an additional vacuum transfer of iodine (for 9 s) was carried out, with mixing at −115 °C. The resultant brown solution was mixed at −115 °C for additional 1.5 h, and then another set of EPR spectra was obtained at 132 K (label: AO876r5).

The sample was warmed up to room temperature (22 °C) for 5 min. The same brown color solution was observed. After obtaining a set of EPR at 132 K (label: AO876r12), the sample was kept at room temperature for additional 10 min, resulting in the same brown solution. Subsequent EPR spectrum was taken at 132 K (label: AO876r13).

The sample was kept at room temperature, with exclusion of light, for overnight, and then it was exposed to air, diluted with benzene and transferred to a vial. The brown crude was washed with $Na_2S_2O_3$ solution. The pink organic layer was washed with brine and dried over $Na_2SO_4$. The organic phase was evaporated under reduced pressure and evacuated on high vacuum for overnight. ^{1}H NMR (600 MHz, acetone-$d_6$, label: AO-8-76-crd) spectrum of this crude reaction mixture showed a mixture of three compounds in 0.5:1.5:1 ratio corresponding to fraction 1:fraction 2:fraction 3. The crude was purified by

preparative TLC under $N_2$ atm (3% deactivated silica, 3% diethyl ether in pentane) to give

2 fractions. $R_f = 0.51$ and 0.38 for fraction 1 and 2, respectively (3% diethyl ether/pentane,

3% deactivated TLC). $^1$H NMR (600 MHz, acetone-$d_6$, label: AO-8-76-fr1) spectrum of

the fraction 1: (aromatic region, $\delta = 7.981$ (dd, $J = 2.4$, 8.4 Hz, 1H), 7.693 (d, $J = 1.8$ Hz,

1H), 7.217 (dd, $J = 1.8$, 8.4 Hz, 1H), 7.056 (s, 1H)) and HR-ESI MS (MeOH/$H_2O$, Figure

C32) which showed $m/z$ 543.4688 may correspond to by-product **43**. $^1$H NMR (400 MHz,

acetone-$d_6$, label: AO-8-76-fr2) spectrum of the fraction 2: (aromatic region, $\delta = 7.570$ (d,

$J = 8.4$ Hz, 2H), 7.125 (d, $J = 8.4$ Hz, 2H), 6.878 (s, 1H)) and ESI MS (0.1% TFA/$CH_2Cl_2$,

label: AO876fr3) which showed $m/z$ 545.2 were coincident with those values found in 4-

*tert*-butylphenyldiamine **28**.

In another experiment, a solution of diradical **11** in 2-MeTHF was prepared from

0.77 mg of diamine **28** according to the procedure described above. After second addition

of $I_2$, similar EPR spectrum (label: AO881r7) was obtained at 132 K with significant

monoradical impurity. The sample was warmed up to room temperature for 5, 10 and 20

min. EPR spectra at 132 K (label: AO881r9, 10, 11) were taken after annealing. After

work up, $^1$H NMR spectrum (600 MHz, acetone-$d_6$, label: AO-8-81-crd) showed a mixture

of two compounds in 0.7:1 ratio (The chemical shift of these two components are identical

to the values found in AO876fr2 and fr3, respectively).

**Aminyl Diradical 11: Reaction with Oxygen (Figures C12, C14, labels: AO941).** 4-*tert*-Butylphenyldiamine **28** (AO-9-21-sld-wsh, MW = 544.9, 0.87 mg, 1.60

µmol) was placed in the EPR sample tube and evacuated overnight at 65 °C and then at

110 °C. THF (~0.1 mL, ~10-mm height) was added to the vessel by vacuum transfer, and

then stirred for 30 min at –30 °C. *n*-BuLi (0.143 M in hexane, 27 µL, 3.83 µmol, 2.4 equiv)

was added to produce initially the yellow homogeneous solution. After stirring at −30 °C for 5 h, the orange reaction mixture was evacuated at −50 °C then immersed in liquid nitrogen. 2-MeTHF (~0.1 mL) was added to the reaction mixture by vacuum transfer. The solution was stirred at −80 °C for 1 min and then the reaction mixture (under vacuum) was immersed in liquid nitrogen. Subsequently, iodine was vacuum transferred (for 16 s) to the sample tube wall, just above the reaction mixture. Iodine was mixed into the reaction mixture at −115 °C, and then the greenish−brown solution was stirred at −115 °C for 3.5 h. The resultant greenish−brown solution was stored in liquid nitrogen; EPR spectra were obtained at 132 K (label: AO941r1−r3).

Subsequently, the sample tube was re-attached to the vacuum line, and an additional vacuum transfer of iodine (for 8 s) was carried out, with mixing at −115 °C. The resultant brown solution was mixed at −115 °C for additional 20 min, and then another set of EPR spectra was obtained at 132 K (label: AO941r4−r6).

The sample was annealed at −78 °C for 10 min with the same brown color solution. After obtaining EPR spectrum at 132 K (label: AO941r7, Figure C12), the sample was annealed at −27 °C for 10 min, resulting in the same brown color solution. Subsequent EPR spectrum was taken at 132 K (label: AO941r9, Figure C12).

The sample tube was attached to high vacuum line. The solution was saturated under dry oxygen atmosphere at −108 °C to produce reddish brown solution. The solution was mixed for 15 min, followed by degassing. The EPR spectrum weas taken at 132 K (label: AO941r10, Figure C12).

The sample was warmed up to room temperature (21 °C) for 45 min to produce yellowish brown solution. The EPR spectra were obtained at 295 K (label:

AO941r16–r19). The sample tube was kept at room temperature for 2 d, exclusion of light. The EPR spectra were taken at 295 K (label: AO941r20–r21). The sample was exposed to air for 10 min, following by degassing. The EPR were taken at 295 K (label: AO941r23–r24).

The sample was transferred to a vial, evaporated by $N_2$ flow and evacuated for overnight. ^{1}H NMR (500 MHz, acetone-$d_6$, label: AO-9-41-crd, Figure C14 (A)) spectrum showed a mixture of three compounds. The crude was purified by preparative TLC under $N_2$ atmosphere (3% diethyl ether in pentane) to give 3 fractions. $R_f$ = 0.56, 0.33 and 0.09 for fraction 1-3, respectively (3% diethyl ether/pentane). ^{1}H NMR (500 MHz, acetone-$d_6$, label: AO-9-41-fr1, Figure C14 (B)) spectrum of the fraction 1: (aromatic region, $\delta$ = 7.989 (d, $J$ = 8.5 Hz, 1H), 7.691 (s, 1H), 7.215 (dd, $J$ = 1.5, 8.5 Hz, 1H), 7.055 (s, 1H)) and ESI MS (0.1% HCOOH/MeOH, label: AO-9-41-fr1) showed $m/z$ 543.9 may identified as by-product **43**. ^{1}H NMR (500 MHz, acetone-$d_6$, label: AO-9-41-fr2, Figure C14 (C)) spectrum of the fraction 2: (aromatic region, $\delta$ = 7.570 (d, $J$ = 8.5 Hz, 2H), 7.123 (d, $J$ = 8.0 Hz, 2H), 6.877 (s, 1H)) is coincident with that for 4-*tert*-butylphenyldiamine **28**. The ESI MS (0.1% HCOOH/MeOH, label: AO-9-41-fr2) showed $m/z$ 545.9 that confirmed 4-*tert*-butylphenyldiamine **28**. ^{1}H NMR (500 MHz, acetone-$d_6$, label: AO-9-41-fr3, Figure C14 (D)) spectrum of the fraction 3: (aromatic region, $\delta$ = 8.200 (s, 2H), 7.529 (d, $J$ = 8.5 Hz, 2H), 7.482 (s, 4H), 6.130 (s, 1 H) ESI MS (0.1% HCOOH/MeOH, label: AO-9-41-fr3, Figure C33) $m/z$ 575.9. HR ESI-MS calcd for $C_{38}H_{58}N_2O_2Na$ (M + $Na^+$) 597.4396 found 597.4369 (Figure C34). The product may be identified as the product of addition of $O_2$ to diradical **11**.

## 1.5. References

1. Gomberg, M. *J. Am. Chem. Soc.* **1900**, *22*, 757−771.

2. IUPAC Compendium of Chemical Terminology, release 2.3.3; International Union of Pure and Applied Chemistry (IUPAC) Research Triangle Park, NC, 2012; p 1003.

3. Ovchinnikov, A. A. *Theor. Chim. Acta.* **1978**, *47*, 297−304.

4. Abe, M. *Chem. Rev.* **2013**, *113*, 7011−7088.

5. Rajca, A. *Adv. Phys. Org. Chem.* **2005**, *40*, 153−199.

6. Rajca, A. *Chem. Rev.* **1994**, *94*, 871−893.

7. Borden, W. T. In Diradicals; Borden, W. T., Ed.; Wiley-Interscience: New York, 1982.

8. Weil, J. A.; Bolton, J. R.; Wertz, J. E.; *Electron Paramagnetic Resonance: Elementary Theory and Practical Applications*; John Wiley & Sons: New York 1994.

9. Pauli, W. Z. *Phys.* **1925**, *31*, 765−783.

10. Fessenden, R. W.; Schuler, R. H. *J. Chem. Phys.* **1963**, 39, 2147−2195.

11. Danen, W. C.; Neugebauer, F. A. *Angew. Chem. Int. Ed.*, **1975**, *14*, 783−789.

12. Danen, W. C.; Kensler, T. T. *J. Am. Chem. Soc.* **1972**, *92*, 5235−5237.

13. Wieland, H. *Liebigs Ann. Chem.* **1911**, *381*, 200–216.

14. Shida, T.; Kira, A. *J. Phys. Chem.* **1969**, *73*, 4315–4320.

15. (a) Neugebauer, F. A.; Fischer, H. *Angew. Chem. Int. Ed.* **1971**, *10*, 732–733; (b) Neugebauer, F. A.; Fischer, H.; Bamberger, S; Smith, H. O. *Chem. Ber.* **1972**, *105*, 2694–2713.

16. Ballester, M.; Castaner, J.; Olivella, S. *Tetrahedron Lett.* **1974**, 615–616.

17. Haider, K.; Soundararajan, N.; Shaffer, M.; Platz, M. S. *Tetrahedron Lett.* **1989**, *30*, 1225–1228.

18. Rajca, A; Shiraishi, K; Pink, M.; Rajca, S. *J. Am. Chem. Soc.* **2007**, *129*, 7232–7233.

19. Boratyński, P. J.; Pink, M.; Rajca, S.; Rajca, A. *Angew. Chem., Int. Ed.*, **2010**, *49*, 5459–5462.

20. Wenthold, P. G.; Kim, J. B.; Lineberger, W. C. *J. Am. Chem. Soc.* **1997**, *119*, 1354–1359.

21. Neuhaus, P.; Grote, D.; Sander, W. *J. Am. Chem. Soc.* **2008**, *130*, 2993–3000.

22. Noodleman, L. *J. Chem. Phys.* **1981**, *74*, 5737–5744.

23. Rajca, A.; Olankitwanit, A.; Rajca, S. *J. Am. Chem. Soc.* **2011**, *133*, 4750–4753.

24. Amiri, S; Schreiner, P. R. *J Phys. Chem. A* **2009**, *113*, 11750–11757.

25. (a) Barone, V.; Boilleau, C.; Cacelli, I.; Ferretti, A.; Monti, S.; Prampolini, G. *J. Chem. Theory Comput.* **2013**, *9*, 300–307; (b) Barone, V.; Cacelli, I.; Ferretti, A.; Monti, S.; Prampolini, G. *Phys. Chem. Chem. Phys.* **2011**, *13*, 4709–4714.

26. Cacchi, S.; Fabrizi, G. *Chem. Rev.* **2011**, *111*, PR215–PR283.

27. Humphrey, G. R.; Kuethe, J. T. *Chem. Rev.* **2006**, *106*, 2875–2911.

28. Sundberg, R. J. *The Chemistry of Indoles*; Academic Press: New York, 1970.

29. Robinson, B. *The Fischer Indole Synthesis*; Wiley-Interscience: New York, 1982.

30. Wagaw, S.; Yang, B. H.; Buchwald, S. L. *J. Am. Chem. Soc.* **1999**, *121*, 10251–10263.

31. Mikhailenko, F. A.; Boguslavskaya, A. N. *Chem. Heterocycl. Comp.* **1971**, *7*, 574–577.

32. Samsoniya, S. A.; Targamadze, N. L.; Tret'yakova, L. G.; Efimova, T. K.; Turchin, K. F.; Gverdtsiteli, I. M.; Suvorov, N. N. *Chem. Heterocycl. Comp.* **1977**, *13*, 757–763

33. Schoutissen, H. A. J. *Rec. Trav. Chim.* **1935**, *54*, 253–255.

34. Solé, D.; Mariani, F.; Fernández, I.; Sierra, M. A. *J. Org. Chem.* **2012**, *77*, 10272–10284.

35. Bloch, R. *Chem. Rev.* **1998**, *98*, 1407–1438.

36. Rodriguez, J. G.; Urrutia, A.; de Diego, J. E.; Martinez-Alcazar, M. P.; Fonseca. I. *J. Org. Chem.* **1998**, *63*, 4332–4337.

37. Gandon, V.; Bertus, P.; Szymoniak, J. *Synthesis* **2002**, 1115–1120.

38. Gottlieb, H. H.; Kotlyar, V.; Nudelman, A. *J. Org. Chem.* **1997**, *62*, 7512–7515.

39. Rajca, A.; Boratyński, P. J.; Olankitwanit, A.; Shiraishi, K.; Pink, M.; Rajca, S. *J. Org. Chem.* **2012**, *77*, 2107–2120.

40. Blanksby, S. J.; Ellison, G. B. *Acc. Chem. Res.* **2003**, *36*, 255–263.

41. Tu, T.; Sun, Z.; Fang, W.; Xu, M.; Zhou, Y. *Org. Lett.* **2012**, *14*, 4250–4253.

42. Wu, L, Drinkel, E.; Gaggia, F.; Capolicchio, S.; Linden, A.; Falivene, L.; Cavallo, L.; Dorta, R. *Chem. Eur. J.* **2011**, *17*, 12886–12890.

43. Altenhoff, G.; Goddard, R.; Lehmann, C. W.; Glorius, F. *J. Am. Chem. Soc.* **2004**, *126*, 15195–15201.

44. Organ, M. G.; Çalimsiz, S.; Sayah, M.; Hoi, K. H.; Lough, A. J. *Angew. Chem. Int. Ed.* **2009**, *48*, 2383–2387

45. Schmidt, A.; Rahimi, A. *Chem. Commun.* **2010**, *46*, 2995–2997.

46. Chartoire, A.; Lesieur, M.; Falivene, L.; Slawin, A. M. Z.; Cavallo, L.; Cazin, C. S. J.; Nolan, S. P. *Chem. Eur. J.* **2012**, *18*, 4517–4521.

47. Ackermann, L.; Potukuchi, H. K.; Althammer, A.; Born. R.; Mayer, P. *Org. Lett.* **2010**, *12*, 1004–1007.

48. Yin, J.; Rainka, M. P.; Zhang, X,-X.; Buchwald, S. L. *J. Am. Chem. Soc.* **2002**, *124*, 1162–1163.

49. Walker, S. D.; Barder, T. E.; Martinelli, J. R.; Buchwald, S. L. *Angew. Chem. Int. Ed.* **2004**, *43*, 1871–1876.

50. Zhao, Q.; Li, C.; Senanayake, C. H.; Tang. W. *Chem. Eur. J.* **2013**, *19*, 2261–2265.

51. Barder, T. E.; Walker, S. D.; Martinelli, J. R.; Buchwald, S. L. *J. Am. Chem. Soc.* **2005**, *127*, 4685–4696.

52. Littke, A. F.; Dai, C.; Fu, G. C. *J. Am. Chem. Soc.* **2000**, *122*, 4020–4028.

53. Sridharan, V.; Suryavanshi, P. A.; Menéndez, J. C. *Chem. Rev.* **2011**, *111*, 7157–7259.

54. Katritzky, A. R.; Rachwal, S.; Rachwal, B. *Tetrahedron* **1996**, *52*, 15031–15070.

55. Hamann, L. G.; Higuchi, R. I.; Zhi, L.; Edwards, J. P.; Wang, X.-N.; Marschke, K. B.; Kong, J. W.; Farmer, L. J.; Jones, T. K. *J. Med. Chem.* **1998**, *41*, 623–639.

56. Yoo, S.-E.; Kim, J. H.; Yi, K. Y. *Bull. Korean Chem. Soc.* **1999**, *20*, 139–140.

57. Morimoto, Y.; Shirahama, H. *Tetrahedron*, **1996**, *32*, 10631–10652.

58. Bunce, R, A.; Herron, D. M.; Ackerman, M. L. *J. Org. Chem.* **2000**, *65*, 2847–2850.

59. Baldwin, J. E. *J. Chem. Soc., Chem. Commun.,* **1976**, 734–736.

60. Pisaneschi, F.; Sejberg, J. J. P.; Blain, C.; Ng, W. H.; Aboagye, E. O.; Spivey, A. C. *Synlett* **2011**, 241–244.

61. Clentsmith, G. K. B.; Field, L. D.; Messerle, B. A.; Shasha, A.; Turner, P. *Tetrahedron Lett.* **2009**, *50*, 1469–1471.

62. Seebach, D. *Angew. Chem. Int. Ed.* **2011**, *50*, 96–101.

63. Meisters, A.; Mole, T. *Aust. J. Chem.* **1974**, *27*, 1655–1663.

64. Reetz, M. T.; Westermann, J.; Steinbach, R. J. *Chem. Soc. Chem. Commun.* **1981**, 237–239.

65. Semmelhack, M. F.; Chong, B. P.; Stauffer, R. D.; Rogerson, T. D.; Chong, A; Jones, L. D. *J. Am. Chem. Soc.* **1975**, *97*, 2507–2516.

66. Xiao, K.-J.; Luo, J.-M.; Ye, K.-Y.; Wang, Y.; Huang, P.-Q. *Angew. Chem.* **2010**, *122*, 3101–3104.

67. Bubnov, Y. N.; Pastukhov, F. V.; Yampolsky, I.; Ignatenko, A. V. *Eur. J. Org. Chem.* **2000**, 1503–1505.

68. Li, Z.; Zhang, Y. *Tetrahedron Letters* **2001**, *42*, 8507–8510.

69. Frisch, M. J. *et al.*, *Gaussian 09, Revision A.01*, Gaussian, Wallingford, CT, 2009.

70. Rajca, A.; Olankitwanit, A.; Wang, Y.; Boratyński, P. J.; Pink, M.; Rajca, S. *J. Am. Chem. Soc.* **2013**, *135*, 18205–18215.

71. Scott, A. P.; Radom, L. *J. Phys. Chem.* **1996,** *100,* 16502–16513.

72. Gennett, T.; Milner, D. F.; Weaver, M. J. *J. Phys. Chem.* **1985**, *89*, 2787−2794.

73. Connelly, N. G.; Geiger, W. E. *Chem. Rev.* **1996**, *96*, 877–910.

74. Gerson, F.; Huber, W. *Electron Spin Resonance Spectroscopy of Organic Radicals*; WILEY-VCH Verlag GmbH & Co. KGaA: Weinheim, 2003.

75. Nelsen, S. F.; Landis, R. T.; Kiehle, L. H.; Leung, T. H. *J. Am. Chem. Soc.* **1972**, *94*, 1610–1614.

76. Suffert, J. *J. Org. Chem.* **1989**, *54*, 509–510.

77. Gennett, T.; Milner, D. F.; Weaver, M. J. *J. Phys. Chem.* **1985**, *89*, 2787–2794.

78. Rajca, S.; Rajca, A.; Wongsriratanakul, J.; Butler, P.; Choi, S. *J. Am. Chem. Soc.* **2004**, *126*, 6972–6986.

79. Rajca, A.; Mukherjee, S.; Pink, M.; Rajca, S. *J. Am. Chem. Soc.* **2006**, *128*, 13497–13507.

80. Rajca, A.; Wongsriratanakul, J.; Rajca, S. *J. Am. Chem. Soc.* **2004**, *126*, 6608–6626.

81. Mikhailenko, F. A.; Boguslavskaya, A. N. *Chem. Heterocycl. Comp.* **1971**, *7*, 574–577.

82. Clentsmith, G. K. B.; Field, L. D.; Messerle, B. A.; Shasha, A.; Turner, P. *Tetrahedron Lett.* **2009**, *50*, 1469–1471.

83. Olankitwanit, A.; Pink, M.; Rajca, S.; Rajca, A. *J. Am. Chem. Soc.* **2014**, *136*, 14277–14288.

# CHAPTER 2

# CALIX[4]ARENE NITROXIDE TETRA- AND OCTARADICALS

Portions of the work described in this chapter have been reported:   Olankitwanit, A.; Kathirvelu, V.; Rajca, S.; Eaton, G. R.; Eaton, S. S.; Rajca, A. "Calix[4]arene nitroxide tetraradical and octaradical", *Chem. Commun.* **2011**, *47*, 6443–6445.

## 2.1. Introduction

Calixarenes are an important family of macrocycles which are extensively studied in the field of supramolecular chemistry.[1,2]   Because of their remarkable structural properties and the wide range of possible chemical modifications, functionalized calixarenes are attractive to researchers in many areas of study including ion and molecular recognition, host-guest chemistry, and catalysis.[3]   These studies are targeting calixarenes for many novel applications such as chemical sensors and gas storage.[4]   We are interested in the development of high-spin organic radicals by the modification of calix[4]arenes with stable nitroxide radicals in order to produce stable paramagnetic compounds with conformations "locked" by the calixarene macrocycle.   This chapter will focus on the general background of calix[4]arenes, high-spin nitroxide radicals, as well as synthesis and magnetic study of calix[4]arene functionalized nitroxide radicals.

### 2.1.1. Background on calixarenes

Calixarenes were first discovered in 1872 by Adolph von Baeyer[5] who investigated the reaction of phenols and formaldehyde in the presence of strong acids.   However, he

was not able to obtain pure materials for chemical structure analysis, and therefore the chemical structures were not established.  In 1944, a cyclic tetrameric structure, obtained from the base-catalyzed condensation of *p-tert*-butylphenol and formaldehyde, was first proposed by Zinke and Zeigler[6].  The structure of the product, later named *p-tert*-butylcalix[4]arene, was confirmed in 1979 by Andreetti and co-workers[7] using an X-ray crystallographic determination.  The pioneering work was carried out in the late 1970s and extending into 1980s by C. David Gutsche and co-workers.  They also coined the name "calixarene" which derived from calix (Greek word means vase) and arene (the presence of aromatic rings).[8]  Finally, the mixtures from the based-catalyzed conditions, mainly three components as *p-tert*-butylcalix[4]arene, *p-tert*-butylcalix[6]arene and *p-tert*-butylcalix[8]arene as shown in Figure 2.1, were separated by recrystallization and chromatographic methods. The true identity of each component was ascertained based on elemental analysis, mass spectrometry, $^{1}$H- and $^{13}$C-NMR spectroscopy.[9]  In addition, Gutsche and coworkers developed the reproducible and efficient procedures for the synthesis of the *p-tert*-butylcalix[4]arene,[10] *p-tert*-butylcalix[6]arene[11] and *p-tert*-butylcalix[8]arene[12] (Figure 2.1).  Calixarenes with up to 20 repeating units have been reported so far.[13]
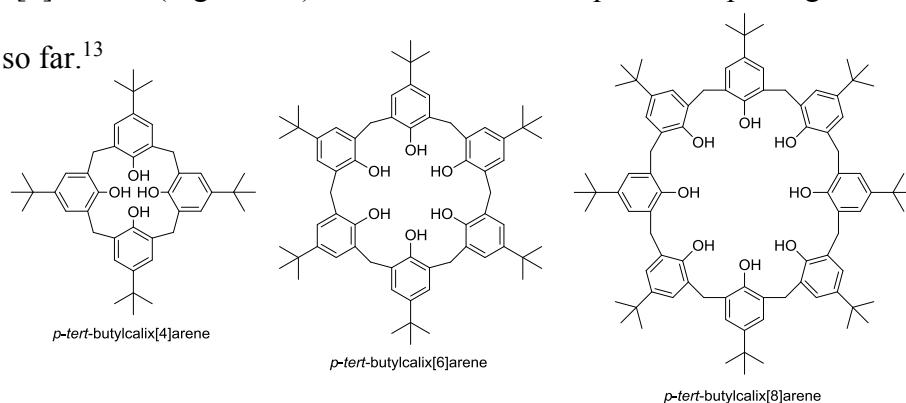


**Figure 2.1.** Structures of *p-tert*-butylcalix[4]arene, *p-tert*-butylcalix[6]arene and *p-tert*-butylcalix[8]arene.

*Conformations of calix[4]arene*

Calix[n]arenes are macrocyclic compounds containing *n* repeating phenolic units connected by methylene groups in the *meta*-position to form a hydrophobic cavity. As illustrated in Figure 2.2, the side of calix[4]arene bearing the hydroxyl group is defined as the lower rim, and the aromatic side bearing *para*-substituents is defined as the upper rim.
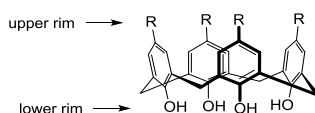


**Figure 2.2.** General structure of *p*-substituted calix[4]arene.

Gutsche and co-workers[14] defined four limiting conformations of calix[4]arene by identifying the aryl groups that point upward (u) or downward (d) with respect to an average plane defined by the bridge methylene groups. These four conformations were cone (u,u,u,u), partial cone (u,u,u,d), 1,2-alternate (u,u,d,d), and 1,3-alternate (u,d,u,d), as shown in Figure 2.3.
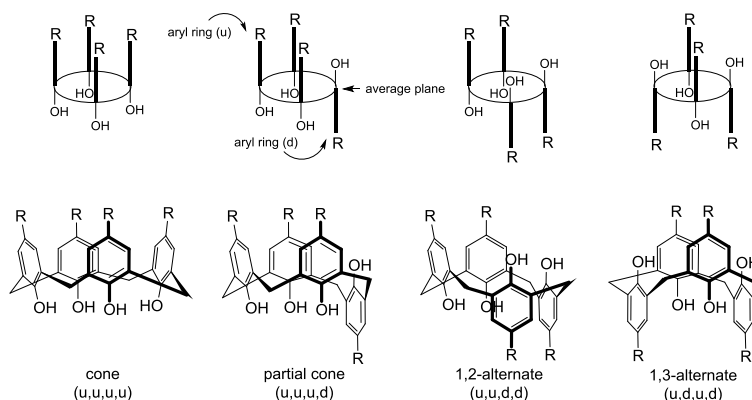


**Figure 2.3.** Conformations of calix[4]arenes.

*Conformationally-locked calix[4]arenes.*

The flexibility and conformational inversion of calixarenes involved two possible pathways: the para-substituent-through-the-annulus and the oxygen-through-the-annulus

[1,15] (Figure 2.4). However, in the case of calix[4]arene, only the latter pathway is considered because even for the smallest *para*-substituent, e.g. *para*-H, the aryl ring too large to pass through the annulus of calix[4]arene. Conditions such as temperature and the presence of metals could influence the conformational inversion, especially for calix[4]arenes with small substituents at the lower rim.
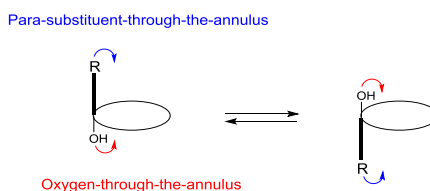


**Figure 2.4.** Two pathways for conformational inversion of calixarenes: oxygen-through-the-annulus rotation and para-substituent-through-the-annulus rotation.

In order to lock the structure of calix[4]arene in the desired conformation, one must prevent the oxygen-through-the-annulus pathway by considering the bulky groups (-OR) attached to the lower rim. Etherification and esterification of the phenolic hydroxyl group (lower rim) are among the most common methods of modification, however, the alkyl group attached must be larger than ethyl group to effectively lock a conformer.[16]

The conformational outcome of calix[4]arenes is generally dependent on solvent, choice of base, reaction temperature, and reactivity of electrophile and the *para*-substituent of the upper rim. There are mainly four conformations that have been synthesized and described in literature: cone, partial cone, 1,3-alternate, and 1,2-alternate conformations. It is possible to lock conformations of the calix[4]arenes by selectively alkylating the phenolic groups under specific conditions. The benzylation of *p-tert*-butylcalix[4]arene with benzyl bromide (BnBr) in the presence of sodium hydride (NaH) exemplified the general method to lock in cone conformations in 63% yield (Scheme 2.1 A).[17] In our lab

such locking to the cone was carried out using 4-*tert*-butylbenzyl bromide.[18]   The partial

cone conformations was a minor product (6-8% yield) upon elevated temperature (24 or

70 °C) and shorter reaction times (1-18 h).   The partial cone conformation could be

generated as a major product (71%) with trace amount of cone and 1,3-alternate conformers

by simply substituting the base with KOSiMe$_3$ (Scheme 2.1B).[17]   Interestingly, 1,3-

alternate conformers were obtained exclusively in 76% isolated yield by alkylating

calix[4]arene with 2-methoxyethyl tosylate as electrophile using Cs$_2$CO$_3$ in DMF (Scheme

2.1C).[19]   1,2-Alternate conformation is generally less common and can be indirectly

prepared by multistep synthesis from *p-tert*-butylcalix[4]arene.[20]

**Scheme 2.1.** Representative synthesis of conformation "lock" calix[4]arenes.
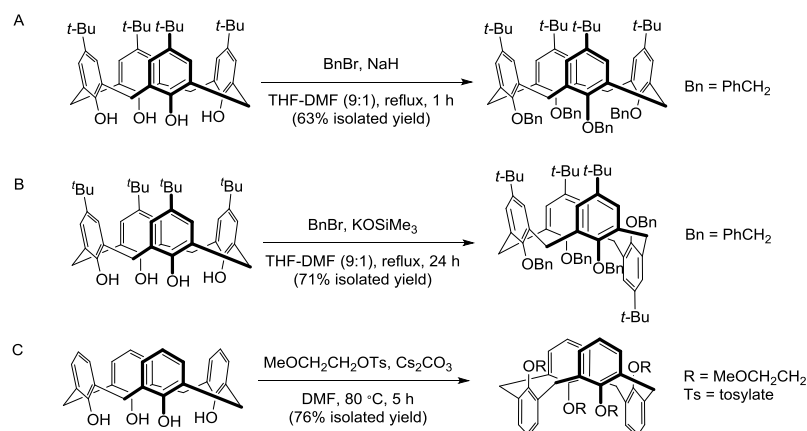


Other modifications to the upper rim are commonly accomplished by electrophilic

aromatic substitution.   These modifications have resulted in calix[n]arenes with many

different functional groups with a variety of different properties such as different sizes,

solubility, flexibilities and binding affinities.   Consequently, these compounds are

becoming important templates for novel applications and materials.

### 2.1.2. Background on nitroxide radicals

Stable radicals defined by Ingold[21] in '1976 Account Chemical Research article were referred to *"a radical so persistent and so unreactive to air, moisture, etc., under ambient conditions and the pure radical can be handled and stored in the lab with no more precautions than would be used for the majority of commercially available organic chemicals."* Nitroxide radicals are generally considered to be stable radicals due to the delocalization of one electron between N and O as presented by two resonance structures in Figure 2.5 with a bond order 1.5. This is supported by the bond dissociation energy (~100 kcal mol$^{-1}$) and the bond length of N–O of nitroxides (~1.23-1.29 Å)[22] which is intermediate between N–OH single bond (53 kcal mol$^{-1}$; 1.43 Å) and N=O double bond (145 kcal mol$^{-1}$; 1.20 Å).[22-23]
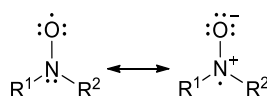


**Figure 2.5.** Resonance structures of nitroxide radical.

Such delocalization contributes to the lack of dimerization in most of the nitroxide radicals as the consequence of O–O bond formation destroys the resonance stability. Although the nitroxide radicals are typically persistent by their electronic structure, bulky substituents with quaternary carbons on nitroxides such as *tert*-butyl groups improve the kinetic stability. For example, as shown in Figure 2.6, the commercially available 2,2,6,6-tetramethyl-1-piperidinyloxy (TEMPO) and di-*tert*-butyl nitroxide are stable at ambient temperature. While bulky substituents and the delocalization of the radical between the nitrogen and oxygen atoms stabilizes the compound, some substituents like phenyl moieties decrease the persistency due to degradation pathways from the delocalization of

the radical into the phenyl ring. Therefore, the sterically hindering group such as *p-tert-*butylphenyl-*tert*-butyl nitroxide[24] (Figure 2.6) is generally attached at *para-* position to minimize such decomposition.
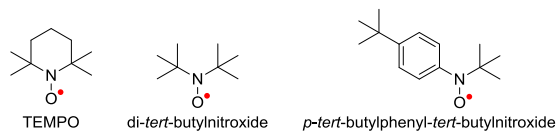


**Figure 2.6.** Examples of some stable nitroxides.

Because of their paramagnetic properties, the applications for stable nitroxide radicals are diverse. For example, they are widely used as spin labels,[25] as mediators for living radical polymerization,[26,27], as charge-storage components in organic battery,[28,29] as ferromagnetic organic materials,[30,31] as paramagnetic relaxation enhancement (PRE) or dynamic nuclear polarization (DNP) techniques,[32-35] and as MRI contrast agents.[36-39]

*Nitroxide diradicals*

Monoradicals refer to a molecule containing an unpaired electron, which possesses a spin quantum number of $S = \frac{1}{2}$ and therefore the spin multiplicity $2S + 1 = 2$ (doublet state). A molecule which possesses two unpaired electrons is called either biradical or diradical depending on how the two electron interact with each other. The term biradical refers to the species in which the two unpaired electrons are far apart and act independently as in two monoradicals; the electron exchange interaction ($J$) is practically negligible. Meanwhile diradicals are the molecules in which the two unpaired electrons are in close enough proximity to have the electron exchange interaction that can produce two spin

states; i.e., singlet state ($S = 0$, spin multiplicity = 1, antiparallel spins, antiferromagnetic coupling)  and triplet state ($S = 1$, spin  multiplicity = 3, parallel spin,  ferromagnetic coupling) as shown in Figure 2.7.  In this case, the energy difference of the singlet (S) and triplet state (T) can be determined by the electron exchange interaction with $\Delta E_{ST} = E_S - E_T = 2J$.  The negative value of $J$ designates singlet ground state and the positive number indicates the triplet ground state. The explanation of how to determine the ground state multiplicity of diradicals is described in Chapter 1.
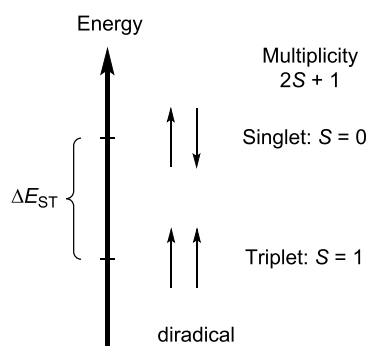


**Figure 2.7.** Energy diagram for singlet and triplet states of diradicals: the case of ferromagnetic coupling.

While there are many studies on nitroxide monoradicals ($S = \frac{1}{2}$), high-spin nitroxide radicals ($S \geq 1$) gained less attention.  Typically, *m*-phenylene is used as a ferromagnetic coupling unit to produce a strong exchange coupling in nitroxide di- or triradicals.   Nitroxide diradical **1**[40] exemplifies a simple structure of nitroxide diradical that shows a strong intramolecular exchange coupling ($2J/k >> 600$ K; $\Delta E_{ST} >> 1.19$ kcal mol$^{-1}$).[41] However, the nitroxide diradical **1** decomposes easily in solution into an isomeric aminoquinone imine *N*-oxide due to the large spin density at the *ortho-* and *para-* position of the phenylene unit (Figure 2.8).
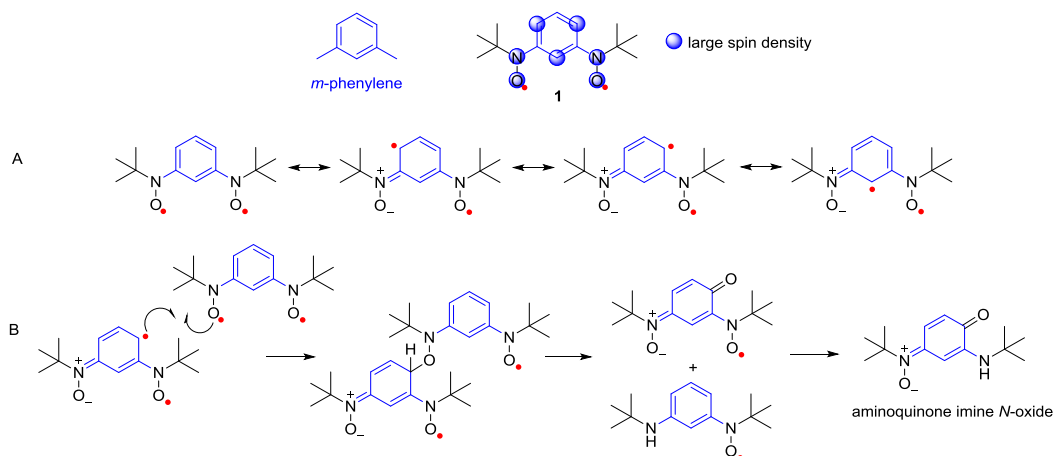
**Figure 2.8.** (A) Resonance structures of **1**. (B) Decomposition pathway of **1.**

When the large spin density positions at *ortho-* and *para-* positions of the *m*-phenylene unit are protected by the bulky substituents, this can lead to stable nitroxide diradicals such as nitroxide diradical **2**[42], **3**[43] and **4**[44] (Figure 2.9).  However, the severe bond twisting of the nitroxide moieties with respect to the 1,3-phenylene moiety weakens intramolecular exchange coupling by an order of magnitude in **2** – **4** and, in some cases, such as crystalline **2**, reverses sign of the coupling from ferromagnetic ($J > 0$) to antiferromagnetic ($J < 0$): ($2J/k = -7.0$ K, $\Delta E_{ST} = -0.014$ kcal mol$^{-1}$, and, in solution, $2J/k = -74$ K, $\Delta E_{ST} = -0.15$ kcal mol$^{-1}$, and, in solution, for **3**, $2J/k = -132$ K, $\Delta E_{ST} = -0.26$ kcal mol$^{-1}$, and $2J/k = -162$ K, $\Delta E_{ST} = -0.32$ kcal mol$^{-1}$, for *syn* and *anti* conformation. In **4**, $2J/k = 80$ K, $\Delta E_{ST} = 0.16$ kcal mol$^{-1}$ are reported.
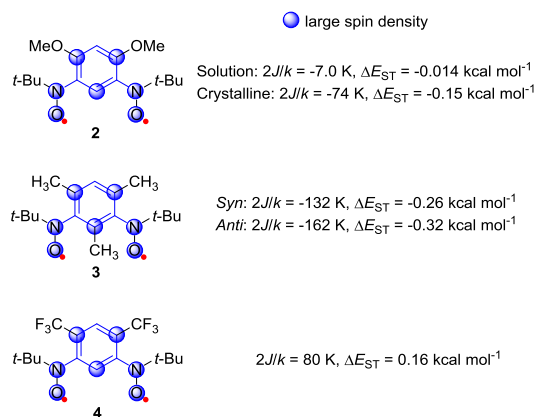
**Figure 2.9.** Structures of nitroxide diradical **2**–**4**.

To ensure the planarity for strong electron exchange interaction between radicals, the nitroxide radicals (**5**, **6**, and **7**) were designed as shown in Figure 2.10. As anticipated, the nitroxide diradical **5**[45] retains a strong exchange coupling ($2J/k > 200$ K, $\Delta E_{ST} > 0.40$ kcal mol$^{-1}$, in solution and $>> 300$ K, $\Delta E_{ST} >> 0.60$ kcal mol$^{-1}$, in solid state).[46] To further study the impact of steric hindrance to the planarity as well as the electron exchange coupling, in 2007, Rajca and co-workers[46] designed and prepared **6** and **7**. The substitution of geminal dimethyl group with spirocyclohexyl groups **6** as shown in Figure 2.10 is designed to shield the nitroxide radical. In addition, 4-*tert*-butylphenyl pendant is substituted at *ortho, ortho'* position to protect the large spin as illustrated by **7** in Figure 2.10. As the results, the large values of $2J/k$ in those nitroxide diradicals were obtained in both solution and solid state which indicated the triplet ($S = 1$) ground states with a strong exchange coupling as in diradical **5**. Nonetheless, the stability of **6** is less than **5**. The decrease in population of triplet ground state of **7** was observed at near room temperature because of the moderate twist out of planarity of the nitroxides.
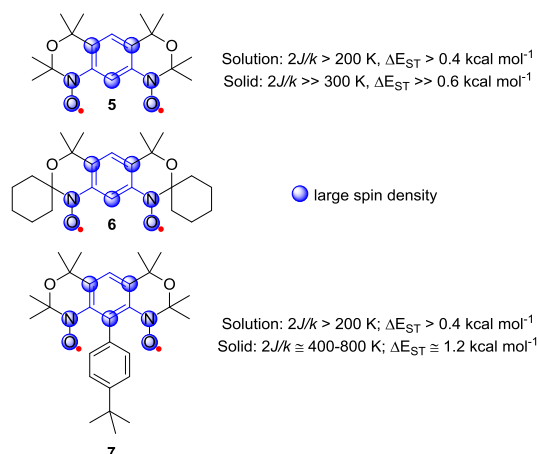
**Figure 2.10.** Structures of nitroxide diradical **5**, **6** and **7**.

In 2009, Rajca and co-workers designed diradical **8** (Figure 2.11) based on tetrahydrodiazapentacene structure where the two aryl groups are annelated by the geminal dimethyl group, to maintain the planarity and to protect the large spin position from decomposition.[47] Furthermore, the *para-* positions of outer rings with respect to the nitroxide radicals, which are unhindered and contain small spin density, are also shielded with *tert*-butyl groups to avoid the decomposition. Thus, the diradical **8** is stable at room temperature in the solid state, as well as possesses a triplet ($S = 1$) ground state with the large singlet-triplet energy gap ($2J/k \geq 300$ K, $\Delta E_{ST} \geq 0.60$ kcal mol$^{-1}$). The calculation by broken-symmetry density functional theory (BS-DFT) predicts the values of $\Delta E_{ST} = 2.0$ kcal mol$^{-1}$ for **8**. Recently, Barone and co-workers also reported the value of $\Delta E_{ST} = 0.6$ kcal mol$^{-1}$ for **8** by Dedicated Difference Configuration Interaction (DDCI) calculation (Figure 2.11).[48]

diazapentacene

tetrahydrodiazapentacene

$2J/k \geq 300$ K, $\Delta E_{ST} \geq 0.6$ kcal mol$^{-1}$

BS-DFT: $\Delta E_{ST} = 2.0$ kcal mol$^{-1}$

DDCI: $\Delta E_{ST} = 0.6$ kcal mol$^{-1}$

8

○ large spin density
○ small spin density
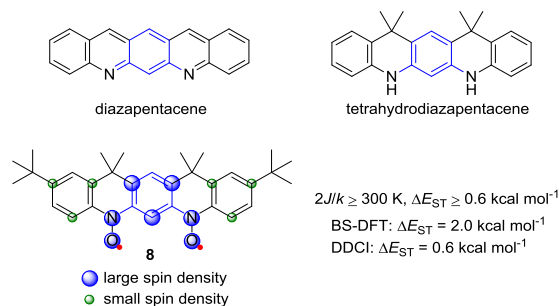
**Figure 2.11.** Structure of nitroxide diradical **8**.

Substitutions, with a bulky group such as *tert*-butyl moiety, at *meta*-position of the *m*-phenylene coupling unit are also known to increase the stability of nitroxide diradicals. These groups provide no disruption to the planarity of nitroxide diradical such that the strong intramolecular exchange coupling between nitroxide radicals is still maintained. For instance, nitroxide diradical **9** is stable in both solution and solid state with strong exchange coupling (solid: $2J/k = 840$ K, $\Delta E_{ST} = 1.67$ kcal mol$^{-1}$) as shown in Figure 2.12.[49] In the development of novel MRI contrast agents, in 2005, Rajca and co-workers[50] reported the synthesis of triplet ($S = 1$) ground state nitroxide diradical **10** in which water-solubilizing group, triethylene glycol methyl ether, was attached at the *meta*-position of the *m*-phenylene unit (Figure 2.12). The diradical **10** possesses large singlet-triplet energy gap (neat: $2J/k = 650$ K, $\Delta E_{ST} = 1.29$ kcal mol$^{-1}$). However, the significant thermal population of singlet excited state was observed at room temperature in aqueous solution. The authors suggest that the twisting out of plane *m*-phenylene of nitroxide radicals weakens the exchange coupling, and therefore reducing the singlet-triplet energy gap.

2$J/k$ = 840 K, $\Delta E_{ST}$ = 1.67 kcal mol$^{-1}$

⬤ large spin density

2$J/k$ = 650 K, $\Delta E_{ST}$ = 1.29 kcal mol$^{-1}$
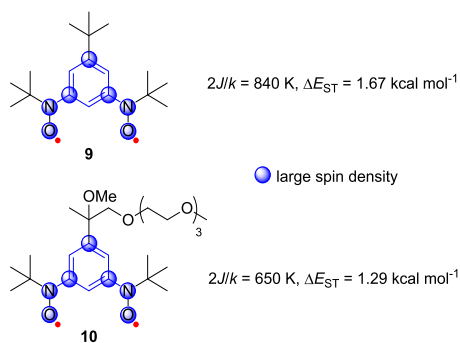
**Figure 2.12.** Structures of nitroxide diradical **9** and **10**.

High-spin nitroxide triradicals have rarely been reported. Nitroxide triradical can be connected through *m*-phenylene units by two 1,3-phenylene (*m*-phenylene) units in a linear version or 1,3,5-connected benzene unit. The energy gap between the ground quartet state and the lowest excited doublet state of linear version ($\Delta E_{DQ} = J$) is smaller compared to the 1,3,5-connected benzene ($\Delta E_{DQ} = 3J$). For example, nitroxide triradical **11** (Figure 3.11) is stable in solution and solid state with strong ferromagnetic coupling ($J/k$ = 240 K, $\Delta E_{DQ}$ = 0.48 kcal mol$^{-1}$).[41] Meanwhile, nitroxide triradical **12**, which was found to be unstable in concentrated solution and used immediately after purification, showed an intramolecular ferromagnetic coupling ($J/k \geq$ 300 K, $\Delta E_{DQ} \geq$ 1.79 kcal mol$^{-1}$).[49] Nitroxide **13** revealed a weak intramolecular ferromagnetic coupling (crystalline: $J/k$ = 6.8 K, $\Delta E_{DQ}$ = 0.041 kcal mol$^{-1}$; Tween 40 matrix: $J/k$ = 5.3 K, $\Delta E_{DQ}$ = 0.032 kcal mol$^{-1}$, Figure 2.13).[49] These $J/k$ values of nitroxide **13** are roughly two orders of magnitude smaller than that estimated for nitroxide **12** due to the extended benzene rings between the nitroxides.
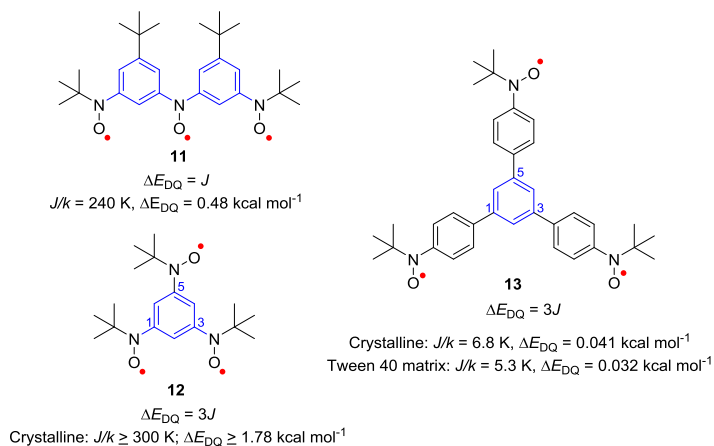
**Figure 2.13.** Structures of nitroxide triradical **11**, **12** and **13**.

### 2.1.3. Calixarenes functionalized with nitroxide radicals

Calixarenes functionalized with high-spin radicals have long been studied. Among them, calix[4]arene-based carbon-centered triphenylmethyl radicals were successfully synthesized and characterized. Delocalization of spin density from the carbon-centered radical to the aromatic rings may stabilize the radical and enhance exchange coupling, thus providing the opportunity to design the building blocks for high-spin polyradicals. For example, when two carbon-centered radicals are connected through *m*-phenylene, the diradical may possess a triplet ($S = 1$) ground state according to Ovchinikov's model.[51] Calix[4]arene macrocycle may provide such *m*-phenylene units, and thus as illustrated in Figure 2.14, high-spin tetraradical **14** with $S = 2$ ground state.[52]
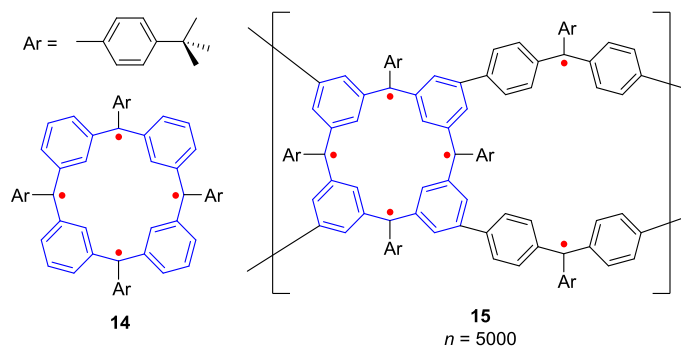
**Figure 2.14.** Structures of high-spin tetraradical **14** and polyradical **15**.

Such macrocyclic tetraradicals ($S = 2$) can also be used to design more complex macromolecules, i.e., high-spin polyradicals with an average $S \geq 5000$ (**15**, Figure 2.14).[53] Although organic magnets generated from these carbon-centered radicals are promising, they are relatively unstable and need to be handled at low temperature.

Because the carbon-centered radicals are relatively unstable, other stable radicals, especially nitroxides, have gained more recent interest for the functionalization of calix[4]arenes. In the majority of the studies, calix[4]arenes, with covalently attached nitroxide radicals on either the lower or upper rims, for potential applications as chemical sensors, have been reported. Since calix[4]arenes conformations can be locked by the substituents attached on the lower and/or upper rim, information gain from the studies is differ from other building blocks. In addition, calix[4]arenes conformations provide the relatively rigid molecular framework for interactions between the radicals. Two types of electron exchange interactions may be identified: (1) through bond and (2) through space. Thus, the idea behind most of the work is to design and study of paramagnetic calix[4]arenes functionalized with nitroxide radicals in order to control the exchange interaction among the unpaired electrons.

The attachment of nitroxide radicals to the lower rim of conformational locked calix[4]arenes was first explored by Shinkai and co-workers[54] and Ziessel and co-workers.[55] These research groups studied the interaction of unpaired electrons in the presence and absence of cations based on intramolecular spin-spin exchange interaction between unpaired electrons using EPR and NMR spectroscopy. Shinkai and co-workers[54] designed a calix[4]arene derivative **16** (Figure 2.15) with the two nitroxide attached diagonally in the locked cone conformation. The observed EPR spectra in THF-toluene (2:3, v/v) at ambient temperature revealed a quintet resonance corresponding to the hyperfine coupling of two equivalent nitrogen nuclei placed in closed proximity. This is a clear evidence of intramolecular exchange interaction between the two nitroxide radicals. There is no clear evidence of the change in EPR spectrum induced by $Na^{+}$.[54] In 1996, Ziessel and co-workers[55] reported another locked cone conformation of calix[4]arene derivative **17** (Figure 2.15) bearing nitronyl-nitroxide radicals on the lower rim. The longer distance of the radicals in the presence of $Zn^{2+}$ for the nitronyl-nitroxide calix[4]arene has been indicated by EPR spectra. The nine-line spectrum at room temperature was observed as the indication of the hyperfine coupling of four equivalent nitrogen nuclei. This is a clear evidence of the intramolecular exchange interaction between the two nitronyl-nitroxide radicals. In the presence of $Zn^{2+}$ the spectrum collapsed to five lines, suggesting that the metal coordination disrupted the through-space exchange interaction between the two nitronyl-nitroxide subunits.[55]
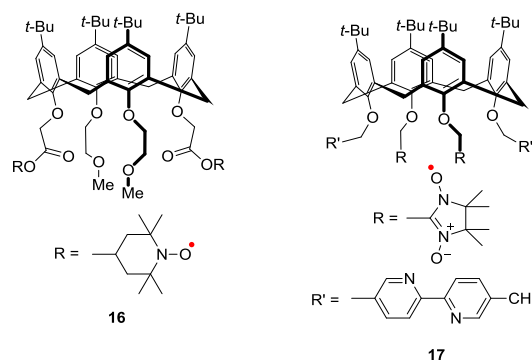
**Figure 2.15.** Structures of calix[4]arene nitroxide **16** and **17**.

In 2002, Li and co-workers reported calix[4]arenes modified by nitroxide radicals on the upper rim.[56] The synthesized calix[4]arene **18** (Figure 2.16) bearing two nitroxide radicals on the upper rim was designed to be flexible for conformational changes by substitution of methyl ether groups which are small enough for oxygen-through-annulus rotation at the lower rim.[16] The structure of **18** was assigned to be partial cone conformation based on the NMR spectroscopic study and the X-ray crystal structure analysis of the hydroxylamine precursor. The EPR spectrum of **18** at room temperature composed of two sets of overlapping signals: a broad triplet from nitrogen hyperfine coupling for the separated nitroxide radicals and a quintet for two nitroxide radicals that are in close proximity. The broad triplet peak also suggested that the "separated" nitroxide radicals, which have negligible spin-spin exchange coupling, are in proximity (partial cone conformation) to have some dipole-dipole interaction to broaden the peak. Upon heating from room temperature to 353 K, the broad triplet spectrum was converted to sharp 3×3 peaks and the additional splitting was assigned to hydrogen hyperfine coupling from two hydrogen nuclei at *ortho* position of the phenyl ring. The change in EPR pattern induced by heating could be explained by the conformation flexibility from partial cone to 1,2-alternate where the triplet spectrum is sharpen due to motional averaging of the dipole-

dipole interaction at higher temperatures and/or the nitroxide radicals being too far apart to have detectable dipole-dipole interaction.

In 2006, Li and co-workers prepared calix[4]arene derivative **19** (Figure 2.16) with nitroxide monoradical on the upper rim and studied the effect of temperature and silver ion ($Ag^+$) complexation to the conformational mobility of calix[4]arene by EPR spectroscopy.[57] The EPR spectra of **19** at 290 K in toluene show a typical monoradical with a broad equivalent triplet from a nitrogen hyperfine coupling. The triplet spectrum split into 3×3 pattern upon bubbling in nitrogen gas probably due to the hydrogen hyperfine coupling with one nitrogen and two *ortho* hydrogen nuclei. After study of the monoradical, in 2008, Li and co-workers prepared calix[4]arene derivatives **18**, **20**, **21** and **22** functionalized with two nitroxide radicals at the diagonal position of the upper rim, to study spin-spin exchange interaction using EPR spectroscopy (Figure 2.16).[58] A similar EPR spectral pattern was observed for **20**, **21**, **22**, and **18** in toluene solution at room temperature: two set of overlapping signal of a broad triplet and a quintet. The higher proportion of the quintet signal corresponding to two nitroxide radicals that are in close proximity was observed for compound **21** and **22** (almost 100% quintet). This is because the propyl groups are attached at the lower rim of compounds **21** and **22** to lock the cone conformation of the calix[4]arenes resulting in closer in proximity between two nitroxide radicals. Likewise, the EPR spectrum of **20** and **22** became nearly coalesced by increasing the temperature to 370 K, showing triplet and quintet in different proportion: **20** quintet (~60%); **22** quintet (~100%). This is explained by the increase in the conformation exchange between cone, partial-cone, and pinched cone conformation at high temperature. In addition, the presence of $Ag^+$ ion in dichloromethane solvent cause the quintet spectrum

of compound **20** and **22** convert to 3×3 pattern as a result of the separation of the nitroxide

radicals due to the Ag$^+$ complexation.
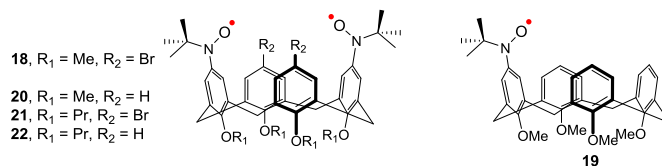


**Figure 2.16.** Structures of calix[4]arene nitroxide **18–22**.

The calix[4]arenes with multiple nitroxide radicals on the upper rim have been also

synthesized and studied by the Rajca group as part of the development of organic magnets

and MRI contrast agents.  Calix[4]arenes conformationally locked cone or 1,3-alternate,

which are functionalized with two or four nitroxides, have been prepared, and employed in

the studies of intramolecular spin-spin interactions between the unpaired electrons or

exchange coupling.  The locked cone or 1,3-alternate conformation was introduced by

bulky substituents on the lower rim, e.g., ethylene glycol methyl ether, which are known

to inhibit the conformational flexibility through the annulus rotation.[16]  Locked

conformations were typically confirmed by spectroscopic techniques (NMR and/or EPR

spectroscopy) and X-ray crystallography.  The locked conformation is important to the

study of exchange coupling because such through-bond interactions are highly dependent

on the geometry (e.g., bond angles) of the through-bond coupling pathways connecting two

interacting radicals.  Predictable exchange interactions may in turn help to attain targeted

magnetic properties.

In cone and 1,3-alternate conformations of calix[4]arene, the EPR spectroscopic

and SQUID magnetometry studies of nitroxide tetraradical **23**, **24** and diradical **25** (Figure

2.17) revealed the intramolecular interactions from exchange couplings between unpaired

electrons through bonds and through space. The through-bond interaction is generally described from the exchange couplings of the adjacent nitroxides generated via the nitroxide-*m*-phenylene-$CH_2$-*m*-phenylene-nitroxide coupling pathways as shown in Figure 2.17. Based on SQUID magnetic studies in frozen solutions, the through bond exchange couplings between adjacent nitroxide radicals is ferromagnetic in cone conformation ($2J/k$ ~ 2 K, $\Delta E_{ST}$ ~ 0.004 kcal mol$^{-1}$ for **23**) whereas antiferromagnetic in 1,3-alternate conformation calix[4]arene ($2J/k$ ~ –2 K for **24**, $\Delta E_{ST}$ ~ –0.004 kcal mol$^{-1}$).[59] Based on analyses of EPR spectra in frozen matrices and X-ray crystallographic studies, the distance between diagonal nitroxide radicals is approximately 5-6 Å in both conformers; magnetic studies indicated through-space antiferromagnetic exchange couplings. In diradical **25**, the magnetic studies in THF reveal weak intramolecular antiferromagnetic exchange coupling ($J/k$ ~ –0.7 K for **25**, $\Delta E_{ST}$ ~ –0.001 kcal mol$^{-1}$). It must be noted that dimerization of one diagonal pair of nitroxide radicals is possible in the cone conformation calix[4]arene tetraradical **23**. This phenomenon forced conformational change to a pinched cone calix[4]arene in solid state with $|2J/k|$ = 400-600 K, $\Delta E_{ST}$ ~ –1.0 kcal mol$^{-1}$.[18] These studies demonstrated that the paramagnetic exchange coupling interaction could be controlled through the locked conformers of calix[4]arenes.
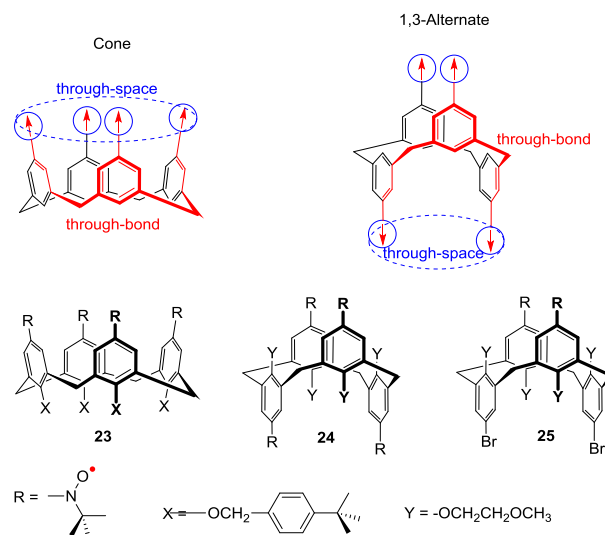
**Figure 2.17.** Coupling pathway of nitroxide radical in cone and 1,3-alternate conformations demonstrating through-space and through-bond interactions and structures of calix[4]arene nitroxides **23–25**.

In 2008, Sawai and co-workers reported the synthesis and characterization of a calix[4]arene tetraradical **26** using mesityl nitroxide group as a building block (Figure 2.18).[60] The authors claimed that the steric hindrance caused by three methyl groups on each benzene ring (mesityl) immobilized the conformation of calix[4]arene. The X-ray crystallography confirmed the 1,3-alternate conformation of calix[4]arene functionalized with four nitroxide radicals. The authors indicated that the quintet state (a spin quantum number of $S = 2$, the spin multiplicity ($2S + 1$) of 5, the four spins are parallel) of the tetraradical **26** was observed from 2-dimensional pulse-based electron spin transient nutation (2D-ESTN) spectroscopy at 3.8 K. However, the spectra also indicated presence of mono-, di-, and triradicals as well. Therefore, the two-dimensional EPR spectrum did not provide clear-cut evidence for a quintet state, in the impure samples of **26**.
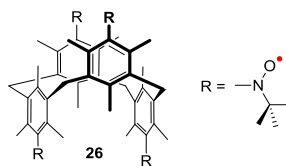
**Figure 2.18.** Structure of calix[4]arene tetranitroxide **26**.

With the results discussed above, stable high-spin calix[4]arenes bearing with nitroxide radicals are still under explored. The investigation of the calix[4]arene functionalized with stable nitroxide radicals possessing a high-spin ground state is indeed essential. In this work, we designed nitroxide tetraradical **27** and octaradical **28** (Figure 2.19). The calix[4]arenes were locked in the 1,3-alternate conformation to control the interactions between unpaired electrons. Instead of attaching the nitroxide radical directly to each benzene ring as seen in tetraradical **24**, we envisioned that the increased distance of the nitroxides through *p*-phenylene spacers could weaken the through-bond exchange interaction and maintain the through-space exchange coupling similar to that for tetraradical **24**. Octaradical **28** could be viewed as the first calix[4]arene with high-spin nitroxide radicals. In addition, water-solubilizing group, i.e. hexaethylene glycol methyl ether (HEG), was introduced to calix[4]arene nitroxide tetraradical and octaradical to increase the solubility in polar solvents such as water or ethanol which may be useful in biomedical applications. The synthesis and characterization of these HEG-functionalized calix[4]arene nitroxides is described later in this chapter.

**2.2. Results and Discussion**

This section described the synthesis, characterization and magnetic measurements of tetraradical **27** and octaradical **28**, in which the calix[4]arene macrocycles are locked in 1,3-alternate conformation.
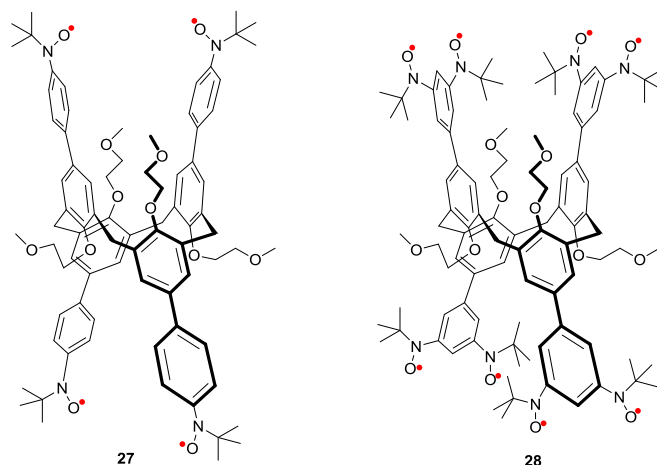
**Figure 2.19.** Structures of calix[4]arene nitroxide tetraradical **27** and octaradical **28** locked in 1,3-alternate conformation.

### 2.2.1. Synthesis of calix[4]arene nitroxide tetraradical 27

### Synthetic plan for calix[4]arene nitroxide tetraradical 27

As illustrated in Scheme 2.2, nitroxide tetraradical **27** could be prepared in two steps from *tert*-butyldimethylsilyl-protected (TBDMS) hydroxylamine **30**: (1) deprotection of TBDMS groups to produce hydroxylamine **29** and (2) oxidation of hydroxylamine **29** to nitroxide **27**. The TBDMS-protected hydroxylamine **29** is obtained in the critical step in the synthesis of **30**, which is the introduction of *p*-phenylene spacers bearing TBDMS-protected hydroxylamine on the upper rim of calix[4]arene by palladium-catalyzed Negishi cross-coupling reaction between (4-bromo)phenyl TBDMS-protected hydroxylamine **31** and 1,3-alternate tetrabromocalix[4]arene **32**. The (4-bromo)phenyl TBDMS-protected hydroxylamine **31** can be prepared from 1,4-dibromobenzene by selective Br/Li exchange with *n*-BuLi and quenched with 2-methyl-2-nitrosopropane dimer followed by protection of hydroxylamine with TBDMS group using *tert*-butyldimethylsilyl chloride (TBDMSCl) according to the typical procedure.[61,62] Another coupling partner, tetrabromocalix[4]arene

**32** locked in the 1,3-alternate conformation, is obtained from bromination reaction of tetra-*O*-alkylated calix[4]arene which in turn is derived from etherification at the lower rim of calix[4]arene with 2-methoxyethyl tosylate using the procedure reported by Reinhoudt.[19]

**Scheme 2.2.** Retrosynthetic analysis of calix[4]arene nitroxide tetraradical **27**.
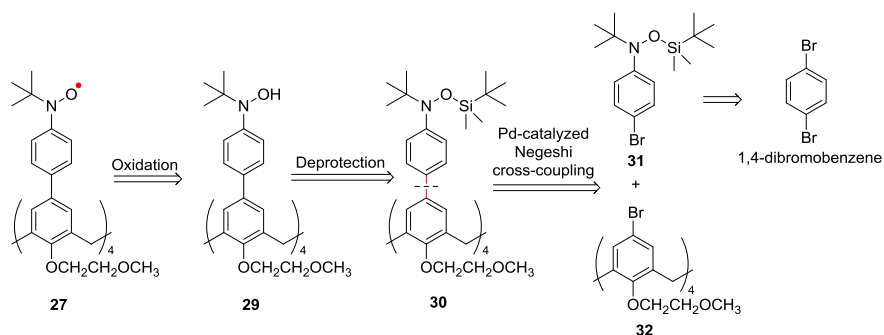


### Synthesis of calix[4]arene nitroxide tetraradical 27

The synthesis of calix[4]arene nitroxide tetraradical **27** started with the preparation of TBDMS-protected hydroxylamine **31** according to the published procedure.[61,62] As presented in Scheme 2.3, the Br/Li exchange on the 1,4-dibromobenzene, using *n*-BuLi (1.0 equiv) in diethyl ether, was followed by the addition of solid 2-methyl-2-nitrosopropane dimer (0.5 equiv) at −78 °C to give a hydroxylamine intermediate. After washing with hexane, a colorless crystalline solid of *N*-(4-bromophenyl)-*tert*-butylhydroxylamine was obtained. The ^{1}H NMR (400 MHz, chloroform-*d*, AO-4-55-solid) spectrum of hydroxylamine precursor showed two sets of doublet at $\delta = 7.370$ ppm ($J = 8.4$ Hz) and 7.117 ppm ($J = 8.4$ Hz) ppm assigned to four aromatic protons and a broad singlet at $\delta = 5.632$ ppm assigned to hydroxyl groups. These values are in agreement with those reported in the literature.[61] The hydroxylamine moiety was protected by TBDMS groups using TBDMSCl in the presence of imidazole in dimethyl formamide (DMF) at 80 °C to yield TBDMS-protected hydroxylamines **31** as colorless sticky oil in 50% yield (2

steps). ${}^1$H NMR (400 MHz, chloroform-*d*, AO-4-56-flt2) spectrum of **31** showed a sharp doublet at $\delta$ = 7.335 ppm (*J* = 8.8 Hz), assigned to two aromatic protons, and a broad doublet at $\delta$ = 7.115 ppm (*J* = 7.6 Hz), assigned to two aromatic protons at *ortho*/*ortho* position with respect to nitrogen on TBDMS group. Also, a broad peak at $\delta$ = −0.136 ppm was assigned to two methyl groups on TBDMS moiety. The broad peaks were caused by two conformations associated with the two diastereotopic methyl groups of TBDMS. Two diastereotopic methyl groups are exchangeable because of the rotation along N–C(aromatic) bonds and Si–O bonds. These values and observation are in agreement with previous report.[61]

**Scheme 2.3.** Synthesis of (4-bromo)phenyl TBDMS-protected hydroxylamine **31**.
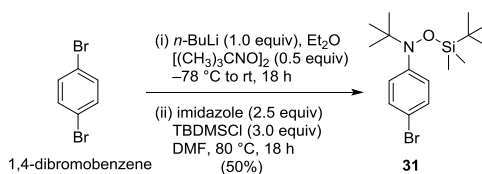


Tetrabromocalix[4]arene **32** was obtained from Dr. Sumit Mukherjee, a former graduate student in our group, who previously reported the synthesis and characterization of tetrabromocalix[4]arene **32** in his dissertation.[19,63]

The procedure for palladium-catalyzed Negishi cross-coupling reaction of (4-bromo)phenyl TBDMS-protected hydroxylamine **31** with tetrabromocalix[4]arene **32** was adapted from literature, e.g., Negishi cross-coupling of **31** with tritoluyl-protected 5-iodo-2′-deoxyuridine.[64,65] As shown in Scheme 2.4, the TBDMS-protected hydroxylamine **31** was converted to organozinc reagent, while tetrabromocalix[4]arene **32** was a coupling partner. The organozinc reagent was prepared by first generating organolithium of **31** with Br/Li exchange using *t*-BuLi (12.6 equiv) in THF, followed by transmetalation with ZnCl$_2$

(72 equiv) in THF at −78 °C. An excess of ZnCl$_2$ was used to minimize formation of homocoupling product, as previously reported.[61] In general, arylhalide (coupling partner) should be electron deficient to favor the oxidative addition of palladium catalyst. Alternatively, it could be accelerated using strong σ-donating ligands, such as trialkylphosphines to increase electron density around the metal. While tetrabromocalix[4]arene **32** contained ether group at *para*-position (the lower rim) could be classified as electron rich arylhalide, Pd[P(*t*-Bu)$_3$]$_2$ (80 mol% based on **32**) was used since the tri-*tert*-butyl phosphine was a strong σ-donating ligand and its steric hindrance facilitated the reductive elimination step.

**Scheme 2.4.** Synthesis of nitroxide tetraradical **27**.

(i) *t*-BuLi, THF, −78 °C, 2 h
(ii) ZnCl$_2$, THF, −78 °C to r.t., 10 min
(iii) Pd[P(*t*-Bu)$_3$]$_2$, **32**, THF, −78 °C to r.t., 72 h
(24-37%)

**31** **32**

*n*-Bu$_4$NF, THF, 15 h
(93-100%)

**30**

Ag$_2$O, CHCl$_3$, 18 h
(52%)

**29**

**27**

OCH$_2$CH$_2$OCH$_3$
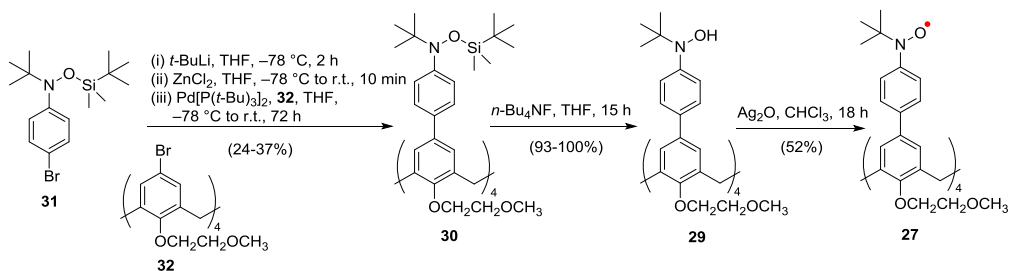
$^1$H NMR (400 MHz, chloroform-*d*, Figure 2.20A, AO-3-87-crd) spectrum of the crude mixture of Negishi cross-coupling reaction showed a doublet at $\delta \approx 7.50$ ppm, a broadened doublet at $\delta \approx 7.22$ ppm and a singlet at $\delta \approx 7.38$ ppm, which were corresponding to aromatic protons of the desired product. The small peak at $\delta \approx 7.36$ ppm and a broadened peak at $\delta = 7.10$ ppm may correspond to the unreacted TBDMS-protected hydroxylamine **31**. These reaction conditions were proved to be effective because, after addition of tetrabromocalix[4]arene **32** (1 equiv) in THF, the coupled product **30** was obtained in 24-37% yield after purification by column chromatography. The obtained yield is reasonable considering the substrates and the fact that four carbon-carbon bonds were formed in one

step. Not only tetrabromocalix[4]arene **32**, an electron rich substrate, can decelerate the rate determining step of the coupling reaction but the steric hindrance after the first coupling with arylzinc compound may also hinder the second reaction leading to incomplete reaction. The $^1$H NMR (600 MHz, chloroform-*d*, Figure 2.20B) and Figure D1 in Appendix D, AO-3-87-col1) spectrum of the tetra-coupled product **30** showed the doublet peak at $\delta$ = 7.518 ppm (*J* = 8.4 Hz) assigned to eight aromatic protons (Figure 2.20B, H$_a$) and the singlet peak at $\delta$ = 7.394 ppm assigned to eight aromatic protons (Figure 2.20B, H$_b$) on calix[4]arene scaffold. The broad peak at $\delta$ = 7.268 ppm was assigned to eight aromatic protons on spacer moieties (Figure 2.20B, H$_c$) at *ortho, ortho'* position with respect to nitrogen. The singlet peak at $\delta$ = 4.012 ppm was assigned to eight methylene bridge protons (Figure 2.20B, H$_d$) of 1,3-alternate conformation of calix[4]arene. The triplet peaks at $\delta$ = 3.701 and 2.875 ppm were assigned to two sets of eight protons (Figure 2.20B, H$_e$ and H$_f$, respectively) on –OCH$_2$CH$_2$OMe group. The singlet peak at $\delta$ = 2.800 ppm was assigned to 12 methoxy protons (Figure 2.20B, H$_g$). The singlet peaks at $\delta$ = 1.319 and 0.901 ppm were assigned to two sets of 36 *t*-Bu protons (Figure 2.20B, H$_h$ and H$_i$). The broadened singlet peak at $\delta$ = –0.124 ppm was assigned to 24 methyl protons (Figure 2.20B, H$_j$). The broadenings were caused by the rotation along N–C(aromatic) bonds, each partially averaging at least two conformations.[61] The $^{13}$C NMR (150 MHz, chloroform-*d*, Figure D2 in Appendix D) confirmed the assignment of **30**.
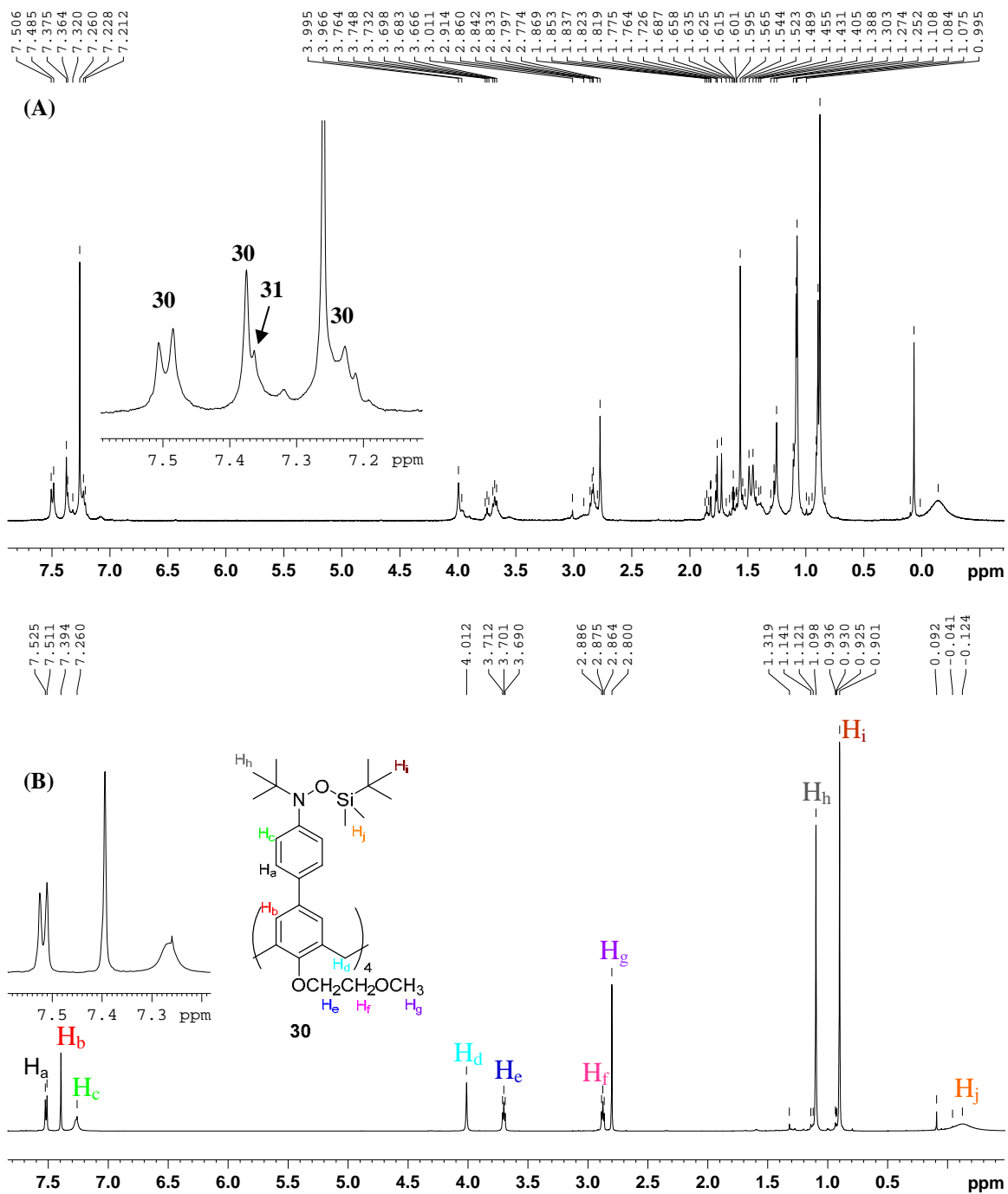
**Figure 2.20.** (A) $^1$H NMR (400 MHz, chloroform-*d*, label: AO-3-87-crd) spectrum of the crude mixture of Negishi cross-coupling reaction. (B) $^1$H NMR (600 MHz, chloroform-*d*, AO-3-87-col1) spectrum of TBDMS-protected tetrahydroxylamine **30**.

Deprotection of TBDMS group of TBDMS-protected tetrahydroxylamine **30** using tetrabutylammonium fluoride (*n*-Bu$_4$NF) in THF at room temperature provides hydroxylamine **29** in almost quantitative yield. $^1$H NMR (500 MHz, acetone-$d_6$, Figure D4 in Appendix D, label: AO-3-90-flt) spectrum revealed a singlet peak at $\delta$ = 9.124 ppm assigned to four protons of hydroxylamine groups. The same pattern of broadened doublet of eight aromatic protons at *ortho*, *ortho′* position with respect to nitrogen could still be observed at $\delta$ = 6.843 ppm ($J$ = 7.5 Hz). Also, the IR (ZnSe, Figure D6 in Appendix D) spectrum of hydroxylamine **29** showed a broad absorption at $\nu_{O\text{-}H}$ = 3232 cm$^{-1}$ which indicated the presence of hydroxyl group. The N–O stretching bands of aromatic and aliphatic hydroxylamines are generally in a range of 1250 ± 50 and 960 ± 20 cm$^{-1}$, respectively.[66-68] There are seven absorption bands ($\nu$ = 1029, 1057, 1081, 1124, 1172, 1200 and 1233 cm$^{-1}$) found in the IR spectrum of hydroxylamine **29** that are in the 1250 ± 50 cm$^{-1}$ range. The band at 1200 cm$^{-1}$ may be assigned as the N–O stretching as it disappears after oxidation to the corresponding nitroxide radical (see the discussion below).

The oxidation of tetrahydroxylamine **29** by an excess (40 equiv) of freshly prepared Ag$_2$O in CHCl$_3$ at room temperature with exclusion of light delivered the nitroxide tetraradical **27** in 52% yield after purification by flash column chromatography. Unfortunately, attempts to grow good quality single crystal of **27** for X-ray crystallography were unsuccessful. However, the nitroxide tetraradical **27** was characterized by $^1$H NMR, IR spectroscopy, high-resolution mass spectrometry (HR FAB-MS) and melting point. The IR (ZnSe, Figure D9 in Appendix D, label: AO-4-20-colfr2-3) spectrum of **27** showed a sharp peak at 1364 cm$^{-1}$ corresponding to N–O$^\bullet$ bond stretching vibration that is in agreement with the reported N–O$^\bullet$ stretching band of *t*-butylphenylnitroxide ($\nu_{N\text{-}O\cdot}$ = 1370

cm$^{-1}$).[68]    The wavenumber of the nitroxide **27** ($v_{N-O\cdot}$ = 1370 cm$^{-1}$) is higher than hydroxylamine **29** ($v_{N-O}$ = 1200 cm$^{-1}$) because N–O bond in the nitroxide radical is shorter (and stronger) than that of the hydroxylamine.   A broad peak assigned to the hydroxyl groups (at $v_{O-H}$ ≈ 3200 cm$^{-1}$) was also practically undetectable which confirmed the disappearance of O–H group.

### 2.2.2. $^1$H NMR spectra of nitroxide tetraradical 27

Paramagnetic shift in $^1$H NMR spectra of organic radicals refers to the shift in resonance signal of a proton nucleus caused by the presence of the unpaired electron.  The direction and magnitude of the shifts, determined relative to the corresponding proton from the precursor of the organic radicals or the closely related diamagnetic molecules, can therefore be used to correlate with the sign and magnitude of the electron-nucleus hyperfine coupling constant in the studied organic radicals.  Basically, the spin polarization explain such correlation.  A proton resonance of an organic radical shifts to the higher field possesses the opposite direction of spins with the radical and therefore has a negative value of the hydrogen hyperfine coupling constant.   While those shifts in the lower field contain the similar spin of the radical and have a positive value of the hydrogen hyperfine coupling constant. For example, the paramagnetic shifts of β-CH$_2$ and β-CH$_3$ protons in TEMPO are in the upfield direction corresponding to the opposite spin density from the nitroxide radical and having the negative sign value of hydrogen hyperfine coupling constants. (Figure 2.21) Whereas the opposite properties were observed for γ-CH$_2$ proton.  The magnitude of the shift is also correlated to the magnitude of the hyperfine coupling constant as the higher

values of the hyperfine coupling constant in β-CH$_2$ is relative to the larger paramagnetic

shift of β-CH$_2$ in comparison with β-CH$_3$ protons.[69]



β–CH$_3$, $\Delta H$ = -14.85 ppm; $a$ = -0.23 G
β–CH$_2$, $\Delta H$ = -25.92 ppm; $a$ = -0.30 G
γ–CH$_2$, $\Delta H$ = +12.37 ppm; $a$ = +0.18 G
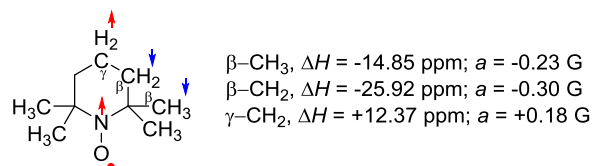
**Figure 2.21.** Spin distribution and estimated ^{1}H hyperfine coupling of TEMPO.

^{1}H NMR spectra of nitroxide tetraradical **27** were taken in concentrated solution at room temperature (295 K). Broad peaks, caused by paramagnetic shift, were observed (Figure 2.23). Because sharp peaks expected for diamagnetic by-products integrated to relatively few protons, ^{1}H NMR spectrum confirmed the high purity of nitroxide tetraradical **27** (~92% purity) (Figure D7 in Appendix D). The analyses of paramagnetic ^{1}H NMR spectra of tetraradicals and octaradicals describing the % purity of each compound are summarized in Table 2.1.

**Table 2.1.** Analyses of paramagnetic ^{1}H NMR spectra for tetranitroxide **27**, **36** and octaradicals **28**, **37**

| Compd | Label | Paramagnetic integrals | | Diamagnetic integrals | | Conc. of nitroxide (mM) | Minimun apparent purity (%)[a] |
|---|---|---|---|---|---|---|---|
| | | Values | Σ | Values | Σ | | |
| **27** | AO-4-33-col1&2-500 | 28.000, 44.343, 8.636 | 80.979 | 2.298, 4.815 | 7.113 | 77 | 92 |
| **28** | AO-4-37-col-500 | 5.761, 8.071, 28.000, 72.515 | 114.347 | 6.192, 0.571 | 6.763 | 60 | 94 |
| **36** | AO-4-80-col | 108.000, 30.321 | 138.321 | 3.453, 13.749 | 17.202 | 53 | 89 |
| **37** | AO-4-79-col | 1.682, 108.000, 46.647 | 156.329 | 21.026, 5.815 | 26.841 | 27 | 85 |

[a] Minimum apparent purity (%) is calculated based on the assumption that some of the paramagnetic peaks are missed (or under-integrated) because they are too broadened to be detected at relatively low concentrations of nitroxides.

The oxidation reaction of tetrahydroxylamine **29** to nitroxide tetraradical **27** proved to be quite challenging because a mixture of products, i.e. nitroxide tetra-, tri-, di- and monoradical was expected from the incomplete reaction.  As a result, ^{1}H NMR spectra would show a combination of complicatedly broad and sharp resonances due to the mixture of paramagnetic and diamagnetic molecules.  ^{1}H NMR (500 MHz, chloroform-*d*, Figure 2.22, label: AO-4-33-col1&2-500) spectrum of 77 mM tetraradical **27** contained four broadened peaks at $\delta$ = 4.004 and 3.634 (br, br, 28H), −3.180 (br, 36H), −5.415 (br, 8H) and −13.95 (br, 8H) ppm.
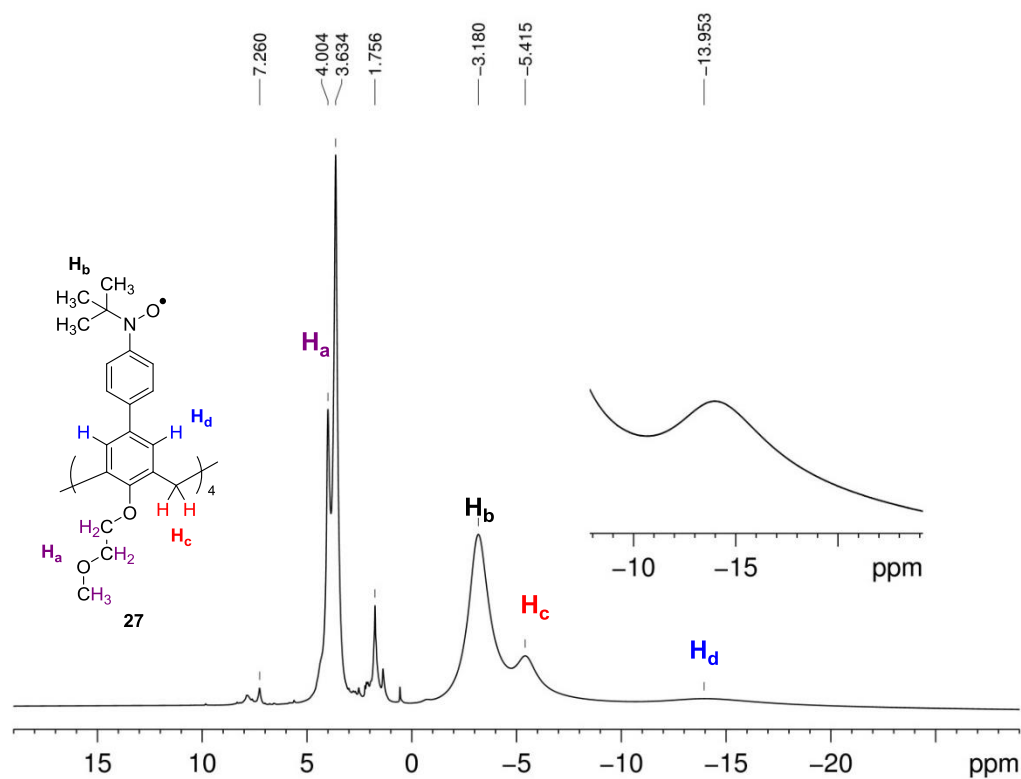


**Figure 2.22.** ^{1}H NMR (500 MHz, chloroform-*d*, conc. 77 mM, AO-4-33-col1&2-500) spectrum of nitroxide tetraradical **27** (~92% purity, see Table 2.1, Figure D7 in Appendix D).  Reproduced from Ref. 72 with permission from The Royal Society of Chemistry.

The resonances at $\delta = 4.00$ and 3.63 ppm corresponded to the 28 protons ($\mathbf{H_a}$) of methyl ($CH_3$) and dimethylene ($CH_2CH_2$) of the methoxyethyleneoxy ($-OCH_2CH_2OCH_3$) groups, respectively. These chemical shifts nearly coincided with those of the corresponding hydroxylamine **29**. This suggested that the spin densities at the hydrogen atoms of $-OCH_2CH_2OCH_3$ groups are negligible due to the twisting of the methoxyethyleneoxy group out of conjugation with the benzene ring and the nitroxide analogously to the methoxy group in the previously reported 3,5-dimethyl-4-methoxyphenyl-*tert*-butylnitroxide.[70]

The 36 protons ($\mathbf{H_b}$) at $\delta = -3.18$ ppm were assigned to the *tert*-butyl group on the nitroxide moieties. The $^1H$ NMR resonance of *tert*-butyl groups on nitroxides of tetraradical **27** was shifted upfield at $\delta = -3.18$ ppm compared to those of the corresponding hydroxylamine **29** at $\delta = 1.21$ ppm (Figure D5 in Appendix D). Similar shifts were found in tetraradical **24**, diradical **25** and *N-tert*-butylnitroxide.[43,59,71] The significant upfield shift by several ppm for *tert*-butyl protons may be explained by the substantial amount of negative spin densities (spin down, ↓, Figure 2.23) at the hydrogen atoms of *tert*-butyl group causing by spin polarization through σ-bonds of the positive spin density at the nitrogen atom.

The broad singlet signal at $\delta = -5.42$ ppm represented the bridge methylene protons ($\mathbf{H_c}$) which was also shifted upfield compared at $\delta = 3.61$ ppm for that of the corresponding hydroxylamine **29**. The negative spin density at the bridge methylene hydrogen atoms also cause by spin polarization from the positive spin density at the nitroxide radical through σ-bonds as found in tetraradical **24** and diradical **25**.[70]
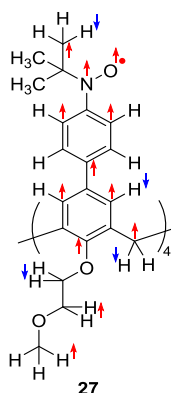
**Figure 2.23.** Spin distribution by spin polarization of tetraradical **27**.
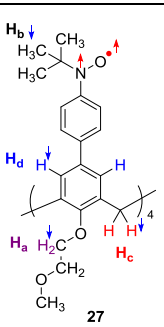
Finally, the very broad signal at the most upfield region $\delta = -13.95$ ppm was assigned to aromatic protons (**H_d**) on calix[4]arene moiety. This upfield shift can be compared to the resonance for aromatic protons of hydroxylamine **29** at $\delta = 7.37$ ppm. The resonances of aromatic protons on benzene rings (spacers) directly attached to nitroxides were not visible because delocalization of significant spin density is expected on these nuclei.

Calculation of proton hyperfine coupling $|A(^1H)|$, spin density as well as geometry optimization of $D_2$-symmetric structure of simplified derivative of **27**, in which the $-OCH_2CH_2OCH_3$ group was replaced with $-OCH_3$ group (**27a**), were performed at DFT level. Summary of calculation can be found in the literature.[72] As expected, the sign and magnitude of the calculated hyperfine coupling constants ($A(^1H)$) in **27a** were in qualitative agreement with the assigned paramagnetic shifts of **27** (Figure D42 in Appendix D). Above all, the proton resonance signals of the aromatic protons on benzene ring directly attached to nitroxide radicals are invisible as the estimated values of the $A(^1H)$ are very large. In addition, the negative signs and relative values of the calculated hyperfine coupling constants of "**H_a**", "**H_c**", and "**H_d**" are in agreement with the sign and magnitude of the

paramagnetic shifts. The sign of the proton paramagnetic shift on the *t*-butyl group labelled as "**H**b" is negative as in agreement with the opposite spin from nitroxide radical by the spin polarization. However, the computed hyperfine coupling constant on the "**H**b" gives the opposite sign compared to the sign of the proton paramagnetic shift probably due to the average between hyperfine coupling constant "**H**b" of spin polarization through σ-bond and a direct interaction of protons to the radical spin through space.

Lastly, the sign and the proton resonances of "**H**a", "**H**b", and "**H**c" tentatively correspond to the previous observation of the 1,3-alternate conformer of nitroxide tetraradical **24**.[63] These ^{1}H NMR spectroscopic assignments confirmed the structure and purity of the locked 1,3-alternate conformation of tetraradical **27**.

**Table 2.2**. Paramagnetic shift of tetraradical **27**

| | Atoms | Shift of hydroxylamine **29** (ppm)[a] | Shift of nitroxide **27** (ppm)[a] | Paramagnetic shift $\Delta\delta$ (ppm) | Computed ^{1}H hyperfine coupling of **27a** (MHz)[b] |
|---|---|---|---|---|---|
|  | $H_a$ | 3.99 | 3.63 | −0.36 | −0.0101 |
| | $H_b$ | 1.21 | −3.18 | −4.39 | +0.0410 |
| | $H_c$ | 3.61 | −5.42 | −9.03 | −0.1712 |
| | $H_d$ | 7.37 | −13.95 | −21.32 | −0.3742 |

[a] ^{1}H NMR chemical shift. [b] isotropic hyperfine couplings computed at the UB3LYP/EPR-II level of **27a**; for example, isotropic hyperfine coupling of $H_b$ is the average from nine hydrogen atoms of *t*-Bu group.

### 2.2.3. EPR spectra of nitroxide tetraradical 27

CW-EPR (X-band) spectra of tetraradical **27** at room temperature (294-295 K) in solution of 2-MeTHF (Figure D10 in Appendix D), 2-MeTHF/MeOH (2:1) (Figure D11A in Appendix D) and toluene/CHCl3 (4:1) (Figure D12A in Appendix D) showed a very

broad peak which may be explained by incomplete motion averaging of the anisotropy, i.e., the anisotropy observed in the rigid lattice spectrum in Figure 2.24 shown below.

The spin counting experiment of tetraradical **27** was carried out in chloroform at room temperature (294–295 K) to determine the number of unpaired electrons per molecule as well as the purity. 4-Oxo-TEMPO and 3-carboxy-PROXYL (1.5 mM in chloroform) were used as intensity references. The spin counting revealed 3.90 ± 0.34 unpaired electrons per molecule confirming the purity of tetraradical **27** (four unpaired electrons). The average value of $\chi T = 1.47 \pm 0.13$ emu K mol$^{-1}$ obtained by EPR spin counting is in agreement with the theoretical value of $\chi T = 1.50$ emu K mol$^{-1}$ for four weakly coupled $S = \frac{1}{2}$ radicals.

**Table 2.3.** Summary of EPR spin count measurements for tetraradical **27** (1.5 mM in chloroform) at 294–295 K

| Run | Sample | Double Integration | SW[a] | Number of unpaired electrons | Avg. $\chi T$ (emu K mol$^{-1}$) |
|---|---|---|---|---|---|
| AO421r1 | AO-4-20-colfr2-3 | 3.84e7 | 400 | 3.79 | |
| AO421r3 | 4-Oxo-TEMPO | 2.53e8 | 80 | | |
| AO421r1 | AO-4-20-colfr2-3 | 3.84e7 | 400 | 3.62 | $1.47 \pm 0.13$[b] |
| AO421r2 | 4-Oxo-TEMPO | 1.06e7 | 400 | | |
| AO559r1 | AO-4-33-col1&2 | 7.076e7 | 400 | 4.28 | |
| AO560r1 | 3-Carboxy-PROXYL | 1.654e7 | 400 | | |

[a] SW = sweep width; [b] mean ± standard deviation

CW-EPR (X-band) spectra of tetraradical **27** at 133 K in 2-MeTHF at a series of concentrations (0.03, 0.06 and 0.25 mM) are shown in Figure D13 in Appendix D and (1.0 mM) Figure 2.24. The spectra showed two distinct spectral features: broad and sharp bands which we assigned to two conformations **27$_b$** and **27$_s$**, respectively (Figure 2.25).
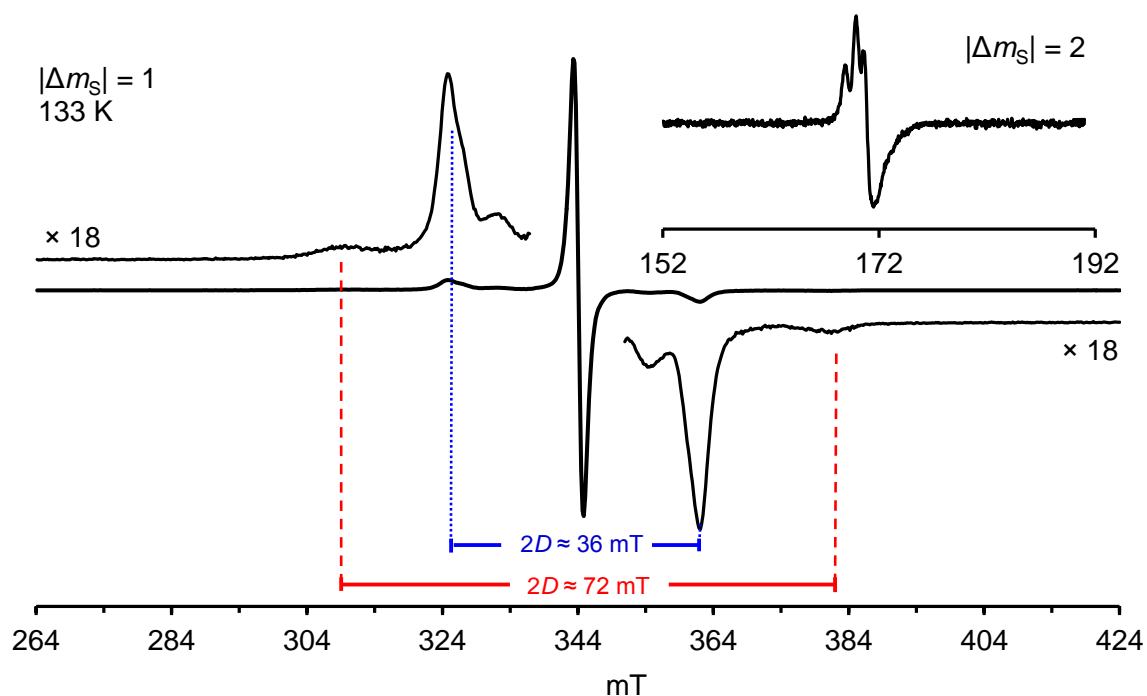
**Figure 2.24.** CW EPR (X-Band, ν = 9.6531 GHz, $|\Delta m_s|$ = 1) spectrum of 1 mM calix[4]arene nitroxide tetraradical **27** in 2-MeTHF at 133 K, 4-mm tube, sample label: AO420colfr2-3, EPR label: AO434r16/r12. Inset plot: $|\Delta m_s|$ = 2 region, ν = 9.6529 GHz. Adapted from Ref. 72 with permission from The Royal Society of Chemistry.

The conformation **27b** where the distance between the two co-facial pairs of nitroxide radicals is shorter for one diagonal pair of nitroxides compared to the other pair was assigned based on the EPR spectra. First, broad side bands with dipolar splitting $2D_\perp$ ~ 72 mT in the $|\Delta m_s|$ = 1 region supported the presence of the dipole-dipole interaction between one diagonal pair of nitroxide radicals and corresponded to $S$ = 1 state. The observation of strong half-field transition, $|\Delta m_s|$ = 2. Since dipolar spitting parameter $D$ is derived from dipole-dipole interaction, it can be related to the distance $r$ between two

unpaired electrons from the shorter distance of one cofacial pair of the nitroxide radicals by the point dipole approximation as given in eq. (1),[73]

$$D = 2781/r^3 \qquad \text{(eq. 1)}$$

where $D$ is the dipolar splitting parameter in mT units, and $r$ is the average distance between the unpaired electrons in Å units.  The distance of a cofacial pair of nitroxide radicals estimated by the point-dipole approximation is around 4.3 Å.  The distance of another cofacial pair (the longer distance) of nitroxide radicals is then about ~5.3 Å by constructing the conformation **27b** using a molecular model kit.  The roughly estimated distance is corresponded to the dipolar splitting ($2D$) of 36 mT (Figure 2.25).  Thus, the conformation **27b** can be viewed as containing two separated spin systems.  The broad band ($2D_\perp \sim 72$ mT) is a characteristic of 1,3-alternate nitroxide radicals calix[4]arene derivatives but somewhat larger since $2D = 29\text{-}31$ mT is found in 1,3-alt diradical **24** with point-dipole distance of 5.6-5.8 Å. [74]



**27b**

estimated by point-dipole approximation

**27s**

estimated by DFT calculation
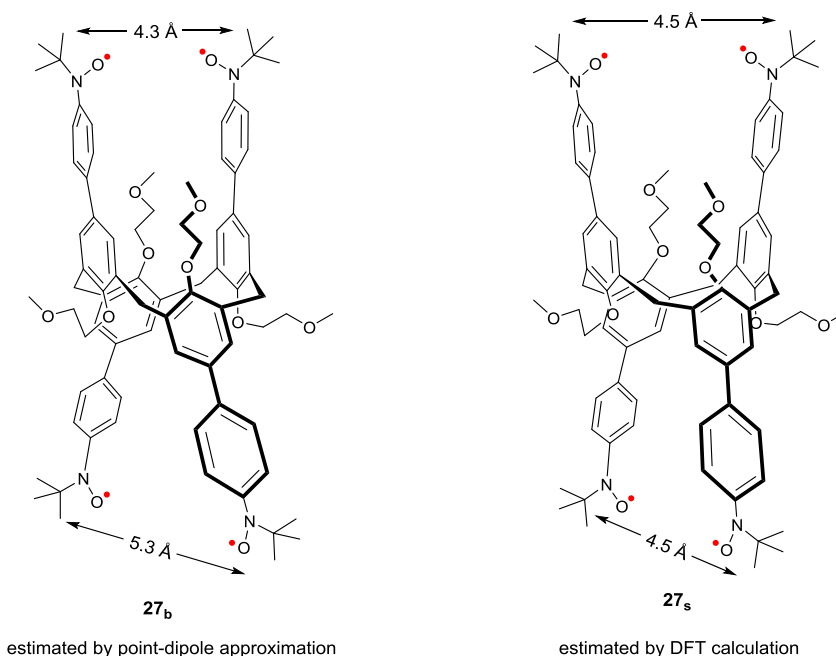
**Figure 2.25.**  Conformation of tetraradical **27b** and **27s**

Second, the sharp peak at the center of the spectrum with a peak-to-peak linewidth ($\Delta B_{pp}$) ~ 1.5 mT was assigned to highly symmetric conformation of tetraradical **27$_s$**. The EPR spectrum pattern of tetraradical **27$_s$** is also similar to previously reported tetraradical **24** in which the though-bond exchange coupling was about 1 K and no dipolar spitting was observed due to high symmetry of the molecule.[59]

There is no aggregation observed of tetraradical **27** since the spectral features of EPR spectra are independent of concentration (Figure D13 in Appendix D). In addition, the EPR spectra of **27** reveal the solvent dependence; double integration of the sharp band **27$_s$** is about 30% in 2-MeTHF but approximately 10% in 2-MeTHF/MeOH (2:1) as summarized in Table 2.4. The two distinct spectra were also obtained between 2-MeTHF/MeOH (2:1) and toluene/CHCl$_3$ (4:1) which were taken at 133 K (Figure D11B and D12B in Appendix D).

**Table 2.4.** % Content of **27$_s$** in different solvents for EPR samples of tetraradical **27**.

| EPR label | Solvent | % Content **27$_s$** |
|---|---|---|
| AO434 | 2-MeTHF | 30 |
| AO563 | 2-MeTHF/MeOH (2:1) | 10 |
| AO564 | toluene/CHCl$_3$ (4:1) | 30 |

### 2.2.4. Magnetic studies of tetraradical 27

The magnetic studies of tetraradical **27** were carried out by SQUID magnetometry in solid and solution. As presented in Figure 2.26, the flat plot between $\chi T$ and $T$ where $\chi$ is molar magnetic susceptibility and $T$ is temperature is observed in 100-290 K range (high temperature). The experimental value of $\chi T = 1.47$ emu K mol$^{-1}$ for tetraradical **27**, which can be considered as four weakly coupled $S = \frac{1}{2}$ radicals, is in good agreement with the

theoretical value of $\chi T = 1.50$ emu K mol$^{-1}$ of four independent $S = \frac{1}{2}$ radicals.  At low temperatures, the $\chi T$ versus $T$ plot for **27** in the solid state showed a downward turn due to typical intermolecular antiferromagnetic exchange coupling.  However, the magnetic studies of **27** in 7-9 mM solution of 2-MeTHF and 2-MeTHF/THF also showed similar downward turns presumably because of the aggregation or precipitation at low temperature.  As a result, the low temperature SQUID studies of weak intramolecular exchange coupling by SQUID magnetometry were problematic, and therefore the intramolecular exchange couplings were evaluated from $^1$H-NMR spectroscopic data and DFT calculations.
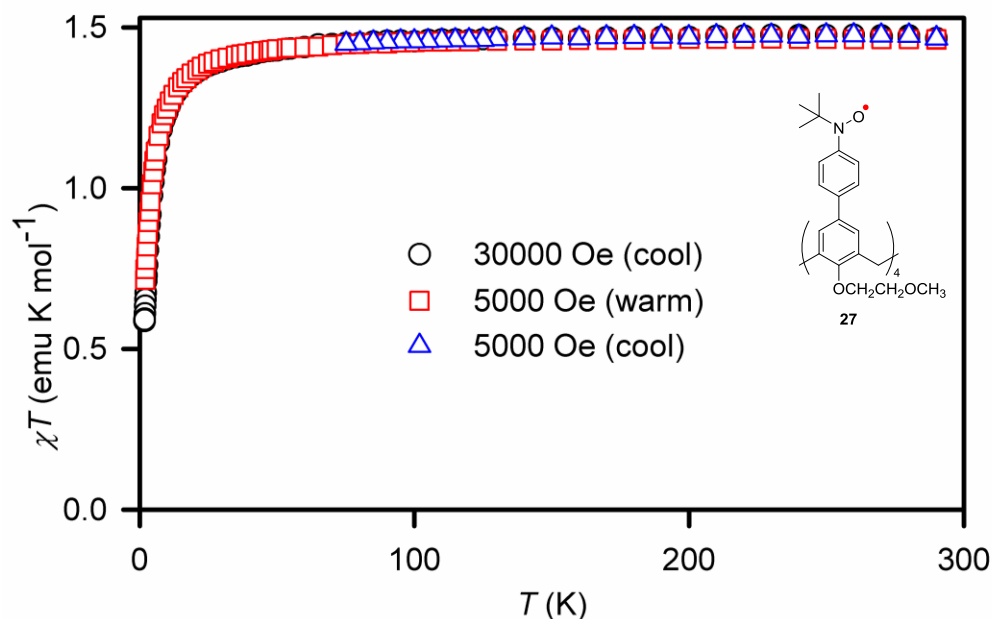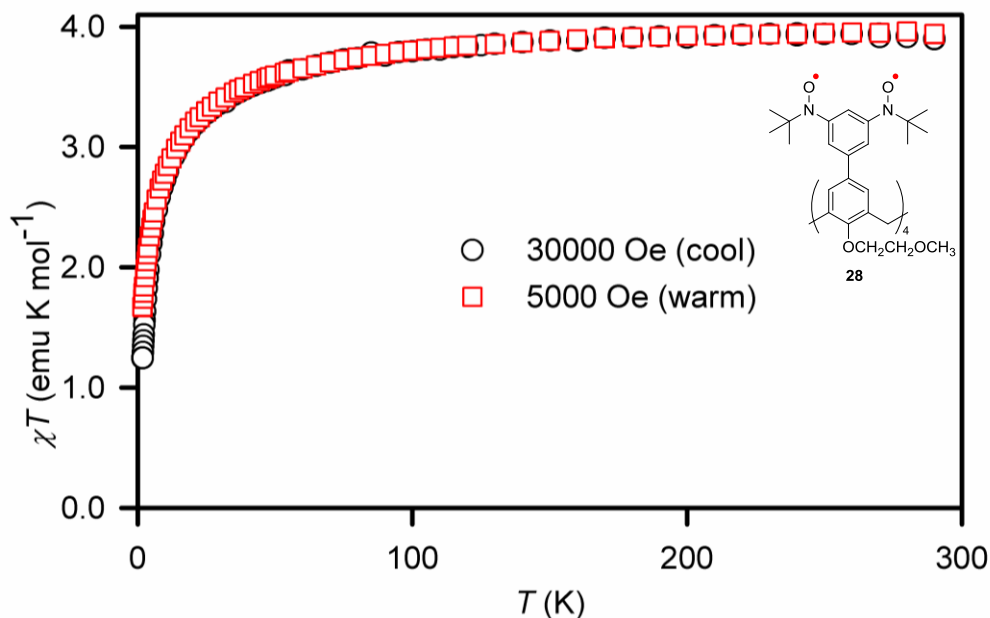


**Figure 2.26.** SQUID magnetometry of solid nitroxide tetraradical **27** (sample label: AO433col1&2, SQUID label: AO507s1).  Reproduced from Ref. 72 with permission from The Royal Society of Chemistry.

Intramolecular exchange coupling of calix[4]arene scaffold may be dissected into through-space and/or through-bond components. The through-space exchange coupling between cofacial nitroxides for tetraradical **27** is expected to be similar ($J/k \approx -1$ K) to tetraradical **24** because the distances between cofacial nitroxides (N⋯N) in $D_2$-symmetry of optimized **24a** and **27a** (similar conformation as **27$_s$**) are in the same range (4-5 Å; see Table D1 in Appendix D). The through-bond exchange coupling through nitroxide–*p*-phenylene spacer–*m*-phenylene–$CH_2$–*m*-phenylene–*p*-phenylene spacer–nitroxide for tetraradical **27** is expected to be much smaller ($|J/k| < 1$ K) than those for tetraradical **24** because the *p*-phenylene spacers of tetraradical **27** extend the through-bond exchange coupling pathway (between "adjacent" nitroxides). Based on the previous studies, one *p*-phenylene spacer in high-spin polyradicals could decrease $|J/k|$ by a factor of 5-6. Thus, $|J/k|$ was expected to decrease by a factor of 30 due to *p*-phenylene spacers in the coupling pathway.[75,76]

In addition, the average spin density at carbon atoms at the $CH_2$ methylene group that act as coupling units, in tetraradical **27a** (0.0012) is much smaller than those in tetraradical **24a** (0.0060) (C8 and C11 in Figure D42 in Appendix D). Also, isotropic ^{1}H hyperfine couplings ($A_H$) for methylene protons ($CH_2$) are much smaller for **27a** (–0.17 MHz) than **24a** (–0.93 MHz). These results supported the weaker through-bond interaction of **27** than **24** due to decreased average spin density in the coupling unit. The values and signs of isotropic hyperfine coupling, $|A(^1H)|$, may be determined by ^{1}H NMR spectroscopy of concentrated solutions of radicals.[77] DFT-computed signs and magnitudes of $A(^1H)$ in $D_2$-optimized geometry of **27a** are in qualitative agreement with the observed paramagnetic shifts for **27**.

**2.2.5. Synthesis of calix[4]arene nitroxide octaradical 28**

**Synthetic plan for calix[4]arene nitroxide octaradical 28**

As presented in Scheme 2.5, nitroxide octaradical **28** is prepared in two steps from TBDMS-protected hydroxylamine **34**: (1) deprotection of TBDMS groups to yield hydroxylamine **33** and (2) oxidation of hydroxylamine **33** to nitroxide **28**. TBDMS-protected hydroxylamine **34** is prepared by palladium-catalyzed Negishi cross-coupling reaction between TBDMS-protected hydroxylamine **35** and 1,3-alternate tetrabromocalix[4]arene **32**. TBDMS-protected hydroxylamine **35** is synthesized from 1,3,5-tribromobenzene according to the previous report.[61,62]

**Scheme 2.5.** Retrosynthetic analysis of calix[4]arene nitroxide octaradical **28**.
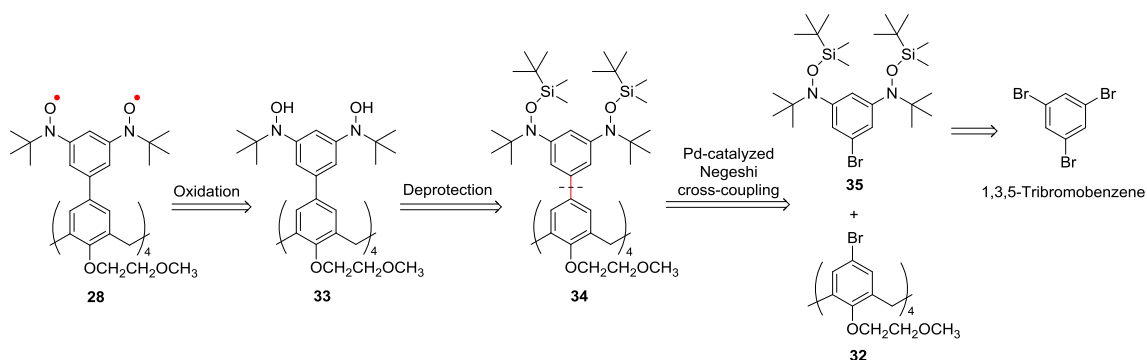


**Synthesis of calix[4]arene nitroxide octaradical 28**

The synthesis of calix[4]arene nitroxide octaradical **28** started with preparation of TBDMS-protected hydroxylamine **35** according to the published procedure.[61] The Br/Li exchange on the 1,3,5-tribromobenzene, using *t*-BuLi (4.0 equiv) in diethyl ether, was followed by the addition of solid 2-methylnitrosopropane dimer (1.2 equiv) at −78 °C to give dihydroxylamine intermediate product. After work up, dihydroxylamine precursor as a light brown solid was obtained. The $^1$H NMR spectrum (400 MHz, chloroform-*d*) showed a broad singlet signal at $\delta = 8.03$ ppm corresponding to two protons of

hydroxylamine groups. The broad singlet peaks at $\delta = 6.92$ and 6.83 ppm were assigned

to two and one aromatic protons, respectively. These values are in good agreement with

the previous report.[61] The hydroxylamine moiety was then protected by TBDMS groups

using TBDMSCl in presence of imidazole in DMF at 80 °C to yield TBDMS-protected

hydroxylamine **35** as a colorless sticky oil in 74% yield.

**Scheme 2.6.** Synthesis of TBDMS-protected hydroxylamine **35**
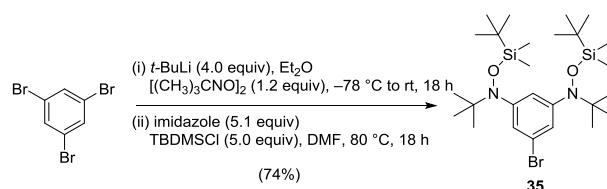


The procedure for synthesis of octaradical **28** is similar to the synthesis of

tetraradical **27** described in the section 2.2.1. The synthetic scheme is shown in Scheme

2.7. The Br/Li exchange on TBDMS-protected hydroxylamine **35** (6 equiv), using *t*-BuLi

(12.6 equiv) in THF gave the organolithium which was converted to the organozinc by

reacting with ZnCl$_2$ in THF (72 equiv) at −78 °C, and then warming the resultant reaction

mixture to room temperature. Pd[P(*t*-Bu)$_3$]$_2$ (80 mol% based on **32**) in THF was added at

−78 °C. Finally, tetrabromocalix[4]arene **32** (1 equiv) in THF was added at −78 °C. The

$^1$H NMR (400 MHz, chloroform-*d*, Figure 2.27A) spectrum of the crude mixture revealed

a singlet peak and a broad peak overlapping at $\delta \approx 7.30$ ppm which may correspond to

aromatic protons on benzene rings of calix[4]arene scaffold and spacer, respectively. The

resonances at $\delta \approx 7.10$ ppm and $\delta \approx 2.0 - 1.5$ ppm correspond to unknown impurities.

The coupled product **34** was obtained in 7-25% yield, which was lower than

preparation of **28** (24-37% yield), possibly due to the difficulties in separation by column

chromatography. The $^1$H NMR (400 MHz, chloroform-*d*, Figure 2.27B and Figure D14 in

Appendix D, AO-3-88-hv) spectrum of tetra-coupled TBDMS-protected hydroxylamine **34** exhibited a broad singlet peak at $\delta = 7.315$ ppm which was assigned to eight aromatic protons (Figure 2.29, $H_a$) on calix[4]arene scaffold. A very broad peak underneath the same region (~7.2 ppm) corresponded to 12 aromatic protons (Figure 2.27B, $H_b$ and $H_c$) on benzene ring directly attached to nitroxides (*p*-phenylene spacers). The characteristic singlet peak at $\delta = 4.017$ ppm assigned to eight methylene bridge protons (Figure 2.27B, $H_d$) of 1,3-alternate conformer of calix[4]arene moiety. Two sets of eight protons (Figure 2.27B, $H_e$ and $H_f$) corresponding to $-OCH_2CH_2OMe$ group are at $\delta = 3.572$ and 2.911 ppm. Another singlet peak overlapping at $\delta = 2.911$ ppm corresponded to 12 methoxy protons (Figure 2.27B, $H_g$). Singlet peaks at $\delta = 1.120$ and 0.950 ppm were assigned to two sets of each 72 *t*-Bu protons (Figure 2.27B, $H_h$ and $H_i$). The broadened singlet peak at $\delta = -0.061$ ppm was assigned to 48 methyl protons (Figure 2.27B, $H_j$). The broadenings were caused by the rotation along N–C(aromatic) bonds, each partially averaging at least two conformations.[61] $^{13}$C NMR (100 MHz, chloroform-*d*, Figure D15 in Appendix D, AO-3-88-hv) spectrum confirmed the assignment of TBDMS-protected hydroxylamine **34**.
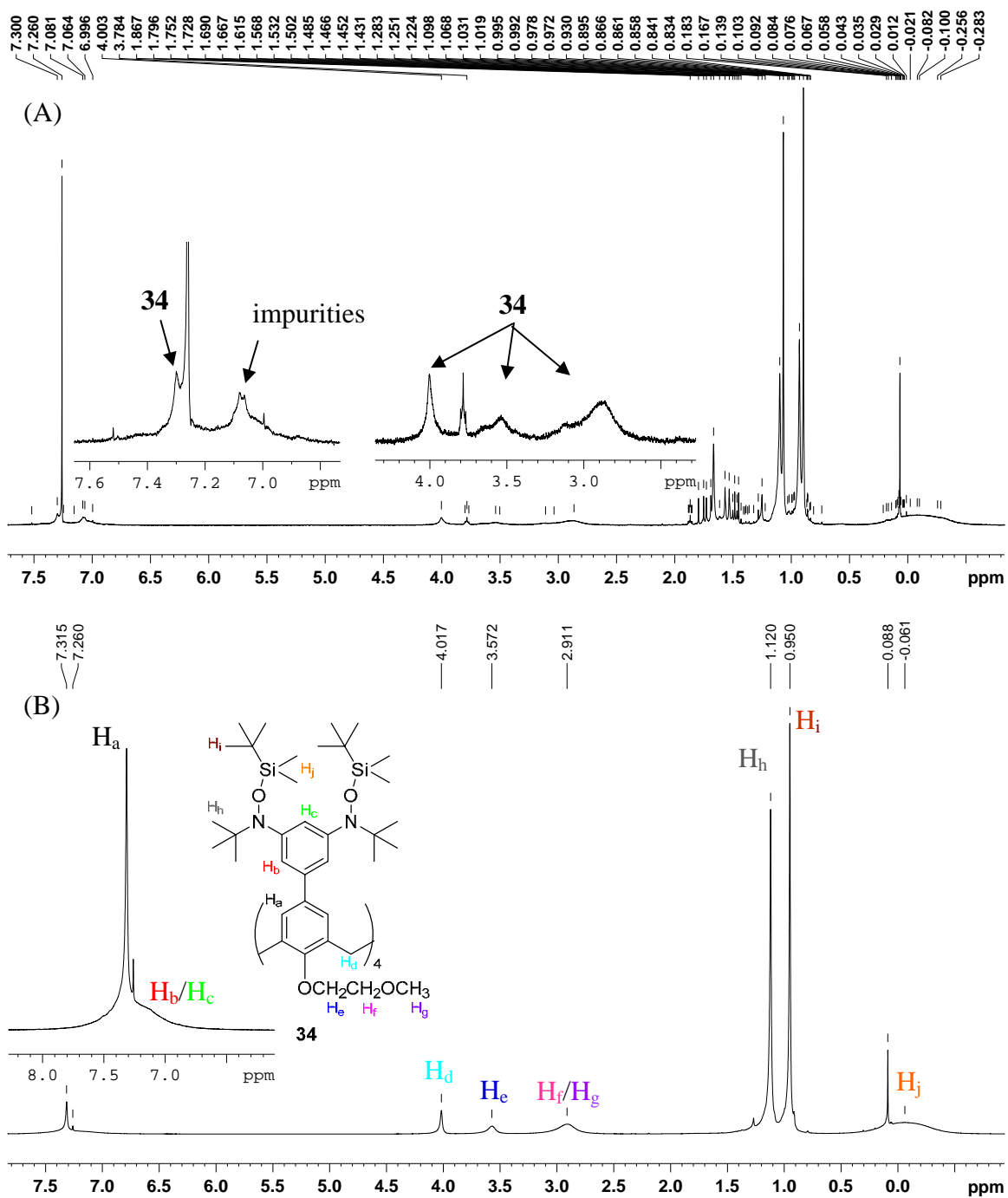
**Figure 2.27.** (A) $^{1}$H NMR (400 MHz, chloroform-*d*) spectrum of crude mixture of **34**. (B) $^{1}$H NMR (400 MHz, chloroform-*d*, label: AO-3-88-hv) spectrum of tetra-coupled TBDMS-protected tetrahydroxylamine **34**.

**Scheme 2.7.** Synthesis of nitroxide octaradical **28**.
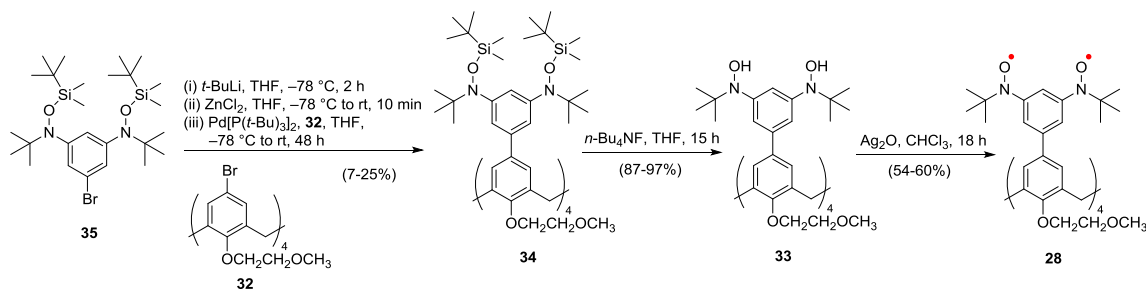


Deprotection of TBDMS groups of **34** using $n$-Bu$_4$NF in THF for overnight at room temperature gave octahydroxylamine **33** in 87-97% yield. $^1$H NMR (400 MHz, chloroform-$d$, Figure D17 in Appendix D) spectrum showed a broad resonance at $\delta = 9.028$ ppm corresponding to eight protons of hydroxyl groups. In addition, IR (cm$^{-1}$, Figure D18 in Appendix D) spectra of **33** confirmed the presence of hydroxylamine groups indicating by the absorption at $\nu_{O-H} \approx 3172$ cm$^{-1}$.

The octahydroxylamine **33** was then oxidized by freshly prepared Ag$_2$O in CHCl$_3$ at room temperature for overnight, exclusion of light. After purification by column chromatography, the nitroxide octaradical **28** was successfully obtained in 54-60% yield. The octaradical **28** was characterized by $^1$H NMR, IR spectroscopy, high-resolution mass spectrometry (HR FAB-MS) and melting point. IR (ZnSe, cm$^{-1}$, Figure D21 in Appendix D) spectrum of **28** no longer showed the absorption of hydroxylamine, $\nu_{O-H} \approx 3200$ cm$^{-1}$ and $\nu_{N-O}$ at 1199 cm$^{-1}$.

### 2.2.6. $^1$H NMR spectra of nitroxide octaradical 28

$^1$H NMR (500 MHz, chloroform-$d$, label: AO-4-37-col-500, conc. 60 mM, Figure 2.28 and Figure D19 in Appendix D) spectrum of octaradicals **28** was taken at room temperature (295 K) showed four broadened peaks at $\delta = 22.92$ (br, 8H), 12.44 (br, 8H),

4.74 and 4.17 (br, br, 28H) and −2.80 (br, 72H). Two broad peaks at $\delta$ = 4.74 and 4.17 corresponded to the 28 protons ($H_a$) on the −$CH_2CH_2OCH_3$ chain. The broad peak at the most upfield region ($\delta$ = −2.80 ppm) were assigned to 72 protons ($H_b$) from the *tert*-butyl groups on the nitroxide moieties. These two types of protons were presented at the same region compared to those in tetraradical **27**. On the other hand, the broad signal at +12.44 ppm which represented the bridge methylene protons ($H_c$) and very broad signal at the most downfield region which assigned to aromatic protons ($H_d$) on calix[4]arene presented in opposite region between tetraradical **27** and octaradical **28**. Specifically, the paramagnetic shifts for resonances labeled $H_c$ are −5.42 and +12.44 ppm in **27** and **28**. Also, paramagnetic shifts for resonances labeled $H_d$ are −13.95 and +22.91 ppm in **27** and **28**, respectively. This can be explained by spin up (↑) on $H_c$ and $H_d$ atoms causing by connectivity of nitroxide radicals to *meta*- position in octaradical **28** vs. spin down (↓) on $H_c$ and $H_d$ atoms causing by connectivity of nitroxides to *para*- position in tetraradical **27**, as shown in spin density distribution in Figures 2.23 and 2.29.
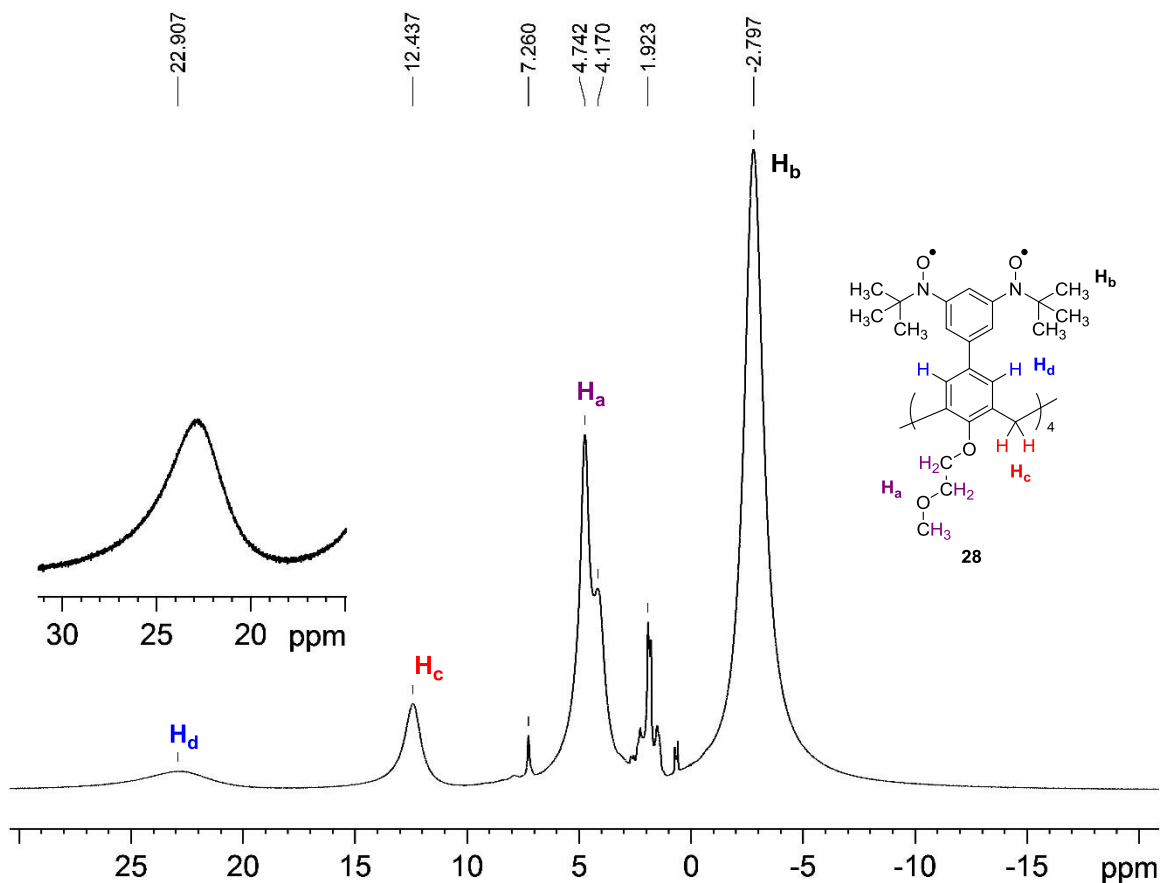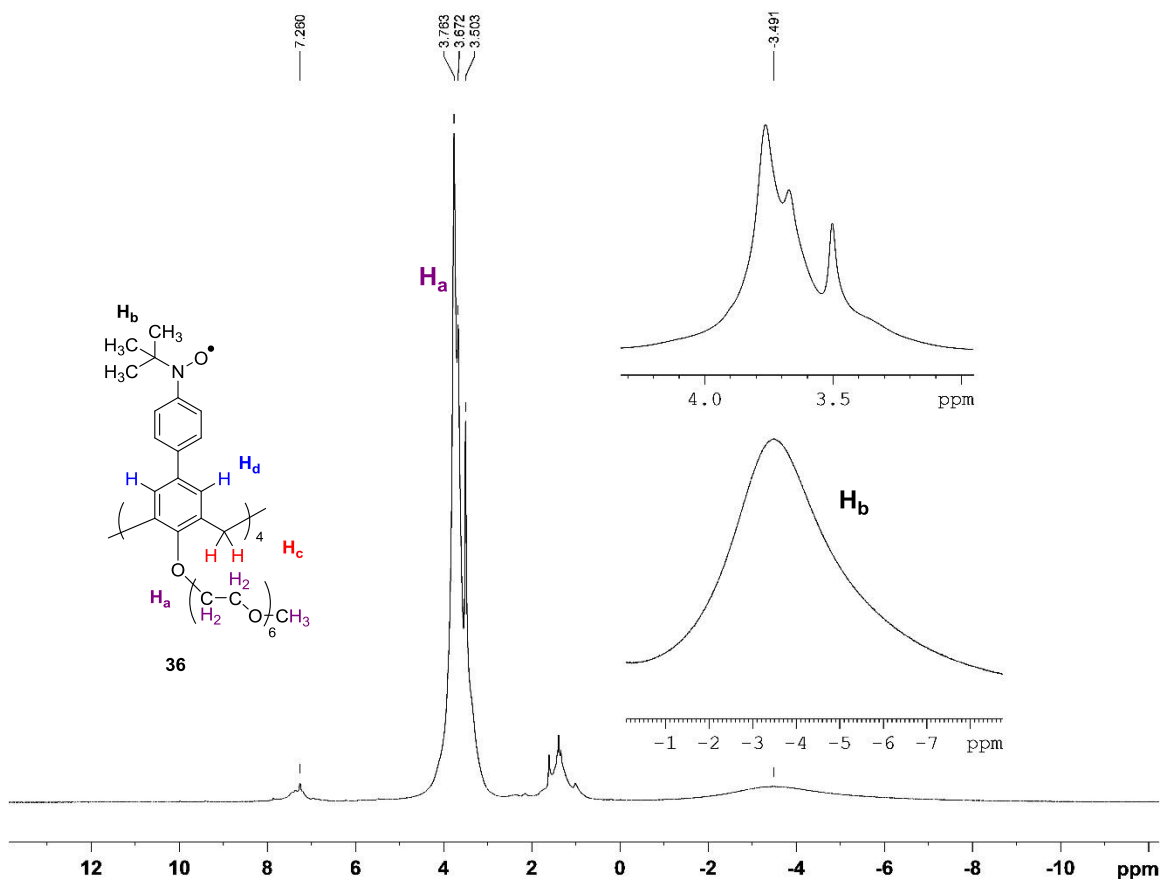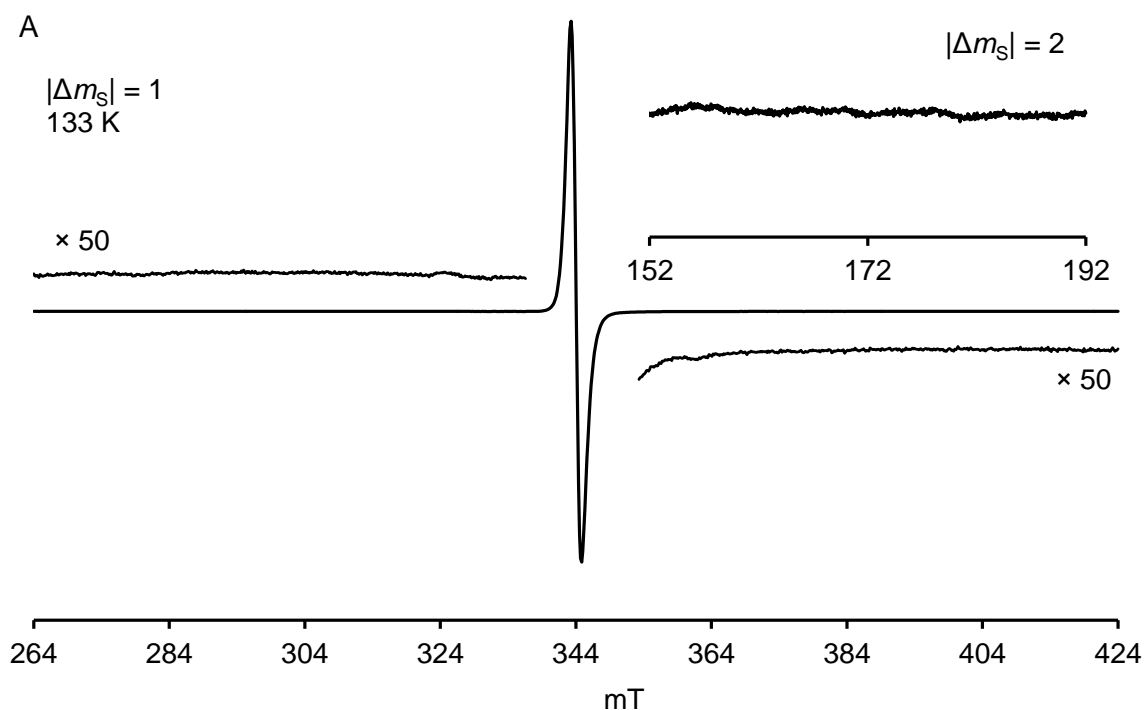
**Figure 2.28.** $^1$H NMR (500 MHz, chloroform-*d*, conc. 60 mM, label: AO-4-37-col-500) spectrum of nitroxide tetraradical **28** (~94% purity, see: Table 2.1 and Figure D19 in Appendix D).  Reproduced from Ref. 72 with permission from The Royal Society of Chemistry.
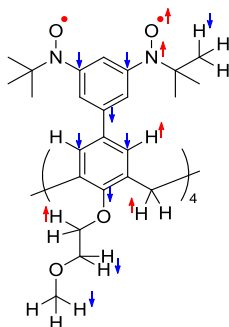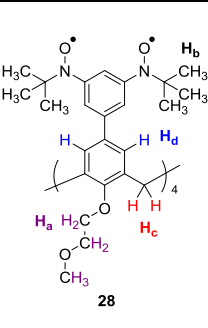


**Figure 2.29.**  Spin density distribution of octaradical **28**.

In addition, $^1$H NMR (500 MHz, chloroform-$d$, label: AO-4-32-col, conc. 44 mM, Figure D20 in Appendix D) spectrum of octaradical **28** from another experiment was also presented.

**Table 2.5.** Paramagnetic shift of octaradical **28**

| | Atoms | Shift of hydroxylamine **33** (ppm) | Shift of octaradical **28** (ppm) | Paramagnetic shift Δδ (ppm) | Computed $^1$H hyperfine coupling of **28a** (MHz)[b] |
|---|---|---|---|---|---|
| | $H_a$ | 4.04 | 4.74 | 0.70 | +0.0030 |
| | $H_b$ | 1.22 | −2.80 | −4.02 | +0.0261 |
| | $H_c$ | 3.64 | 12.44 | 8.80 | +0.0537 |
| | $H_d$ | 7.42 | 22.91 | 15.49 | +0.1118 |

[a] $^1$H NMR chemical shift. [b] Average isotropic hyperfine couplings computed at the UB3LYP/EPR-II level of theory of **28a**; for example, isotropic hyperfine coupling of $H_b$ is the average from 18 hydrogen atoms of $t$-Bu group

### 2.2.7. EPR spectra of nitroxide octaradical 28

CW EPR (X-band) spectrum of octaradical **28** in 2-MeTHF solution at room temperature (295 K) was relatively narrower than that of tetraradical **27** as shown in Figure D22A in Appendix D.

Spin counting measurement of octaradical **28** was carried out (1.5 mM in chloroform) at room temperature (294–295 K) to determine the number of unpaired electrons per molecule as well as the purity of the compound. 3-Carboxy-PROXYL (1.5 mM in chloroform) was used as intensity reference for spin counting. The spin counting exhibited 10.8 unpaired electrons per molecule. The average value of $\chi T = 3.87$ emu K

mol$^{-1}$ obtained by EPR spin counting is in agreement with the theoretical value of $\chi T = 4.0$ emu K mol$^{-1}$ for four $S = 1$ radicals.

**Table 2.6.** Summary of EPR spin counting measurement for octaradical **28** (1.5 mM in chloroform) at 294–295 K

| Run | Sample | Double Integration | SW[a] | Number of unpaired electrons | $\chi T$ (emuK mol$^{-1}$) |
|---|---|---|---|---|---|
| AO558r1 | AO-4-37-col | 1.703e8 | 400 | 10.3 | 3.87 |
| AO560r1 | 3-Carboxy-PROXYL | 1.654e7 | 400 | | |

[a] SW = sweep width

CW EPR spectrum of octaradical **28** was taken at 133 K in 2-MeTHF (Figure 2.30) and showed the similar spectral features as observed in tetraradical **27**. A center band superimposed on broad side-bands with dipolar splittings of about 10 and 20 mT which are slightly smaller than *m*-phenylene diradicals ($D \sim 12$ to 17 mT, depending on solvent).[50] These two spectral features are assigned to two conformations by the same analogy with tetraradical **27**. The center peak corresponds to conformation **28$_s$**. The broad dipolar splitting corresponds to conformation **27$_b$**. The observation of half-field transition, $|\Delta m_s| = 2$, which is relatively weak compared to tetraradical **27**, is consistent with the modest population of through-space interaction.
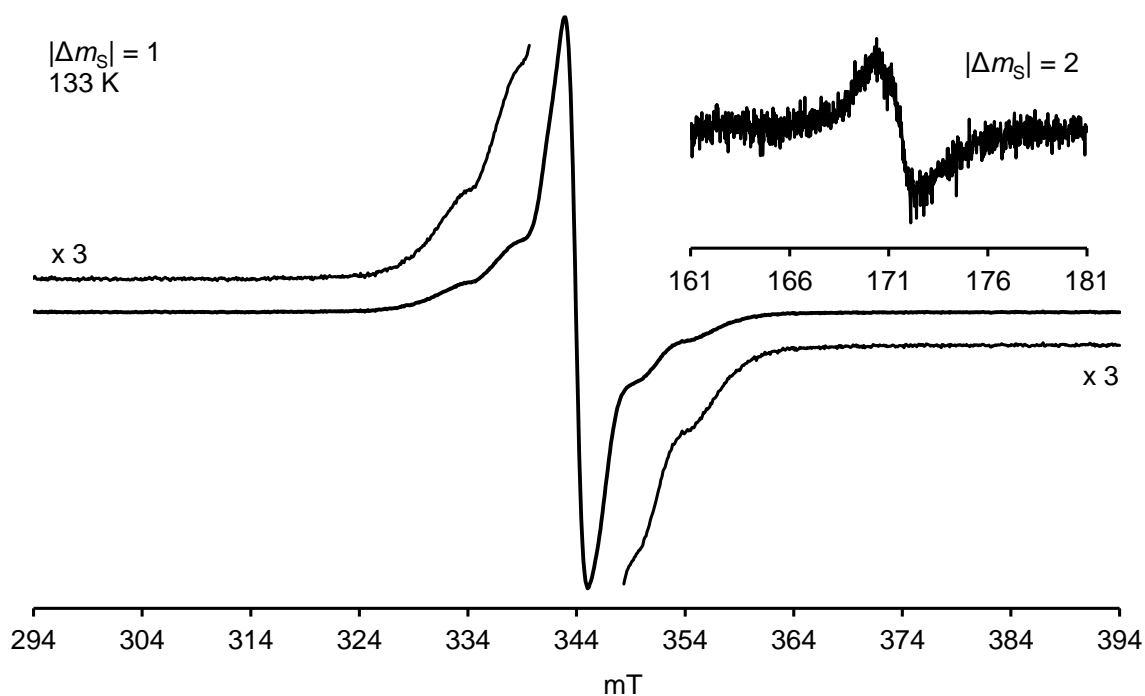
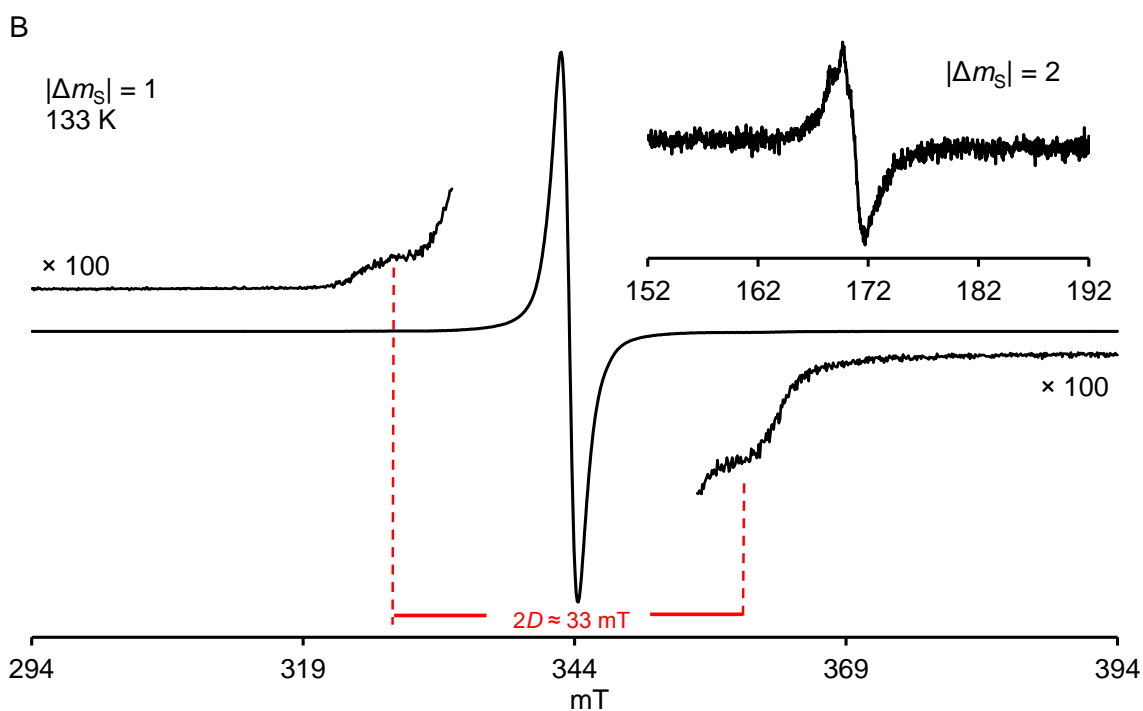**Figure 2.30.** CW EPR (X-Band, ν = 9.6554 GHz, $|\Delta m_s|$ = 1) spectrum of 1 mM calix[4]arene nitroxide octaradical **28** in 2-MeTHF at 133 K, 4-mm tube, sample label: AO437col, EPR label: AO556r2. Inset plot: $|\Delta m_s|$ = 2 region, ν = 9.6504 GHz. Reproduced from Ref. 72 with permission from The Royal Society of Chemistry.

### 2.2.8. Magnetic studies of octaradical 28

The magnetic studies of octaradical **28** were carried out using SQUID magnetometry in solid and solution. As shown in Figure 2.31, the flat plot between $\chi T$ and $T$ where $\chi$ is molar magnetic susceptibility and $T$ is temperature is observed in 100-290 K range (high temperature). The experimental value of $\chi T \approx 3.9$ emu K mol$^{-1}$ for octaradical **28** is in good agreement with the theoretical value of $\chi T = 4.0$ emu K mol$^{-1}$ for four independent $S = 1$ diradicals with strong ferromagnetic exchange coupling through *m*-phenylene and weak coupling between diradicals. This value of $\chi T$ is in a good agreement

with the value of $\chi T \approx 3.9$ emu K mol$^{-1}$ obtained from EPR spin counting for the same sample of octaradical **28** in chloroform at 295 K.



**Figure 2.31.** SQUID magnetometry of solid nitroxide octararadical **28** (sample label: AO4-37col, SQUID label: AO534s2). Reproduced from Ref. 72 with permission from The Royal Society of Chemistry.

DFT geometry optimization of $D_2$-symmetric **28a**, in which –OCH$_2$CH$_2$OCH$_3$ groups were replaced by –OCH$_3$ groups, was performed. The computed ONCC torsional angles of **28a** are in the range of 15-25° (Table D1 in Appendix D) revealed that nitroxides are near-coplanarity with $m$-phenylene unit. As a result, a strong ferromagnetic coupling of $S = 1$ diradical is expected. The through-space exchange coupling between cofacial nitroxides for octaradical **28** is expected to be somewhat smaller ($J/k > -1$ K) compared to tetraradicals **24** and **27** because the distances between cofacial nitroxides (N···N) in $D_2$-symmetry of optimized **28a** is slightly longer (6 Å; see Table D1 in Appendix D). The through-bond exchange coupling through nitroxide–$m$-phenylene–$m$-phenylene–CH$_2$–$m$-

phenylene–*m*-phenylene–nitroxide for octaradical **28** is expected to be smaller than that in tetraradical **24** by because of the additional *m*-phenylene units in the coupling pathway ($|J/k|$ < 1 K). The summary of selected torsional angles and intramolecular distances for computed tetraradical **24a**, tetraradical **27a** and octaradical **28a** is shown in Table D1 in Appendix D.

The current interest in developing water-soluble nitroxide for using in biological application such as MRI imaging.[36] Mukherjee[63] reported the synthesis of water-soluble calix[4]arene nitroxide tetraradical **24-HEG** with hexaethylene glycol methyl ether groups. Thus, we would like to explore the synthesis of water-soluble calix[4]arene nitroxide radicals for the future investigation. The goal of this section is to synthesize calix[4]arene nitroxide tetra- and octaradical in 1,3-alternate conformation with attachment of hydrophilic groups at lower rims, i.e. hexaethylene glycol methyl ether (HEG) groups. We report the synthesis and preliminary characterization of nitroxide tetraradical **36** and octaradical **37** as shown in Figure 2.32. However, tetraradical **36** and octaradical **37** are not soluble in water but soluble in polar organic solvents such as ethanol. More hydrophilic groups need to be used in this calix[4]arene scaffolds to synthesis of water-soluble nitroxides.
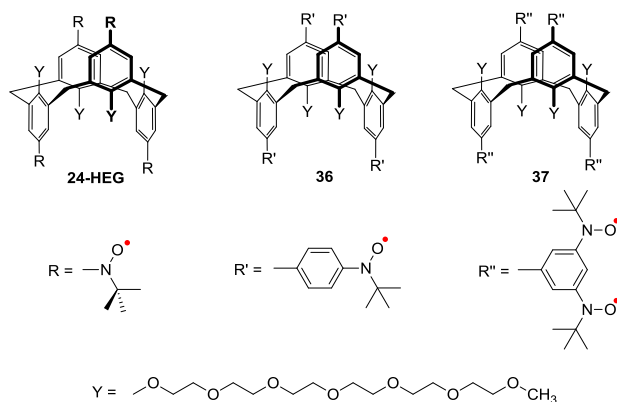
**Figure 2.32.** Structures of calix[4]arene nitroxide tetraradical **24-HEG**, **36** and octaradical **37** in 1,3-alternate conformation with hexaethylene glycol methyl ether (HEG) groups.

### 2.2.9. Synthesis of calix[4]arene nitroxide tetraradical 36

As shown in Scheme 2.8, the plan for synthesis of nitroxide tetraradical **36** could be adopted from the synthesis of nitroxide tetraradical **27** by (1) deprotection of TBDMS groups of **39** and followed by (2) oxidation of the corresponding tetrahydroxylamine **38**. Palladium-catalyzed Negishi cross-coupling reaction using two partners, i.e. (4-bromo)phenyl TBDMS-protected hydroxylamine **29** (Section 2.2.1) and tetrabromocalix[4]arene **40** containing hexaethylene glycol methyl ether chains leads to couple product **39**. Tetrabromocalix[4]arene **40** could be synthesized from commercially available *p-tert*-butylcalix[4]arene.

**Scheme 2.8.** Retrosynthetic analysis of calix[4]arene nitroxide tetraradical **36**.
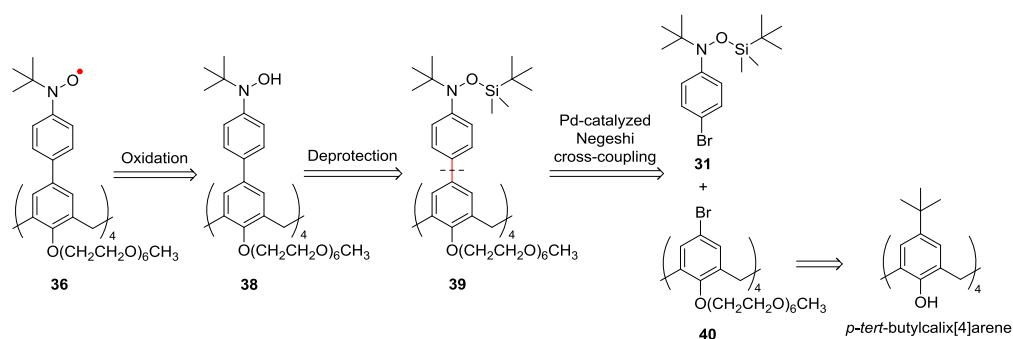
Synthesis of tetrabromocalix[4]arene **40**, which was previously reported and prepared by Dr. Sumit Mukherjee, was reproduced.[19,63]  As illustrated in Scheme 2.9., the synthesis started with the removal of *tert*-butyl groups of *p-tert*-butylcalix[4]arene with anhydrous AlCl₃ in presence of phenol in toluene to give calix[4]arene in 83% yield compared to 75% yield from the literature.[78]  Etherification at the lower rim of calix[4]arene with hexaethylene glycol tosylate which was previously synthesized by Mukherjee[63] was performed in refluxing CH₃CN with Cs₂CO₃ to give 1,3-alternate conformation of tetra-HEG calix[4]arene in 29% yield compared to 55% yield as previously reported due to difficulties in separation by column chromatography.  Although the obtained yield was lower than the previous report, the present sample had better purity. The ¹H NMR (400 MHz, chloroform-*d*, Figure D23A in Appendix D) spectrum of tetraHEG-calix[4]arene showed the impurities' peaks, and the ¹H NMR (400 MHz, chloroform-*d*, Figure D23B in Appendix D) spectrum showed pure sample of tetraHEG-calix[4]arene.

**Scheme 2.9.** Synthesis of tetrabromocalix[4]arene **40**.
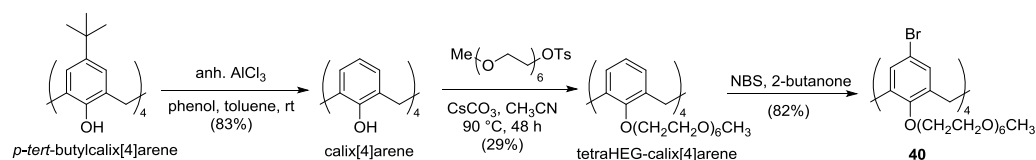


The resonance of characteristic methylene protons for 1,3-alternate conformation was not clearly observed by ¹H NMR spectrum.  However, ¹³C NMR (100 MHz, chloroform-*d*, label: AO-1-35starting, Figure D24 in Appendix D) spectrum of tetraHEG-calix[4]arene showed the characteristic peak at $\delta = 34.92$ ppm which is in agreement with

$\delta = 37$ ppm[19] for $C$H$_2$ methylene carbon of 1,3-alternate conformation. Bromination of tetra-HEG calix[4]arene with NBS in 2-butanone at room temperature, with exclusion of light gave tetrabromo tetra-HEG calix[4]arene **40** in 82% yield which is comparable to 81% yield from the previous report.[63] $^1$H NMR spectrum showed a singlet peak at $\delta = 7.290$ ppm corresponding to two aromatic protons. The characteristic peak for the 1,3-alternate conformation showed at $\delta = 3.427$ ppm which is in good agreement with previous report.[63]

**Scheme 2.10.** Synthesis of calix[4]arene nitroxide tetraradical **36**.
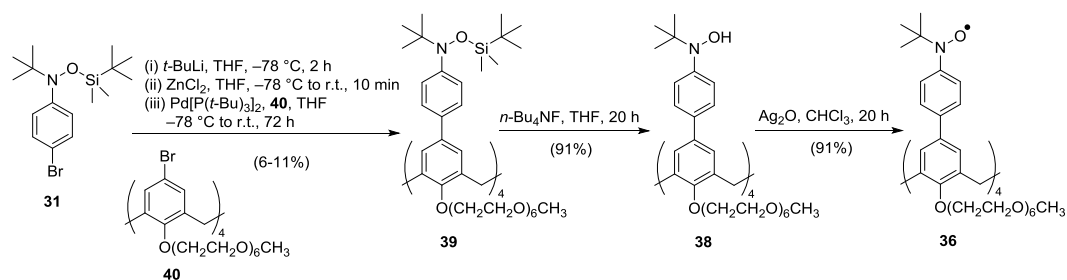


The synthesis of nitroxide tetraradical **36** was based on the established procedure for the synthesis of nitroxide tetraradical **27** shown in section 2.2.1. As presented in Scheme 2.10, the synthesis started with palladium-catalyzed Negishi cross-coupling reaction between TBDMS-protected hydroxylamine **31** and 1,3-alternate tetrabromocalix[4]arene **40**.[64,65] The hydroxylamine **31** was converted to organo-zinc reagent by generating organolithium with Br/Li exchange using $t$-BuLi (12.6 equiv) at $-78$ °C followed by ZnCl$_2$ at $-78$ °C to room temperature. The organozinc was then cross-coupled with tetrabromocalix[4]arene **40** using Pd[P($t$-Bu$_3$)$_2$] (80mol%) gave the crude mixture as shown in Figure 2.33A. $^1$H NMR (500 MHz, chloroform-d, label: AO-4-60-crd) of the crude reaction mixture of **39** showed a small doublet at $\delta \approx 7.5$ ppm which may correspond to aromatic protons on p-phenylene spacers. Another doublets may overlap

with unknown impurities' signals at $\delta \approx 7.2$ ppm. After purification by column chromatography and preparative TLC, cross-coupled product **39** is obtained in 6-11% yield. ^{1}H NMR (400 MHz, chloroform-*d*, AO-4-60-ptlc, Figure 2.33B and D25 in Appendix D) spectrum in aromatic region of **39** showed doublets at $\delta$ = 7.425 (2H, *J* = 8.8 Hz) and 7.221 (2H, *J* = 7.2 Hz) ppm which corresponded to aromatic protons on *p*-phenylene spacers. A singlet at $\delta$ = 7.327 (2H) ppm may correspond to aromatic protons on calix[4]arene moiety.
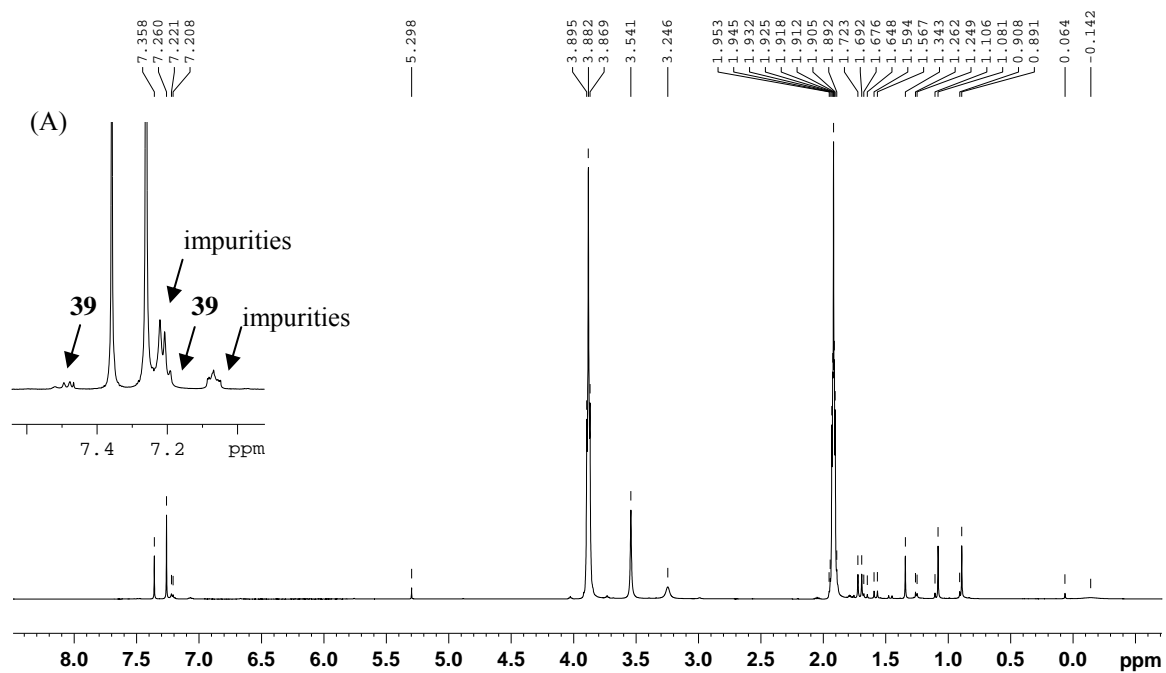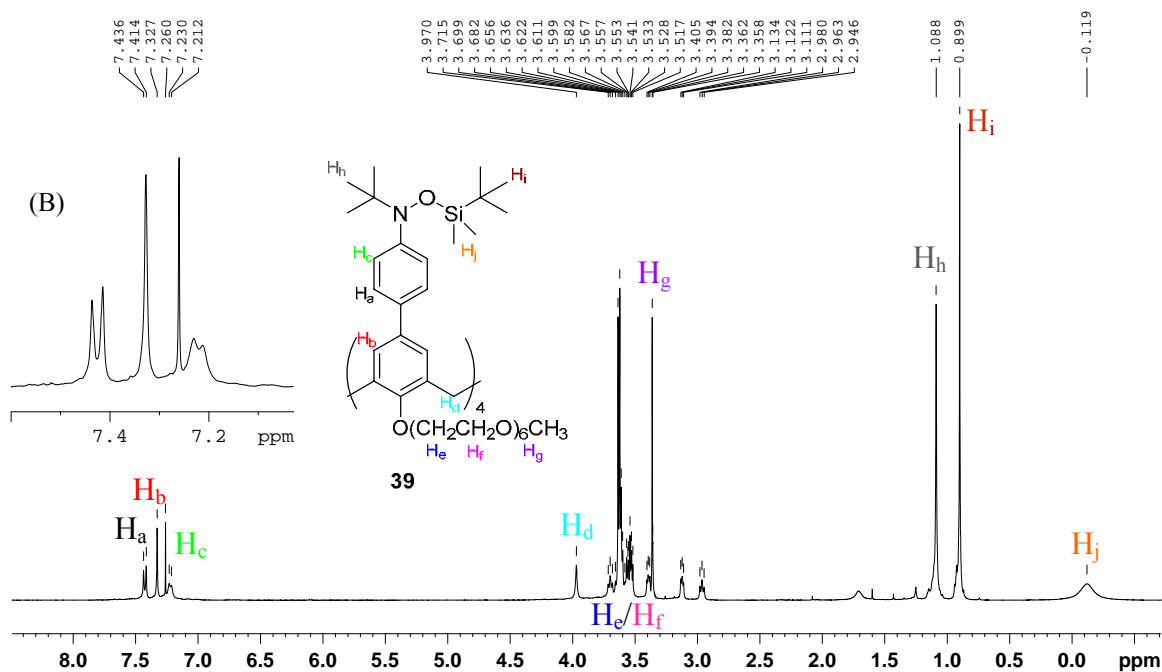
**Figure 2.33.** (A) $^1$H NMR (500 MHz, chloroform-*d*, label: AO-4-60-crd) spectrum of the tetra-coupled crude mixture of Negishi cross-coupling reaction. (B) $^1$H NMR (400 MHz, chloroform-*d*, AO-4-60-ptlc) spectrum of TBDMS-protected tetrahydroxylamine **39**.

TBDMS groups of the coupled calix[4]arene **39** were removed using *n*-Bu$_4$N$^+$F$^-$ to yield tetrahydroxylamine **38** in 91% yield. $^1$H NMR (400 MHz, chloroform-*d*, Figure D28 in Appendix D) spectrum showed a broad singlet at $\delta = 9.26$ ppm corresponding to four protons of hydroxylamine. IR (Figure D29 in Appendix D) spectrum confirmed the presence of hydroxyl groups indicated by absorption at $\nu_{O\text{-}H} = 3208$ cm$^{-1}$. The absorption at $\nu_{O\text{-}H} = 1203$ cm$^{-1}$ corresponded to the N–O stretching bands hydroxylamine **38**. Subsequently, oxidation of tetrahydroxylamine **38** with freshly prepared Ag$_2$O in CHCl$_3$ produced nitroxide tetraradical **36** in 91% yield. Nitroxide tetraradical **36** was characterized by $^1$H NMR, IR spectroscopy and HR mass spectrometry. IR

(Figure D31 in Appendix D) spectrum of **36** no longer showed the absorption of hydroxyl groups (at $v_{O-H} \approx 3200$ cm$^{-1}$). The absorption at 1352 cm$^{-1}$ may correspond to the N–O$^{\bullet}$ stretching bands tetraradical **36**.

### 2.2.10. $^1$H NMR spectroscopy of nitroxide tetraradical 36

$^1$H NMR spectra of nitroxide tetraradical **36** were taken at 295 K showing broad peaks causing by paramagnetic shift. The $^1$H NMR (500 MHz, chloroform-*d*, Figure 2.34 and Figure D30 in Appendix D, AO-4-80-col) spectrum of 53 mM calix[4]arene nitroxide tetraradical **36** contained two broadened peaks at $\delta$ = 3.76-3.51 (br, 108H) and –3.49 (br, 36H) ppm. The downfield resonances at $\delta$ = 3.76-3.51 ppm corresponded to the 108 protons (**H$_a$**) on the –O(CH$_2$CH$_2$O)$_6$CH$_3$ (HEG) groups. The resonances in this region of **36** appeared relatively in good agreement with nitroxide tetraradical **24-HEG**.[63] The upfield resonance at $\delta$ = –3.49 ppm corresponded to 36 protons on *tert*-butyl groups on nitroxide moieties. The lower number of eight protons from methylene-bridge calix[4]arene and eight aromatic protons may not be able to observed at this concentration probably due to overlapping or too broad peaks. The assignment for $^1$H NMR spectrum for nitroxide tetraradical **36** with HEG groups is analogous to nitroxide tetraradical **27** due to similar structure except HEG side chains.

**Figure 2.34.** $^1$H NMR (500 MHz, chloroform-*d*, conc. 53 mM, label: AO-4-80-col) spectrum of nitroxide tetraradical **36** (~89% purity, see: Table 2.1 and Figure D30 in Appendix D).

### 2.2.11. EPR spectra of nitroxide tetraradical 36

CW-EPR (X-band, Figure D32 in Appendix D) spectra of **36** in 2-MeTHF solution at room temperature showed much sharper signal compared to tetraradical **27**. EPR spectrum is split into 5 lines because of equivalent interaction between two nitrogens. EPR (Figure D33A in Appendix D) spectrum of **36** in EtOH solution at room temperature show unresolved signal.

The EPR (Figure 2.35A) spectra of glassy matrix of 2-MeTHF for **36** (133 K) showed a sharp signal with peak-to-peak line width ($\Delta B_{pp}$) ~ 1.5 mT. This is similar to **27$_s$** in EPR spectrum of **27**. The absence of half-field transition, $|\Delta m_s| = 2$, indicates much weaker electron-electron dipolar interaction, consistent with the absence of resolved dipolar splitting in the $|\Delta m_s| = 1$ signal. However, the EPR (Figure 2.35B) spectrum of rigid matrix of EtOH revealed the dipolar split side bands which is similar to **27$_b$**. This is in consistent with the presence of half-field transition, $|\Delta m_s| = 2$.

B

$|\Delta m_S| = 1$
133 K

× 100

$|\Delta m_S| = 2$

152     162     172     182     192

× 100

2D ≈ 33 mT

294            319            344            369            394
mT

**Figure 2.35. (A)** CW EPR (X-Band, $v = 9.6534$ GHz, $|\Delta m_s| = 1$) spectrum of 1 mM calix[4]arene nitroxide tetraradical **36** (R = HEG) in 2-MeTHF at 133 K, 4-mm tube, sample label: AO480col, EPR label: AO587r2/r4 (SW1600, 20dB, 5G); inset plot: $|\Delta m_s| = 2$ region, $v = 9.6517$ GHz (SW400, 10dB, 5G). **(B)** CW EPR (X-Band, $v = 9.6419$ GHz, $|\Delta m_s| = 1$) spectrum of 1 mM calix[4]arene nitroxide tetraradical **36** (R = HEG) in EtOH at 133 K, 4-mm tube, sample label: AO480col, EPR label: AO545r5 (SW1000, 20dB, 4G); inset plot: $|\Delta m_s| = 2$ region, $v = 9.6419$ GHz (SW400, 5dB, 4G). Reproduced from Ref. 72 with permission from The Royal Society of Chemistry.

### 2.2.12. Synthesis of calix[4]arene nitroxide octaradical 37

As illustrated in Scheme 2.11, the plan for synthesis of nitroxide octaradical **37** is similar to nitroxide octaradical **28** using palladium-catalyzed Negishi cross-coupling

reaction between TBDMS-protected hydroxylamine **35** and tetrabromo[4]arene **40** containing hexaethylene glycol chains.

**Scheme 2.11.** Retrosynthetic analysis of calix[4]arene nitroxide octaradical **37**
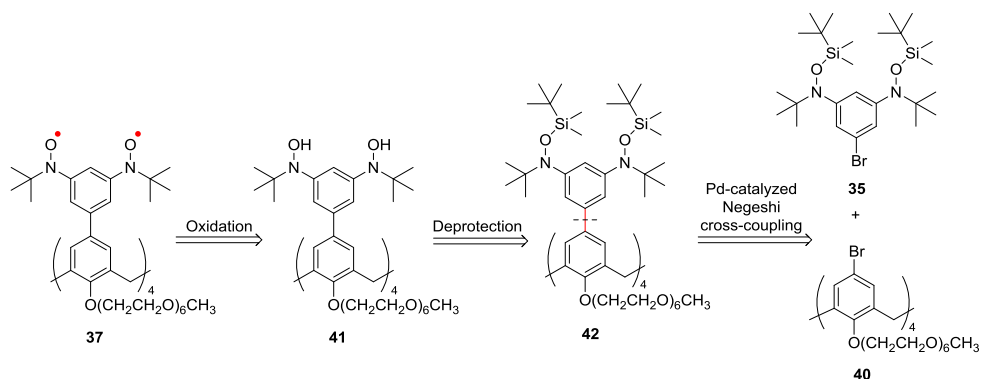


The synthesis of nitroxide octaradical **37** based on the established procedure for synthesis of nitroxide octaradical **28**. As shown in Scheme 2.12, TBDMS-protected hydroxylamine **35** was converted to organozinc by Br/Li exchange using $t$-BuLi at $-78\ °C$ and followed by $ZnCl_2$ at $-78\ °C$ to room temperature. The corresponding organozinc intermediate was coupled with tetrabromocalix[4]arene **40** by Negishi cross-coupling using Pd[P($t$-Bu$_3$)$_2$] (80 mol%) to give the crude mixture of **42**. $^1$H NMR (400 MHz, chloroform-$d$, label: AO-4-12-crd) spectrum of the crude reaction mixture showed a broad peak at $\delta\sim7.2$ ppm which may correspond to the aromatic protons on $p$-phenylene spacers as shown in Figure 2.36A. After purification by column chromatography, the target product **42** is obtained in 11-23% yield. $^1$H NMR (400 MHz, chloroform-$d$, AO-4-16-fr2-1) spectrum of target product **42** showed a broad peak at $\delta\sim7.2$ ppm. This observation is similar to **34**.
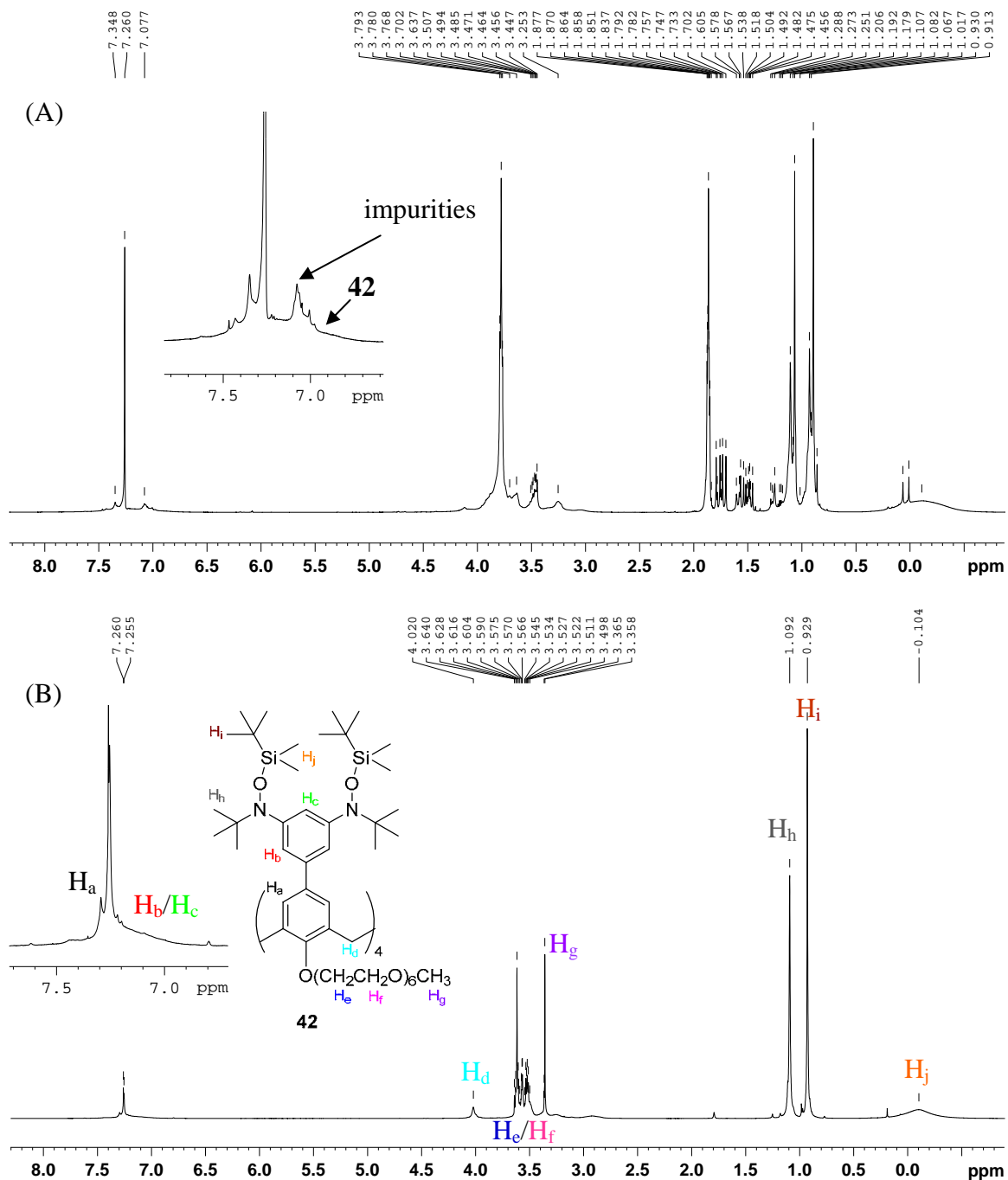
**Figure 2.36.** (A) $^1$H NMR (400 MHz, chloroform-$d$, AO-4-12-crd) spectrum of crude mixture of **42**. (B) $^1$H NMR (400 MHz, chloroform-$d$, label: AO-4-16-fr2-1) spectrum of tetra-coupled TBDMS-protected tetrahydroxylamine **42**.

**Scheme 2.12.** Synthesis of nitroxide octaradical **37**.
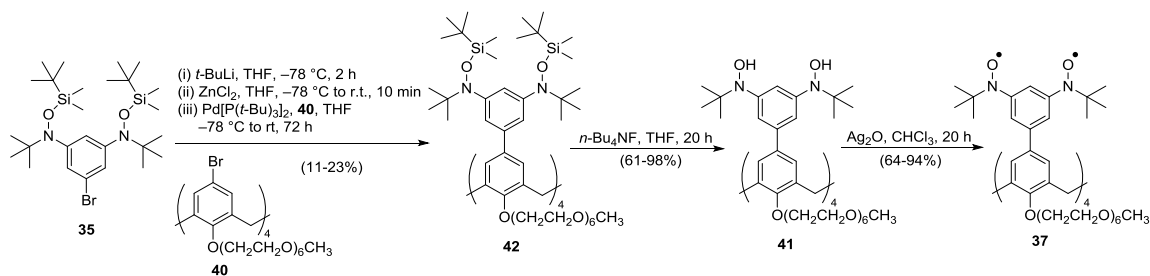


Deprotection of TBDMS groups using $n$-Bu$_4$NF in THF at ambient temperature gave octahydroxylamine **41** in 61-98% yield. $^1$H NMR (400 MHz, chloroform-$d$, Figure D37 in Appendix D) spectrum revealed the broad singlet peak at $\delta$ = 8.996 ppm corresponding to eight protons of hydroxylamine groups on octahydroxylamine **41**. IR (Figure D38 in Appendix D) spectrum showed the absorption of hydroxylamine at $\nu_{O-H}$ = 3240 cm$^{-1}$. The absorption at $\nu_{O-H}$ = 1202 cm$^{-1}$ may correspond to the N–O stretching bands hydroxylamine **41**. Oxidation of octahydroxylamine **41** using freshly prepared Ag$_2$O in CHCl$_3$ at room temperature produced nitroxide octaradical **37** in 64-94% yield. IR (Figure D40 in Appendix D) spectrum no longer showed the absorption at 3240 and 1202 cm$^{-1}$ of hydroxylamine **41**.

### 2.2.13. $^1$H NMR spectroscopy of nitroxide octaradical 37

$^1$H NMR (500 MHz, chloroform-$d$, conc. 27 mM, Figure 2.37 and Figure D39 in Appendix D, AO-4-79-col) spectra of nitroxide octaradical **37** were taken at 295 K consisting of three broad peaks causing by paramagnetic effect. The resonances at $\delta$ = 11.65 (br, 8H), 3.85-3.59 (br, 108H) and −1.89 (br, 72H) ppm. The small broad peak at the most downfield resonance centered at $\delta$ = 11.65 ppm was assigned to eight methylene-bridge protons (**H$_c$**) of calix[4]arene. The broad resonances at $\delta$ = 3.85-3.59 ppm

corresponded to 108 protons (**H$_a$**) on the –O(CH$_2$CH$_2$O)$_6$CH$_3$ groups. The resonances in this region of **37** appeared relatively in good agreement with nitroxide tatraradical **36** shown in earlier section. The most upfield resonance at $\delta = -1.89$ ppm corresponded to 72 protons on *tert*-butyl groups on nitroxide moieties. The eight aromatic protons (**H$_d$**) may not be able to be observed at this concentration probably due to overlapping or too broad peaks. The assignment for $^1$H NMR of nitroxide octaradical **37** is analogous to nitroxide octaradical **28** because of similar structure except HEG side chains.
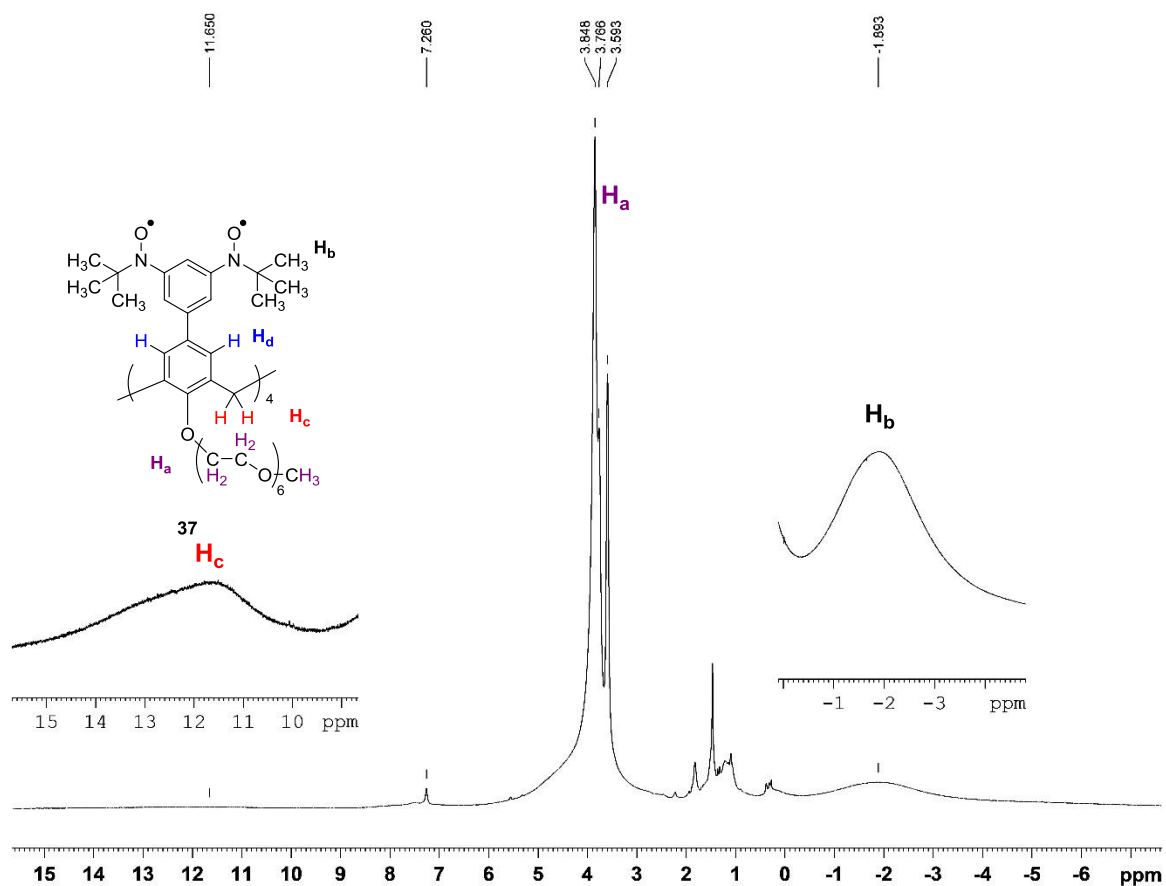


**Figure 2.37.** $^1$H NMR (500 MHz, chloroform-*d*, conc. 27 mM, label: AO-4-79-col) spectrum of nitroxide octaradical **37** (~85% purity, see: Table 2.1 and Figure D39 in Appendix D).

### 2.2.14. EPR spectra of nitroxide octaradical 37

CW EPR (X-band, Figure D41 in Appendix D) spectra of octaradical **37** in EtOH at room temperature showed a relatively broad peak compared to tetraradical **36**. The EPR spectra of octaradical **37** in EtOH showed unresolved signal that is similar to tetraradical **36**.

CW EPR (X-band, Figure 2.38) spectrum of rigid matrix of EtOH for nitroxide octaradical **37** at 133 K is similar to octaradical **28**. However, the dipolar coupling side-bands are relatively weaker compared to octaradical **28**. The half-field transition, $|\Delta m_s| = 2$ is observed.
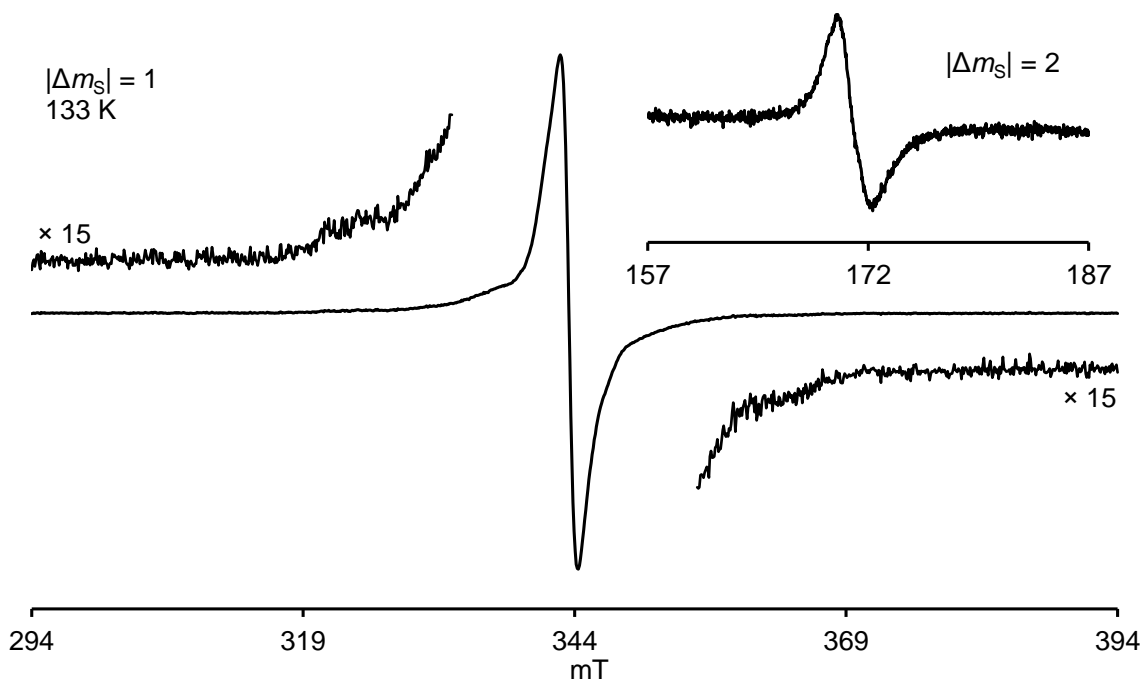


**Figure 2.38.** CW EPR spectra of 1.00 mM calix[4]arene nitroxide octaradical **37** in EtOH (sample label: AO479col); $|\Delta m_s| = 1$ at 133 K; X-Band, $\nu = 9.6408$ GHz, 4-mm tube, EPR label: AO546r1/r3 (SW1000, 30dB, 1G); inset plot: $|\Delta m_s| = 2$ region, $\nu = 9.6410$ GHz

(SW300, 10dB, 4G).  Reproduced from Ref. 72 with permission from The Royal Society of Chemistry.

## 2.3. Conclusions

The 1,3-alternate calixarene nitroxide tetraradicals **27**, **36** and octaradicals **28**, **37** were prepared and characterized.  Tetraradical **27** and octaradical **28** showed high purity from the evidence of $^1$H NMR spectra and spin counting measurement of EPR spectroscopy.  Values of $\chi T \approx 1.47$ and 3.9 emu K mol$^{-1}$ for **27** and **28** are in good agreement with to the theoretical values of 1.5 and 4.0 emu K mol$^{-1}$, respectively. Through-space exchange coupling in tetraradical **27** is comparable to previously reported tetraradical **24**.  Through-bond exchange coupling in tetraradical **27** and octaradical **28** is much smaller than that in tetraradical **24**.  Tetraradical **36** and octaradical **37** are not soluble in water but well soluble in EtOH.  The optimization of water-soluble groups this calix[4]arene scaffold are necessary for preparing water-soluble calix[4]arene nitroxide.

## 2.4. Experimental Section

**General procedures and materials.**  Tetrahydrofuran (THF) was freshly distilled from sodium benzophenone.  Palladium catalyst, Pd[P(*t*-Bu)₃]₂, was obtained from Streck Laboratories, and stored in a freezer inside Vacuum Atmospheres glovebox.  Per-deuterated solvents for NMR spectroscopy were obtained from Cambridge Isotope Laboratories.  *n*-BuLi in hexane and *t*-BuLi in pentane were obtained from Aldrich; prior to use, the concentration was determined by titration with *N*-pivaloyl-*o*-toluidine.[79]  All other commercially available chemicals were obtained from either Aldrich or Acros, unless

indicated otherwise. Column chromatography was carried out with flash silica gel, particle size 40-63 μm obtained from EMD chemicals, with TLC grade silica gel obtained from Sigma-Aldrich, or with Premium $R_f$ grade silica gel, particle size 40-75 μm obtained from Sorbent Technologies using 0–20 psig pressure. Preparative thin layer chromatography was carried out using Analtech silica plate (tapered with preadsorbent zone). Standard techniques for synthesis under inert atmosphere, using Schlenk glassware and gloveboxes (Vacuum Atmospheres), were employed.

Silver oxide ($Ag_2O$) for oxidation of hydroxylamines to nitroxides was freshly prepared before use as follows. A concentrated aqueous solution of sodium hydroxide (5.4 M, 500 μL, 2.34 mmol, 1.5 equiv) was added to an aqueous solution of silver nitrate (0.53 g, 3.12 mmol, 2 equiv), exclusion of light to produce a brown precipitate of silver oxide. The reaction was stirred at room temperature in the dark for 30 min, then the precipitate was filtered off and washed with water (100 mL), acetone (50 mL) and diethyl ether (50 mL), respectively. Silver oxide was dried under high vacuum for overnight under protection from light.[63]

**NMR spectroscopy.** NMR spectra were obtained with a Bruker spectrometer ($^1$H, 400 MHz, 500 MHz and 600 mHz) using chloroform-$d$ ($CDCl_3$) and acetone-$d_6$ as solvent; the 500 MHz instrument was equipped with a cryoprobe. The chemical shift references were as follows: ($^1$H) chloroform-$d$, 7.26 ppm; ($^{13}$C) chloroform-$d$, 77.00 ppm (chloroform-$d$), ($^1$H) acetone-$d_5$, 2.05 ppm; ($^{13}$C) acetone-$d_5$, 29.92 ppm (acetone-$d_6$). Typical 1D FID was subjected to exponential multiplication with a line broadening exponent (LB) of 0.3 Hz (for $^1$H) and 1.0 – 2.0 Hz (for $^{13}$C). For selected spectra, smaller (or negative) values

of LB and additional Gaussian multiplication (GB) were used, to resolve closely spaced resonances, as indicated in the spectral data summaries.

Paramagnetic $^1$H NMR spectra were obtained on concentrated solutions of tetraradical **27** and octaradical **28** in chloroform-*d*, using 3-mm samples tube and 500 MHz NMR instrument with a cryoprobe. The employed concentrations were limited by the available amounts of **27** and **28** and their solubility. Examples of $^1$H NMR spectra for specific samples of **27** and **28** are presented in Appendix D.

**IR spectroscopy.** IR spectra were obtained using a Nicolet Avatar 360 FT-IR instrument, equipped with an ATR sampling accessory (Spectra Tech, Inc.). A few drops of the compound in $CH_2Cl_2$ were applied to the surface of a ZnSe ATR plate horizontal parallelogram (45°, Wilmad). After the solvent evaporated, the spectrum was acquired (2-cm$^{-1}$ resolution).

**Mass spectrometry.** HRFAB MS analyses were carried out in 3-nitrobenzyl alcohol (3-NBA) or *o*-nitrophenyl octyl ether (ONPOE) matrices at the Nebraska Center for Mass Spectrometry. HR-ESI-MS analyses were carried out in NaI + CsI in methanol/water solution.

**EPR spectroscopy.** CW X-band EPR spectra for tetraradicals **27** and **36**, and octaradical **28** and **37** were acquired on a Bruker EMX instrument, equipped with a frequency counter and dual mode cavity. Temperature was controlled with nitrogen flow system (130–300 K). The samples were contained in either 4-mm EPR quartz tubes or 5-mm SQUID sample tubes. All spectra were obtained with the oscillating magnetic field perpendicular (TE$_{102}$) to the swept magnetic field. The *g*-values were referenced using DPPH (*g* = 2.0037, powder, Aldrich).

**SQUID magnetometry.** 5-Tesla AC/DC SQUID magnetometer, with continuous temperature control and operating in the DC-mode, was used.

Solid octaradical **28** (8.26 mg) was loaded to the 3-piece gelatin capsule. Following the measurements, the capsule was partially emptied (1.47 mg was retained), and then identical sequences of measurements was carried out for the point-by-point correction for diamagnetism. Additional correction was based upon Pascal constants: $\chi_{dia} = -1.078 \times 10^{-3}$ emu mol$^{-1}$, as well as a small correction for residual ferromagnetic impurities. Solid tetraradical **27** (12.64 mg) was measured using similar procedure but without point-by-point correction; correction for diamagnetism was implemented by extrapolation of the $\chi$ vs. $1/T$ plots in the 180–290 K temperature range ($R^2 = 0.9998 - 1.0000$).

All solution samples were contained in home-made 5-mm O.D. EPR quality quartz tubes, modified to possess a thin bottom, which is 6 cm from the end of the tube (referred to as "SQUID tubes").[59,80] Tetraradical **27** (1.15 mg, or for the second sample 0.88 mg) was loaded into the SQUID tube, and then placed under vacuum. THF and/or 2-MeTHF were vacuum transferred, to obtain 8.8 mM (or for second sample 6.7 mM) concentration of tetraradical, and after the tube was flame sealed under vacuum, the samples were carefully inserted to the magnetometer, as described elsewhere.[59,80] Correction for diamagnetism was implemented by extrapolation of the $\chi$ vs. $1/T$ plots in the 60–130 K ($R^2 = 0.9998$) range.

Numerical curve fitting for magnetic data was carried out with the SigmaPlot for Windows software package. The reliability of a fit is measured by the parameter dependence, which is defined as follows: *dependence = 1 − ((variance of the parameter,*

*other parameters constant)/(variance of the parameter, other parameters changing))*.
Values close to 1 indicate overparametrized fit.
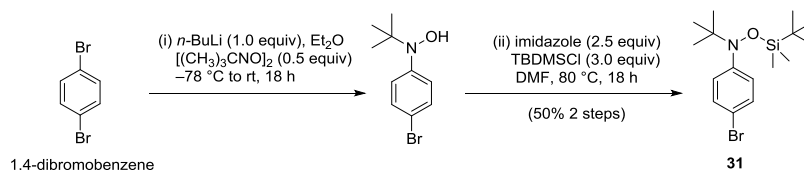


| Run | 1,4-Dibromobenzene (g/mmol) | *n*-BuLi (mL/mmol) | [(CH$_3$)$_3$CNO]$_2$ (g/mmol) | Imidazole (g/mmol) | TBDMSCl (g/mmol) | Yield (g/%) |
|---|---|---|---|---|---|---|
| AO-4-55 | 2.61/11.1 | 6.37/11.1 | 0.965/5.54 | 0.970/14.2 | 2.58/17.1 | 1.99/50 |

**TBDMS-protected hydroxylamine 31.** TBDMS-protected hydroxylamine **31** was
prepared previously by Dr. Kausik Das using the reported procedure.[61,62] 1,4-
Dibromobenzene was evacuated on high vacuum for 30 min and then charged with
nitrogen. Ether was added to the reaction flask. A solution of 1,4-dibromobenzene in ether
was cooled to −78 °C for 15 min. *n*-BuLi was added and the solution was stirred at −78
°C for 6 h. 2-Methyl-2-nitrosopropane dimer was added as a solid to the reaction. The
reaction mixture was stirred at room temperature for 18 h. The crude reaction mixture was
extracted with water (2 × 20 mL) and brine (2 × 20 mL). The combined organic layer was
dried over anh. Na$_2$SO$_4$ then evaporated in vacuo. The crude product was washed with
hexane (2 × 20 mL) and the solid was filtered to yield the corresponding hydroxylamine
intermediate. The corresponding hydroxylamine and imidazole were evacuated under high
vacuum for 30 min then DMF (10 mL) was added. TBDMSCl was added to the solution
and the reaction mixture was heated at 80 °C for 18 h. The crude reaction mixture was
filtered through a plug of silica gel using hexane to yield the corresponding product **31** as

a colorless liquid. $R_f = 0.57$ (hexane). $^1$H NMR (400 MHz, chloroform-$d$, AO-4-56-flt): $\delta$ = 7.335 (d, $J$ = 8.8 Hz, 2H), 7.115 (br d, $J$ = 7.6 Hz, 2H), 1.067 (s, 9H), 0.892 (s, 9H), −0.136 (br, 6H). Lit.[61] $^1$H NMR (400 MHz, chloroform-$d$, KD-12-20-col): $\delta$ = 7.335 (d, $J$ = 8.8 Hz, 2H), 7.115 (br d, $J$ = 7.6 Hz, 2H), 1.067 (s, 9H), 0.892 (s, 9H), −0.135 (br, 6H).
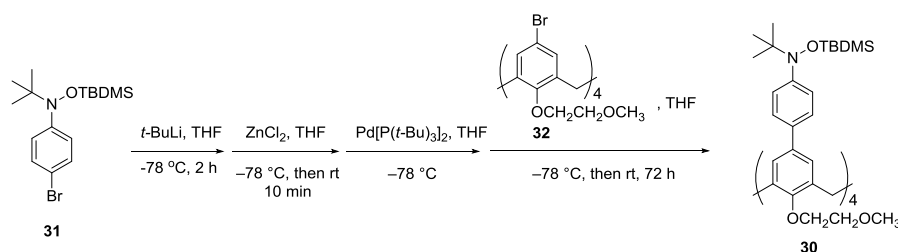


| Run | 31 | $t$-BuLi | 1 M ZnCl$_2$ | Pd[P($t$-Bu$_3$)$_2$] | 32 | Yield |
| | (mg/mmol) | (mL/mmol) | (mL/mmol) | (mg/mmol) | (mg/mmol) | (mg/%) |
| AO-3-77 | 130/0.362 | 0.48/0.76 | 4.4/4.34 | 24.7/0.048 | 58.6/0.060 | 25.9/24 |
| AO-3-87 | 170/0.474 | 0.63/1.00 | 5.7/5.69 | 32.3/0.063 | 76.9/0.079 | 52.0/37 |
| AO-4-27 | 253/0.698 | 0.92/1.46 | 8.4/8.37 | 48.0/0.093 | 113.0/0.116 | 60.2/29 |

**TBDMS-protected tetrahydroxylamine 30 (AO-3-87).** The procedure for Negishi cross-coupling reaction of TBDMS-protected hydroxylamine **31** with tetrabromocalix[4]arene **32** was followed the previous report.[64] TBDMS-protected hydroxylamine **31** (170.0 mg, 0.474 mmol), tetrabromocalix[4]arene **32** (76.9 mg, 0.0791 mmol) were introduced separately in the screw capped Schlenk vessels equipped with magnetic stirring bars and dried for overnight. Freshly distilled THF (2 mL) was added to both of the starting materials under N$_2$ flow. $t$-BuLi in pentane (1.59 M, 0.63 mL, 0.996 mmol) was added dropwise to a solution of TBDMS-protected hydroxylamine **31** at −78 °C under N$_2$ flow. The resulting yellow solution was stirred at −78 °C for 2 h. A solution of ZnCl$_2$ (1.00 M, 5.7 mL, 5.69 mmol) was added dropwise under N$_2$ flow at −78 °C. The resulting solution was warmed to the ambient temperature to obtain a clear organo-zinc solution for 10 min and then was cooled to at −78 °C. Pd[P($t$-Bu)$_3$]$_2$ (32.3 mg, 0.0632

mmol) was weighed and transferred into a Schlenk vessel inside the glove box. The Pd catalyst solution was prepared by adding freshly distilled THF (1 mL) into the Schlenk vessel under $N_2$ flow. This catalyst solution was added to the organo-zinc solution under $N_2$ flow at −78 °C. The solution of the tetrabromocalix[4]arene **32** was added dropwise to the reaction mixture under $N_2$ flow at −78 °C. The reaction mixture was stirred at room temperature for 72 h. The resulting solution was filtered through a Celite pad and concentrated in vacuo to give a crude mixture. The crude was purified by column chromatography (silica gel, ethyl acetate/pentane, 5:95) to give the desired Negishi cross-coupling product **30** (52.0 mg, 37%) as a white solid. M.p. 218-220 °C (under air). $^1$H NMR (600 MHz, chloroform-*d*, AO-3-87-col1): $\delta$ = 7.518 (d, *J* = 8.4 Hz, 8H), 7.394 (s, 8H), 7.265 (br, 8H), 4.012 (s, 8H), 3.701 (t, *J* = 6.6 Hz, 8H), 2.875 (t, *J* = 6.6 Hz, 8H), 2.800 (s, 12H), 1.098 (s, 36H), 0.901 (s, 36H), −0.124 (br, 24H). $^{13}$C NMR (150 MHz, chloroform-*d*, AO-3-87-col1): $\delta$ = 155.4, 149.9, 136.9, 134.8, 134.3, 127.3, 125.4, 125.2, 70.4, 67.9, 60.9, 58.6, 38.4, 26.1, 26.1, 17.9, −4.8. IR (ZnSe, cm$^{-1}$, AO-3-87-col1): 2956, 2926, 2850, 1466, 1387, 1359, 1246, 1120, 1125, 1082, 1036, 944, 860, 834, 780. LRFAB–MS (ONPOE matrix, AO-3-77-col1): *m/z* ion type (%RA for *m/z* = 600-2500): 1766 [M+H]$^+$ (100%). HRFAB–MS (ONPOE matrix, AO-3-77-col1): *m/z* ion type (%RA for *m/z* = 1762-1770): 1767.0952 [M+2H]$^+$ (77%, 0.1 ppm for $^{12}$C$_{104}$$^1$H$_{158}$$^{14}$N$_4$$^{16}$O$_{12}$$^{28}$Si$_4$), 1766.0908 [M+H]$^+$ (100%, −1.9 ppm for $^{12}$C$_{104}$$^1$H$_{157}$$^{14}$N$_4$$^{16}$O$_{12}$$^{28}$Si$_4$), 1765.0852 [M]$^+$ (69%, −3.1 ppm for $^{12}$C$_{104}$$^1$H$_{156}$$^{14}$N$_4$$^{16}$O$_{12}$$^{28}$Si$_4$).
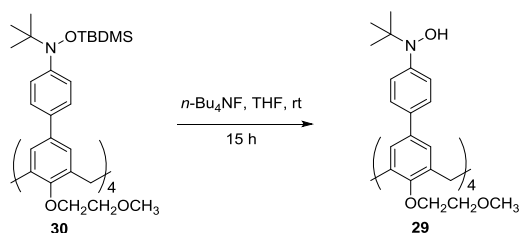
| Run | SM (mg/μmol) | $n$-Bu$_4$NF (mL/μmol) | Yield (mg/%) | TM label |
|---|---|---|---|---|
| AO-3-85 | 2.5/1.42 | 0.013/13.0 | 0.9/49 | AO-3-85-flt1 |
| AO-3-90 | 25.6/14.5 | 0.14/133 | 18.0/95 | AO-3-90-flt |
| AO-4-07 | 52.0/29.4 | 0.28/271 | 35.7/93 | AO-4-07-flt |
| AO-4-31 | 60.0/34.0 | 0.31/312 | 44/100 | AO-4-31-flt |

**Tetrahydroxylamine 29 (AO-4-31).** $n$-Bu$_4$NF (0.31 mL, 312 μmol) was added

dropwise to a solution of TBDMS-protected tetrahydroxylamine **30** (60.0 mg, 34.0 μmol)

in freshly distilled THF (2 mL). The resultant solution was protected from light and stirred

at room temperature for overnight (15 h). The crude mixture was rapidly filtered through

a silica gel pad using ethyl acetate (100 mL). Concentration in vacuo and drying under

high vacuum gave the tetrahydroxylamine **29** (44.4 mg, 100%) as a red solid. M.p. 225-

228 °C (brown liquid). $^1$H NMR (500 MHz, acetone-$d_6$, AO-3-90-flt): $\delta$ = 9.116 (d, $J$ =

8.5 Hz, 4H), 7.462 (s, 8H), 7.204 (br d, $J \approx$ 8 Hz, 8H), 6.886 (br d, $J \approx$ 8 Hz, 8H), 4.001-

3.909 (m, 16H), 3.661 (s, 8H), 3.576 (s, 12H), 1.207 (s, 36H). $^1$H NMR (500 MHz,

chloroform-$d$, AO-4-31-flt): $\delta$ = 9.336 (s, 4H), 7.372 (s, 8H), 7.110 (br, 8H), 6.843 (br,

8H), 3.991-3.856 (m, 16H), 3.608 (s, 8H), 3.560 (s, 12H), 1.206 (s, 36H). IR (ZnSe, cm$^-$

$^1$, AO-3-90-flt): 3232, 2961, 2924, 2872, 1466, 1454, 1389, 1362, 1233, 1200, 1172, 1124,

1081, 1057, 1029, 835, 800. LRFAB–MS (3-NBA matrix, AO-3-85-flt): $m/z$ ion type

(%RA for $m/z$ = 500-2000): 1310 [M+H]$^+$ (100%). HRFAB–MS (3-NBA matrix, AO-3-

85-flt): $m/z$ ion type (%RA for $m/z$ = 1306-1312): 1309.7391 [M+H]$^+$ (90%, 1.9 ppm for

$^{12}C_{80}{}^1H_{101}{}^{14}N_4{}^{16}O_{12}$), 1308.7362 [M]$^+$ (100%, −1.9 ppm for $^{12}C_{80}{}^1H_{100}{}^{14}N_4{}^{16}O_{12}$).
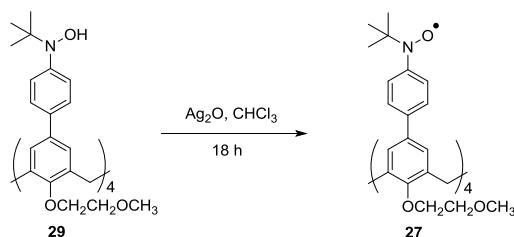
| Run | SM (mg/μmol) | Ag$_2$O (mg/mmol) | Yield (mg/%) | TM label |
|---|---|---|---|---|
| AO-3-89 | 1.5/1.15 | 10.6/0.0458 | N.A. | N.A. |
| AO-3-93 | 18.3/14.0 | 130.0/0.559 | 7.8/43 | AO-3-95-col |
| AO-4-10 | 35.7/27.3 | 253.0/1.09 | 5.6/16 | AO-4-20-colfr2-3 |
| AO-4-33 | 44.4/33.9 | 315.0/1.36 | 23.0/52 | AO-4-33-col |

**Nitroxide tetraradical 27 (AO-4-33).** Freshly prepared silver oxide (315.0 mg, 1.36 mmol) was added to a solution of tetrahydroxylamine **29** (44.4 mg, 33.9 μmol) in CHCl$_3$ (2 mL). After being stirred at room temperature in darkness for 18 h, the reaction mixture was filtered through a cotton plug. The red filtrate was evaporated to dryness to give the crude product. The crude was purified by column chromatography (silica gel, CHCl$_3$/ethyl acetate, 4:1) to give the nitroxide tetraradical **27** (23.0 mg, 52%) as a red solid. M.p. 130 °C (dec.). $^1$H NMR (500 MHz, chloroform-$d$, AO-4-33-col1&2-500, conc. 77.1 mM): $\delta$ = 4.00–3.63 (br, br, 28H), –3.18 (br, 36H), –5.42 (br, 8H), –13.95 (br, 8H). $^1$H NMR (500 MHz, chloroform-$d$, AO-4-20-colfr2-3, conc. 5.7 mM): $\delta$ = 3.53–3.18 (br, br, 28H), –3.67 (br, 44H). IR (ZnSe, cm$^{-1}$, AO-4-20-colfr2-3): 2981, 2929, 2875, 1585, 1466, 1455, 1364, 1237, 1176, 1125, 1082, 1057, 1032, 831, 756. LRFAB–MS (3-NBA matrix, AO-4-20-colfr2-3): $m/z$ ion type (%RA for $m/z$ = 500-1600): 1309 [M+4H]$^+$ (100%). HRFAB–MS (3-NBA matrix, AO-4-20-colfr2-3): $m/z$ ion type (%RA for $m/z$ = 1304-1313): 1308.7362 [M+4H]$^+$ (100%, –1.9 ppm for $^{12}$C$_{80}$$^1$H$_{100}$$^{14}$N$_4$$^{16}$O$_{12}$), 1307.7271 [M+3H]$^+$ (49%, –0.9 ppm for $^{12}$C$_{80}$$^1$H$_{99}$$^{14}$N$_4$$^{16}$O$_{12}$).
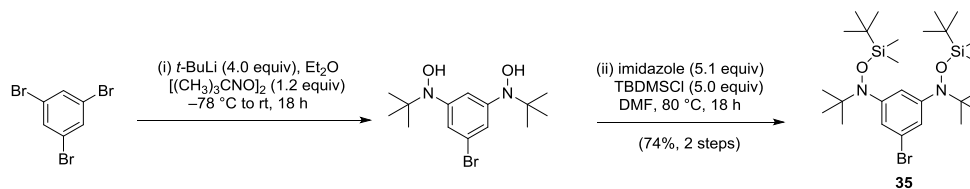
| Run | 1,3,5-Tribromobenzene (g/mmol) | $t$-BuLi (mL/mmol) | $[(CH_3)_3CNO]_2$ (g/mmol) | Imidazole (g/mmol) | TBDMSCl (g/mmol) | Yield (g/%) |
|---|---|---|---|---|---|---|
| AO-3-71 | 0.109/0.346 | 0.87/1.38 | 0.0724/0.416 | 3.24/48.0 | 7.10/47.1 | 4.64/74 |
| AO-3-75 | 0.928/2.95 | 7.41/11.8 | 0.617/3.54 | | | |
| AO-3-78 | 2.50/7.95 | 20.0/31.8 | 1.66/9.53 | | | |

**TBDMS-protected hydroxylamine 35.** TBDMS-protected hydroxylamine **35** was prepared previously by Dr. Kausik Das using the reported procedure.[61,62] 1,3,5-Tribromobenzene was evacuated on high vacuum for 30 min and then charged with nitrogen. Ether was added to the reaction flask. A solution of 1,3,5-tribromobenzene in ether was cooled to −78 °C for 20 min. $t$-BuLi was added and the solution was stirred at −78 °C for 1.5 h then stirred at −30 °C for 40 min. The reaction was cooled back to −78 °C for 20 min; and then 2-methyl-2-nitrosopropane dimer was added as a solid to the reaction. The reaction mixture was stirred at room temperature for 18 h. The crude reaction mixture was diluted with diethyl ether and extracted with water (2 × 20 mL) and brine (2 × 20 mL). The combined organic layer was dried over anh. $MgSO_4$, evaporated in vacuo and evacuated on high vacuum for overnight to yield the crude hydroxylamine. The crude hydroxylamine and imidazole were transferred to a Schlenk vessel and evacuated under high vacuum for overnight then DMF (10 mL) was added under nitrogen flow. TBDMSCl was added to the solution and the reaction mixture was heated at 80 °C for 18 h. The crude reaction mixture was purified by column chromatography using pentane to yield the target product **35** as a colorless liquid. $R_f$ = 0.63 (hexane). ^{1}H NMR (400 MHz, chloroform-$d$,

AO-3-81-col): $\delta$ = 7.221 (bs, 2H), 6.962 (bs, 1H), 1.076 (s, 18H), 0.904 (s, 18H), −0.109 (br, 12H).  Lit.[61] ^{1}H NMR (400 MHz, chloroform-$d$, KD-12-50-col): $\delta$ = 7.221 (bs, 2H), 6.951 (bs, 1H), 1.078 (s, 18H), 0.907 (s, 18H), −0.109 (br, 12H).
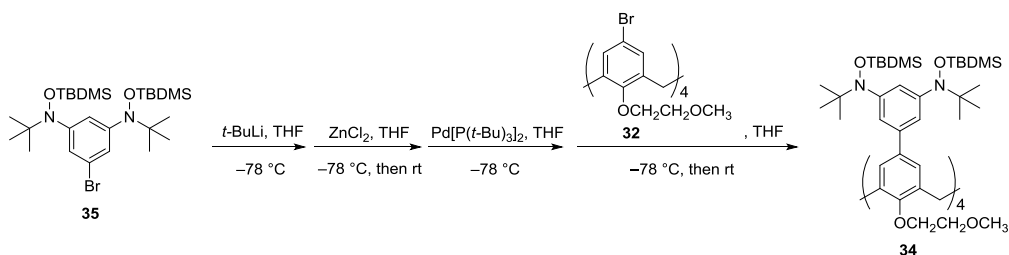


| Run | 35 (mg/mmol) | $t$-BuLi (mL/mmol) | 1 M ZnCl$_2$ (mL/mmol) | Pd[P($t$-Bu$_3$)$_2$] (mg/µmol) | 32 (mg/µmol) | Yield (mg/%) |
|---|---|---|---|---|---|---|
| AO-3-63 | 146/0.261 | 0.35/0.548 | 3.2/3.132 | 17.8/34.8 | 42.0/43.5 | 17.0/15 |
| AO-3-72 | 209/0.374 | 0.50/0.785 | 4.5/4.485 | 25.5/49.8 | 61.0/62.3 | 32.0/7 |
| AO-3-88 | 420/0.750 | 1.00/1.576 | 9.0/9.00 | 51.1/100 | 122.0/125 | |
| AO-4-13 | 466/0.833 | 1.10/1.75 | 10.0/10.0 | 57.0/111 | 135.0/139 | 8.7/2[*] |
| AO-4-17 | 518/0.926 | 1.25/1.94 | 11.1/11.1 | 63.0/123 | 150.0/154 | 99.8/25 |
| AO-4-49 | 411/0.734 | 1.04/1.54 | 8.8/8.81 | 50.0/97.9 | 119.0/122 | 79.6/25 |

[*] Low yield was caused by difficulty for separation pure product by chromatography.

**TBDMS-protected octahydroxylamine 34 (AO-4-17).**    TBDMS-protected dihydroxylamine **35** (518.0 mg, 0.926 mmol), tetrabromocalix[4]arene **32** (150.0 mg, 0.154 mmol) were introduced separately in the screw capped Schlenk vessels equipped with magnetic stirring bars and dried for overnight.  Freshly distilled THF (10 mL) was added to both of the starting materials under N$_2$ flow.  $t$-BuLi in pentane (1.56 M, 1.25 mL, 1.94 mmol) was added dropwise to a solution of TBDMS-protected dihydroxylamine **35** at −78 °C under N$_2$ flow.  The resulting yellow solution was stirred at −78 °C for 2 h. A solution of ZnCl$_2$ (1.00 M, 11.1 mL, 11.1 mmol) was added dropwise under N$_2$ flow at −78 °C.  The resulting solution was warmed to the ambient temperature to obtain a clear organo-zinc solution for 10 min and then was cooled to at −78 °C. Pd[P($t$-Bu)$_3$]$_2$ (63.0 mg,

0.123 mmol) was weighed and transferred into a Schlenk vessel inside the glove box. The Pd catalyst solution was prepared by adding freshly distilled THF (2 mL) into the Schlenk vessel under $N_2$ flow. The resulting catalyst solution was added to the organo-zinc solution under $N_2$ flow at −78 °C. The solution of the tetrabromocalix[4]arene **32** was added dropwise to the reaction mixture under $N_2$ flow at −78 °C. The reaction mixture was stirred at room temperature for 48 h. The resulting solution was filtered through a Celite pad and concentrated in vacuo to give a crude mixture. The crude was purified by column chromatography (silica gel, ethyl acetate/pentane, 1:200) to give the desired coupled product **34** (99.8 mg, 25%) as a white solid. M.p. 265 °C (dec.). $^1$H NMR (400 MHz, chloroform-*d*, AO-3-88-hv): $\delta$ = 7.315 (br, 20H), 4.017 (s, 8H), 3.572 (br, 8H), 2.911 (br, 20H), 1.120 (s, 72H), 0.950 (s, 72H), −0.050 (br, 48H). $^{13}$C NMR (100 MHz, chloroform-*d*, AO-3-88-hv): $\delta$ = 155.9, 150.6, 138.5, 135.3, 134.1, 127.7, 120.0, 70.6, 68.9, 61.0, 58.9, 38.5, 26.3, 26.1, 17.9, −4.5. IR (ZnSe, cm$^{-1}$, AO-3-88-hv): 2956, 2927, 2855, 1591, 1577, 1472, 1438, 1387, 1358, 1246, 1197, 1129, 1090, 1026, 952, 892, 854, 833, 778, 734. LRFAB–MS (ONPOE matrix, AO-3-66-colfr1): *m/z* ion type (%RA for *m/z* = 800-3500): 2572 [M+2H]$^+$ (100%). HRFAB–MS (ONPOE matrix, AO-3-66-colfr1): *m/z* ion type (%RA for *m/z* = 2568-2576): 2571.7024 [M+2H]$^+$ (100%, 4.9 ppm for $^{12}C_{144}{}^1H_{250}{}^{14}N_8{}^{16}O_{16}{}^{28}Si_8$), 2570.6996 [M+H]$^+$ (83%, 2.9 ppm for $^{12}C_{144}{}^1H_{249}{}^{14}N_8{}^{16}O_{16}{}^{28}Si_8$), 2569.7001 [M]$^+$ (41%, −0.3 ppm for $^{12}C_{144}{}^1H_{248}{}^{14}N_8{}^{16}O_{16}{}^{28}Si_8$).
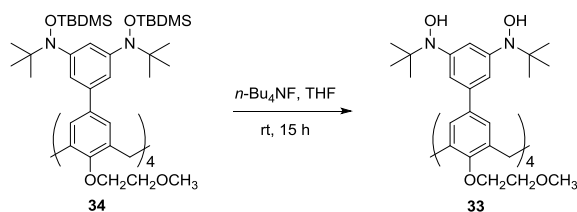
| Run | SM (mg/μmol) | *n*-Bu₄NF (mL/mmol) | Yield (mg/%) | TM label |
|---|---|---|---|---|
| AO-3-91 | 10.5/4.08 | 0.076/0.0751 | 6.0/89 | AO-3-91-flt |
| AO-4-08 | 28.0/10.9 | 0.20/0.200 | 15.7/87 | AO-4-08-flt |
| AO-4-25 | 8.7/3.38 | 0.063/0.0622 | 5.3/95 | AO-4-25-flt |
| AO-4-29 | 29.2/11.4 | 0.21/0.209 | 18.2/97 | AO-4-29-flt |
| AO-4-58 | 21.9/8.51 | 0.16/0.157 | 10.9/77 | AO-4-58-flt |

**Octahydroxylamine 33 (AO-4-29).** *n*-Bu₄NF (0.21 mL, 0.209 mmol) was added dropwise to a solution of TBDMS-protected octahydroxylamine **34** (29.2 mg, 0.0114 mmol) in freshly distilled THF (1 mL). The resultant solution was protected from light and stirred at room temperature for overnight (15 h). The crude mixture was rapidly filtered through a silica gel pad using chloroform (100 mL). Concentration in vacuo and drying under high vacuum gave the octahydroxylamine **33** (18.2 mg, 97%) as a yellow solid. M.p. 160 °C (dec.). $^1$H NMR (400 MHz, chloroform-*d*, AO-3-91-flt): $\delta$ = 9.028 (br, 8H), 7.419 (s, 4H), 7.162 (br, 8H), 7.000 (br, overlapping signal, 4H), 4.035 (s, 16H), 3.641 (s, 8H), 3.624 (s, 12H), 1.221 (s, 72H). IR (ZnSe, cm$^{-1}$, AO-3-88-hv): 3172, 2965, 2925, 2872, 2850, 1594, 1442, 1390, 1361, 1257, 1199, 1161, 1125, 1090, 1048, 1025, 951, 902, 868, 801, 731. LRFAB–MS (3-NBA matrix, AO-3-91-flt): *m/z* ion type (%RA for *m/z* = 600-2500): 1658 [M+H]$^+$ (100%). HRFAB–MS (3-NBA matrix, AO-3-91-flt): *m/z* ion type (%RA for *m/z* = 1655-1662): 1658.0079 [M+H]$^+$ (100%, 4.4 ppm for $^{12}C_{96}{}^1H_{137}{}^{14}N_8{}^{16}O_{16}$), 1657.0039 [M]$^+$ (71%, 2.2 ppm for $^{12}C_{96}{}^1H_{136}{}^{14}N_8{}^{16}O_{16}$).
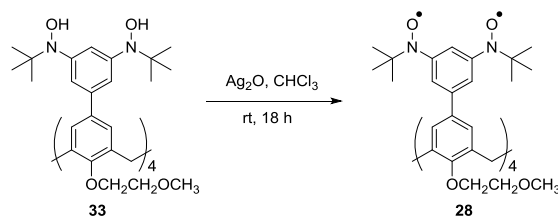
| Run | SM (mg/μmol) | Ag₂O (mg/mmol) | Yield (mg/%) | TM label |
|---|---|---|---|---|
| AO-3-94 | 6.0/3.62 | 34.0/0.145 | 5.0/84 | AO-3-94-wsh |
| AO-4-11 | 15.7/9.47 | 176.0/0.757 | no reaction | n.a. |
| AO-4-28 | 5.3/3.20 | 30.0/0.128 | 2.9/55 | AO-4-28-col |
| AO-4-30 | 18.2/11.0 | 102.0/0.439 | 10.8/60 | AO-4-32-col |
| AO-4-37 | 40.7/24.5 | 227.8/0.982 | 21.7/54 | AO-4-37-col |

**Nitroxide octaradical 28 (AO-4-30).**  Freshly prepared silver oxide (102.0 mg, 0.439 mmol) was added to a solution of octahydroxylamine **33** (18.2 mg, 0.0110 mmol) in chloroform (2 mL).  After being stirred at room temperature in darkness for 18 h, the reaction mixture was filtered through a cotton plug.  The yellow filtrate was evaporated to dryness to obtain the crude product.  The crude product was purified by column chromatography (silica gel, ethyl acetate/pentane, 1:1) to give nitroxide octaradical **28** (10.8 mg, 60%) as an orange solid. M.p. 150 °C (dec.).  $^1$H NMR (500 MHz, chloroform-*d*, AO-4-37-col, conc. 60.2 mM): $\delta$ = 22.91 (br, 8H), 12.44 (br, 8H), 4.74–4.17 (br, br, 28H), –2.80 (br, 72H).  $^1$H NMR (500 MHz, chloroform-*d*, AO-4-32-col, conc. 43.6 mM): $\delta$ = 11.93 (br, 8H), 4.19–3.60 (br, br, 28H), –3.38 (br, 72H).  IR (ZnSe, cm$^{-1}$, AO-4-32-col): 2981, 2874, 2817, 1581, 1476, 1444, 1267, 1249, 1192, 1125, 1047, 859, 743, 706.  LRFAB–MS (3-NBA matrix, AO-4-32-col): *m/z* ion type (%RA for *m/z* = 700-1900): 1658 [M+8H]$^+$ (100%).  HRFAB–MS (3-NBA matrix, AO-4-32-col): *m/z* ion type (%RA for *m/z* = 1653-1662): 1657.0081 [M+8H]$^+$ (100%, –0.4 ppm for $^{12}C_{96}{}^{1}H_{136}{}^{14}N_8{}^{16}O_{16}$), 1656.0079 [M+7H]$^+$ (67%, –5.0 ppm for $^{12}C_{96}{}^{1}H_{135}{}^{14}N_8{}^{16}O_{16}$).
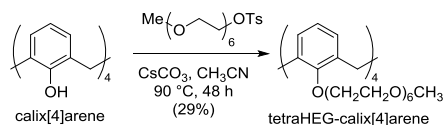
**25,26,27,28-Tetrakis(1-(2-(2-(2-(2-(2-methoxy-ethoxy)-ethoxy)-ethoxy)-ethoxy)-ethoxy)-ethoxy))calix[4]arene (TetraHEG-calix[4]arene).** A mixture of 25,26,27,28-tetrahydroxycalix[4]arene (0.884 g, 2.00 mmol), and hexaethylene glycol tosylate (4.50 g, 10.0 mmol) in a Schlenk flask, was evacuated under high vacuum for 3 h. $Cs_2CO_3$ (3.91 g, 12.0 mmol) and dry acetonitrile (35 mL) were then added under nitrogen and the reaction mixture was heated at 90 °C for 48 h. The acetonitrile was removed in vacuo and the reaction mixture was taken up in DCM (300 mL) and water (300 mL). The organic layer was further washed with water (2 × 200 mL), dried over MgSO4, filtered, and evaporated in vacuo to give a crude product as a yellow oil. Column chromatography with TLC standard silica gel (2 – 5% MeOH in DCM) on a 4-inch diameter column equipped with fraction collecter carried out overnight. The pure fractions were combined, evaporated in vacuo and evacuated on high vacuum to provide tetraHEG-calix[4]arene as a faint yellow oil (0.602 g, 29%). ^{1}H NMR (400 MHz, chloroform-$d$, AO-1-34bc1L): $\delta$ = 7.031 (d, $J$ = 7.6 Hz, 8H), 6.593 (t, $J$ = 7.6 Hz, 4H), 3.79 (t, $J$ = 5.0 Hz, 8H), 3.719 – 3.505 (m, 96H), 3.349 (s, 12H). lit.[63] ^{1}H NMR (400 MHz, chloroform-$d$, sm-9-9col1.2): $\delta$ 7.00 (d, $J$ = 7.2 Hz, 8H, Ar$H$), 6.57 (t, $J$ = 7.2 Hz, 4H, Ar$H$), 3.79 (t, $J$ = 5.2 Hz, 8H, ArOC$H$2), 3.69 – 3.58 (m, 80H, OC$H$2 + ArC$H$2Ar), 3.53 – 3.47 (m, 16H, OC$H$2), 3.32 (s, 12H, OC$H$3). [13]C NMR (100 MHz, chloroform-$d$, AO-1-34bc1L): $\delta$ = 155.59, 133.36, 129.82, 121.62, 77.20, 71.82, 71.08, 70.60, 70.50, 70.47, 70.41, 70.28, 58.92, 34.92, 29.57. IR (ZnSe, cm$^{-1}$, AO-1-34bc1L): 2866, 1451, 1387, 1350, 1249, 1198, 1091, 940, 847, 770. HR FAB−MS (AO-

1-34fr2): theoretical for $^{12}C_{80}{}^{1}H_{128}{}^{16}O_{28}{}^{23}Na_1$ 1559.8490; found 1559.8495 $[M+Na]^+$ (100, −0.3 ppm).
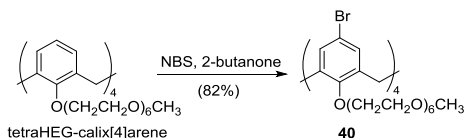


**Tetrabromocalix[4]arene 40.** *N*-bromosuccinimide (0.529 g, 2.97 mmol) was added to a solution of tetraHEG-calix[4]arene (0.520 mg, 0.338 mmol) in 17 mL of methyl ethyl ketone to produce the yellow solution. The reaction mixture was stirred at room temperature for 24 h, protected from light. The reaction mixture was then quenched with 5 mL of 10% aqueous NaHSO$_3$. The resulting mixture was taken up in 100 mL of DCM. The organic layer was washed with water, and then dried over MgSO$_4$. Filtration and concentration in vacuo, followed by column chromatography (DCM to 5% MeOH in DCM), provided **40** as a light yellow oil (0.559 mg, 82%). $^1$H NMR (400 MHz, chloroform-*d*, AO-1-36hivac): $\delta$ = 7.274 (s, 8H), 3.880 − 3.80 (m, 32H), 3.701 − 3.607 (m, 56H), 3.534 − 3.511 (m, 8H), 3.414 (s, 8H), 3.354 (s, 12H). lit.[63] $^1$H NMR (400 MHz, chloroform-*d*, sm-9-13col1-r8910) 7.27 (s, 8H, Ar*H*), 3.90 − 3.78 (m, 32H, OC*H*2), 3.73 − 3.57 (m, 56H, OC*H*2), 3.51 (m, 8H, OC*H*2), 3.41 (s, 8H, ArC*H*2Ar), 3.35 (s, 12H, OC*H*3).
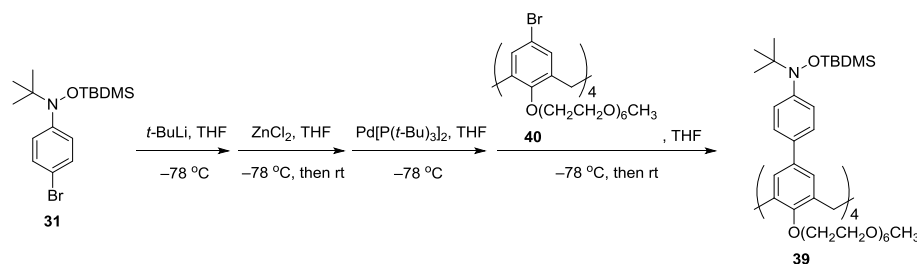
| Run | N-OTBDMS (mg/mmol) | t-BuLi (mL/mmol) | 1M ZnCl₂ (mL/mmol) | Pd[P(t-Bu₃)₂] (mg/mmol) | Tetrabromo calixarene (mg/mmol) | Yield (mg/%) |
|-----|-----|-----|-----|-----|-----|-----|
| AO-4-60 | 185/0.517 | 0.85/1.09 | 6.2/6.21 | 35.3/0.0690 | 159.8/0.0862 | 14.3/6 |
| AO-4-66 | 702/1.96 | 2.91/4.11 | 23.5/23.5 | 134/0.261 | 605.0/0.326 | 96.8/11 |

**TBDMS-protected hydroxylamine 39 (AO-4-66).** TBDMS-protected hydroxylamine **31** (701.9 mg, 1.96 mmol), tetrabromocalix[4]arene **40** (605.0 mg, 0.326 mmol) were introduced separately in the screw capped Schlenk vessels equipped with magnetic stirring bars and dried for overnight. Freshly distilled THF (2 mL) was added to both of the starting materials under N₂ flow. t-BuLi in pentane (1.41 M, 2.91 mL, 4.11 mmol) was added dropwise to a solution of TBDMS-protected hydroxylamine **31** at –78 °C under N₂ flow. The resulting yellow solution was stirred at –78 °C for 2 h. A solution of ZnCl₂ (1.00 M, 23.5 mL, 23.5 mmol) was added dropwise under N₂ flow at –78 °C. The resulting solution was warmed to the ambient temperature for 10 min to obtain a clear organo-zinc solution and then was cooled to at –78 °C. Pd[P(t-Bu)₃]₂ (133.5 mg, 0.261 mmol) was weighed and transferred into a Schlenk vessel inside the glove box. The Pd catalyst solution was prepared by adding freshly distilled THF (2 mL) into the Schlenk vessel under N₂ flow. The resulting catalyst solution was added to the organo-zinc solution under N₂ flow at –78 °C. The solution of the tetrabromocalix[4]arene **40** was added dropwise to the reaction mixture under N₂ flow at –78 °C. The reaction mixture was stirred at room temperature for 72 h. The resulting solution was filtered through a Celite pad and

concentrated in vacuo to give a crude mixture. The crude was purified by column chromatography (silica gel, methanol/dichloromethane, 5:95) to give the desired Negishi coupling product **39** (96.8 mg, 11%) as a yellow oil. $^1$H NMR (400 MHz, chloroform-$d$, AO-3-60-ptlc): $\delta$ = 7.425 (d, $J$ = 8.8 Hz, 8H), 7.327 (s, 8H), 7.221 (br, $J$ = 7.2 Hz, 8H), 3.970 (s, 8H), 3.699 (t, $J$ = 6.6 Hz, 8H), 3.656-3.517 (m, 64H), 3.405-3.382 (m, 8H), 3.362 (s, 12H), 3.134-3.111 (m, 8H), 2.963 (t, $J$ = 6.8 Hz, 8H), 1.088 (s, 36H), 0.899 (s, 36H), – 0.119 (br, 24H). $^{13}$C NMR (100 MHz, chloroform-$d$, AO-4-60-ptlc): $\delta$ = 155.59, 149.71, 137.18, 134.82, 134.11, 127.46, 125.41, 125.34, 71.90, 70.56, 70.53, 70.49, 70.39, 70.36, 69.06, 67.91, 60.84, 59.01, 38.18, 26.16, 26.15, 17.92, –4.64. IR (ZnSe, cm$^{-1}$, AO-4-60-ptlc): 3023, 2954, 2927, 2858, 1464, 1387, 1358, 1246, 1198, 1107, 1032, 944, 910, 861, 834, 781. HR ESI−MS (NaI/CsI, AO-4-60-ptlc) $m/z$ (% RA for $m/z$ = 1345-1349): calculated for $^{12}C_{72}{}^{1}H_{118}{}^{14}N_2{}^{16}O_{16}{}^{28}Si_2{}^{23}Na_1$ [M+2Na]$^{2+}$ calculated 1345.7918 (55%), found 1345.8049 (68%, 9.8 ppm); [M+2Na+1]$^{2+}$ calculated 1346.2933 (99%), found 1346.2994 (100%, 4.6 ppm); [M+2Na+2]$^{2+}$ calculated 1346.7944 (100%), found 1346.7953 (100%, 0.7 ppm); [M+2Na+3]$^{2+}$ calculated 1347.2954 (70%), found 1347.2982 (78%, 2.1 ppm).
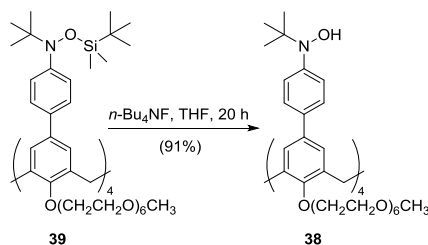


| Run | SM (mg/μmol) | $n$-Bu$_4$NF (mL/mmol) | Yield (mg/%) | TM Label |
|---|---|---|---|---|
| AO-4-74 | 49.8/18.8 | 0.17/0.173 | 37.6/91 | AO-4-74-flt |

**Tetrahydroxylamine 38 (AO-4-74).** *n*-Bu$_4$NF (0.17 mL, 0.173 mmol) was added

dropwise to a solution of TBDMS-protected hydroxylamine **39** (49.8 mg, 18.8 μmol) in

freshly distilled THF (1 mL). The resulting solution was protected from light and stirred

at room temperature for overnight (20 h). The crude mixture was rapidly filtered through

a silica gel pad using methanol/dichloromethane, 5:95 (100 mL). Concentration in vacuo

and drying under high vacuum gave the tetrahydroxylamine **38** (37.6 mg, 91%) as a red

oil. $^1$H NMR (400 MHz, chloroform-*d*, AO-4-74-flt): $\delta$ = 9.264 (s, 4H), 7.303 (s, 8H),

6.813 (br, 8H), 4.010-3.923 (m, 16H), 3.786-3.691 (m, 16H), 3.645-3.568 (m, 56H), 3.530-

3.507 (m, 8H), 3.353 (s, 12H), 1.197 (s, 36H). IR (ZnSe, cm$^{-1}$, AO-4-74-flt): 3208, 2920,

2875, 1719, 1466, 1359, 1239, 1203, 1109, 1056, 944, 837. ESI-MS (NaCl in H$_2$O/MeOH,

AO-4-74-flt): calculated for $^{12}$C$_{60}$$^1$H$_{90}$$^{14}$N$_2$$^{16}$O$_{16}$$^{23}$Na$_1$ [M+2Na]$^{2+}$ calculated 1117.6188

(77%), found 1117.7 (88%); [M+2Na+1]$^{2+}$ calculated 1118.1205 (100%), found 1118.2

(100%); [M+2Na+2]$^{2+}$ calculated 1118.6222 (64%), found 1118.7 (67%).
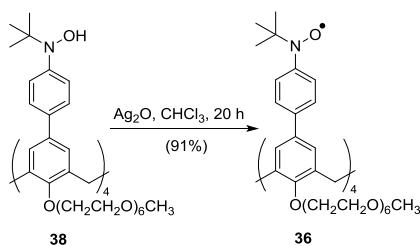


| Run | SM (mg/μmol) | Ag$_2$O (mg/mmol) | Yield (mg/%) | TM Label |
|---|---|---|---|---|
| AO-4-80-1 | 26.2/12.0 | 111/0.478 | 34.5/91 | AO-4-80-col |
| AO-4-80-2 | 11.4/5.20 | 48.3/0.208 | | |

**Nitroxide tetraradical 36 (AO-4-80-1).** Freshly prepared silver oxide (111.0 mg,

0.478 mmol) was added to a solution of tetrahydroxylamine **38** (26.2 mg, 0.0120 mmol) in

chloroform (2 mL). After being stirred at room temperature in darkness for 20 h, the

reaction mixture was filtered through a cotton plug. The red filtrate was evaporated to dryness to obtain the crude product. The combined crude product was purified by column chromatography (silica gel, methanol/dichloromethane, 5:95) to give the nitroxide tetraradical **36** (34.5 mg, 91%) as a red sticky liquid. $^1$H NMR (500 MHz, chloroform-$d$, AO-4-80-col): $\delta$ = 3.763-3.503 (br, 108H), –3.491 (br, 36H). IR (ZnSe, cm$^{-1}$, AO-4-80-col): 2920, 2854, 1464, 1352, 1239, 1190, 1103, 1055, 943, 832. HR ESI−MS (NaI/CsI, AO-4-80-col) $m/z$ ion type (% RA for $m/z$ = 1115-1119): calculated for $^{12}C_{60}{}^{1}H_{88}{}^{14}N_2{}^{16}O_{16}{}^{23}Na_1$ [M+2Na]$^{2+}$ calculated 1115.6032 (75%), found 1115.6057 (71%, 2.3 ppm); [M+2Na+1]$^{2+}$ calculated 1116.1048 (100%), found 1116.1116 (100%, 6.1 ppm); [M+2Na+2]$^{2+}$ calculated 1116.6064 (72%), found 1116.6073 (79%, 0.8 ppm); [M+2Na+3]$^{2+}$ calculated 1117.1080 (34%), found 1117.1099 (44%, 1.7 ppm).
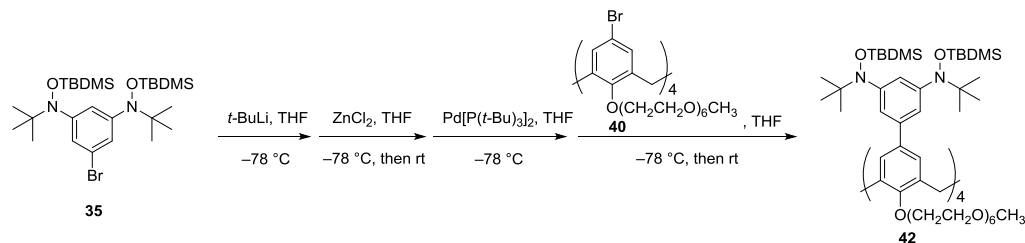


| Run | N-OTBDMS (mg/mmol) | $t$-BuLi (mL/mmol) | 1M ZnCl$_2$ (mL/mmol) | Pd[P($t$-Bu$_3$)$_2$] (mg/μmol) | Tetrabromo calixarene (mg/μmol) | Yield (mg/%) |
|---|---|---|---|---|---|---|
| AO-3-99 | 44.0/0.0774 | 0.10/0.162 | 0.93/0.928 | 6.0/10.3 | 23.9/12.9 | 4.8/11 |
| AO-4-12 | 272/0.486 | 0.64/1.020 | 6.0/5.827 | 33.0/64.7 | 150/80.9 | 42/15 |
| AO-4-39 | 326/0.553 | 0.77/1.224 | 7.0/6.992 | 39.7/77.7 | 180/97.1 | 78.4/23 |

**TBDMS-protected hydroxylamine 42 (AO-4-39).** TBDMS-protected hydroxylamine **35** (326.2 mg, 0.583 mmol), tetrabromocalix[4]arene **40** (180.0 mg, 0.0971 mmol) were introduced separately in the screw capped Schlenk vessels equipped with magnetic stirring bars and dried for overnight. Freshly distilled THF (6 mL) was added to

both of the starting materials under N$_2$ flow. *t*-BuLi in pentane (1.59 M, 0.77 mL, 1.22 mmol) was added dropwise to a solution of TBDMS-protected hydroxylamine **35** at −78 °C under N$_2$ flow. The resulting yellow solution was stirred at −78 °C for 2 h. A solution of ZnCl$_2$ (1.00 M, 7.00 mL, 6.99 mmol) was added dropwise under N$_2$ flow at −78 °C. The resulting solution was warmed to the ambient temperature for 10 min to obtain a clear organo-zinc solution and then was cooled to at −78 °C. Pd[P(*t*-Bu)$_3$]$_2$ (39.7 mg, 0.0777 mmol) was weighed and transferred into a Schlenk vessel inside the glove box. The Pd catalyst solution was prepared by adding freshly distilled THF (1 mL) into the Schlenk vessel under N$_2$ flow. The resulting catalyst solution was added to the organo-zinc solution under N$_2$ flow at −78 °C. The solution of the tetrabromocalix[4]arene **40** was added dropwise to the reaction mixture under N$_2$ flow at −78 °C. The reaction mixture was stirred at room temperature for 72 h. The resulting solution was filtered through a Celite pad and concentrated in vacuo to give a crude mixture. The crude was purified by column chromatography (silica gel, methanol/dichloromethane, 2:98) to give the desired Negishi coupling product **42** (78.4 mg, 23%) as a light yellow oil. $^1$H NMR (400 MHz, chloroform-*d*, AO-4-16-fr2-1): $\delta$ = 7.255 (s, 20H), 4.020 (s, 8H), 3.640-3.498 (m, 104H), 3.358 (s, 12H), 1.092 (s, 144H), 0.929 (s, 144H), −0.104 (br, 48H). $^{13}$C NMR (100 MHz, chloroform-*d*, AO-4-16-fr2-1): $\delta$ = 156.3, 150.7, 138.6, 135.2, 134.0, 127.4, 120.2, 71.9, 70.5, 70.5, 70.5, 70.4, 70.4, 61.0, 59.0, 38.6, 26.4, 26.2, 17.9, −4.4. IR (ZnSe, cm$^{-1}$, AO-4-16-fr2): 2956, 2928, 2857, 1593, 1574, 1472, 1439, 1388, 1359, 1247, 1200, 1110, 1030, 951, 892, 894, 857, 835, 780. LRFAB–MS (3-NBA+Na matrix, AO-3-99ptlcfr1): *m/z* ion type (%RA for *m/z* = 700-3500): 3473.1 [M+Na]$^+$ (100%). HRFAB–MS (3-NBA+Na matrix, AO-3-99ptlcfr1): *m/z* ion type (% RA for *m/z* = 3472-3479): calculated for

$^{12}C_{184}{}^{1}H_{328}{}^{14}N_8{}^{16}O_{36}{}^{23}Na_1{}^{28}Si_8$ [M+Na]$^+$ calculated 3473.2133 (31%), found 3473.2260

(41%, 3.7 ppm); [M+Na+1]$^+$ calculated 3474.2160 (75%), found 3474.2183 (80%, 0.7

ppm); [M+Na+2]$^+$ calculated 3475.2179 (100%), found 3475.2231 (100%, 1.5 ppm);

[M+Na+3]$^+$ calculated 3476.2194 (99%), found 3476.2221 (99%, 0.8 ppm).
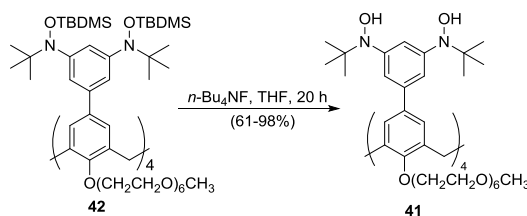


| Run | SM (mg/μmol) | $n$-Bu$_4$NF (mL/mmol) | Yield (mg/%) | TM Label |
|---|---|---|---|---|
| AO-4-59 | 14.4/4.17 | 0.08/0.0768 | 6.5/61 | AO-4-59-flt |
| AO-4-70 | 40.7/11.8 | 0.22/0.217 | 24.1/80 | AO-4-70-flt |
| AO-4-76 | 30.1/8.70 | 0.16/0.160 | 21.8/98 | AO-4-76-flt |

**Octahydroxylamine 41 (AO-4-76).** $n$-Bu$_4$NF (0.16 mL, 0.160 mmol) was added

dropwise to a solution of TBDMS-protected hydroxylamine **42** (30.1 mg, 0.00870 mmol)

in freshly distilled THF (2 mL). The resulting solution was protected from light and stirred

at room temperature for overnight (20 h). The crude mixture was rapidly filtered through

a silica gel pad using methanol/dichloromethane, 5:95 (100 mL). Concentration in vacuo

and drying under high vacuum gave the octahydroxylamine **41** (21.8 mg, 98%) as a yellow

oil. $^1$H NMR (400 MHz, chloroform-$d$, AO-4-59-flt): $\delta$ = 8.996 (br, 8H), 7.327 (s, 12H),

7.095 (br, 8H), 4.141-4.051 (m, 16H), 3.930-3.756 (m, 16H), 3.685-3.605 (m, 56H), 3.533-

3.510 (m, 8H), 3.356 (s, 12H), 1.214 (s, 36H). IR (ZnSe, cm$^{-1}$, AO-4-59-flt): 3240, 2868,

1595, 1439, 1389, 1359, 1255, 1202, 1106, 1050, 947, 866. HR ESI−MS (NaI/CsI, AO-4-

59-flt) $m/z$ (% RA for $m/z$ = 1290-1295): calculated for $^{12}C_{68}{}^{1}H_{108}{}^{14}N_4{}^{16}O_{18}{}^{23}Na_1$

[M+2Na]$^{2+}$ calculated 1291.7557 (65%), found 1291.7633 (90%, 5.9 ppm); [M+2Na+1]$^{2+}$

calculated 1292.2573 (100%), found 1292.2605 (100%, 2.5 ppm); [M+2Na+2]$^{2+}$ calculated 1292.7590 (79%), found 1292.7633 (70%, 3.3 ppm); [M+2Na+3]$^{2+}$ calculated 1293.2604 (46%), found 1293.2655 (40%, 4.0 ppm).
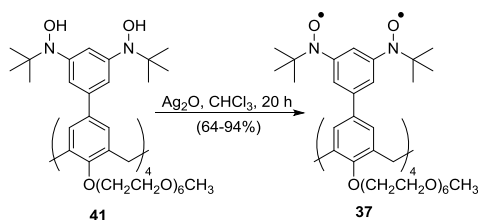


| Run | SM (mg/μmol) | Ag$_2$O (mg/mmol) | Yield (mg/%) | TM Label |
|---|---|---|---|---|
| AO-4-64 | 6.5/2.56 | 23.8/0.102 | n.a. | n.a. |
| AO-4-78-1 | 13.8/5.44 | 50.4/0.217 | 12.9/94 | AO-4-78-col1 |
| AO-4-78-2 | 9.9/3.90 | 36.2/0.156 | 9.3/94 | AO-4-78-col2 |
| AO-4-79 | 21.0/8.27 | 76.7/0.331 | 13.5/64 | AO-4-79-col |

**Nitroxide octaradical 37 (AO-4-79).** Freshly prepared silver oxide (76.7 g, 0.331 mmol) was added to a solution of octahydroxylamine **41** (21.0 mg, 0.00827 mmol) in chloroform (2 mL). After being stirred at room temperature in darkness for 20 h, the reaction mixture was filtered, and then the yellow filtrate was evaporated to dryness to obtain the crude product (24.4 mg). The crude product was purified by column chromatography on silica gel using methanol/dichloromethane (5:95) to give nitroxide octaradical **37** (13.5 mg, 64%) as a yellow oil. $^1$H NMR (500 MHz, chloroform-*d*, AO-4-79-col): $\delta$ = 11.650 (br, 8H), 3.848-3.593 (br, 108H), −1.893 (br, 72H). IR (ZnSe, cm$^{-1}$, AO-4-79-col): 2920, 2869, 1460, 1445, 1356, 1248, 1192, 1106, 1044, 859. HR ESI−MS (NaI/CsI, AO-4-79-col) *m/z* (% RA for *m/z* = 1287-1291): calculated for $^{12}$C$_{68}$$^1$H$_{104}$$^{14}$N$_4$$^{16}$O$_{18}$$^{23}$Na$_1$ [M+2Na]$^{2+}$ calculated 1287.7244 (65%), found 1287.7323 (46%, 6.2 ppm); [M+2Na+1]$^{2+}$ calculated 1288.2260 (100%), found 1288.2439 (88%, 13.9 ppm);

$[M+2Na+2]^{2+}$ calculated 1288.7276 (82%), found 1288.7336 (100%, 4.7 ppm);

$[M+2Na+3]^{2+}$ calculated 1289.2291 (46%), found 1289.2372 (87%, 6.3 ppm).

## 2.5. References

1. Gutsche, C. D. *Calixarenes Revisited*, 1st ed.; RSC, Cambridge, 1998.

2. Sliwa, W.; Kozlowski, C. *Calixarenes and Resorcinarenes: Synthesis, Properties and Applications*, 1st ed.; Wiley-VCH, Weinheim, 2009.

3. Böhmer, V. *Angew. Chem. Int. Ed. Engl.* **1995**, *34*, 713−745.

4. Vicens, J.; Harrowfield, J. Eds. *Calixarenes in the Nanoworld*; Springer, Dordrecht, 2007.

5. Baeyer, A. *Berlin* **1872**, *5*, 25.

6. Zinke, A.; Zeigler, E. *Ber.* **1941**, *74*, 1729−1736.

7. Andreetti, G. D.; Ungaro, R.; Pochini, A. *J. Chem. Soc., Chem. Commun.* **1979**, 1005−1007.

8. Gutsche, C. D.; Muthukrishnan, R. *J. Org. Chem.* **1978**, *43*, 4905–4906.

9. Gutsche, C. D.; Dhawan, B.; Levine, J. A.; No, K. H.; Muthukrishnan, R. *J. Am. Chem. Soc.* **1981**, *103*, 3782–3792.

10. Gutsche, C. D. Iqbal, M. *Org. Synth.* **1990**, *68*, 234–237.

11. Gutsche, C. D.; Dhawan, B.; Leonis, M.; Stewart, D. *Org. Synth.* **1990**, *68*, 238−242.

12. Munch, J. H.; Gutsche, C. D. *Org. Synth.* **1990**, *68*, 243−246.

13. Stewart, D. R.; Gutsche, C. D. *J. Am. Chem. Soc.* **1999**, *121*, 4136–4146.

14. Gutsche, C. D.; Dhawan, B.; Levine, J. A.; No, K. H.; Bauer, L. J. *Tetrahedron* **1983**, *39*, 409–426.

15. Ikeda, A.; Shinkai, S. *Chem. Rev.* **1997**, *97*, 1713–1734.

16. Araki, K.; Iwamoto, K.; Shinkai, S.; Matsuda, T. *Chem. Lett.* **1989**, 1747–1750.

17. Gutsche, C. D.; Reddy, P. A. *J. Org. Chem.* **1991**, *56*, 4783–4791.

18. Rajca, A.; Pink, M.; Rojsajjakul, T.; Lu, K.; Wang, H.; Rajca, S. *J. Am. Chem. Soc.* **2003**, *125*, 8534−8538.

19. Verboom, W.; Datta, S.; Asfari, Z.; Harkema, S.; Reinhoudt, D. N. *J. Org. Chem.* **1992**, *57*, 5394–5398.

20. Groenen, L. C.; van Loon, J, -D.; Verboom, W.; Harkema, S.; Casnati, A.; Ungaro, R.; Pochini, A.; Ugozzoli, F.; Reinhoudt, D. N. *J. Am. Chem. Soc.* **1991**, *113*, 2385–2392.

21. Griller, D.; Ingold, K. U. *Acc. Chem. Res.* **1976**, *9*, 13–19.

22. Breuer, E.; Aurich, H. G.; Nielsen, A. In Nitrones, Nitronates and Nitroxides, Wiley, New York, 1989, p.313.

23. Hass, H. B.; Riley, E. F. *Chem. Rev.* **1943**, *32*, 373–430.

24. Calder, A.; Forrester, A. R. *J. Chem. Soc. (C)*, **1969**, *10*, 1459−1469.

25. Rivera, E. J.; Sethi, R.; Qu, F.; Krishnamurthy, R.; Muthupillai, R.; Alford, M.; Swanson, M. A.; Eaton, S. S.; Eaton, G. R.; Wilson, L. J. *Adv. Funct. Mater.* **2012**, *22*, 3691–3698.

26. Sciannamea, V; Jérôme, R.; Detrembleur, C. *Chem. Rev.* **2008**, *108*, 1104–1126.

27. Hawker, C. J.; Bosman, A. W.; Harth, E. *Chem. Rev.* **2001**, *101*, 3661−3688.

28. Janoschka, T.; Hager, M. D.; Schubert, U. S. *Adv. Mater.* **2012**, *24*, 6397–6409.

29. Nesvadba, P.; Bugnon, L.; Maire, P.; Novák, P. *Chem. Mater.* **2010**, *22*, 783–788.

30. Tretyakov, E. V.; Ovcharenko, V. I. *Russ. Chem. Rev.* **2009**, *78*, 971–1012.

31. Lahti, P. M. *Magnetic Properties of Organic Materials*, Marcel Dekker, New York, 1999.

32. Ni, Q, Z.; Daviso, E.; Can, T. V.; Markhansin, E.; Jawla, S. K.; Swager, T. M.; Temkin, R. J.; Herzfelf, J.; Griffin, R. G. *Accounts of Chemical Research* **2013**, *46*, 1933–1941.

33. Haze, O.; Corzilius, B.; Smith, A. A.; Griffin, R. G.; Swager, T. M. *J. Am. Chem. Soc.* **2012**, *134*, 14287–14290.

34. Clore, G. M.; Iwahara, J. *Chem. Rev.* **2009**, *109*, 4108–4139.

35. Hu, K. N.; Yu, H.; Swager, T. M.; Griffin, R. G. *J. Am. Chem. Soc.* **2004**, *126*, 10844–10845.

36. Rajca, A.; Wang, Y.; Boska, M.; Paletta, J. T.; Olankitwanit, A.; Swanson, M. A.; Mitchell, D. G.; Eaton, S. S.; Eaton, G. R.; Rajca, S. *J. Am. Chem. Soc.* **2012**, *134*, 15724–15727.

37. Zhelev, Z.; Bakalova, R.; Aoki, I.; Matsumoto, K.; Gadjeva, V.; Anzai, K.; Kanno, I. *Chem. Commun.* **2009**, 53–55.

38. Winalski, C. S.; Shortkroff, S.; Schneider, E.; Yoshioka, H.; Mulkern, R. V.; Rosen, G. M. *Osteoarthritis Cartilage* **2008**, *16*, 815–822.

39. Gallez, B.; Lacour, V.; Demeure, R.; Debuyst, R.; Dejehet, F.; De Keyser, J. L.; Dumont, P. *Magn. Reson. Imaging* **1994**, *12*, 61–69.

40. Calder, A.; Forrester, A. R.; James, P. G.; Luckurst, G. R. *J. Am. Chem. Soc.* **1969**, *91*, 3724–3727.

41. Ishida, T.; Iwamura, H. *J. Am. Chem. Soc*. **1991**, *113*, 4238–4241.

42. Kanno, F.; Inoue, K.; Koga, N.; Iwamura, H. *J. Am. Chem. Soc*. **1993**, *115*, 847–850.

43. Dvolaitzky, M.; Chiarelli, R.; Rassat, A. *Angew. Chem. Int. Ed*. **1992**, *31*, 180−181.

44. Rajca, A.; Lu, K.; Rajca, S.; Ross, C. R., *Chem. Commun*. **1999**, 1249–1250

45. Rassat, A.; Sieveking, U. *Angew. Chem., Int. Ed. Engl.* **1972**, *11*, 303–304.

46. Rajca, A.; Takahashi, M.; Pink, M.; Spagnol, G.; Rajca, S. *J. Am. Chem. Soc.* **2007**, *129*, 10159–10170.

47. Rajca, A.; Shiraishi, K.; Rajca, S. *Chem. Commun.* **2009**, 4372–4374.

48. (A) Barone, V.; Boilleau, C.; Cacelli, I.; Ferretti, A.; Monti, S.; Prampolini, G. *J. Chem. Theory Comput.* **2013**, *9*, 300−307. (B) Barone, V.; Cacelli, I.; Ferretti, A.; Monti, S.; Prampolini, G. *Phys. Chem. Chem. Phys.* **2011**, *13*, 4709–4714.

49. Kanno, F.; Inoue, K.; Koga, N.; Iwamura, H. *J. Phys. Chem*. **1993**, *97*, 13267–13272.

50. Spagnol, G.; Shiraishi, K.; Rajca, S.; Rajca, A. *Chem. Commun.* **2005**, 5047–5049.

51. Ovchinnikov, A. A. *Theor. Chim. Acta.* **1978**, *47*, 297−304.

52. Rajca, A.; Rajca, S.; Desai, S. R. *J. Am. Chem. Soc.* **1995**, *117*, 806–816.

53. Rajca, A.; Wongsriratanakul, J; Rajca, S. *Science* **2001**, *295*, 1503–1505.

54. Araki, K.; Nakamura, R.; Otsuka, H.; Shinkai, S. *J. Chem. Soc., Chem. Commun.,* **1995**, *20*, 2121–2122.

55. Ulrich, G.; Turek, P.; Ziessel, R. *Tetrahedron Lett.* **1996**, *37*, 8755–8758.

56. Wang, Q.; Li, Y.; Wu, G. S. *Chem. Commun.*, **2002**, 1268–1269.

57. Hu, X.; Li, Y.; Yang, H.; Luo, Y. *Tetrahedron Lett.* **2006**, *47*, 7463–7465.

58. Hu, X.; Yang, H.; Li, Y. *Spectrochim. Acta, Part A* **2008**, *70*, 439–444.

59. Rajca, A.; Mukherjee, S.; Pink, M.; Rajca, S. *J. Am. Chem. Soc.* **2006**, *128*, 13497–13507.

60. Sawai, T.; Sato, K.; Ise, T.; Shiomi, D.; Toyota, K.; Morita, Y.; Takui, T. *Angew. Chem. Int. Ed.* **2008**, *47*, 3988–3990.

61. Das, K. Syntheses of Building Blocks for Organic Materials: Spin-Labeled Nucleosides and Thiophene-Based Oligomers. Ph.D. Dissertation, University of Nebraska – Lincoln, Lincoln, NE, July 2007.

62. Iwamura, H.; Inoue, K. *Angew. Chem., Int. Ed.* **1995**, *34*, 927–928.

63. Mukherjee, S. Syntheses of Nitroxide Diradicals and Tetraradicals. Ph.D. Dissertation, University of Nebraska – Lincoln, Lincoln, NE, July 2006.

64. Das, K.; Pink, M.; Rajca, S.; Rajca, A. *J. Am. Chem. Soc.* **2006**, *128*, 5334–5335.

65. Miyasaki, M.; Rajca, A. *Synlett* **2004**, 177–181.

66. Chapelet-Letourneux, G.; Lemaire, H.; Rassat, A. *Bull. Soc. Chim. France* **1965**, *11*, 444–450.

67. Davies, M.; Spiers, N. A. *J. Chem. Soc.* **1959**, 3971–3988.

68. American University of Beirut Home Page. http://staff.aub.edu.lb/~tg02/IR.pdf (accessed Sep 2014).

69. Kreilick, R. W. *J. Chem. Phys.* **1967**, *46*, 4260−4264.

70. Forrester, A. R.; Hepburn, S. P.; McConnachie, G. *J. Chem. Soc., Perkin Transaction I* **1974**, *19* , 2213–2219.

71. Rassat, A.; Ray, P. *Tetrahedron* **1973**, 29, 2845–2848.

72. Olankitwanit, A.; Kathirvelu, V.; Rajca, S.; Eaton, G. R.; Eaton, S. R.; Rajca, A. *Chem. Commun.* **2011**, *47*, 6443−6445.

73. Gerson, F.; Huber, W. *Electron Spin Resonance Spectroscopy of Organic Radicals*; WILEY-VCH Verlag GmbH & Co. KGaA: Weinheim, 2003.

74. Sato, H.; Kathirvelu, V.; Spagnol, G.; Rajca, S.; Eaton, S. S.;  Eaton, G. R. *J. Phys. Chem. B* **2008**, *112*, 2818–2828.

75. Rajca, A. *Adv. Phys. Org. Chem.* **2005**, *40*, 153−199.

76. Rajca, A.; Wongsriratanakul, J.; Rajca, S. *J. Am. Chem. Soc*. **1997**, *119*, 11674–11686.

77. Rastrelli, F.; Bagno, A. *Chem. Eur. J.* **2009**, *15*, 7990–8004.

78. Percec, V.; Bera, T. K.; De, B. B.; Sanai, Y.; Smith, J.; Holerca, M. N.; Barboiu, B.; Grubbs, R. B.; Fréchet, J. M. J. *J. Org. Chem.* **2001**, *66*, 2104–2117.

79. Suffert, J. *J. Org. Chem.* **1989**, *54*, 509−510.

80. Rajca, A.; Takahashi, M.; Pink, M.; Spagnol, G.; Rajca, S. *J. Am. Chem. Soc.* **2007**, *129*, 10159–10170.

**Appendix A**

**$^1$H, $^{13}$C NMR, IR Spectra, X-ray data (Chapter 1)**
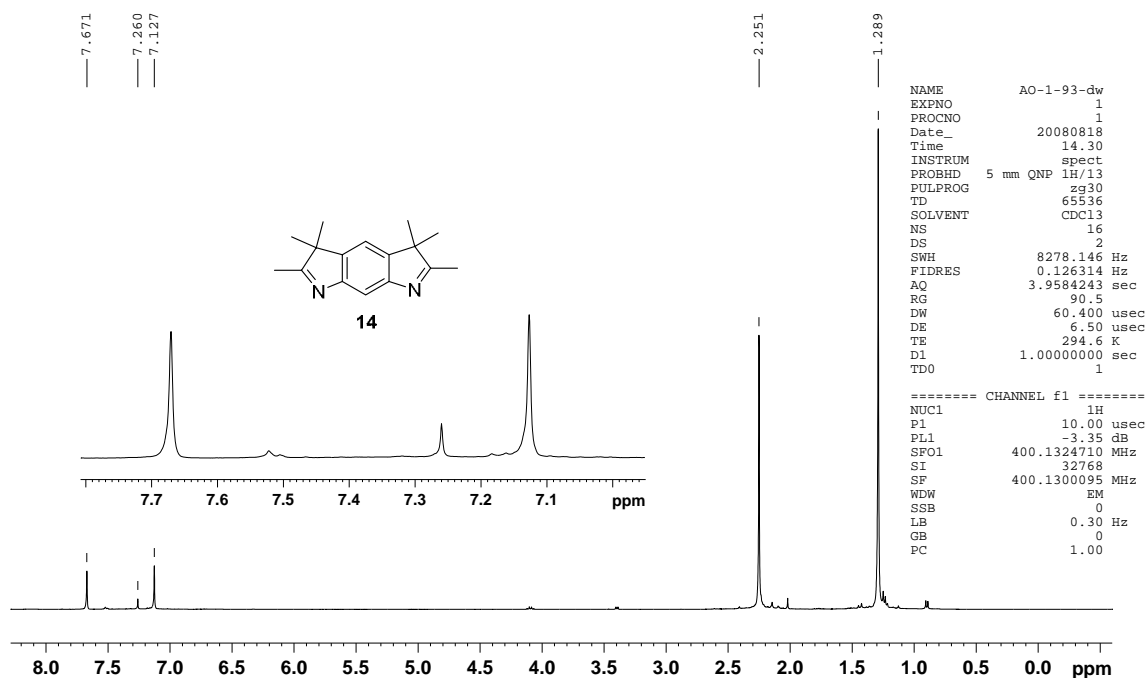
**Figure A1.** ^{1}H NMR (400 MHz, chloroform-*d*) spectrum of **14** (AO-1-93-dw).
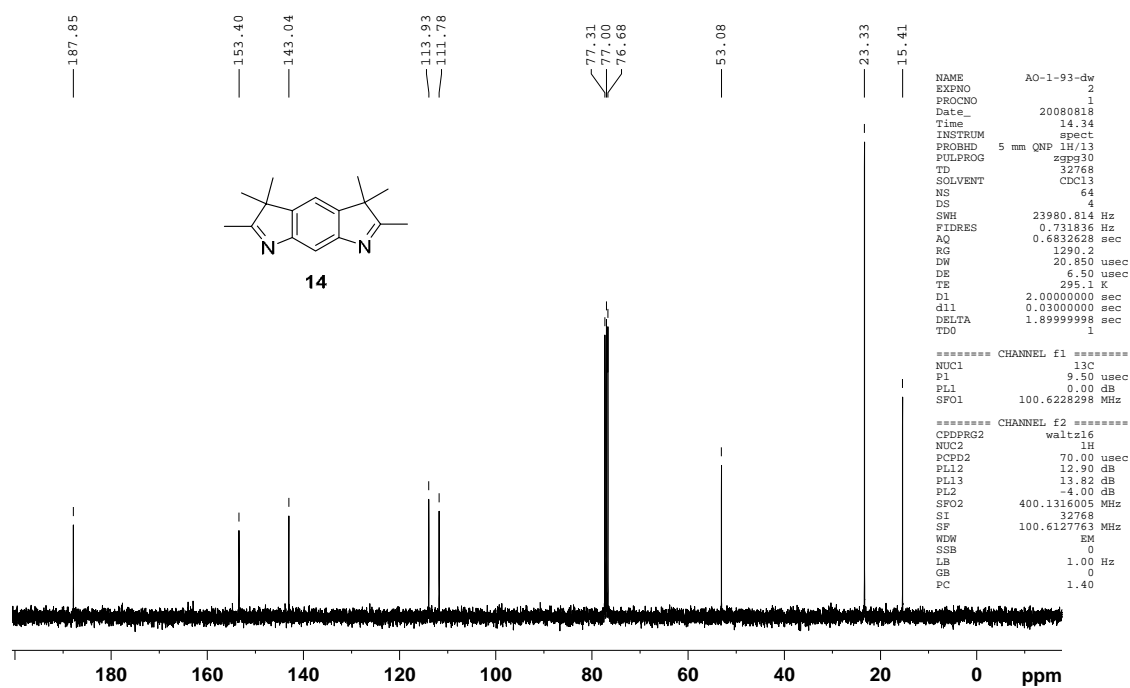


**Figure A2.** ^{13}C NMR (100 MHz, chloroform-*d*) spectrum of **14** (AO-1-93-dw).
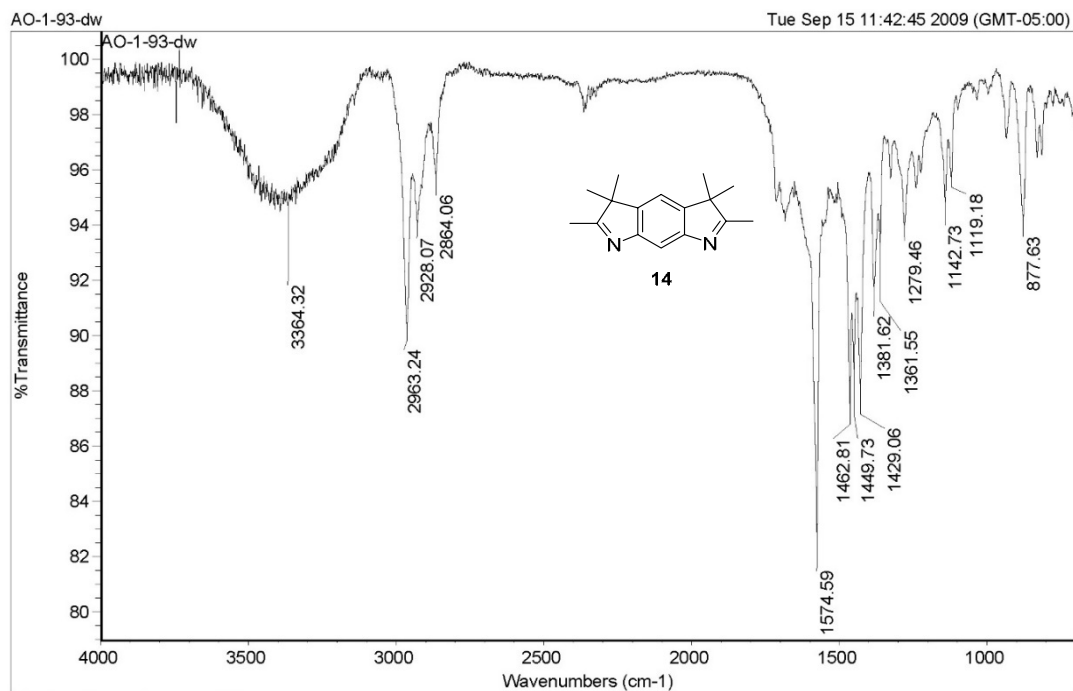
**Figure A3.** IR (ATR, ZnSe, cm$^{-1}$) spectrum of **14** (AO-1-93-dw).
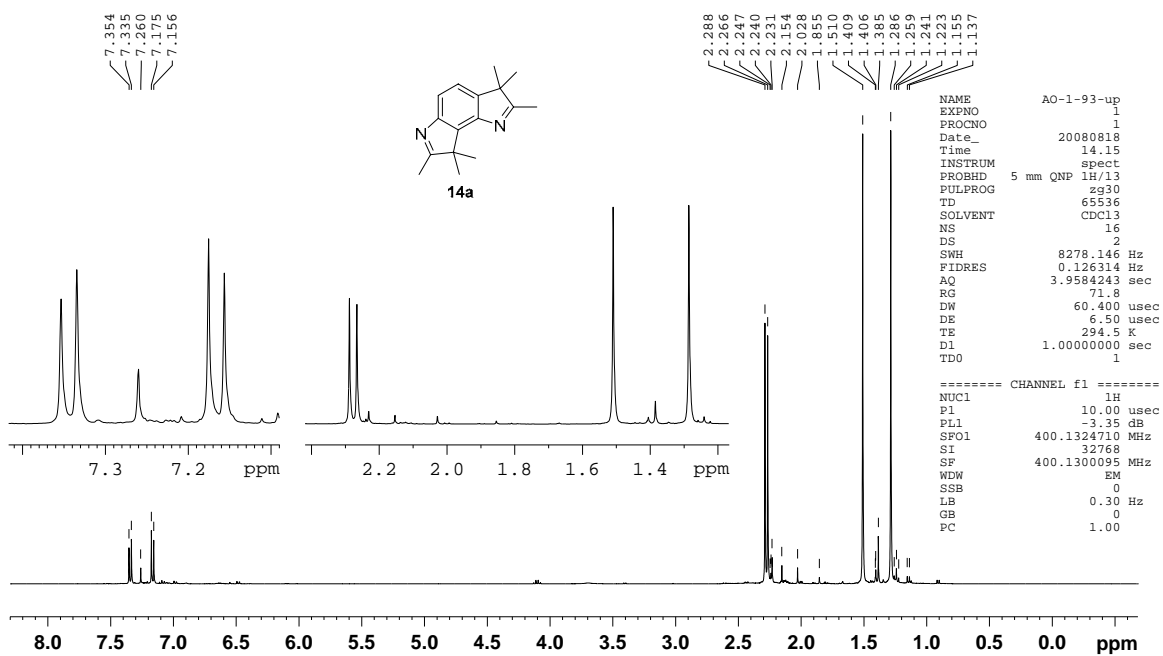


**Figure A4.** $^1$H NMR (400 MHz, chloroform-*d*) spectrum of **14a** (AO-1-93-up).
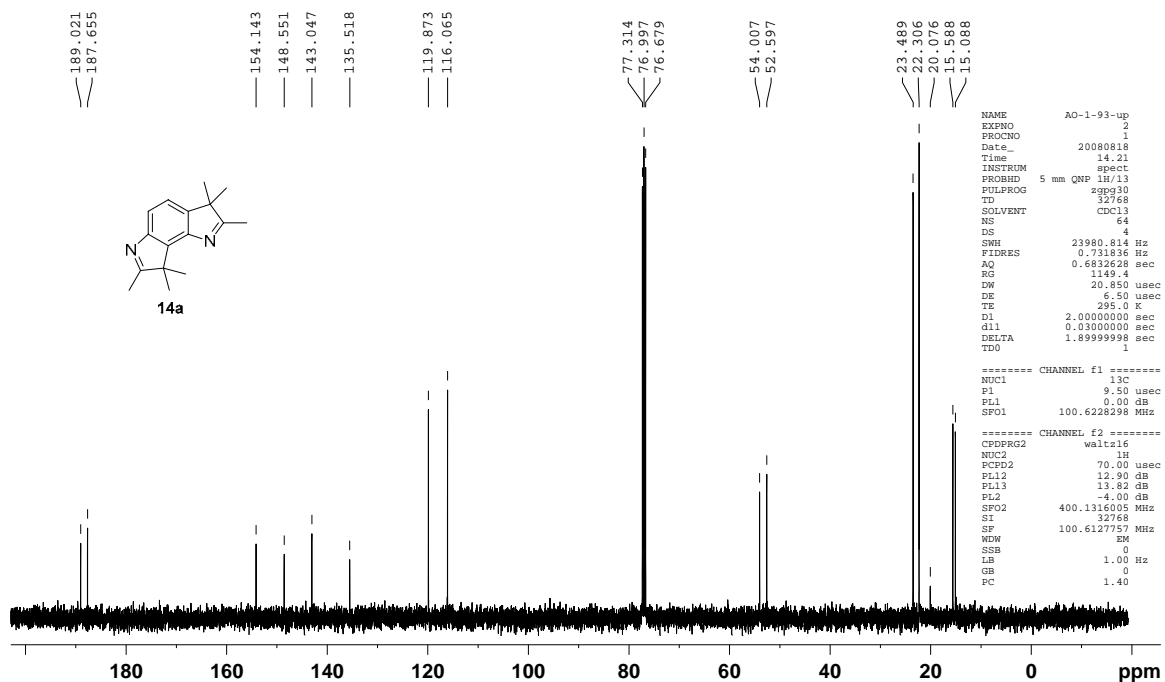
**Figure A5.** $^{13}$C NMR (100 MHz, chloroform-*d*) spectrum of **14a** (AO-1-93-up).
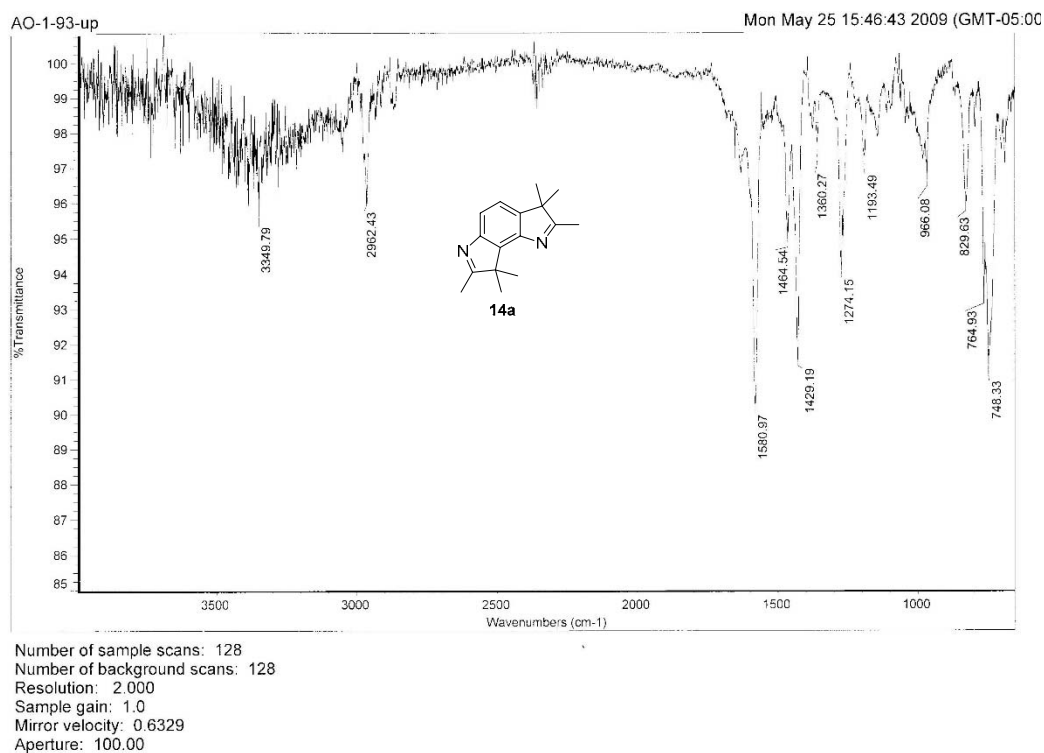


**Figure A6.** IR (ATR, ZnSe, cm$^{-1}$) spectrum of **14a** (AO-1-93-up).
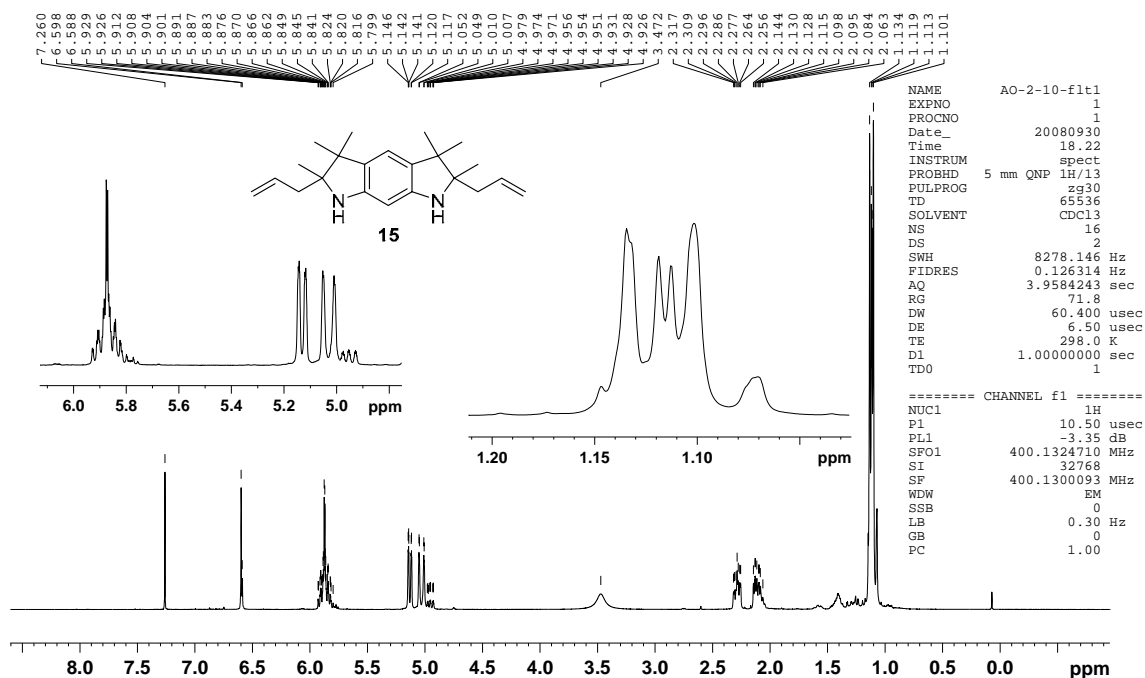
**Figure A7.** ^{1}H NMR (400 MHz, chloroform-*d*) spectrum of diallyldiamine **15** (AO-2-10-flt).
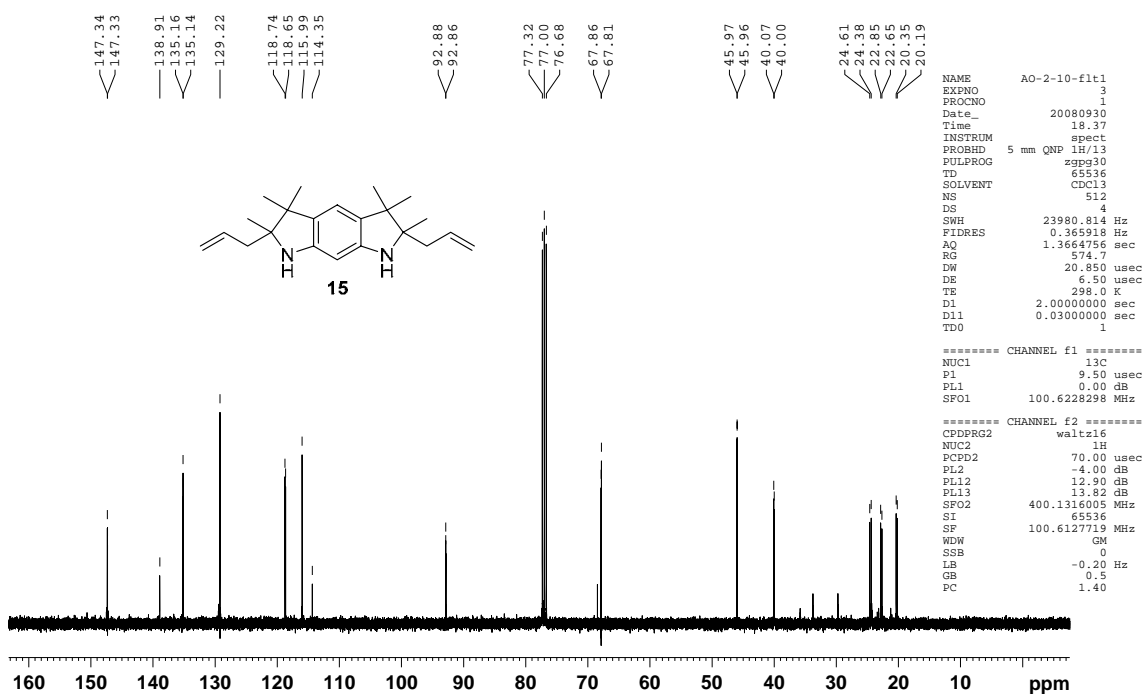


**Figure A8.** ^{13}C NMR (100 MHz, chloroform-*d*) spectrum of diallyldiamine **15** (AO-2-10-flt1).
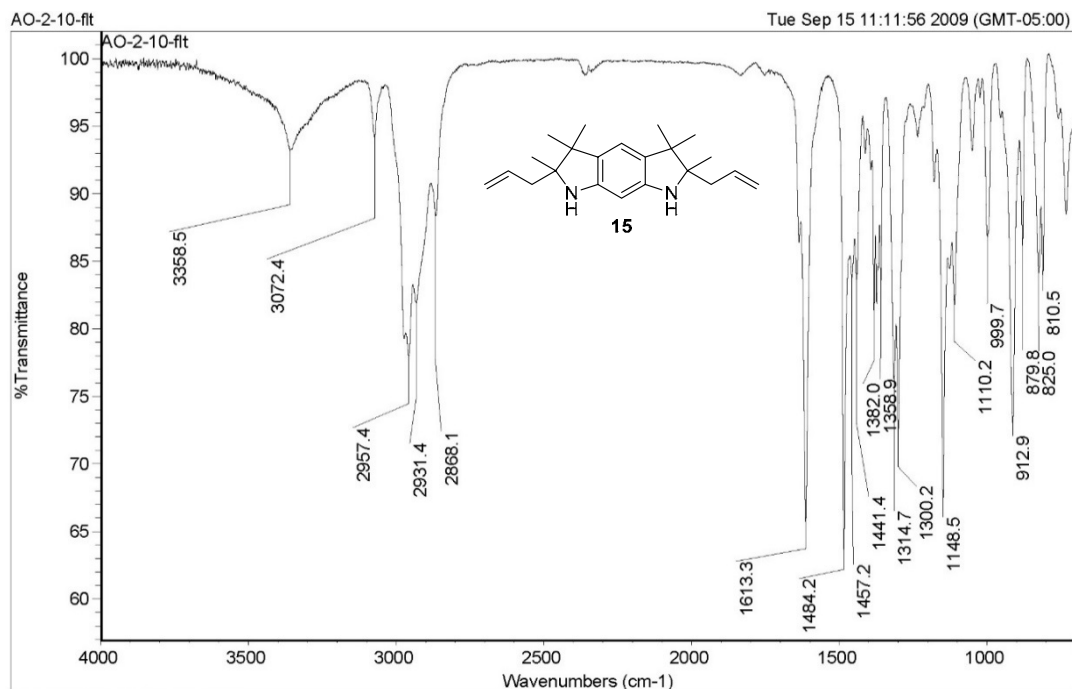
**Figure A9.** IR (ATR, ZnSe, cm$^{-1}$) spectrum of diallyldiamine **15** (AO-2-10-flt).
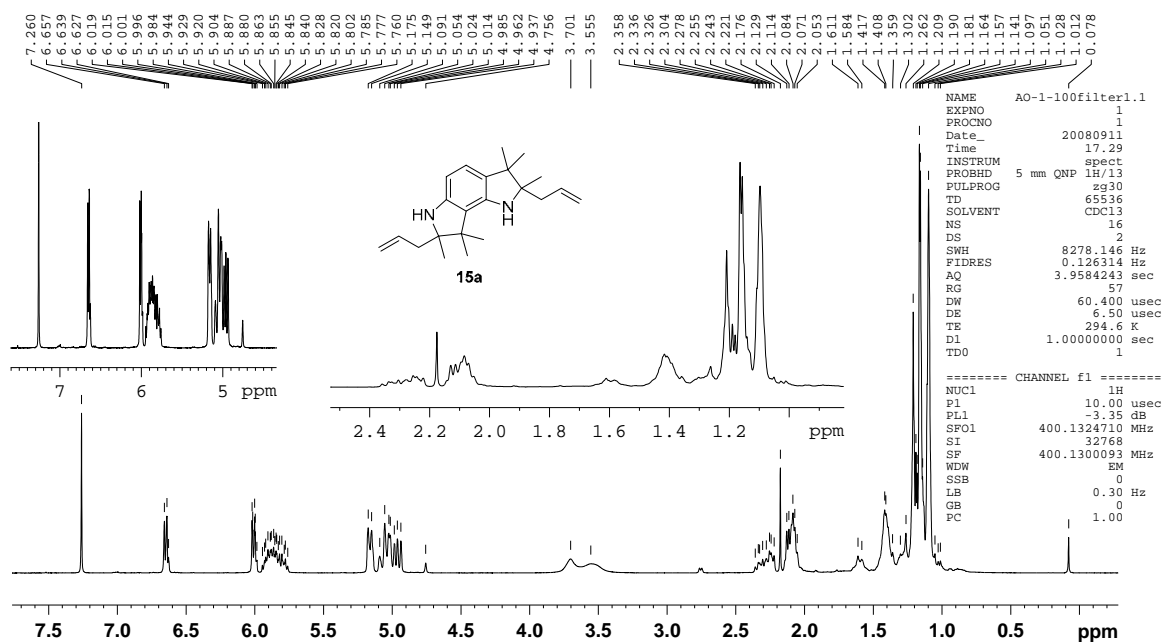


**Figure A10.** $^1$H NMR (400 MHz, chloroform-*d*) spectrum of **15a** (AO-1-100-filter).
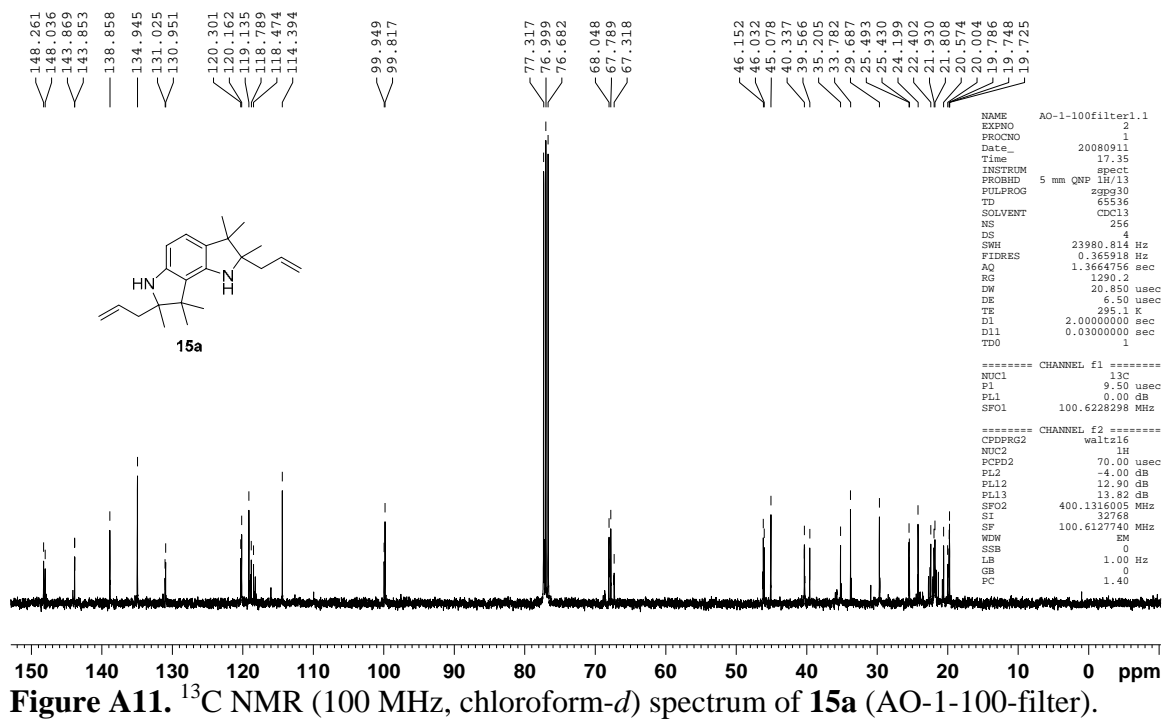
**Figure A11.** $^{13}$C NMR (100 MHz, chloroform-$d$) spectrum of **15a** (AO-1-100-filter).
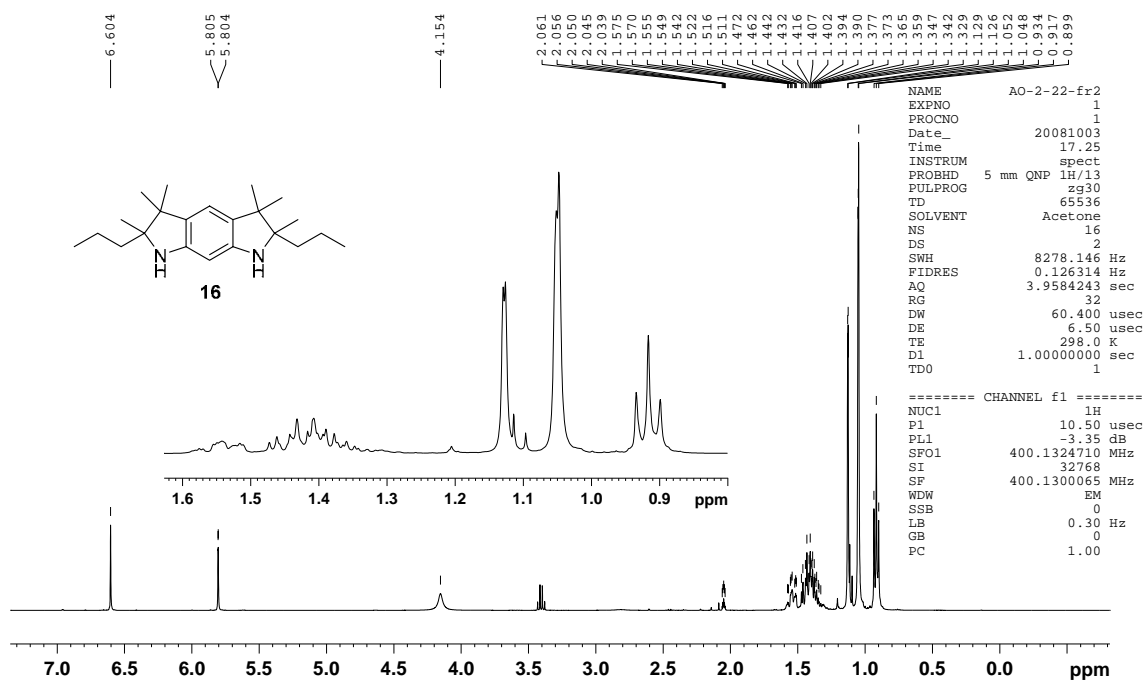


**Figure A12.** $^{1}$H NMR (400 MHz, acetone-$d_6$) spectrum of dipropyldiamine **16** (AO-2-22-fr2).
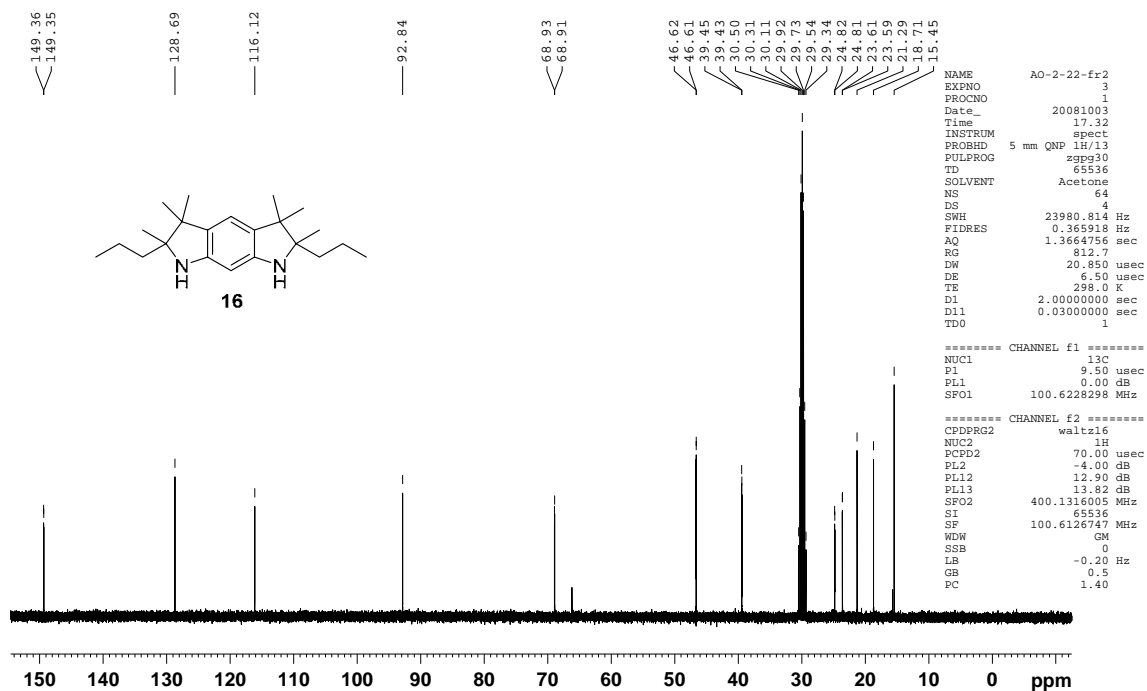
**Figure A13.** $^{13}$C NMR (100 MHz, acetone-$d_6$) spectrum of dipropyldiamine **16** (AO-2-22-fr2).
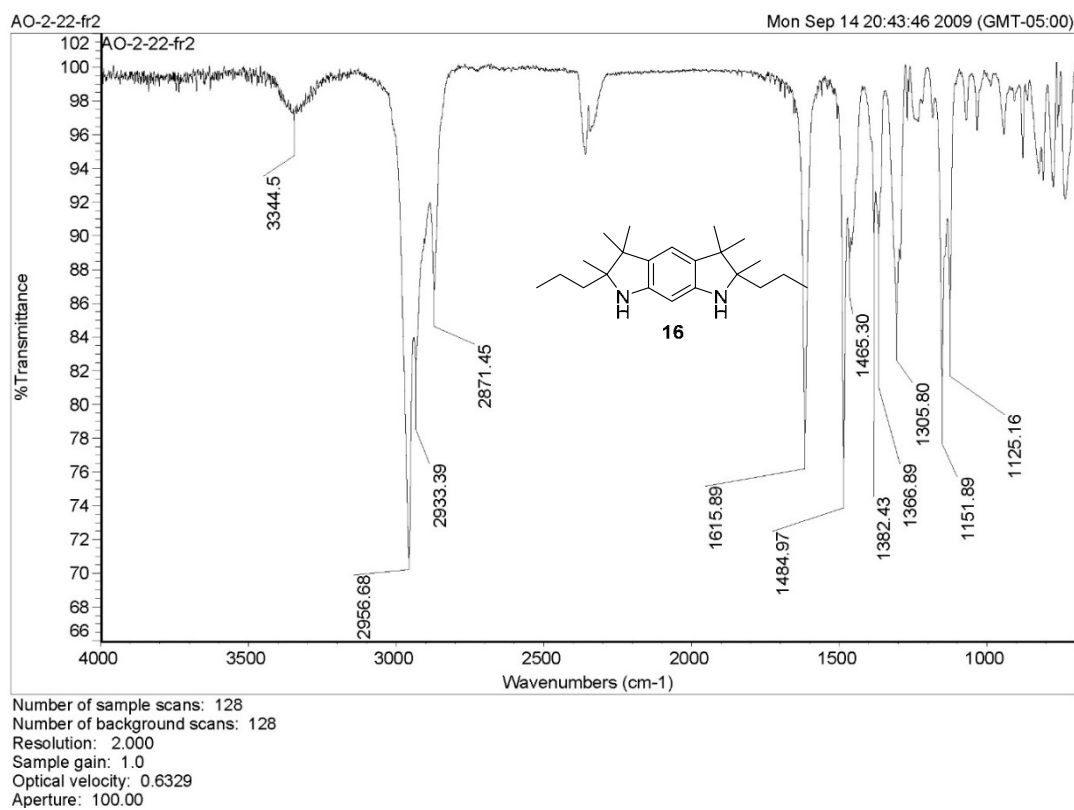


**Figure A14.** IR (ATR, ZnSe, cm$^{-1}$) spectrum of dipropyldiamine **16** (AO-2-22-fr2).
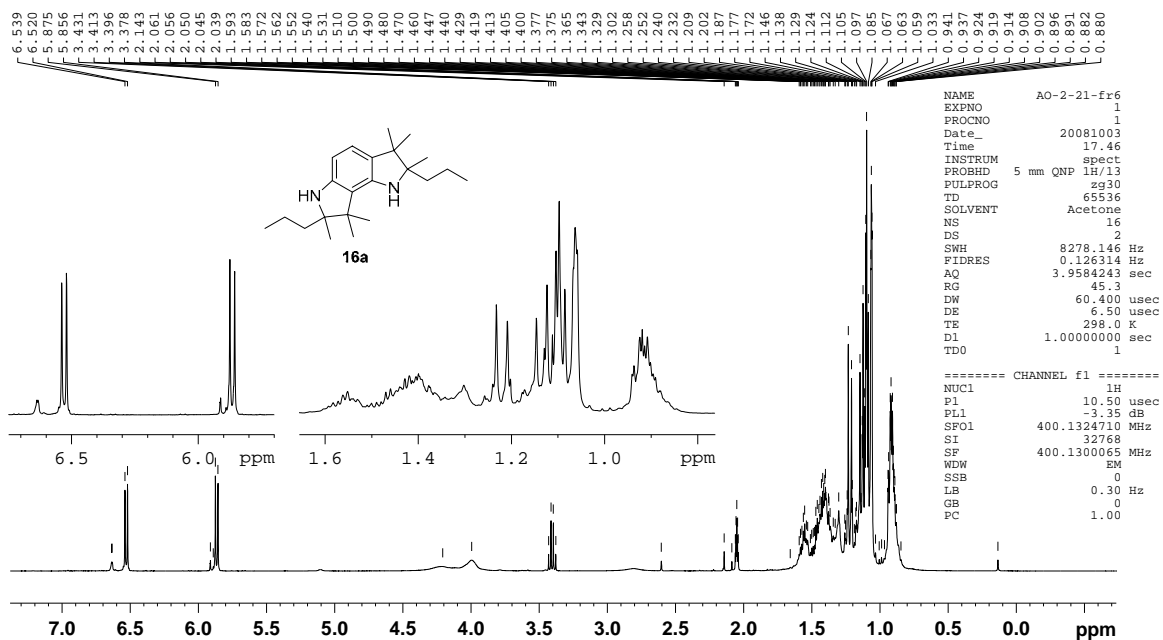
**Figure A15.** [^1]H NMR (400 MHz, acetone-*d*₆) spectrum of dipropyldiamine **16a** (AO-2-21-fr6).
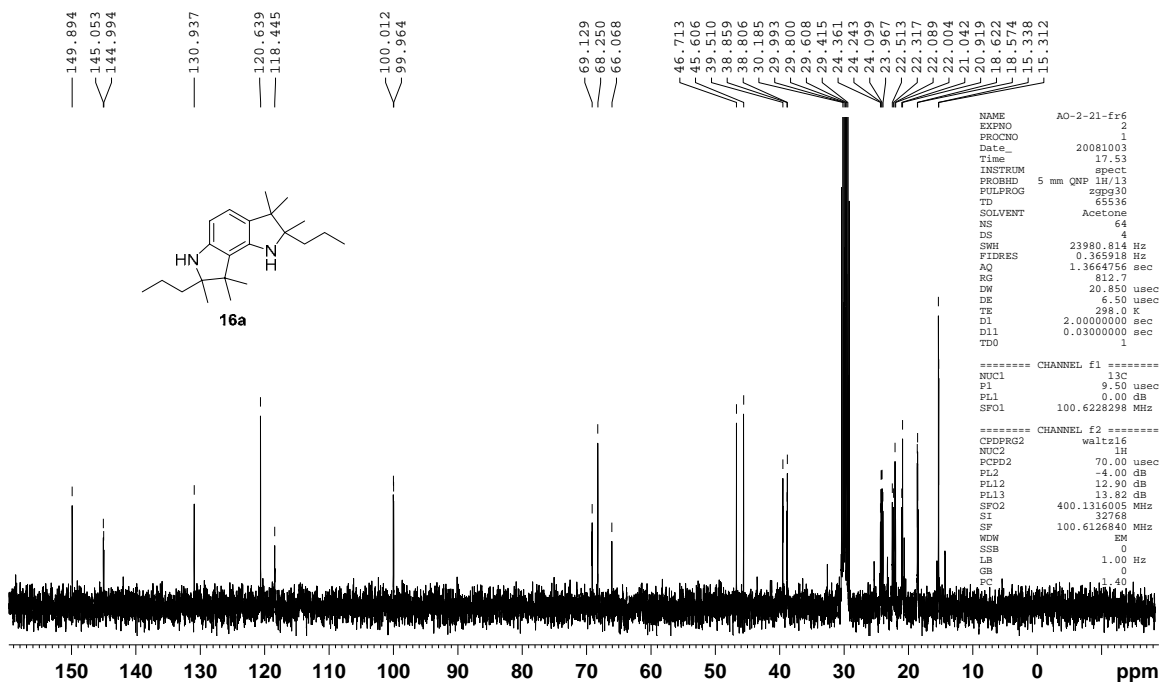


**Figure A16.** [^13]C NMR (100 MHz, acetone-*d*₆) spectrum of dipropyldiamine **16a** (AO-2-22-fr6).
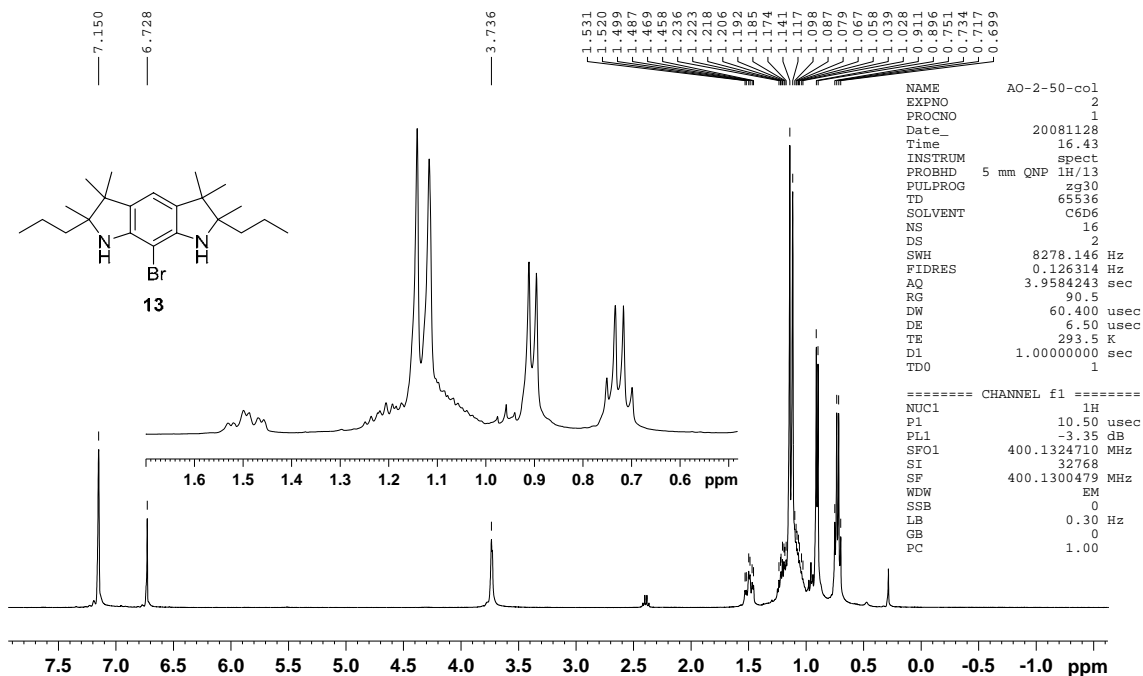
**Figure A17.** $^1$H NMR (400 MHz, benzene-$d_6$) spectrum of bromodiamine **13** (AO-2-50-col).
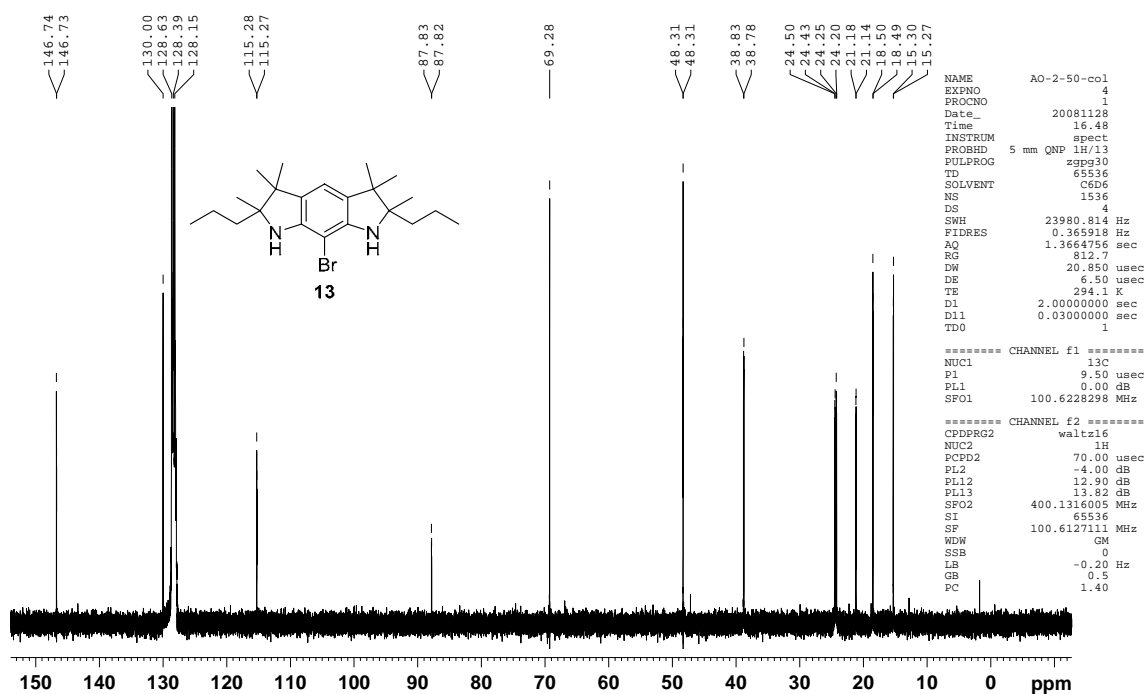


**Figure A18.** $^{13}$C NMR (100 MHz, benzene-$d_6$) spectrum of bromodiamine **13** (AO-2-50-col).
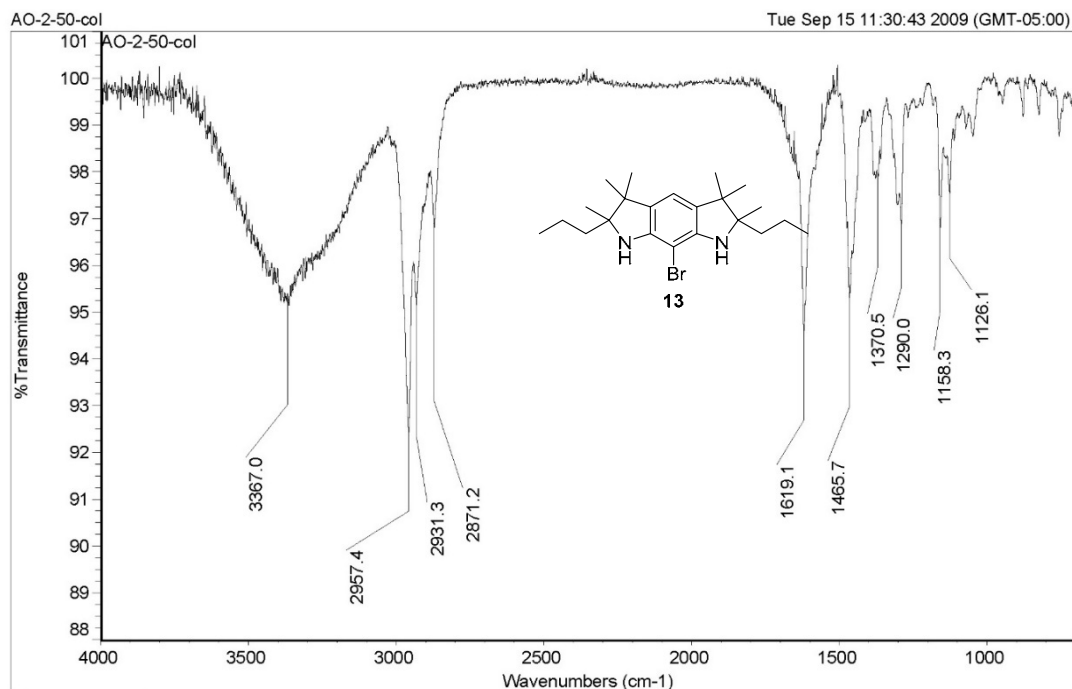
**Figure A19.** IR (ATR, ZnSe, cm$^{-1}$) spectrum of bromodiamine **13** (AO-2-50-col).
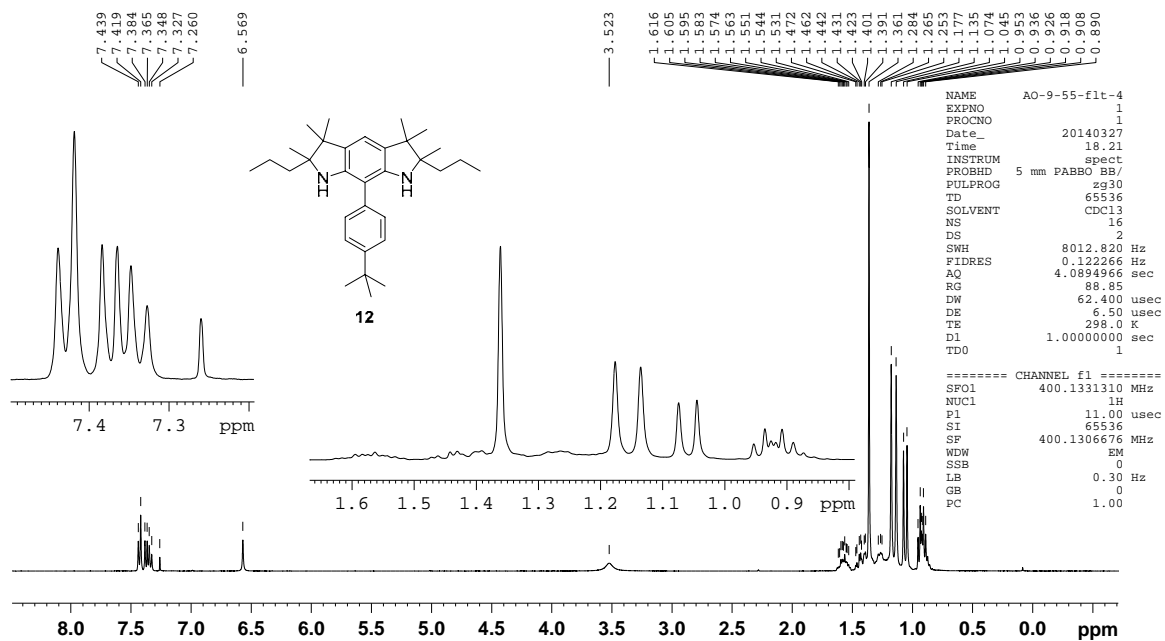


**Figure A20.** $^{1}$H NMR (500 MHz, chloroform-*d*) spectrum of diamine **12** (AO-9-55-flt-4).
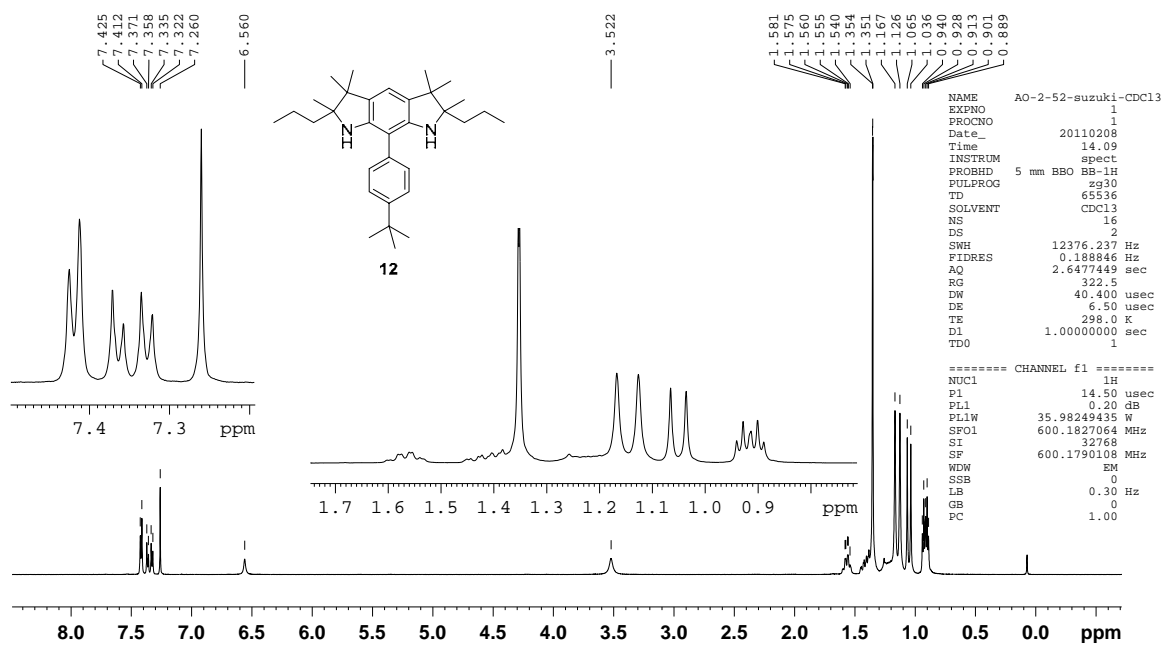
**Figure A21.** ^{1}H NMR (600 MHz, chloroform-*d*) spectrum of diamine **12** (AO-2-52-suzuki-CDCl3).
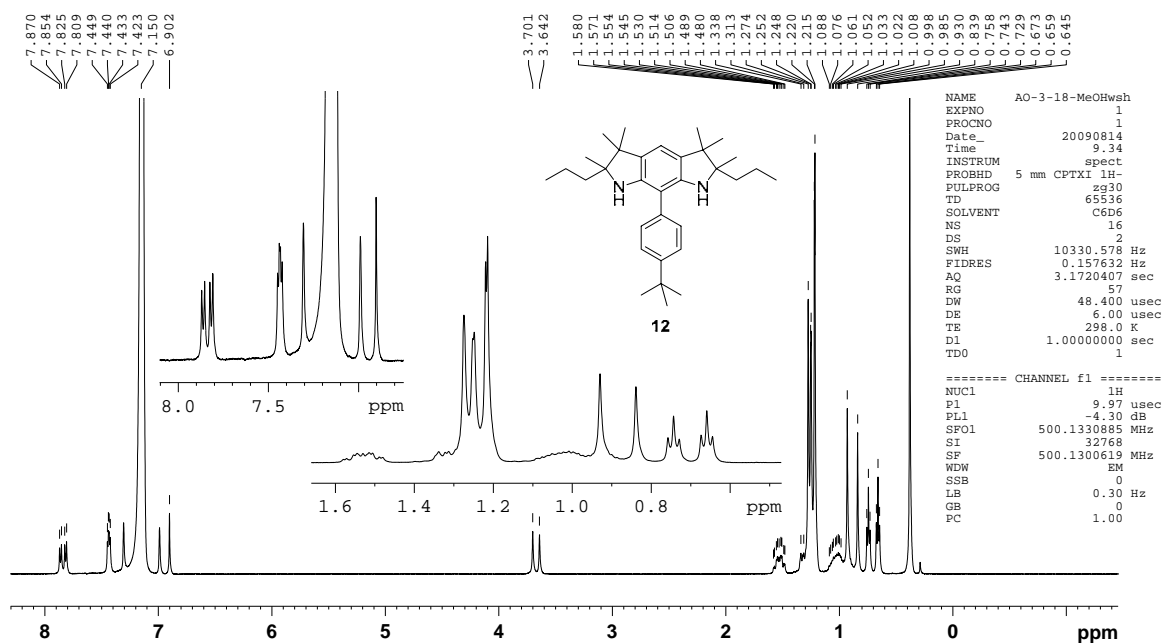


**Figure A22.** ^{1}H NMR (500 MHz, benzene-*d*$_6$) spectrum of diamine **12** (AO-3-18-MeOHwsh).
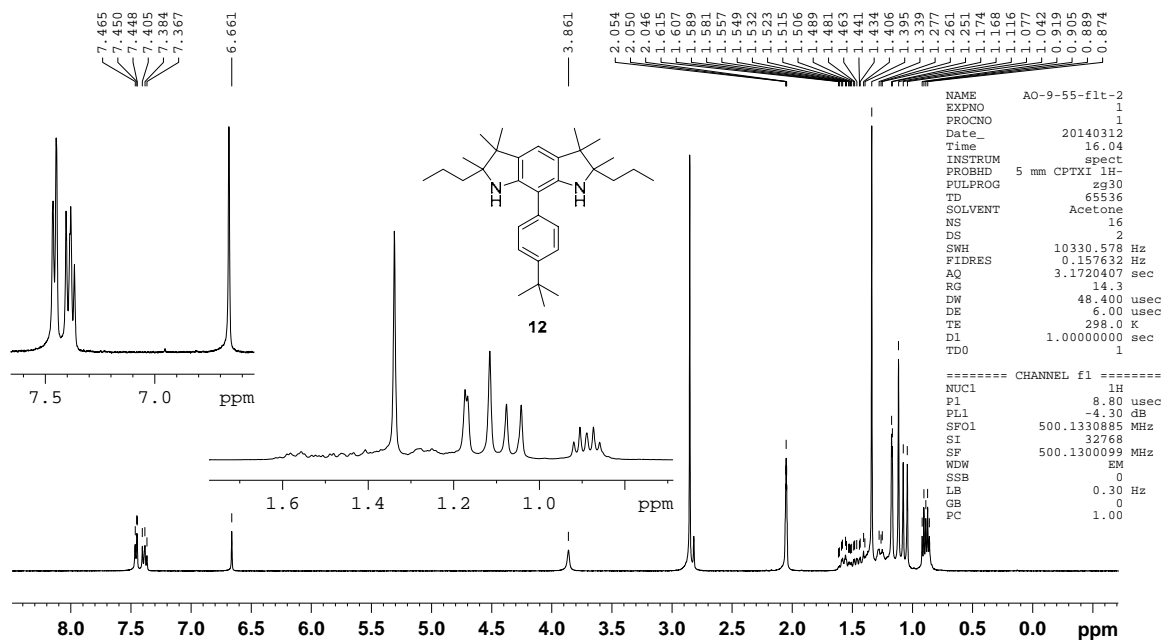
**Figure A23.** $^1$H NMR (500 MHz, acetone-$d_6$) spectrum of diamine **12** (AO-9-55-flt-2).
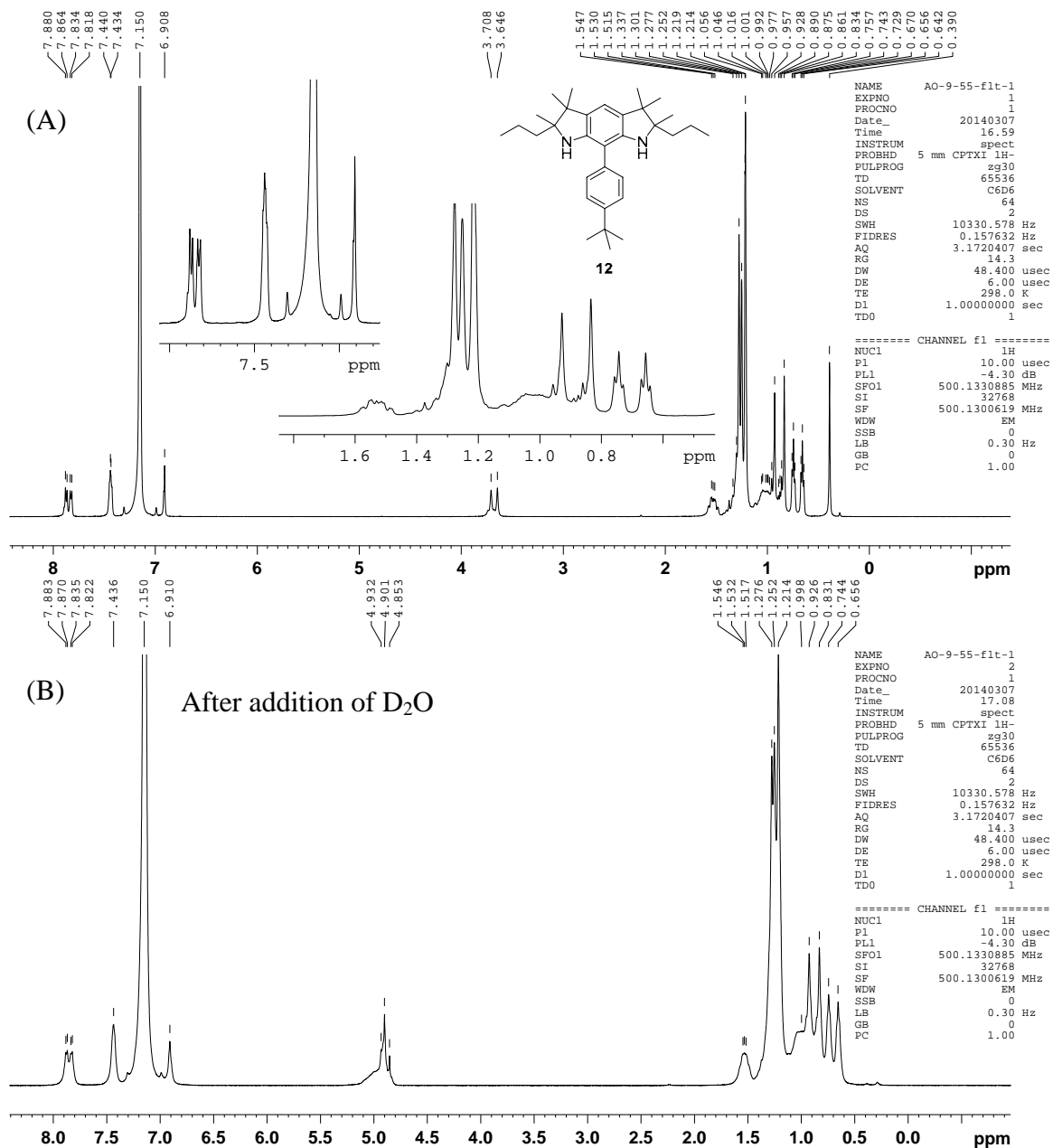
**Figure A24.** (A) ${}^1$H NMR (500 MHz, benzene-$d_6$) spectrum of diamine **12** (AO-9-55-flt1). (B) After addition 2 drops of D$_2$O, N-H peaks at $\delta$ = 3.708, 3.646 ppm are D$_2$O exchangeable.
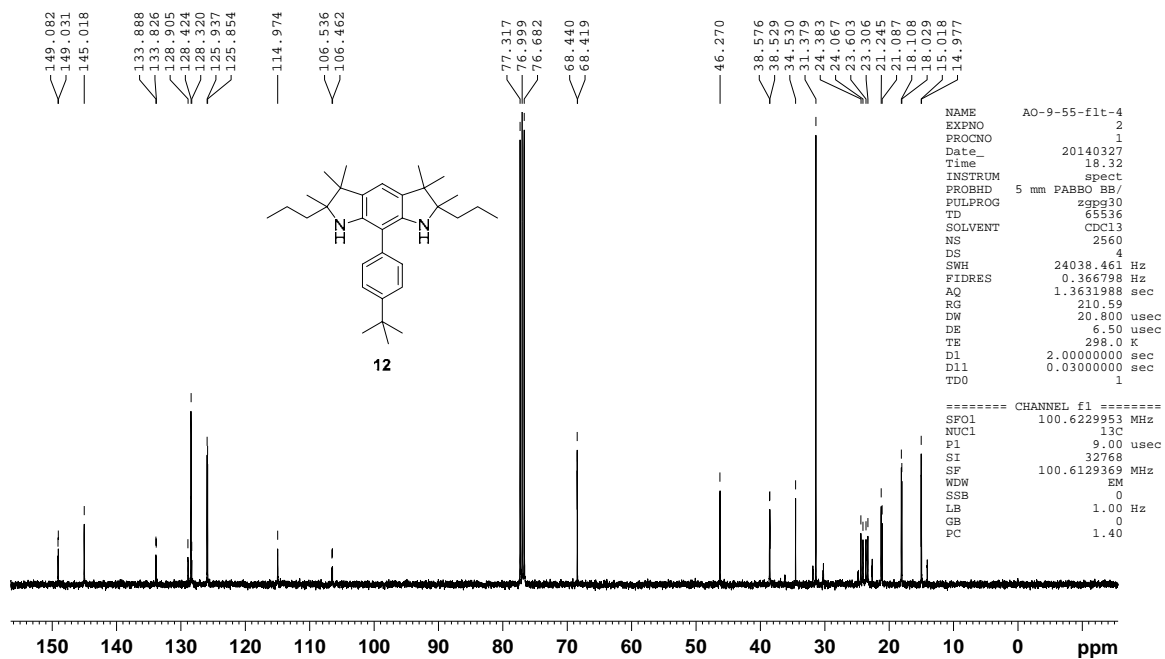
**Figure A25.** $^{13}$C NMR (100 MHz, chloroform-*d*) spectrum of diamine **12** (AO-9-55-flt-4).
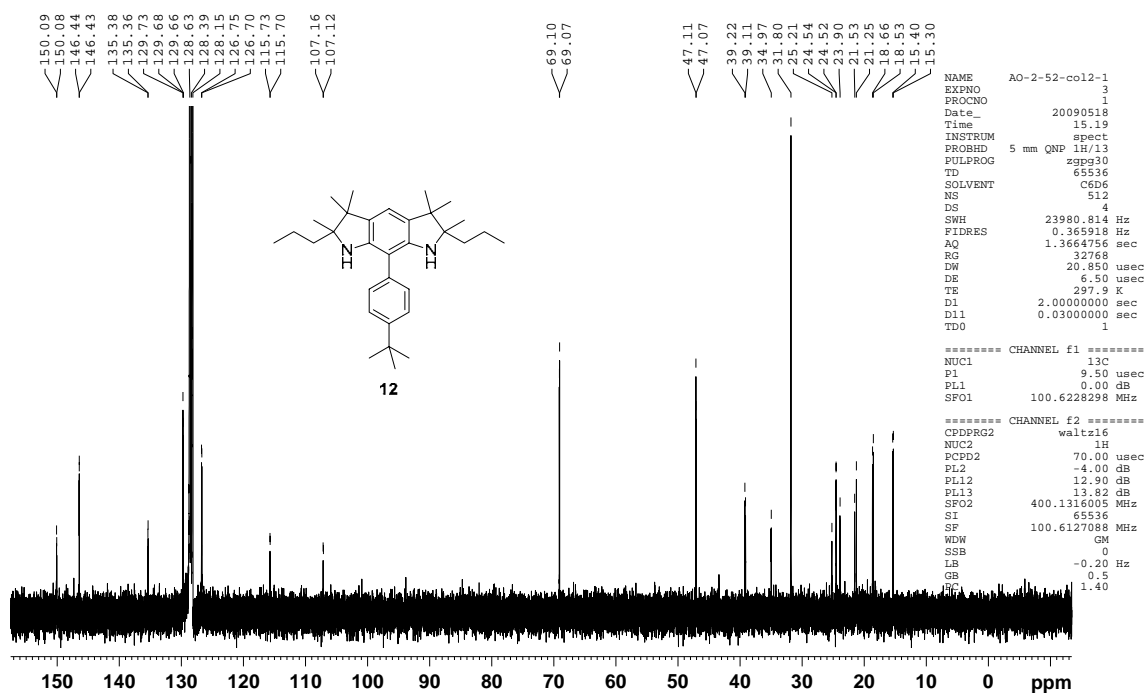


**Figure A26.** $^{13}$C NMR (100 MHz, benzene-$d_6$) spectrum of diamine **12** (AO-2-52-col2).
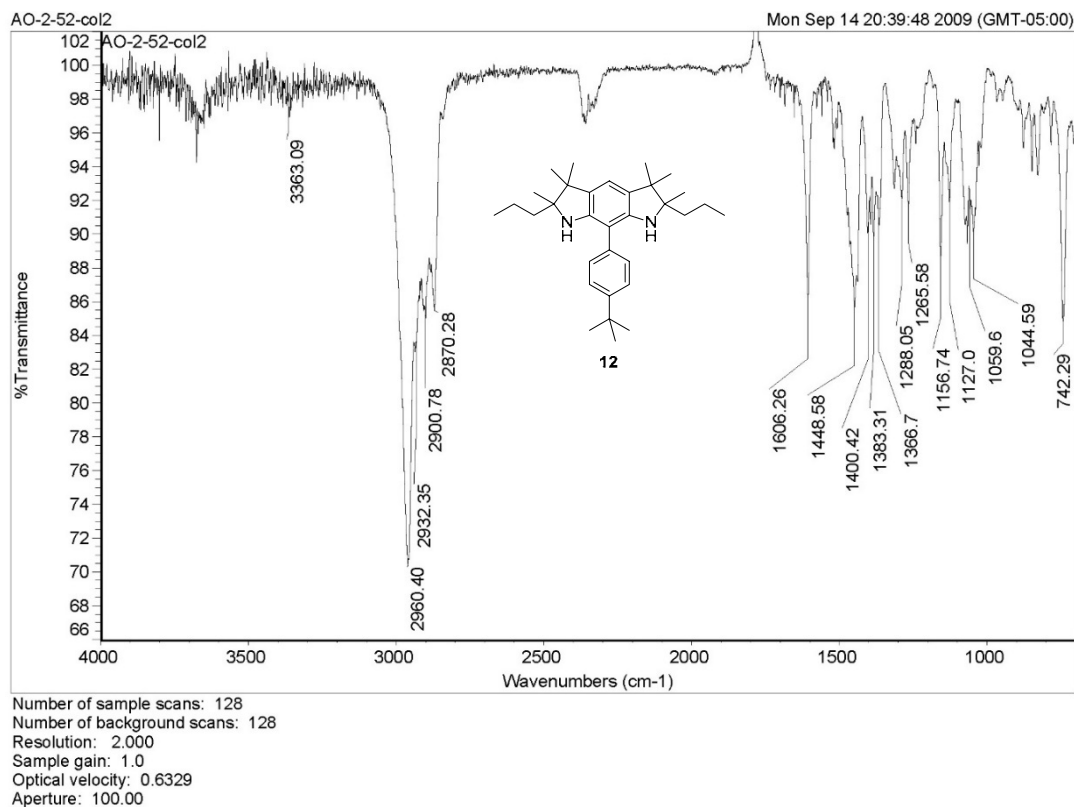
**Figure A27.** IR (ATR, ZnSe, cm$^{-1}$) spectrum of diamine **12** (AO-2-52-col2).
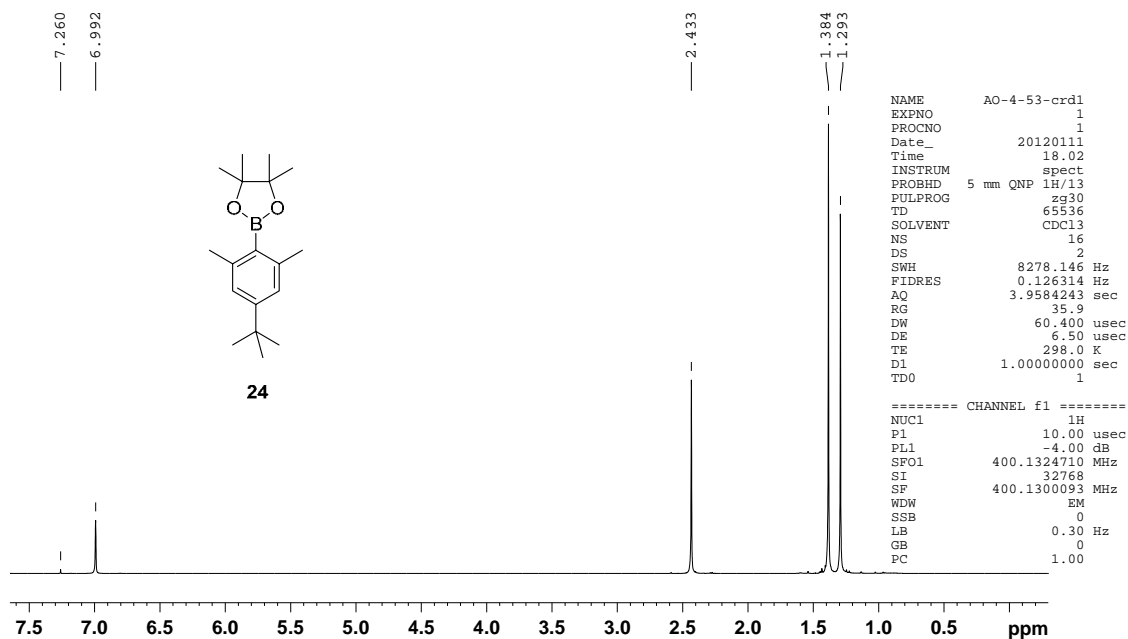


**Figure A28.** $^{1}$H NMR (400 MHz, chloroform-*d*) spectrum of pinacolboronate **24** (AO-4-53-crd1).
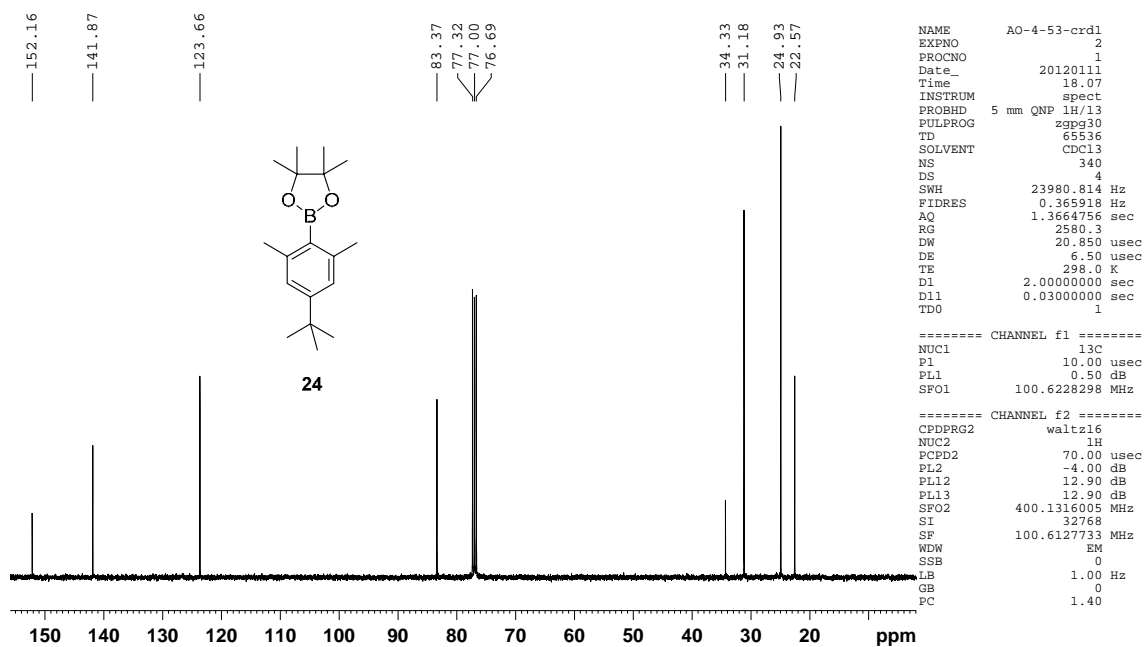
**Figure A29.** $^{13}$C NMR (100 MHz, chloroform-*d*) spectrum of pinacolboronate **24** (AO-4-53-crd1).
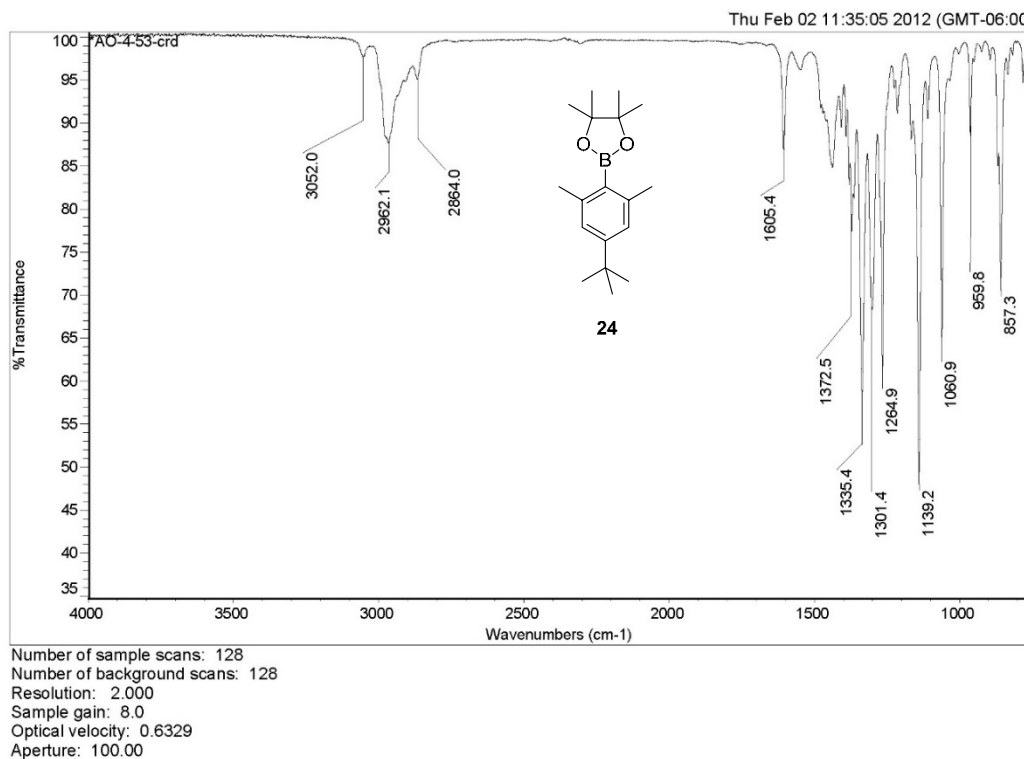


**Figure A30.** IR (ATR, ZnSe, cm$^{-1}$) spectrum of diamine **24** (AO-4-53-crd1).
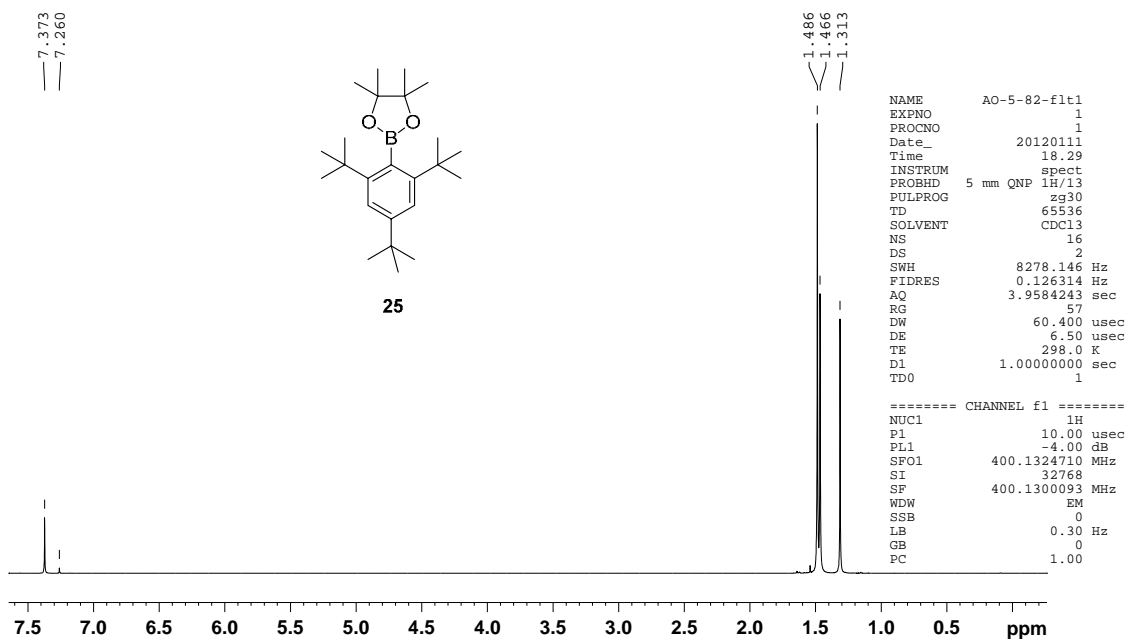
**Figure A31.** $^1$H NMR (400 MHz, chloroform-*d*) spectrum of pinacolboronate **25** (AO-5-82-flt1).
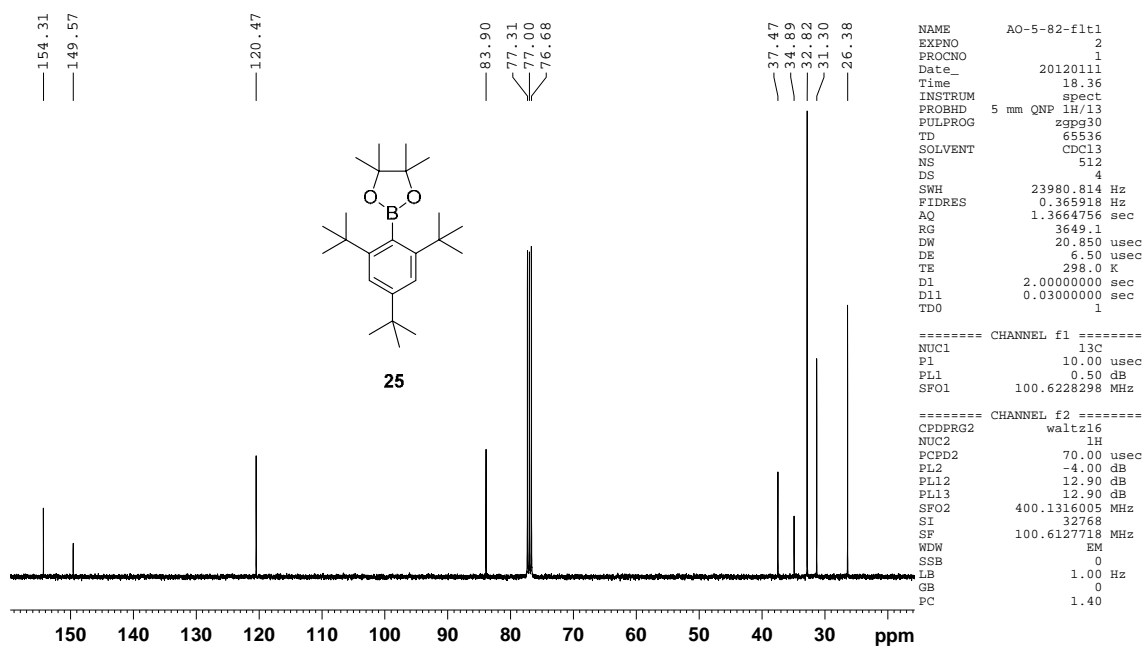


**Figure A32.** $^{13}$C NMR (100 MHz, chloroform-*d*) spectrum of pinacolboronate **25** (AO-5-82-flt1).
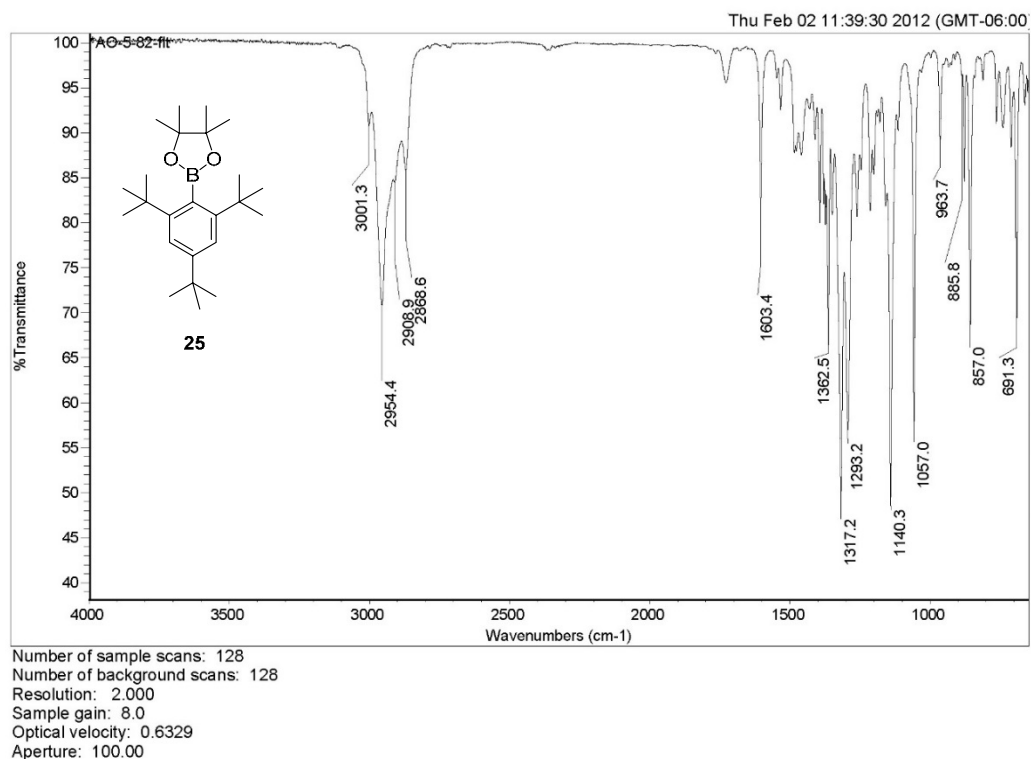
**Figure A33.** IR (ATR, ZnSe, cm$^{-1}$) spectrum of pinacolboronate **25** (AO-5-82-flt).
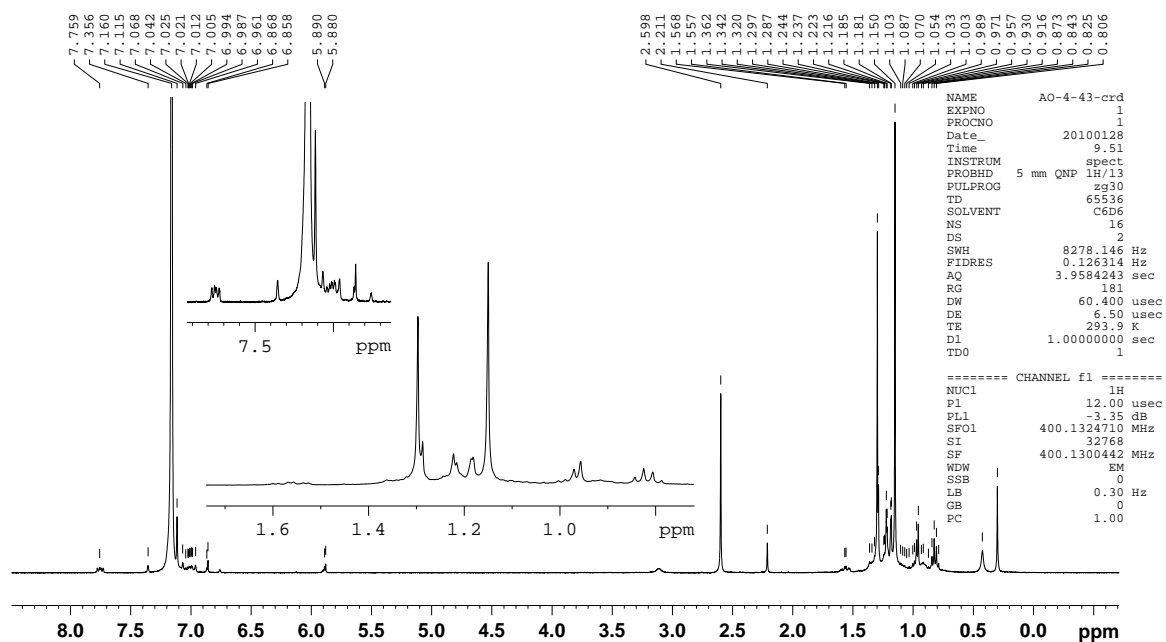


**Figure A34.** $^1$H NMR (400 MHz, chloroform-*d*) spectrum of attempted synthesis of **22** (AO-4-43-crd).
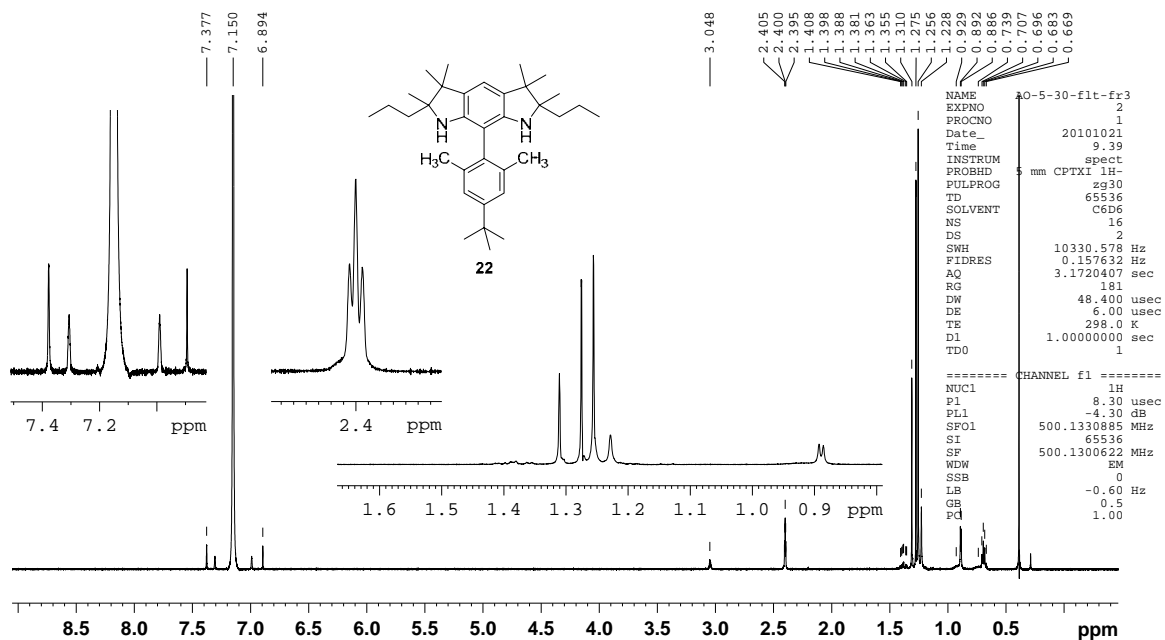
**Figure A35.** ¹H NMR (500 MHz, benzene-*d₆*) spectrum of diamine **22** (AO-5-30-flt-fr3).
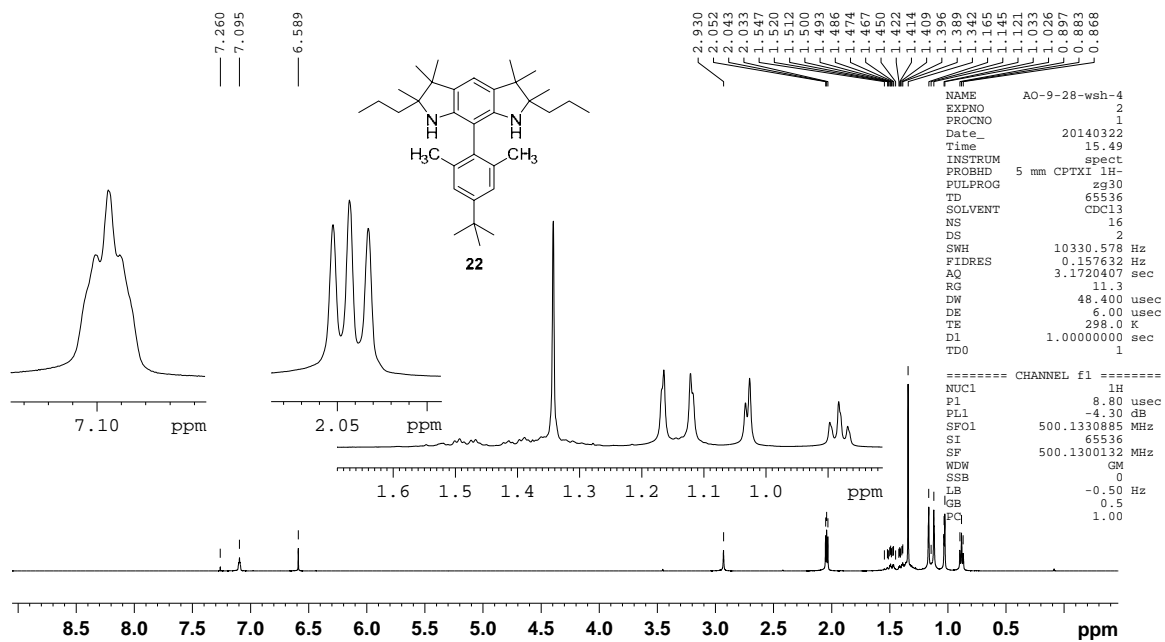


**Figure A36.** ¹H NMR (500 MHz, chloroform-*d*) spectrum of diamine **22** (AO-9-28-wsh-4).
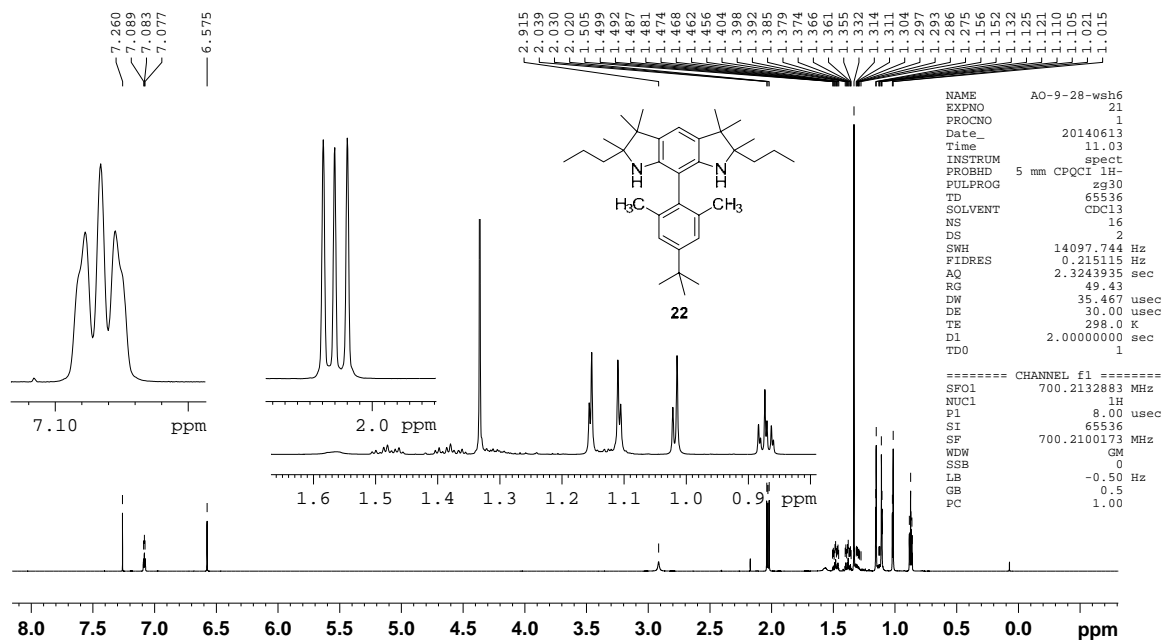
**Figure A37.** ^{1}H NMR (700 MHz, chloroform-*d*) spectrum of diamine **22** (AO-9-28-wsh-6).
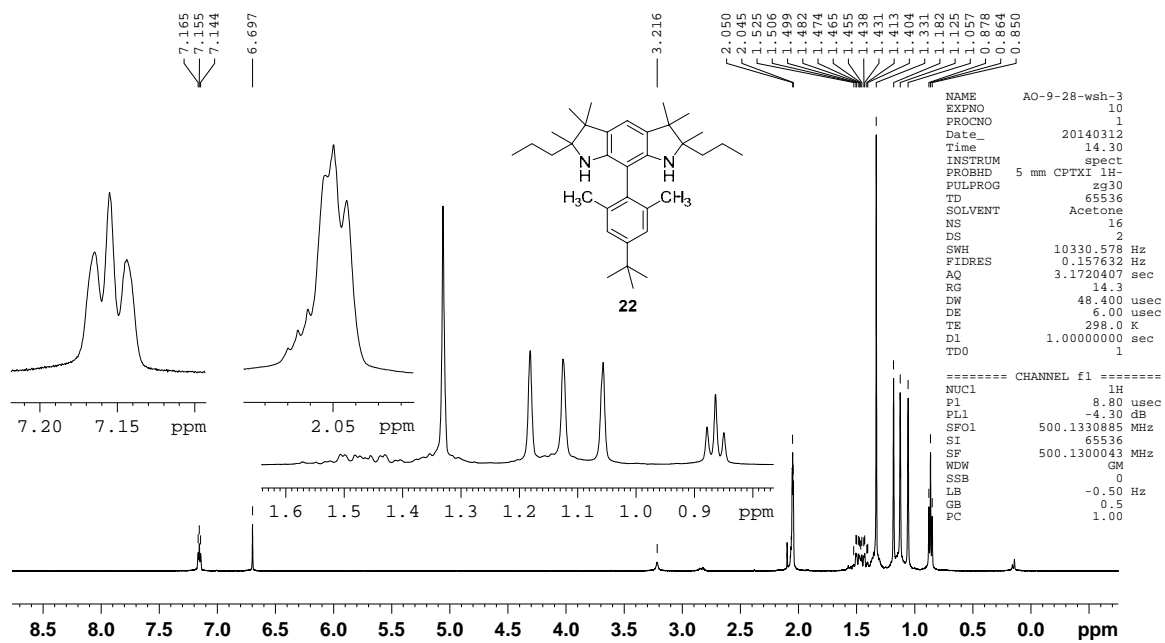


**Figure A38.** ^{1}H NMR (500 MHz, acetone-*d*₆) spectrum of diamine **22** (AO-9-28-wsh-3).
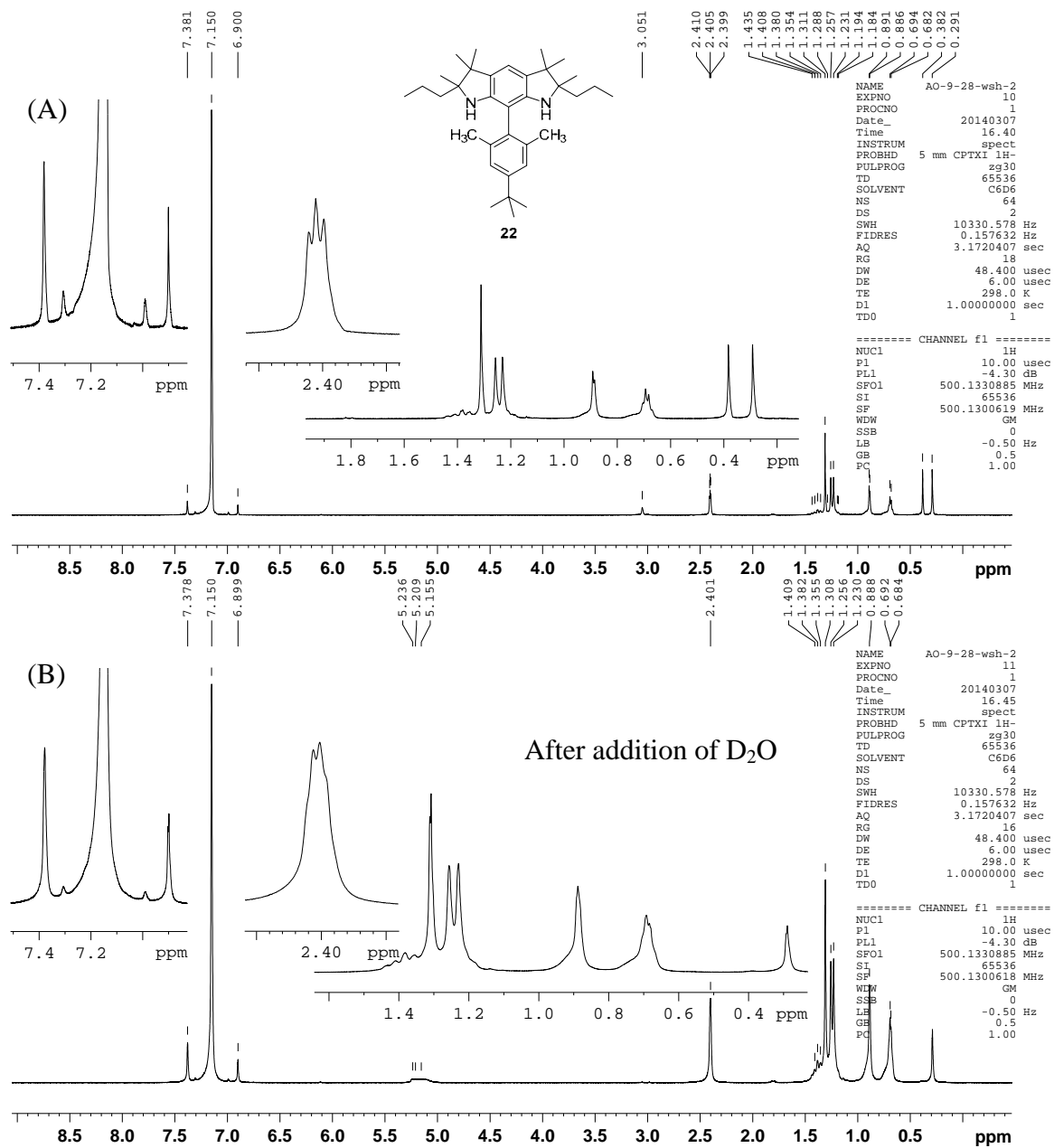
**Figure A39.** (A) $^1$H NMR (500 MHz, benzene-$d_6$) spectrum of diamine **22** (AO-9-28-wsh-2). (B) After addition 2 drops of D$_2$O, N-H peak at $\delta$ = 3.051 ppm is D$_2$O exchangeable.
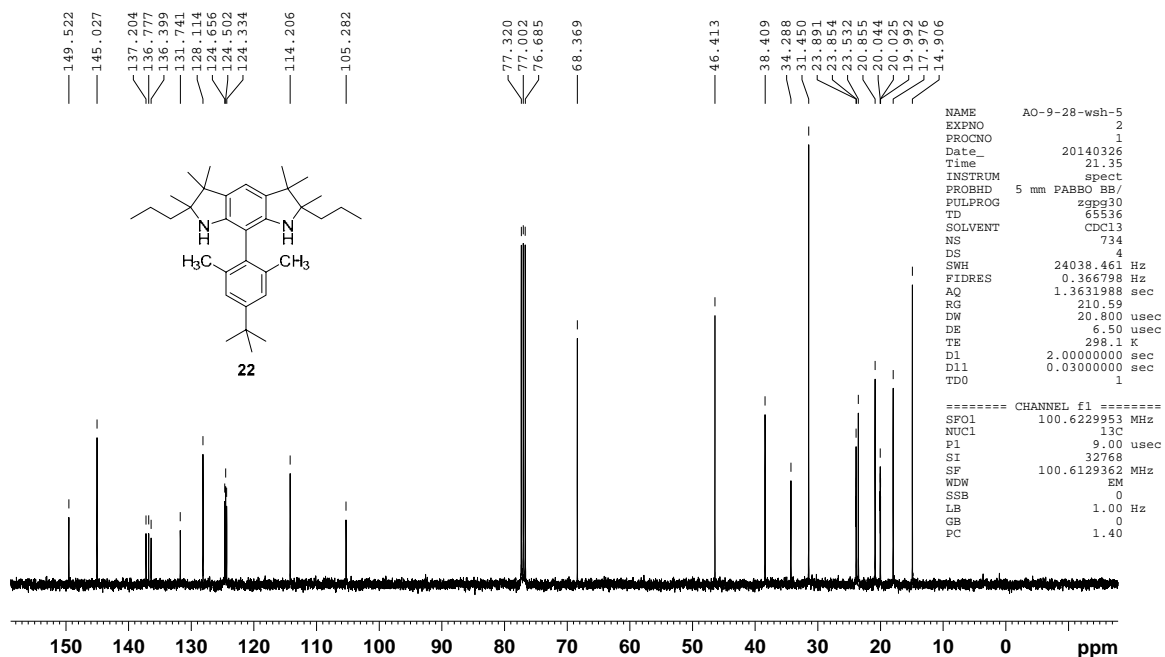
**Figure A40.** $^{13}$C NMR (100 MHz, chloroform-*d*) spectrum of diamine **22** (AO-9-28-wsh-5).
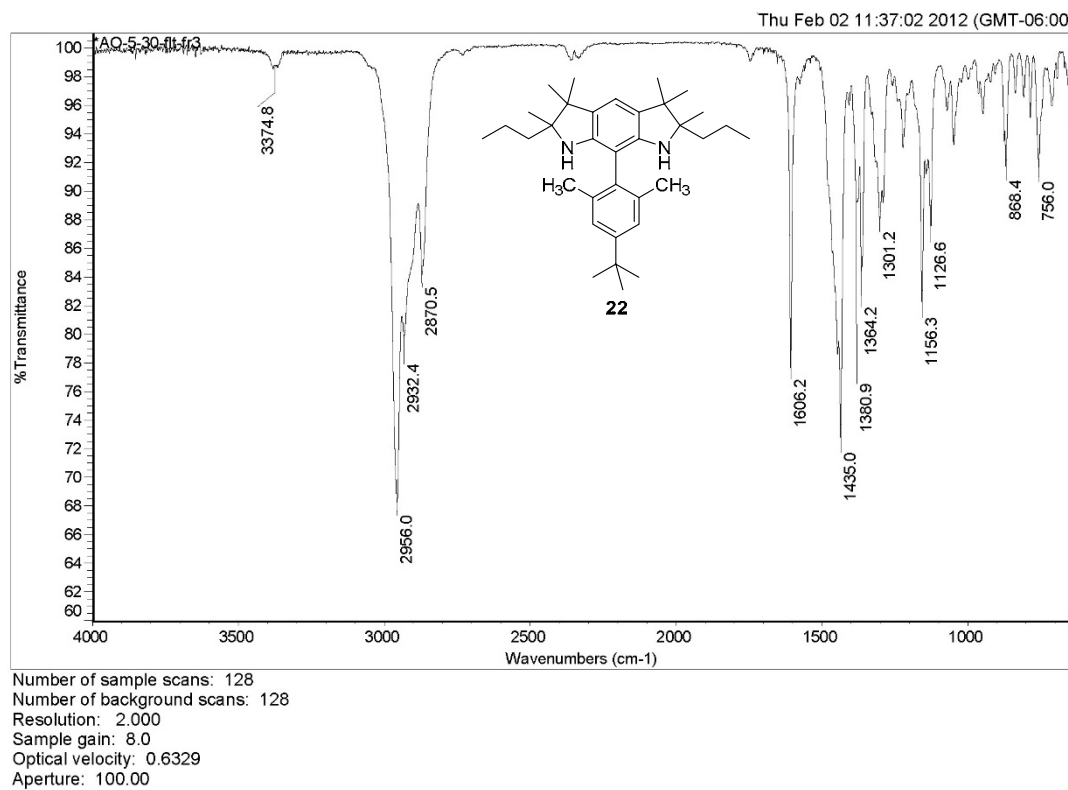


**Figure A41.** IR (ATR, ZnSe, cm$^{-1}$) spectrum of diamine **22** (AO-5-30-flt-fr3).
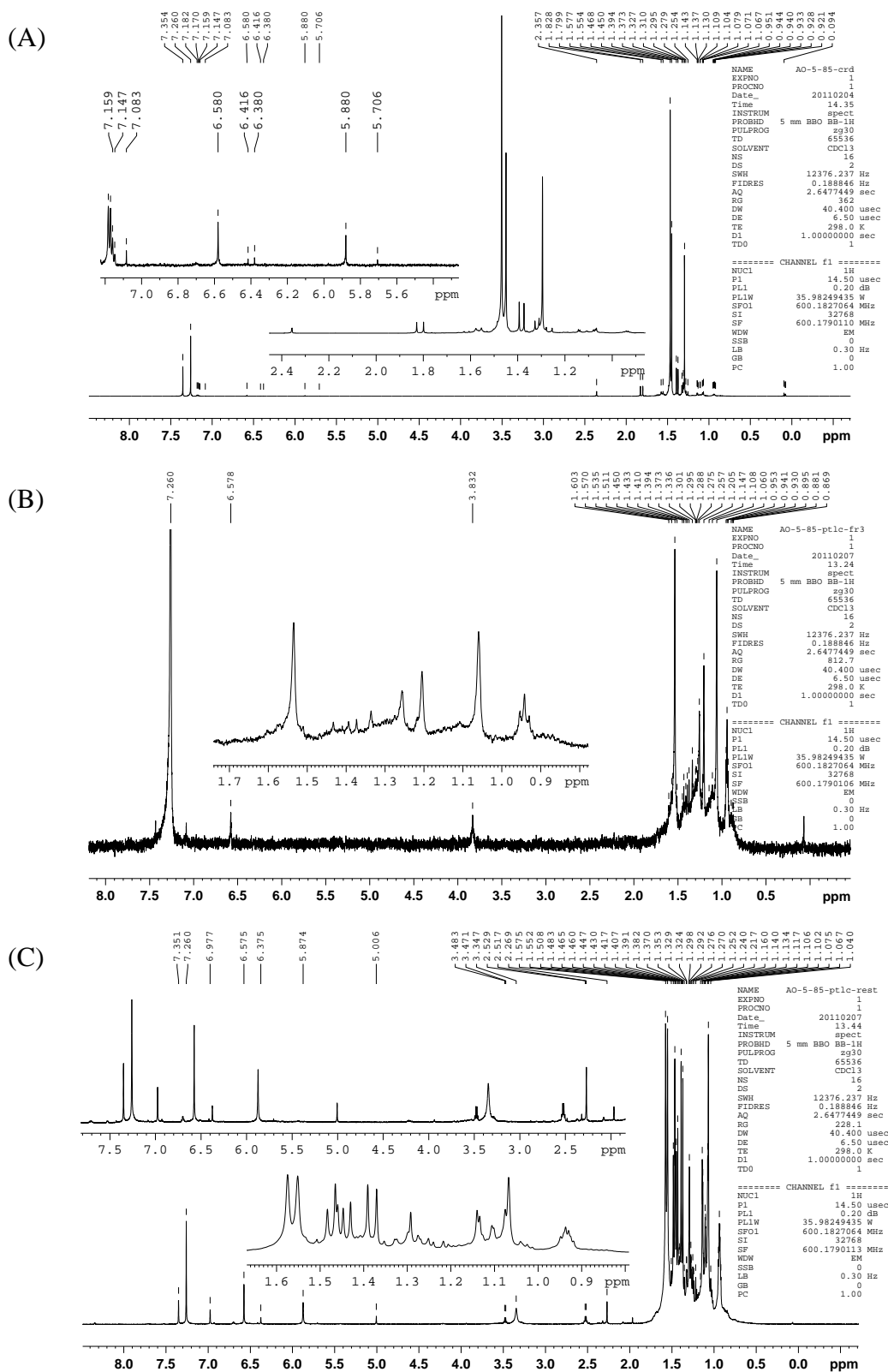
**Figure A42.** ^{1}H NMR (600 MHz, chloroform-*d*, label: AO-5-85) spectra of attempted synthesis of diamine **23**. (A) Crude reaction mixture. (B) Fraction 3. (C) Residue.
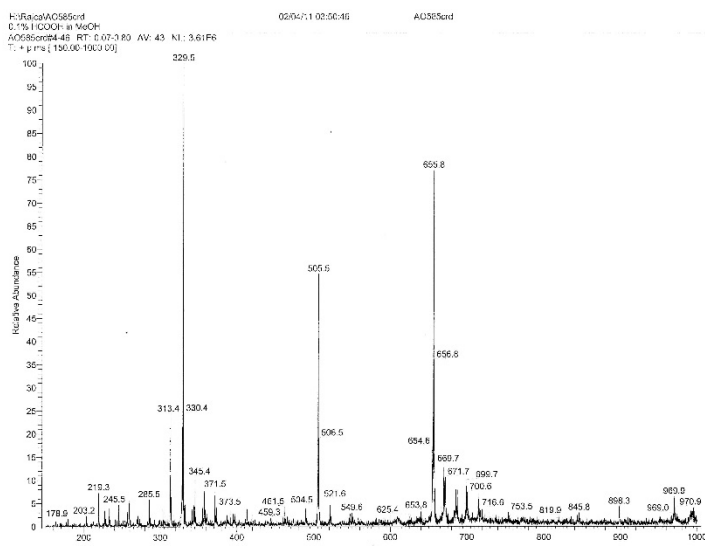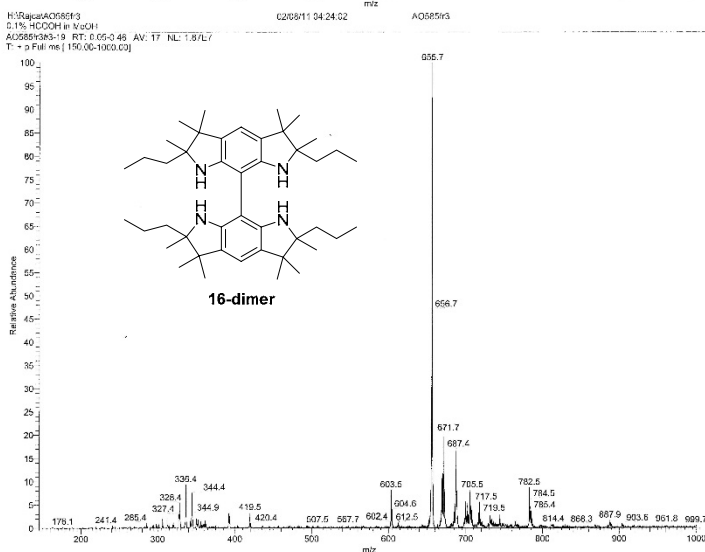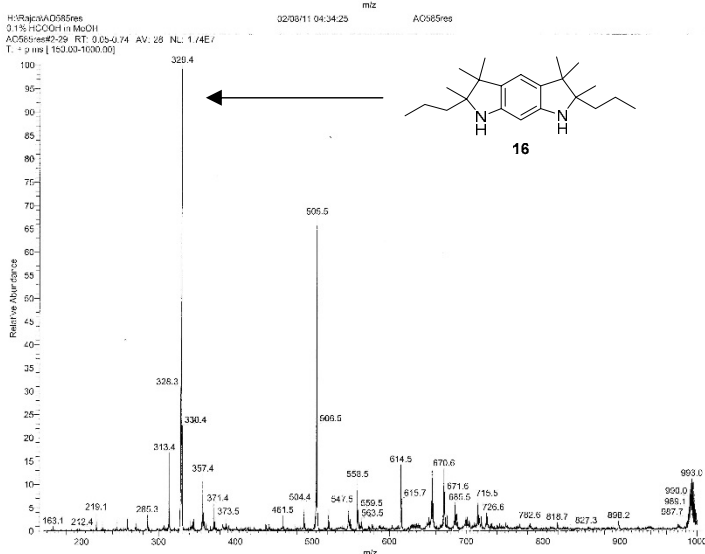
**Figure A43.** ESI-MS (label: AO-5-85) spectra of attempted synthesis of diamine **23**. (A) Crude reaction mixture. (B) Fraction 3. (C) Residue.
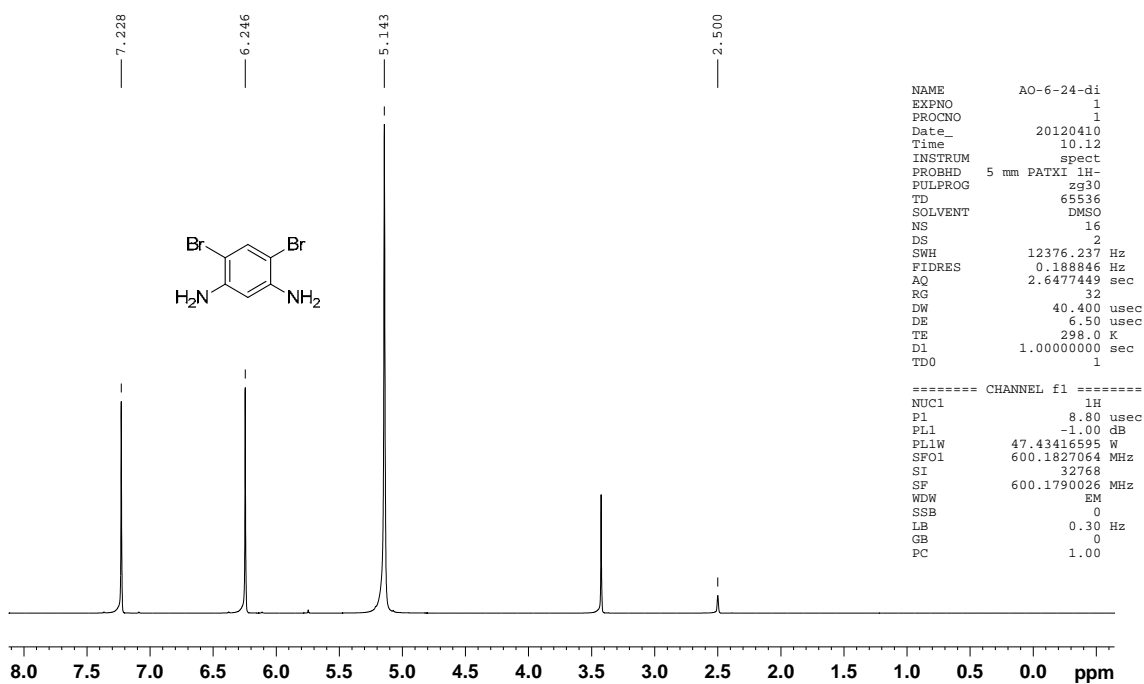
**Figure A44.** $^1$H NMR (600 MHz, dimethyl sulfoxide-$d_6$) spectrum of 1,3-dibromo-4,6-diaminobenzene (AO-6-24-di).
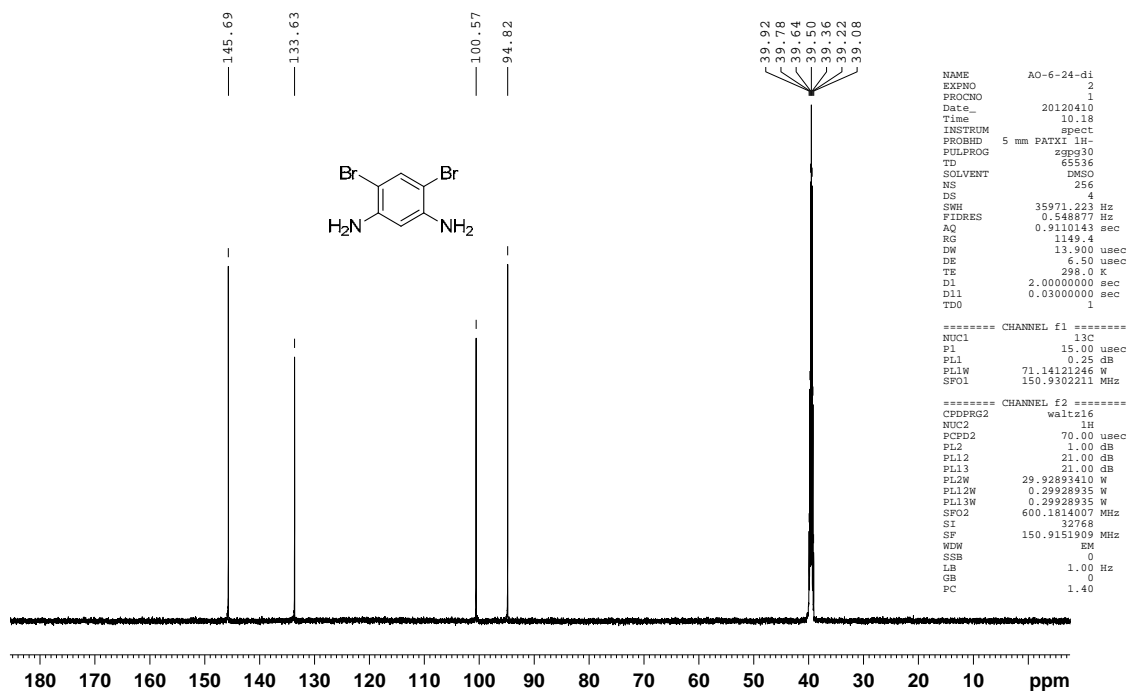


**Figure A45.** $^{13}$C NMR (150 MHz, dimethyl sulfoxide-$d_6$) spectrum of 1,3-dibromo-4,6-diaminobenzene (AO-6-24-di).
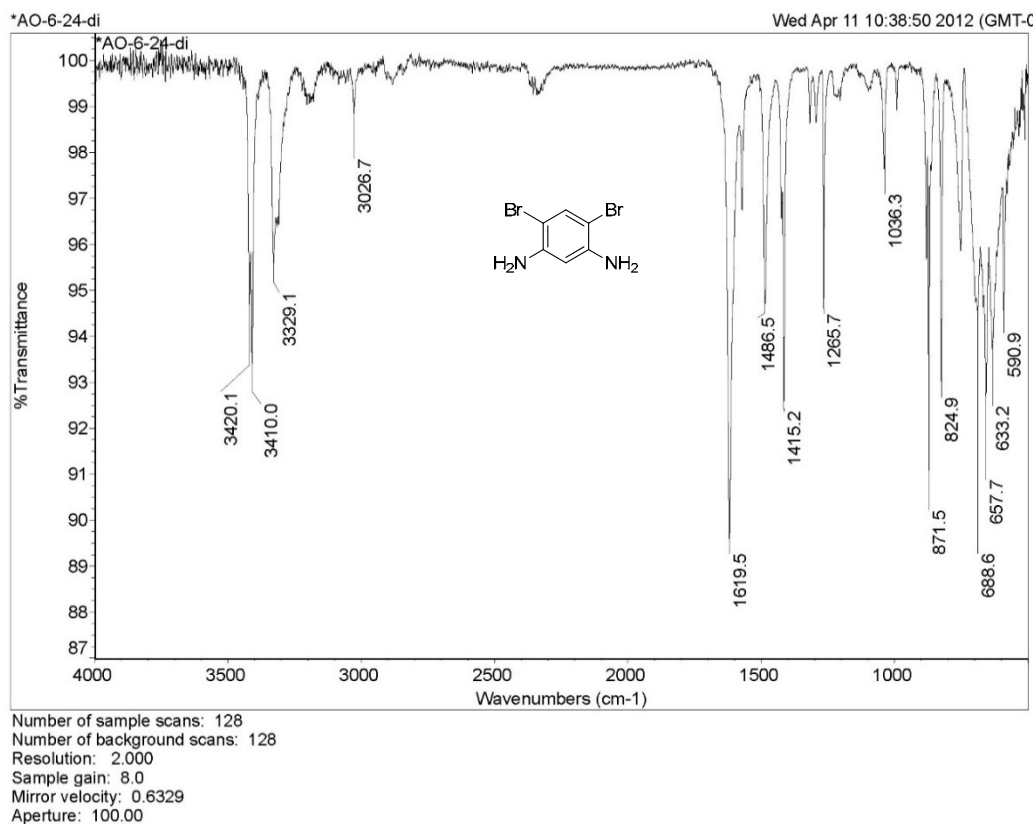
**Figure A46.** IR (ATR, ZnSe, cm$^{-1}$) spectrum of 1,3-dibromo-4,6-diaminobenzene (AO-6-24-di).
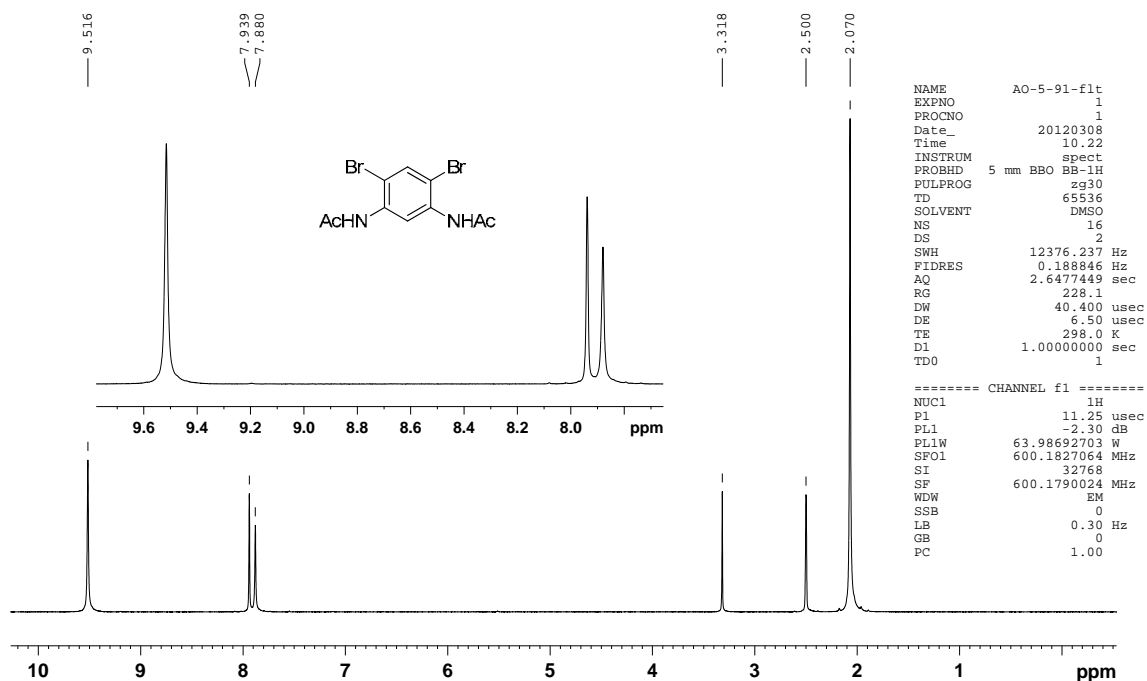


**Figure A47.** $^1$H NMR (600 MHz, dimethyl sulfoxide-$d_6$) spectrum of 1,3-dibromo-4,6-bis(acetamido)benzene (AO-5-91-flt).
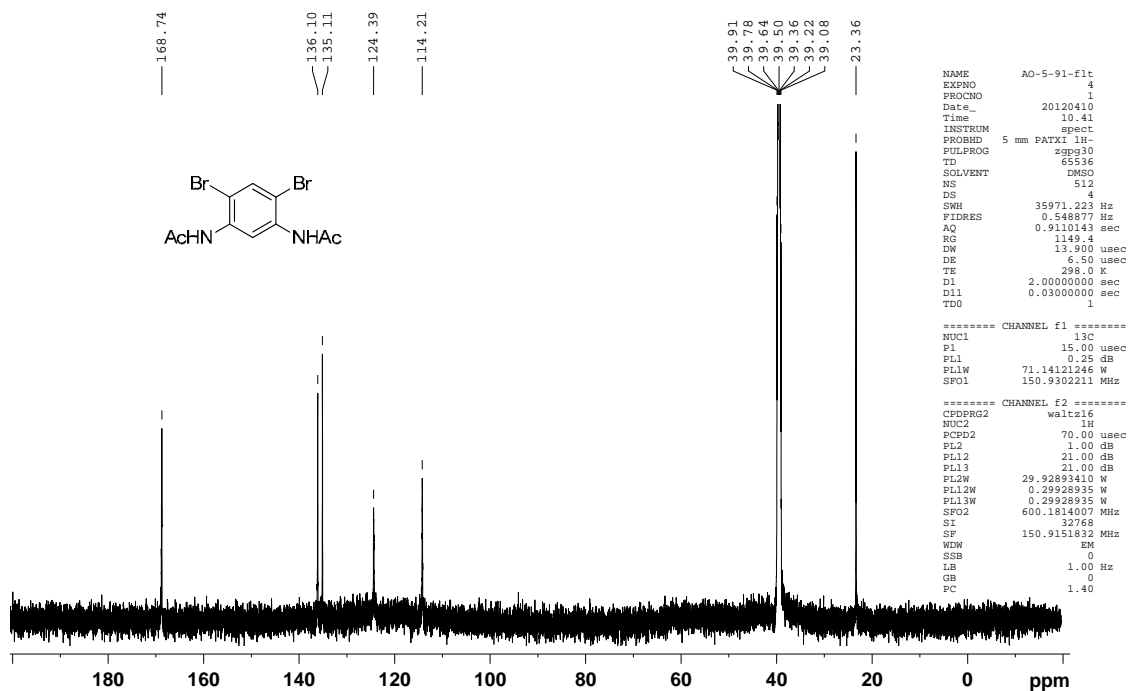
**Figure A48.** $^{13}$C NMR (150 MHz, dimethyl sulfoxide-$d_6$) spectrum of 1,3-dibromo-4,6-bis(acetamido)benzene (AO-5-91-flt).
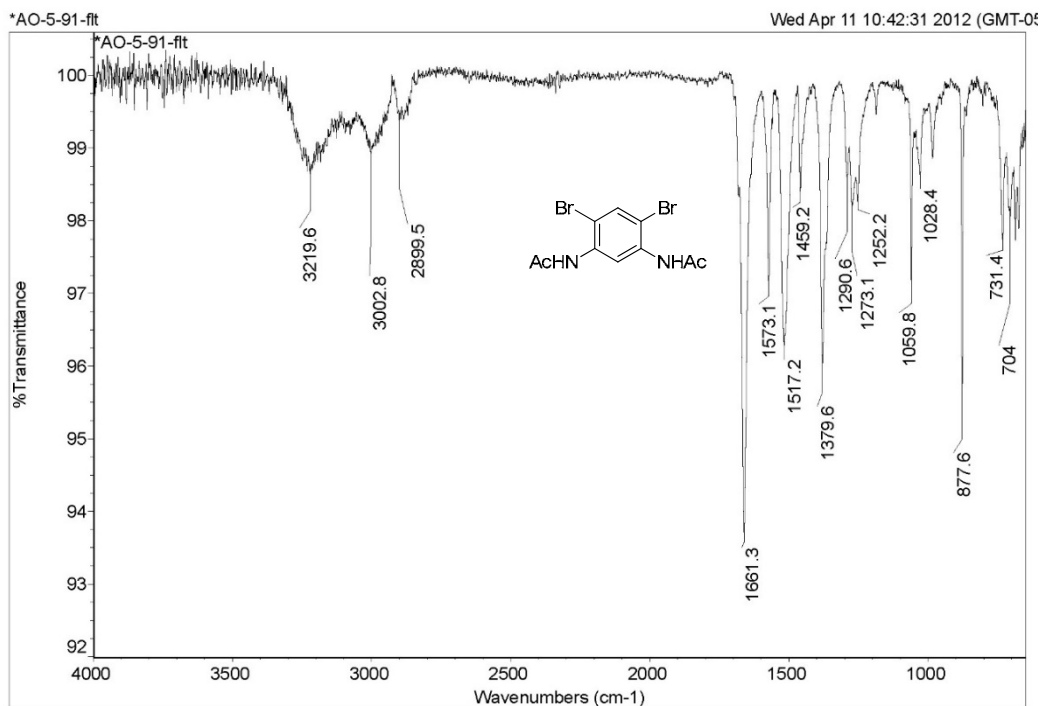


Number of sample scans: 128
Number of background scans: 128
Resolution: 2.000
Sample gain: 8.0
Mirror velocity: 0.6329
Aperture: 100.00

**Figure A49.** IR (ATR, ZnSe, cm$^{-1}$) spectrum of 1,3-dibromo-4,6-bis(acetamido)benzene (AO-5-91-flt).
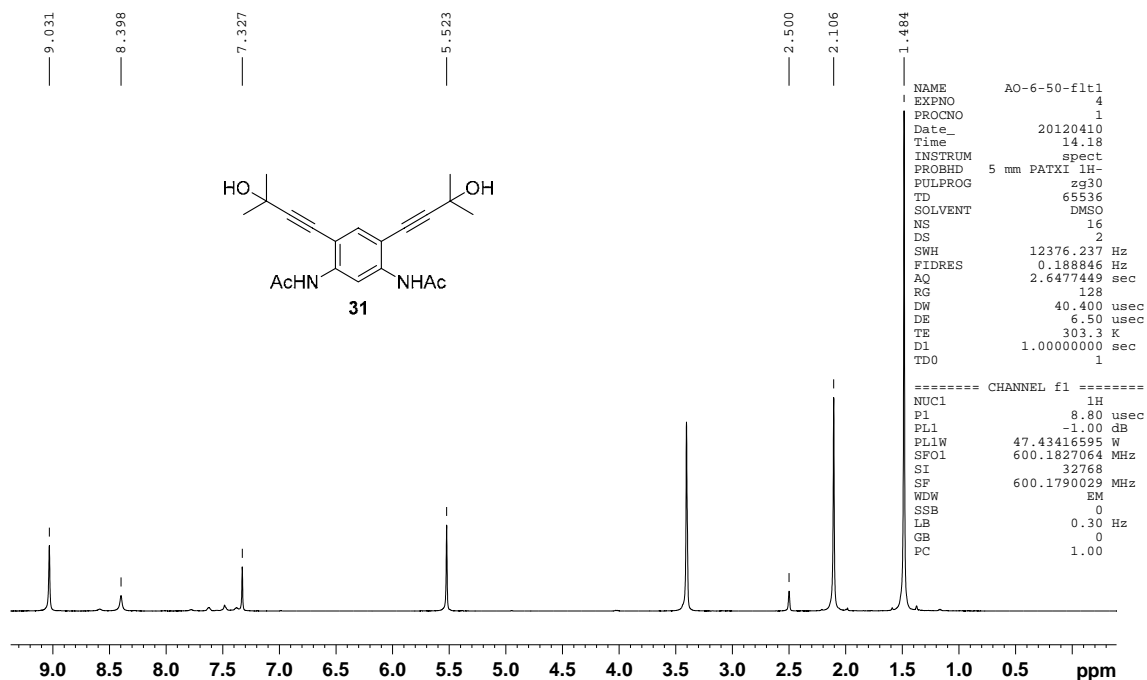
**Figure A50.** $^1$H NMR (600 MHz, dimethyl sulfoxide-$d_6$) spectrum of **31** (AO-6-50-flt1).
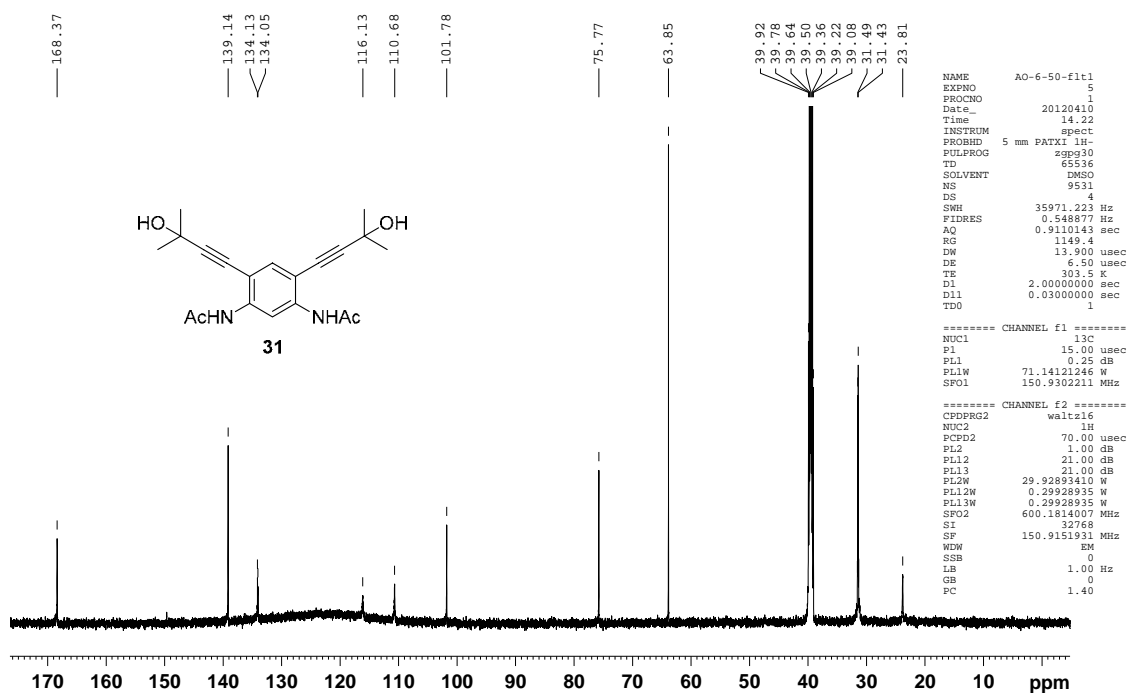


**Figure A51.** $^{13}$C NMR (150 MHz, dimethyl sulfoxide-$d_6$) spectrum of **31** (AO-6-50-flt1).
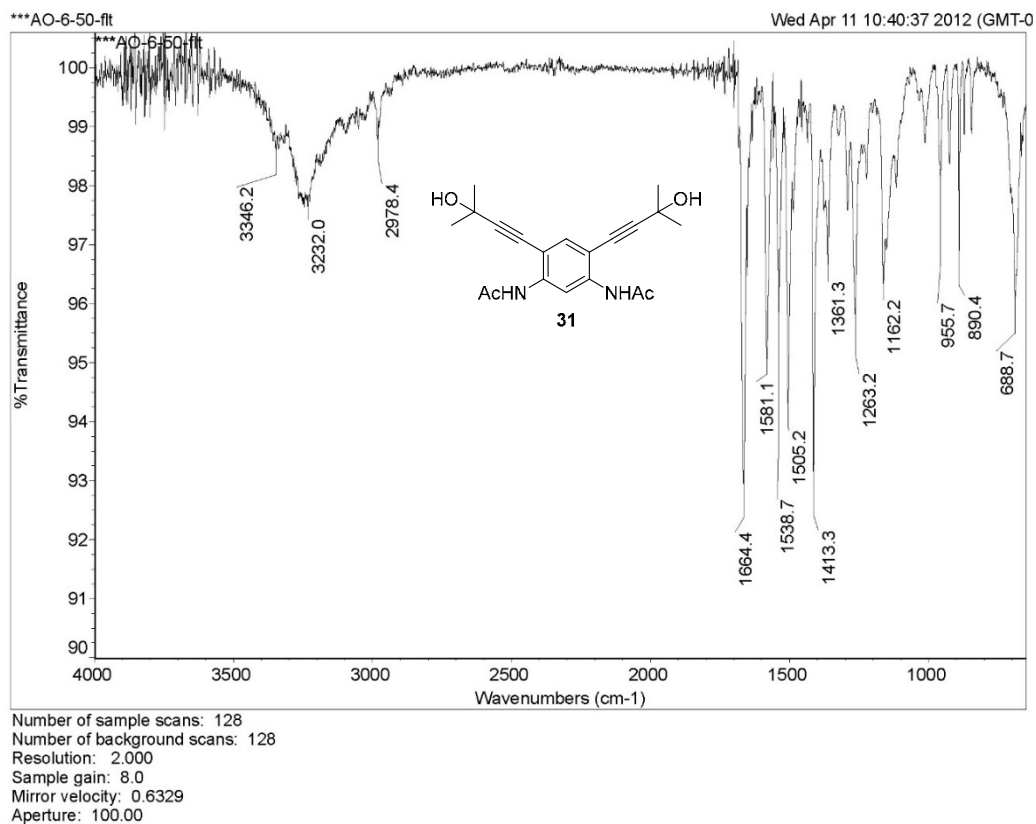
**Figure A52.** IR (ATR, ZnSe, cm$^{-1}$) spectrum of **31** (AO-6-50-flt).
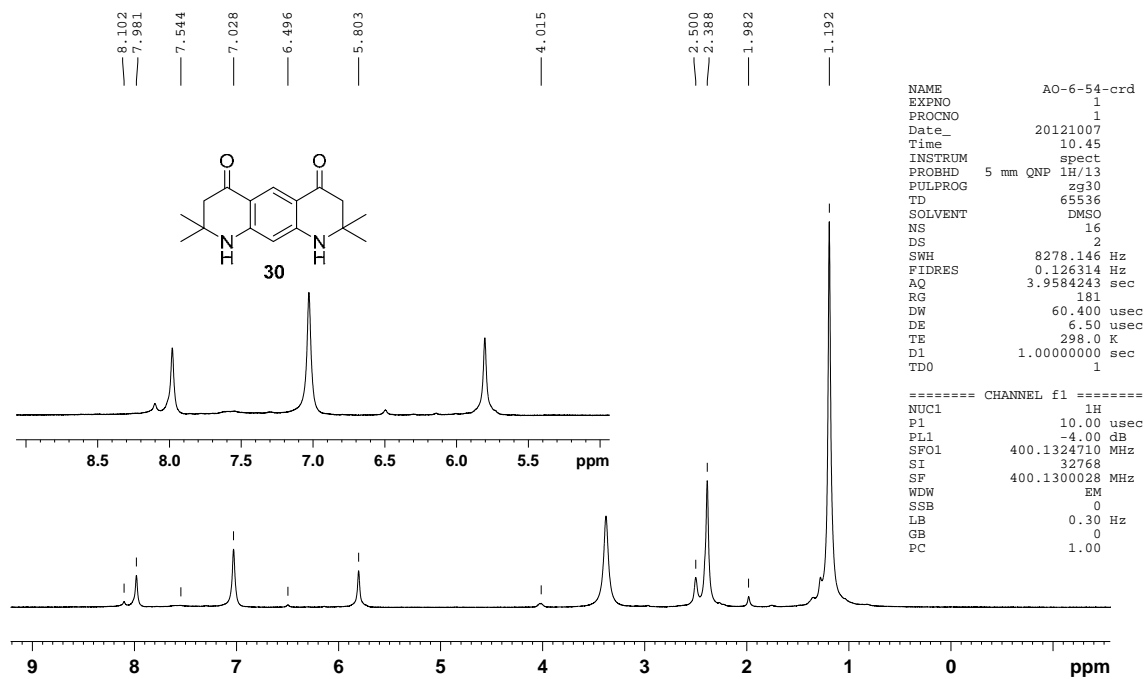


**Figure A53.** $^1$H NMR (400 MHz, dimethyl sulfoxide-$d_6$) spectrum of diketone-diamine **30** (AO-6-54-crd).
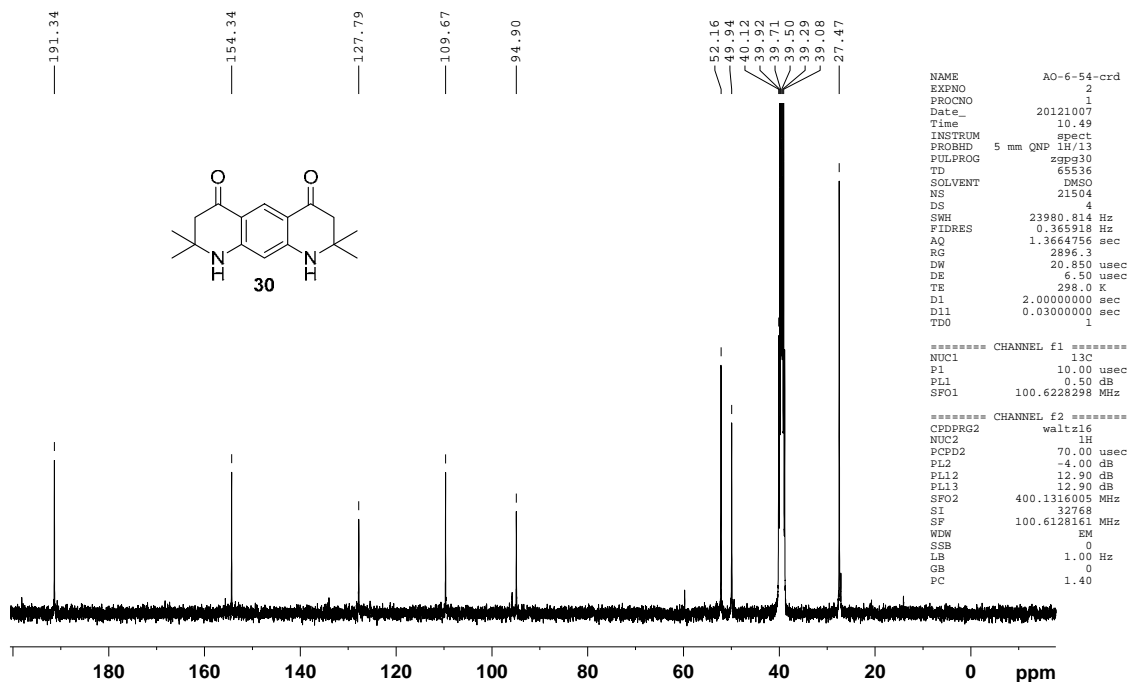
**Figure A54.** $^{13}$C NMR (100 MHz, dimethyl sulfoxide-$d_6$) spectrum of diketo-diamine **30** (AO-6-54-crd).
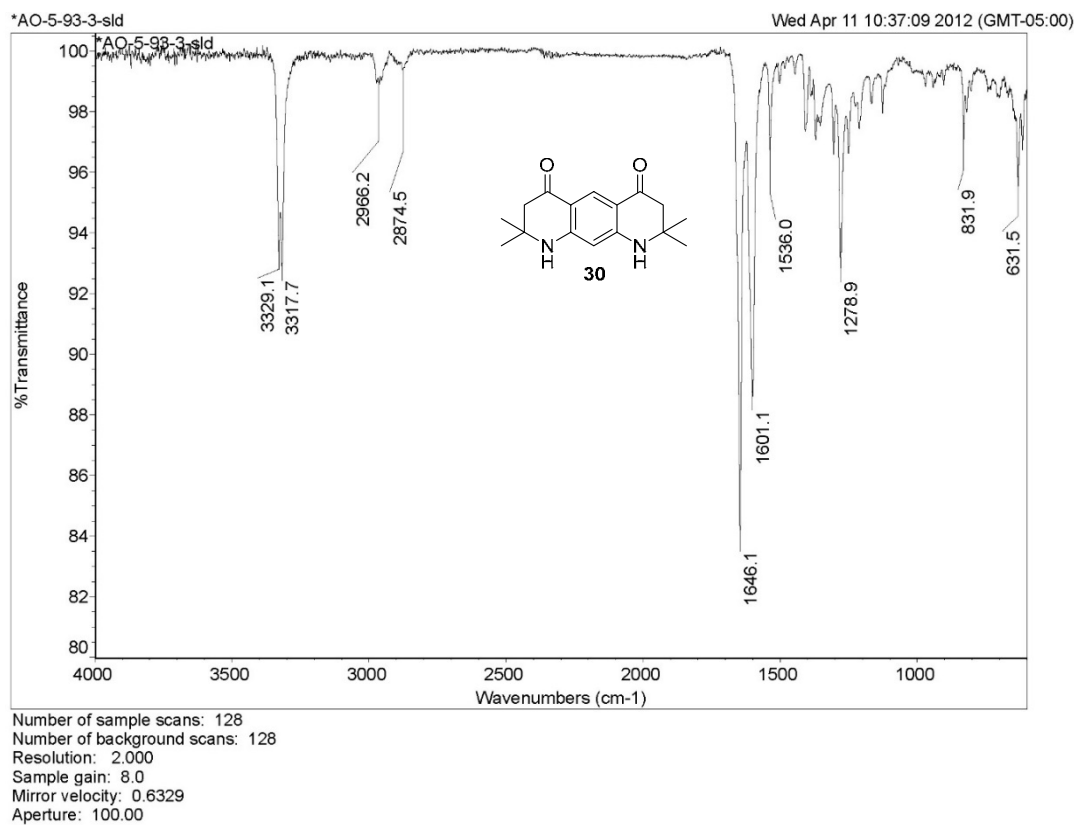


**Figure A55.** IR (ATR, ZnSe, cm$^{-1}$) spectrum of diketo-diamine **30** (AO-5-93-3-sld).
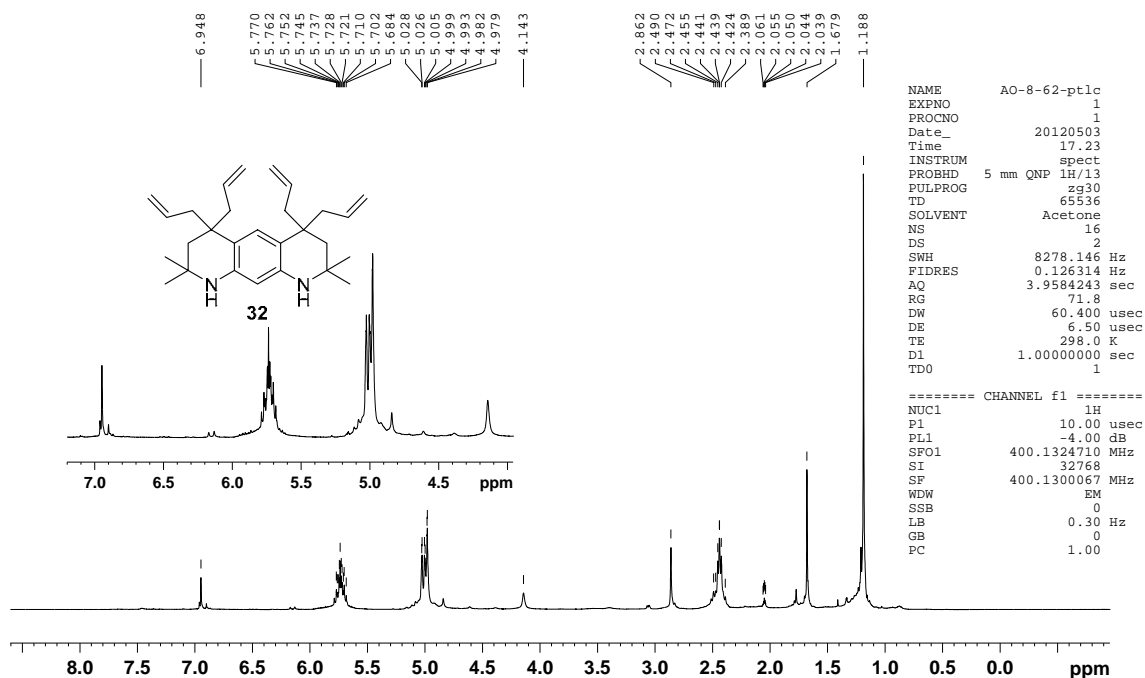
**Figure A56.** ¹H NMR (400 MHz, acetone-$d_6$) spectrum of bis(*gem*-diallyl)diamine **32** (AO-8-62-ptlc).
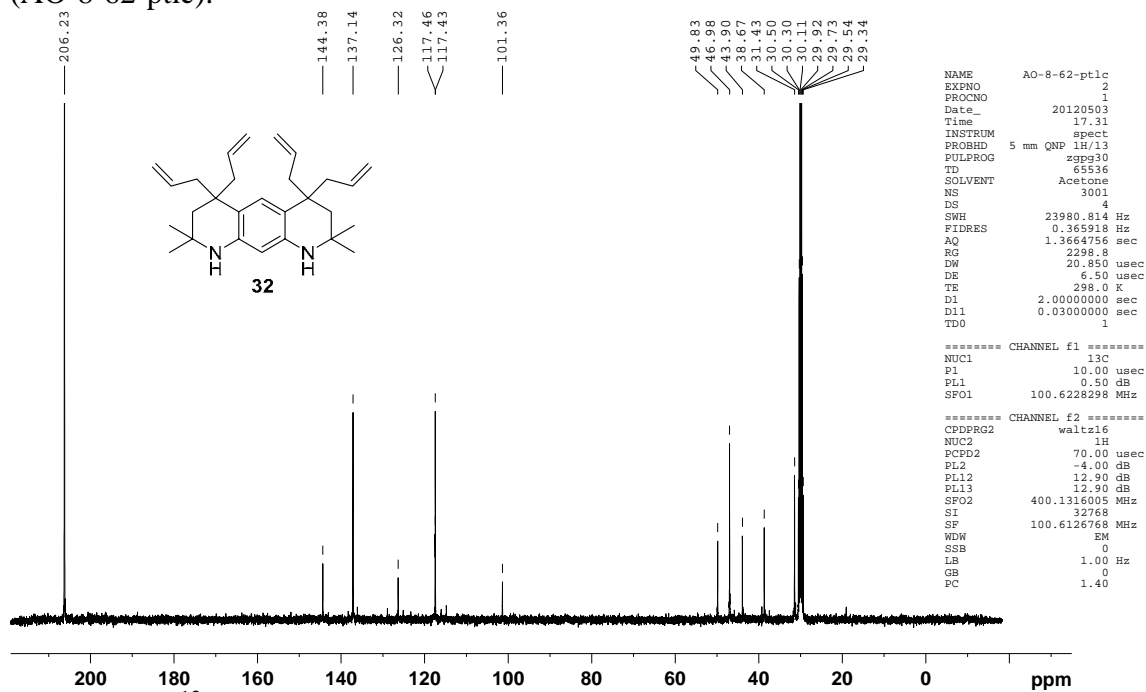


**Figure A57.** ¹³C NMR (100 MHz, acetone-$d_6$) spectrum of bis(*gem*-diallyl)diamine **32** (AO-8-62-ptlc).
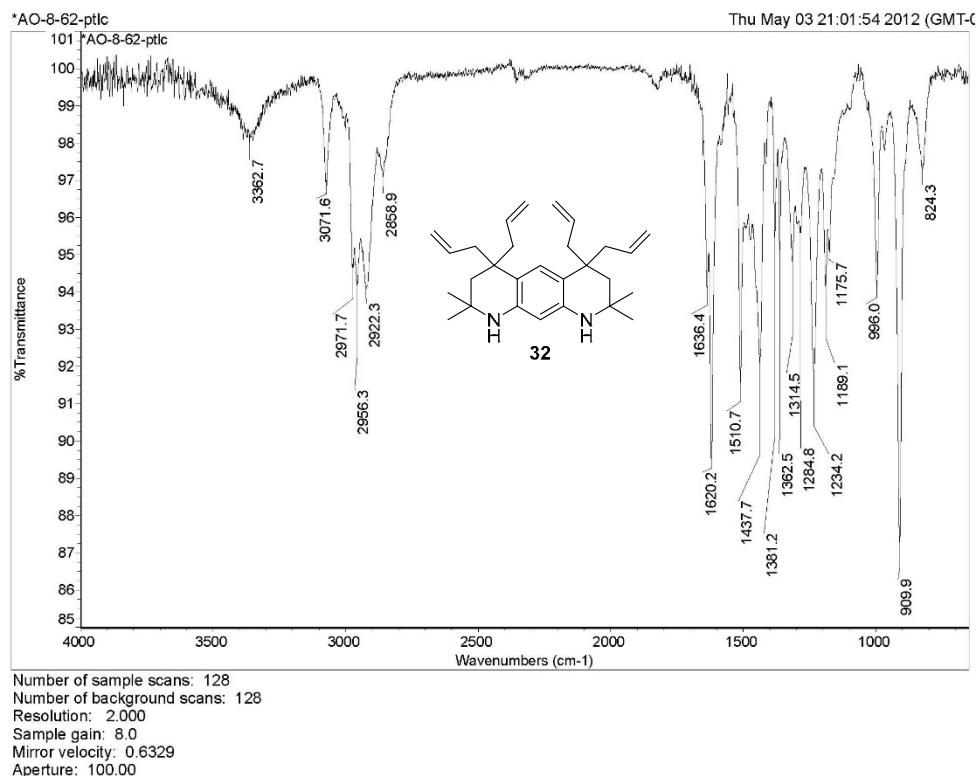
**Figure A58.** IR (ATR, ZnSe, cm$^{-1}$) spectrum of bis(*gem*-diallyl)diamine **32** (AO-8-62-ptlc).
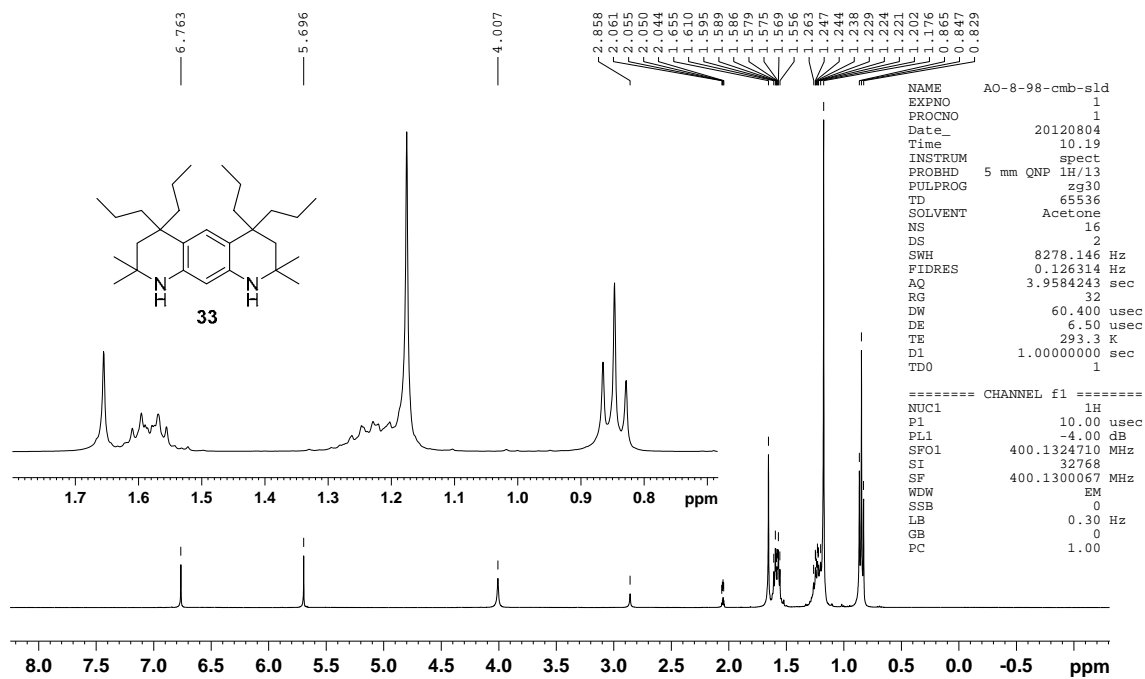


**Figure A59.** $^1$H NMR (400 MHz, acetone-$d_6$) spectrum of bis(*gem*-di-*n*-propyl)diamine **33** (AO-8-98-cmb-sld).
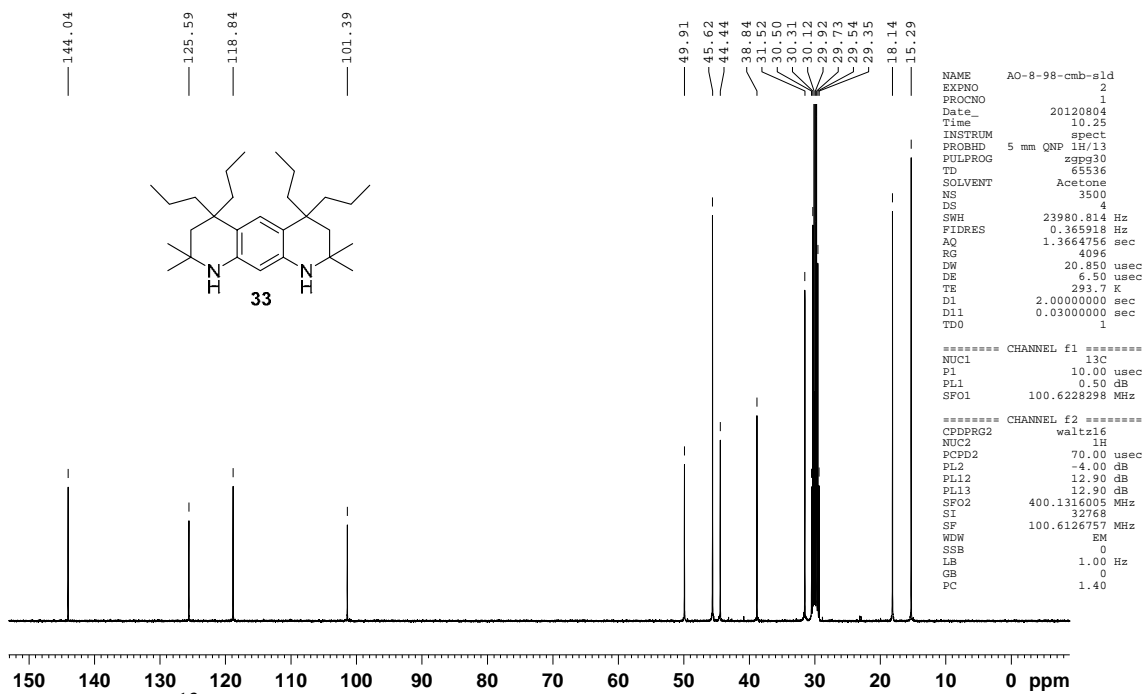
**Figure A60.** ^{13}C NMR (100 MHz, acetone-$d_6$) spectrum of bis(*gem*-di-*n*-propyl)diamine **33** (AO-8-98-cmb-sld).
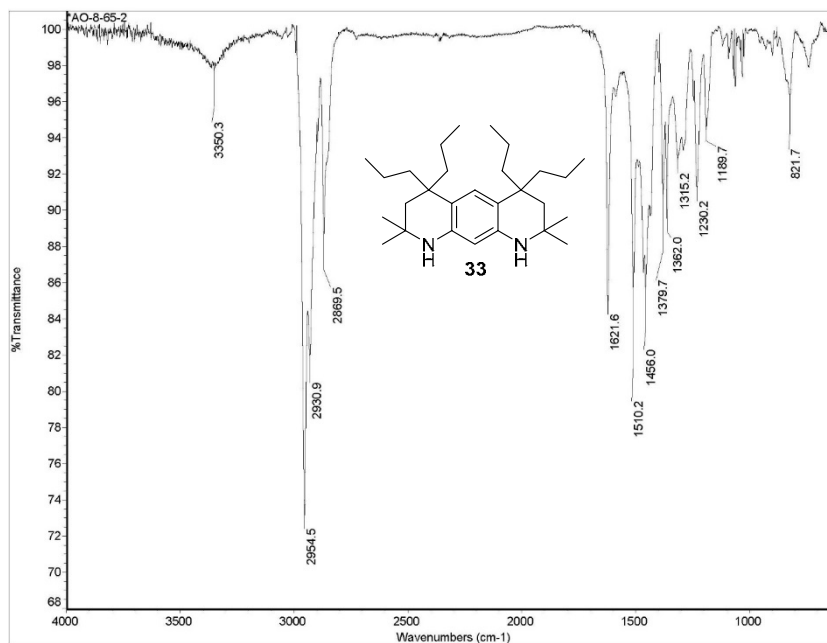


**Figure A61.** IR (ATR, ZnSe, cm[−1]) spectrum of bis(*gem*-di-*n*-propyl)diamine **33** (AO-8-65-2).
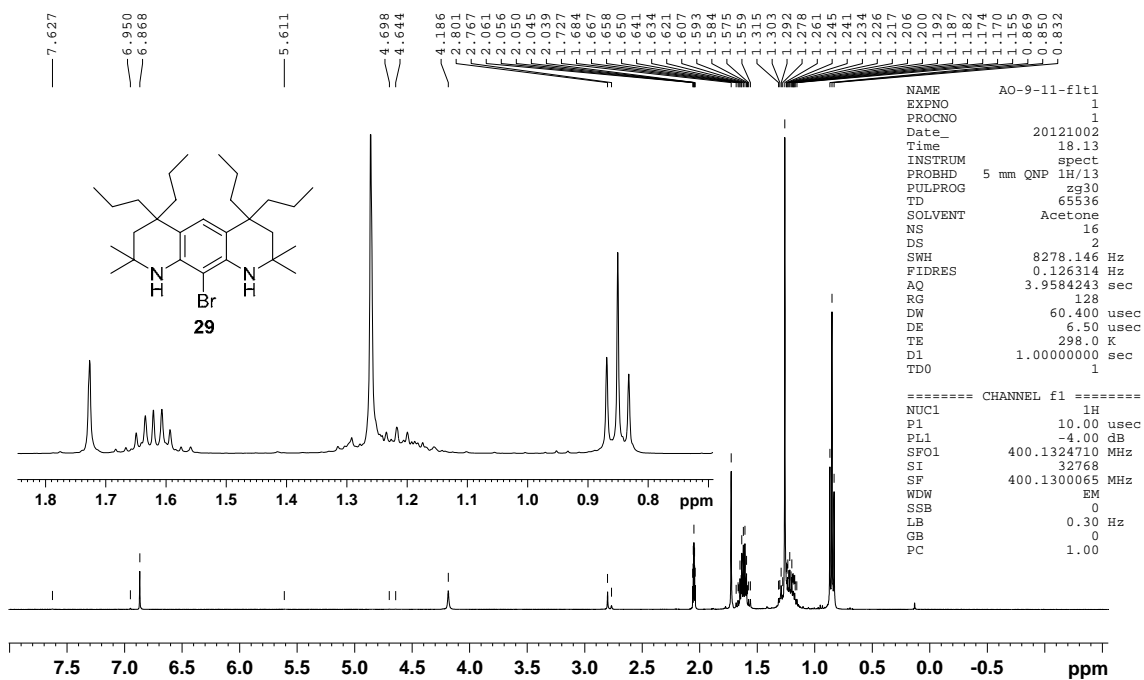
**Figure A62.** ¹H NMR (400 MHz, acetone-$d_6$) spectrum of bromodiamine **29** (AO-9-11-flt1).
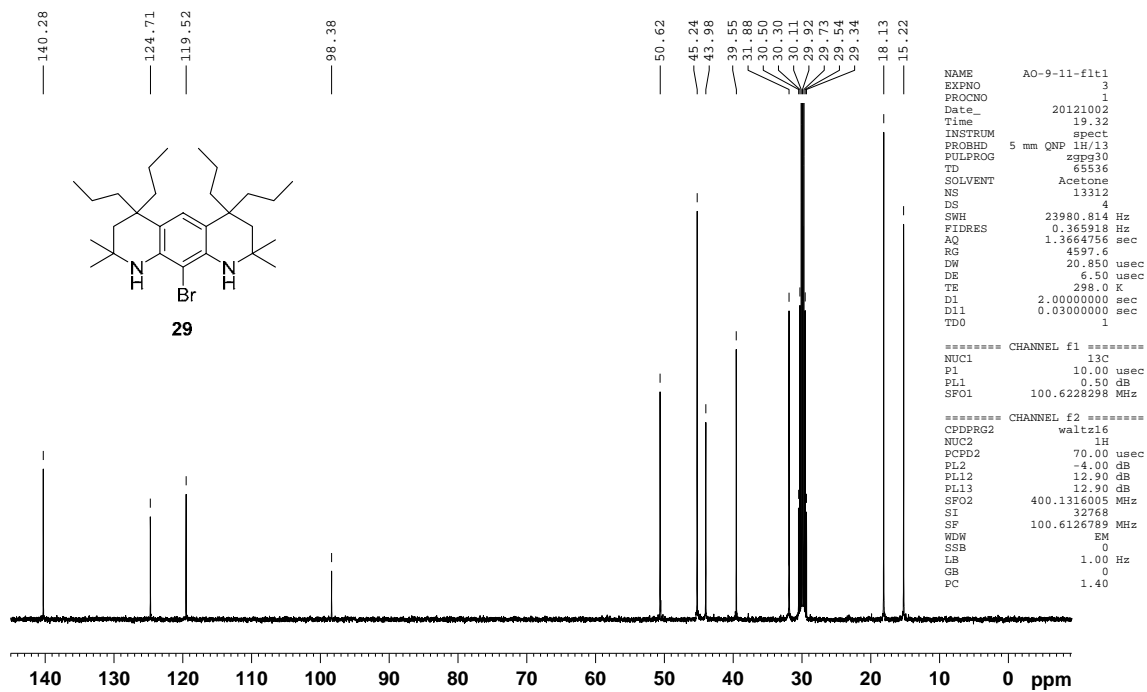


**Figure A63.** ¹³C NMR (100 MHz, acetone-$d_6$) spectrum of bromodiamine **29** (AO-9-11-flt1).
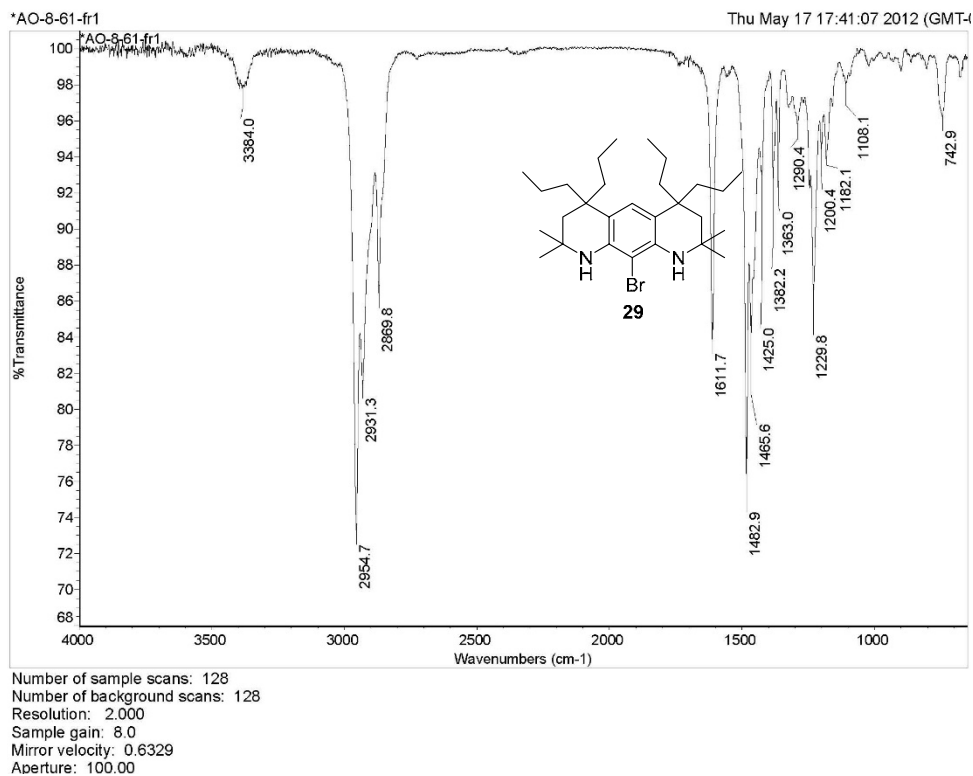
**Figure A64.** IR (ATR, ZnSe, cm$^{-1}$) spectrum of bromodiamine **29** (AO-8-61-fr1).
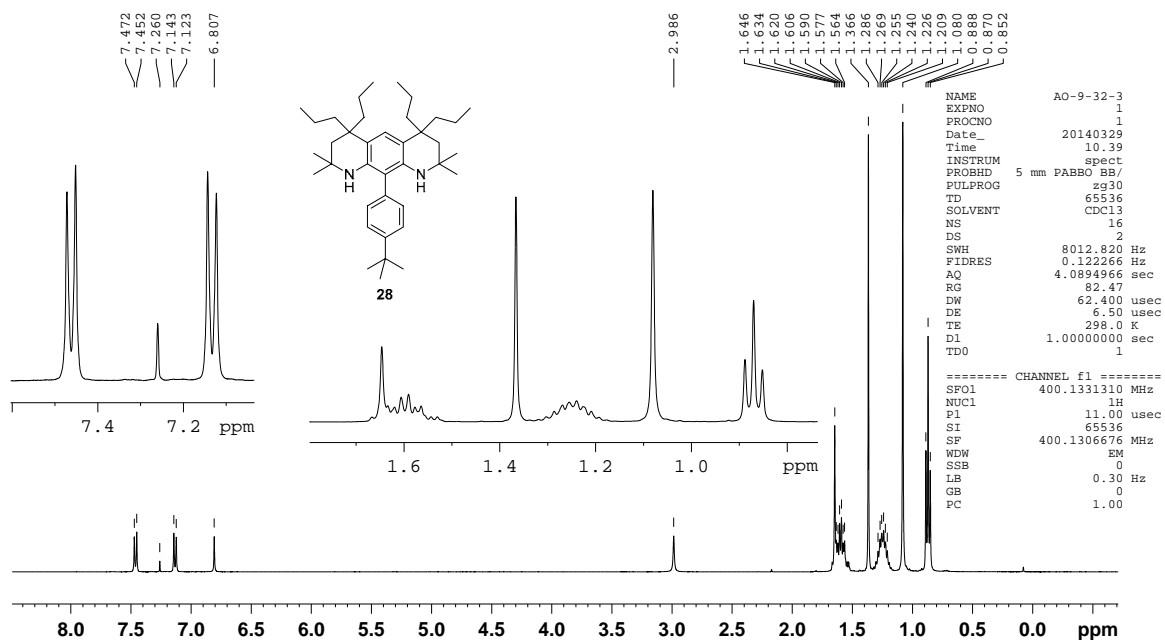


**Figure A65.** $^1$H NMR (500 MHz, chloroform-*d*) spectrum of diamine **28** (AO-9-32-2).
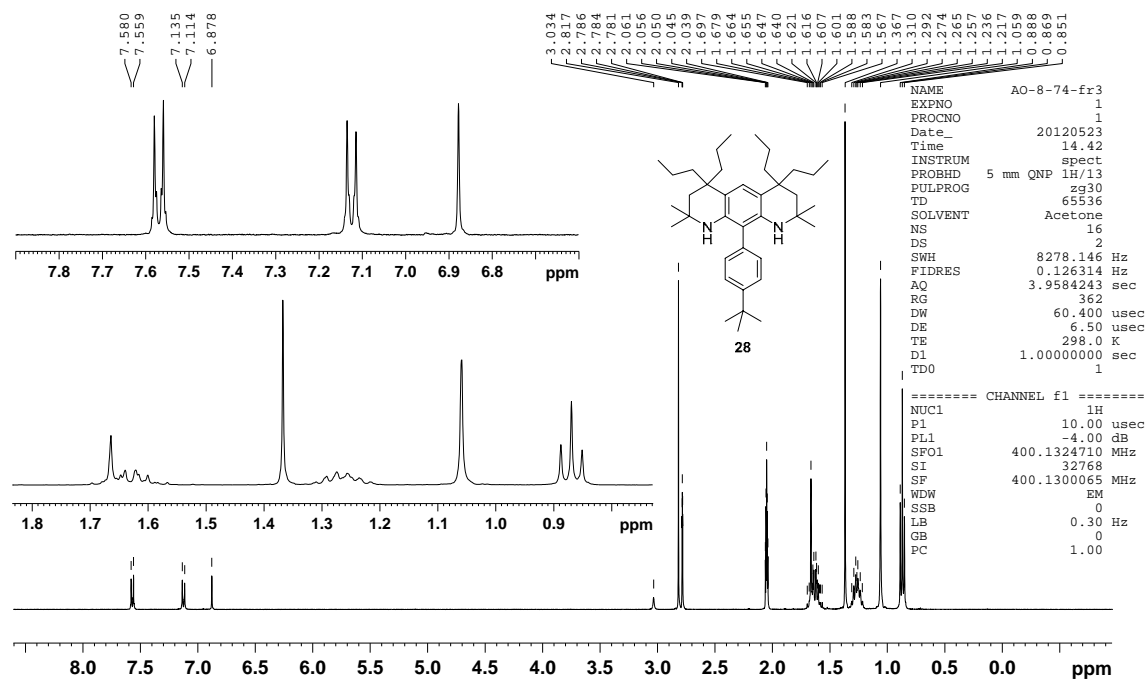
**Figure A66.** $^{1}$H NMR (400 MHz, acetone-$d_6$) spectrum of diamine **28** (AO-8-74-fr3).
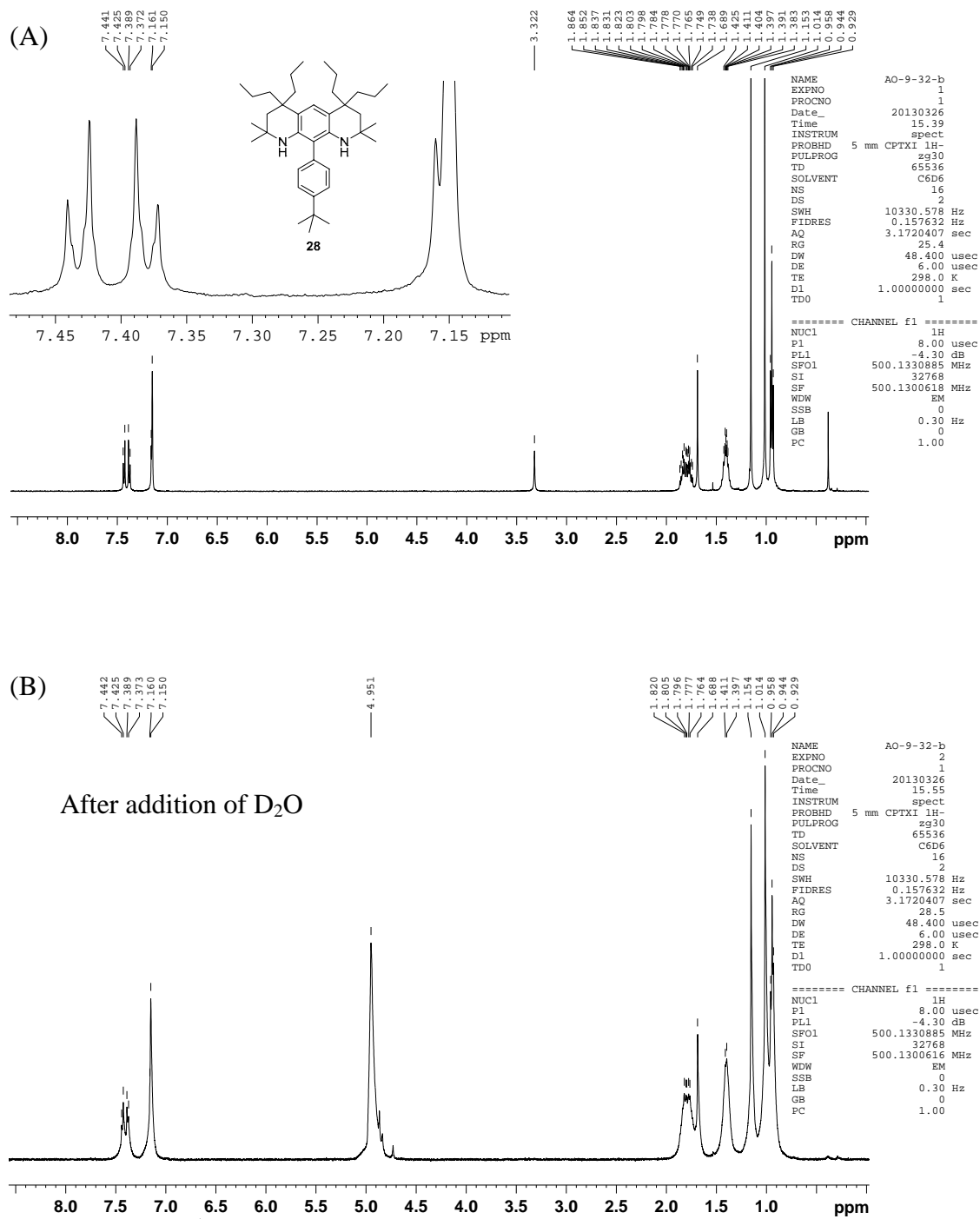
**Figure A67.** (A) $^1$H NMR (500 MHz, benzene-$d_6$) spectrum of diamine **28** (AO-9-32-b). (B) After addition 2 drops of $D_2O$, N-H peak at $\delta = 3.322$ ppm is $D_2O$ exchangeable.
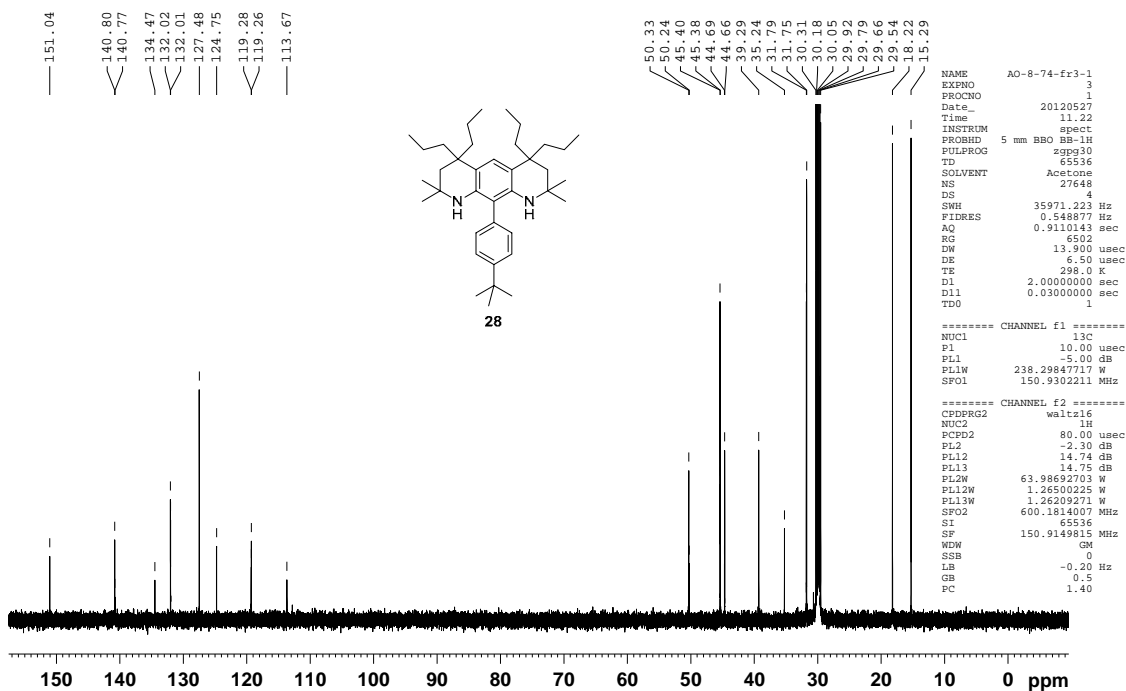
**Figure A68.** $^{13}$C NMR (150 MHz, acetone-$d_6$) spectrum of diamine **28** (AO-8-74-fr3).
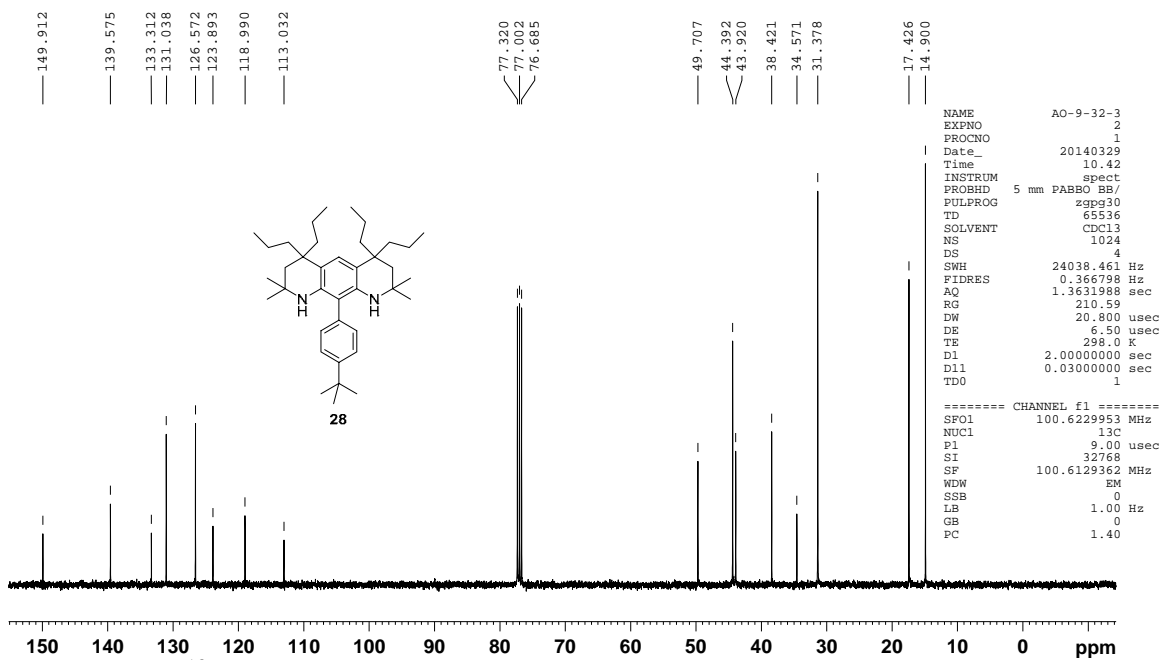


**Figure A69.** $^{13}$C NMR (100 MHz, chloroform-$d$) spectrum of diamine **28** (AO-9-32-3).
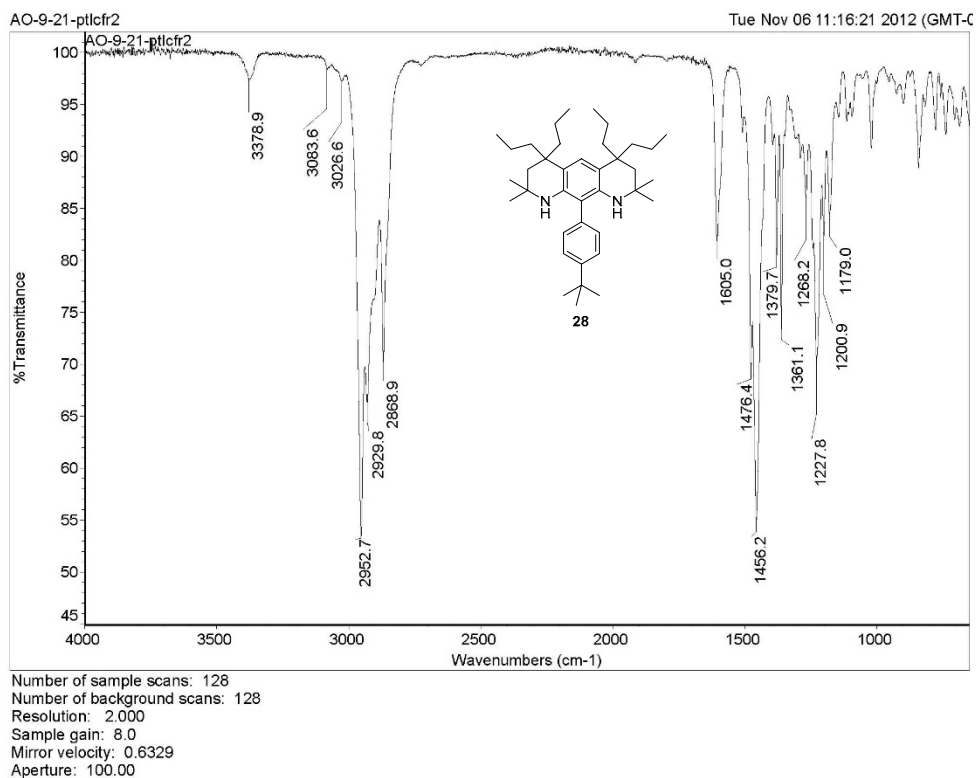
**Figure A70.** IR (ATR, diamond, cm$^{-1}$) spectrum of diamine **28** (AO-9-21-ptlcfr2).
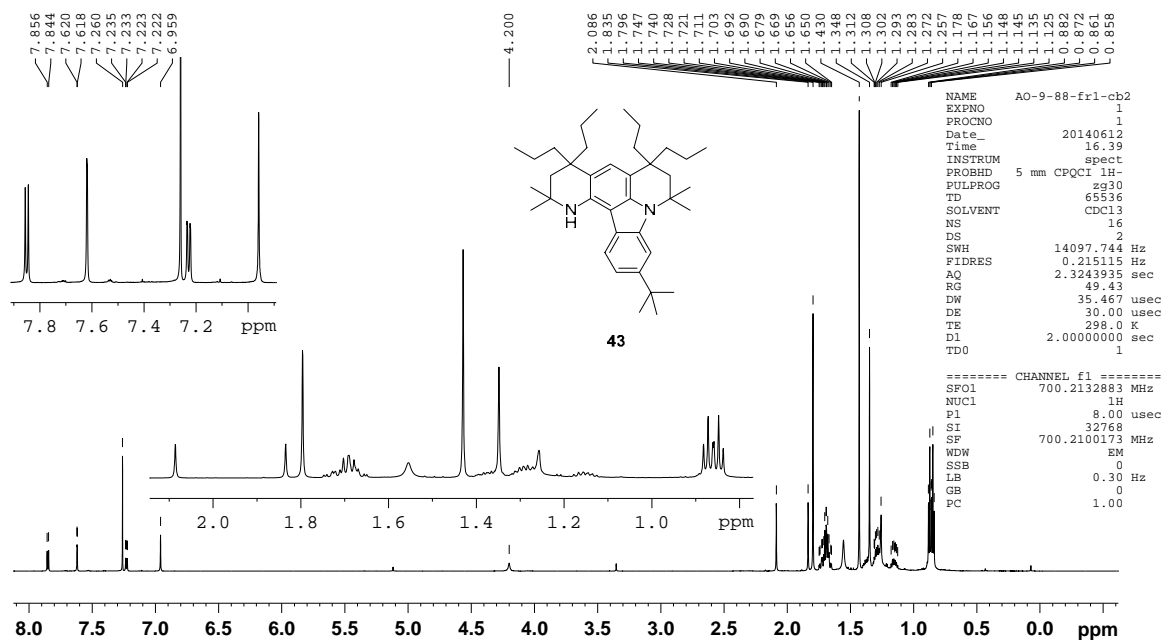


**Figure A71.** $^1$H NMR (700 MHz, chloroform-*d*) spectrum of by-product **43** (AO-9-88-fr1-cb2).

**Table A1.** Crystal data and structure refinement for diketone-diamine **30** (X-ray label: 11502) and diamine **28** (X-ray label: 12511).

| | Diketone-diamine **30** | Diamine **28** |
|---|---|---|
| Empirical formula | C16 H20 N2 O2 | C38 H60 N2 |
| Formula weight | 272.34 | 544.88 |
| Crystal color, shape, size | yellowish block, $0.01 \times 0.01 \times 0.008$ mm$^3$ | colorless block, $0.01 \times 0.005 \times 0.002$ mm3 |
| Temperature | 150(2) K | 100(2) K |
| Wavelength | 0.41328 Å | 0.41328 Å |
| Crystal system, space group | Monoclinic, P2(1)/c | Monoclinic, P2$_1$/c |
| Unit cell dimensions | a = 6.9085(9) Å   $\alpha$= 90°<br>b = 10.0392(12) Å  $\beta$= 93.407(2)°<br>c = 21.009(3) Å   $\gamma$= 90° | a = 16.0042(15) Å   $\alpha$= 90°<br>b = 9.8362(8) Å  $\beta$= 100.198(2)°<br>c = 22.3583(19) Å   $\gamma$= 90° |
| Volume | 1454.5(3) Å$^3$ | 3464.0(5) Å$^3$ |
| Z | 4 | 4 |
| Density (calculated) | 1.244 Mg/m$^3$ | 1.045 Mg/m$^3$ |
| Absorption coefficient | 0.053 mm$^{-1}$ | 0.029 mm$^{-1}$ |
| F(000) | 584 | 1208 |
| ***Data collection*** | | |
| Diffractometer | APEX II on a D8 platform, Bruker, at CMC, APS Chicago | SMART6000 Platform CCD, Bruker |
| Theta range for data collection | 1.13 to 20.15° | 0.75 to 15.59° |
| Index ranges | -7<=h<=11, -16<=k<=15, -34<=l<=28 | -20<=h<=18, -12<=k<=10, -29<=l<=29 |
| Reflections collected | 28020 | 28319 |
| Independent reflections | 7050 [R(int) = 0.0596] | 7581 [R(int) = 0.1246] |
| Observed Reflections | 5318 | 4097 |
| Completeness to theta | 99.5 % | 94.9 % |
| ***Solution and Refinement*** | | |
| Absorption correction | Semi-empirical from equivalents | Semi-empirical from equivalents |
| Max. and min. transmission | 0.9996 and 0.9995 | 0.9999 and 0.9997 |
| Solution | Direct methods | Direct methods |
| Refinement method | Full-matrix least-squares on F$^2$ | Full-matrix least-squares on F$^2$ |
| Weighting scheme | w = [ $^2$Fo$^2$+ AP$^2$+ BP]$^{-1}$, with P = (Fo$^2$+ 2 Fc$^2$)/3, A = 0.0993, B = 0.0130 | w = [ $^2$Fo$^2$+ AP$^2$+ BP]$^{-1}$, with P = (Fo$^2$+ 2 Fc$^2$)/3, A = 0.0671 |
| Data / restraints / parameters | 7050 / 0 / 199 | 7581 / 0 / 380 |
| Goodness-of-fit on F$^2$ | 1.066 | 0.991 |
| Final R indices [I>2sigma(I)] | R1 = 0.0512, wR2 = 0.1540 | R1 = 0.0690, wR2 = 0.1340 |
| R indices (all data) | R1 = 0.0664, wR2 = 0.1645 | R1 = 0.1470, wR2 = 0.1627 |
| Largest diff. peak and hole | 0.445 and -0.291 e.Å$^{-3}$ | 0.478 and -0.309 e.Å$^{-3}$ |

Goodness-of-fit = $[\Sigma[w(F_o^2 - F_c^2)^2]/N_{observns} - N_{params})]^{1/2}$, all data.  R1 = $\Sigma(|F_o| - |F_c|) / \Sigma |F_o|$.  $w$R2 = $[\Sigma[w(F_o^2 - F_c^2)^2] / \Sigma [w(F_o^2)^2]]^{1/2}$.

**Table A2.** Hydrogen bonds for diketone-diamine **30** [Å and °] (X-ray label: 11502).

| D-H...A | d(D-H) | d(H...A) | d(D...A) | <(DHA) |
|---|---|---|---|---|
| N1-H1N...O1#1 | 0.875(12) | 2.121(12) | 2.9601(10) | 160.5(11) |
| N2-H2N...O2#1 | 0.863(13) | 2.077(13) | 2.9219(10) | 166.1(11) |

Symmetry transformations used to generate equivalent atoms: #1 x+1,y,z

**Appendix B**

**NMR Spectral Assignment for diamines 12, 22, 28 and by-product 43**

NMR Spectral Assignment for Diamines **12**, **22**, **28** and by-product **43**: correlations between DFT-calculated and experimental $^{13}$C and $^{1}$H NMR chemical shifts. DFT-calculated and experimental $^{15}$N NMR chemical shifts.
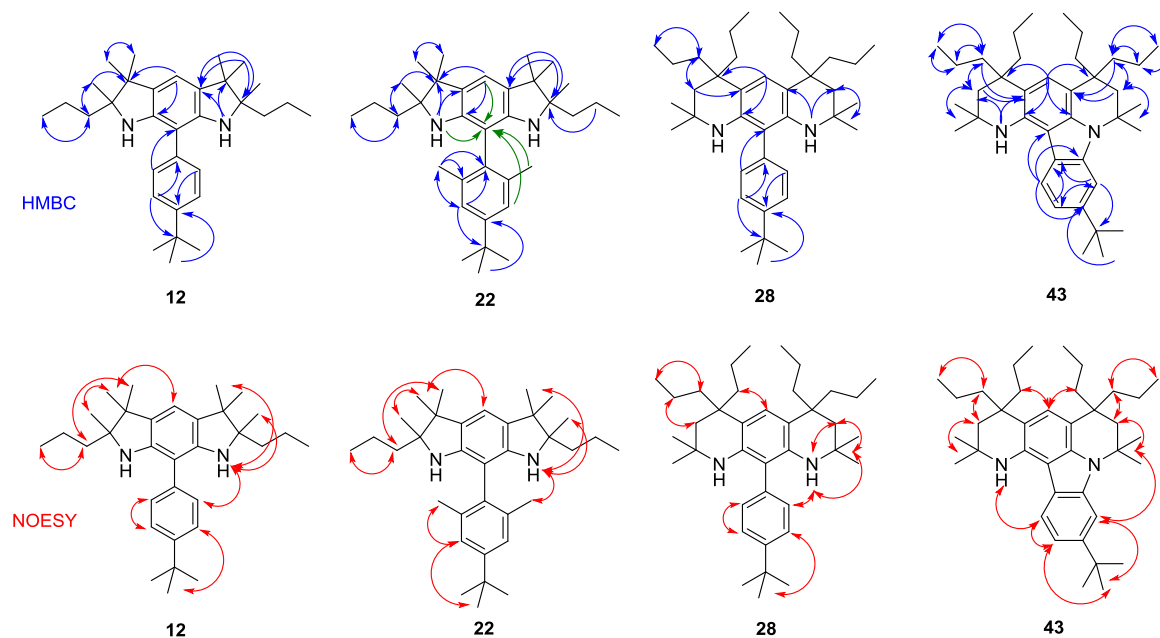


**Figure B1.** Summary of 2D NMR experiments for diamines **12**, **22**, **28** and by-product **43**. $^{1}$H-$^{13}$C HMBC couplings are indicated in blue; and weak correlations are indicated in green. $^{1}$H-$^{1}$H NOESY correlations are indicated in red.

$^{1}$H-$^{13}$C HSQC spectra allowed for assignment of the resonances to the corresponding nuclei. $^{1}$H-$^{13}$C HMBC spectra showed most of the expected 1-3 couplings. Also, weak cross-correlations of the protons of NH groups and surrounding hydrogens were also observed in NOESY experiments allowing to confirm atom connectivity for **12**, **22**, **28** and by-product **43**.
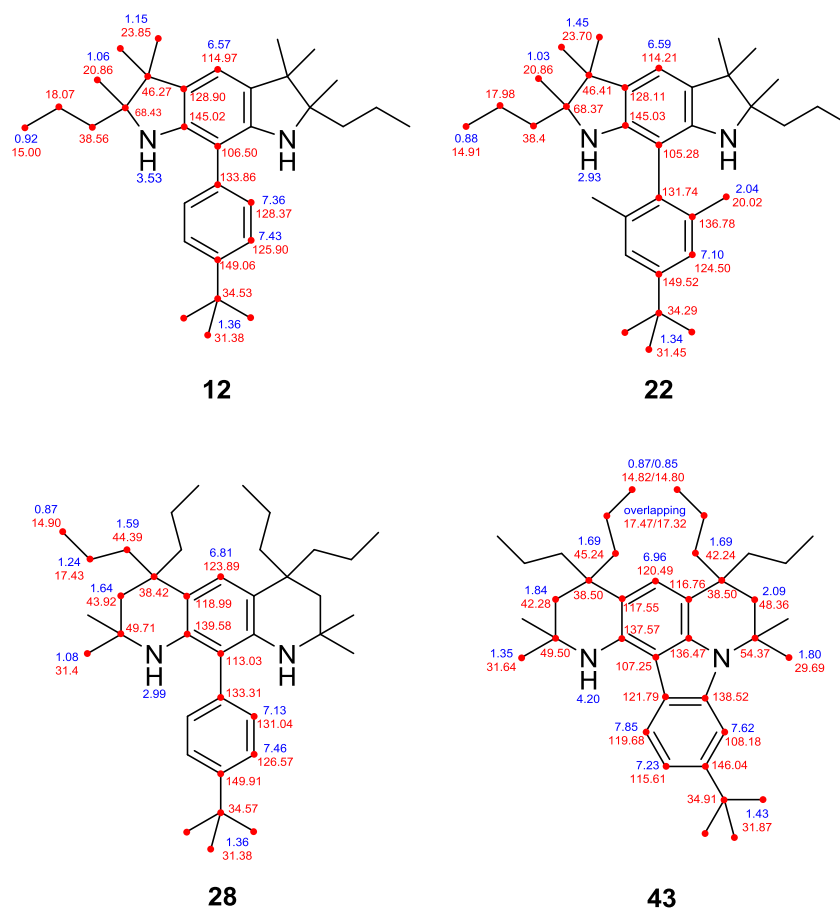
**Figure B2.** ^{1}H and ^{13}C NMR chemical shift assignments for diamines **12**, **22**, **28** and by-product **43** in chloroform-*d* (sample label: AO-9-55-flt, AO-9-28-wsh, AO-9-32, respectively) using HSQC, HMBC, COSY and NOESY 2D NMR experiments. The ^{1}H and ^{13}C NMR chemical shifts are indicated in blue and red, respectively.

**Table B1.** Statistical Parameters for the Correlations of $^{13}$C and $^1$H NMR Chemical Shifts.[a]

| | $a$ | $b$ | $R^2$ | MaxErr | CMAE ($n$) |
|---|---|---|---|---|---|
| **12/12a** ($^{13}$C) | 4.4232 | 0.9374 | 0.9986 | 2.85 | 1.641 (14) |
| **12/12a** ($^1$H) | −0.1195 | 1.0507 | 0.9946 | 0.482 | 0.145 (7) |
| **22/22a** ($^{13}$C) | 4.1059 | 0.9463 | 0.9989 | 2.76 | 1.495 (15) |
| **22/22a** ($^1$H) | −0.0490 | 1.0378 | 0.9934 | 0.468 | 0.134 (7) |
| **28/28a** ($^{13}$C) | 1.4469 | 0.9633 | 0.9938 | 10.1 | 2.356 (15) |
| **28/28a** ($^1$H) | −0.2205 | 1.0867 | 0.9959 | 0.279 | 0.153 (8) |
| **43/43a** ($^{13}$C) | 1.4317 | 0.9629 | 0.9909 | 10.8 | 2.651 (24) |
| **43/43a** ($^1$H) | −0.1762 | 1.0577 | 0.9949 | 0.415 | 0.161 (12) |

[a] $a$ and $b$ are the intercept and slope of the linear fit to $\delta_{DFT} = a + b\ \delta_{expt}$, and $R^2$ is its correlation coefficient. MaxErr is the maximum corrected absolute error with respect to the linear fit ($|\delta_{scaled} - \delta_{expt}|$). CMAE is the corrected mean absolute error for $n$ chemical shifts ($\Sigma|\delta_{scaled} - \delta_{expt}|/n$).

**12a**: R = CH$_3$ (DFT calculation)
**12**: R = C$_3$H$_7$ (Experiment)
Solvent: chloroform
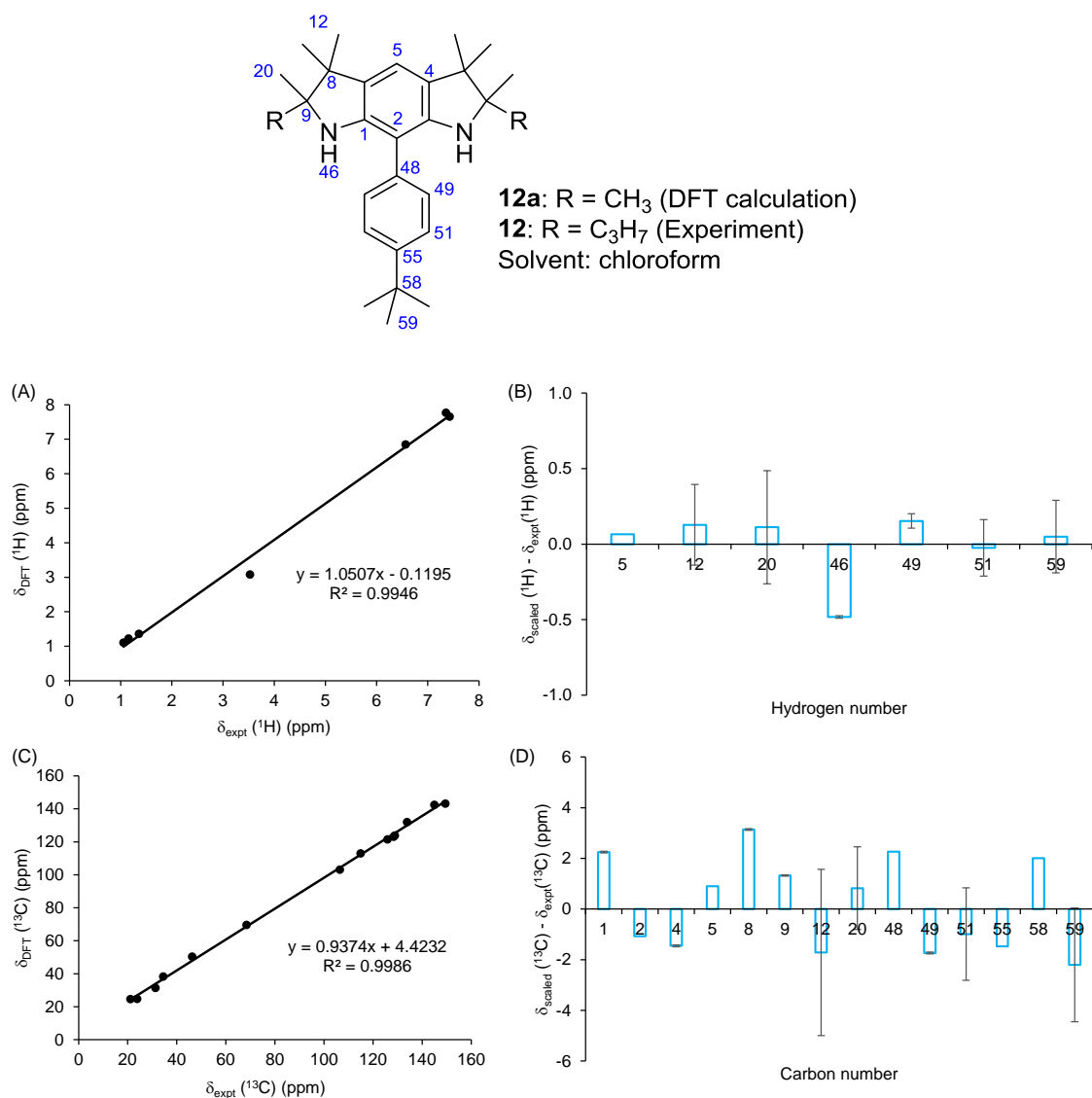
**Figure B3.** Correlation between the calculated ($\delta_{DFT}$) and experimental ($\delta_{expt}$) $^1$H NMR (A) and $^{13}$C NMR (C) shifts for diamine **12a** in the IEF-PCM-UA0 solvent model for acetone and **12** in chloroform-*d*, respectively. Solid line is the best fit to $\delta_{DFT} = a + b\ \delta_{expt}$. Difference between scaled calculated ($\delta_{scaled} = (\delta_{DFT} - a)\ /\ b$) and experimental ($\delta_{expt}$) $^1$H NMR (B) and $^{13}$C NMR (D) chemical shifts for diamine **12** in chloroform-*d*. Calculated structure **12a** was simplified by replacing R = C$_3$H$_7$ with R = CH$_3$. Error bars correspond to the standard deviation of chemical shifts calculated for carbon atoms that are magnetically equivalent by symmetry and rotation.
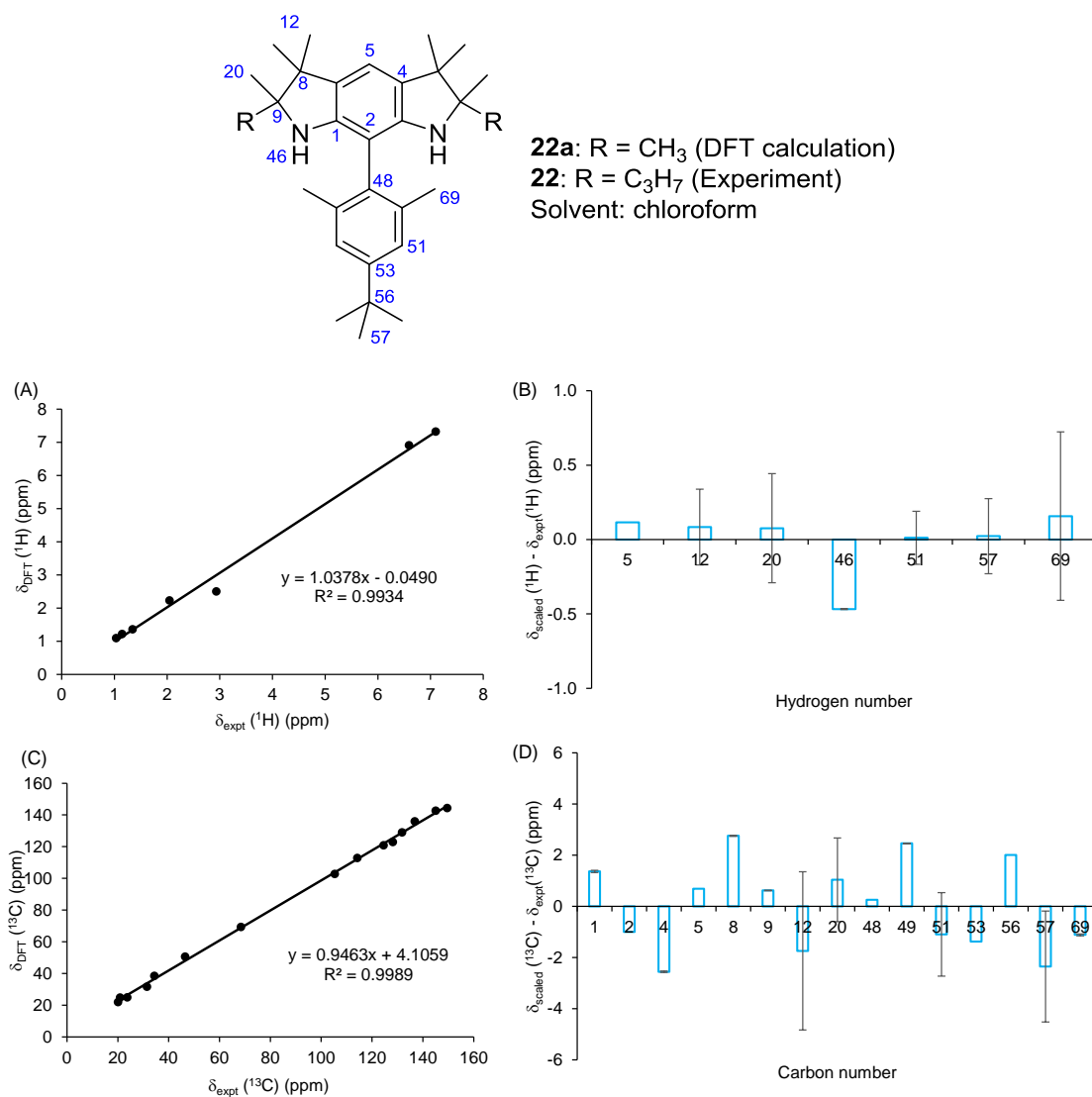
**Figure B4.** Correlation between the calculated ($\delta_{DFT}$) and experimental ($\delta_{expt}$) $^1$H NMR (A) and $^{13}$C NMR (C) shifts for diamine **22a** in the IEF-PCM-UA0 solvent model for acetone and **22** in in chloroform-*d*, respectively. Solid line is the best fit to $\delta_{DFT} = a + b\ \delta_{expt}$. Difference between scaled calculated ($\delta_{scaled} = (\delta_{DFT} - a) / b$) and experimental ($\delta_{expt}$) $^1$H NMR (B) and $^{13}$C NMR (D) chemical shifts for diamine **22** in chloroform-*d*. Calculated structure **22a** was simplified by replacing R = $C_3H_7$ with R = $CH_3$. Error bars correspond to the standard deviation of chemical shifts calculated for carbon atoms that are magnetically equivalent by symmetry and rotation.

**28a**: R = CH₃ (DFT calculation)
**28**: R = C₃H₇ (Experiment)
Solvent: chloroform
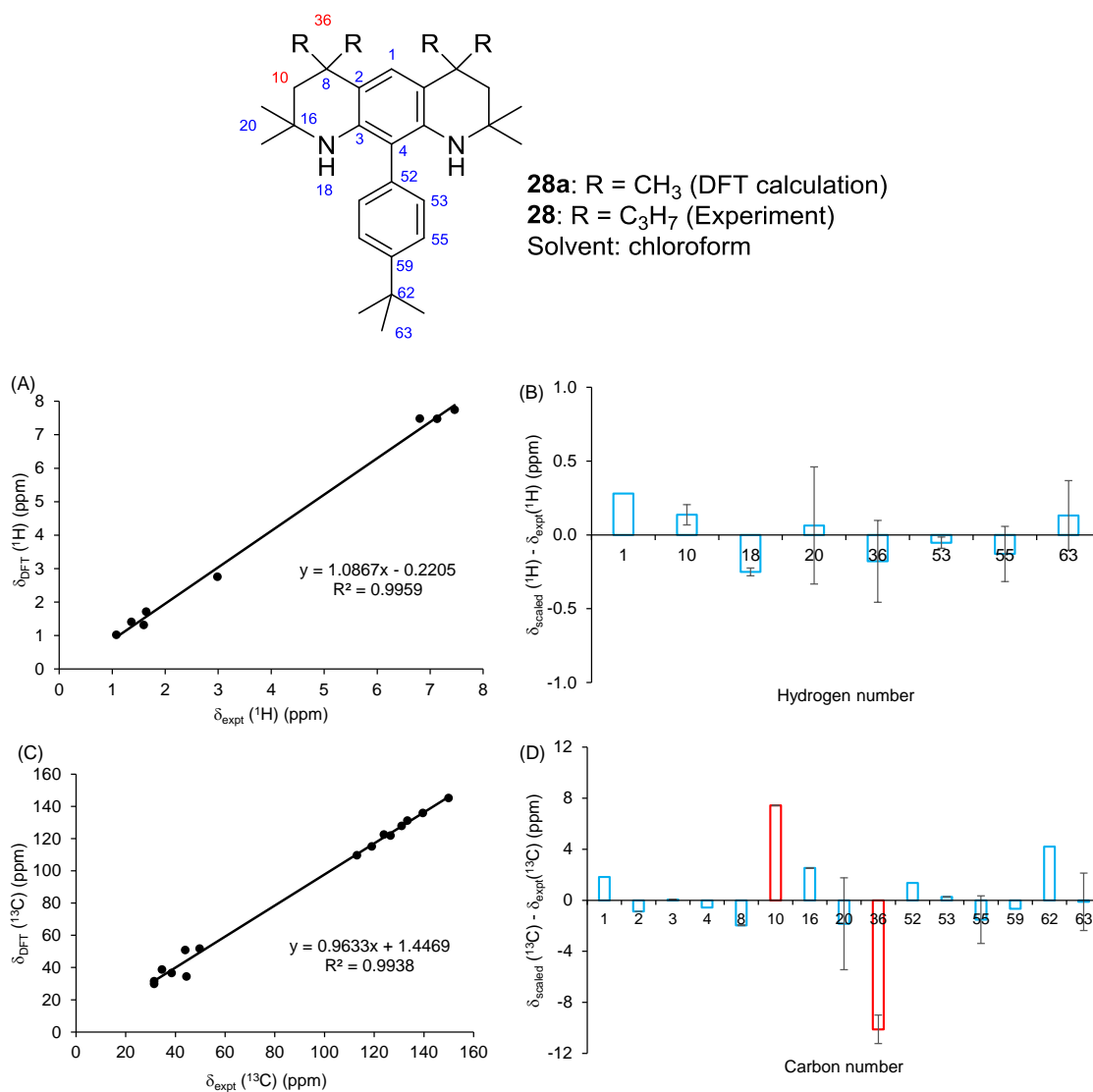
**Figure B5.** Correlation between the calculated ($\delta_{DFT}$) and experimental ($\delta_{expt}$) ¹H NMR (A) and ¹³C NMR (C) shifts for diamine **28a** in the IEF-PCM-UA0 solvent model for acetone and **28** in in chloroform-*d*, respectively. Solid line is the best fit to $\delta_{DFT} = a + b\ \delta_{expt}$. Difference between scaled calculated ($\delta_{scaled} = (\delta_{DFT} - a)\ /\ b$) and experimental ($\delta_{expt}$) ¹H NMR (B) and ¹³C NMR (D) chemical shifts for diamine **28** in chloroform-*d*. Calculated structure **28a** was simplified by replacing R = C₃H₇ with R = CH₃. Error bars correspond to the standard deviation of chemical shifts calculated for carbon atoms that are magnetically equivalent by symmetry and rotation. Shift corresponding to aliphatic carbon atoms affected from different sidechains (*n*-propyl in **28** and methyl in **28a**) are marked in red.
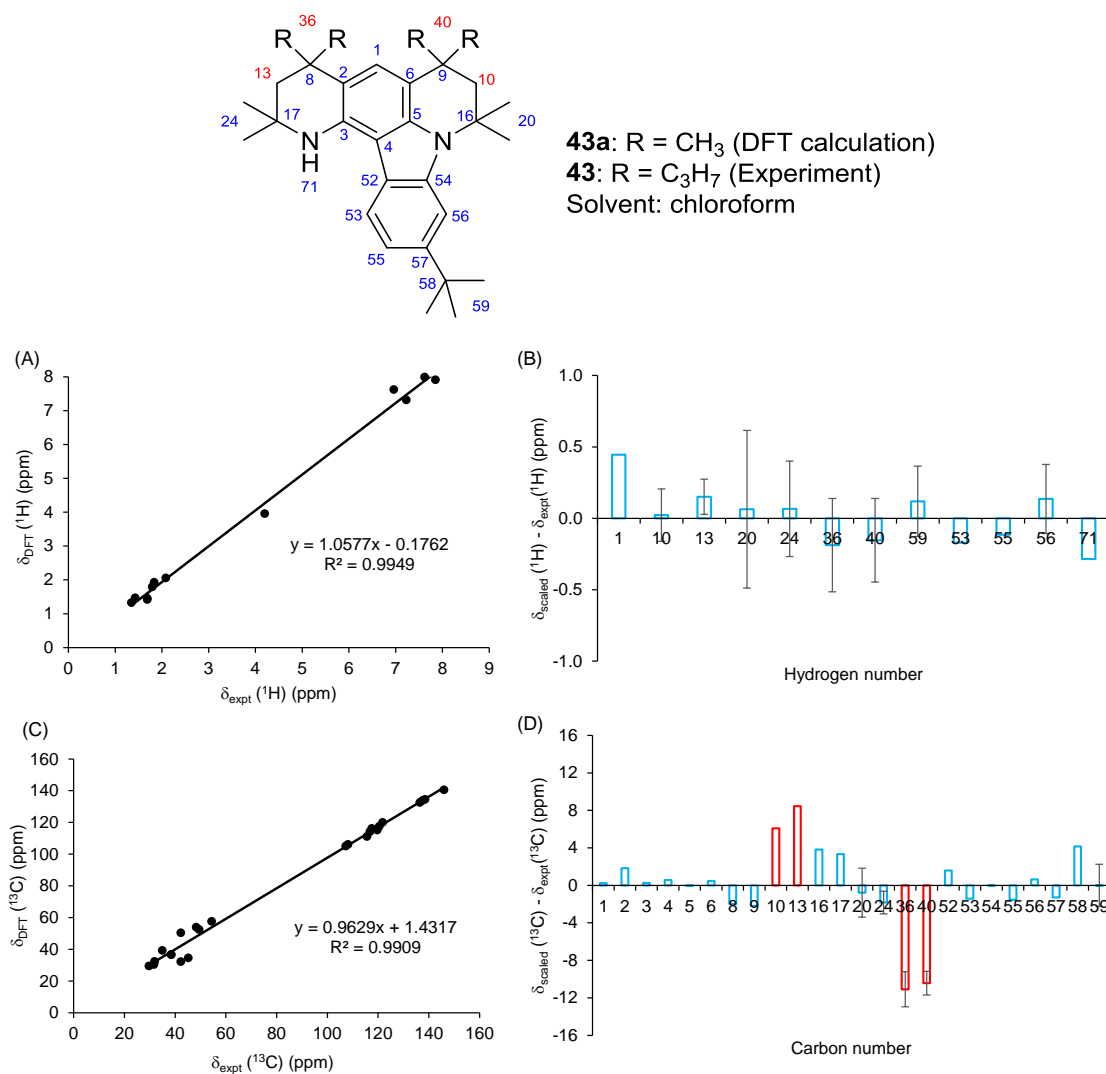
**Figure B6.** Correlation between the calculated ($\delta_{DFT}$) and experimental ($\delta_{expt}$) $^1$H NMR (A) and $^{13}$C NMR (C) shifts for by-product **43a** in the IEF-PCM-UA0 solvent model for chloroform and **43** in chloroform-*d*, respectively. Solid line is the best fit to $\delta_{DFT} = a + b\ \delta_{expt}$. Difference between scaled calculated ($\delta_{scaled} = (\delta_{DFT} - a)\ /\ b$) and experimental ($\delta_{expt}$) $^1$H NMR (B) and $^{13}$C NMR (D) chemical shifts for by-product **43** in chloroform-*d*. Calculated structure **43a** was simplified by replacing R = C$_3$H$_7$ with R = CH$_3$. Error bars correspond to the standard deviation of chemical shifts calculated for carbon atoms that are magnetically equivalent by symmetry and rotation. Shift corresponding to aliphatic carbon atoms affected from different sidechains (*n*-propyl in **43** and methyl in **43a**) are marked in red.

**Table B2.** ^{1}H and ^{13}C NMR spectral assignments for diamines **12**, **22**, **28** and by-product **43**, experimental ($\delta_{expt}$), calculated ($\delta_{DFT}$), and scaled ($\delta_{scaled}$) NMR chemical shifts,[a] as well as calculated NMR isotropic shieldings ($\sigma_{DFT}$).[b] Values of $\sigma_{DFT}$ and $\delta_{DFT}$ are for simplified structures **12a**, **22a**, **28a**, and **43a**.

| Diamine **12** | | | | | | | | | | Diamine **22** | | | | | | | | |
| [13]C | | | | | [1]H | | | | | [13]C | | | | | [1]H | | | |
| C no. | $\sigma_{DFT}$ | $\delta_{expt}$ | $\delta_{DFT}$ | $\delta_{scaled}$ | H no. | $\sigma_{DFT}$ | $\delta_{expt}$ | $\delta_{DFT}$ | $\delta_{scaled}$ | C no. | $\sigma_{DFT}$ | $\delta_{expt}$ | $\delta_{DFT}$ | $\delta_{scaled}$ | H no. | $\sigma_{DFT}$ | $\delta_{expt}$ | $\delta_{DFT}$ | $\delta_{scaled}$ |
|---|---|---|---|---|---|---|---|---|---|---|---|---|---|---|---|---|---|---|---|
| 1 | 49.65 | 145.02 | 142.53 | 147.33 | 5 | 24.896 | 6.570 | 6.852 | 6.635 | 1 | 49.55 | 145.03 | 142.64 | 146.40 | 5 | 24.839 | 6.589 | 6.909 | 6.704 |
| 2 | 88.99 | 106.50 | 103.17 | 105.34 | 12 | 30.374 | 1.154 | 1.227 | 1.281 | 2 | 89.37 | 105.28 | 102.78 | 104.28 | 12 | 30.345 | 1.143 | 1.225 | 1.227 |
| 4 | 68.25 | 128.90 | 123.88 | 127.44 | 20 | 30.682 | 1.057 | 1.108 | 1.169 | 4 | 69.22 | 128.11 | 122.92 | 125.56 | 20 | 30.646 | 1.030 | 1.099 | 1.106 |
| 5 | 79.16 | 114.97 | 112.99 | 115.82 | 46 | 28.672 | 3.528 | 3.081 | 3.046 | 5 | 79.32 | 114.21 | 112.84 | 114.90 | 46 | 29.243 | 2.931 | 2.508 | 2.463 |
| 8 | 141.71 | 46.27 | 50.47 | 49.12 | 49 | 24.011 | 7.356 | 7.770 | 7.509 | 8 | 141.53 | 46.41 | 50.63 | 49.17 | 51 | 24.548 | 7.095 | 7.326 | 7.107 |
| 9 | 122.53 | 68.43 | 69.61 | 69.54 | 51 | 24.221 | 7.428 | 7.659 | 7.403 | 9 | 122.76 | 68.37 | 69.39 | 68.99 | 57 | 30.154 | 1.343 | 1.368 | 1.366 |
| 12 | 170.17 | 23.85 | 24.82 | 21.75 | 59 | 30.184 | 1.359 | 1.361 | 1.409 | 12 | 169.95 | 23.70 | 24.89 | 21.96 | 69 | 28.827 | 2.043 | 2.235 | 2.200 |
| 20 | 166.04 | 21.17 | 24.68 | 21.61 | | | | | | 20 | 165.90 | 20.86 | 24.83 | 21.90 | | | | | |
| 48 | 60.11 | 133.86 | 132.04 | 136.14 | | | | | | 48 | 63.14 | 131.74 | 129.02 | 132.00 | | | | | |
| 49 | 69.07 | 128.37 | 123.11 | 126.62 | | | | | | 49 | 56.29 | 136.78 | 135.87 | 139.24 | | | | | |
| 51 | 71.95 | 125.90 | 121.49 | 124.89 | | | | | | 51 | 72.43 | 124.50 | 120.88 | 123.40 | | | | | |
| 55 | 48.95 | 149.46 | 143.20 | 148.05 | | | | | | 53 | 47.86 | 149.52 | 144.30 | 148.15 | | | | | |
| 58 | 153.79 | 34.53 | 38.37 | 36.21 | | | | | | 56 | 153.70 | 34.29 | 38.45 | 36.30 | | | | | |
| 59 | 163.31 | 31.38 | 31.44 | 28.82 | | | | | | 57 | 163.01 | 31.45 | 31.64 | 29.10 | | | | | |
| | | | | | | | | | | 69 | 170.14 | 20.02 | 22.00 | 18.91 | | | | | |

## Table B2. contd.

| | Diamine 12 | | | | | | | | | | Diamine 22 | | | | | | | | |
| | $^{13}$C | | | | $^{1}$H | | | | | $^{13}$C | | | | | $^{1}$H | | | | |
| C no. | $\sigma_{DFT}$ | $\delta_{expt}$ | $\delta_{DFT}$ | $\delta_{scaled}$ | H no. | $\sigma_{DFT}$ | $\delta_{expt}$ | $\delta_{DFT}$ | $\delta_{scaled}$ | C no. | $\sigma_{DFT}$ | $\delta_{expt}$ | $\delta_{DFT}$ | $\delta_{scaled}$ | H no. | $\sigma_{DFT}$ | $\delta_{expt}$ | $\delta_{DFT}$ | $\delta_{scaled}$ |
|---|---|---|---|---|---|---|---|---|---|---|---|---|---|---|---|---|---|---|---|
| 1 | 69.60 | 123.89 | 122.55 | 125.72 | 1 | 24.269 | 6.806 | 7.479 | 7.085 | 1 | 74.60 | 120.49 | 117.56 | 120.60 | 1 | 24.125 | 6.959 | 7.623 | 7.374 |
| 2 | 76.93 | 118.99 | 115.23 | 118.11 | 10 | 29.973 | 1.644 | 1.714 | 1.781 | 2 | 75.89 | 117.55 | 116.26 | 119.26 | 10 | 29.561 | 2.086 | 2.187 | 2.112 |
| 3 | 56.18 | 139.58 | 135.96 | 139.64 | 18 | 28.975 | 2.988 | 2.754 | 2.737 | 3 | 58.21 | 137.57 | 133.94 | 137.62 | 13 | 29.733 | 1.835 | 2.015 | 1.990 |
| 4 | 82.38 | 113.03 | 109.78 | 112.46 | 20 | 30.631 | 1.080 | 1.023 | 1.144 | 4 | 86.97 | 107.25 | 105.19 | 107.75 | 20 | 30.222 | 1.796 | 1.526 | 1.864 |
| 8 | 155.58 | 38.42 | 36.56 | 36.45 | 36 | 30.785 | 1.594 | 1.317 | 1.415 | 5 | 59.56 | 136.47 | 132.60 | 136.22 | 24 | 30.358 | 1.348 | 1.389 | 1.422 |
| 10 | 141.22 | 43.92 | 50.92 | 51.36 | 53 | 24.249 | 7.132 | 7.472 | 7.079 | 6 | 77.95 | 116.76 | 114.20 | 117.12 | 36 | 30.669 | 1.690 | 1.078 | 1.509 |
| 16 | 140.40 | 49.71 | 51.77 | 52.24 | 55 | 23.868 | 7.461 | 7.747 | 7.332 | 8 | 155.32 | 38.50 | 36.83 | 36.77 | 40 | 30.432 | 1.690 | 1.316 | 1.543 |
| 20 | 159.13 | 31.38 | 29.90 | 29.54 | 63 | 30.506 | 1.363 | 1.404 | 1.495 | 9 | 155.52 | 38.50 | 36.63 | 36.56 | 59 | 30.441 | 1.430 | 1.307 | 1.556 |
| 36 | 158.66 | 44.39 | 34.47 | 34.28 | | | | | | 10 | 138.15 | 48.36 | 54.01 | 54.60 | 53 | 23.835 | 7.850 | 7.913 | 7.648 |
| 52 | 60.98 | 133.31 | 131.18 | 134.67 | | | | | | 13 | 141.70 | 42.28 | 50.45 | 50.91 | 55 | 24.430 | 7.229 | 7.318 | 7.085 |
| 53 | 64.24 | 131.04 | 127.93 | 131.31 | | | | | | 16 | 134.54 | 54.37 | 57.62 | 58.35 | 56 | 23.756 | 7.619 | 7.992 | 7.722 |
| | | | | | | | | | | 17 | 139.68 | 49.50 | 52.48 | 53.02 | 71 | 27.792 | 4.200 | 3.956 | 3.907 |
| | | | | | | | | | | 20 | 160.48 | 29.69 | 31.68 | 29.20 | | | | | |
| | | | | | | | | | | 24 | 158.66 | 31.64 | 33.50 | 30.09 | | | | | |
| | | | | | | | | | | 36 | 158.66 | 45.24 | 33.50 | 34.41 | | | | | |
| | | | | | | | | | | 40 | 159.07 | 42.24 | 33.09 | 32.07 | | | | | |
| | | | | | | | | | | 52 | 72.06 | 121.79 | 120.09 | 123.23 | | | | | |
| | | | | | | | | | | 53 | 76.97 | 119.68 | 115.18 | 118.13 | | | | | |
| | | | | | | | | | | 54 | 57.55 | 138.52 | 134.61 | 138.31 | | | | | |
| | | | | | | | | | | 55 | 80.96 | 115.61 | 111.19 | 113.99 | | | | | |
| | | | | | | | | | | 56 | 86.02 | 108.18 | 106.13 | 108.74 | | | | | |
| | | | | | | | | | | 57 | 51.56 | 146.04 | 140.59 | 144.52 | | | | | |
| | | | | | | | | | | 58 | 152.87 | 34.91 | 39.29 | 39.31 | | | | | |
| | | | | | | | | | | 59 | 158.74 | 31.87 | 33.41 | 32.13 | | | | | |

$^{1}$H–$^{15}$N HSQC spectra for **12**, **22**, **28** and by-product **43** in acetone-$d_6$ show $^{1}$H–$^{15}$N cross-peaks for the NH groups (Figures B7, B12, B17 and B22).  The $^{15}$N NMR chemical shifts are in the $\delta = -288 - (-287)$ ppm range (relative to nitromethane at 0.0 ppm), which is within the typical range for NH groups in amines. DFT-calculated $^{15}$N NMR chemical shifts for these NH groups are in good agreement compared to the experimental values.

**Table B3**.  Experimental ($\delta_{expt}$) and calculated ($\delta_{DFT}$) $^{15}$N NMR chemical shift assignments of NH groups for **12**, **22**, **28** and by-product **43** in acetone-$d_6$.

| Structure | $\sigma_{DFT}$[a] | $\delta_{expt}$ | $\delta_{DFT}$ |
|---|---|---|---|
| Diamine **12** and **12a** | 161.43 | −287.4 | −287.68 |
| Diamine **22** and **22a** | 161.47 | −288.2 | −287.72 |
| Diamine **28** and **28a** | 165.84 | −287.9 | −292.08 |
| By-product **43** and **43a** | 164.53 | −287.5 | −290.77 |

[a] $\sigma_{DFT}$ for nitromethane: −126.2466 ($^{15}$N). Experimental ($\delta_{expt}$) and calculated ($\delta_{DFT}$) NMR chemical shifts relative to nitromethane, as well as calculated NMR isotropic shieldings ($\sigma_{DFT}$).[a] Values of $\sigma_{DFT}$ and $\delta_{DFT}$ are for simplified structures **12a**, **22a**, **28a** and **43a**.

2D-NMR Spectra for diamines **12**, **22**, **28** and by-product **43**.
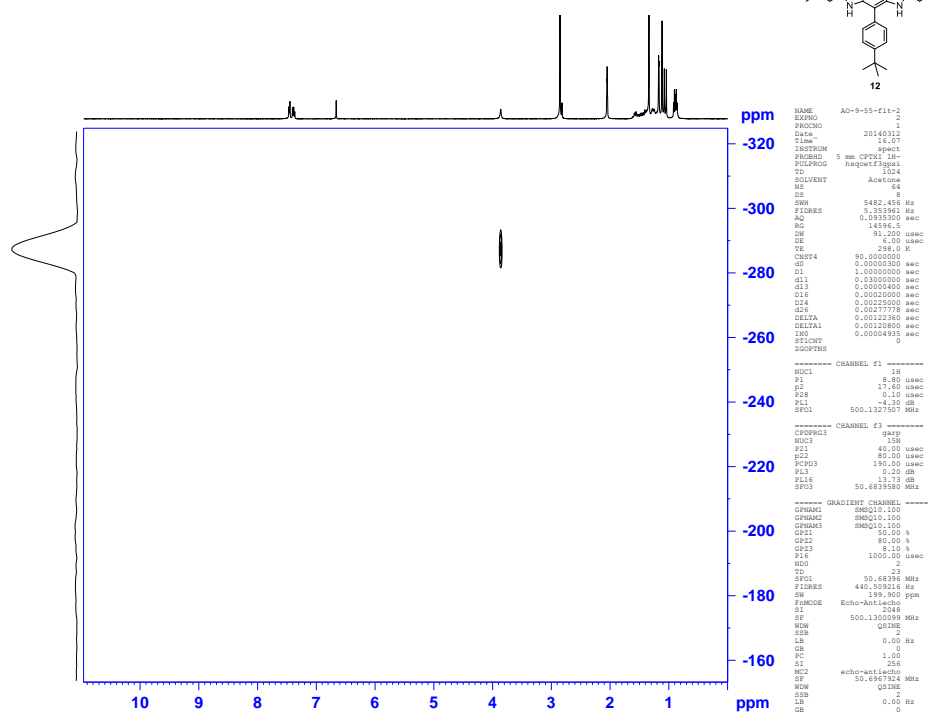


**Figure B7.** $^1H$–$^{15}N$ HSQC experiment (500 MHz, acetone-$d_6$, label: AO-9-55-flt2) of diamine **12**.
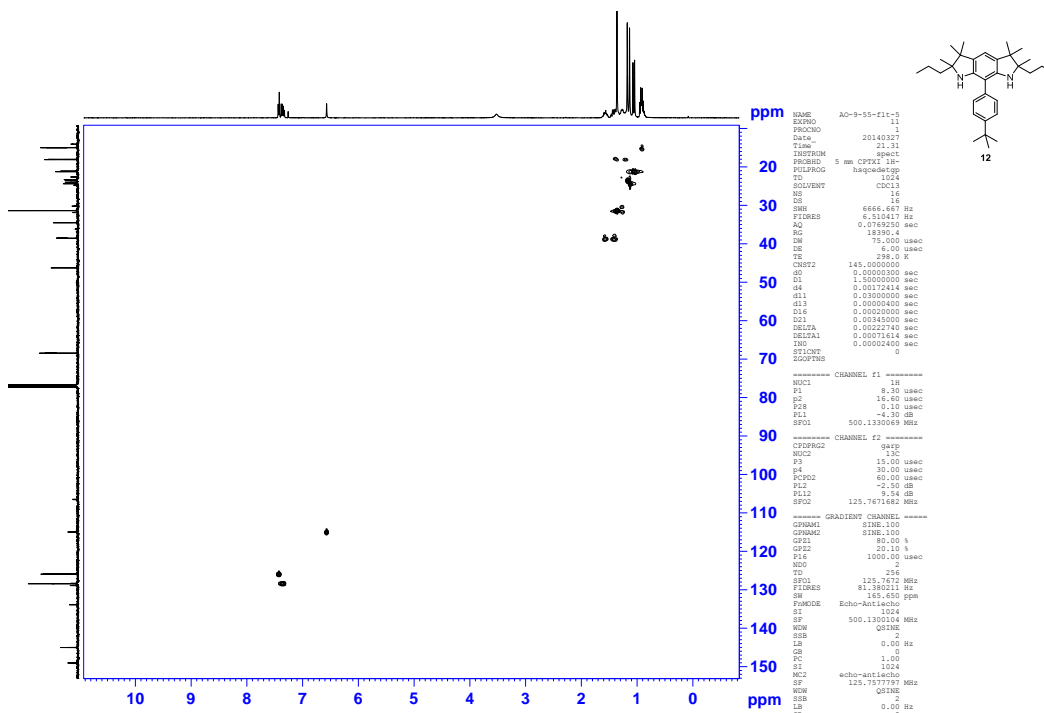


**Figure B8.** $^1H$–$^{13}C$ HSQC experiment (500 MHz, chloroform-$d$, label: AO-9-55-flt5) of diamine **12**.
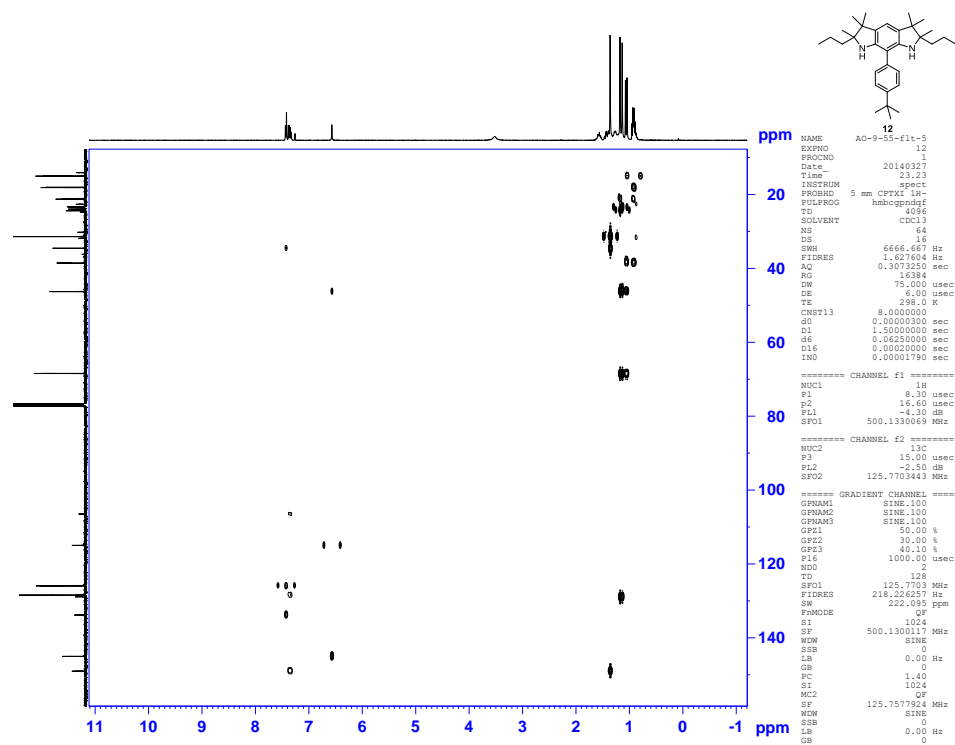
**Figure B9.** $^{1}$H–$^{13}$C HMBC experiment (500 MHz, chloroform-*d*, label: AO-9-55-flt5) of diamine **12**.
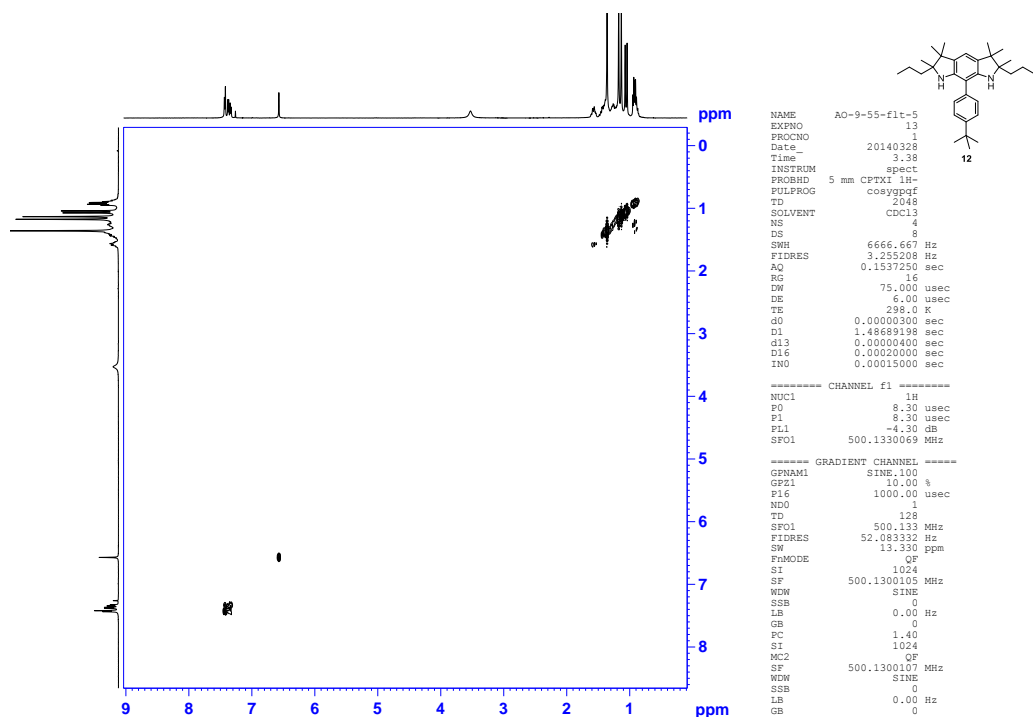


**Figure B10.** $^{1}$H–$^{1}$H COSY experiment (500 MHz, chloroform-*d*, label: AO-9-55-flt5) of diamine **12**.
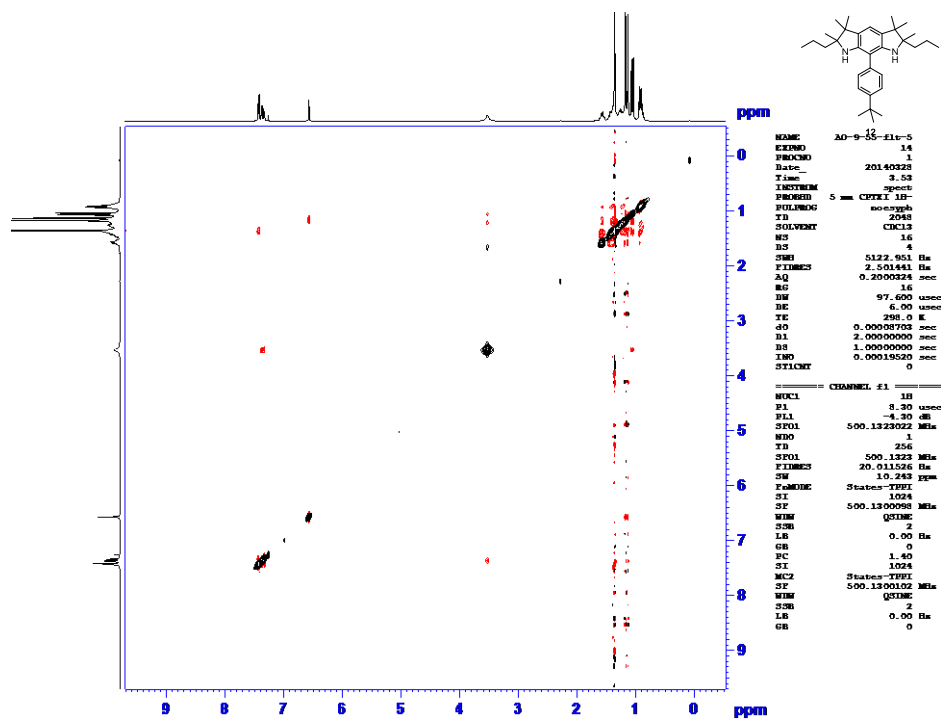
**Figure B11.** $^1$H–$^1$H NOESY experiment (500 MHz, chloroform-*d*, label: AO-9-55-flt5) of diamine **12**.
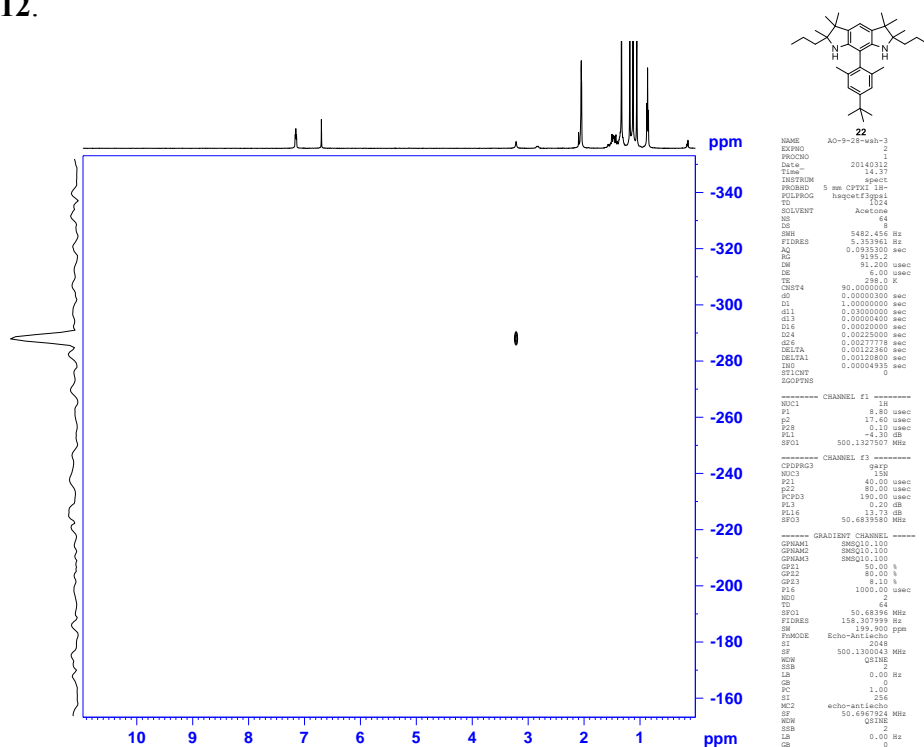


**Figure B12.** $^1$H–$^{15}$N HSQC experiment (500 MHz, acetone-*d*$_6$, label: AO-9-28-wsh3) of diamine **22**.
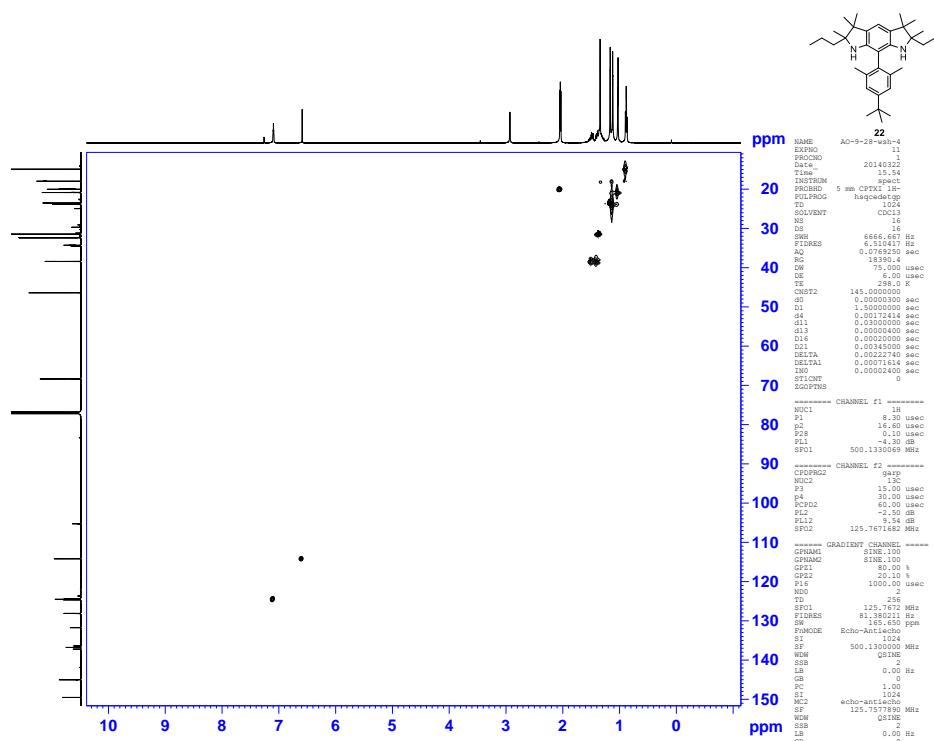
**Figure B13.** $^{1}$H–$^{13}$C HSQC experiment (500 MHz, chloroform-*d*, label: AO-9-28-wsh4) of diamine **22**.
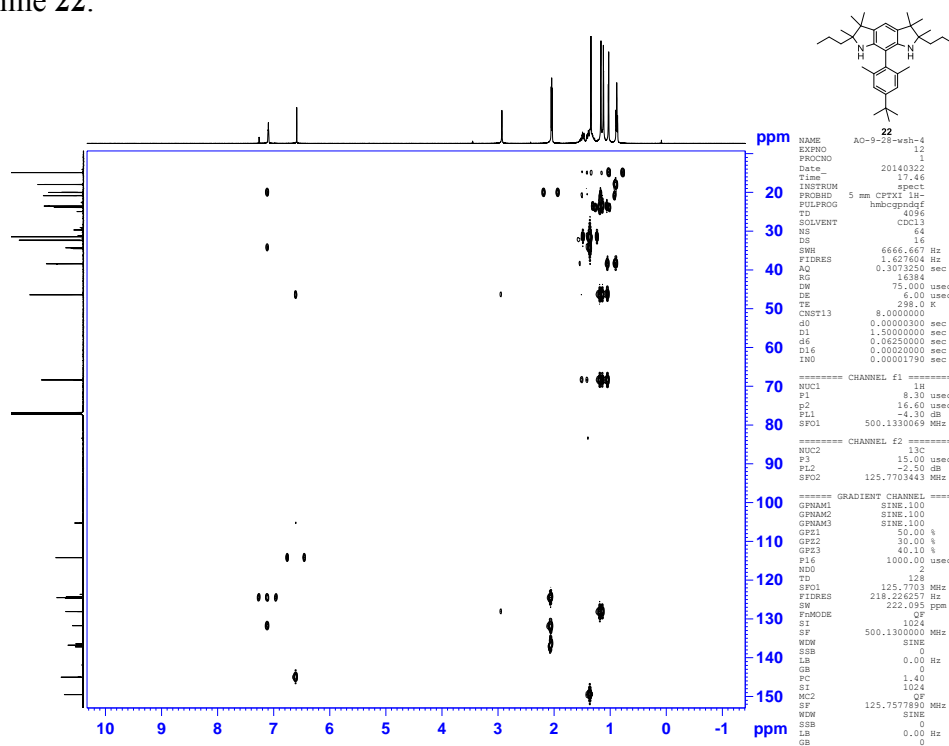


**Figure B14.** $^{1}$H–$^{13}$C HMBC experiment (500 MHz, chloroform-*d*, label: AO-9-28-wsh4) of diamine **22**.
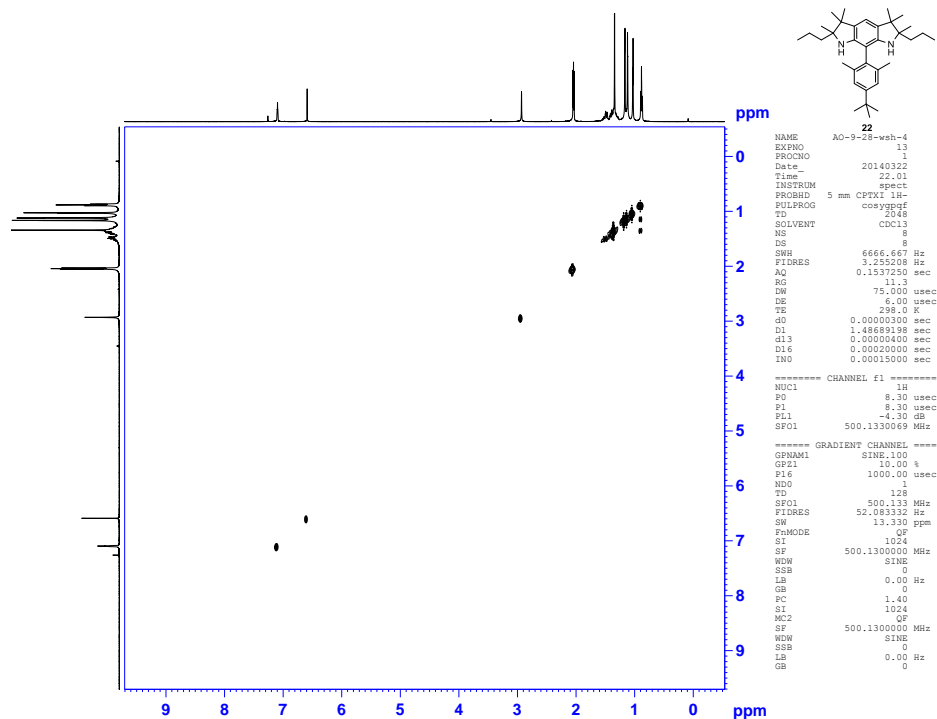
**Figure B15.** ¹H–¹H COSY experiment (500 MHz, chloroform-*d*, label: AO-9-28-wsh4) of diamine **22**.
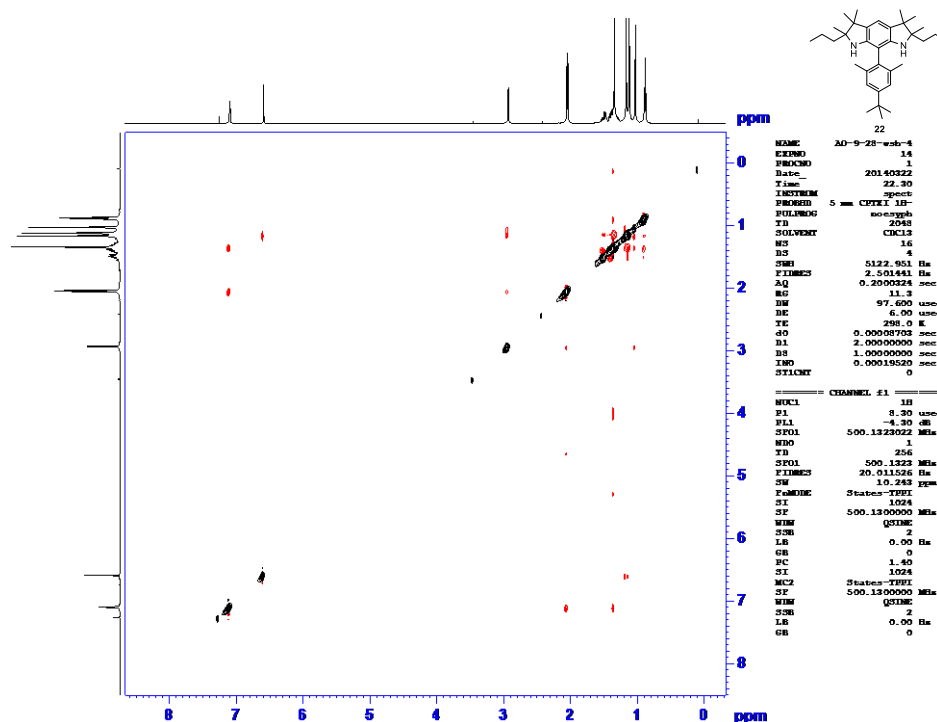


**Figure B16.** ¹H–¹H NOESY experiment (500 MHz, chloroform-*d*, label: AO-9-28-wsh4) of diamine **22**.
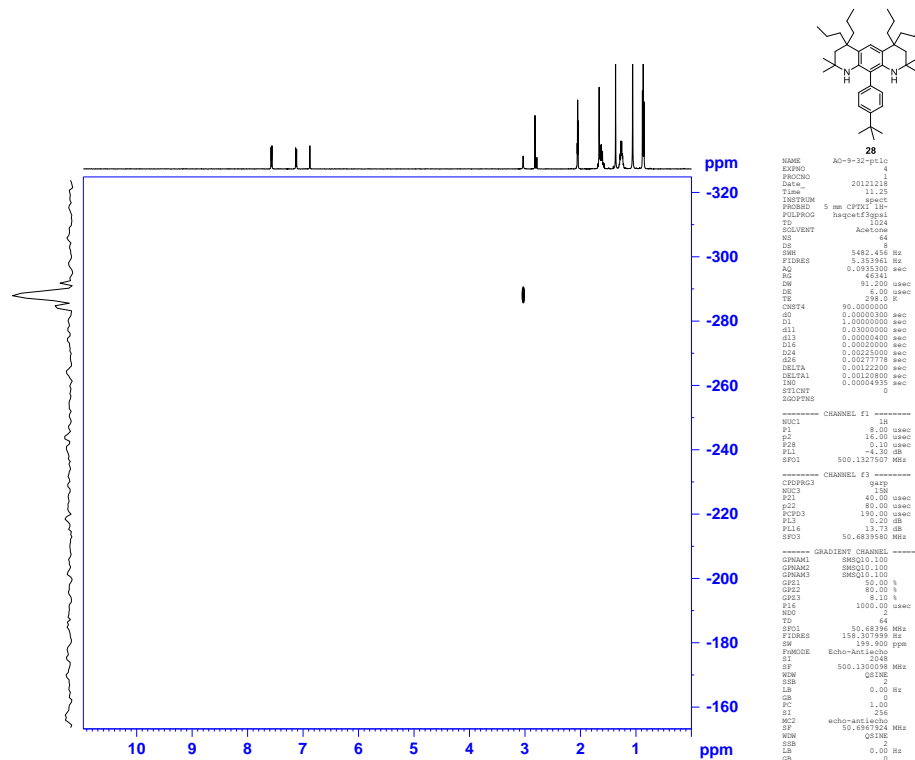
**Figure B17.** $^1$H–$^{15}$N HSQC experiment (500 MHz, acetone-$d_6$, label: AO-9-32-ptlc) of diamine **28**.
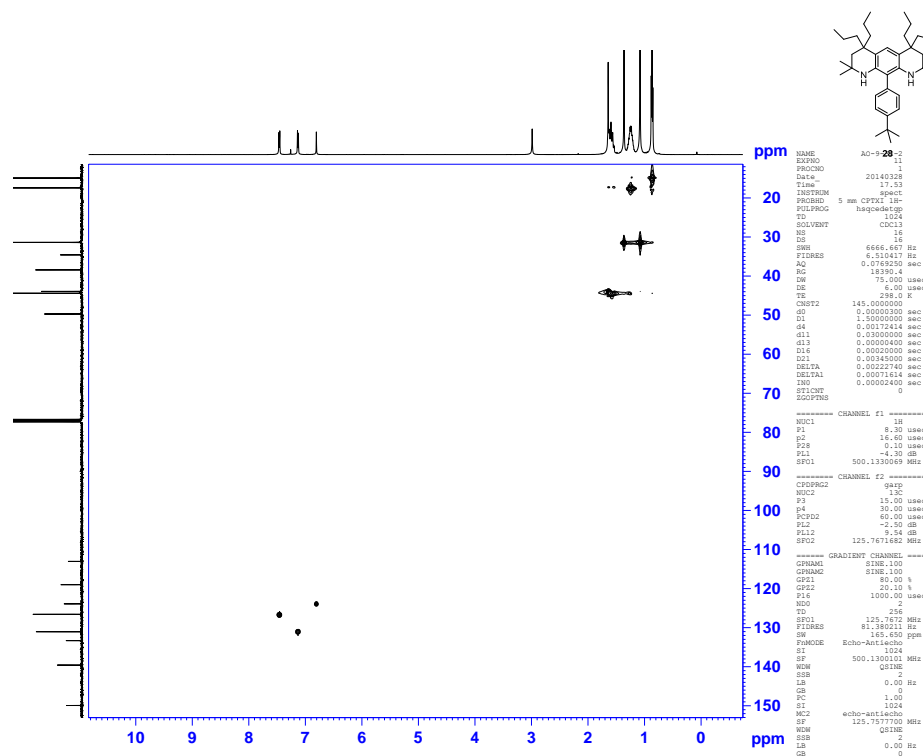


**Figure B18.** $^1$H–$^{13}$C HSQC experiment (500 MHz, chloroform-$d$, label: AO-9-32-2) of diamine **28**.
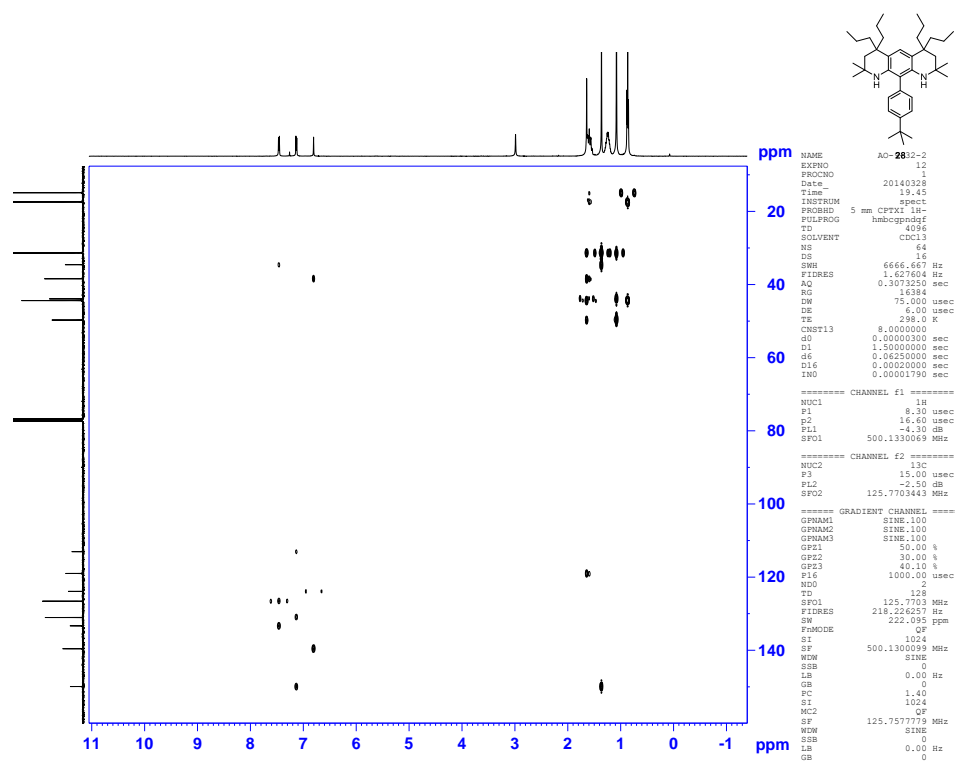
**Figure B19.** $^1H$–$^{13}C$ HMBC experiment (500 MHz, chloroform-*d*, label: AO-9-32-2) of diamine **28**.
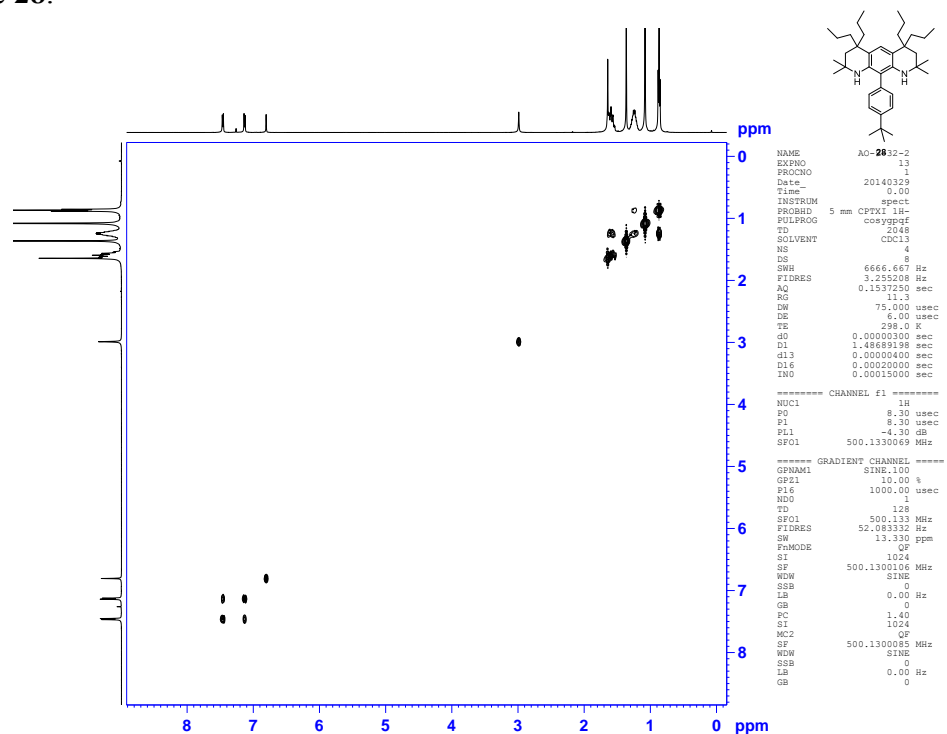


**Figure B20.** $^1H$–$^1H$ COSY experiment (500 MHz, chloroform-*d*, label: AO-9-32-2) of diamine **28**.
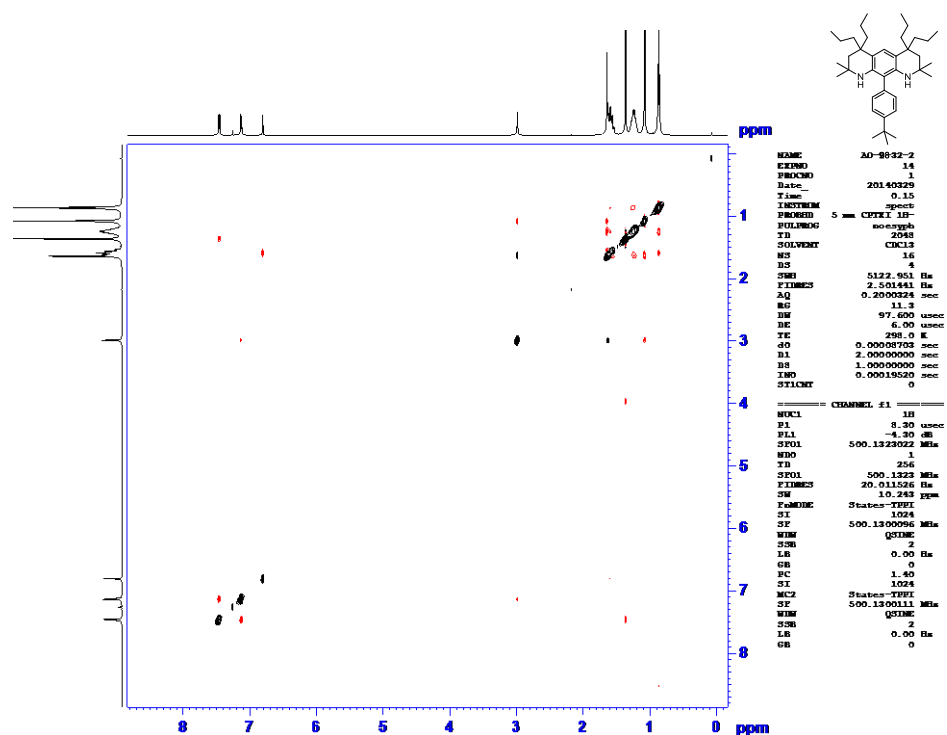
**Figure B21.** $^1$H–$^1$H NOESY experiment (500 MHz, chloroform-$d$, label: AO-9-32-2) of diamine **28**.
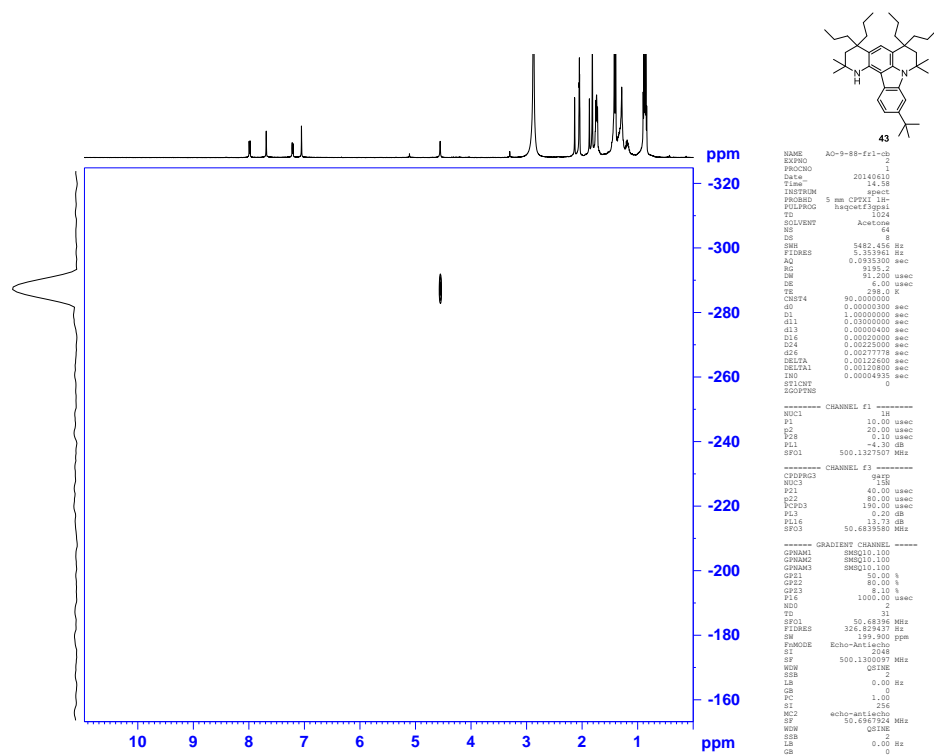


**Figure B22.** $^1$H–$^{15}$N HSQC experiment (500 MHz, acetone-$d_6$, label: AO-9-88-fr1-cb) of by-product **43**.
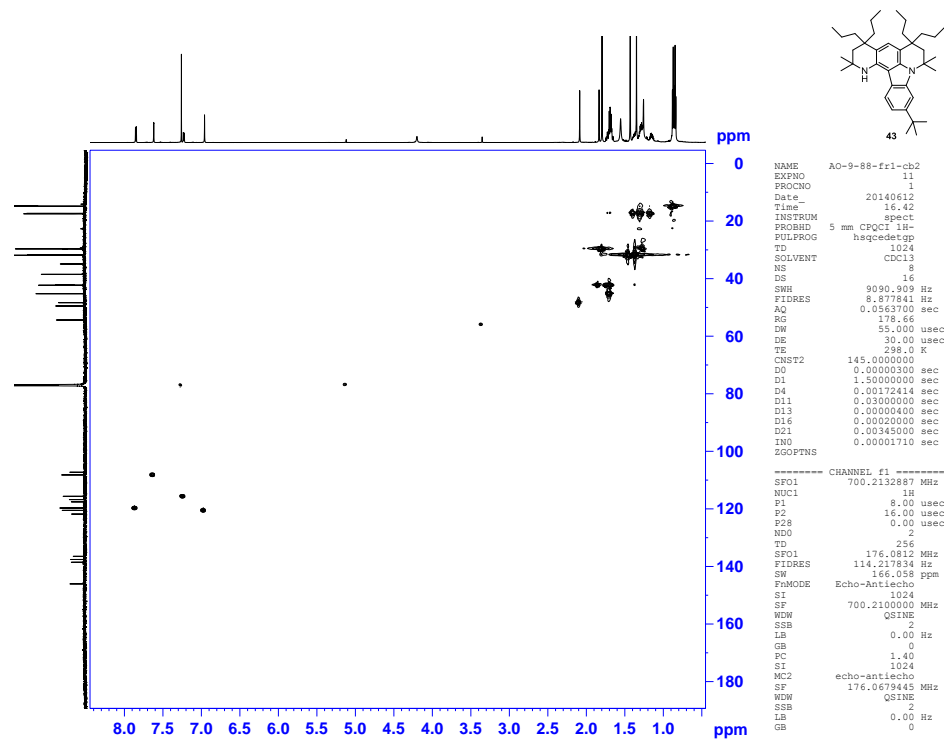
**Figure B23.** $^1$H–$^{13}$C HSQC experiment (500 MHz, chloroform-*d*, label: AO-9-88-fr1-cb2) of by-product **43**.
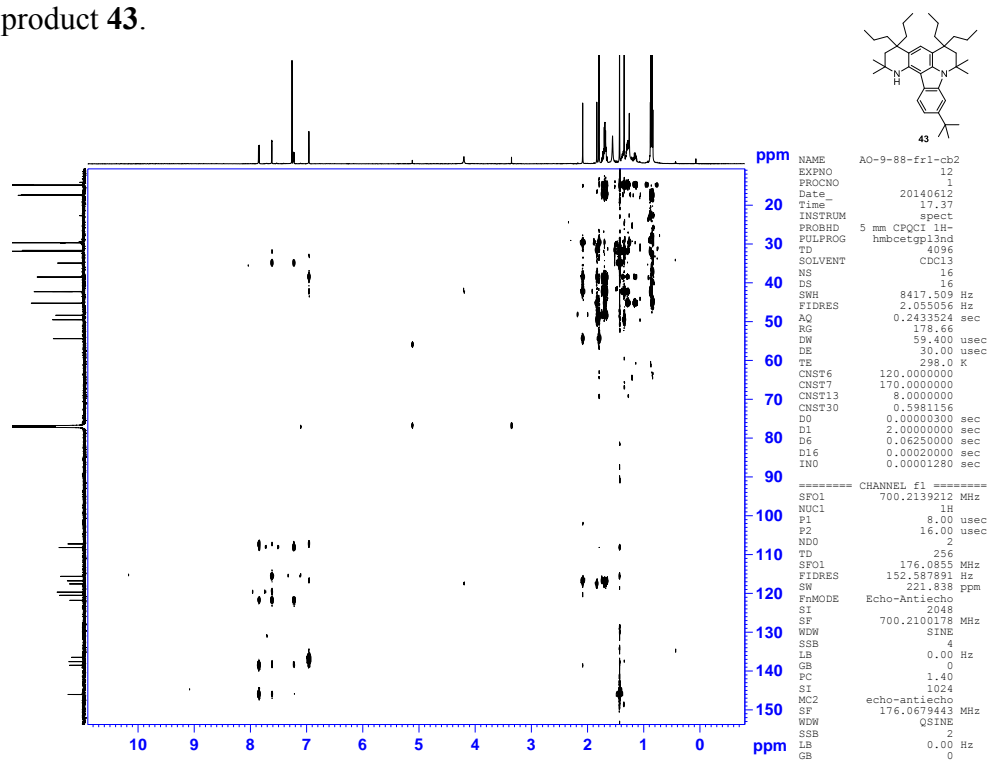


**Figure B24.** $^1$H–$^{13}$C HMBC experiment (500 MHz, chloroform-*d*, label: AO-9-88-fr1-cb2) of by-product **43**.
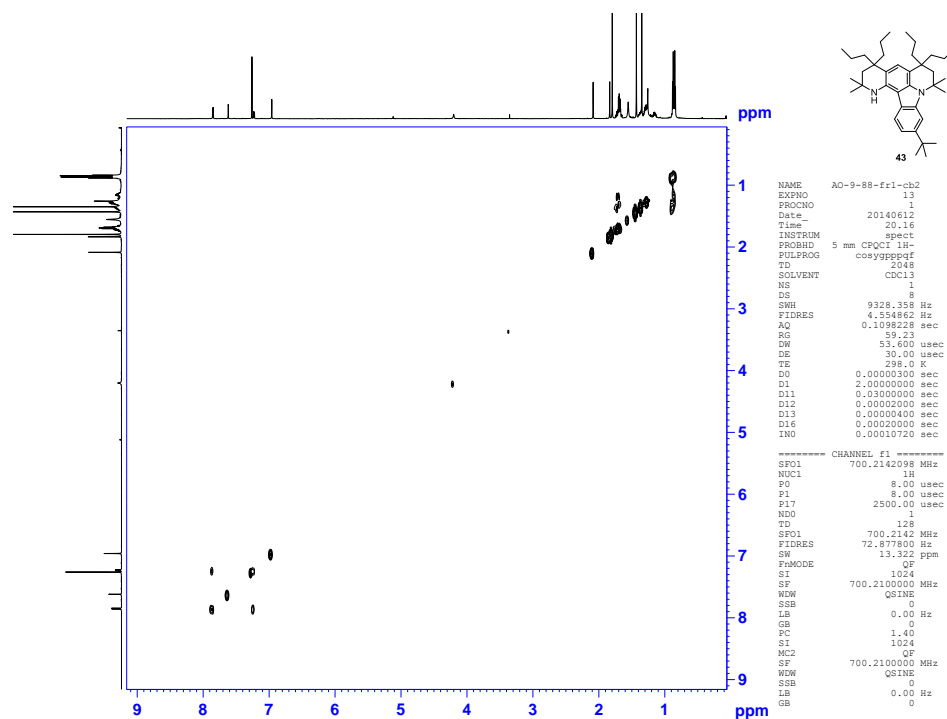
**Figure B25.** ^{1}H–^{1}H COSY experiment (500 MHz, chloroform-*d*, label: AO-9-88-fr1-cb2) of by-product **43**.
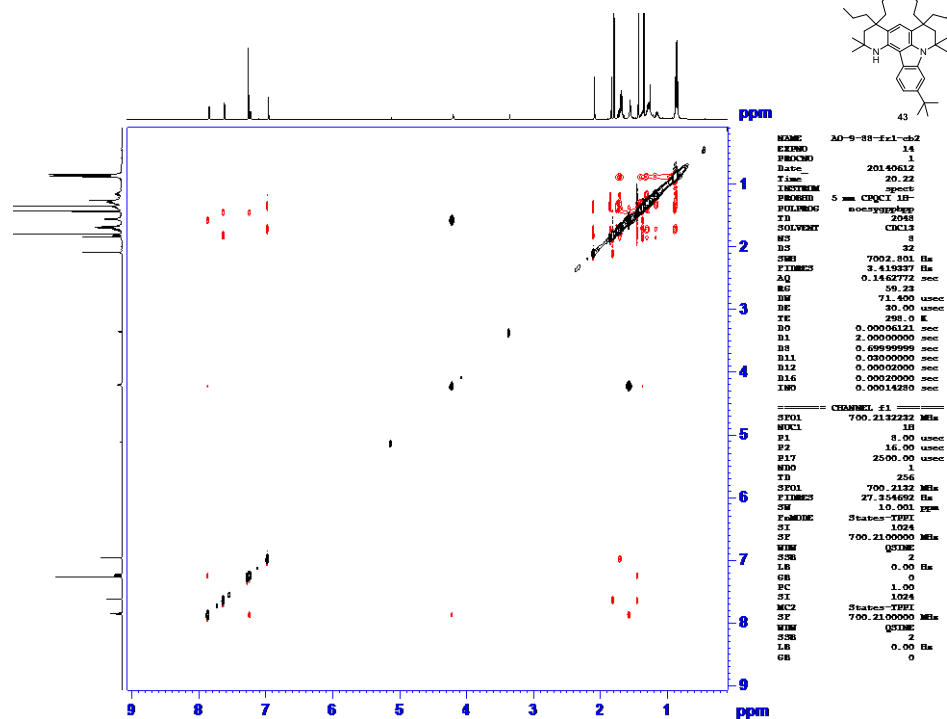


**Figure B26.** [1]H–[1]H NOESY experiment (500 MHz, chloroform-*d*, label: AO-9-88-fr1-cb2) of by-product **43**.

**Appendix C**

**EPR, ^{1}H NMR Spectra, and Decay Experiments**
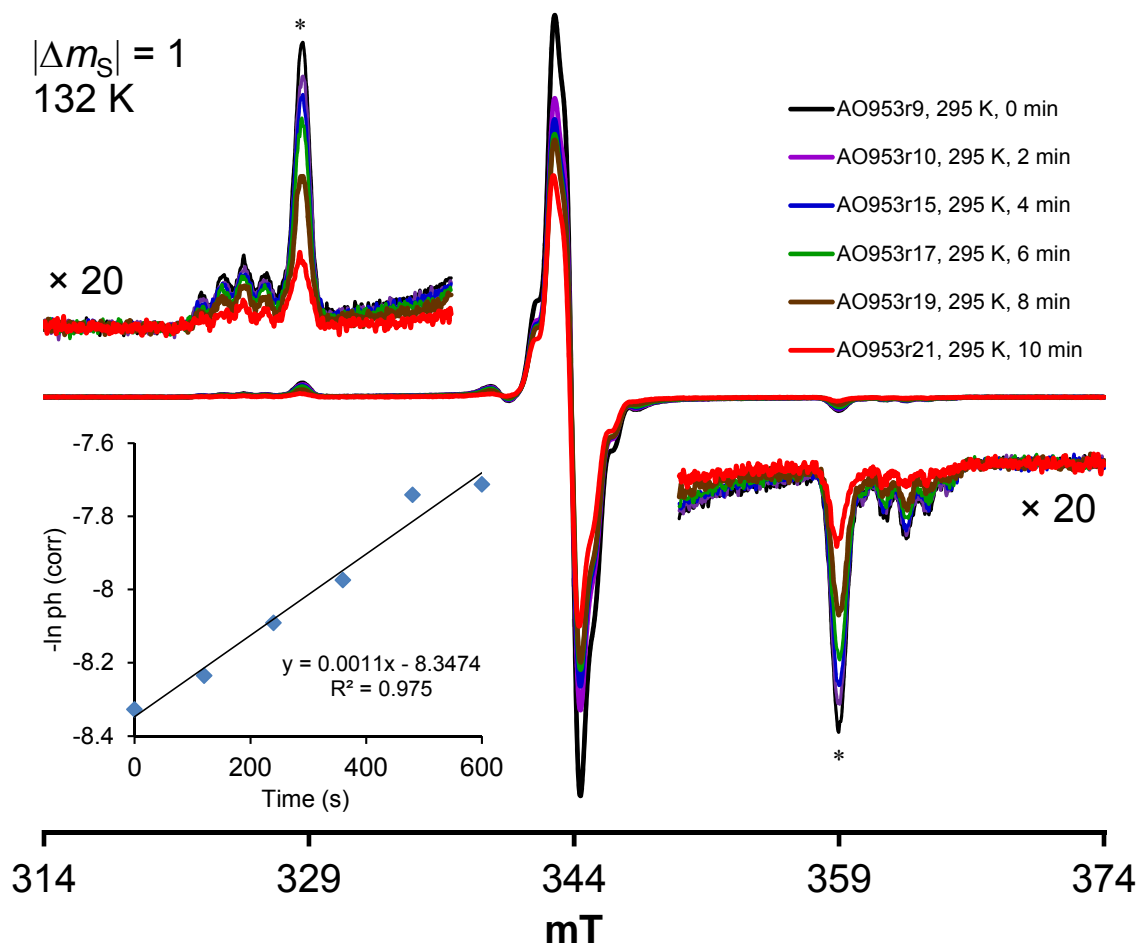
**Figure C1.** Decay kinetics for diradical **9** in 2-MeTHF at room temperature (AO-9-53).
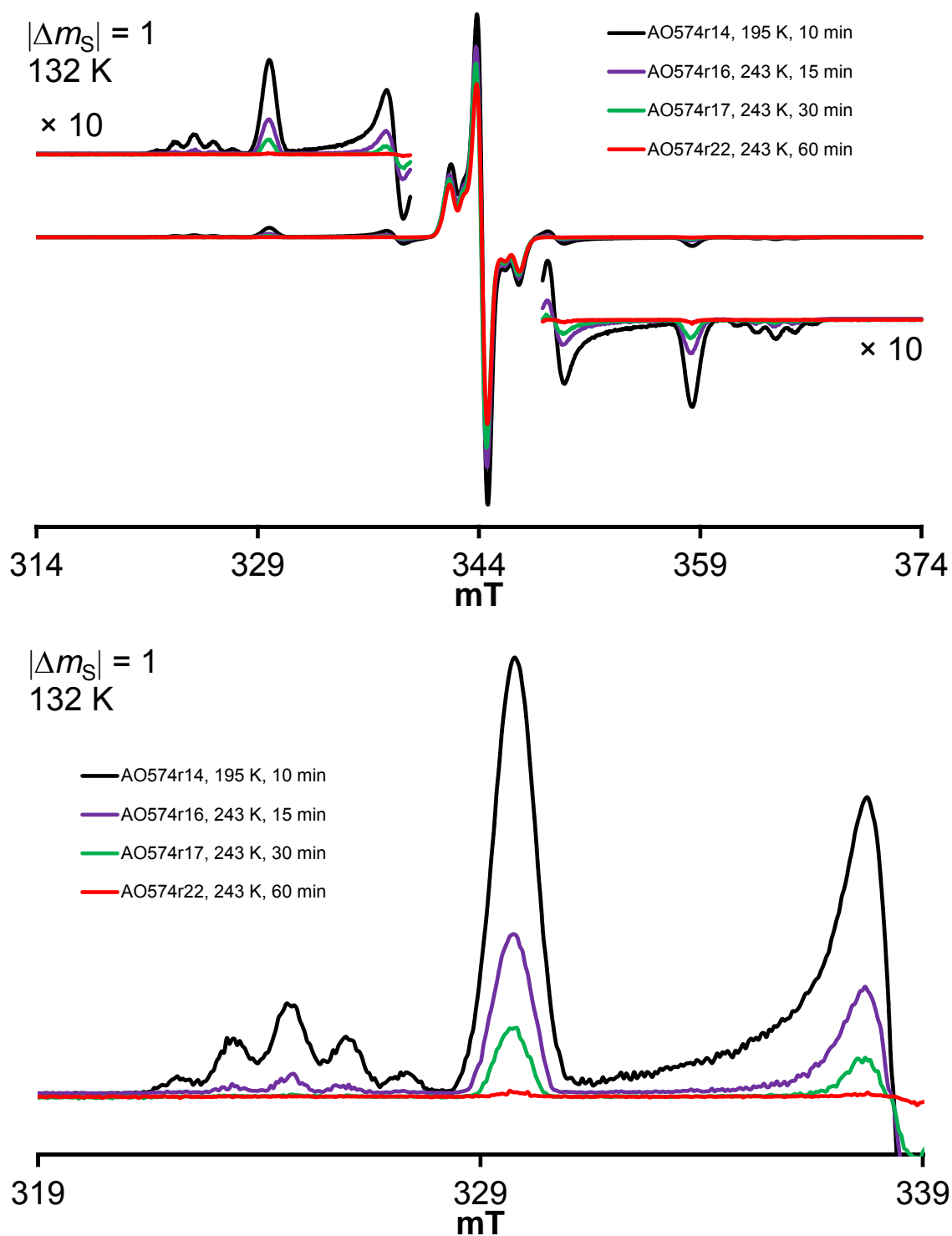
**Figure C2.** Decay kinetics for diradical **10** in 2-MeTHF at 195 and 243 K (AO-5-74).

$|\Delta m_S| = 1$
132 K

× 5

- AO983r33, 4.89 mM
- AO983r35, 246 K, 15 min
- AO983r37, 246 K, 30 min
- AO983r39, 246 K, 45 min
- AO983r41, 246 K, 60 min

× 5

314    329    344    359    374

**mT**

$|\Delta m_S| = 1$
132 K

- AO983r33, 4.89 mM
- AO983r35, 246 K, 15 min
- AO983r37, 246 K, 30 min
- AO983r39, 246 K, 45 min
- AO983r41, 246 K, 60 min

317    322    327    332    337

**mT**
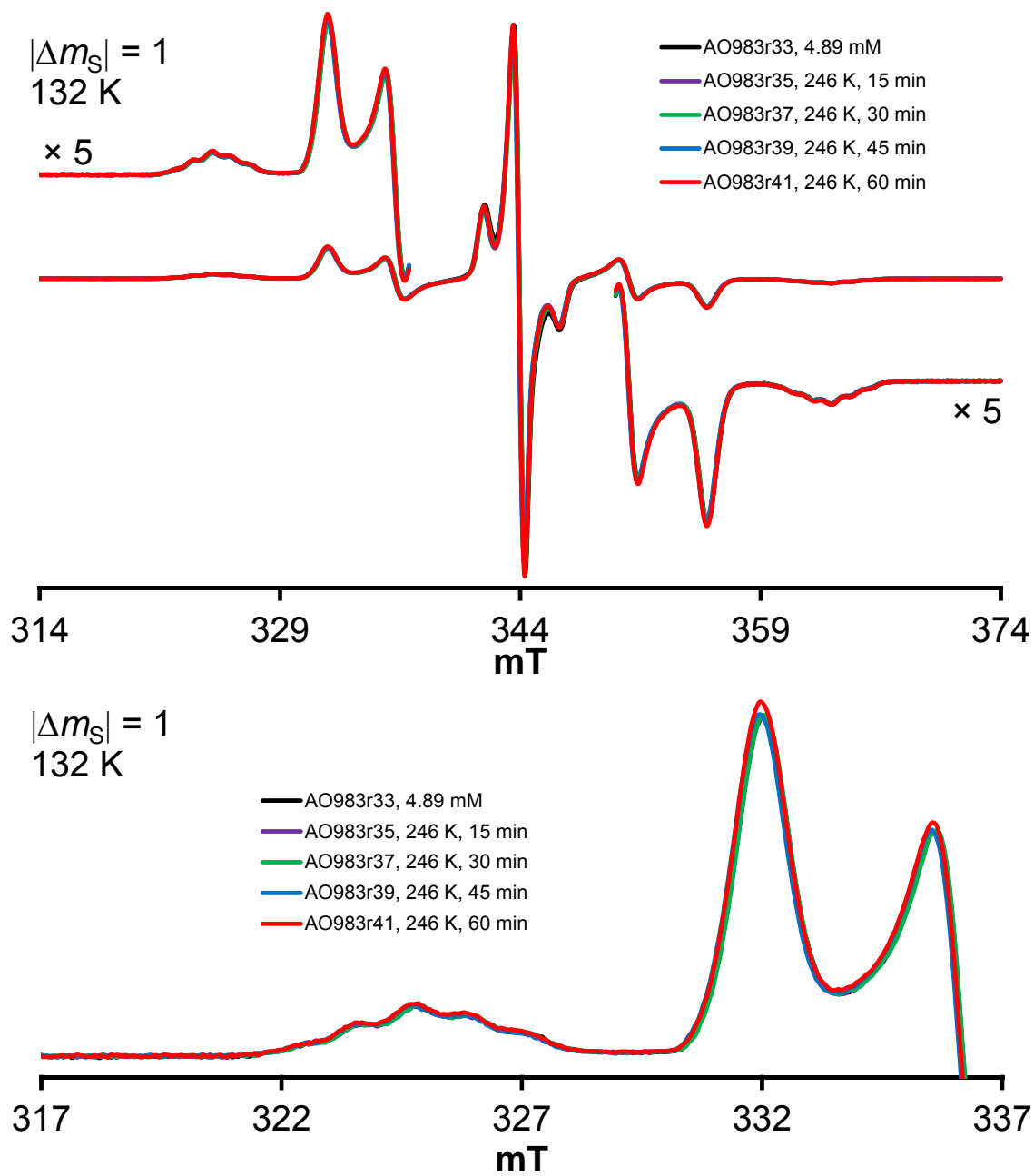
**Figure C3.** Decay kinetics for 5.1 mM diradical **11** in 2-MeTHF at 246 K (AO-9-83).
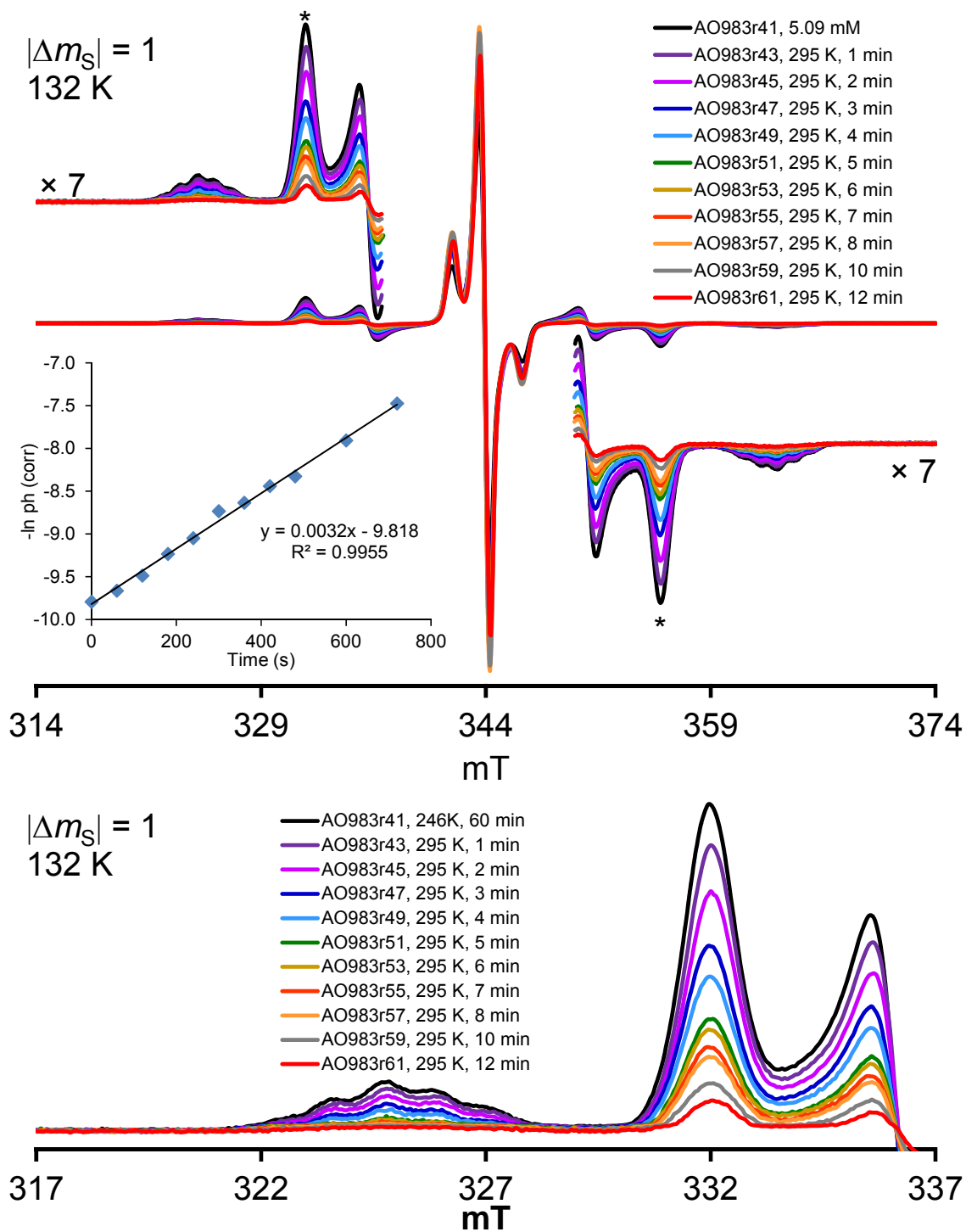
**Figure C4.** Decay kinetics for 5.1 mM diradical **11** in 2-MeTHF at room temperature (AO-9-83).

Plot inset: $y = 0.0028x - 8.9757$, $R^2 = 0.9792$
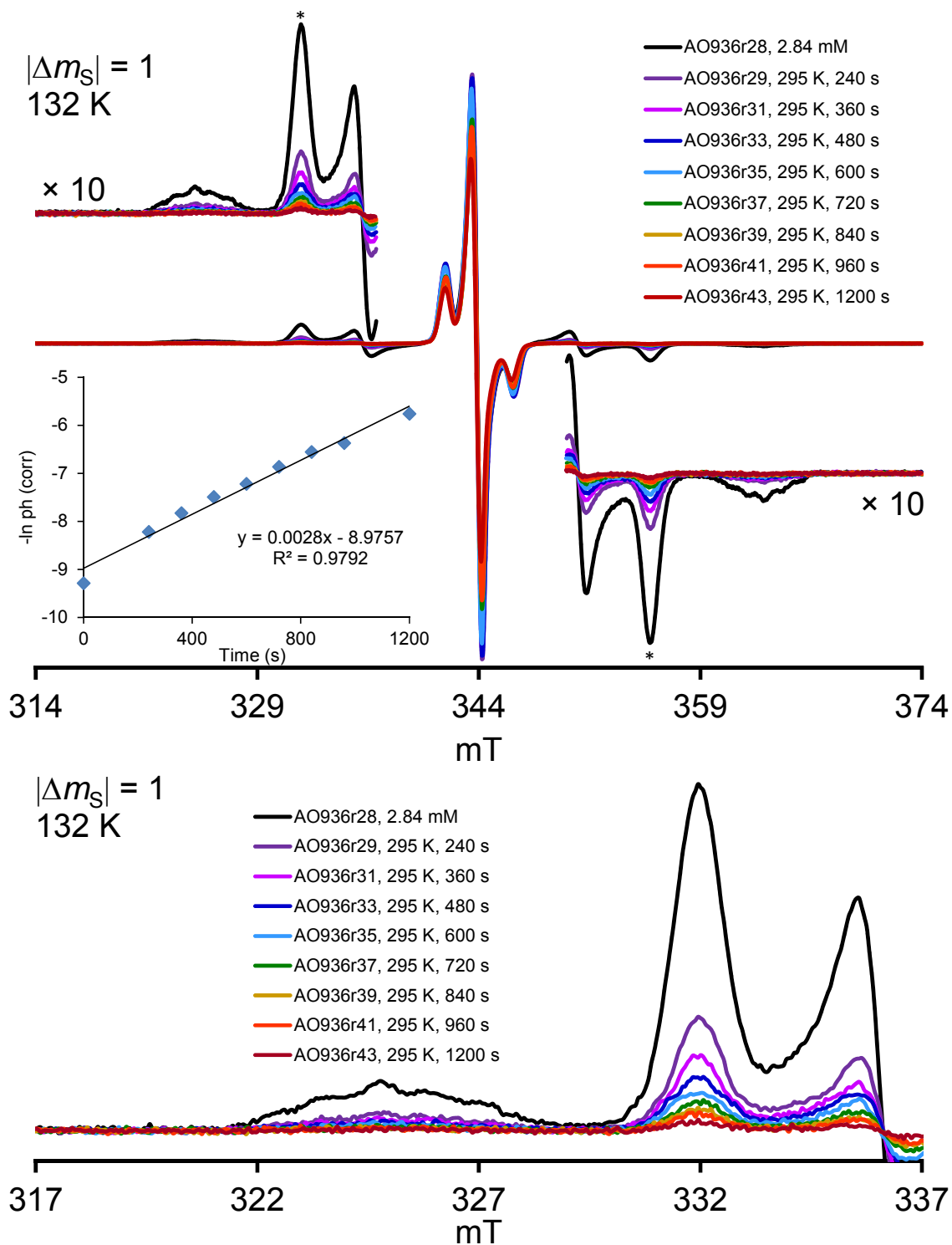
**Figure C5.** Decay kinetics for 2.8 mM diradical **11** in 2-MeTHF at room temperature (AO-9-36).

The NMR peak labels along the top include:
7.872, 7.856, 7.826, 7.810, 7.450, 7.440, 7.433, 7.423, 6.903, 3.702, 1.554, 1.545, 1.530, 1.514, 1.505, 1.481, 1.449, 1.275, 1.253, 1.248, 1.220, 1.214, 0.929, 0.910, 0.899, 0.838, 0.758, 0.743, 0.729, 0.673, 0.659, 0.644

Acquisition parameters:

```
NAME       AO-3-07-diaminyl
EXPNO                     2
PROCNO                    1
Date_              20090406
Time                  19.39
INSTRUM               spect
PROBHD    5 mm CPTXI 1H-
PULPROG               zg30
TD                    65536
SOLVENT               C6D6
NS                      128
DS                        2
SWH             10330.578 Hz
FIDRES           0.157632 Hz
AQ             3.1720407 sec
RG                     35.9
DW                48.400 usec
DE                 6.00 usec
TE                  298.0 K
D1            1.00000000 sec
TD0                       1

======== CHANNEL f1 ========
NUC1                     1H
P1                 8.30 usec
PL1                -4.30 dB
SFO1          500.1330885 MHz
SI                    32768
SF            500.1300618 MHz
WDW                      EM
SSB                       0
LB                  0.30 Hz
GB                        0
PC                     1.00
```

**Figure C6.** $^1$H NMR spectrum (500 MHz, aromatic region, benzene-$d_6$, label: AO-3-07-diaminyl) of the crude reaction mixture following EPR spectroscopic monitoring of aminyl diradical **9**,  The $^1$H NMR spectrum indicates that the major product is diamine **12**.
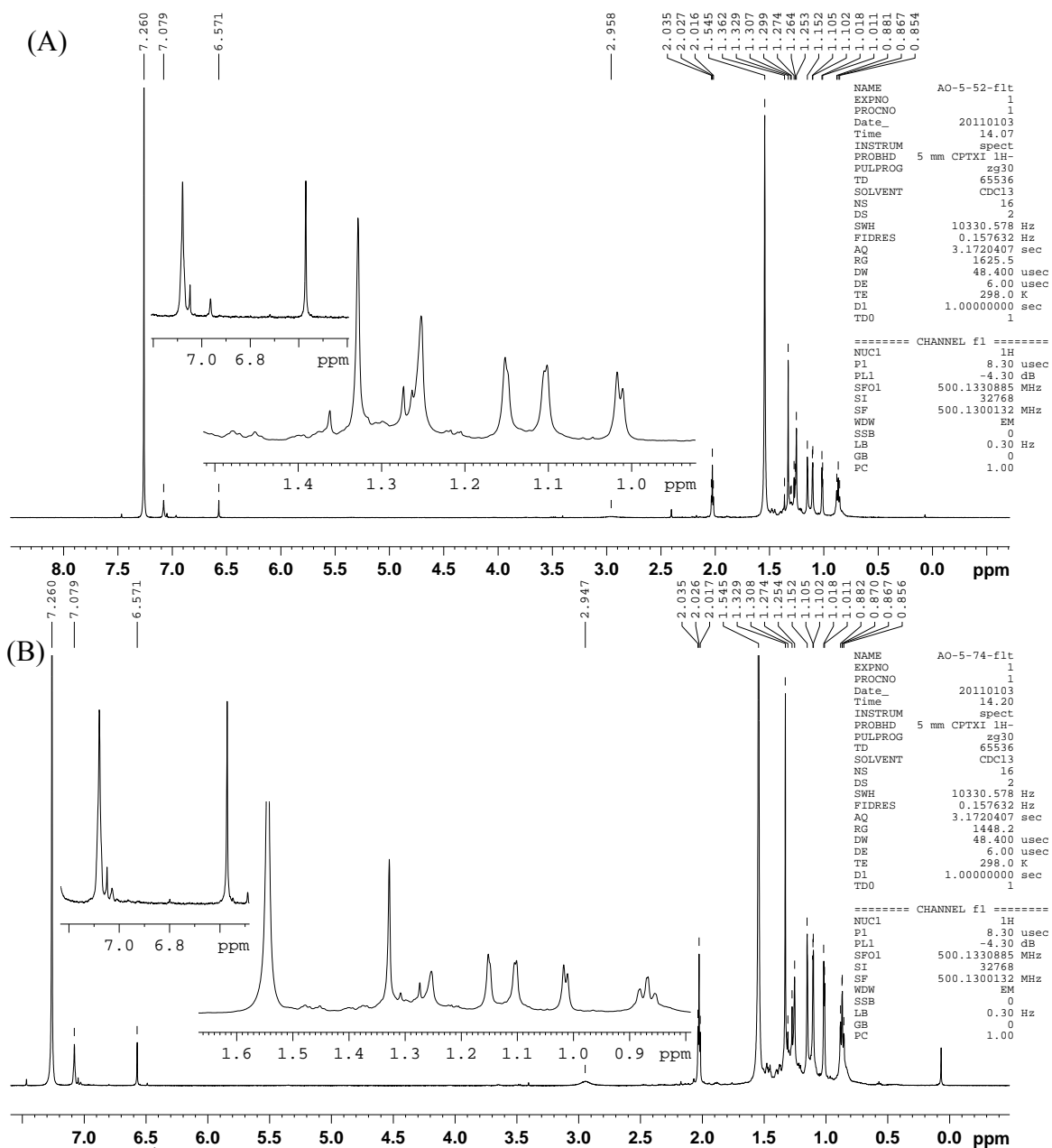
**Figure C7.** ¹H NMR spectra (500 MHz, chloroform-*d*, label: (A) AO-5-52-flt, (B) AO-5-74-flt) of the crude reaction mixture following EPR spectroscopic monitoring of aminyl diradical **10**. The ¹H NMR spectra indicate that the major product is diamine **22**.
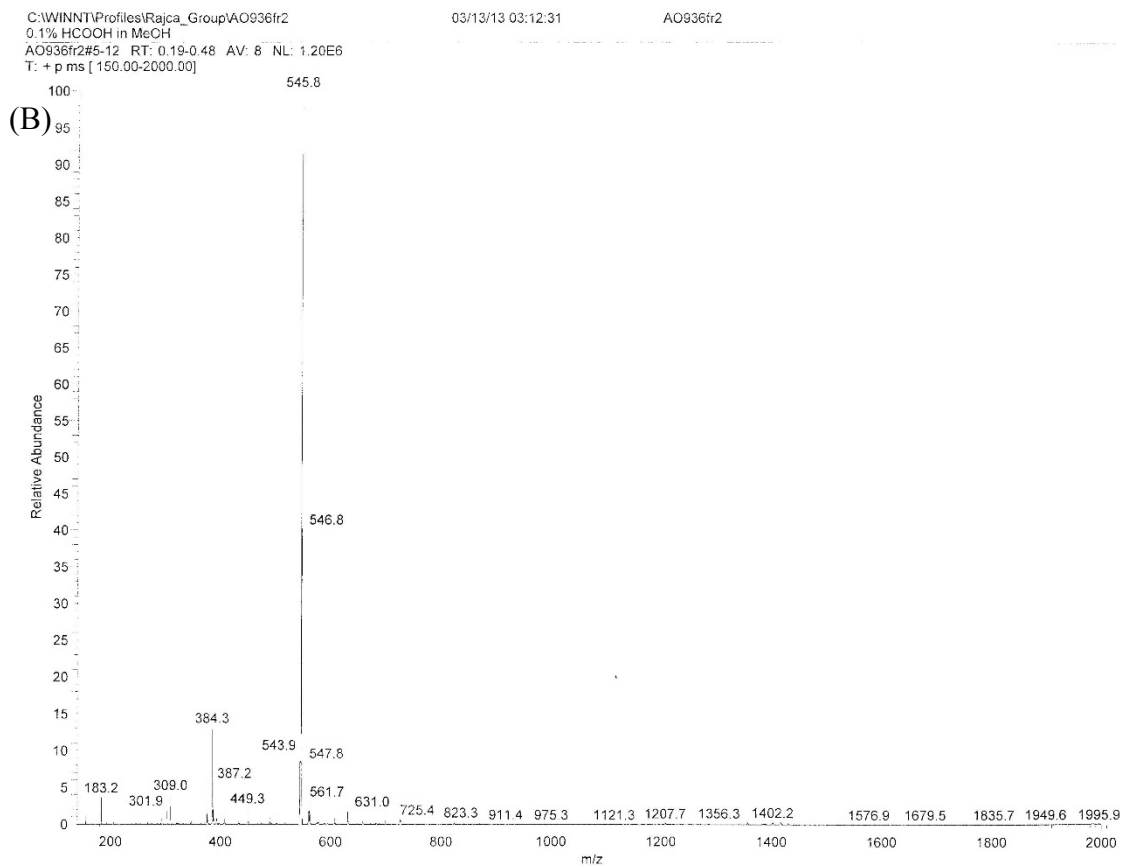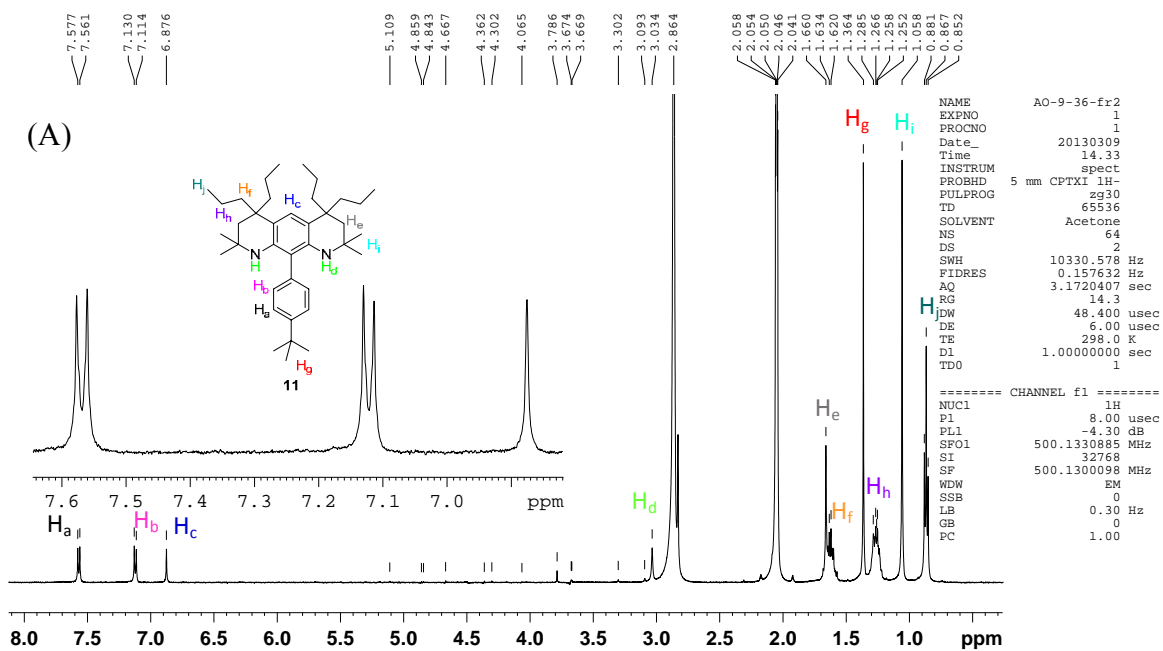
**Figure C8.** (A) $^1$H NMR spectrum (500 MHz, acetone-$d_6$, label: AO-9-36-fr2) of the purified sample following EPR spectroscopic monitoring of aminyl diradical **28**. (B) ESI MS of the purified sample. Fraction 2 corresponds to diamine **28**.
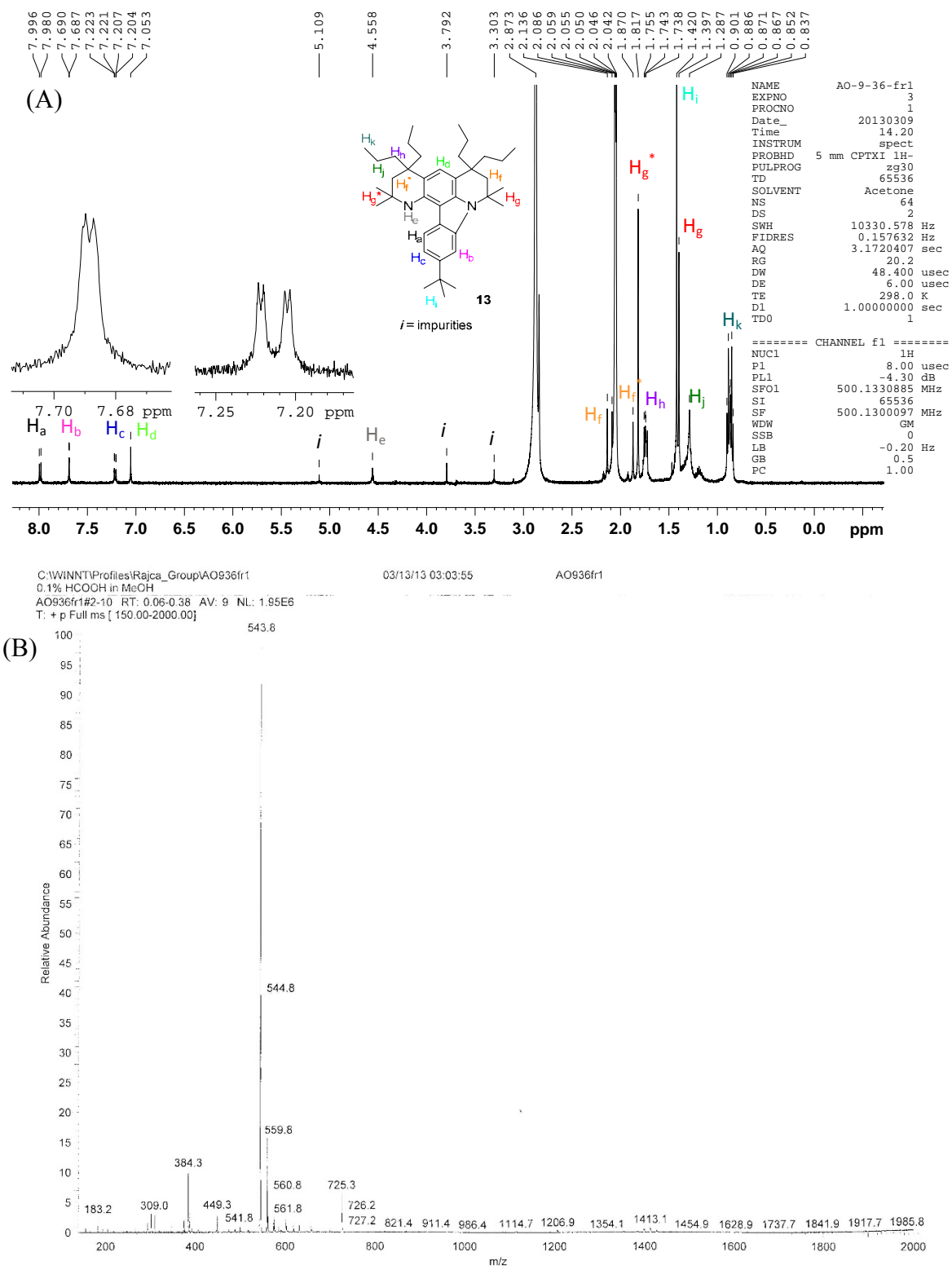
**Figure C9.** (A) $^1$H NMR spectrum (500 MHz, acetone-$d_6$, label: AO-9-36-fr1) of the purified sample following EPR spectroscopic monitoring of aminyl diradical **11**. (B) ESI MS of the purified sample. The $^1$H NMR spectrum and MS spectrum indicate that the major product is by-product **43**.
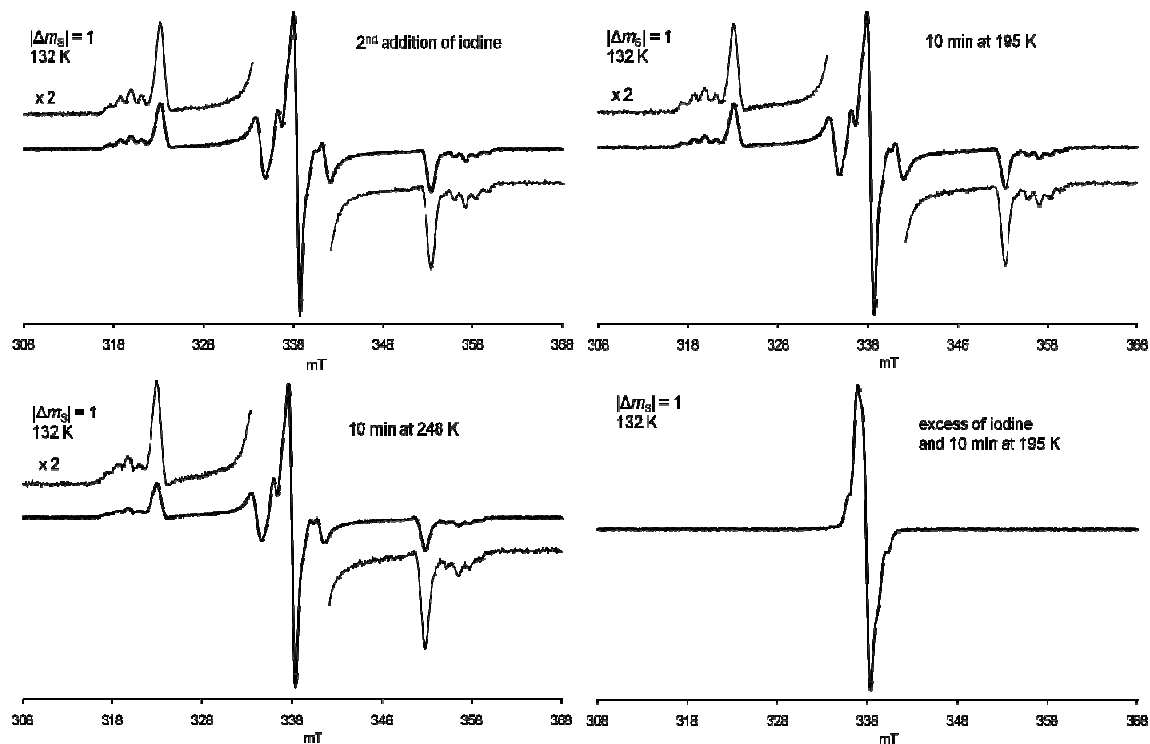
**Figure C10.** Reaction of aminyl diradical **9** with iodine in 2-MeTHF monitored by EPR spectroscopy. EPR (X-Band, $\nu$ = 9.4863 GHz; $\nu$ = 9.4834 GHz; $\nu$ = 9.4759 GHz; $\nu$ = 9.4732 GHz) spectra in 2-MeTHF at 132−133 K (5-mm EPR tube, label: AO328r3/r5/r6/r7). Sequence of the EPR spectra: (1) top-left, after the 2$^{nd}$ addition of iodine; (2) top-right, after annealing at 195 K (–78 °C) for 10 min; (3) after annealing at 246 K (–27 °C) for 10 min; (4) after addition of an excess of iodine, and then annealing at 195 K (–78 °C) for 10 min.
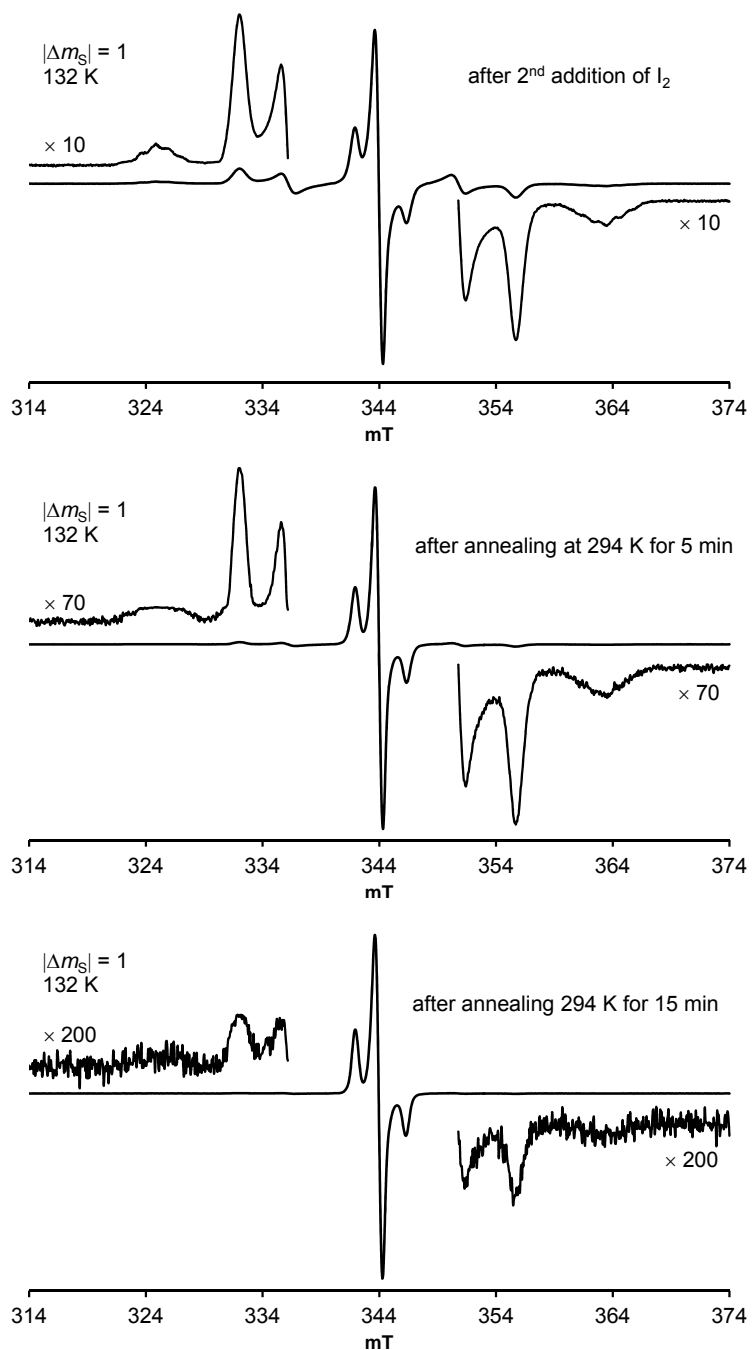
**Figure C11.** Reaction of aminyl diradical **11** with iodine in 2-MeTHF monitored by EPR spectroscopy. EPR (X-Band, $\nu$ = 9.6428 GHz (top); $\nu$ = 9.6430 GHz (middle); $\nu$ = 9.6423 GHz (bottom)) spectra in 2-MeTHF at 132−133 K (5-mm EPR tube, label: AO876r5/r12/r13). Sequence of the EPR spectra: (top) after the 2nd addition of iodine; (middle) after annealing at 294 K for ~ 5 min; (3) after annealing at 294 K for 15 min.
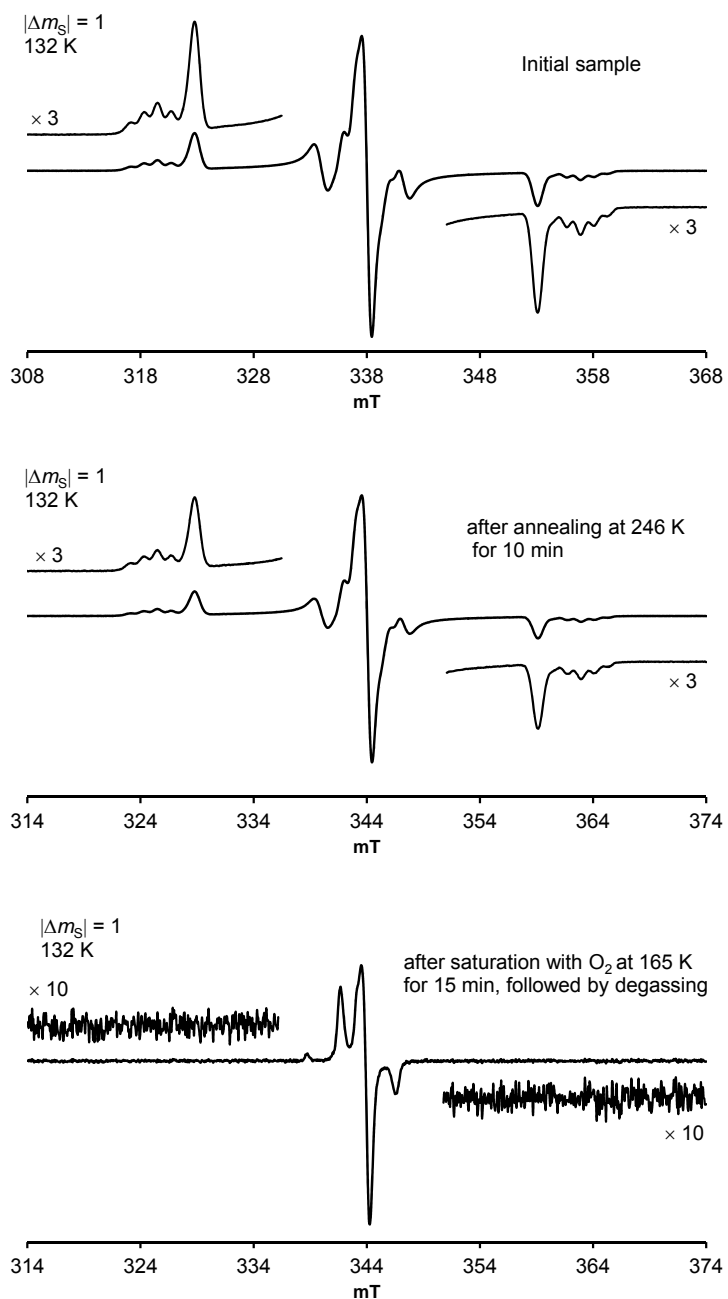
**Figure C12. (A)** Reaction of aminyl diradical **9** with oxygen in 2-MeTHF (in the presence of LiI). EPR (X-Band, $\nu$ = 9.4762 GHz (top); $\nu$ = 9.6447 GHz (middle); $\nu$ = 9.6435 GHz (bottom)) spectra in 2-MeTHF at 132 K (5-mm tube, label: AO367). (top) Initial sample (label: AO367r1/r2). (middle) After annealing at 246 K (–27 °C) for 10 min (label: AO367r3). (bottom) After saturation with $O_2$ at 168 K (–105 °C) for 15 min, followed by degassing (label: AO367r5).
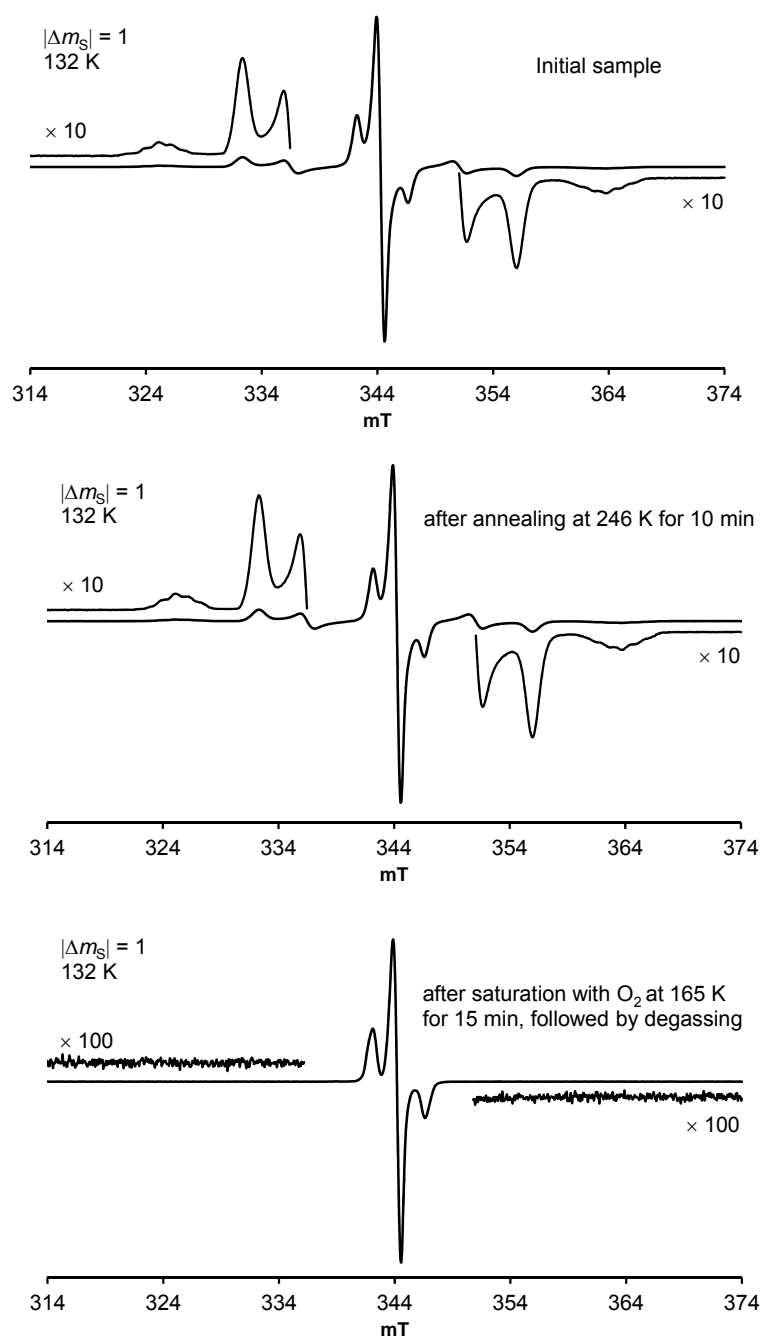
**Figure C12. (B)** Reaction of aminyl diradical **11** with oxygen in 2-MeTHF (in the presence of LiI). EPR (X-Band, $\nu$ = 9.6520 GHz (top); $\nu$ = 9.6504 GHz (middle); $\nu$ = 9.6499 GHz (bottom)) spectra in 2-MeTHF at 132 K (5-mm tube, label: AO941). (top) Initial sample (label: AO941r7). (middle) After annealing at 246 K (–27 °C) for 10 min (label: AO941r9). (bottom) After saturation with $O_2$ at 165 K (–108 °C) for 15 min, followed by degassing (label: AO941r10).
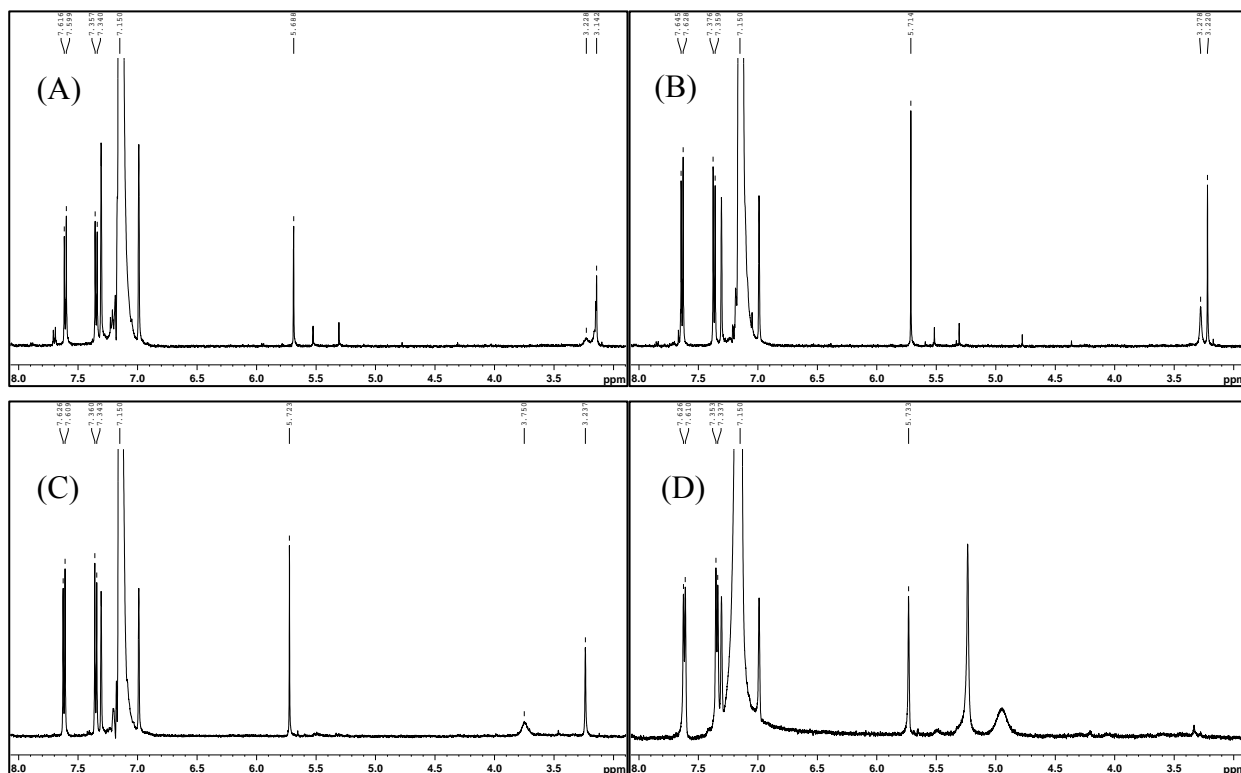
**Figure C13.** $^1$H NMR spectra (500 MHz, benzene-$d_6$, 3–8 ppm) of diamagnetic "diol product", isolated after EPR monitoring of reaction of aminyl diradical **9** with oxygen as illustrated in the preceding figure (Figure S13). (A). Fraction 1, label: AO-3-67-ptlc-fr1-bz. (B). Fraction 2, label: AO-3-67-ptlc-fr2-bz. (C). Fraction 3, label: AO-3-67-ptlc-fr3-bz.  (D), Fraction 3 after D$_2$O exchange, label: AO-3-67-ptlc-fr3-bz-ex.

**AO-3-67-CHK**
57240 1028 (17.136) Cm (1000:1028-63:176)

TOF MS EI+
7.89e4

Chemical Formula: $C_{32}H_{48}N_2O_2$
Exact Mass: 492.3716
Molecular Weight: 492.7480
m/z: 492.3716 (100.0%), 493.3749 (34.6%), 494.3783 (5.8%)
Elemental Analysis: C, 78.00; H, 9.82; N, 5.69; O, 6.49
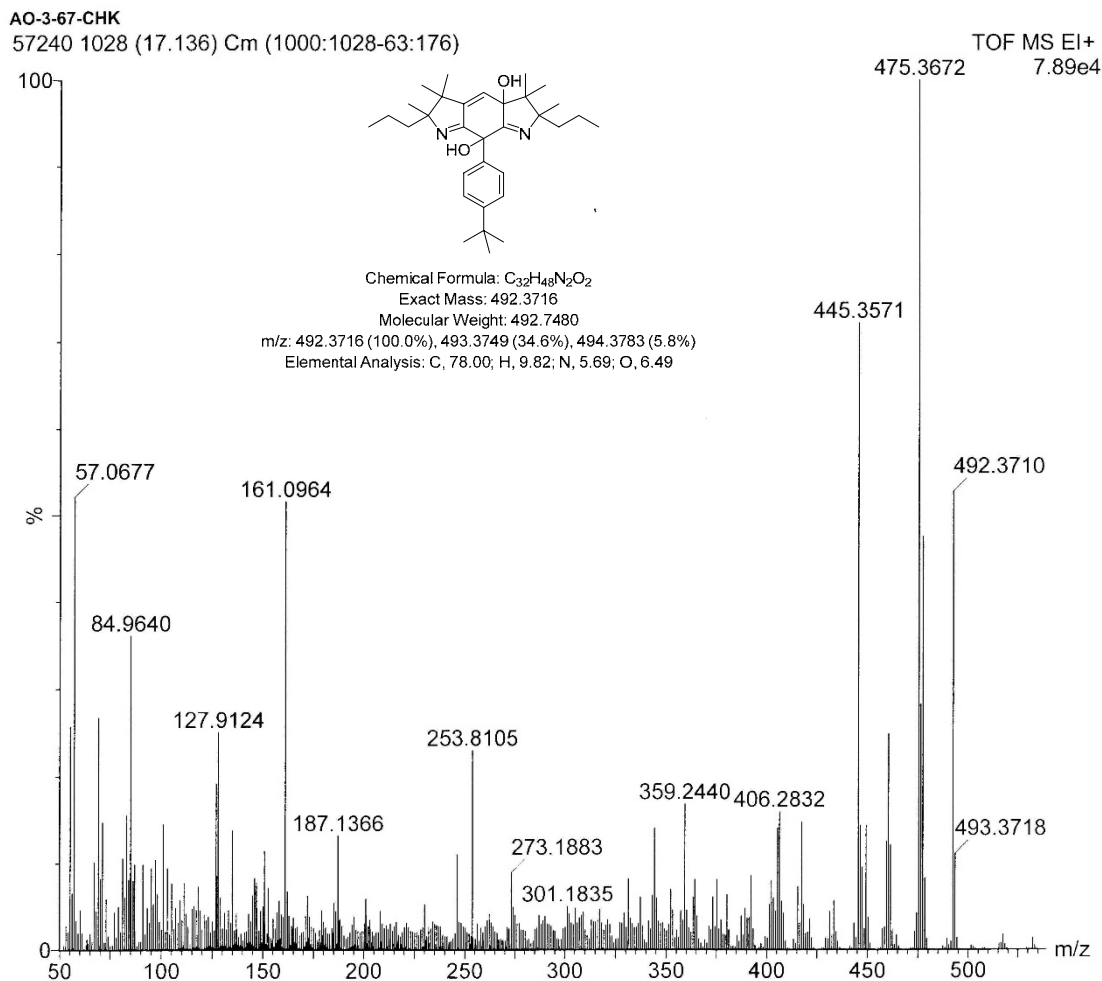
**Figure C13. (E)** HR EI mass spectrum of the product obtaining after the reaction of aminyl diradical **9** with oxygen.

**Figure C14.** (A) ¹H NMR spectrum (500 MHz, acetone-$d_6$, label: AO-9-41-crd) of the crude reaction mixture following reaction with oxygen of aminyl diradical **11**. (B) ¹H NMR (500 MHz, acetone-$d_6$, label: AO-9-41-fr1) spectrum of the fraction 1 corresponds to by-product **43**.

**Figure C14. (cont)** (C) $^1$H NMR (500 MHz, acetone-$d_6$, label: AO-9-41-fr2) spectrum of the purified sample (fraction 2) corresponds to 4-*tert*-butylphenyldiamine **28**. (D) $^1$H NMR (500 MHz, acetone-$d_6$, label: AO-9-41-fr3) spectrum of the purified sample (fraction 3) may correspond to the product of addition of O$_2$ to **11**.
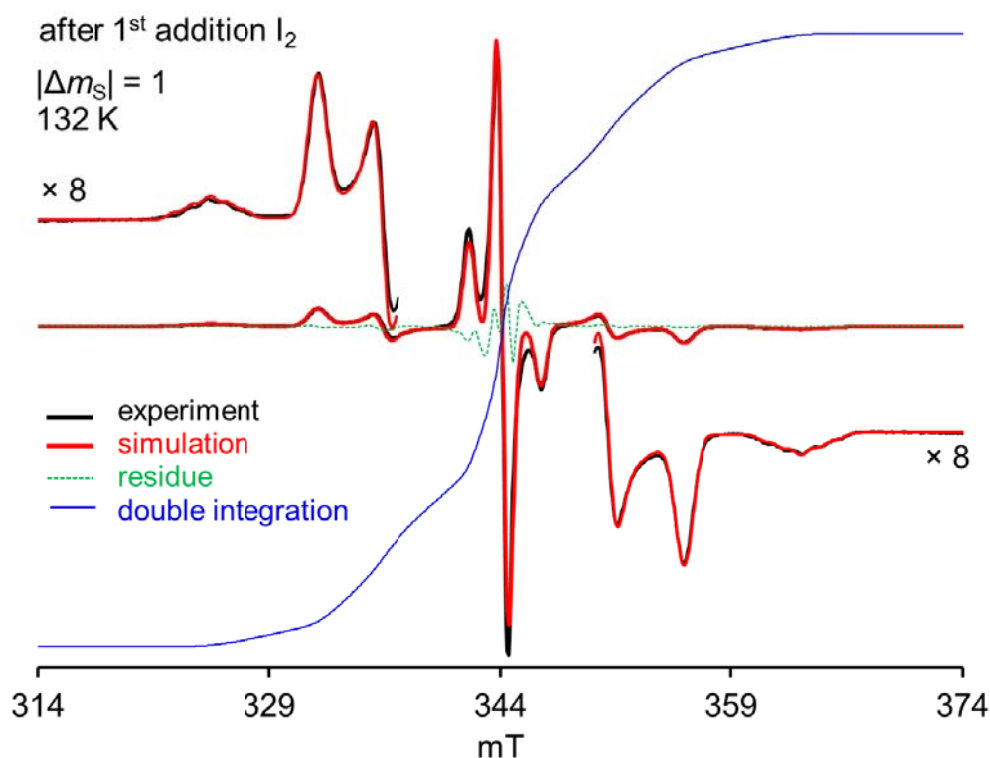
**Figure C15.** EPR (X-Band, ν = 9.4796 GHz, $|\Delta m_s|$ = 1) spectrum of aminyl diradical **9** in 2-MeTHF (5-mm tube, label: AO335r1/r2) at 132 K; inset plot: $|\Delta m_s|$ = 2 region, ν = 9.4798 GHz. These spectra are obtained following the initial addition of iodine to the precursor dianion. The EPR spectra following the final addition of iodine to this sample are shown in the following figure (Figure C16).
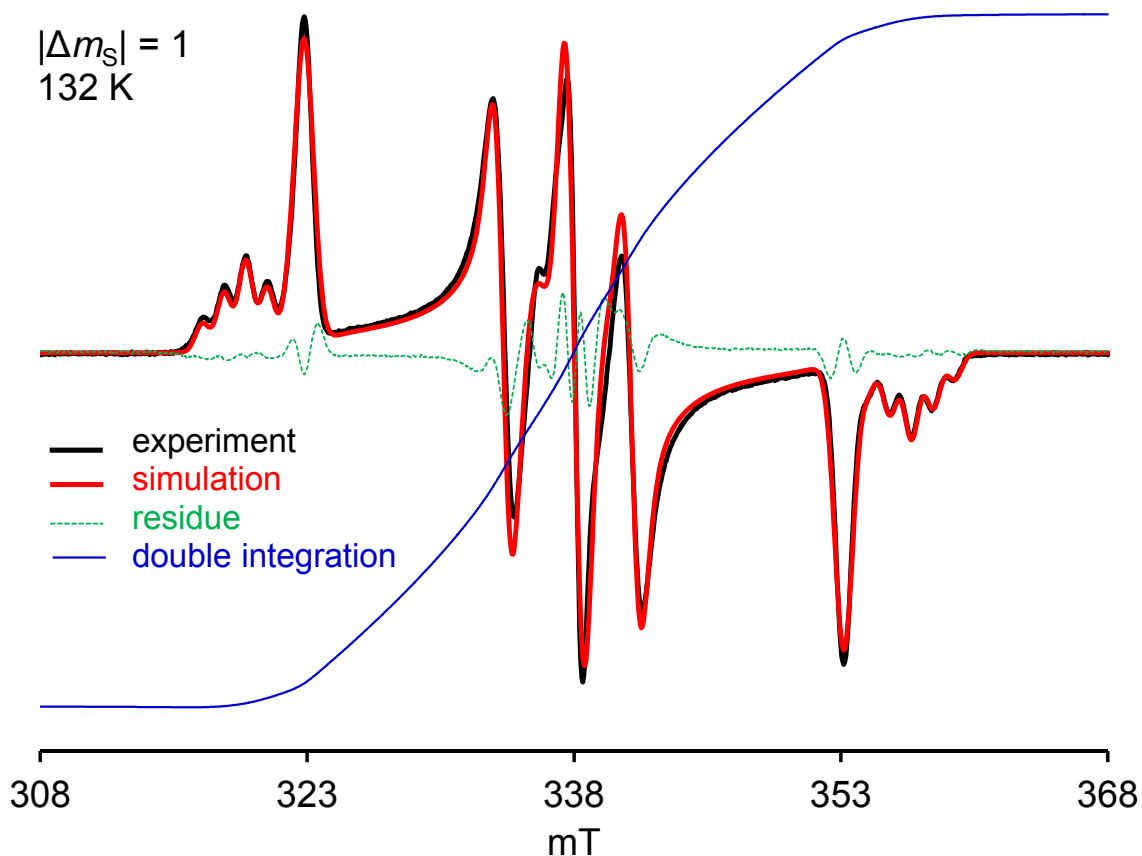
**Figure C16.** Plot and complete simulation of the EPR spectrum in Figure 1.31. EPR (X-Band, $\nu$ = 9.4780 GHz) spectrum of aminyl diradical **9** in 2-MeTHF at 132 K (5-mm tube, label: AO335r3). The simulation parameters for the $S$ = 1 state are: $|D/hc|$ = 17.5 × $10^{-3}$ cm$^{-1}$ ($|D/g\mu_B|$ = 18.7 mT), $|E/hc|$ = 3.60 × $10^{-3}$ cm$^{-1}$ ($|E/g\mu_B|$ = 3.85 mT), $|A_{zz}/2hc|$ = 11.34 × $10^{-3}$ cm$^{-1}$ ($|A_{zz}/2g\mu_B|$ = 1.21 mT), $g_x$ = 2.0046, $g_y$ = 2.0030, $g_z$ = 2.0019, Gaussian line ($L_x$ = 0.90, $L_y$ = 1.05, $L_z$ = 0.80 mT). The center lines correspond to an $S$ = ½ (monoradical) by-product simulated with the identical $g$-values, $|A_{zz}/hc|$ = 22.68 × $10^{-3}$ cm$^{-1}$ ($|A_{zz}/g\mu_B|$ = 2.42 mT) and Gaussian line ($L_x$ = 0.85, $L_y$ = 0.94, $L_z$ = 1.40 mT). The EPR spectra for this sample after the initial addition of iodine are shown in the preceding figure (Figure C15).
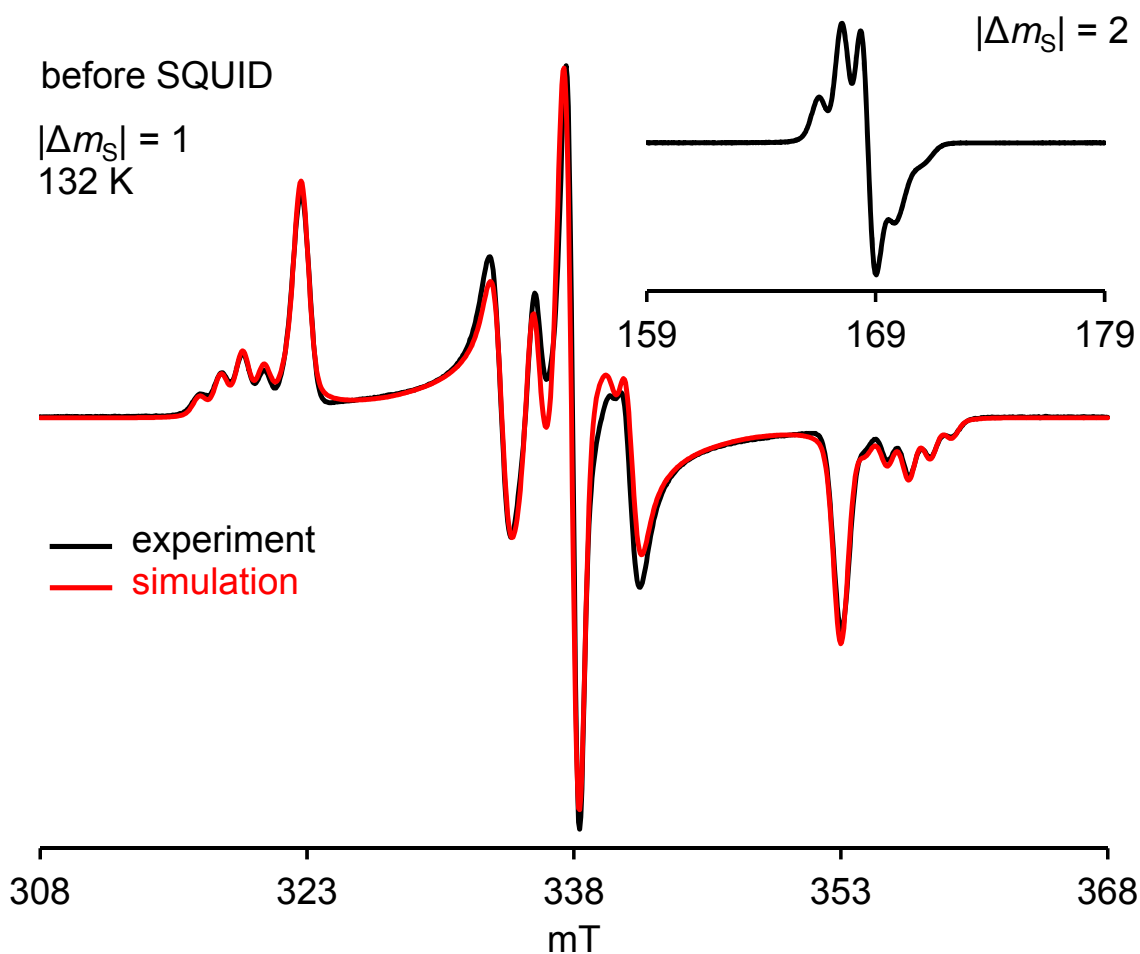
**Figure C17.** EPR (X-Band, $\nu = 9.4737$ GHz, $|\Delta m_s| = 1$) spectrum of aminyl diradical **9** in 2-MeTHF (5-mm SQUID tube, label: AO358r1/r2/sm1/sm3) at 132 K before SQUID magnetic studies shown in Figure 2, main text. The simulation parameters for the $S = 1$ state are: $|D/hc| = 1.75 \times 10^{-2}$ cm$^{-1}$, $|E/hc| = 3.60 \times 10^{-3}$ cm$^{-1}$, $|A_{zz}/2hc| = 1.13 \times 10^{-3}$ cm$^{-1}$, $g_x = 2.0041$, $g_y = 2.0031$, $g_z = 2.0019$, Gaussian/Lorentzian line (0.98, $L_x = 0.9$, $L_y = 0.8$, $L_z = 0.7$ mT). The center lines correspond to an $S = \frac{1}{2}$ (monoradical) by-product simulated with the identical g-values and $|A_{zz}/hc| = 2.20 \times 10^{-3}$ cm$^{-1}$. Inset plot: $|\Delta m_s| = 2$ region, $\nu = 9.4738$ GHz. Following these EPR spectra, magnetic data were obtained as illustrated in Figure C18.
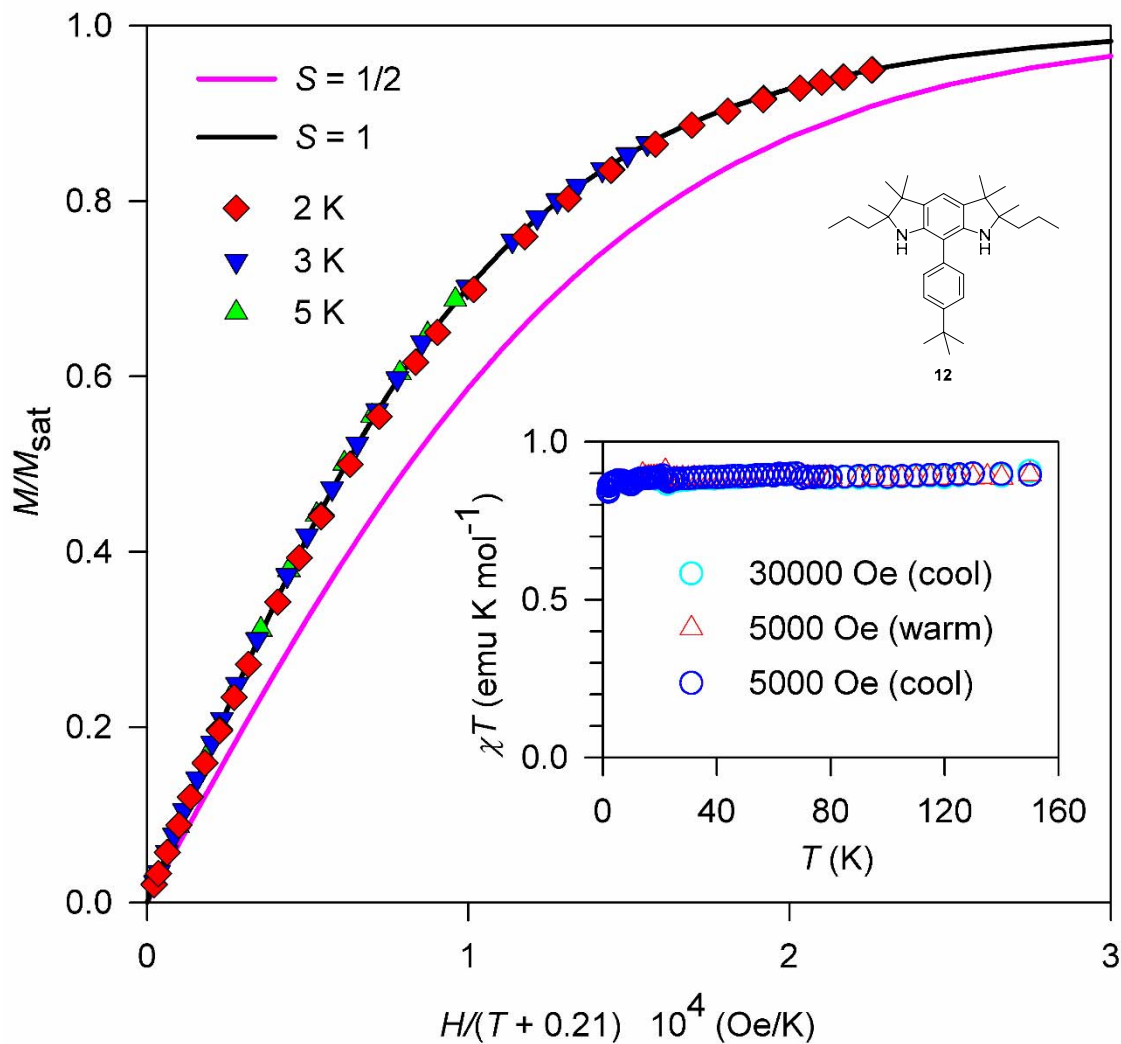
**Figure C18.** The expanded plot of magnetic data for aminyl diradical **9** in 2-MeTHF, shown in Figure 2, main text. The data were obtained after annealing the matrix at 190 K (label: AO358s2). Main plot: $M/M_{sat}$ vs. $H/(T - \theta)$ and $\chi T$ vs. $T$, with $\theta = -0.21$ K, $M_{sat} = 0.89$ $\mu_B$, and $S = 1.0$; inset plot: $\chi T$ vs. $T$ with $\chi T = 0.89$ emu K mol$^{-1}$. Following these magnetic measurements, the sample was withdrawn cold from the SQUID sample space, and then the EPR spectra (Figure C19) were obtained.
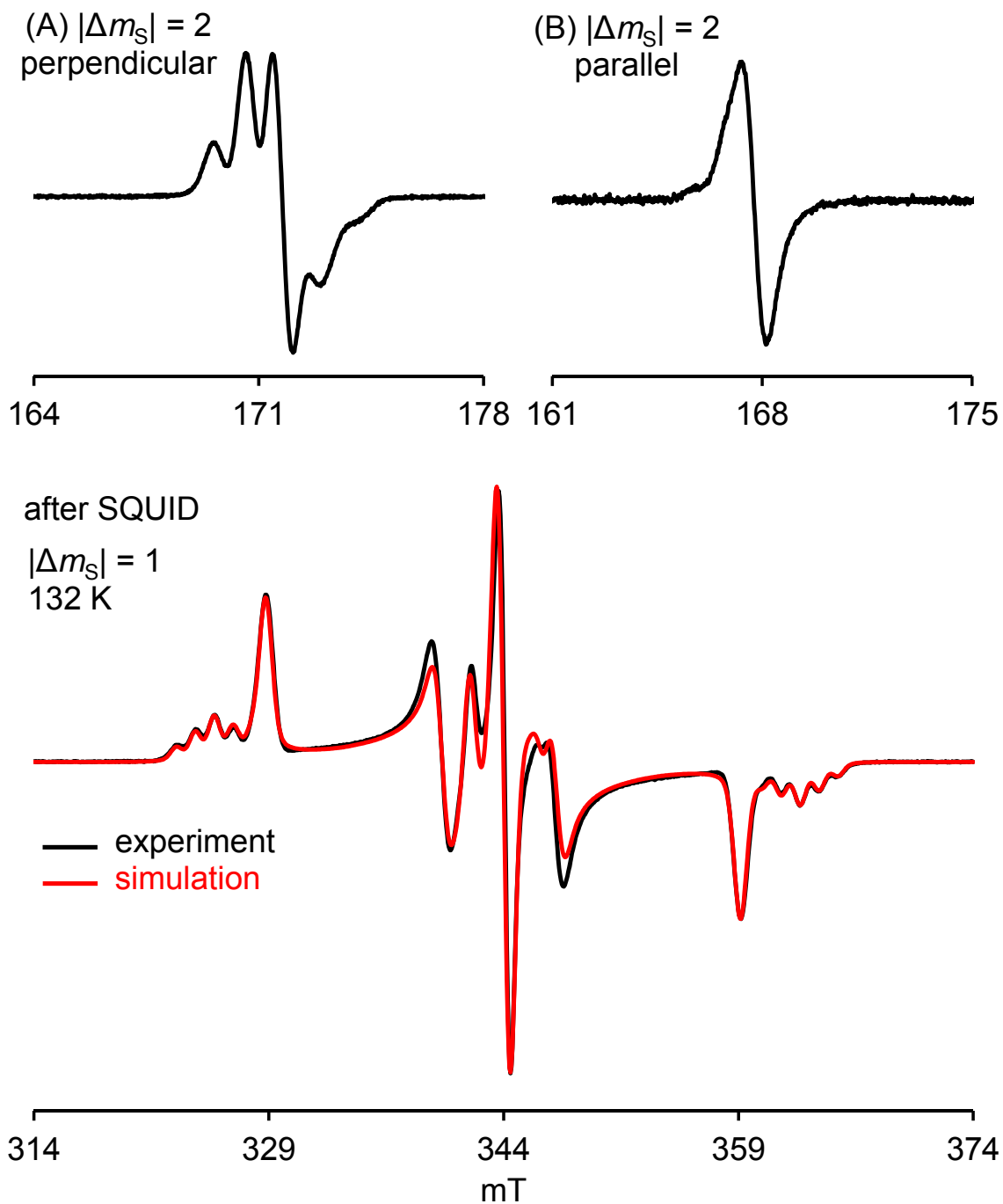
**Figure C19.** EPR (X-Band, $\nu$ = 9.6456 GHz, perpendicular mode in dual-mode cavity, $|\Delta m_s|$ = 1) spectrum of aminyl diradical **9** in 2-MeTHF (5-mm SQUID tube, label: AO358r5) at 132 K after SQUID magnetic studies shown in Figure C18. Inset plots ($|\Delta m_s|$ = 1 region): (A) perpendicular mode, $\nu$ = 9.6455 GHz (label: AO358r6), (B) parallel mode, $\nu$ = 9.4256 GHz (label: AO358r7).
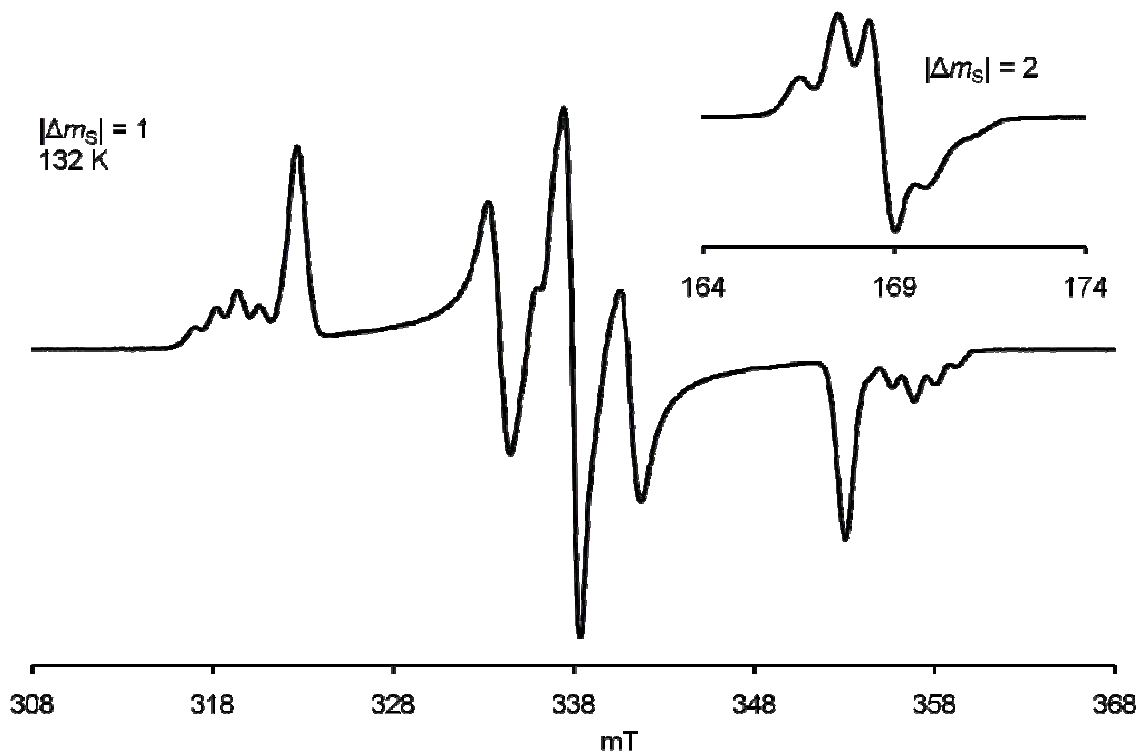
**Figure C20.** EPR (X-Band, ν = 9.4737 GHz, |Δ$m_s$| = 1) spectrum of aminyl diradical **9** in 2-MeTHF (5-mm SQUID tube, label: AO352r3/r4) at 132 K before SQUID magnetic studies shown in Figure C21.
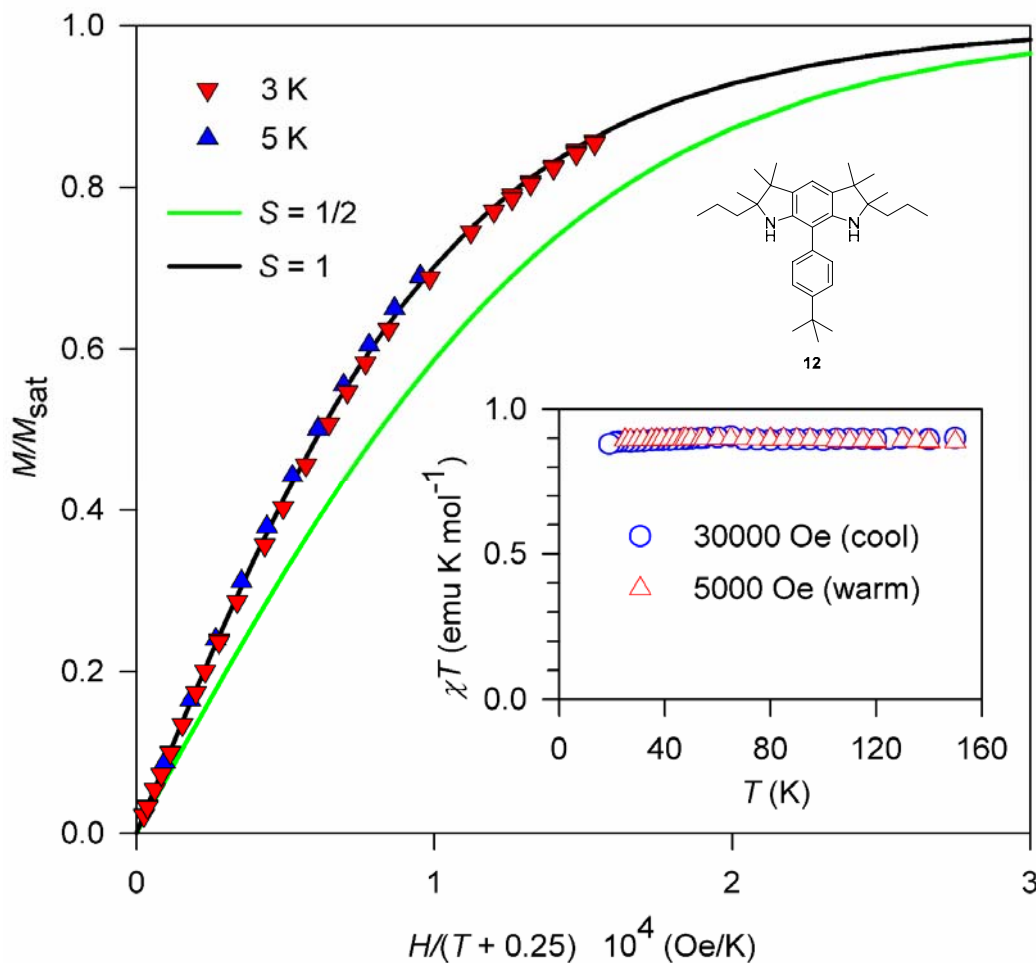
**Figure C21.** SQUID magnetic data for a repeat sample of aminyl diradical **9** in 2-MeTHF. The data are obtained after annealing the matrix at 170 K (label: AO352s1). Main plot: $M/M_{sat}$ vs. $H/(T − \theta)$ and $\chi T$ vs. $T$, with $\theta = −0.25$ K, $M_{sat} = 0.89$ $\mu_B$, and $S = 1.0$; inset plot: $\chi T$ vs. $T$ with $\chi T = 0.89$ emu K mol$^{-1}$. Following these magnetic measurements, the sample was withdrawn cold from the SQUID sample space, and then the EPR spectra were obtained, as illustrated in Figure C22 (label: AO352r5/r6).
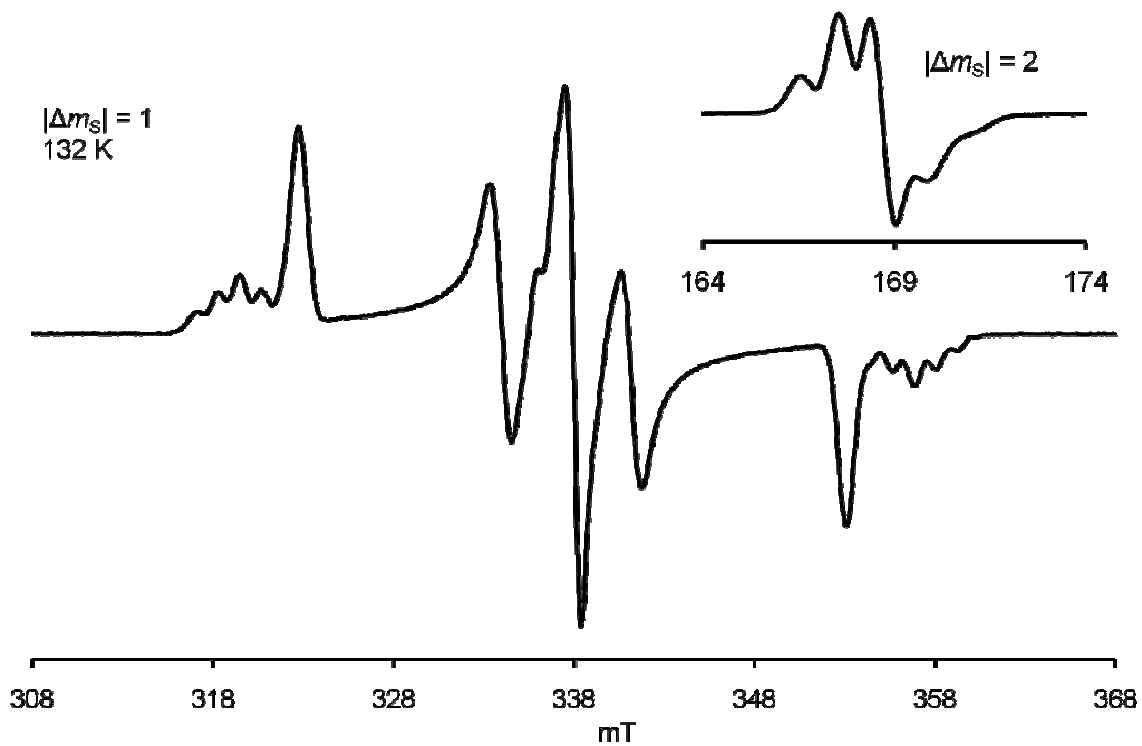
**Figure C22.** EPR (X-Band, $\nu$ = 9.4756 GHz, $|\Delta m_s|$ = 1) spectrum of aminyl diradical **9** in 2-MeTHF (5-mm SQUID tube, label: AO352r5/r6) at 132 K after SQUID magnetic studies shown in Figure S7. Inset plot: $|\Delta m_s|$ = 2 region, $\nu$ = 9.4755 GHz.
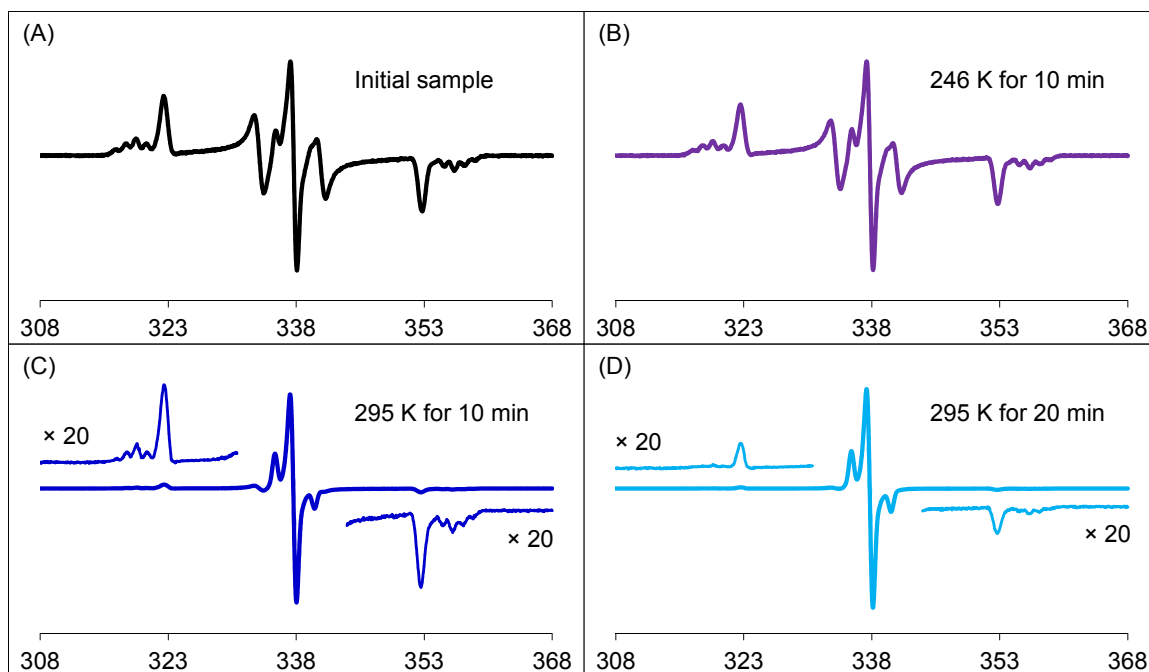
**Figure C23.** Persistence of aminyl diradical **9** in 2-MeTHF monitored by EPR (X-Band, ν = 9.4674 GHz; ν = 9.4696 GHz; ν = 9.4692 GHz; ν = 9.4692 GHz) spectroscopy at 134–136 K (5-mm EPR tube, label: AO306r3/r4/r8/r10).  EPR spectra: (A) starting sample of **9**, (B) after annealing 246 K for 10 min, (C) after annealing at room temperature for 10 min, and (D) after annealing at room temperature for an additional 10 min.  Double integration of the above spectra and spectral simulation for the diradical, suggests the following contents (%) of *S* = 1 diradical for the diradical/monoradical mixtures: 91%, 87%, 34%, 13%; thus, assuming that the monoradical does not decay on the time scale of the experiment, half-life, $\tau_{1/2} \approx 7$ min, is estimated for the diradical in 2-MeTHF at room temperature.
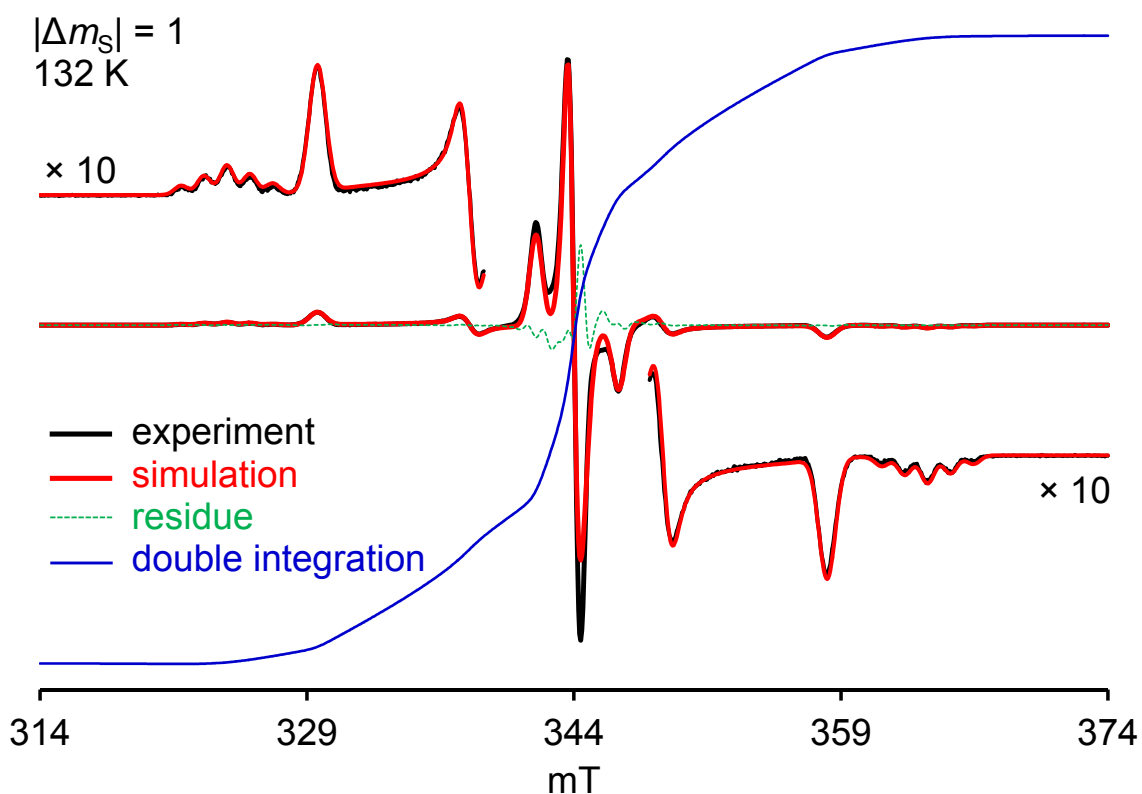
**Figure C24.** EPR (X-Band, $\nu$ = 9.6451 GHz) spectrum of aminyl diradical **10** in 2-MeTHF at 132 K (8 mM, label: AO552r4). The simulation parameters for the $S$ = 1 state are: $|D/hc| = 18.4 \times 10^{-3}$ cm$^{-1}$, $|E/hc| = 2.77 \times 10^{-3}$ cm$^{-1}$, $|A_{zz}/2hc| = 1.20 \times 10^{-3}$ cm$^{-1}$, $g_x$ = 2.0045, $g_y$ = 2.0027, $g_z$ = 2.0014, Gaussian line ($L_x$ = 0.84, $L_y$ = 0.94, $L_z$ = 0.76 mT). The center lines correspond to an $S$ = ½ (monoradical) by-product simulated with the identical $g$-values, $|A_{zz}/hc| = 2.15 \times 10^{-3}$ cm$^{-1}$ and Gaussian line ($L_x$ = 0.80, $L_y$ = 0.80, $L_z$ = 0.90 mT).
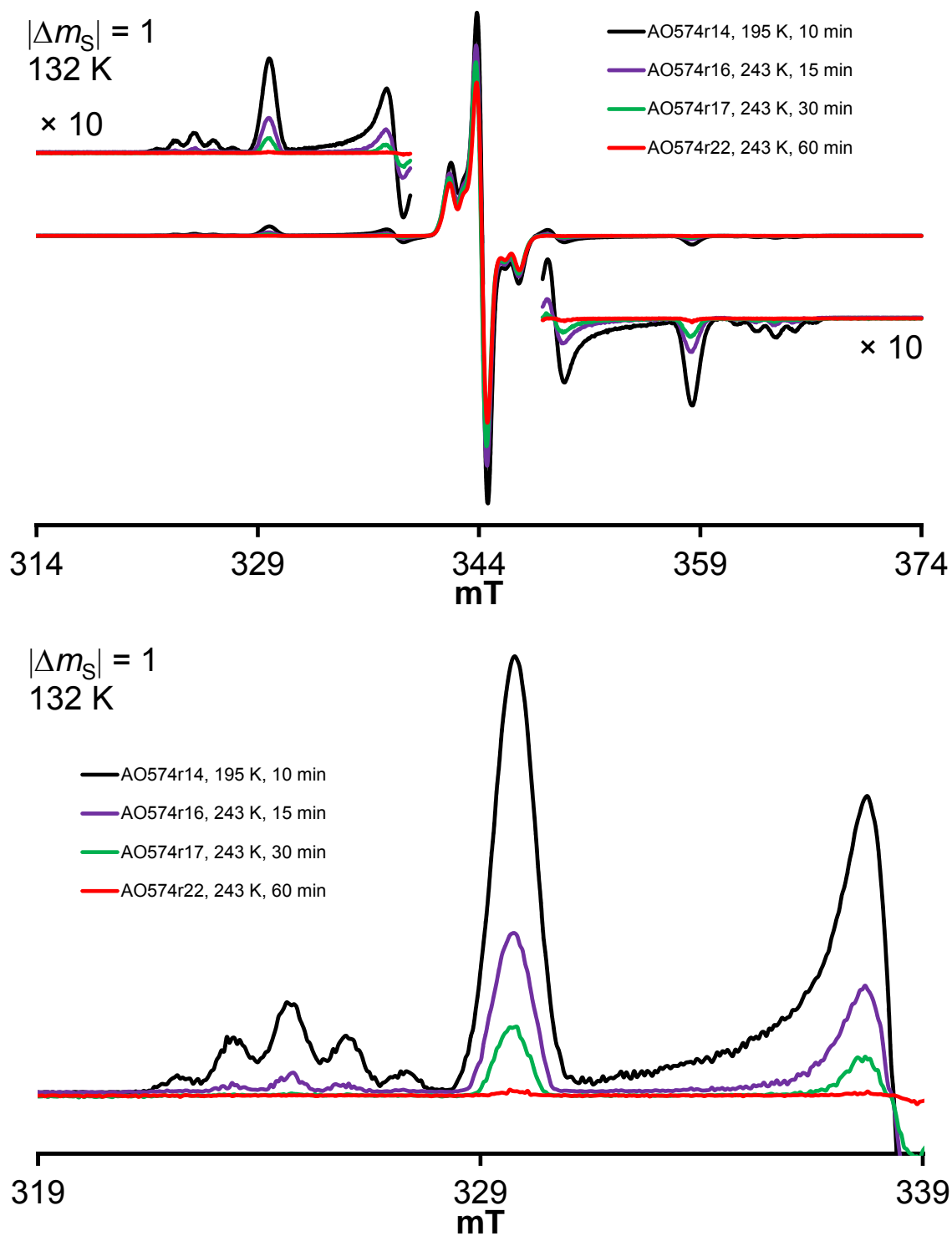
**Figure C25.** EPR spectra at 132 K showing annealing of ~7.2 mM diradical **10** in 2-MeTHF at 243 K for 1 h (label: AO574).
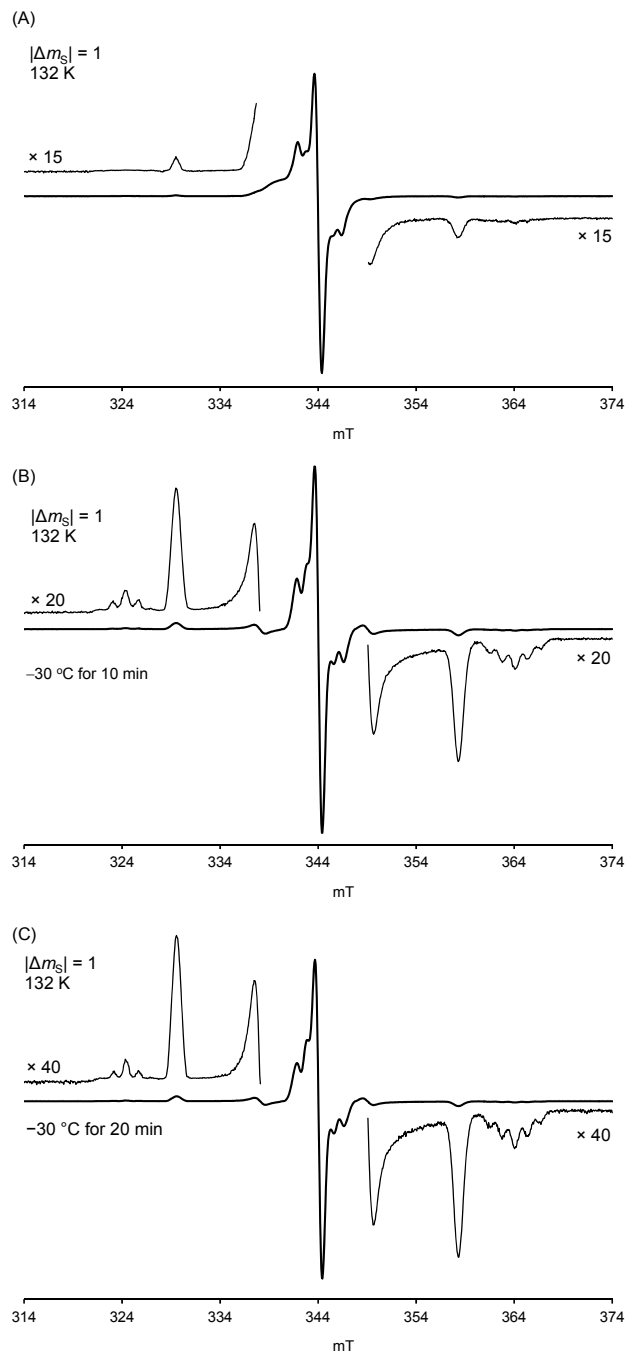
**Figure C26.** (A) EPR (X-Band, $\nu = 9.6442$ GHz) spectra at 132 K of the reaction mixture after addition of iodine in 2-MeTHF and mixing at $-115$ °C for 2 h (label: AO915r1/r2); inset plot: $|\Delta m_s| = 2$ region ($\nu = 9.6451$ GHz). (B) EPR (X-Band, $\nu = 9.6454$ GHz) spectra at 132 K of the reaction mixture after annealing at $-30$ °C for 10 min. (C) EPR (X-Band, $\nu = 9.6459$ GHz) spectra at 132 K of the reaction mixture after annealing at $-30$ °C for 20 min.
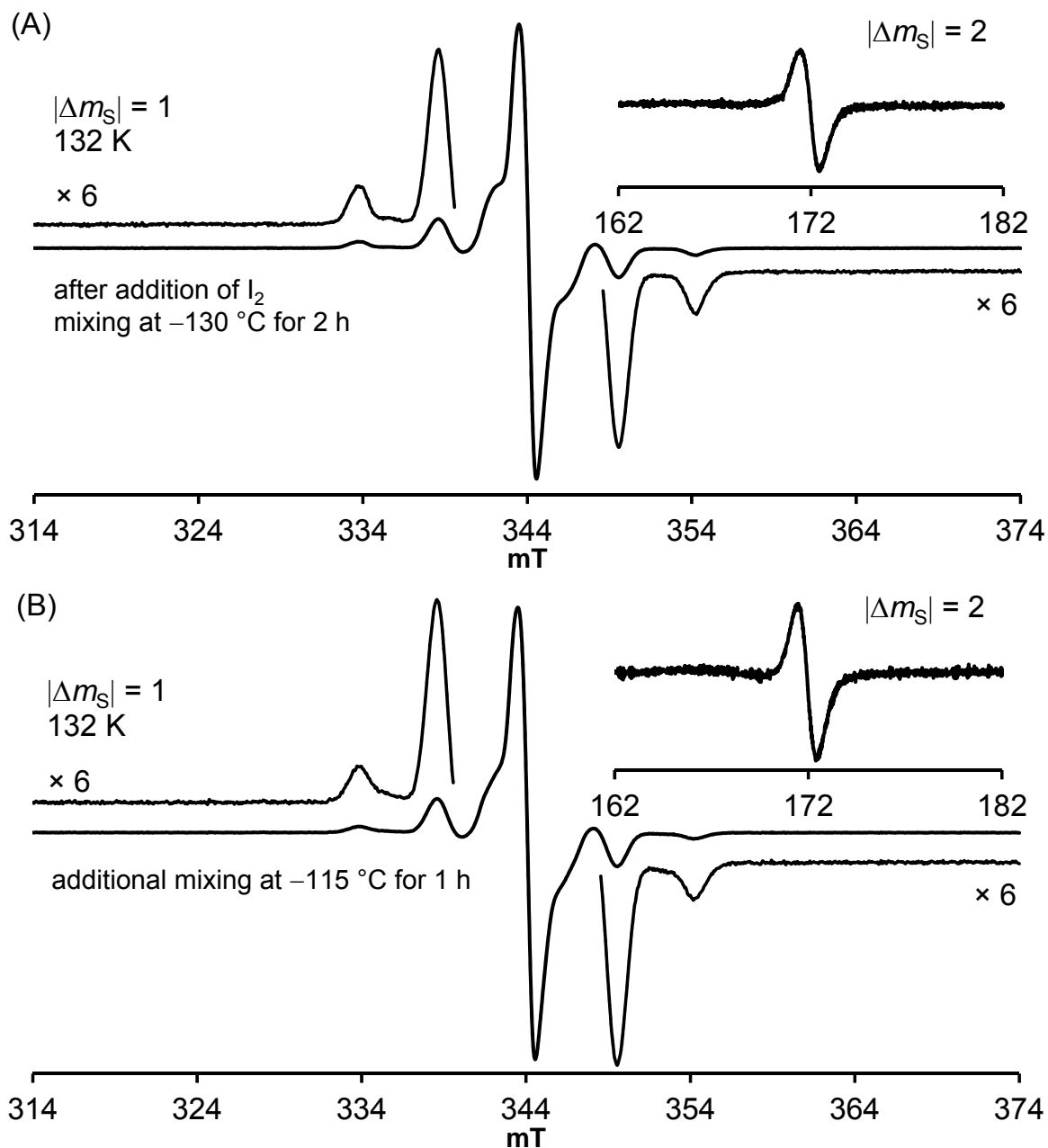
**Figure C27.** (A) EPR (X-Band) spectra at 132 K of the reaction mixture after addition of iodine in 2-MeTHF and mixing at −130 °C for 2 h (label: AO860r1/r2); inset plot: $|\Delta m_s|$ = 2 region. (B) EPR (X-Band) spectra at 132 K of the reaction mixture after additional mixing at −115 °C for 1 h (label: AO860r7/r8); inset plot: $|\Delta m_s|$ = 2 region. After these EPR spectra, the sample was examined by SQUID magnetometry.

**Figure C28.** EPR (X-Band, $\nu$ = 9.6476 GHz, $|\Delta m_s|$ = 1) spectrum of aminyl diradical **11** in 2-MeTHF (5-mm tube, label: AO943r1) at 132 K. This spectrum is obtained following the initial addition of iodine to the precursor dianion. The simulation parameters for the $S$ = 1 state are: $|D/hc|$ = 17.9 × 10$^{-3}$ cm$^{-1}$ ($|D/g\mu_B|$ = 19.1 mT), $|E/hc|$ = 1.42 × 10$^{-3}$ cm$^{-1}$ ($|E/g\mu_B|$ = 1.51 mT), $|A_{zz}/2hc|$ = 1.08 × 10$^{-3}$ cm$^{-1}$ ($|A_{zz}/2g\mu_B|$ = 1.15 mT), $g_x$ = 2.0050, $g_y$ = 2.0031, $g_z$ = 2.0018, Gaussian line ($L_x$ = 0.95, $L_y$ = 1.17, $L_z$ = 0.97 mT). The center lines correspond to an $S$ = ½ (monoradical) by-product simulated with the identical $g$-values, $|A_{zz}/hc|$ = 2.15 × 10$^{-3}$ cm$^{-1}$ ($|A_{zz}/g\mu_B|$ = 2.30 mT) and Gaussian line ($L_x$ = 0.78, $L_y$ = 1.00, $L_z$ = 0.74 mT). The EPR spectra following the addition of FeCp$_2$BF$_4$ to this sample are shown in the following figure (Figure C29).
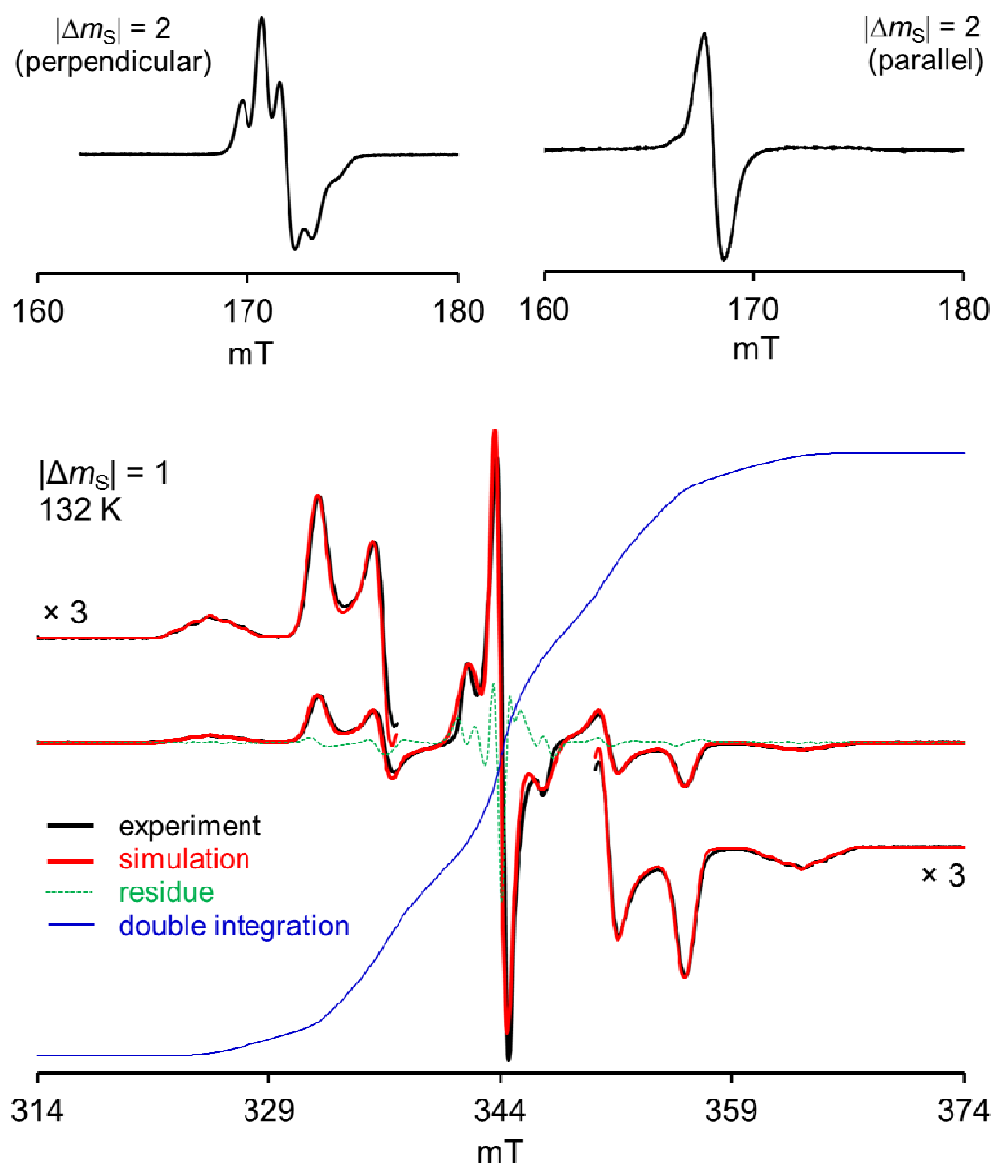
**Figure C29.** EPR (X-Band, $\nu$ = 9.6487 GHz) spectrum of aminyl diradical **11** in 2-MeTHF at 132 K (5-mm tube, labels: AO943r10, r12, 13): $\nu$ = 9.6487 GHz, 9.6496 GHz, and 9.4477 GHz for the $|\Delta m_S|$ = 1 (perpendicular), $|\Delta m_S|$ = 2 (perpendicular), and $|\Delta m_S|$ = 2 (parallel) regions, respectively. This sample was 13 mM based on the starting diamine **28**, and the spectrum was obtained after oxidation of the dianion was carried by addition of iodine, followed by two additions of $[Cp_2Fe]^+[BF_4^-]$ (total of 4 equiv). The simulation parameters for the $S$ = 1 state are: $|D/hc|$ = 17.94 × $10^{-3}$ cm$^{-1}$, $|E/hc|$ = 1.42 × $10^{-3}$ cm$^{-1}$, $|A_{zz}/2hc|$ = 1.08 × $10^{-3}$ cm$^{-1}$, $g_x$ = 2.0050, $g_y$ = 2.0031, $g_z$ = 2.0018, Gaussian line ($L_x$ = 0.95, $L_y$ = 1.17, $L_z$ = 0.97 mT). The center lines correspond to an $S$ = ½ (monoradical) by-product simulated with identical $g$-values and $|A_{zz}/hc|$ = 2.35 × $10^{-3}$ cm$^{-1}$ and Gaussian line ($L_x$ = 0.60, $L_y$ = 0.70, $L_z$ = 1.35 mT).
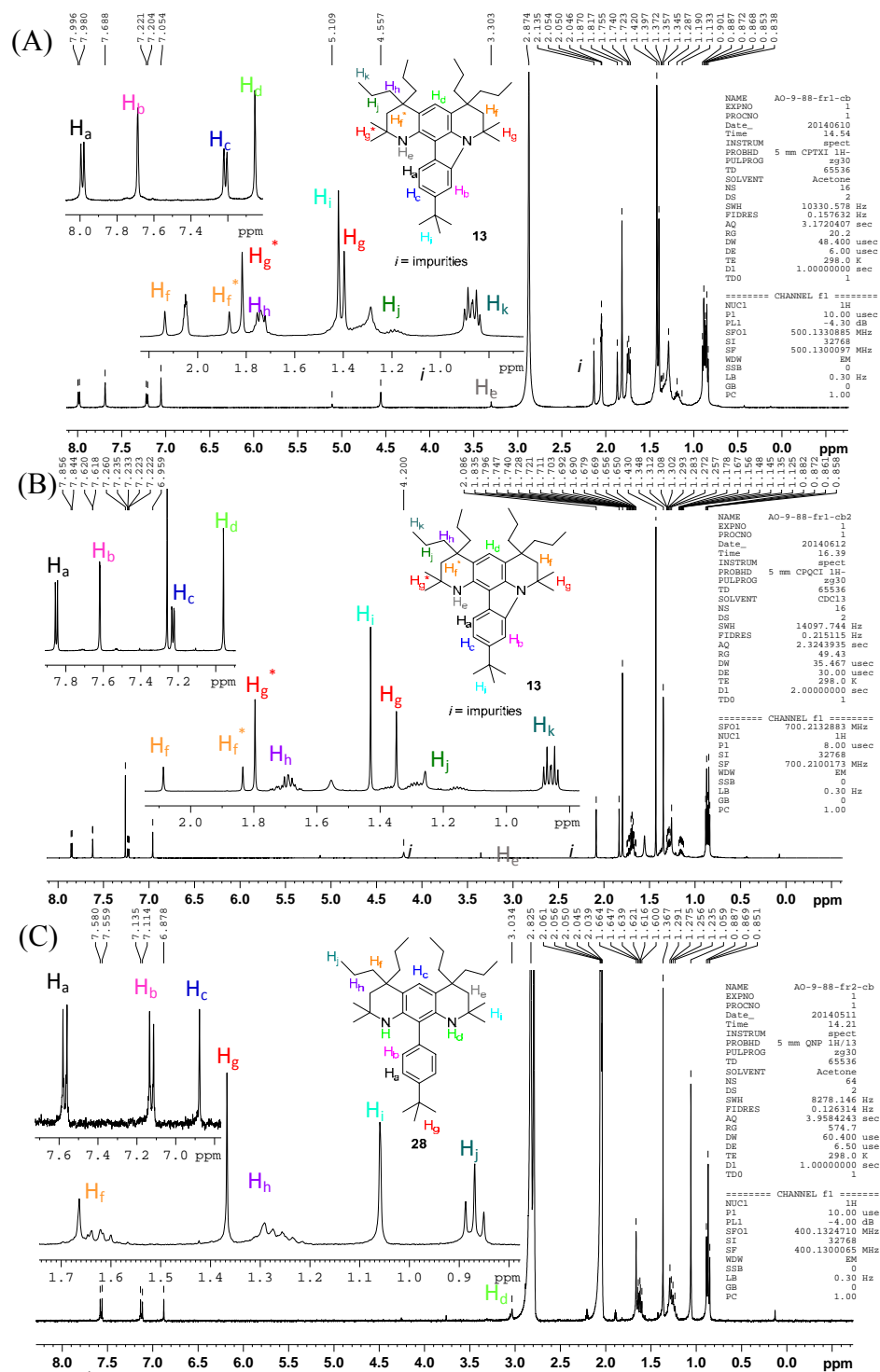
**Figure C30.** ^{1}H NMR ((A) 500 MHz, acetone-$d_6$, label: AO-9-88-fr1-cb, (B) 700 MHz, chloroform-$d$, AO-9-88-fr1-cb2) spectra of the purified sample (fraction 1) corresponds to by-product **43** following $\chi T$ measurement and EPR spectroscopic monitoring of aminyl diradical **11**. (C) ^{1}H NMR (400 MHz, acetone-$d_6$, label: AO-9-88-fr2-cb) spectrum of the purified sample (fraction 2) corresponds to diamine **28**.
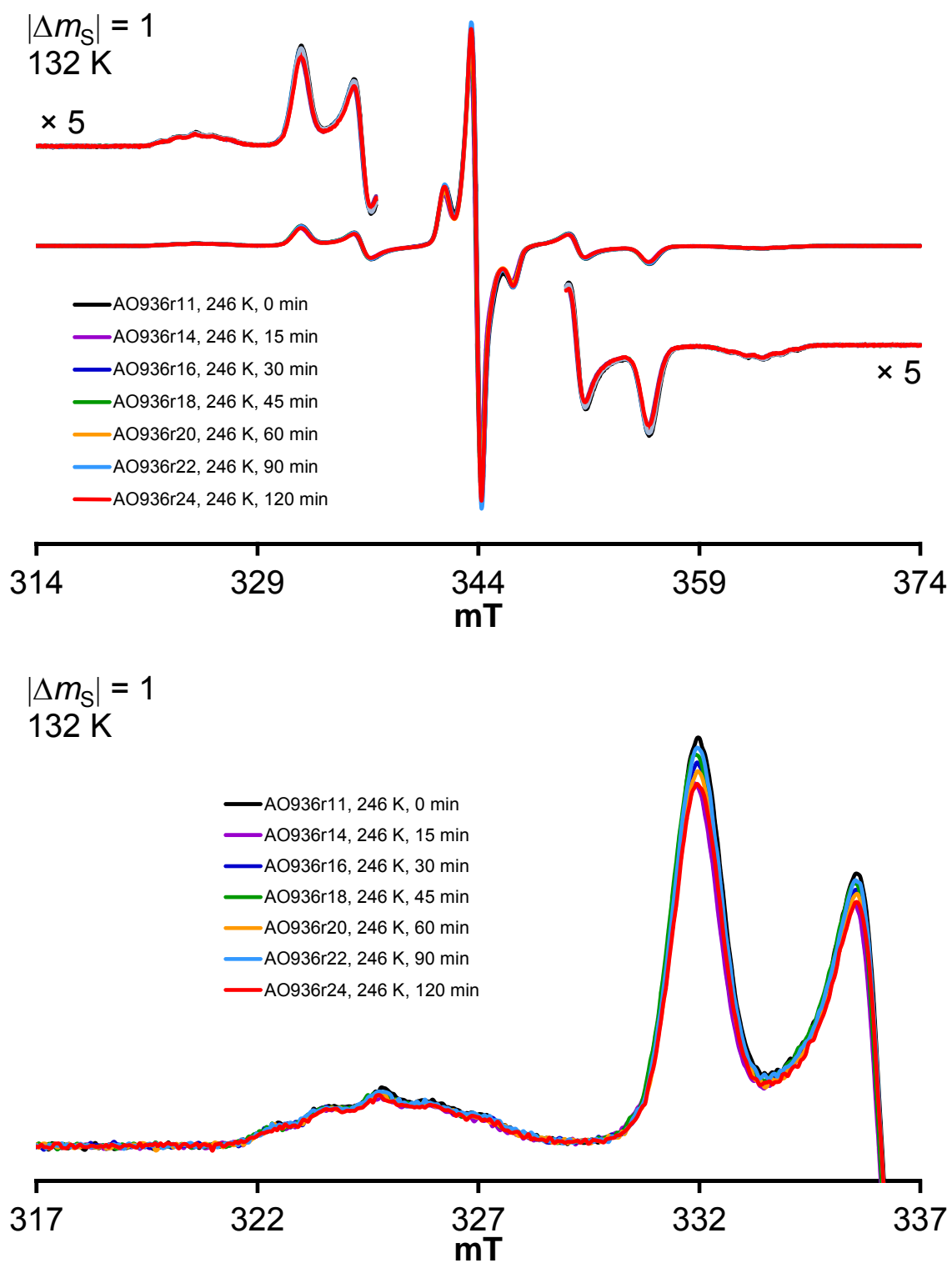
**Figure C31.** EPR spectra at 132 K showing annealing of ~2.8 mM diradical **11** in 2-MeTHF at 246 K for 2 h, prior to the kinetic runs at 295 K (label: AO936).
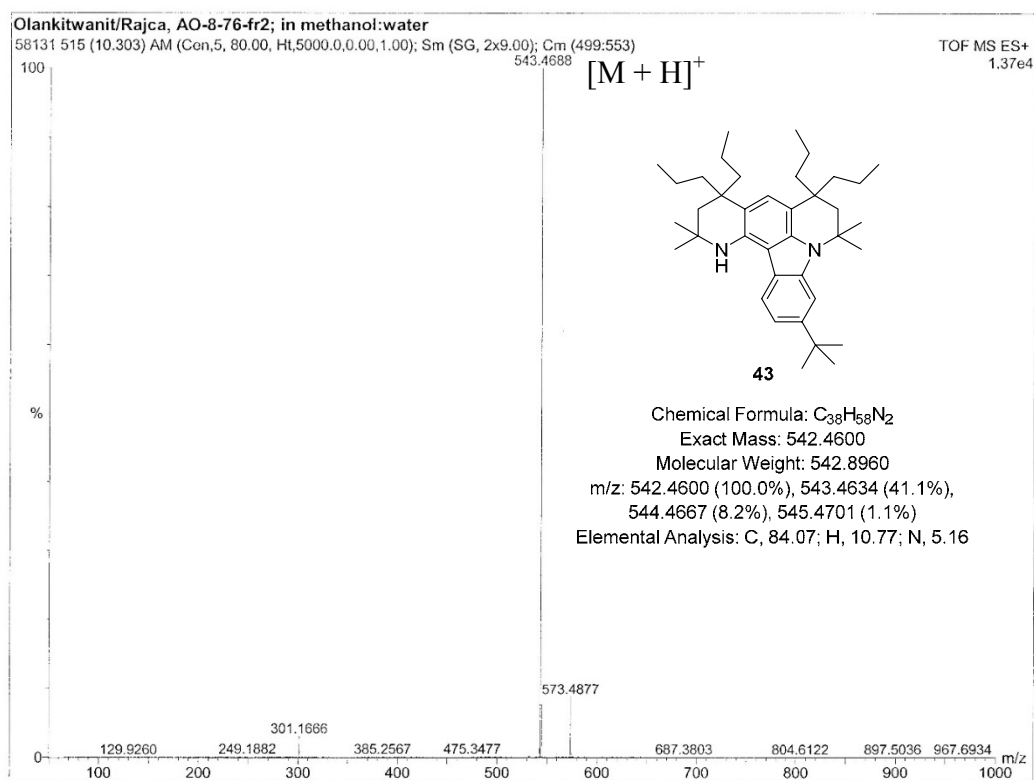
**Figure C32.** HR MS spectra by-product **43**
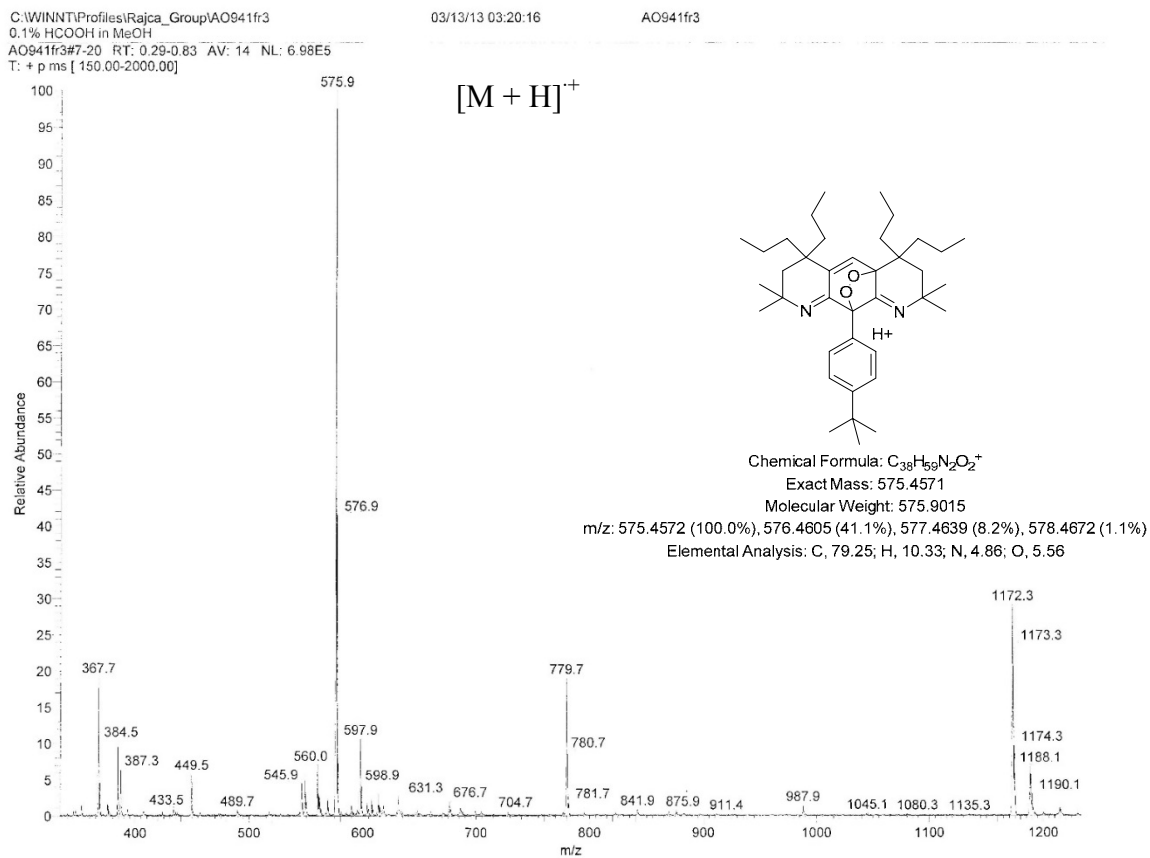
**Figure C33.** ESI MS (label: AO-9-41-fr3) of the purified sample (fraction 3). ¹H NMR

spectrum for the same sample is presented in Figure C14 (D)).
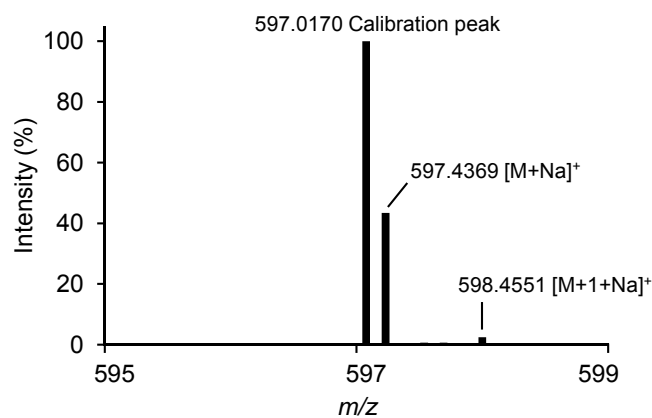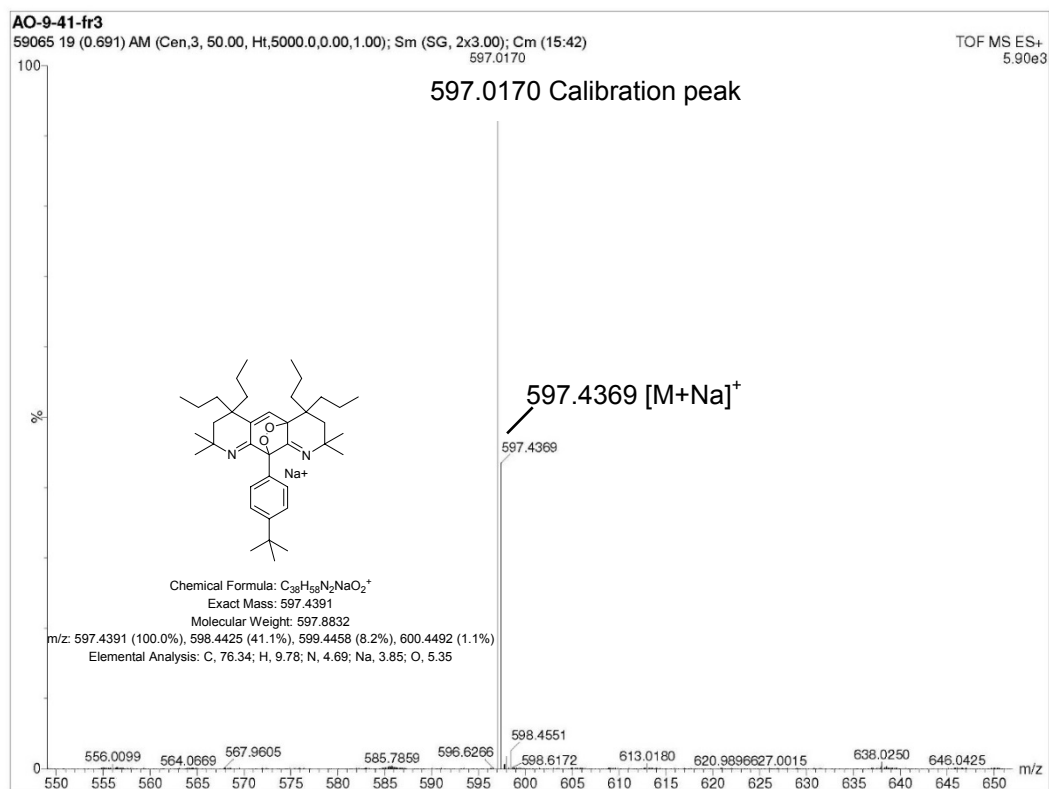
**Figure S34.** HR ESI-MS (sample label: AO-9-41-fr3) of the purified sample (fraction 3) obtained after treatment of aminyl diradical **11** with oxygen (O₂).

**Appendix D**

**$^1$H, $^{13}$C NMR, IR, EPR Spectra (Chapter 2)**
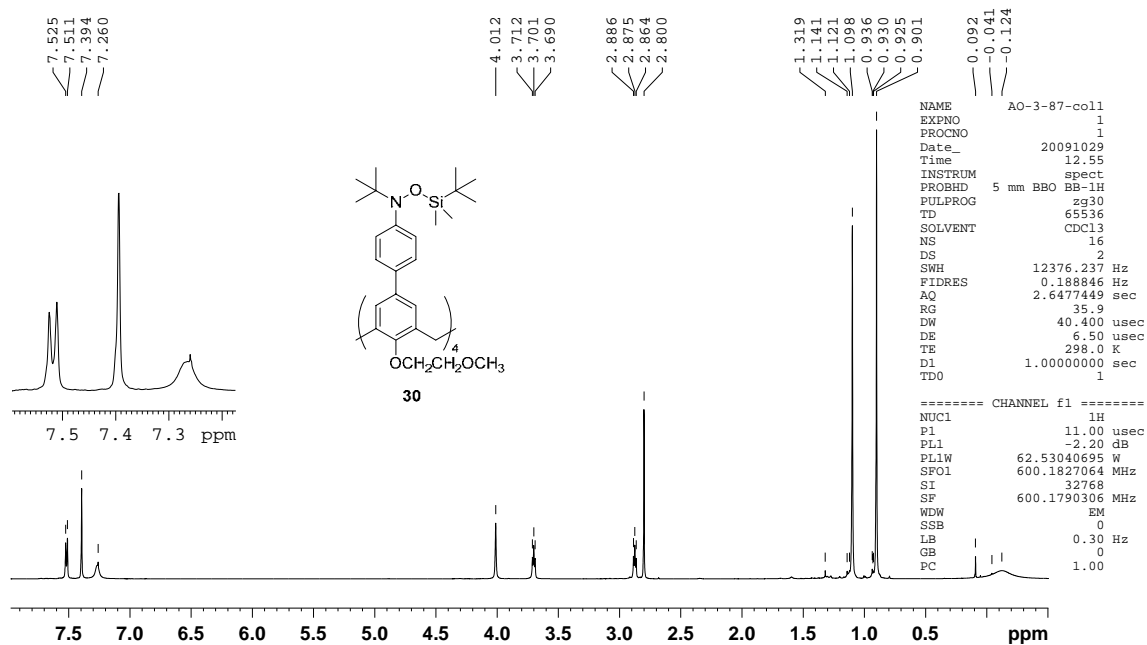
**Figure D1.** $^{1}$H NMR (600 MHz, chloroform-*d*) spectrum of TBDMS-protected calix[4]arene **30** (AO-3-87-col1).
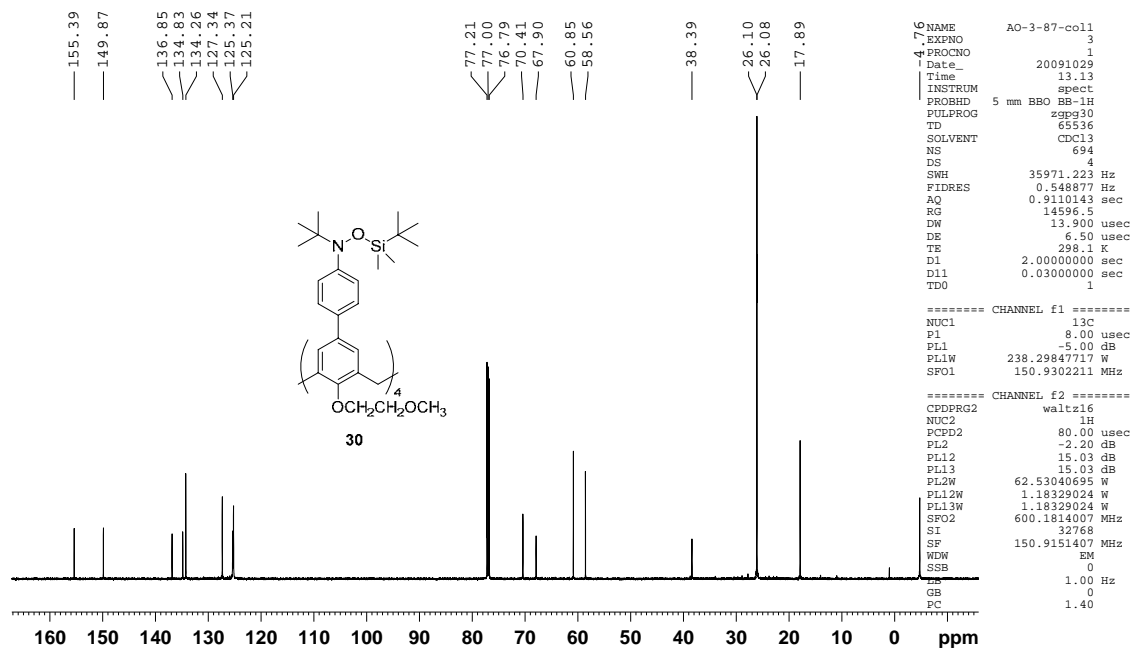


**Figure D2.** $^{13}$C NMR (150 MHz, chloroform-*d*) spectrum of TBDMS-protected calix[4]arene **30** (AO-3-87-col1).
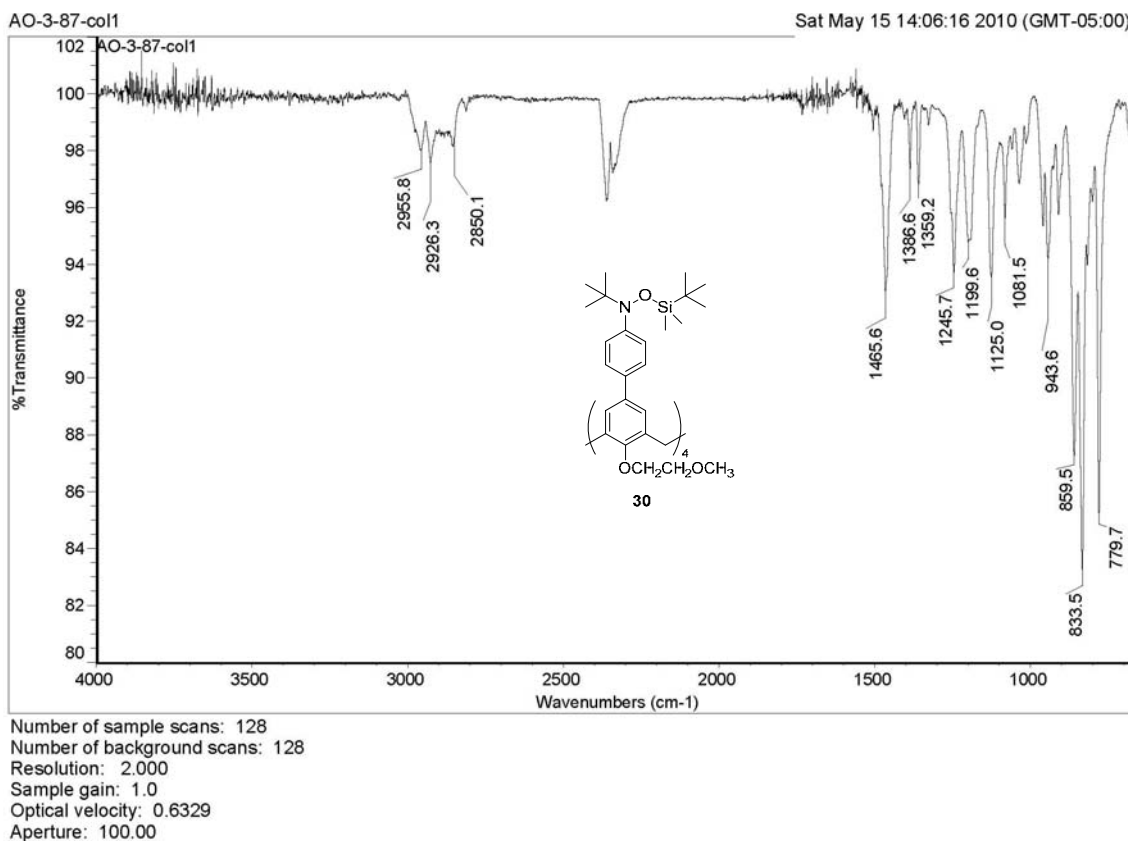
**Figure D3.** IR (ATR, ZnSe, cm$^{-1}$) spectrum of TBDMS-protected calix[4]arene **30** (AO-3-87-col1).
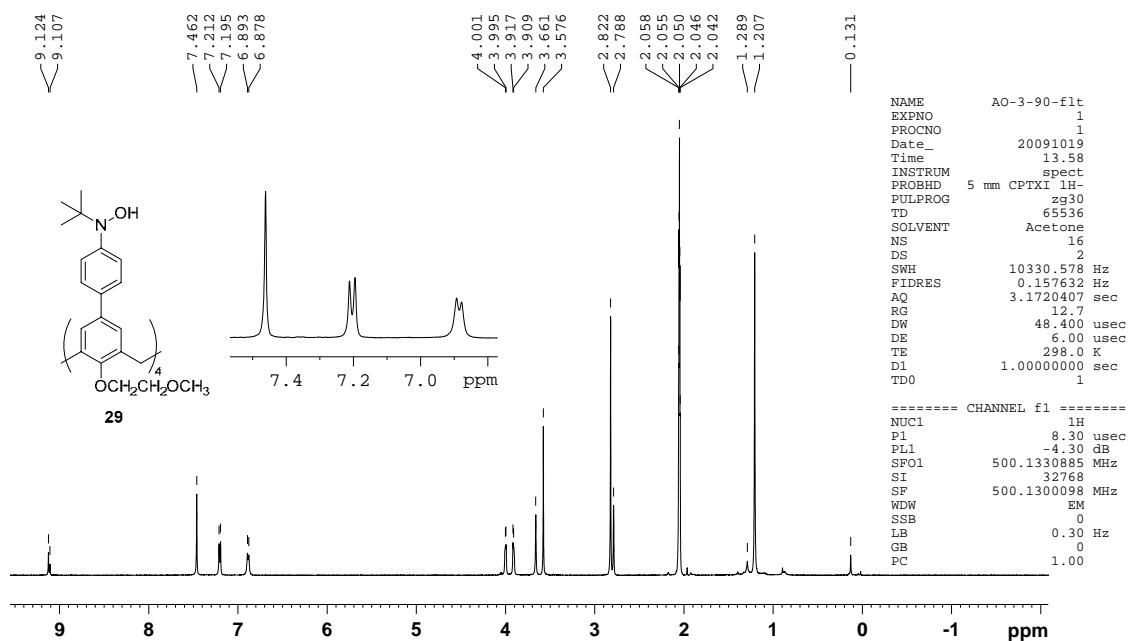


**Figure D4.** $^1$H NMR (500 MHz, acetone-$d_6$) spectrum of tetrahydroxylamine calix[4]arene **29**. (AO-3-90-flt).
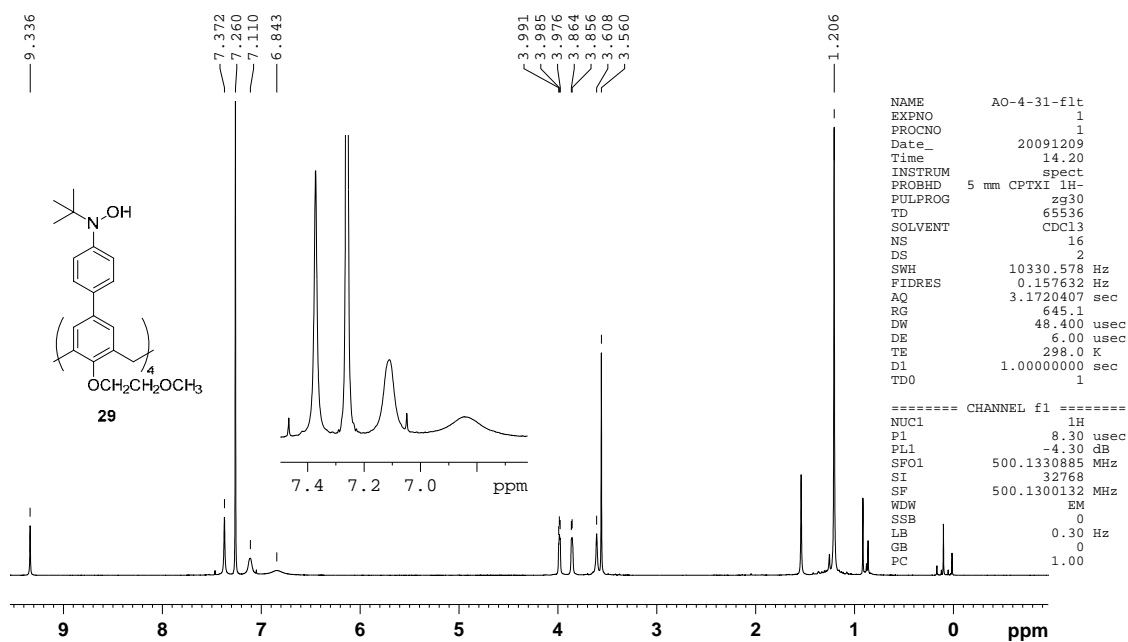
**Figure D5.** ^{1}H NMR (500 MHz, chloroform-*d*) spectrum of tetrahydroxylamine calix[4]arene **29** (AO-4-31-flt).
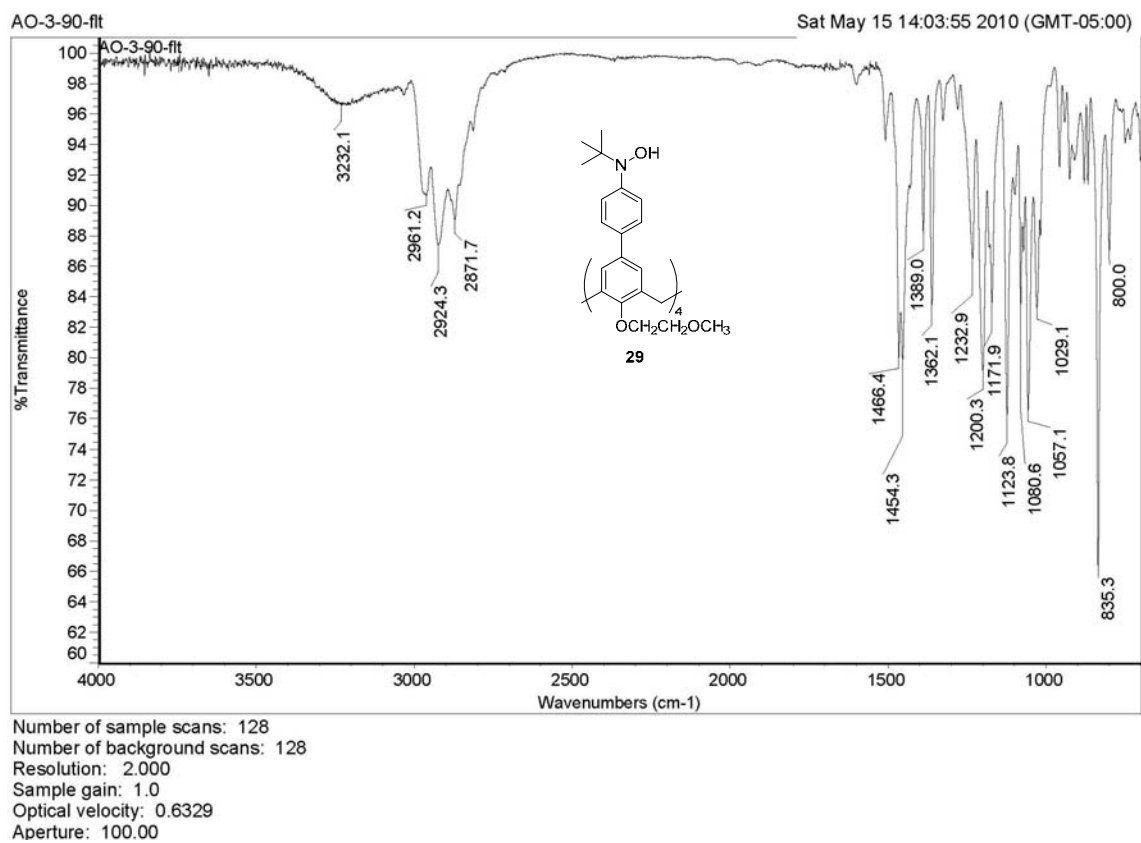


**Figure D6.** IR (ATR, ZnSe, cm[-1]) spectrum of tetrahydroxylamine calix[4]arene **29** (AO-3-90-flt).
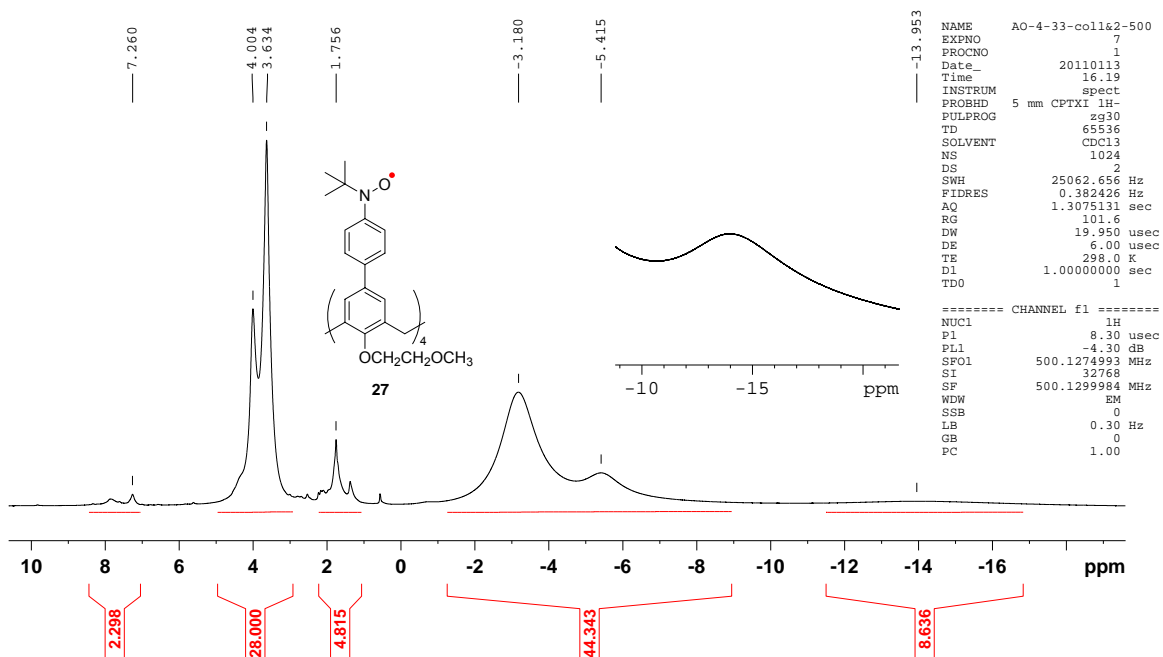
**Figure D7.** ^{1}H NMR (500 MHz, chloroform-*d*, conc. 77 mM) spectrum of nitroxide tetraradical **27** (AO-4-33-col1&2-500).
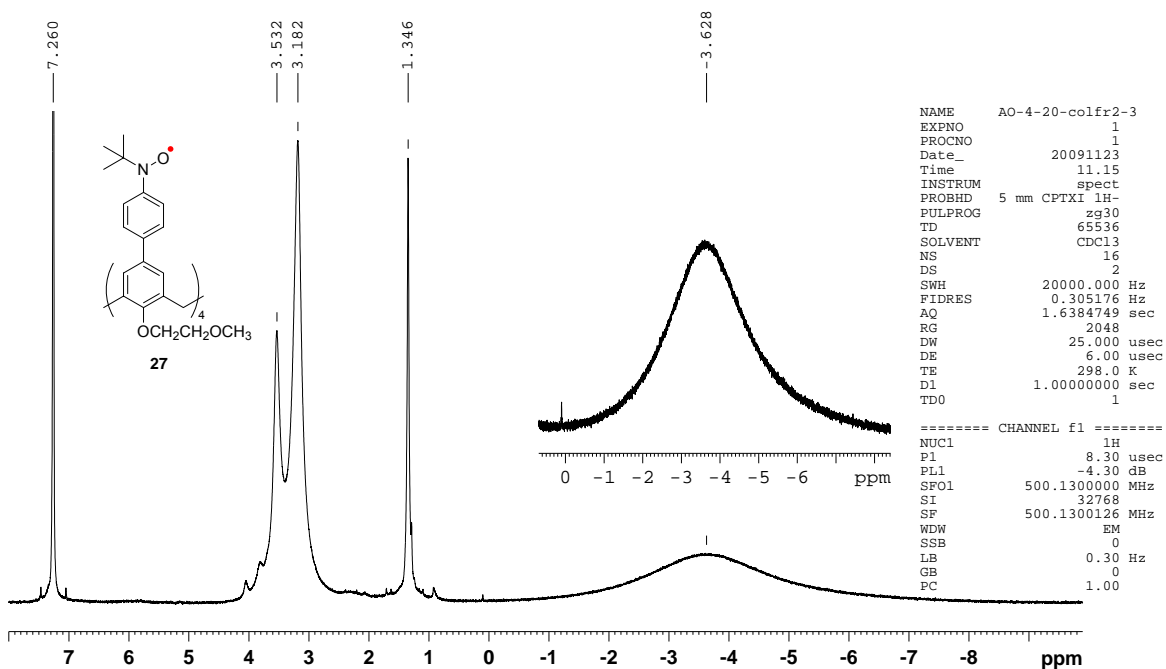


**Figure D8.** ^{1}H NMR (500 MHz, chloroform-*d*, conc. 6 mM) spectrum of nitroxide tetraradical **27** (AO-4-20-colfr2-3).
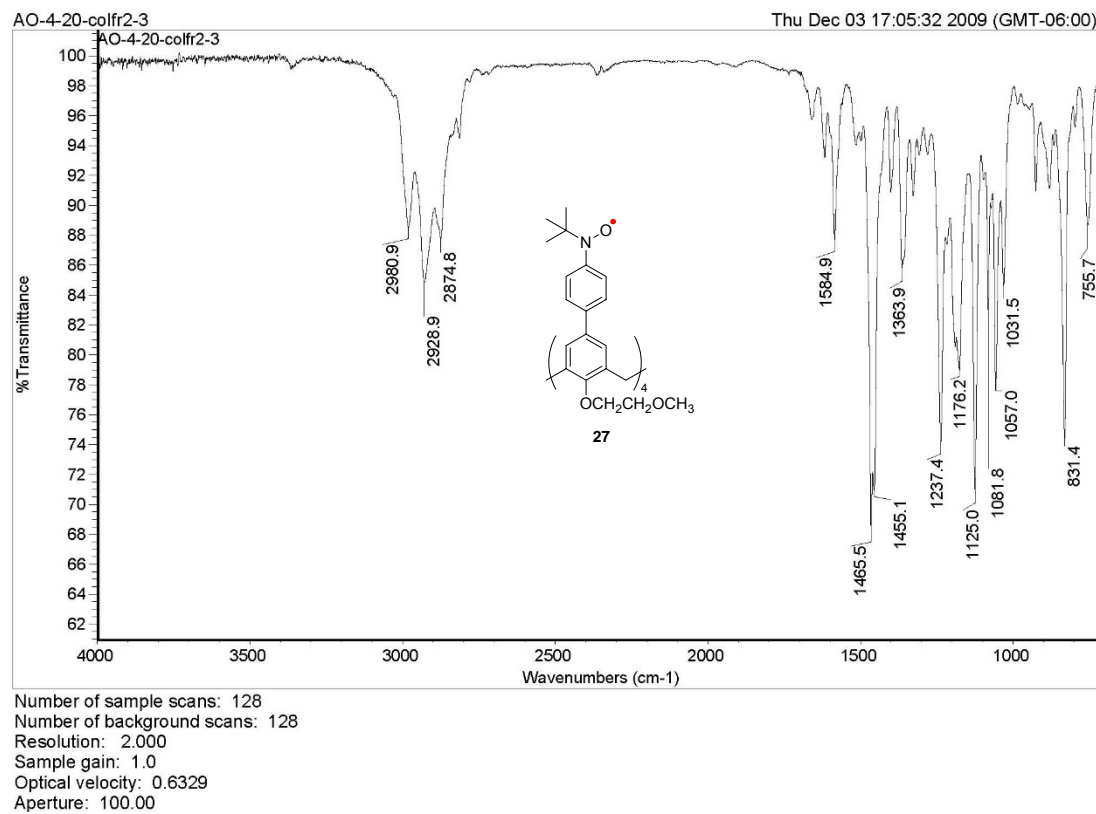
**Figure D9.** IR (ATR, ZnSe, cm$^{-1}$) spectrum of nitroxide tetraradical **27** (AO-4-20-colfr2-3).
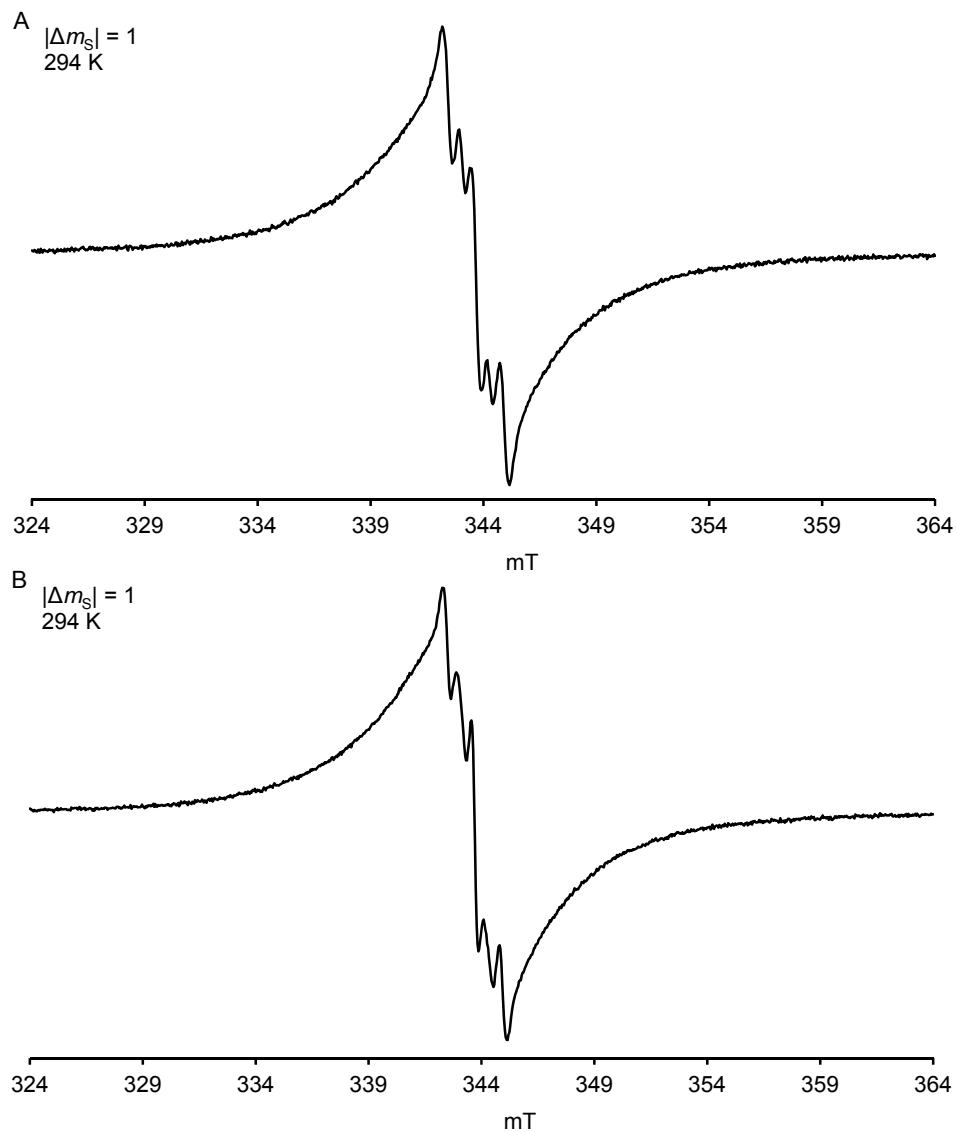
**Figure D10.** CW EPR spectra ($|\Delta m_s| = 1$) of calix[4]arene nitroxide tetraradical **27** in 2-MeTHF at 294 K. **(A) Conc. 1 mM**; X-Band, $\nu = 9.6469$ GHz, 4-mm tube, sample label: AO420colfr2-3, EPR label: AO434r2 (SW400, 20dB, 2G). **(B) Conc. 0.25 mM**; X-Band, $\nu = 9.6481$ GHz, 4-mm tube, sample label: AO433col1&2, EPR label: AO563r5 (SW400, 15dB, 2G).
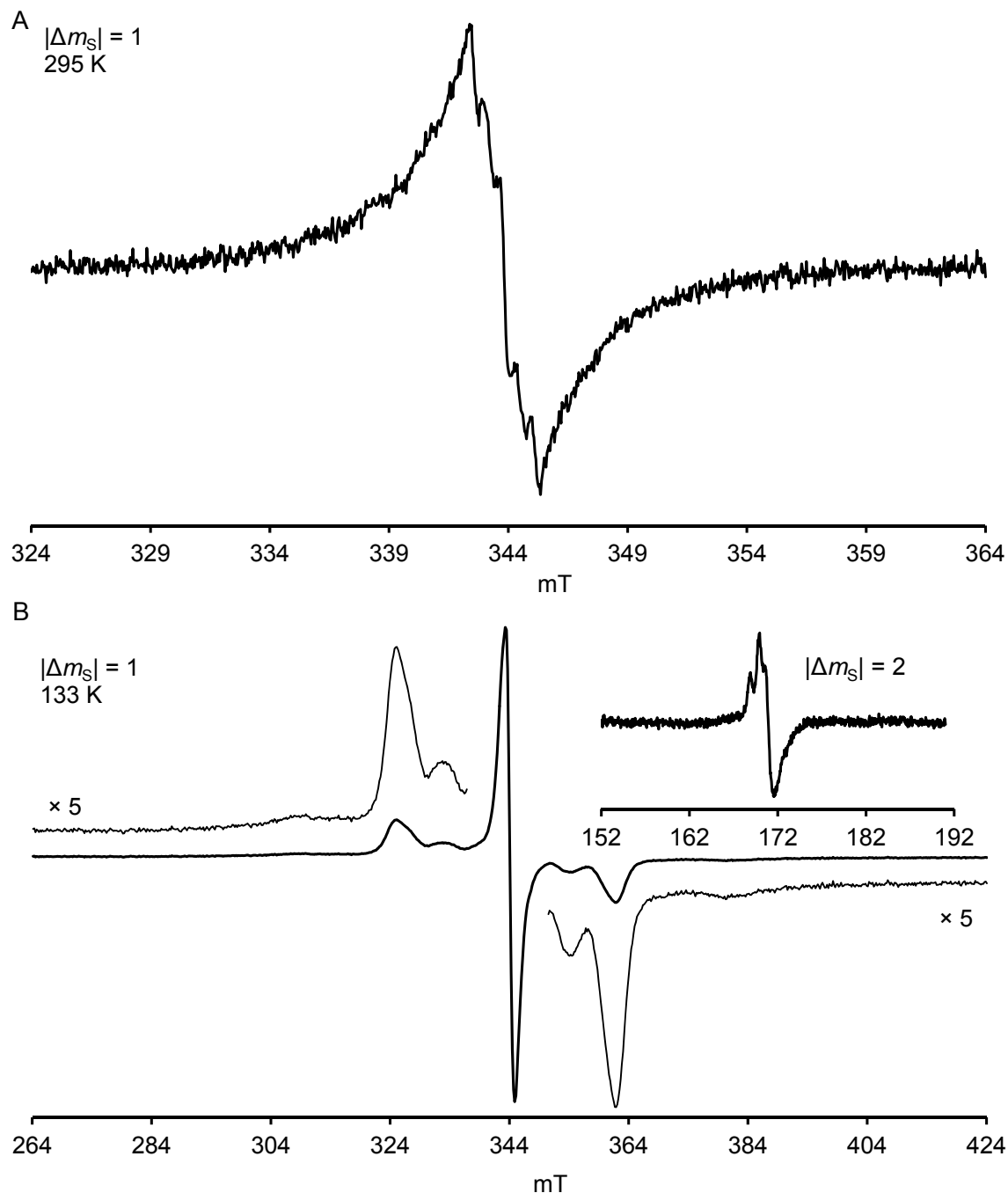
**Figure D11.** CW EPR spectra of 0.17 mM calix[4]arene nitroxide tetraradical **27** in 2-MeTHF/MeOH, 2:1 (sample label: AO433col1&2). **(A) $|\Delta m_s|$ = 1 at 295 K**; X-Band, $\nu$ = 9.6513 GHz, 4-mm tube, EPR label: AO563r9 (SW400, 20dB, 5G). **(B) $|\Delta m_s|$ = 1 at 133 K**; X-Band, $\nu$ = 9.6533 GHz, 4-mm tube, EPR label: AO563r11 (SW1600, 10dB, 3G); inset plot: $|\Delta m_s|$ = 2 region, $\nu$ = 9.6533 GHz (SW400, 10dB, 5G).
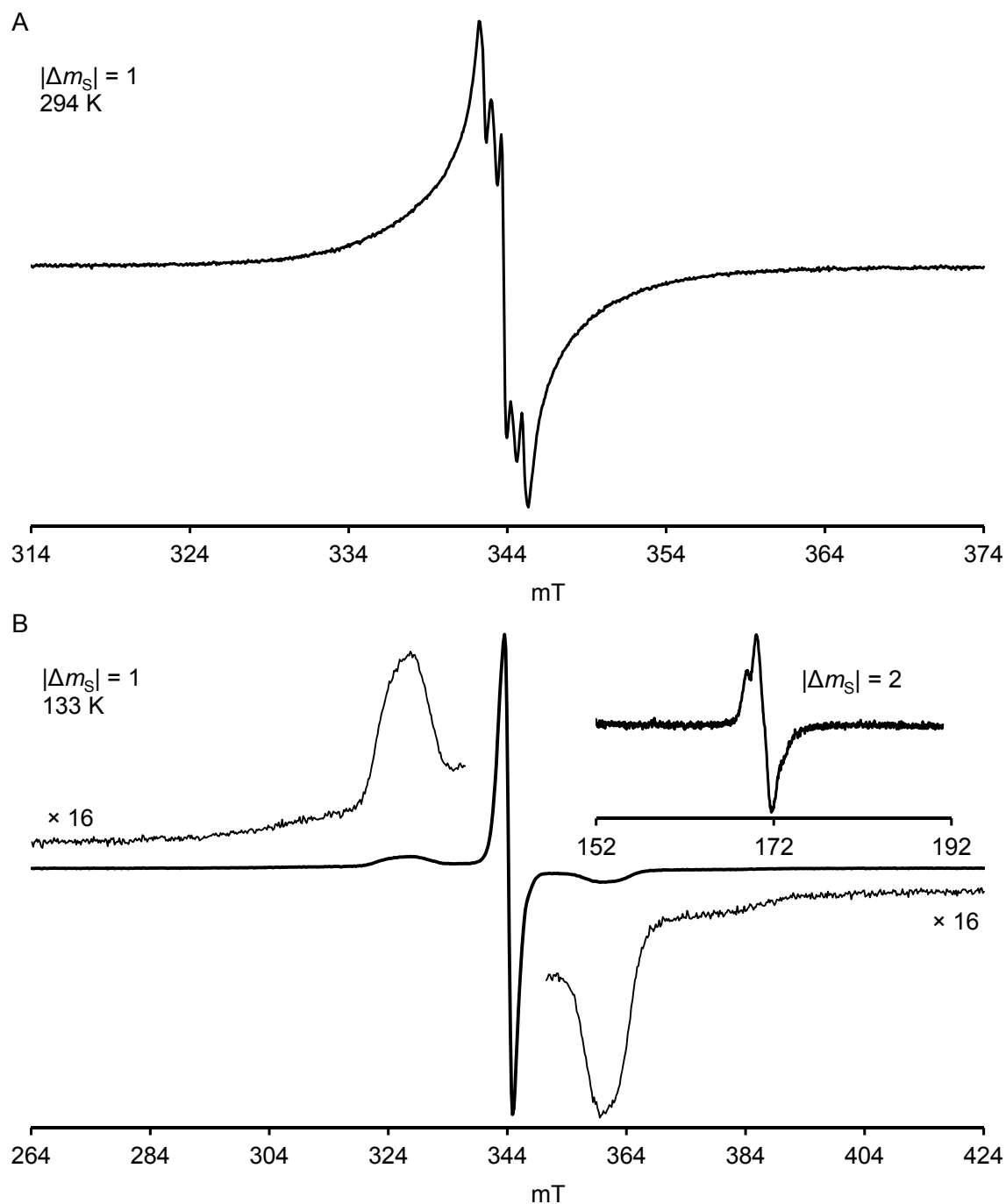
**Figure D12.** CW EPR spectra of 0.2 mM calix[4]arene nitroxide tetraradical **27** in toluene/CHCl$_3$, 4:1 (sample label: AO433col1&2). **(A) $|\Delta m_s| = 1$ at 294 K**; X-Band, $\nu = 9.6488$ GHz, 4-mm tube, EPR label: AO564r21 (SW600, 20dB, 2G). **(B) $|\Delta m_s| = 1$ at 133 K**; X-Band, $\nu = 9.6557$ GHz, 4-mm tube, EPR label: AO564r25 (SW1600, 20dB, 3G); inset plot: $|\Delta m_s| = 2$ region, $\nu = 9.6556$ GHz (SW400, 10dB, 4G).
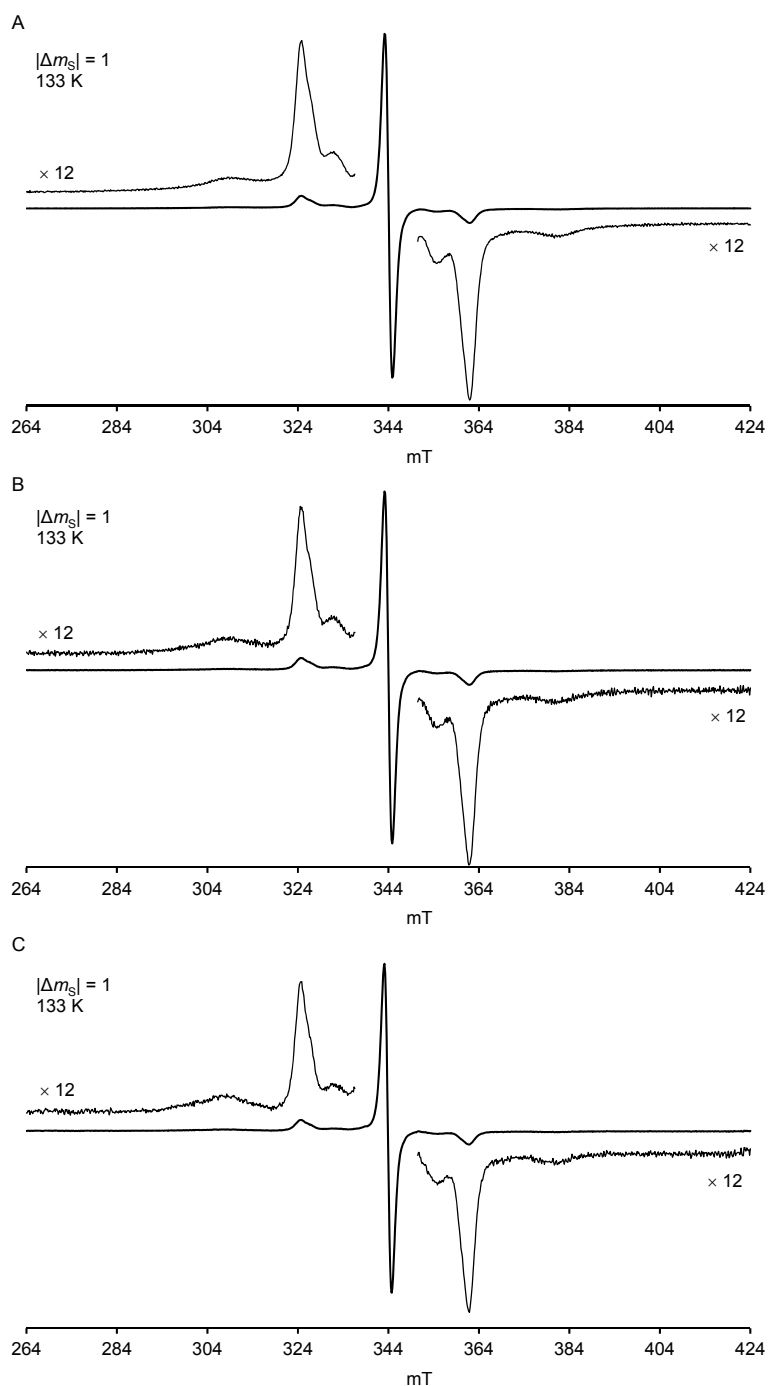
**Figure D13.** CW EPR spectra ($|\Delta m_s| = 1$) calix[4]arene nitroxide tetraradical **27** in 2-MeTHF at 133 K (4-mm tube, sample label: AO433col1&2). **(A) Conc. 0.25 mM**; X-Band, $\nu = 9.6542$ GHz, EPR label: AO586r6 (SW1600, 10dB, 5G). **(B) Conc. 0.06 mM**; X-Band, $\nu = 9.6528$ GHz, 4-mm tube, EPR label: AO586r9 (SW1600, 10dB, 5G). **(C) Conc. 0.03 mM**; X-Band, $\nu = 9.6499$ GHz, 4-mm tube, EPR label: AO586r11 (SW1600, 10dB, 5G).
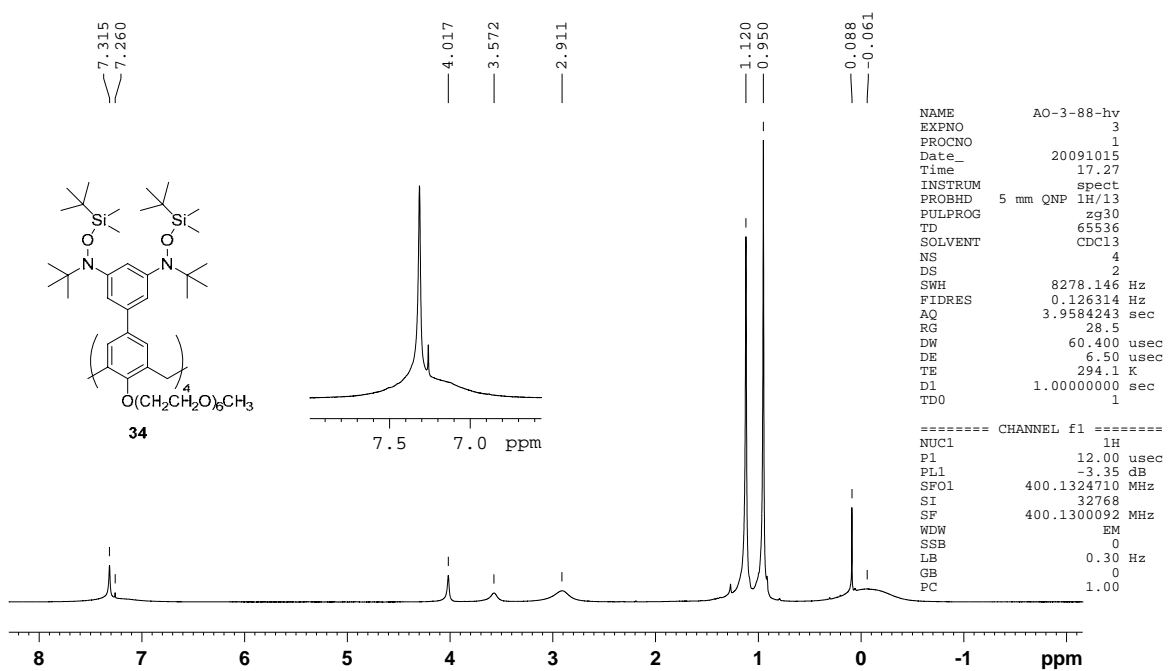
**Figure D14.** $^1$H NMR (400 MHz, chloroform-*d*) spectrum of TBDMS-protected calix[4]arene **34** (AO-3-88-hv).
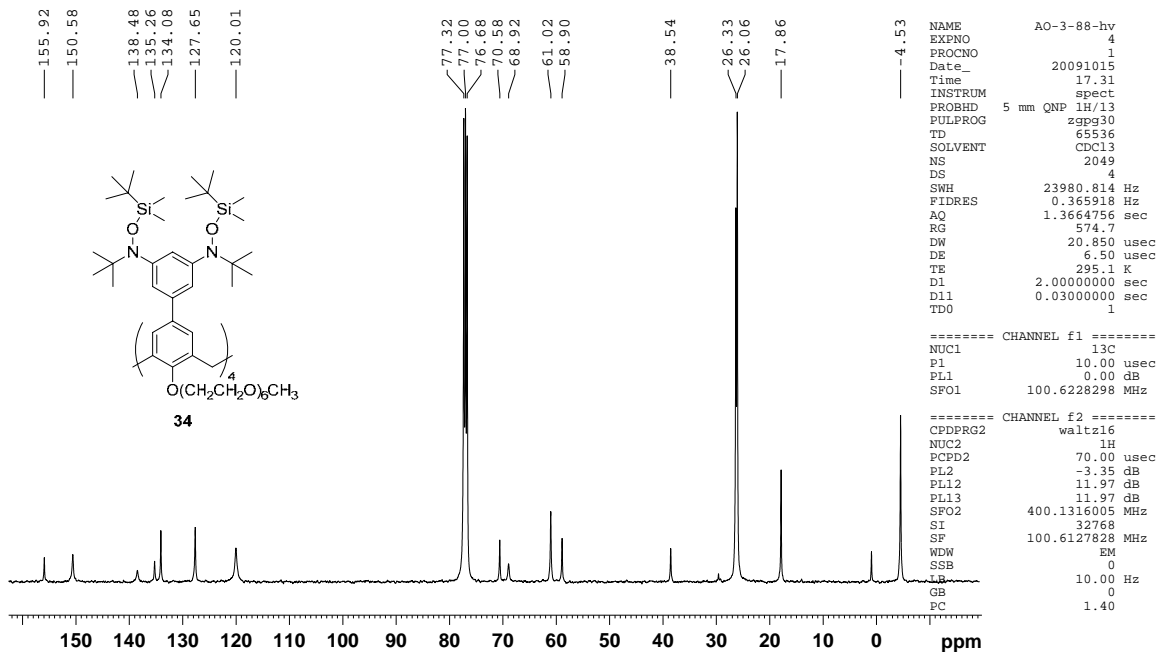


**Figure D15.** $^{13}$C NMR (100 MHz, chloroform-*d*) spectrum of TBDMS-protected calix[4]arene **34** (AO-3-88-hv).
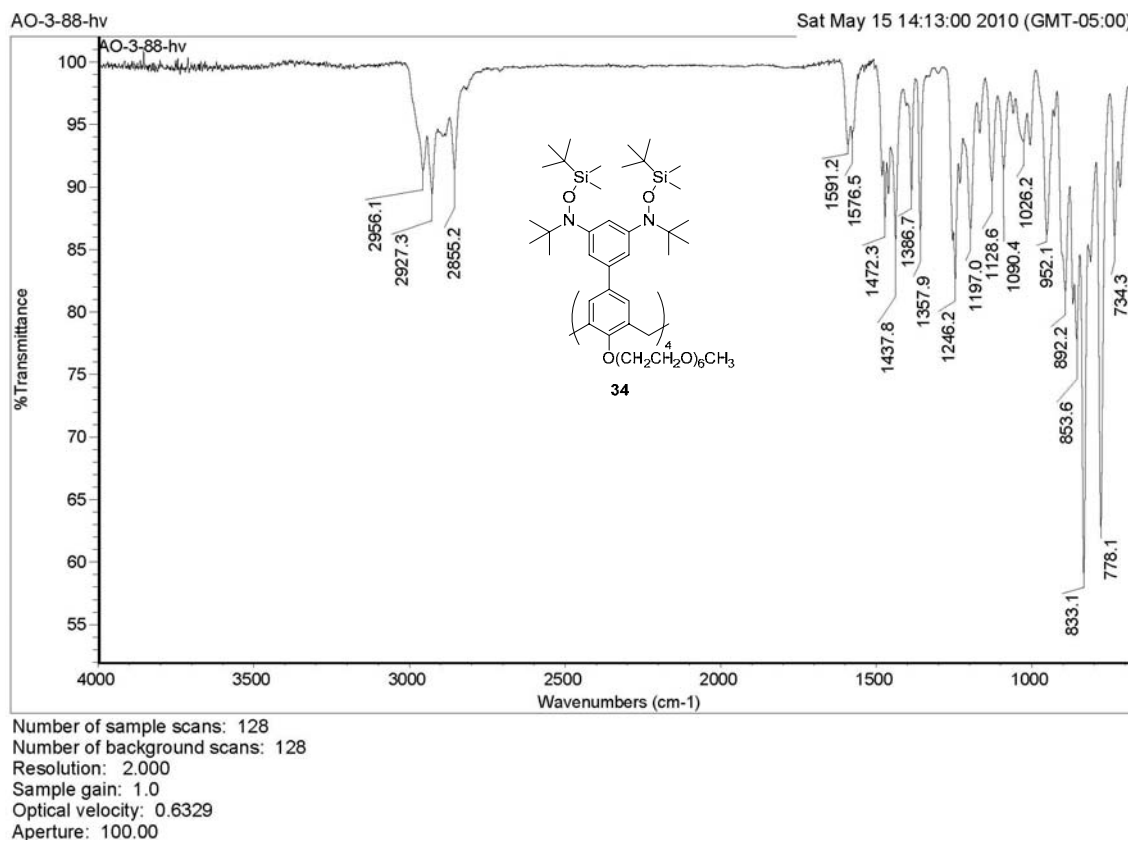
**Figure D16.** IR (ATR, ZnSe, cm$^{-1}$) spectrum of TBDMS-protected calix[4]arene **34** (AO-3-88-hv).
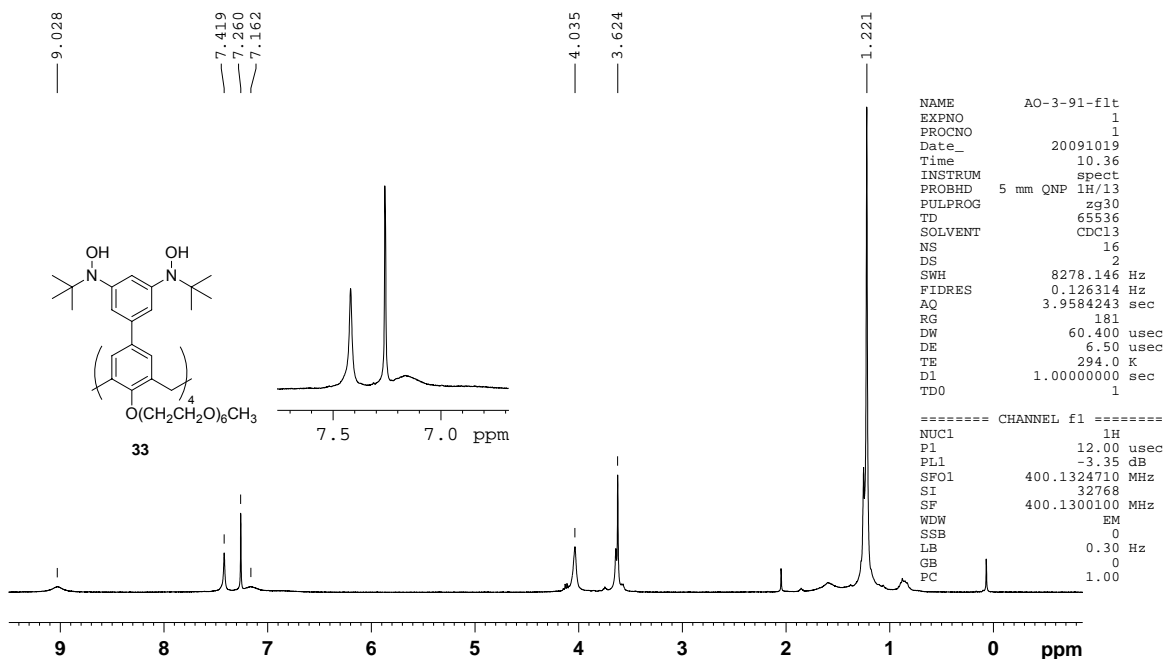
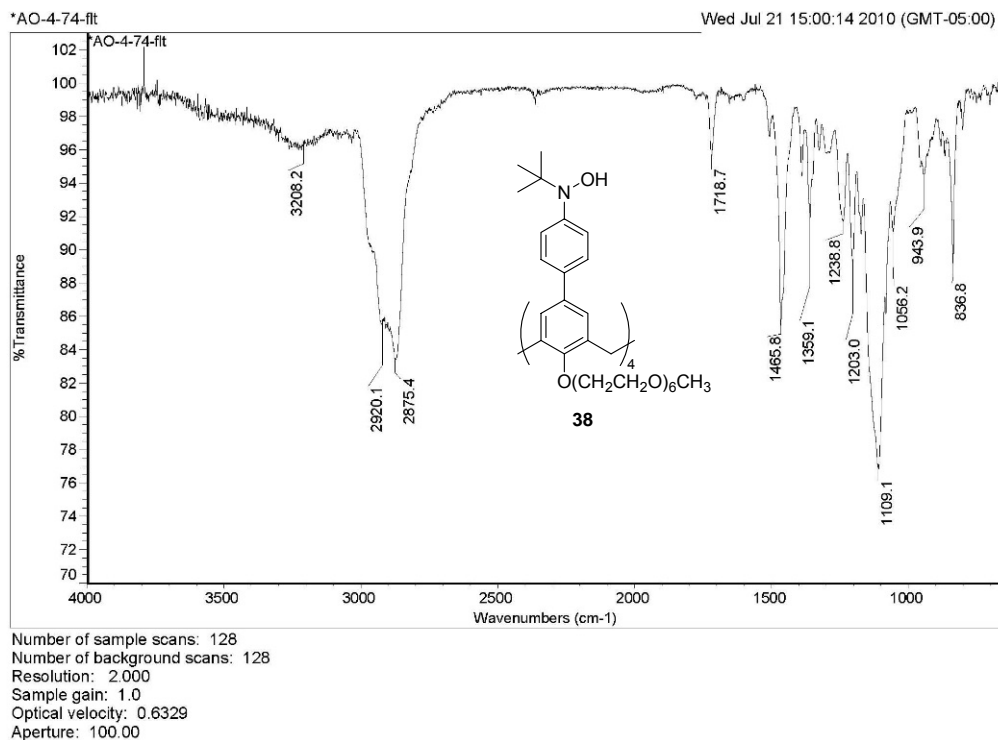**Figure D17.** $^1$H NMR (400 MHz, chloroform-*d*) spectrum of octahydroxylamine calix[4]arene **33** (AO-3-91-flt).
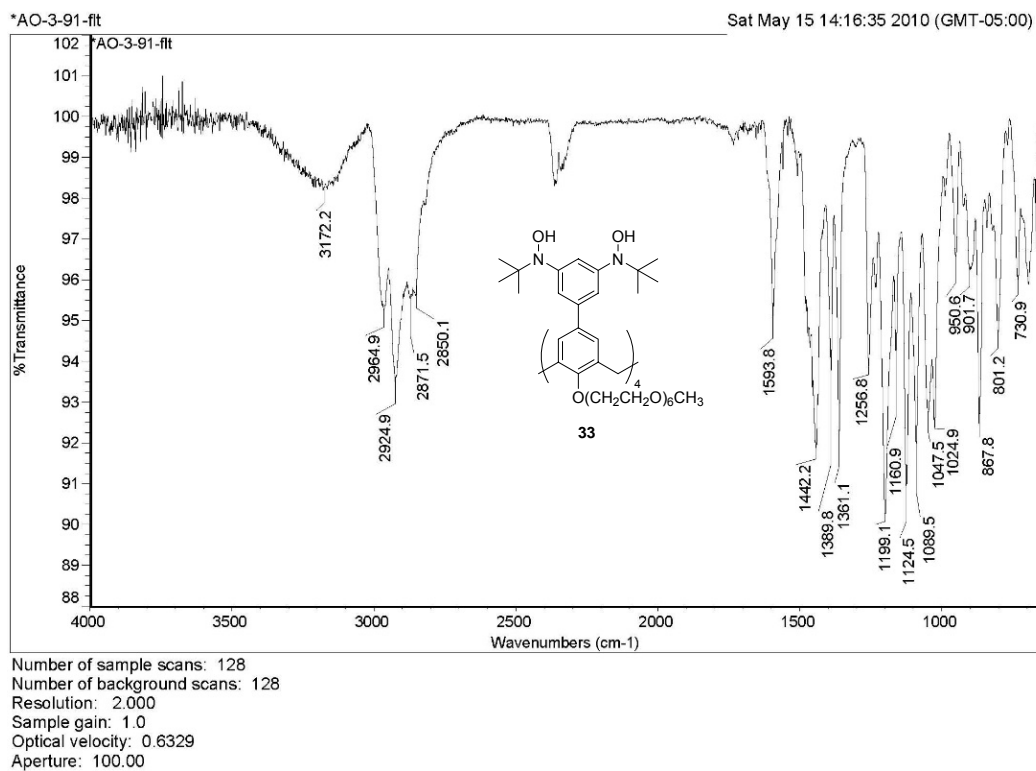


**Figure D18.** IR (ATR, ZnSe, cm$^{-1}$) spectrum of octahydroxylamine calix[4]arene **33** (AO-3-91-flt).
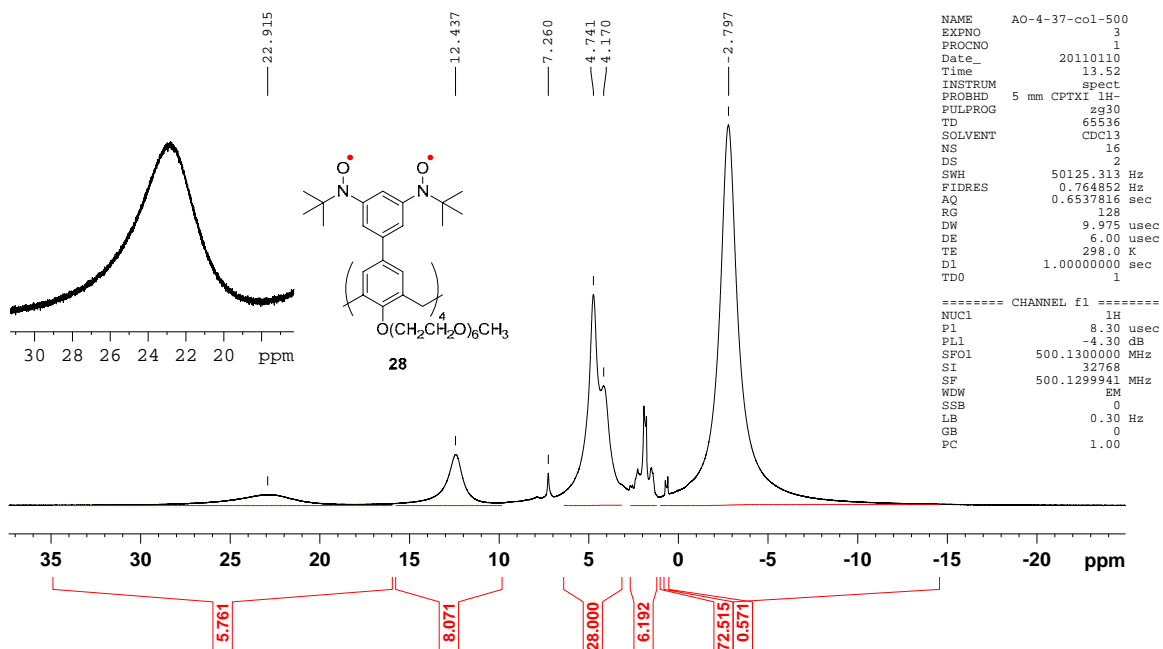
**Figure D19.** $^1$H NMR (500 MHz, chloroform-*d*, conc. 60 mM) spectrum of nitroxide octaradical **28** (AO-4-37-col-500).
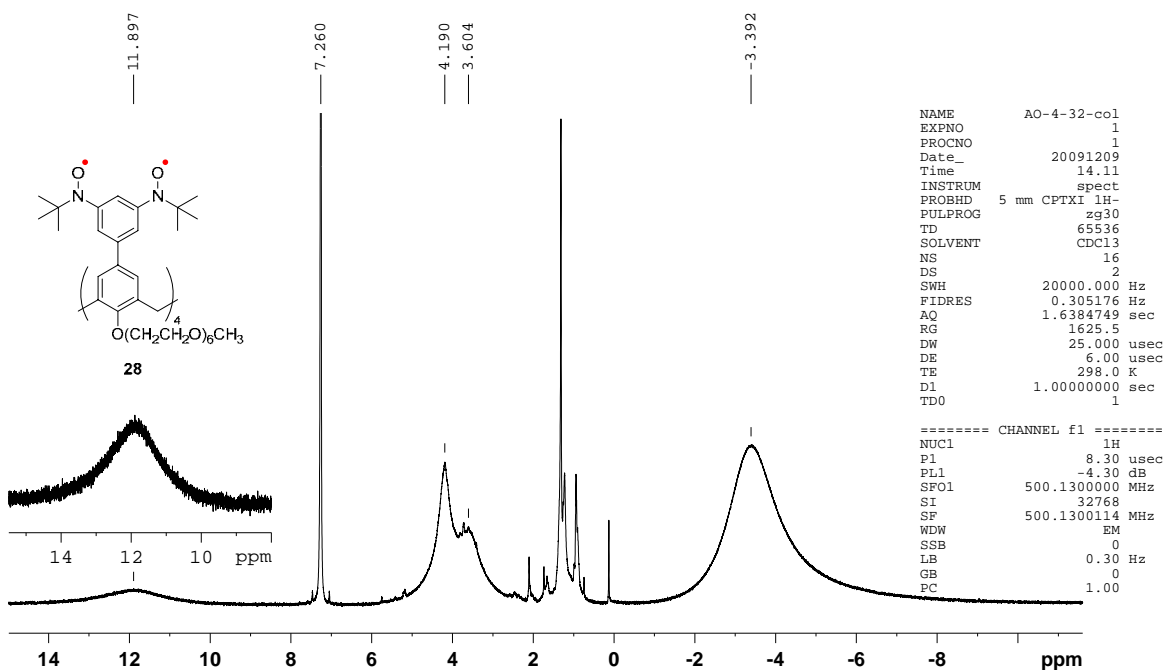


**Figure D20.** $^1$H NMR (500 MHz, chloroform-*d*, conc. 44 mM) spectrum of nitroxide octaradical **28**. (AO-4-32-col).
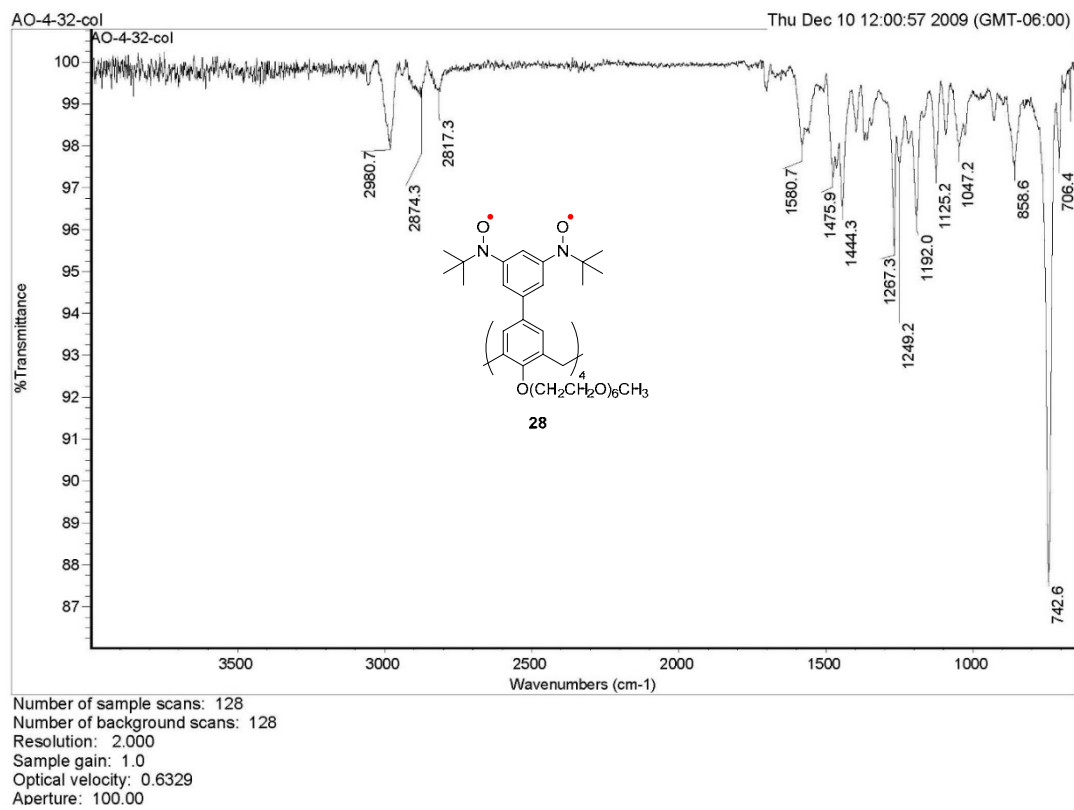
**Figure D21.** IR (ATR, ZnSe, cm$^{-1}$) spectrum of nitroxide octaradical **28** (AO-4-32-col).
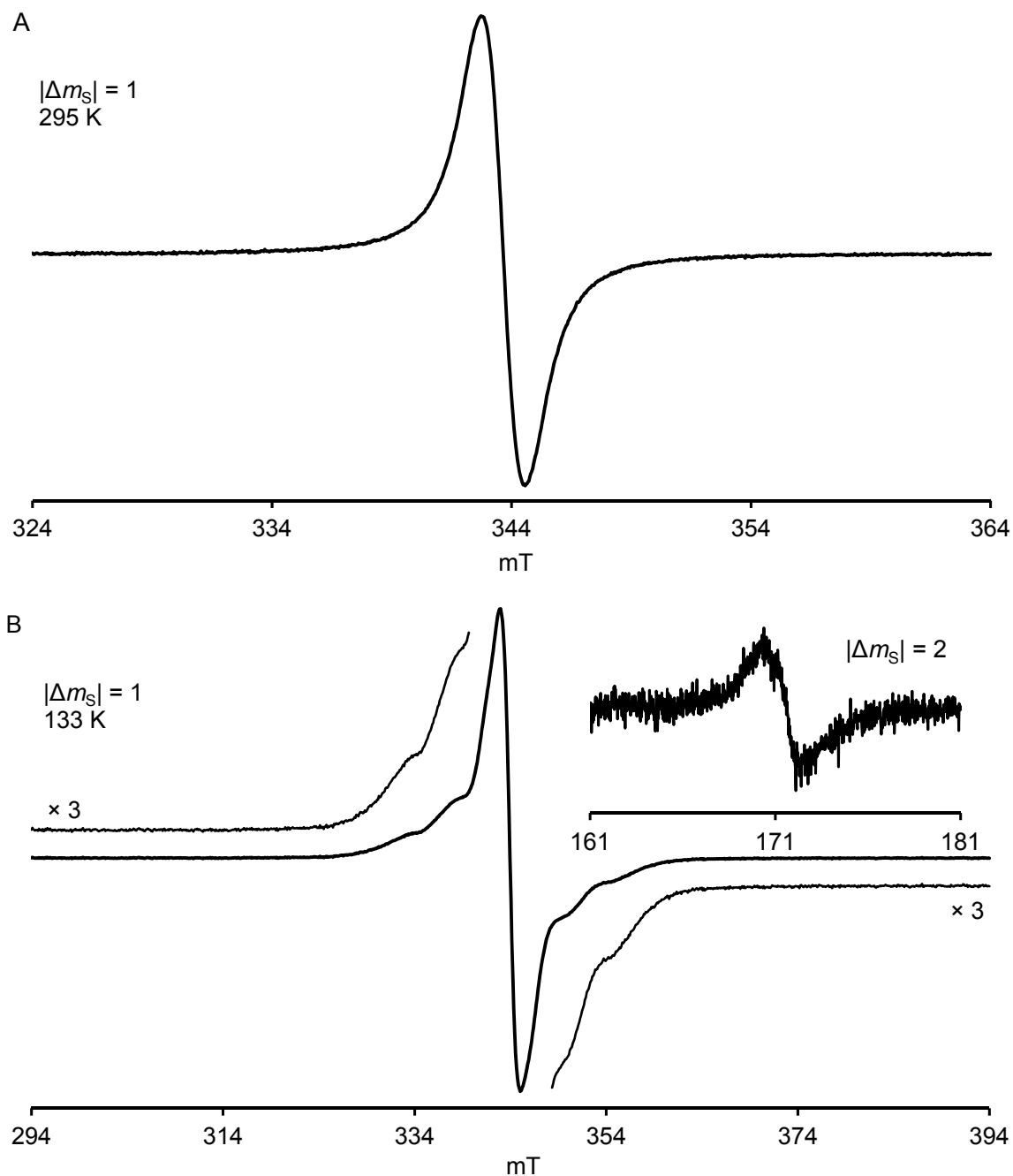
**Figure D22.** CW EPR spectra of 1 mM calix[4]arene nitroxide octaradical **28** in 2-MeTHF (sample label: AO437col). **(A) $|\Delta m_s| = 1$ at 295 K**; X-Band, $\nu = 9.6478$ GHz, 4-mm tube, EPR label: AO556r1 (SW400, 30dB, 1G). **(B) $|\Delta m_s| = 1$ at 133 K**; X-Band, $\nu = 9.6554$ GHz, 4-mm tube, EPR label: AO556r2 (SW1000, 30dB, 1G); inset plot: $|\Delta m_s| = 2$ region, $\nu = 9.6504$ GHz (SW200, 10dB, 5G).

(A)



* impurities

Y = (structure)

(B)

7.260
7.031
7.012
6.612
6.593
6.574
5.276
3.829
3.817
3.804
3.719
3.702
3.682
3.668
3.662
3.656
3.648
3.643
3.637
3.627
3.621
3.610
3.602
3.540
3.529
3.522
3.517
3.506
3.349
2.142
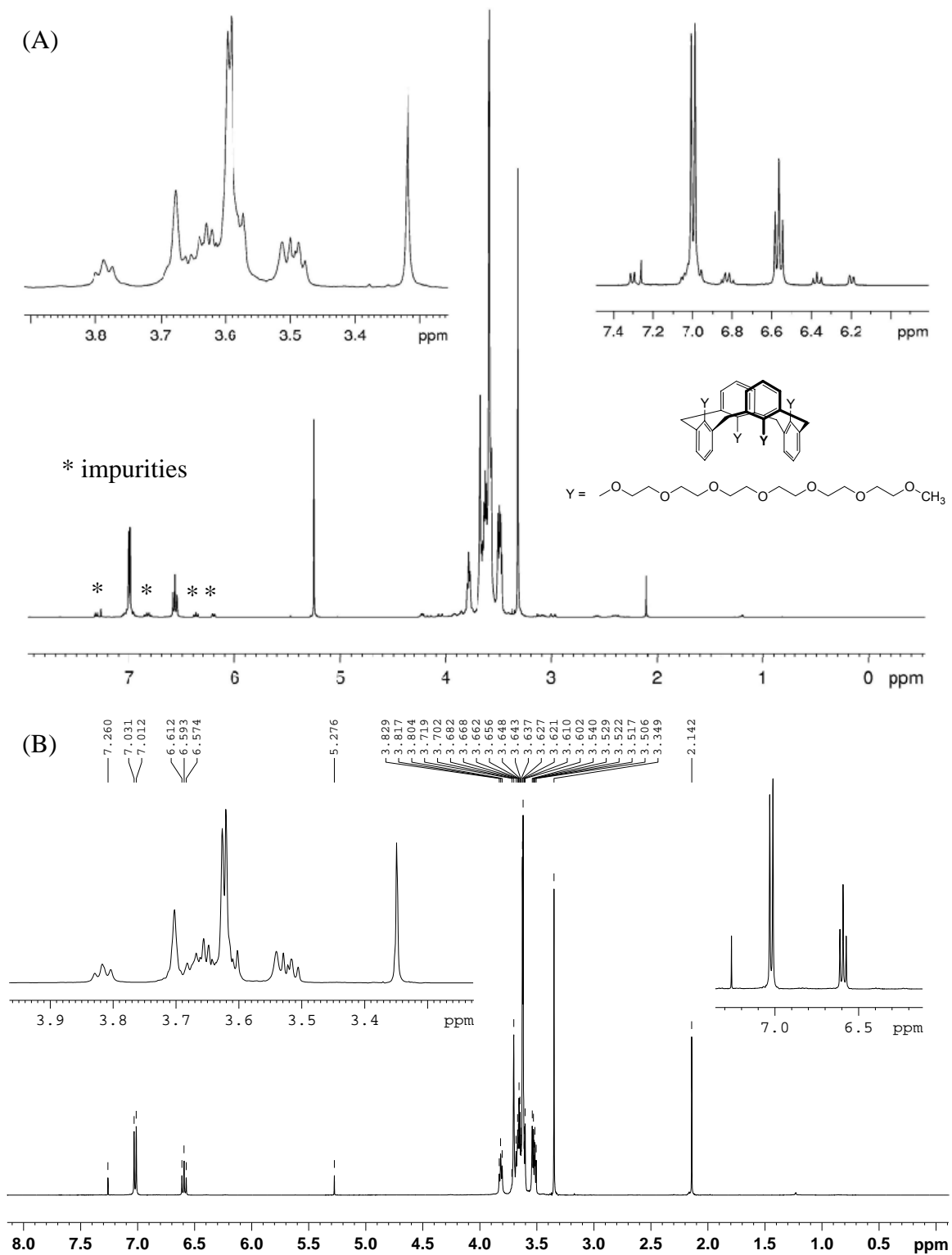
**Figure D23.** $^{13}$C NMR (400 MHz, chloroform-*d*) spectra of tetra-HEG calix[4]arene. (A) label: SM-9-9-col1.2 (B) label: AO-1-35-starting.
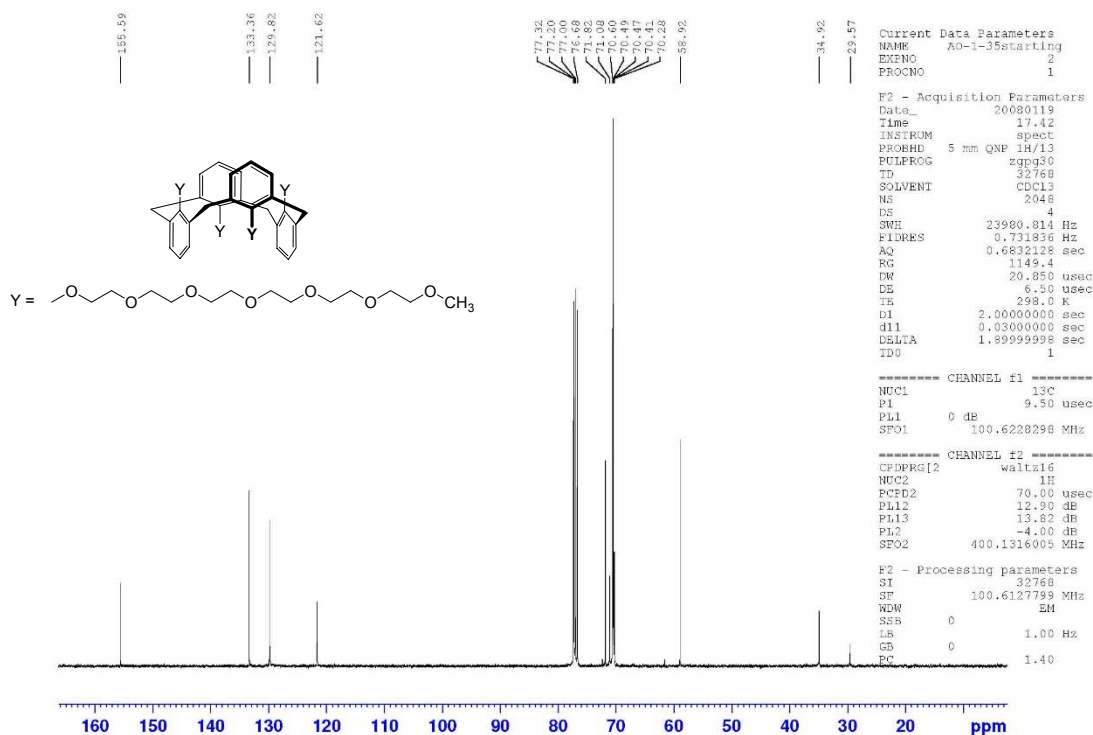
**Figure D24.** $^{13}$C NMR (100 MHz, chloroform-*d*) spectrum of tetra-HEG calix[4]arene (AO-1-35-starting).
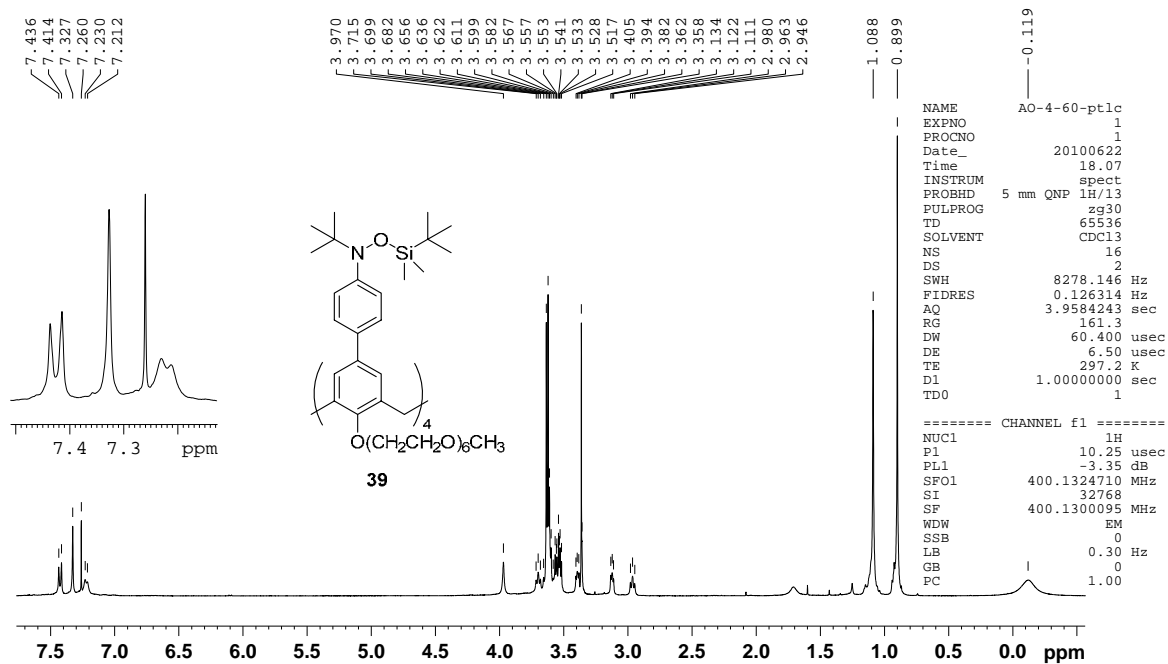


**Figure D25.** $^1$H NMR (400 MHz, chloroform-*d*) spectrum of TBDMS-protected calix[4]arene **39** (AO-4-60-ptlc).
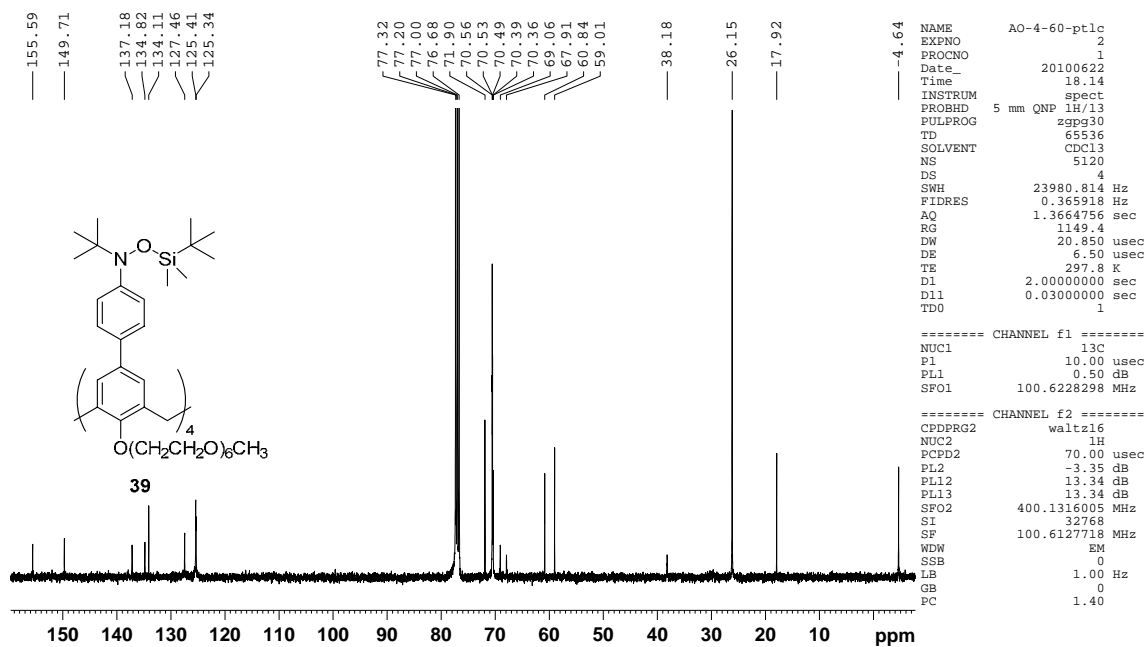
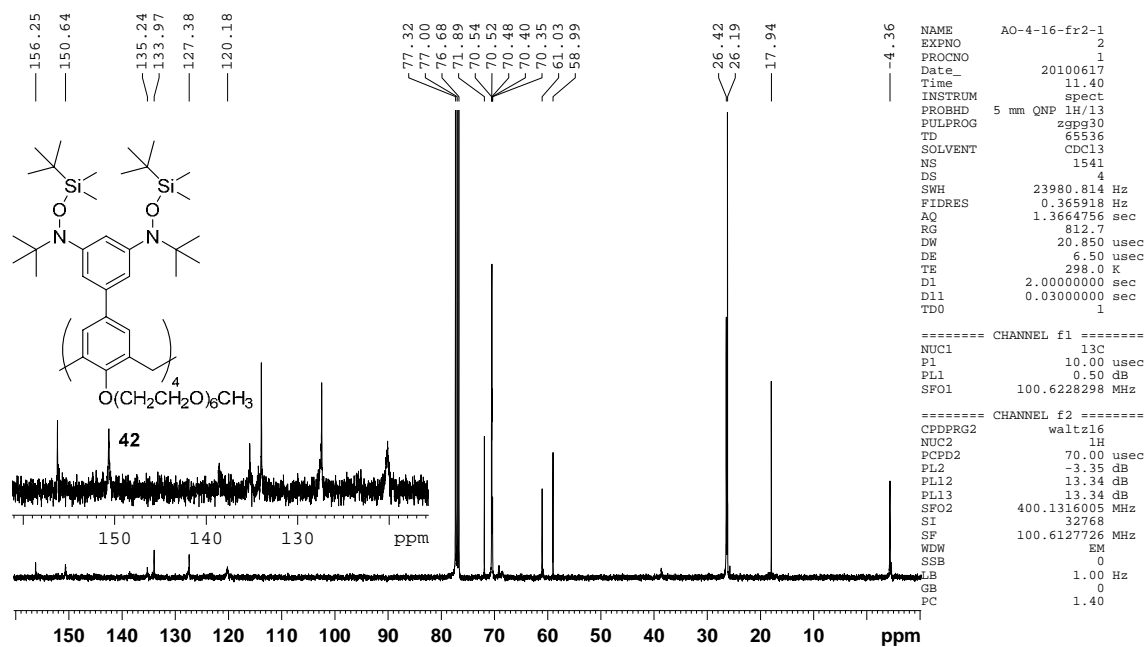**Figure D26.** $^{13}$C NMR (100 MHz, chloroform-*d*) spectrum of TBDMS-protected calix[4]arene **39** (AO-4-60-ptlc).
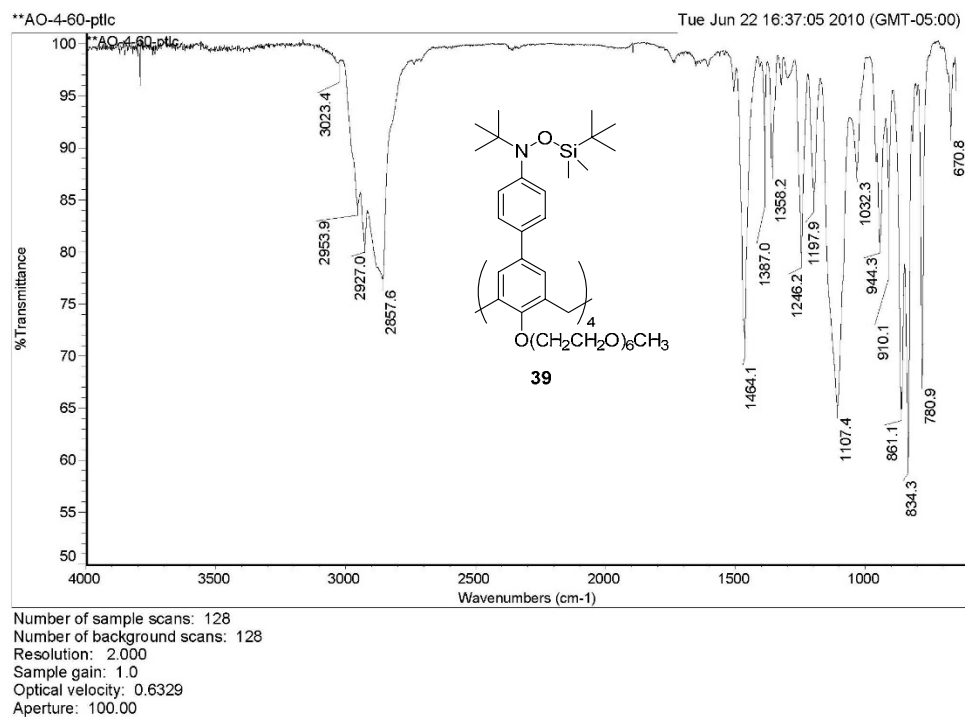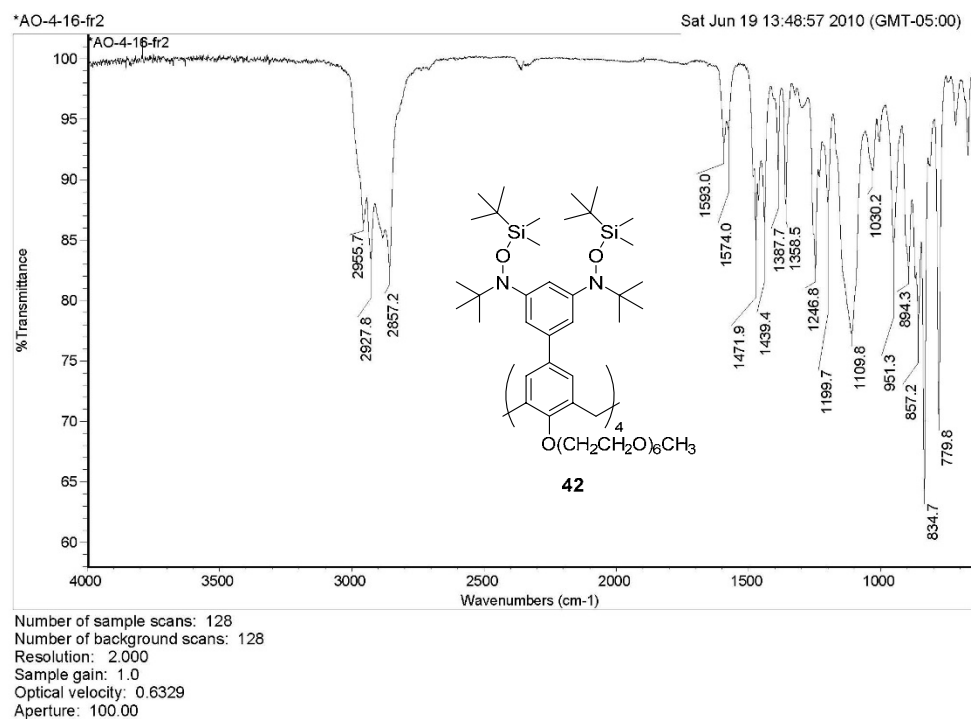


**Figure D27.** IR (ATR, ZnSe, cm$^{-1}$) spectrum of TBDMS-protected calix[4]arene **39** (AO-4-60-ptlc).
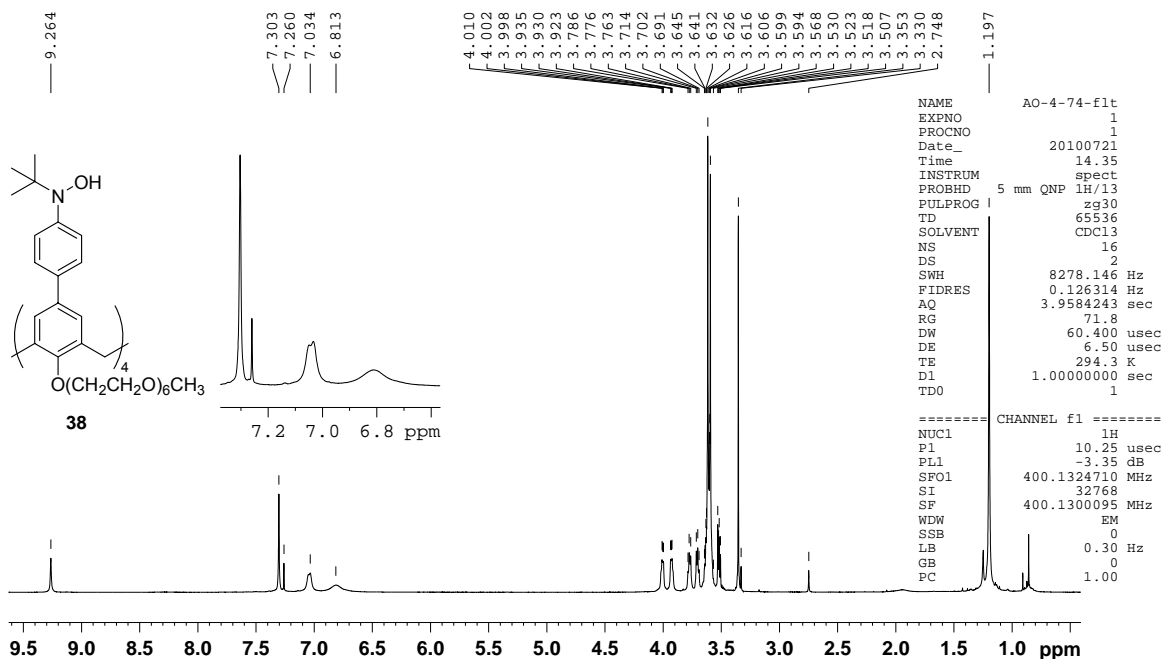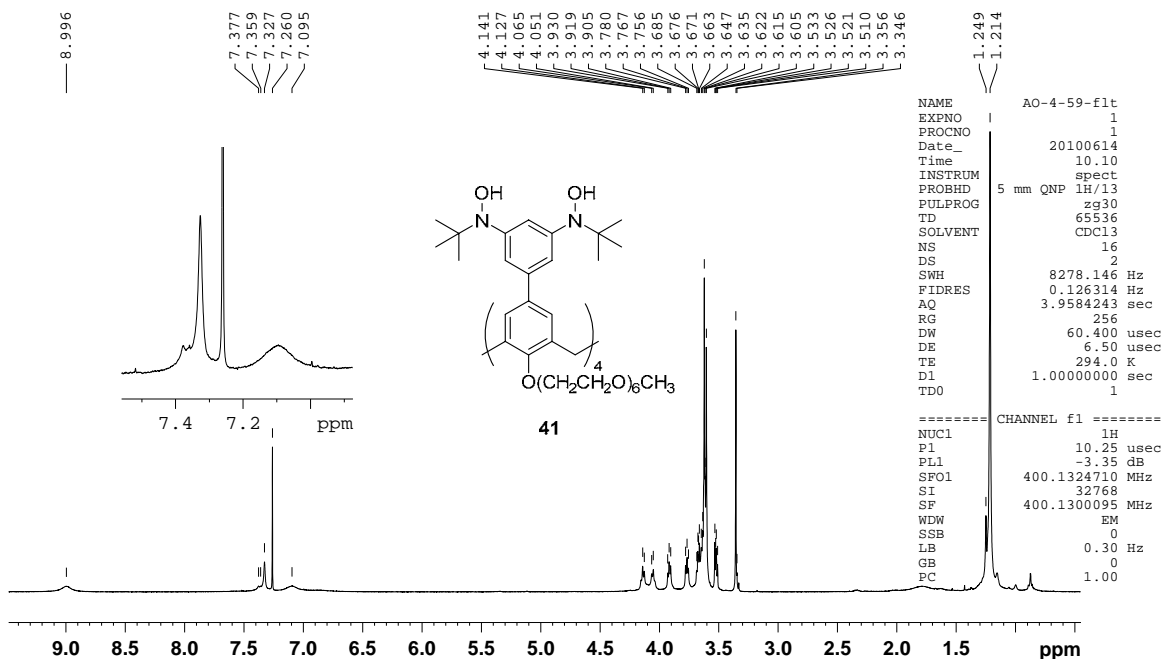
**Figure D28.** $^1$H NMR (400 MHz, chloroform-*d*) spectrum of tetrahydroxylamine calix[4]arene **38** (AO-4-74-flt).
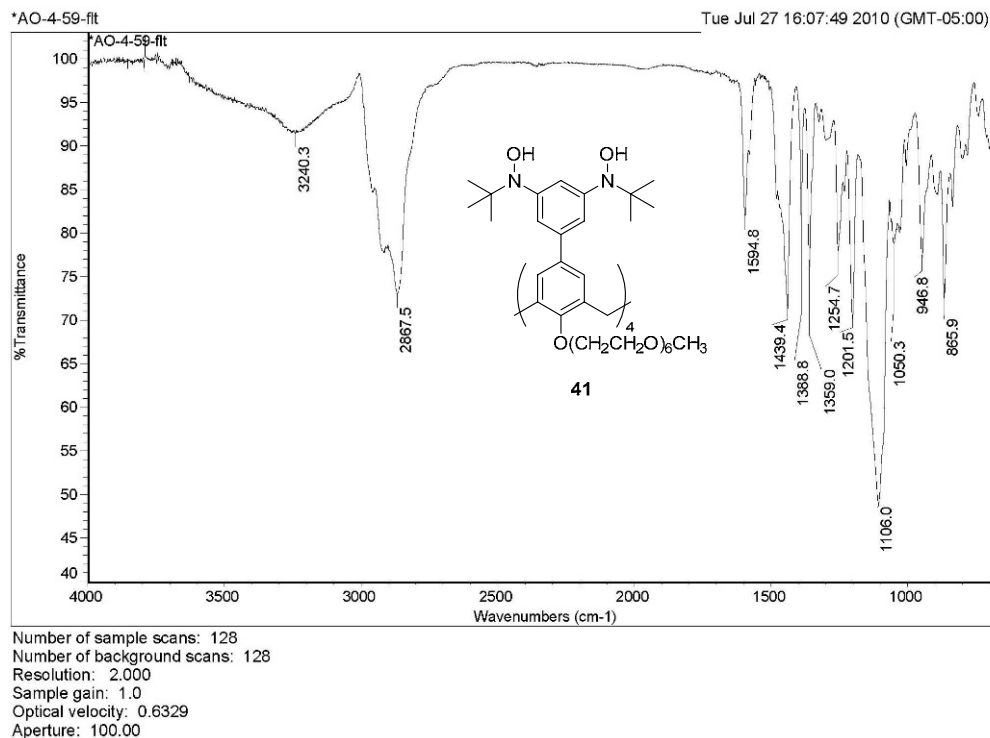


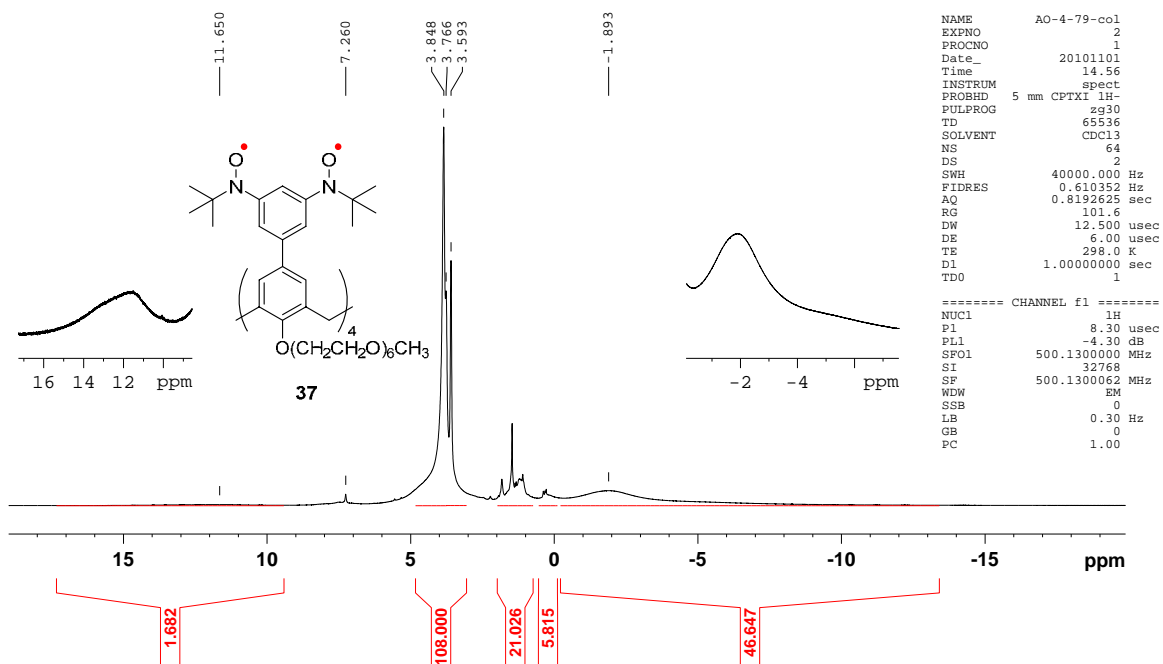**Figure D29.** IR (ATR, ZnSe, cm$^{-1}$) spectrum of tetrahydroxylamine calix[4]arene **38** (AO-4-74-flt).
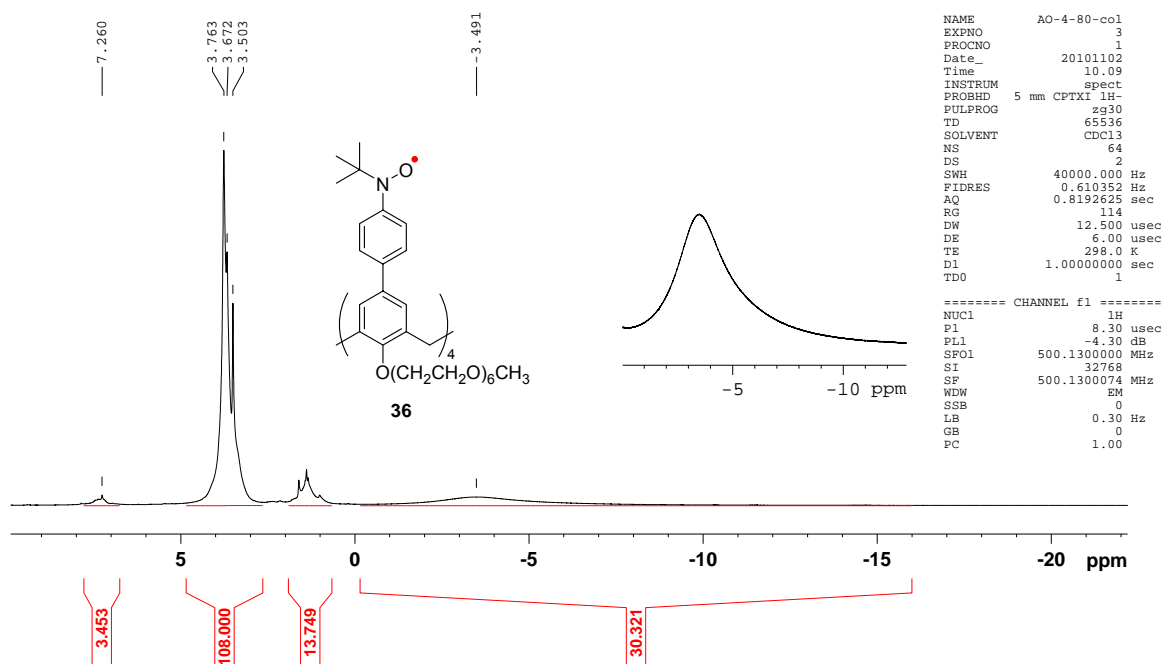
**Figure D30.** $^1$H NMR (500 MHz, chloroform-$d$, conc. 53 mM) spectrum of nitroxide tetraradical **36**. (AO-4-80-col).
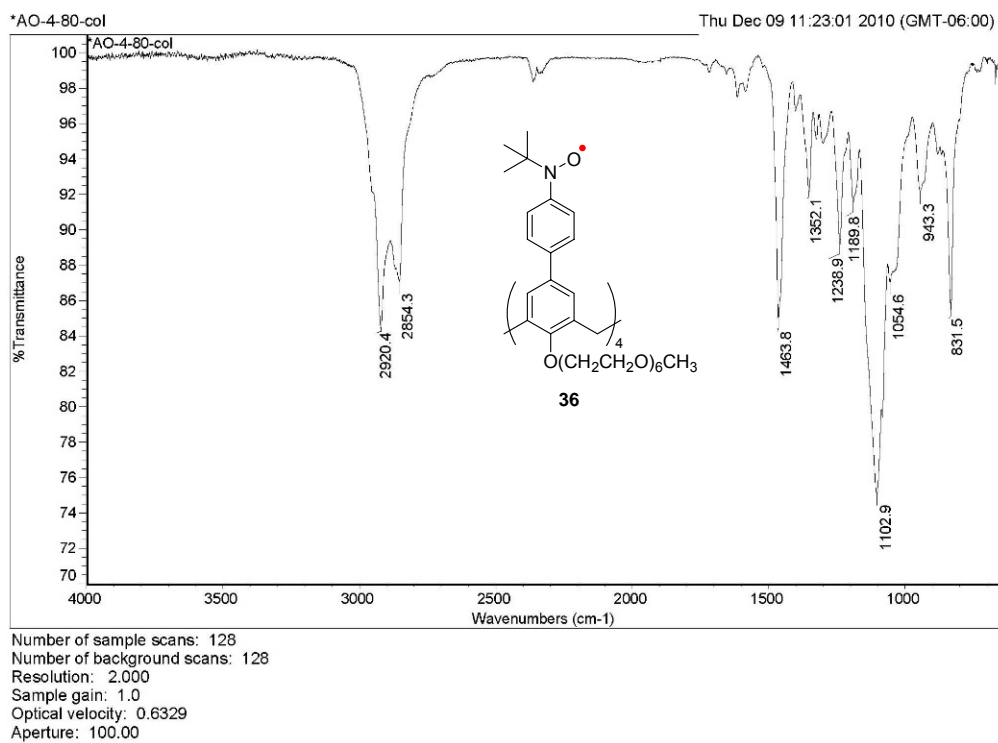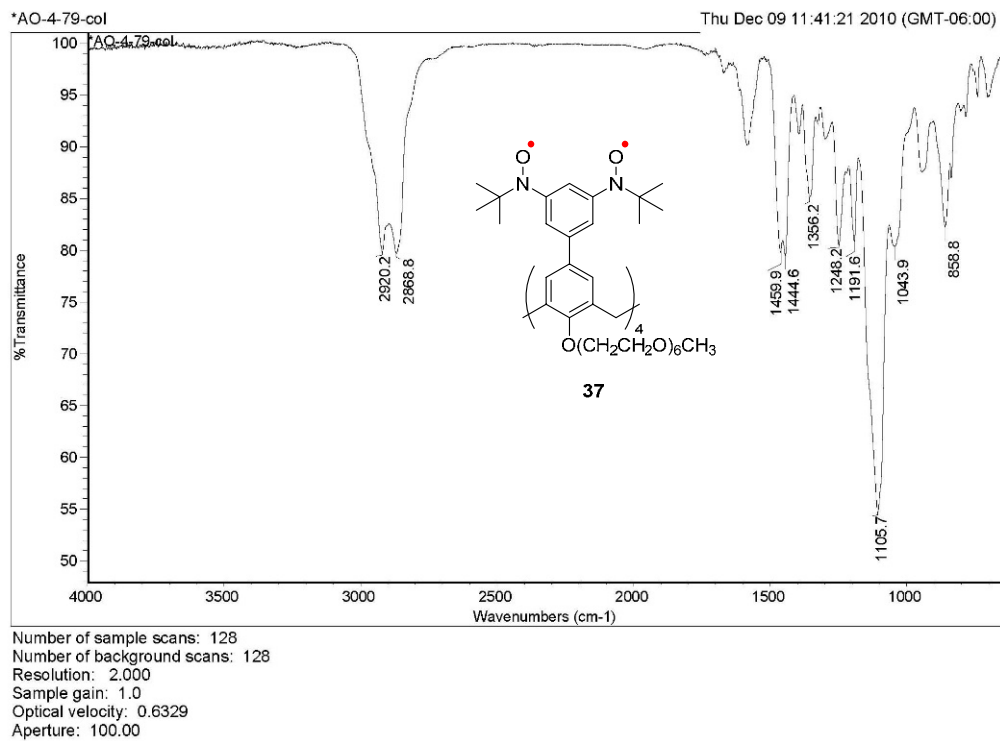


**Figure D31.** IR (ATR, ZnSe, cm$^{-1}$) spectrum of nitroxide tetraradical **36** (AO-4-80-col).
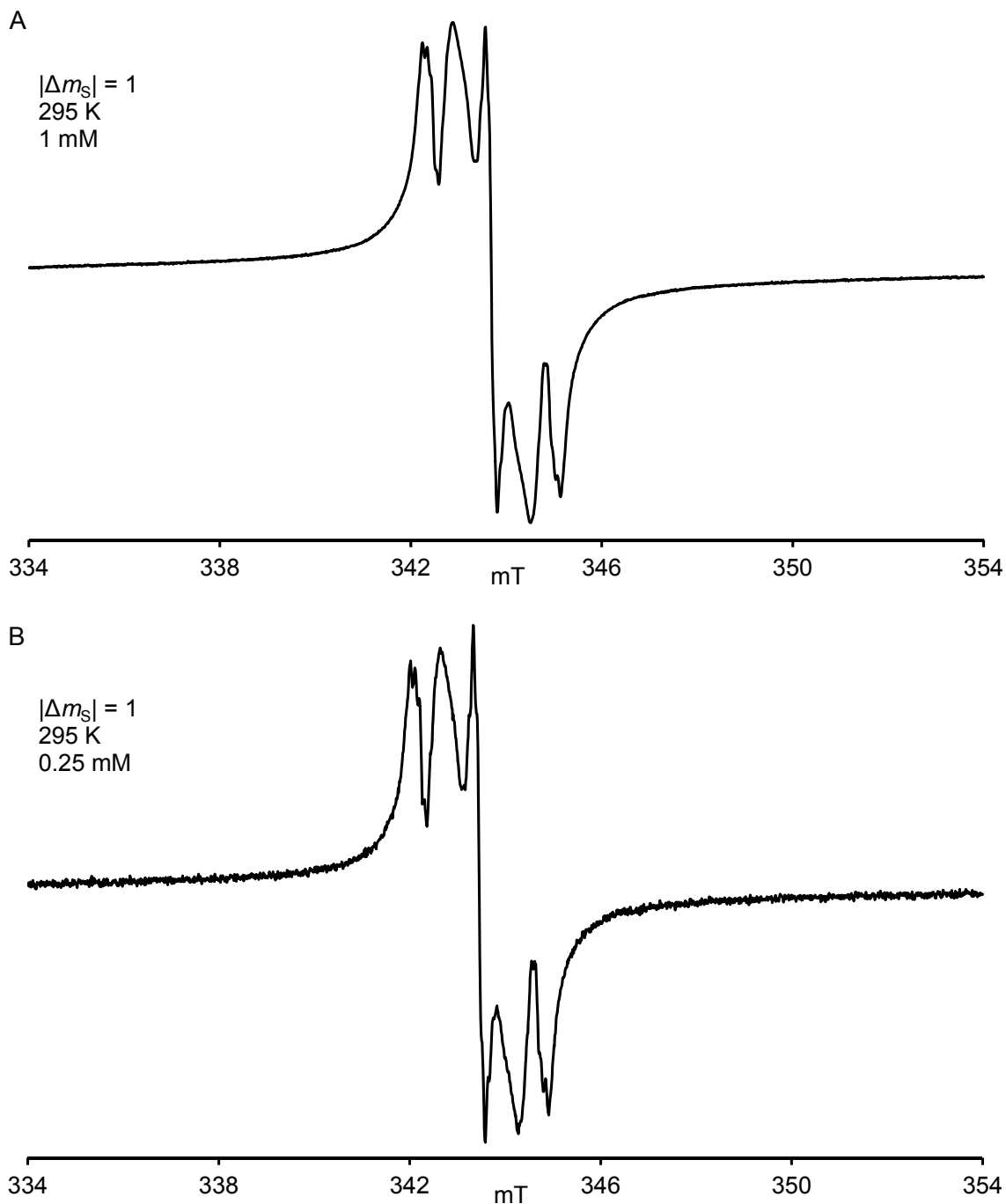
**Figure D32.** CW EPR spectra ($|\Delta m_s| = 1$) of calix[4]arene nitroxide tetraradical **36** (R = HEG) in 2-MeTHF at 295 K. **(A) Conc. 1 mM**; X-Band, $\nu$ = 9.6494 GHz, 4-mm tube, sample label: AO480col, EPR label: AO587r13 (SW200, 10dB, 0.5G). **(B) Conc. 0.25 mM**; X-Band, $\nu$ = 9.6433 GHz, 4-mm tube, sample label: AO480col, EPR label: AO587r23 (SW200, 10 dB, 0.5G).
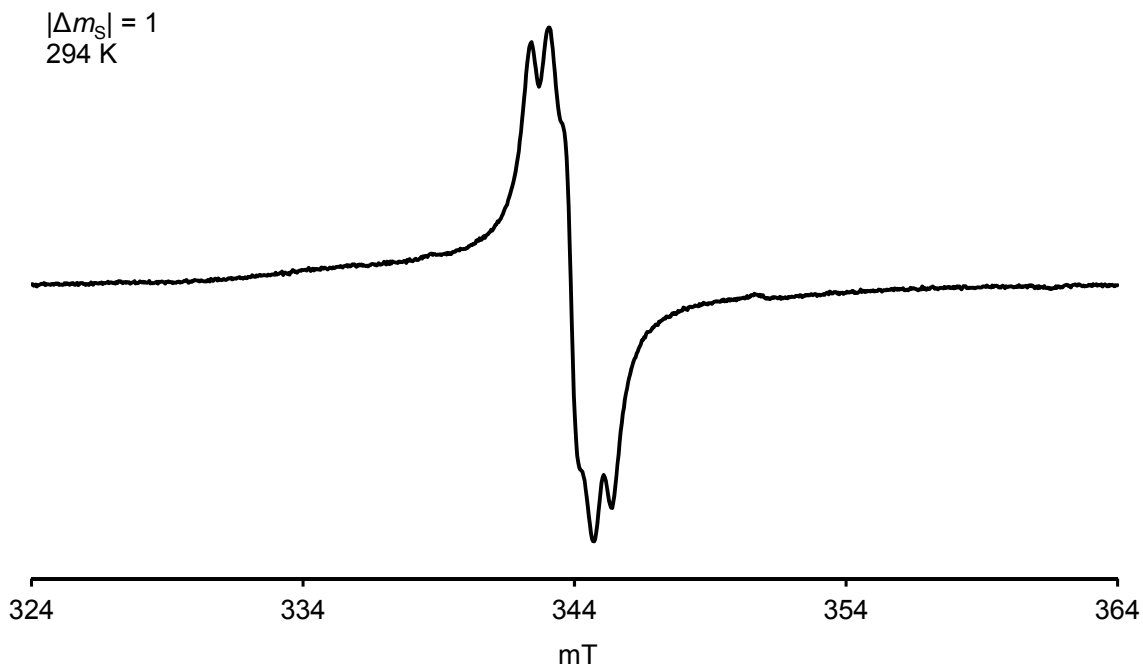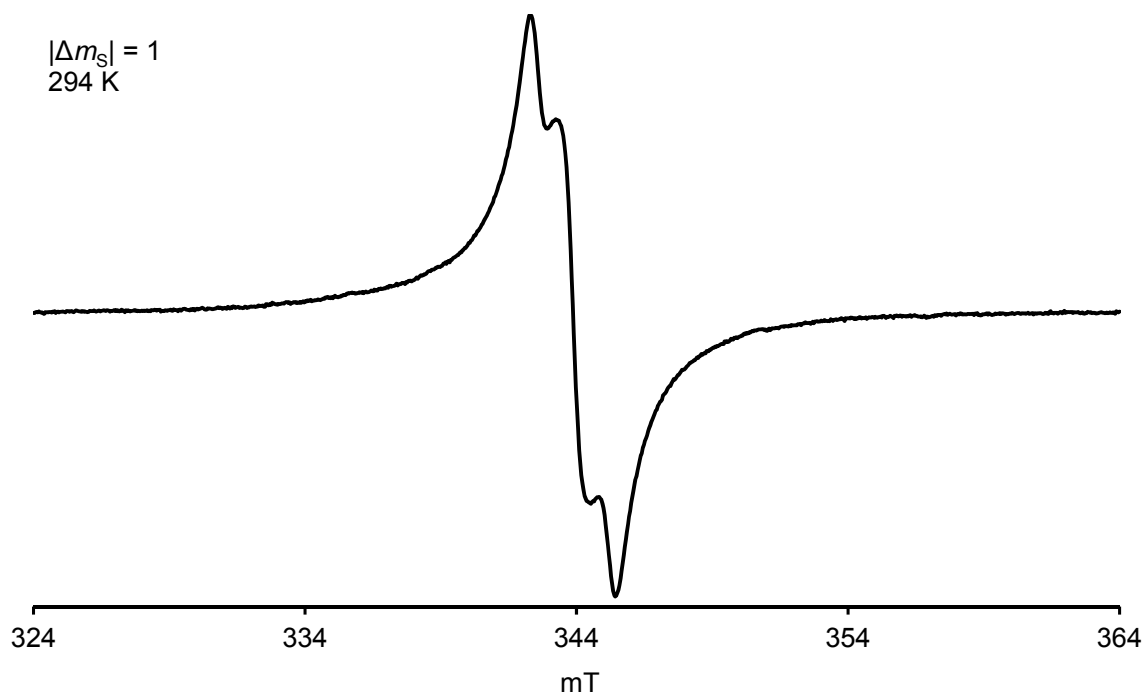
**Figure D33.** CW EPR spectra of 1 mM calix[4]arene nitroxide tetraradical **36** (R = HEG) in EtOH (sample label: AO480col); $|\Delta m_s| = 1$ at 294 K; X-Band, $\nu = 9.6521$ GHz, 4-mm tube, EPR label: AO545r7 (SW400, 10dB, 4G).
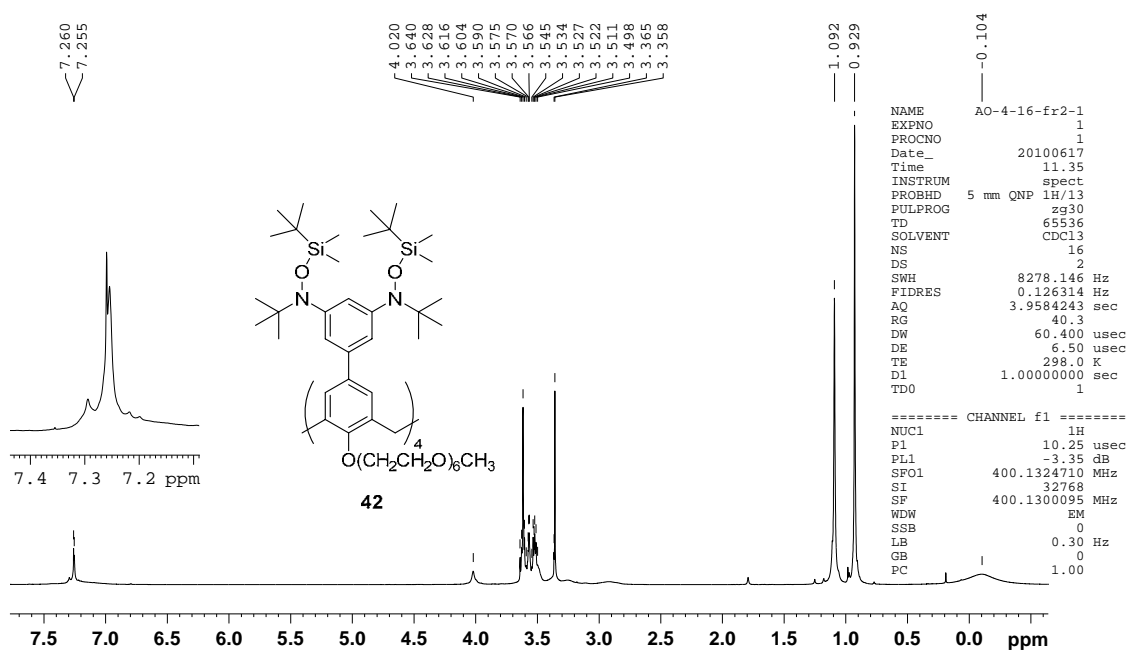


**Figure D34.** $^1$H NMR (400 MHz, chloroform-*d*) spectrum of TBDMS-protected calix[4]arene **42** (AO-4-16-fr2-1).

**Figure D35.** $^{13}$C NMR (100 MHz, chloroform-*d*) spectrum of TBDMS-protected calix[4]arene **42** (AO-4-16-fr2-1).



**Figure D36.** IR (ATR, ZnSe, cm$^{-1}$) spectrum of TBDMS-protected calix[4]arene **42** (AO-4-16-fr2).

**Figure D37.** $^1$H NMR (400 MHz, chloroform-*d*) spectrum of tetrahydroxylamine calix[4]arene **41** (AO-4-59-flt).



**Figure D38.** IR (ATR, ZnSe, cm$^{-1}$) spectrum of tetrahydroxylamine calix[4]arene **41** (AO-4-59-flt).

**Figure D39.** $^1$H NMR (500 MHz, chloroform-*d*, conc. 27 mM) spectrum of nitroxide octaradical **37** (AO-4-79-col).



**Figure D40.** IR (ATR, ZnSe, cm$^{-1}$) spectrum of nitroxide octaradical **37** (AO-4-79-col).

**Figure D41.** CW EPR spectra of 1 mM calix[4]arene nitroxide octaradical **37** (R = HEG) in EtOH (sample label: AO479col); $|\Delta m_s| = 1$ at 294 K; X-Band, $\nu = 9.6527$ GHz, 4-mm tube, EPR label: AO546r5 (SW400, 10dB, 4G).
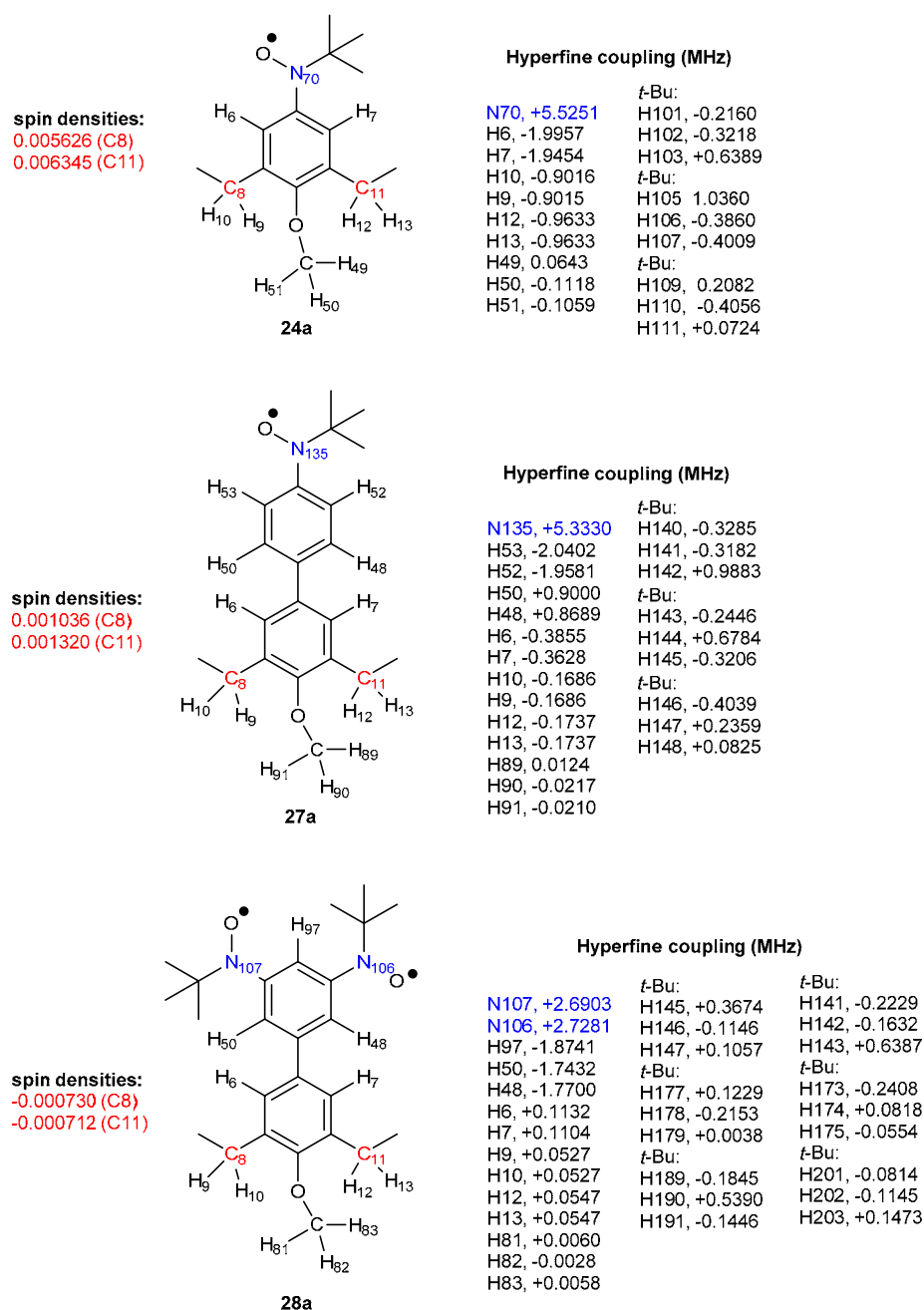
**Figure D42.** Isotropic hyperfine couplings (MHz) and spin densities, computed at the UB3LYP/EPR-II level of theory using ORCA for high-spin states of **24a**, **27a**, and **28a**. [1]H hyperfine couplings (black) and ^{14}N hyperfine couplings (blue) are taken directly from ORCA outputs, i.e., not scaled for values of *S*. Spin densities (red) from ORCA sum to the number of unpaired electrons, i.e., four for **24a** and **27a**, and eight for **28a**. Adapted from Ref. 72 with permission from The Royal Society of Chemistry.

**Table D1.** Selected torsional angles (°) and intramolecular distances (Å) for calix[4]arene nitroxides. Reproduced from Ref. 72 with permission from The Royal Society of Chemistry.

| | | Biphenyl | Cofacial | | | | Adjacent | |
|---|---|---|---|---|---|---|---|---|
| | ONCC | CCCC | C···C | C···C | N···N | O···O | N···N | O···O |
| Tetraradical **24** (X-ray structure) | 15.1, -163.8 -55.7, 121.6 -41.4, 132.8 36.8, -138.1 | - | - | 5.48 5.49 | 5.78 5.70 | 6.92 6.05 | 9.34 9.34 9.45 9.50 | 10.12 10.34 10.67 10.74 |
| Tetraradical **24a** UB3LYP/6-31G(d) gas phase | -10.0, 167.2 | - | - | 4.87 | 4.58 | 4.66 | 9.13 9.18 | 9.64 10.59 |
| Tetraradical **24a** UB3LYP/6-31G(d,p) gas phase | -9.4, 167.9 | - | - | 4.86 | 4.58 | 4.68 | 9.13 9.18 | 9.65 10.60 |
| Tetraradical **27a** UB3LYP/6-31G(d) gas phase | 7.6, -171.5 | -32.8, -35.1 | 4.55 | 4.98 | 4.40 | 4.29 | 17.44 17.57 | 18.15 18.64 |
| Tetraradical **27a** UB3LYP/6-31G(d,p) gas phase | 7.1, -172.1 | -32.6, -35.0 | 4.53 | 4.97 | 4.38 | 4.27 | 17.43 17.56 | 18.14 18.63 |
| Tetraradical **27a** UB3LYP/6-31G(d) THF | 11.0, -167.8 | -32.0, -34.5 | 4.66 | 5.01 | 4.58 | 4.67 | 17.45 17.60 | 18.14 18.72 |
| Octaradical **28a** UB3LYP/6-31G(d) gas phase | -16.5, 162.8 26.0, -151.5 | -28.4, -30.6 | 6.13 | 5.46 | 6.00 6.11 | 6.76 6.86 | 14.37 14.62 15.05 15.71 15.79 16.63 | 12.88 16.06 16.22 16.43 17.00 18.29 |
| Octaradical **28a** UB3LYP/6-31G(d,p) gas phase | 25.1, -152.5, -15.6, 163.7 | -28.8, -30.9 | 6.12 | 5.45 | 5.97 6.10 | 6.70 6.87 | 14.38 14.62 15.04 15.70 15.78 16.63 | 12.87 16.05 16.22 16.43 17.01 18.28 |
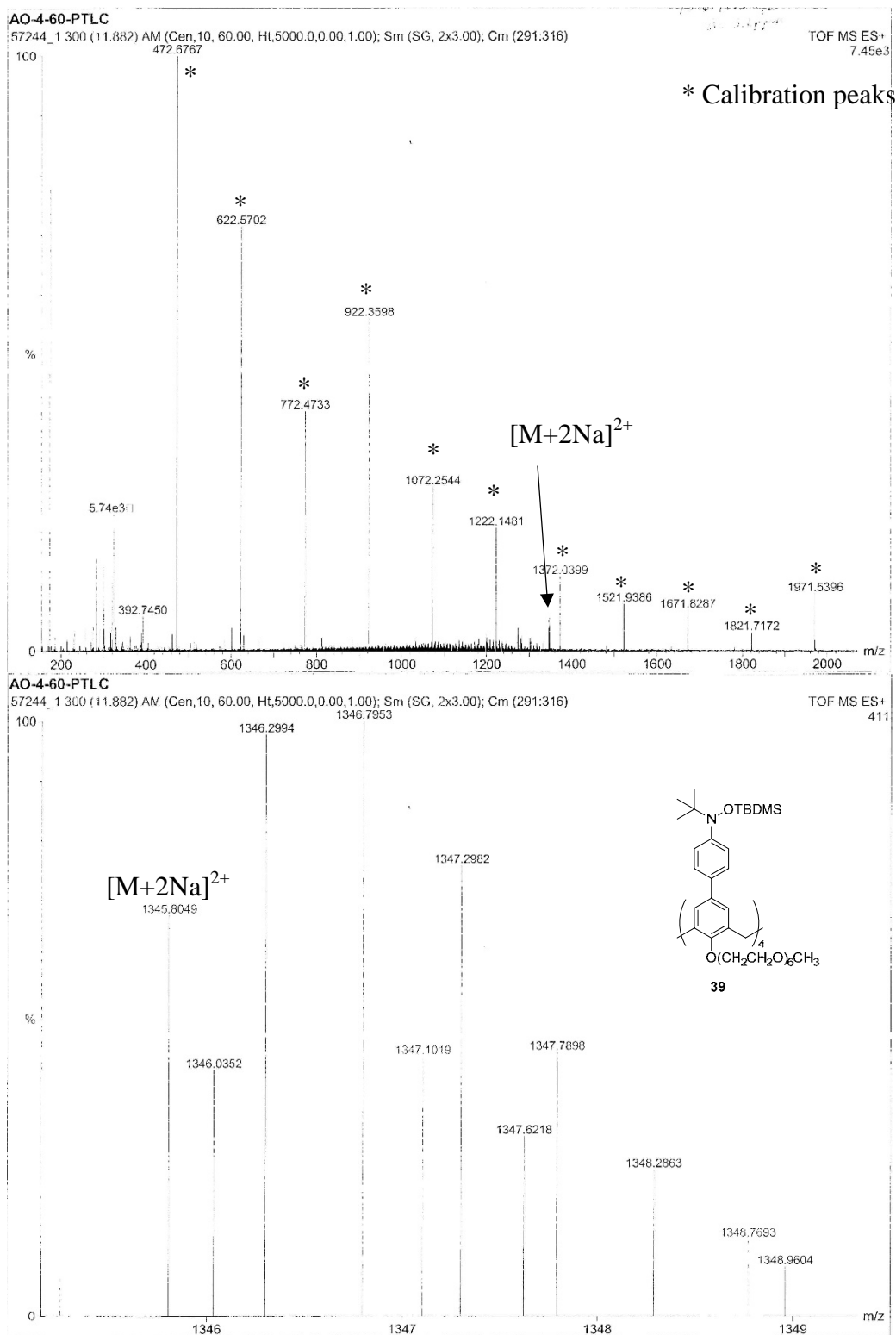
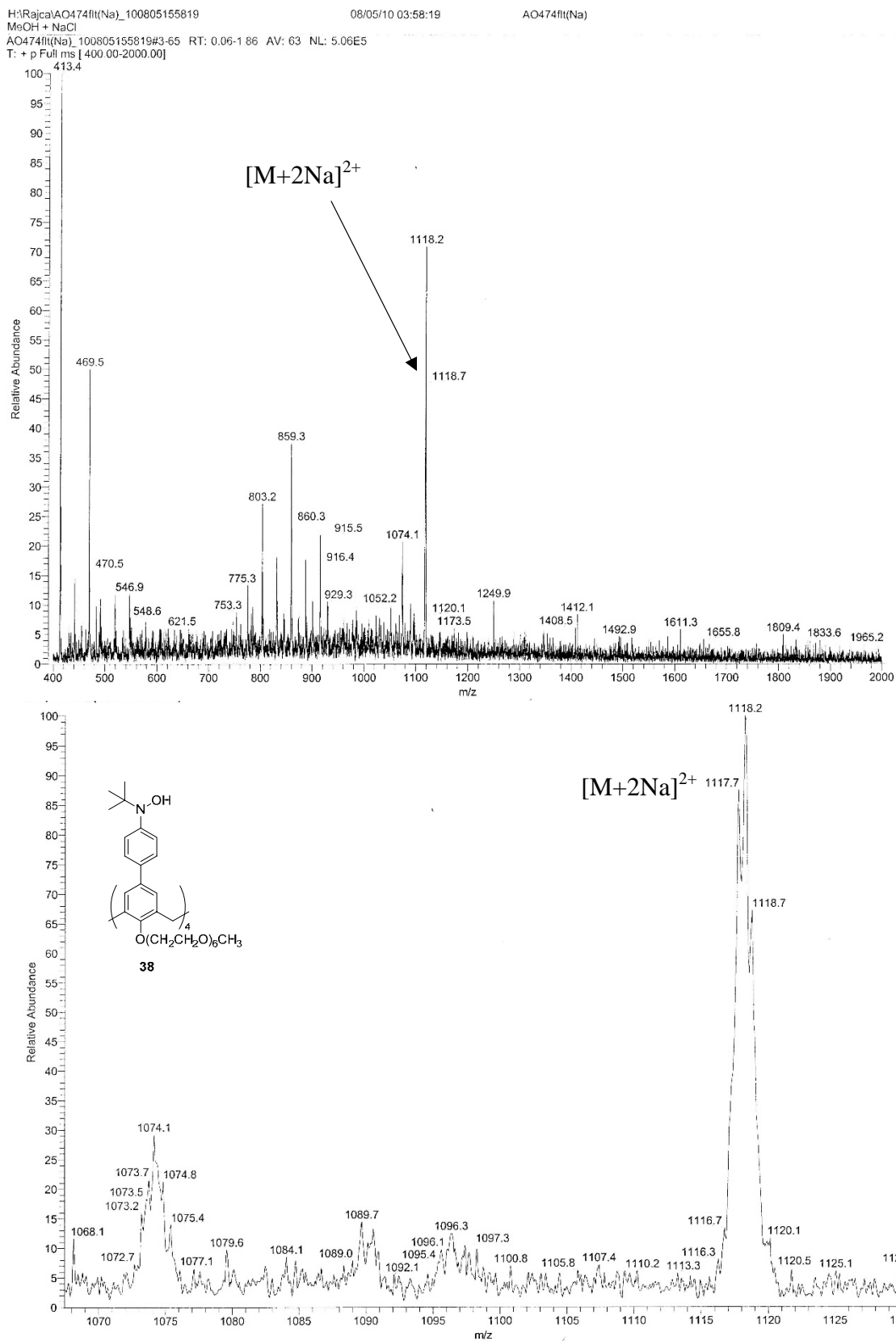**Figure D43.** HR ESI-MS (AO-4-60-ptlc) of TBDMS-protected **39**.

**Figure D44.** LR ESI-MS (AO-4-74-flt) of tetrahydroxylamine **38**.
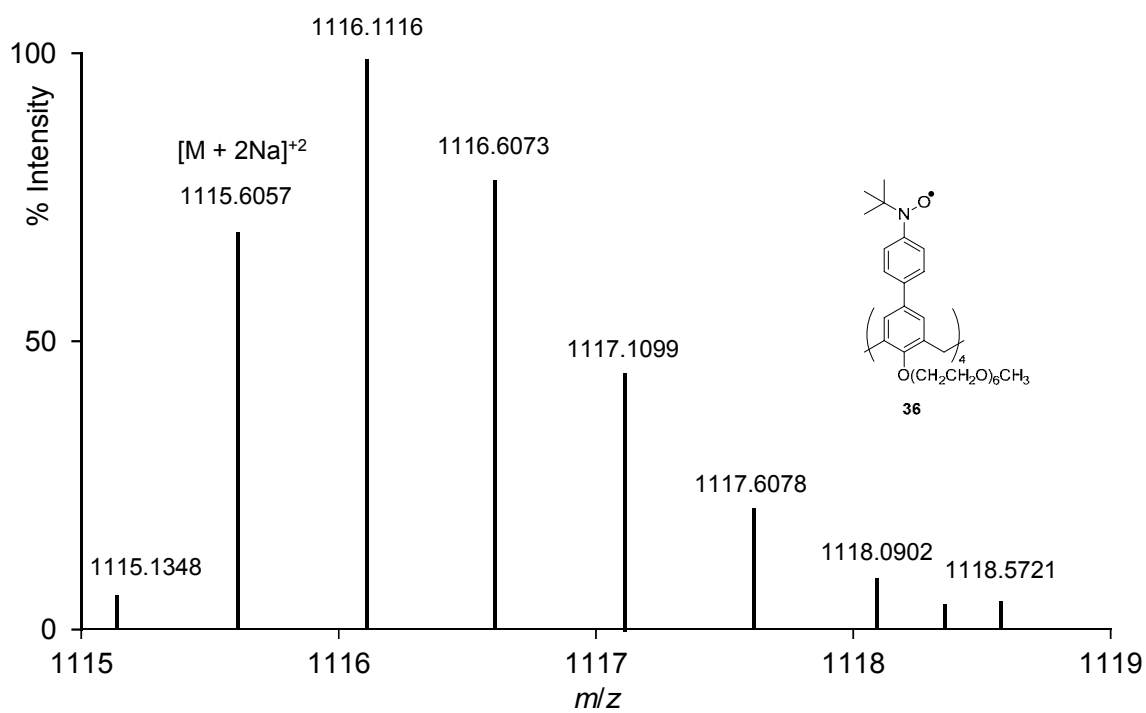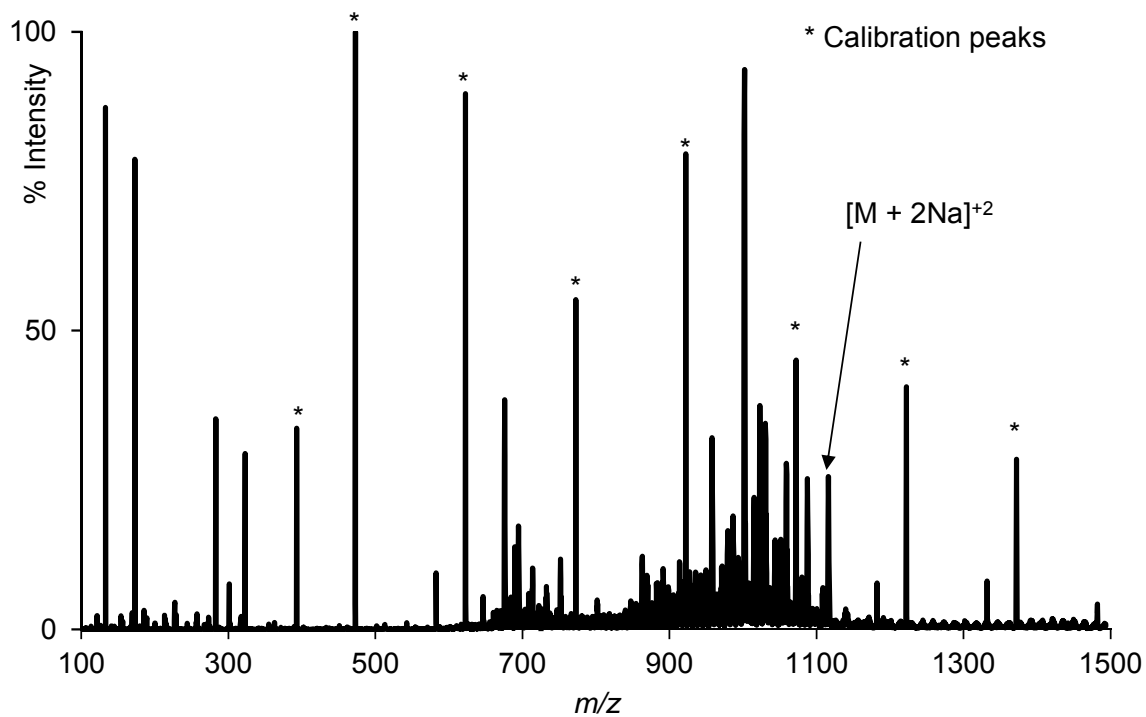
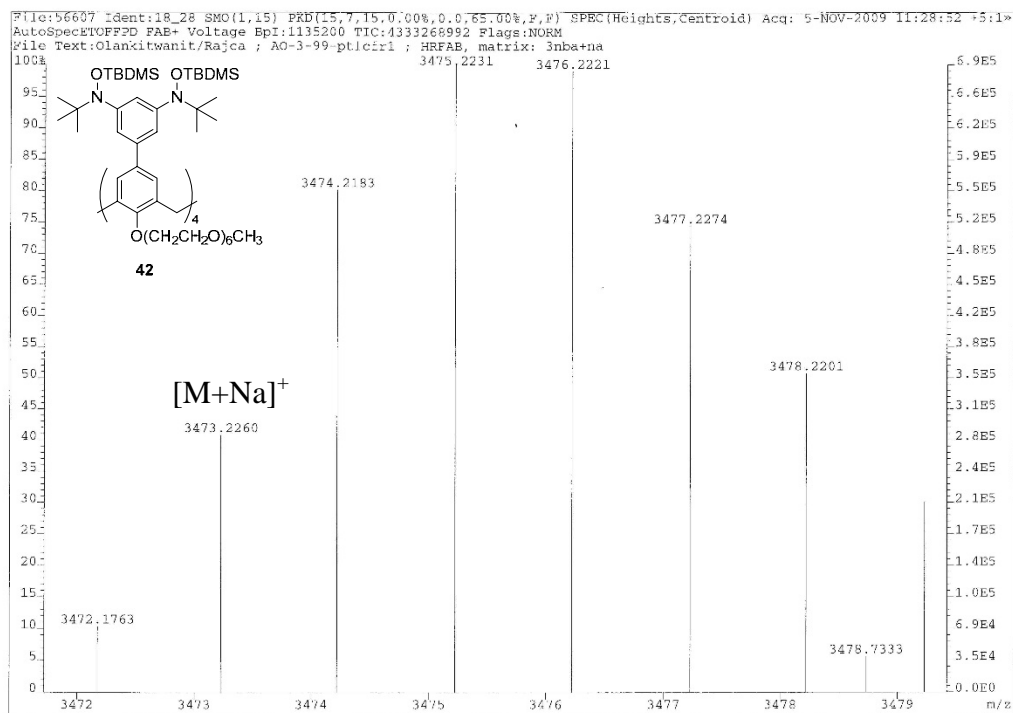**Figure D45.** HR ESI-MS (AO-4-80) of calix[4]arene nitroxide tetraradical **36**.

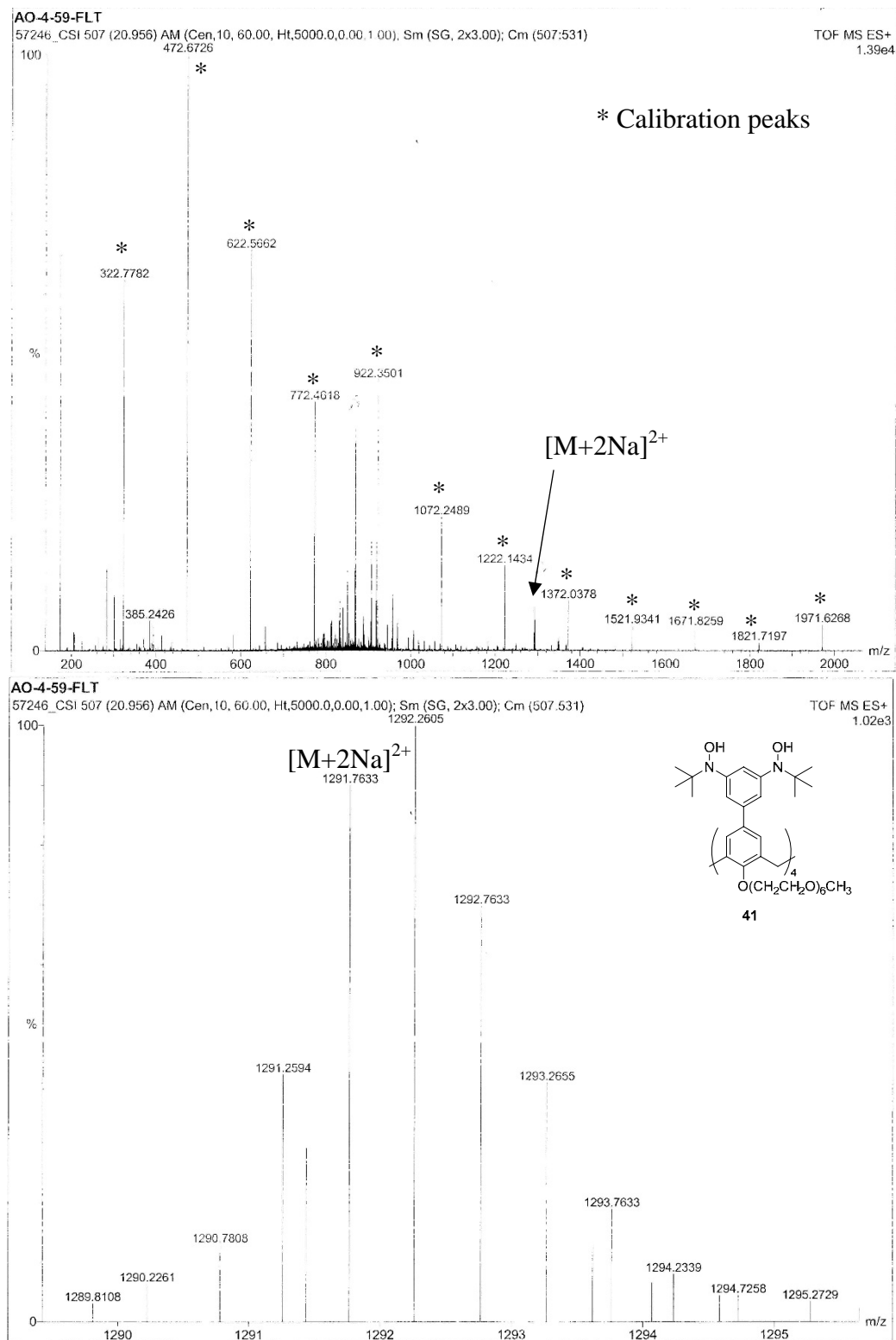**Figure D46.** HR ESI-MS (AO-3-99ptlcfr1) of TBDMS-protected hydroxylamine **42**.

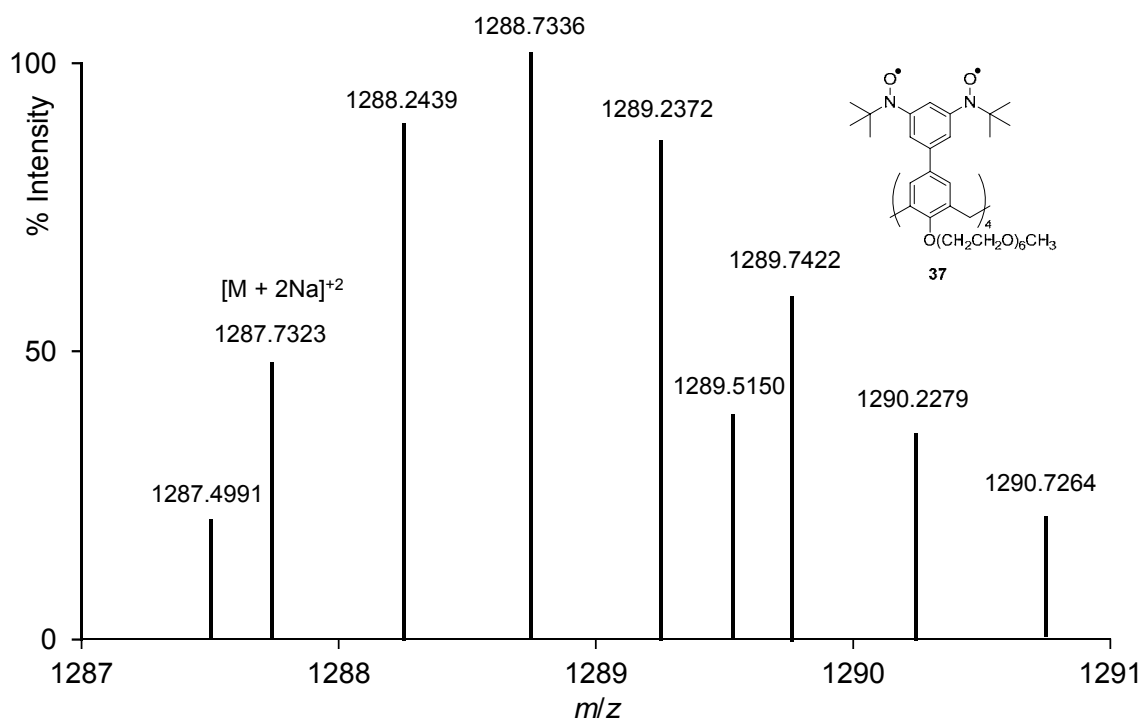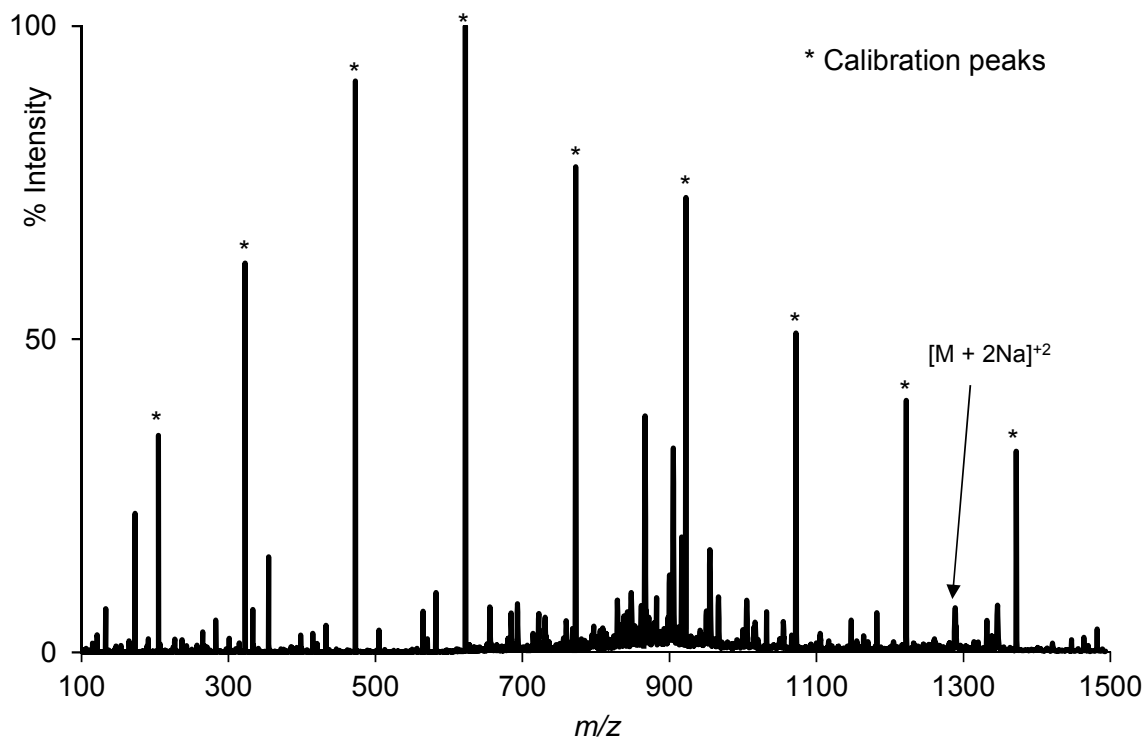**Figure D47.** HR ESI-MS (AO-4-59-flt) of octahydroxylamine **41**.

**Figure D48.** HR ESI-MS (AO-4-79-col) of calix[4]arene nitroxide octaradical **37**.